

ENERGY BUDGET STUDIES IN RELATION TO FAST-ICE BREAKUP PROCESSES IN DAVIS STRAIT

Climatological Overview

R.G. Barry and J.D. Jacobs
with
R.G. Crane, R.A. Keen, R.E. Moritz, E.F. LeDrew,
and R.L. Weaver



Occasional Paper No. 26
1978

ENERGY BUDGET STUDIES
IN RELATION TO FAST-ICE BREAKUP PROCESSES
IN DAVIS STRAIT: CLIMATOLOGICAL OVERVIEW

by

R. G. Barry¹ and J. D. Jacobs²

with R. G. Crane¹, R. A. Keen¹, R. E. Moritz¹, E. F. LeDrew³ and R. L. Weaver¹

¹Institute of Arctic and Alpine Research
University of Colorado, Boulder

²Department of Geography
University of Windsor, Ontario

³Department of Geography
University of Waterloo, Ontario

Final Report to Division of Polar Programs,
National Science Foundation

GV-28218

March 1978

University of Colorado
Institute of Arctic and Alpine Research

Occasional Paper 26
ISSN 0069-6145
INSTAAR/OP-26

Citation of this publication is Institute of Arctic and Alpine Research,
University of Colorado, Occasional Paper No. 26, 1978.

CONTENTS

1. Overview: Program Structure and Major Findings - R. G. Barry	1
A. Program Structure	
B. Major Findings	
2. Regional Climatic Setting - R. G. Barry and R. A. Keen	8
A. Large-scale controls	
B. Synoptic classification and catalog	
C. Synoptic climatology	
3. Synoptic Case Studies - E. F. LeDrew	68
A. Diagnostic analysis of a synoptic situation causing extreme ice melt	
B. Investigation of the heat island effect of the West Greenland Current	
4. Radiation Studies	105
A. Radiation climate of Broughton Island - J. D. Jacobs	
B. A model for estimating global solar radiation - R. E. Moritz	
5. Ice Regime - R. L. Weaver, J. D. Jacobs and R. G. Crane	143
A. Regional setting	
B. Fast ice characteristics at Broughton Island	
6. Microclimatology of the Fast Ice - R. L. Weaver, R. G. Crane and J. D. Jacobs	177
A. Approach and methods	
B. Radiation results	
C. Energy budget of the fast-ice	
D. Synoptic controls on the energy budget	
7. Ice-Climate Interactions	262
A. Seasonal controls of ice melt - R. G. Barry	
B. The response of Baffin Bay ice conditions to changes in atmospheric circulation patterns - R. A. Keen	
Appendix 1	279

Acknowledgments

During the course of this program, many individuals and organizations have assisted us. We particularly wish to thank: Mrs. Margaret Eccles, INSTAAR, who gave indispensable help with computer programming, the Computing Center, University of Colorado, and the Computing Facility, NCAR; John, Clark, INSTAAR and Harold Banton, FOF, NCAR, assisted with field instrumentation; data and imagery requirements were filled with help from NOAA-NESS (E.P. McClain), NCAR(Roy Jenne), Atmospheric Environment Service, Canada, the Ice Forecast Central, Ottawa (H. Hengevelt, W. Markham); logistical and other field operations were facilitated by the North American Air Defense Command (DEW-line), Parks Canada (E. Sieber), the Government of the Northwest Territories, and the Hudson Bay company store, Broughton Island; much of the drafting for the report was carried out by Marilyn Joel, INSTAAR, secretarial and administrative personnel at INSTAAR also assisted in various stages of the study. Finally, the field program was greatly helped by the cooperation of the people of Broughton Island.

Roger G. Barry

SUMMARY OF COMPLETED PROJECT

Please read instructions on reverse carefully before completing this form.

1. INSTITUTION AND ADDRESS Institute of Arctic & Alpine Res. Univ. of Colorado Boulder, CO 80309		2. NSF PROGRAM Division of Polar Programs	3. GRANT PERIOD April 1972- Dec. 1977 from to
4. GRANT NUMBER CV-28218	5. BUDGET DUR. (MOS) 69	6. PRINCIPAL INVESTIGATOR(S) R. G. Barry	7. GRANTEE ACCOUNT NUMBER 1530700

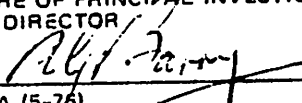
8. SUMMARY (Attach list of publications to form)

The program focused on the climatic factors affecting the shorefast ice regime in western Davis Strait, especially during the decay season. The major components of the program included field study of ice growth and ablation and related microclimatology near Broughton Island, N.W.T. (67°34'N, 64°03'W), from satellite imagery, and synoptic climatological analysis of climatic factors affected the ice.

A five-stage ice melt regime from inception of puddling to breakup has been identified and the timing of these phases during 1971-74 has been examined. Energy balance computations for 1972 enabled the snow-cover removal - puddling phases to be studied in detail. A simple melt model reproduced contrasts between 1972, when the ice did not break-up, and 1973. Air temperature is an important factor until the snow cover becomes isothermal at 0°; then net radiation and advected sensible heat flux strongly determine the progress of melt. Accumulated thawing degree-days (TDD) for mean daily temperature above 0° are probably the most useful simple index of melt conditions. About 180 TDDs are required at Broughton Island (580 meters) for the fast ice to break up; On average, this takes place in late July.

Synoptic analyses show that northerly-easterly airflow tends to retard the melt whereas southerly-westerly flow accelerates it. Although there were too few data to relate specific energy flux regimes to the synoptic pressure patterns, case studies based on field measurements and a modelling study were carried out. An objective catalog of daily pressure patterns over 58° - 80°N, 55°-100°W, grouped into 28 types, has been carried out for 1946-74. Distinctive temperature anomalies and precipitation amounts at Broughton Island are shown to be associated with each of the major types.

The fast ice off eastern Baffin Island in early summer has a typical thickness of 1.5-2.0m. Its extent varies about +15-25 percent from year-to-year. Winter severity has little effect on ice thickness or extent, but severe summer conditions such as 1972 occasionally allow second year ice to develop. A trend towards cooler summers from about 1962 to the early 1970's can be related to an eastward displacement of the mean trough of low pressure aloft, which gave rise to more frequent northerly airflow. This appears to have been linked with northward contraction of the hemispheric westerlies.

9. SIGNATURE OF PRINCIPAL INVESTIGATOR/ PROJECT DIRECTOR 	TYPED OR PRINTED NAME ROGER G. BARRY	DATE 15 Feb. 1978
--	---	----------------------

1. OVERVIEW: PROGRAM STRUCTURE AND MAJOR FINDINGS

R. G. Barry

A. Program Structure

Introduction

The overall program in the Davis Strait - eastern Baffin Island area has focused on climatic conditions, and especially energy budgets, in relation to shorefast ice and its seasonal decay. The research has comprised field studies centered primarily at Broughton Island (Fig.1) and synoptic climatological analyses, including some diagnostic modeling calculations of particular atmospheric processes.

It will be helpful to begin by outlining the major components of the overall research program, together with a summary of the field programs, since these determine the structure of this final report. We have sought to understand:

1. the nature of the shorefast ice in the western Davis Strait and its seasonal regime, with primary emphasis on summer breakup;
2. the role of atmospheric factors, particularly energy transfers, in the breakup process both on the microclimatic and the synoptic scale;
3. the interactions between ice conditions and climate in this area, on both short (daily - weekly) and long (several years) time scales.

Field Program

The field research has involved measurements of ice conditions and related microclimatological measurements in the vicinity of Broughton Island ($67^{\circ} 34'N$, $64^{\circ} 03'W$), just off the east coast of Baffin Island. The sites were mainly located in the harbor area between Broughton Island and the mainland (Fig. 6A.1). The terrain rises to 600 m on the surrounding land. In addition, climatological data were collected at Broughton Village. The periods covered by field measurements, and reference sources, are summarized in Table 1. Additional information on the 1972-1974 ice observations are given in Figs. 6A.2-4. In 1973, the "West Station" was established in mid June. However, melt in early July forced a move to "North Station" which was closer to the 1972 site. In 1974, it had been planned to work in the more exposed coastal environment east of Broughton Island, but extremely rough ice conditions made this impossible. In 1975, the summer work was limited to some ground reconnaissance surveys of ice south of Broughton Island and participation in five Canadian ice patrol flights by R. L. Weaver and J. D. Jacobs to provide a view of regional ice conditions.

Results deriving from these field programs are contained in Jacobs (1973, 1974d) and Weaver (1976) as well as in the contributions of Jacobs and Crane in this report. The primary objectives of the field programs were to collect the following:

- (i) data on ice characteristics and water characteristics during the decay season;
- (ii) concurrent micrometeorological and weather data to use in modelling the ice growth and decay processes.
- (iii) climatological data at Broughton Village, to provide a check on the local representativeness of the data from the regular weather station, "Broughton Island", which is located at the DEW-line site (580 m asl) on the seaward side of the island.

Analytical Data Studies

The central focus of our analyses has been the application of synoptic climatological techniques to meteorological data, in order to isolate the major types of weather systems that shape the character of the decay season and departures from its climatological mean regime. On the large-scale, this has been examined in terms of a synoptic catalog of pressure pattern types. The early work used a subjective classification (Barry, 1974), but an objective catalog has now been developed (Barry, Keen, this report). Local climatic conditions and field data on energy fluxes over the ice from 1972 have been examined with respect to these types (Bradley, 1974; Barry, Keen and Crane, this report). The interaction of large-scale and local processes has also been examined via diagnostic studies of advection situations and via the application of mesoscale numerical models to hypothetical data (LeDrew, 1976 and this report). Finally, the fast-ice regime itself has been examined by satellite imagery (Weaver, 1974; Crane, this report) in addition to its characterization from field surveys (Weaver, 1976; Weaver *et al.*, 1976), and we have attempted to clarify relationships between the controls and the ice regime (Jacobs, 1973; Barry, Jacobs, 1974; Barry *et al.*, 1975).

B. Major Findings

The major results of the program, detailed in the following sections, can be summarized as follows:

1. Maps of ice conditions for 1970-73 show that most of our field data relate to conditions similar to those during the recognized severe ice regime of the 1960's. Breakup in the Broughton Island area generally occurs about late July; the 1972 season, when breakup and clearance did not occur, was a major regional anomaly.

2. The fast ice extent in early summer off eastern Baffin Island varies approximately - 15 - 25 percent with a typical thickness of between 1.5 - 2.0 m.
3. A five-stage melt sequence can be identified. A transition from snow cover to slush occurs late May - early June and then breakup takes place in late July following the accumulation of about 180 thawing degree-days ($^{\circ}\text{C}$), at Broughton Island (581 m. a.s.l.).
4. Air temperature is thus an important factor until the snow cover ripens. Net radiation and advected turbulent heat flux mainly determine the subsequent progress of melt. A simple model to compute ice melt rate using daily totals of solar and net radiation and mean daily albedo, with initial conditions of mean ice temperature, salinity and thickness specified has been outlined. Its estimates for 1973, while overestimating the thickness change, were within one standard deviation (16 cm) of the measured value in early August, confirming the importance of radiative energy sources to melt.
5. Airflow from northerly - easterly directions tends to retard the melt, whereas southerly - westerly airflow accelerates it. However, insufficient cases with similar pressure patterns and variability in the local conditions, during the period with detailed microclimatological data over the ice in 1972, has prevented any firm categorization of synoptic patterns in terms of their energy inputs to the surface.
6. Daily MSL pressure patterns have been catalogued according to an objective scheme of 28 types, based on grid point data for the sector 58°N - 80°N , 50°W - 100°W , for 1946-74. Distinctive temperature departures and precipitation amounts are associated with each of the major types at Broughton Island, showing that the catalog is useful for discriminating local weather conditions.
7. Diagnostic analysis of a cold low system which affected the area in July 1973 and which gave rise to significant ice melt, shows that warm advection from the west was augmented by adiabatic descent over the east coast mountains.
8. Preliminary work with a sea-breeze model (with a dry atmosphere) suggests that local advective energy import associated with a warm surface current, for example, will have little effect on potential melt rate of ice surfaces for reasonable temperature anomalies.
9. The trend towards cooler summers around Baffin Bay since about 1962 can be related to an eastward displacement of the 700 mb trough giving rise to more northerly airflow. This eastward shift is apparently related to stronger hemispheric westerlies in high latitudes as a result of a northward contraction of the westerly wind belt.

Table 1 Periods of Field Measurements

<u>Location</u>	<u>Period</u>	<u>Comments</u>	<u>References</u>
Cape Dyer vicinity	19-26 May 1971	Aircraft transects over Davis Strait	Jacobs <u>et al</u> 1972
Broughton Village	June 1971 - Oct 1974 (except April - May 1972	Twice-daily climatological observarions	<u>Monthly Record</u>
Broughton Village	15 Dec 1971 - 20 Jan 1972	Micrometeorology and ice observations	Jacobs, 1973, 1974d
2 km SSW of Cape Broughton	10 June - 20 July 1972	Micrometeorology and ice observations	Jacobs, 1973 Weaver, 1976 Crane, this report
West Station, North Station, Broughton harbor	20 June - 1 July 1973 2 July - 5 Aug 1973	Micrometeorology and ice observations (See Table 2)	Jacobs, 1974a Weaver, 1976
Broughton Island vicinity	May - Nov 1973 June - July 1975	Water temperature and salinity profiles	Jacobs, 1974b Annual Rep. 1976
South Station Broughton harbor	6 June - 2 July 1974	Micrometeorology and ice observations	Weaver, 1976

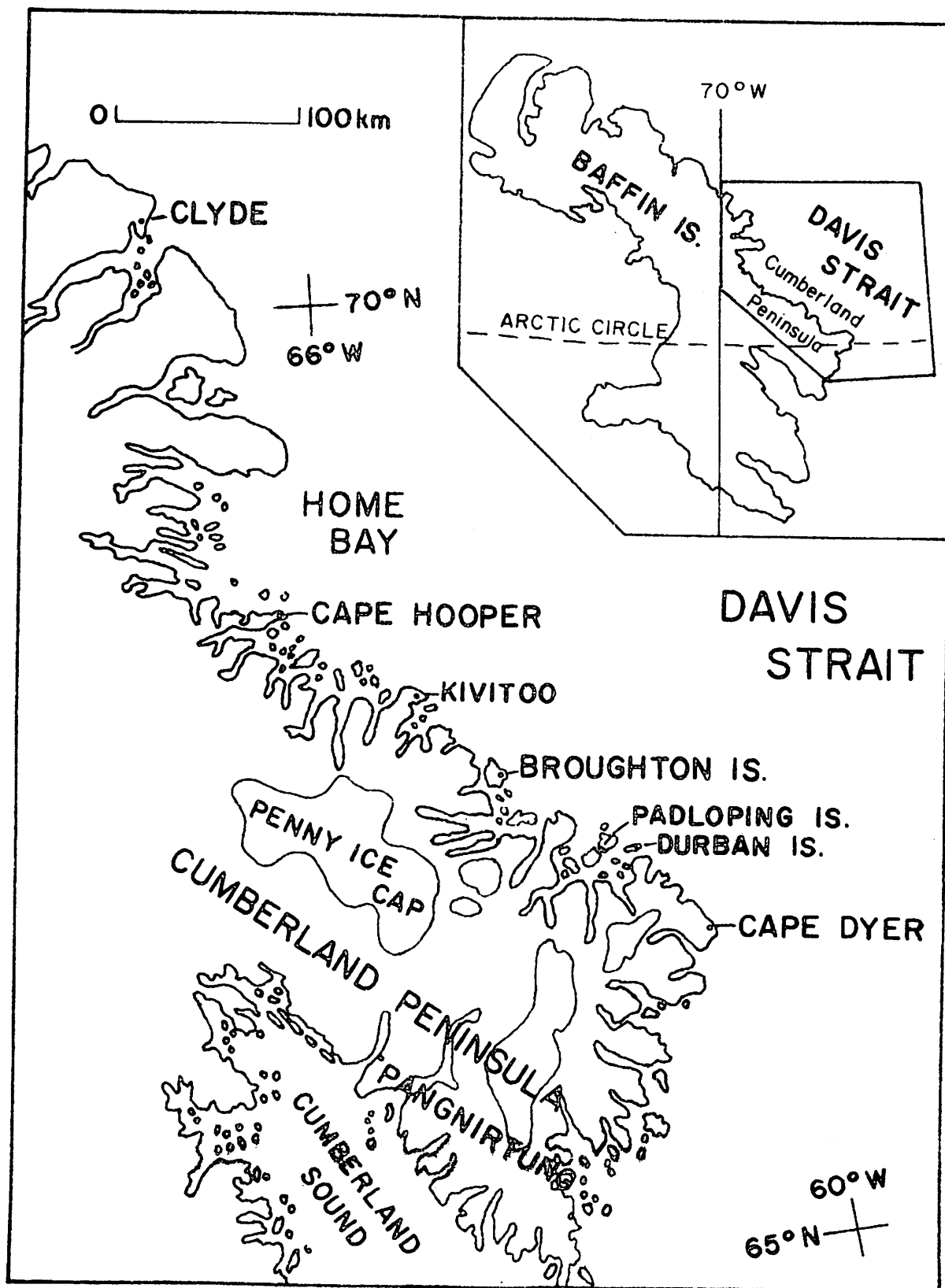


Figure 1. Eastern Baffin Island

References

- Barry, R.G. 1974. Further climatological studies of Baffin Island, Northwest Territories. Inland Waters Directorate, Tech. Bull. No. 65, Environment Canada, Ottawa: 33-38.
- Barry, R.G. and Jacobs, J.D. 1974. Synoptic activity, climate, and ice conditions for summers 1971-1973. In: Jacobs, J.D. et al. (1974): 67-75.
- Barry, R.G., Bradley, R.S. and Jacobs, J.D. 1975. Synoptic climatological studies of the Baffin Island area. In: Weller, G. and Bowling, S.A. (eds.), Climate of the Arctic, Univ. of Alaska Press: 82-90.
- Bradley, R.S. 1974. Climatic conditions in eastern Baffin Island in relation to synoptic pressure patterns. In: Jacobs, J.D. et al. (1974): 17-34.
- Jacobs, J.D. 1973. Synoptic energy budget studies in the eastern Baffin Island - Davis Strait region. Unpub. Ph.D. thesis, Univ. of Colorado, Boulder, 218 pp.
- Jacobs, J.D. 1974a. Research activities during 1973. In: Jacobs et al. (1974): 1-8.
- Jacobs, J.D. 1974b. Seasonal variations in temperatures and salinities on near-shore surface waters around Broughton Island, eastern Baffin Island. In: Jacobs et al. (1974): 59-66.
- Jacobs, J.D. 1974c. A growth equation for fast ice. In: Jacobs et al. (1974): 35-46.
- Jacobs, J.D. 1974d. Solar and radiation data for Broughton Island, eastern Baffin Island, 1971-1973. Univ. of Colorado, Boulder, Inst. Arct. Alp. Res., Occas. Pap. No. 11: 13 pp + appendices.
- Jacobs, J.D., Barry, R.G., Stankov, B. and Williams, J. 1972. Short-term air-sea interactions and surface effects in the Baffin Bay-Davis Strait region from satellite observations. Univ. of Colorado Boulder, Inst. Arct. Alp. Res., Occas. Pap. No. 4: 80 pp.
- Keen, R.A. 1977. The response of Baffin Bay ice conditions to changes in atmospheric circulation patterns. Preprint, 4th International Conference on Port and Ocean Engineering under Arctic Conditions, St. Johns, Newfoundland.
- LeDrew, E.F. 1976. Physical mechanisms responsible for the major synoptic systems in the eastern Canadian Arctic in the winter and summer of 1973. Univ. of Colorado, Boulder, Inst. Arct. Alp. Res., Occas. Pap. No. 22 (NCAR Cooperative Thesis No. 38): 205 pp.
- Weaver, R.L. 1974. Mapping seasonal changes in the fast ice and pack using remote sensing data. In: Jacobs et al. (1974): 47-54.

Weaver, R.L. 1974. Mapping seasonal changes in the fast ice and pack using remote sensing data. In: Jacobs et al. (1974): 47-54.

Weaver, R.L. 1976. Aspects of the radiation budget related to fast ice decay, Broughton Island, Baffin Island, N.W.T. Unpub. M.S. thesis, University of Colorado, Boulder, 158 pp.

Weaver, R.L., Barry, R.G. and Jacobs, J.D. 1976. Fast ice studies in western Davis Strait. In: Proceedings of the Third International Conference on Port and Ocean Engineering under Arctic Conditions, Vol. 1, Univ. of Alaska: 455-466.

2. REGIONAL CLIMATIC SETTING

R. G. Barry and R. A. Keen

A. Large-Scale Controls

Throughout the year the upper air circulation over Baffin Island is dominated by a major trough or closed low within the troposphere westerlies. At the 500 mb level, a closed low is present on the mean monthly charts (1951-60) over or near Baffin Island from November through February and also in May (Titus, 1967). At this level, the atmosphere over the area is the coldest part of the hemisphere and this factor is important in terms of the atmospheric vapor content (Barry and Fogarasi, 1968). Flohn (1952) showed that the frequency of cold lows on the 1000-500 mb thickness charts is a maximum over Baffin Island in winter.

From March through October (excluding May), the 500 mb circulation displays a trough centered over Baffin Island. Consequently, the upper circulation generally tends to be rather weak in winter and summer. At the surface the mean flow in winter is a strong northerly-northwesterly one between the Mackenzie high and the Icelandic low, which has a subsidiary trough along the west coast of Greenland. The circulation weakens in spring when the high tends to shift to the Queen Elizabeth Islands. In summer, the mean circulation at the surface is slack, with a weak low over southern Baffin Island (O'Connor, 1961)

The northern part of Baffin Bay is a major focus of cyclonic in winter (Keegan, 1958). The effects of the Greenland ice sheet in causing stagnation of eastward-moving systems, in promoting secondary disturbances, and in steering lows northward along the west coast of Greenland, are all apparent in this Baffin Bay maximum of cyclone activity (H. Wilson, 1958). The occurrence of the North Water in Smith Sound, with its associated heat and moisture fluxes to the atmosphere, is also a contributory factor to subsynoptic and synoptic scale cyclogenesis (Müller et al., 1976). In summer the frequency of baroclinic disturbances is a maximum over Hudson Strait-David Strait, associated with the Arctic Front (Barry, 1967), with a secondary maximum in northern Baffin Bay (Reed and Kunkel, 1960) which serves as a 'graveyard' for cyclones from east coast of North America and from the continental interior. On the meso-scale, there are indications that the mountains of eastern Baffin Island induce ridging (H. Wilson, 1958), especially in northwesterly flow situations. The station network is too sparse to examine these effects. It is worth noting that the stations at Cape Dyer, Broughton Island, Cape Hooper and Dewar Lakes are on exposed hilltop sites whereas Frobisher Bay is located between low ridges at the head of the long inlet, and Clyde is in a relatively open location on an inlet.

B. Synoptic Classification and Catalog

The earliest studies (Jacobs et al., 1976) made use of an existing subjective catalog of daily surface pressure-pattern types over the area (Barry, 1974, pp. 35-38). In order to provide an objectively-determined classification that could be applied rapidly to a longer time period, a procedure developed by Kirchoffer (1973) for European 500 mb patterns was adopted. This method has also been used for similar classifications for the western United States (Barry, Bradley & Tarleton, 1977) and for Alaska (Barry, 1976). The description below follows methods used by Moritz (1978). An objective classification has been developed for the Baffin Island area by Fogarasi (1972) using the correlation method of Lund. However, it is not readily amenable to large data sets of the type used here, due to the required size of the correlation matrix. Fogarasi's study was restricted only to summer 1968.

The classification scheme was applied to NMC grid-point pressure data (provided by NCAR) for the sector $58^{\circ} - 80^{\circ} \text{ N}$, $50^{\circ} - 100^{\circ} \text{ W}$. The 37 - point NMC grid, and row and column groupings of the points, are shown in Figure 2.1. The first stage of the analysis involved a set of 58 months, selected by inspection of monthly maps of pressure anomaly to represent seasons with a variety of regimes. Table 2.1 summarizes regional indices of geostrophic zonal wind for $55^{\circ} - 70^{\circ} \text{ N}$ between $50^{\circ} - 100^{\circ} \text{ W}$ and geostrophic meridional wind for $60^{\circ} - 75^{\circ} \text{ W}$ averaged at 60° , 65° and 70° N showing that a balanced range of monthly anomalies is indeed represented. This table also lists the actual months selected and the corresponding mean values of the two indices.

The first step in the process is to normalize the 37-point grid for each individual day. The mean (\bar{P}_j) and standard deviation (s_j) of the 36 pressures are calculated for each ("jth") day individually. Each day's grid is then normalized individually so that the actual pressure at the "ith" point on the "jth" map (P_{ij}) is replaced by:

$$Z_i = \frac{P_{ij} - \bar{P}_j}{s_j} \quad (2.1)$$

i.e. the number of standard deviations by which it differs from the map mean. Z_{ij} will be referred to as the normalized grid value of the "ith" point on the "jth" map. The effects of this procedure are twofold:

- 1) All reference to the absolute magnitudes of the pressures are removed. e.g. a closed circular low with a uniform pressure gradient will have the same normalized pattern no matter what the central pressure is.
- 2) Weak actual pressure patterns can become stronger normalized patterns. That this is so can be seen by considering two maps with identical isobar pattern shapes and identical mean pressures, but with different standard deviations. The differences in pressure $P_{ij} - \bar{P}_j$ for the weak pattern (low standard deviation) will be less in each case than the corresponding differences in the strong pattern. However, the weak pattern's standard deviation s_j will be even more strongly reduced, because it is calculated from a sum of squared

deviations from the mean. The net effect is to cause grid patterns of normalized values to become stronger (more isopleths) than their corresponding (weak) actual pressure patterns.

The second step in the procedure is to determine for each day in the sample the number of other days classified as having a similar normalized pattern to that of the given day. Similarity is tested by computing the quantity:

$$(\Delta_j)_{jk} = (z_{ij} - z_{jk}) \quad (2.2)$$

where the subscripts indicate that we take the difference between normalized grid values at the "ith" point of the "jth" and "kth" daily maps. We then square and sum over the 37 points:

$$\text{SUM}_\Delta^2 = (\Delta_i^2)_{jk} \quad (2.3)$$

which yields the total sum of squared differences between corresponding normalized grid point values between the two (j & k) maps. The magnitude of SUM_Δ^2 is then a measure of the dissimilarity of the two maps in question. Previous work with this technique suggests that two patterns can be satisfactorily grouped as similar if SUM_Δ^2 is less than equal to N, the number of grid points (37 in this case). It should be emphasized that the selection of such a "threshold" is a subjective process, involving visual inspection of similar maps and testing of the program with various thresholds. The total sum of squared grid-point differences over the map gives a measure of similarity for the entire field, but it might still be possible to have similar maps with rather undesirable pattern differences concentrated in a small portion of the field. Therefore, the maps were divided into six (approximately) zonal rows and seven meridional columns (Figure 2.1). The SUM_Δ^2 for the points in each of these subdivisions are then calculated for each pair of maps and must be less than or equal to 1.8NN , where NN is the number of points in the subdivision, in order to be classified as similar. This threshold was also determined subjectively, based on previous work. After repeating this procedure for all pairs of maps in the sample, we have a "table" (within the computer) listing against each day, all days passing both similarity tests.

The third step in the classification is to find the key days which serve as pattern-types or representatives for the rest of the sample. The day having the largest number of similar days is designated as key day number one. All days listed as similar to key day number one are then removed from the lists of similar days in the rest of the "table". After these days are cleared from the matrix, the day having the greatest number of remaining similar days in its list is designated as key day number two. This process is repeated until there are no days with greater than or equal to five similar days in their lists. Any residual days are listed as "unclassified".

The final step in the typing procedure is to assign all non-key days in the sample to the key day with which it had the lowest $\text{SUM} \Delta^2$. The need for this step arises when we clear each successive key day's list of similar days from the remaining table. This latter procedure removes from the remaining lists all days which passed with the key day presently under consideration. However, some of the days so removed may have a lower $\text{SUM} \Delta^2$ with respect to a key day generated later in the typing program. (i.e. it was "similar" to more than one key day, and had a lower score with the key day which occurred later in the program).

After completing these steps, we have a set of 28 key days, each with a list of all other days that have the smallest score within one of these key days. Subsequently, all days were typed with reference to the 28 key dates for January 1946 - August 1974.

The pressure maps for the 28 key days are given in Figure 2.2 which shows normalized values, i.e. the isopleth interval is $(0.5 \times \text{standard deviation})$ for each given map. The variability within each type is indicated by Figure 2.3 which plots the absolute frequency of low centers for the first twelve types. In most cases the center is located over a narrow range of grid points.

The complete catalog is presented in Table 2.2. The 28 types account for 98 percent of daily MSL pressure patterns for 1946-74 (Table 2.3). A descriptive name for each pattern is proposed in Table 2.4, together with an indication of the circulation direction and isobaric curvature over the area of Cumberland Peninsula. These are intended as a convenient reference system to obviate continual inspection of the type maps.

Table 2.5 summarizes the mean monthly frequency of the types in days. This emphasizes the dominance of patterns with a low in Davis Strait in winter months. In summer there is a greater variety of cyclonic patterns (see Figure 2.4) with types 1 (Davis Strait Low), 2 (Ungawa Low), 3 (Devon Island Low) and 4 (Hudson Bay Low) each occurring on about 3 days in July. On an annual basis, the first five types, which are all basically cyclonic, account for half of the days in the year and anticyclonic patterns (types 8, 10, 12, 17, 19, 24, 25 and 28) occur on only 17 percent of days (Table 2.5)

C. Synoptic Climatology

The climatic characteristics of the synoptic types have been analyzed for Broughton Island for the period 1959-70 with respect to daily temperature departures, since this element is of primary importance. For this purpose, normals for each day of the year were first determined. It was assumed that the daily temperatures could be represented as a quadratic function of time by $(a + bt + ct^2)$. The

mean temperature on the 15th of a given month ($t = 0$), was assumed to correspond to the published mean value for 1941-70, and likewise for the preceding ($t = -1$) and following ($t = +1$) months. The quadratic function was then fitted to these points. The quantity $c/12$ must be subtracted from the coefficient a in order for the integrated mean value of the quadratic to equal the monthly mean temperature. The coefficients b and c were then adjusted so that the computed mean for the end of one month matched that for the beginning of the next. The derived daily means are tabulated in Table 2.6.

The mean daily departures for each type, and their standard deviations and standard errors, are listed by month and season in Table 2.7. In order to examine these data, each type is plotted as a function of its average temperature anomaly for the summer and winter seasons in Figure 2.5¹. The seasonal anomalies are consistent, in virtually all cases, with what one would expect from advection and radiation considerations. A summary version of the same information is also given in Figure 2.6 to bring out relationships between the types.

Twelve of the synoptic types are characterized by a fairly simple flow pattern between a single low pressure center towards one edge of the grid and higher pressures elsewhere. For type 1, the low is in Davis Strait with northeasterly cyclonic (NE_C) flow over Cumberland Peninsula. Type 6, with a high over Thule, gives similar flow over the Cumberland Peninsula. From Figure 2.6, ten similar types can be identified where the low center is progressively displaced in a clockwise rotation. In sequence, these are type 10 (Thule High, NE flow), type 2 (Ungawa Low, E flow), type 7 (Hudson Strait Low, SE flow), type 4 (Hudson Bay Low, SE_C flow), type 11 (Southampton Island Low, S flow), type 22 (Foxye Basin Low, S flow), type 16 (North Baffin Low, SW_C flow), type 3 (Devon Island Low, W flow), type 9 (North-Central Low, W_C flow), and type 15 (Baffin Bay Low).

In winter the warmest types at Broughton Island (types 7, 4, 11 and 22) all give rise to southerly flow off the relatively warm, open waters of the Labrador Sea, while the coldest types (types 13, 24 and 27) are associated with cold air from north or northwesterly directions, or are high pressure situations (types 8 and 19). Type 21 is a transitional pattern from northerly flow over Davis Strait. Although type 28, with a high cell over Baffin Island, has positive departures in both seasons it should be noted that there are also large standard deviations, especially in winter (Table 2.7).

In summer, the warmest conditions at Broughton Island occur with types giving rise to south or southwesterly flow from southern land areas (types 16 and 22) or are anticyclonic patterns (types 25 and 28). The strongest anticyclonic patterns (types 12, 17, 19, 24, 25 and 28) all give positive departures in summer (Figure 2.6). Evidently,

¹In Figure 2.5, $1.2^{\circ}C$ has been subtracted from the mean winter departures given in Table 2.7, and $0.2^{\circ}C$ added to the summer departures, to account for the differences between the 12-year period used for the calculations and the 30-year mean values.

flow direction is less significant than a tendency for clear skies and high radiation inputs. The cool summer types are those bringing northerly or easterly flow over the relatively cold waters of Baffin Bay (types 1, 2, 6, and 10) or have a low centered over the area with extensive cloud cover (types 5, 15 and 26).

Inspection of Figure 2.5 allows similarities to be identified between some of the more complex pressure patterns and others where single lows are the dominant component. For example, the temperature characteristics of type 16 (a col situation with lows to the west and southeast) are intermediate between those of types 6 and 22 which have, respectively, lows to the southeast and to the west. In the case of the E-W col patterns of types 20 and 23, it is apparent, in view of their similarity to types 3 and 9 in Figure 2.5, that it is the low over Baffin Bay which is controlling the temperature anomalies.

The precipitation characteristics of the types at Broughton Island are indicated in Table 2.8. In winter, easterly flow with a low over Ungava (type 2) accounts for 30 percent of the precipitation and lows in the Davis Strait (types 1 and 6) and Baffin Bay (type 20) provide another 30 percent. In summer, lows over Davis Strait (type 1) give 20 percent of the total, with contributions of 14 percent from lows over Ungava (type 2), 16 percent from lows over Baffin Island and Devon Island (types 5 and 3) and 7 percent from lows over Hudson Strait (type 11). As Table 2.8 shows, there is a wider variety of patterns and airflow directions contributing to summer precipitation. Also, the actual amounts involved are more than 50 percent greater in summer than in winter.

In both seasons, the anticyclonic patterns (types 8, 12, 17, 19, 25 and 28) are almost entirely associated with dry conditions. Average intensities (mean precipitation per day of type occurrence) are generally 3-4 mm/day in summer for the major precipitation-contributing types, whereas in winter type 2 averages 5.2 mm/day and type 20 gives 5.9 mm/day, but averages are much lower for types 1 (2.4 mm/day) and 6 (1.6 mm/day).

These results indicate that the objective classification of daily MSL pressure patterns provide a useful basis for characterizing the climatic conditions of at least temperature and precipitation at Broughton Island. The potential significance of synoptic patterns with respect to summer decay of the fast ice, which has already been explored using the subjective catalog (Weaver *et al.*, 1976) is examined further in sections 6 and 7 of this report.

TABLE 2.1

A. Seasonal Frequency of Meridional Index Values

<u>Seasons</u>	<u>Meridional Index</u>				
	σ anomalies				
	-1.5	-1.4 to -0.5	-0.4 to 0.4	0.5 to 1.4	1.5
D-J-F	1	4	4	5	1
M-A-M	3	5	5	0	1
J-J-A	1	3	8	0	2
S-O-N	2	3	4	6	0
Year	7	15	21	11	4

B. Mean Meridional and Zonal Index For the Sample Months

	<u>Summary of Months</u>	<u>Mean Indices (m s⁻¹)</u>	
		<u>Meridional Index</u>	<u>Zonal Index</u>
January	1958, 63, 64, 70, 72	-4.4	0.3
February	1954, 68, 70, 72, 73	-3.4	0.9
March	1956, 60, 68, 71	-3.8	-0.5
April	1954, 65, 68, 69, 72	-2.5	-0.5
May	1963, 66, 68, 71, 72	-1.0	-1.6
June	1954, 61, 70, 73	-0.4	0.3
July	1952, 58, 64, 66, 69	+0.4	0.3
August	1952, 53, 55, 68, 73	+0.3	0.5
September	1954, 58, 60, 67, 71	-1.2	0.6
October	1953, 54, 64, 69, 72	-1.9	1.4
November	1952, 58, 66, 70, 72	-1.7	1.0
December	1957, 63, 67, 71, 72	-3.9	0.4

All indices are for MSL pressure data.

Table 2.2

Catalog of daily pressure types, 1946-74

(For code see Table 2.4; for key-day maps, see fig. 2.2)

Types for a few days with missing data have been determined subjectively.

YEAR	MON	1	2	3	4	5	6	7	8	9	10	11	12	13	14	15	16	17	18	19	20	21	22	23	24	25	26	27	28	29	30	31			
1946	1	1	21	1	1	8	15	10	1	19	6	1	1	1	1	1	1	1	1	1	1	1	3	12	8	5	5	10	1	1	1	1	1		
	2	1	1	1	14	8	2	2	1	27	23	21	14	15	13	2	1	1	1	3	22	2	6	10	1	1	0	2	2	11	1	1	1		
	3	24	4	4	7	5	9	11	1	1	1	26	26	6	6	6	6	19	8	1	26	15	10	1	8	1	1	0	2	2	11	1	1		
	4	3	9	5	1	1	3	0	1	1	3	0	4	5	20	1	6	1	5	3	18	27	4	4	2	2	2	1	12	2	6	6	6		
	5	1	10	1	1	1	5	0	4	2	10	2	2	23	5	15	20	1	1	21	5	12	2	10	8	2	2	2	6	6	6	6	10		
	6	10	1	1	15	15	20	2	5	11	24	2	2	10	1	1	1	1	10	10	1	1	8	5	5	5	4	1	1	1	15	1	1		
	7	20	2	10	1	3	3	9	9	27	23	23	2	1	1	1	1	1	15	1	1	15	1	8	9	27	11	20	1	27	23	20	3	3	
	8	27	1	27	4	7	25	2	2	10	20	1	11	7	4	11	2	1	1	1	1	9	20	3	3	3	3	3	5	1	10	10	1	23	
	9	23	2	11	11	9	5	18	1	1	15	20	1	15	15	6	26	2	1	15	4	2	6	4	2	6	4	2	7	13	11	20	1	17	
	10	24	0	6	12	2	1	1	3	12	2	2	4	11	9	9	5	24	6	1	6	1	15	23	8	4	2	1	1	1	1	1	1	8	
	11	1	8	8	2	1	6	2	1	1	2	1	5	5	11	1	8	23	2	5	5	21	26	4	7	7	4	4	1	1	1	1	1	1	
	12	1	8	6	1	1	8	1	1	8	6	6	6	2	2	6	1	5	20	1	3	15	20	6	1	2	2	1	1	1	1	1	1	1	3
1947	1	1	1	14	1	1	15	5	1	1	1	1	1	1	1	3	7	5	5	1	15	13	2	1	5	5	16	16	23	2	2	2	6		
	2	6	22	2	2	4	17	10	2	2	2	10	1	6	1	6	1	6	4	4	7	7	2	2	2	2	2	2	23	10	2	2	2	6	
	3	6	17	4	23	2	10	10	1	1	1	1	1	1	1	1	1	1	2	2	5	6	2	4	4	20	1	2	2	2	2	2	6	1	
	4	1	1	1	1	1	1	1	1	1	5	1	14	3	21	2	6	1	1	1	1	1	1	3	3	0	10	1	1	10	2	5	23		
	5	3	27	4	20	1	1	10	14	1	1	1	5	10	1	8	1	1	1	1	1	14	13	12	4	4	4	4	4	4	4	4	4	23	
	6	2	10	14	3	0	8	15	15	5	5	11	10	18	28	6	1	3	3	3	3	27	5	15	15	12	4	4	4	4	4	4	4	2	
	7	1	0	24	4	11	11	2	5	1	23	20	3	27	20	3	15	1	5	2	5	11	11	5	18	14	18	3	9	5	5	9	18		
	8	22	5	0	15	24	17	13	10	26	22	18	5	5	1	1	1	1	3	20	19	21	1	21	1	1	1	1	3	11	6	15	2		
	9	6	13	20	1	1	26	10	1	15	12	13	6	12	23	2	2	1	3	3	27	11	5	9	1	1	1	1	3	27	5	5	5	2	
	10	9	3	26	26	4	2	1	1	3	3	27	13	7	24	11	6	6	12	4	7	10	1	1	1	1	1	1	27	4	20	6	8	8	
	11	5	1	4	1	1	8	8	4	4	4	4	17	4	24	24	23	17	6	15	1	8	22	7	2	4	2	1	5	11	2	14	14		
	12	2	21	21	6	6	10	2	5	6	6	6	6	6	6	6	6	23	10	6	6	6	1	14	8	13	15	1	9	2	6	6	14		
1948	1	12	12	4	22	5	3	28	22	5	5	14	21	1	1	1	1	1	3	8	6	1	1	3	10	1	1	1	1	1	1	1	1	3	
	2	6	1	1	1	1	1	1	1	3	21	21	1	21	1	2	1	1	20	10	5	20	2	3	3	27	2	1	1	3	10	1	1	1	
	3	1	1	1	3	13	20	1	1	2	26	5	14	15	9	5	1	3	3	11	14	1	15	1	1	1	21	1	14	27	13	13	1	1	
	4	15	10	10	1	1	20	1	3	3	12	7	2	14	11	5	5	5	1	1	1	1	1	1	1	1	1	1	12	16	9	9	10	1	
	5	0	1	1	1	15	1	18	3	0	10	1	1	1	1	1	1	1	1	9	16	17	23	23	23	4	2	5	1	1	1	1	1	9	
	6	28	8	23	10	10	2	2	10	16	11	4	2	17	23	23	10	10	25	24	28	28	5	15	20	18	14	8	1	0	10	1	0		
	7	17	10	10	8	3	14	4	4	2	2	2	20	20	2	2	6	17	23	23	10	3	3	3	12	19	15	1	25	24	2	2	2	28	
	8	10	10	1	1	1	3	3	9	9	5	1	3	5	1	1	3	27	16	20	24	4	4	22	16	11	0	9	1	13	3	28	2		
	9	27	11	2	26	4	2	1	23	10	24	24	6	1	18	3	3	16	11	11	20	0	27	26	24	3	18	1	8	10	5	1	3		
	10	5	9	9	16	26	15	24	4	7	7	4	2	1	3	9	3	5	15	5	20	5	1	27	11	5	9	16	5	1	3	5	1	3	
	11	28	3	0	9	18	16	4	7	7	4	2	1	1	1	1	1	1	13	20	1	8	21	24	6	13	1	1	1	1	1	8	23	1	3
	12	17	6	6	6	21	2	23	5	6	24	6	6	6	2	10	1	1	3	18	2	6	1	1	1	1	1	1	1	8	19	14	11	1	1
1949	1	14	1	1	3	24	4	2	23	1	18	14	1	15	1	1	1	1	8	15	20	1	3	1	1	1	1	1	14	9	5	20	6	1	
	2	9	18	6	1	1	3	3	1	10	1	1	3	3	3	8	23	1	1	1	1	3	3	21	1	1	14	3	6	2	2	10	10	24	
	3	6	1	8	4	2	2	26	9	5	9	27	4	10	6	22	4	2	1	1	1	1	3	3	28	18	3	9	24	2	2	10	24		
	4	24	26	12	11	5	15	15	10	24	8	17	1	1	19	3	1	3	9	15	4	2	1	1	1	1	1	8	1	1	12	12	6	6	
	5	23	17	7	2	1	1	1	1	1	3	15	13	2	2	6	1	1	1	10	10	6	6	4	4	4	4	20	23	17	17	12	24		
	6	0	12	4	10	4	22	10	12	4	11	2	24	4	4	4	4	4	4	11	5	3	27	22	0	19	12	17	6	12	1	8	3	1	
	7	4	2	2	2	1	1	3	3	9	5	5	11	7	7	7	4	2	6	1	ND	1	1	1	1	7	28	3	12	17	7	10	10	3	
	8	9	9	11	9	5	5	5	2	10	10	1	1	3	3	3	0	10	1	3	0	2	1	1	1	1	1	3	15	9	20	14	1	4	22
	9	4	7	4	2	10	3	3	9	20	3	3	16	20	0	17	2	10	19	1	1	15	1	0	1	1	0	10	1	15	23	20	15	1	1
	10	1	27	4	2	6	12	12	4	7	6	4	2	2	2	6	6	4	0	5	1	3	3	16	2	5	4	1	1	2	21	1	1	2	
	11	1	1	15	1	8	5	4	2	10	10	6	6	24	6	6	13	2	6	1	1	6	6	6	1	1	1	1	18	1	27	3	2	2	
	12	10	1	8	4	23	2	7	10	2	26	5	23	2	1	1	1	5	14	3	21	21	2	6	10	21	1	19	1	1	1	10	6	12	

Table 2.2 Continued

YEAR	MON	1	2	3	4	5	6	7	8	9	10	11	12	13	14	15	16	17	18	19	20	21	22	23	24	25	26	27	28	29	30	31		
1950	1	2	5	21	7	14	3	21	1	21	3	1	19	22	13	14	13	2	1	1	3	3	3	3	1	1	13	1	1	3	15	10	8	
	2	8	8	1	1	1	1	19	3	1	1	1	1	3	3	14	1	15	1	1	1	3	10	6	1	1	1	1	1	1	1	1	1	
	3	1	10	1	8	2	6	0	2	20	2	2	6	6	6	6	1	1	1	1	1	1	1	8	15	23	10	6	1	1	1	1	1	
	4	9	3	6	1	1	10	1	3	27	20	1	3	3	9	1	12	28	17	4	20	0	20	10	2	2	2	2	2	2	2	2	1	
	5	1	1	14	1	1	23	10	10	6	23	23	2	2	2	2	7	7	4	16	12	4	22	16	11	23	5	3	27	26	2	4	15	
	6	4	4	7	20	2	2	18	14	4	11	2	1	1	7	2	22	7	7	7	7	25	25	1	3	3	3	11	17	0	0	10		
	7	23	10	3	9	0	9	9	26	1	1	1	5	1	3	9	5	9	5	9	4	2	4	4	4	7	11	26	11	2	1	1	20	
	8	1	14	1	1	1	3	9	2	1	13	1	1	3	3	1	1	5	10	1	20	1	26	2	10	25	10	3	15	12	23	23	1	
	9	18	1	3	3	27	2	1	1	1	1	1	3	3	3	1	1	3	9	11	10	1	15	3	12	4	0	1	1	1	1	1	15	
	10	1	20	5	5	5	5	5	1	12	4	5	9	10	10	1	1	1	1	1	1	1	1	1	1	1	1	1	1	1	1	1	1	
	11	22	20	5	9	27	1	3	9	19	23	1	1	1	1	1	1	1	1	1	1	1	1	1	1	1	1	1	1	1	1	1	1	
	12	4	4	22	2	20	3	3	8	4	23	26	23	2	2	2	2	20	1	21	11	21	5	22	6	6	20	10	2	2	2	2	4	
1951	1	6	2	5	21	5	21	1	15	6	1	3	8	8	4	6	2	6	2	2	1	1	1	1	1	1	1	1	1	1	1	1	3	
	2	27	13	13	5	3	21	19	10	2	9	9	21	5	14	3	1	3	28	4	2	17	1	1	1	3	16	1	1	1	1	1	3	
	3	3	3	8	4	4	4	2	2	2	0	3	1	1	14	12	4	7	3	8	23	7	2	22	0	21	10	15	12	17	17	10		
	4	21	3	24	4	7	5	9	5	12	4	23	23	23	2	2	2	2	6	1	3	3	11	2	5	16	3	0	9	6	1	1		
	5	6	6	6	10	10	2	6	20	1	5	5	5	5	1	15	18	3	1	8	23	23	10	6	0	6	6	1	8	13	17	1		
	6	2	2	2	5	18	6	6	2	4	12	16	11	0	16	4	4	4	4	4	4	13	23	2	5	9	18	24	12	23	23	23	1	
	7	2	10	18	14	27	11	4	11	11	5	27	27	11	2	20	20	1	3	11	7	2	2	2	2	10	1	1	18	0	1	1	1	
	8	3	1	20	10	5	26	20	2	5	7	2	6	13	1	18	18	1	15	1	1	1	1	1	1	3	14	5	8	4	2	2	2	
	9	6	17	20	1	2	20	2	2	6	14	12	23	4	4	11	5	11	2	10	1	1	1	1	1	1	1	1	1	1	1	1	1	
	10	1	6	19	19	3	3	14	1	14	5	1	1	8	1	19	1	1	2	3	28	11	5	9	20	8	27	11	0	14	6	6	1	
	11	10	1	8	2	11	5	9	27	24	6	1	1	1	1	10	10	1	1	1	1	1	3	16	4	4	13	1	1	27	6	15	20	1
	12	3	8	4	2	23	8	23	10	1	1	21	2	2	1	1	1	6	1	1	3	8	15	1	1	1	1	1	1	1	1	1	1	27
1952	1	23	1	3	3	3	3	27	5	3	1	3	1	1	8	1	0	24	2	2	6	2	2	2	2	2	12	13	1	1	1	1	3	
	2	1	1	9	3	17	2	2	5	22	26	6	9	1	10	1	1	1	1	3	3	19	19	21	1	8	2	2	2	4	2	2	3	
	3	2	7	24	28	7	3	3	19	28	8	1	10	10	6	6	6	6	8	2	6	1	14	3	12	4	17	6	6	6	6	6	15	
	4	0	6	23	1	3	4	2	20	3	28	18	1	26	6	6	6	6	28	7	10	6	2	2	2	6	1	1	8	12	6	24	4	
	5	10	10	7	7	7	2	11	0	0	17	4	4	23	23	17	1	3	3	3	9	3	9	3	9	15	16	2	2	3	0	4	4	
	6	17	17	4	7	2	20	3	12	17	23	23	11	2	25	7	4	4	2	2	10	6	1	1	1	1	1	1	1	1	1	1	1	
	7	15	1	1	13	0	16	11	5	9	11	8	7	7	26	12	12	10	1	3	3	3	3	3	20	18	22	11	5	11	1	1	4	
	8	7	2	2	2	21	7	4	4	4	4	4	4	7	11	4	2	5	9	1	0	20	18	0	24	2	2	1	1	1	1	1	1	
	9	9	16	7	2	1	1	1	27	11	1	3	9	8	12	22	25	2	2	23	2	1	1	20	20	9	9	2	5	9	9	1		
	10	0	20	27	12	2	1	27	20	1	1	15	1	1	1	2	1	6	6	1	6	6	6	8	1	1	6	23	1	6	6	6	1	
	11	1	9	1	15	20	2	10	1	1	4	2	6	24	24	14	2	3	16	16	4	4	11	9	23	1	1	23	5	9	9	9	1	
	12	9	20	1	19	8	12	2	4	12	4	7	2	20	28	4	7	2	1	1	1	1	14	27	5	9	23	2	2	2	2	2	2	6
1953	1	11	5	5	23	2	6	27	19	8	13	1	10	1	1	3	3	14	21	10	6	15	3	3	21	1	1	1	3	13	7	2	5	
	2	20	10	1	3	28	19	3	1	1	24	24	6	23	1	23	2	2	10	1	1	3	10	1	1	1	1	1	3	1	20	2	2	17
	3	1	3	3	8	23	1	1	1	1	19	19	3	3	19	19	17	17	6	27	8	6	6	12	2	2	2	2	2	2	2	2	1	
	4	7	7	0	28	28	23	6	19	ND	16	2	2	2	2	2	2	2	1	14	13	1	2	2	2	2	2	2	2	2	2	2	1	
	5	1	1	1	1	5	1	5	22	5	6	2	10	17	4	12	12	23	23	4	4	4	4	4	7	5	18	3	1	1	1	1	1	
	6	10	10	1	1	14	5	5	3	3	3	3	3	3	3	3	3	3	0	1	3	23	10	10	24	17	7	7	7	7	7	7	15	
	7	2	17	17	4	4	4	4	7	10	0	18	20	3	9	26	1	8	4	4	20	15	15	2	2	0	1	20	6	4	4	4	4	
	8	1	1	3	3	18	5	5	1	14	15	1	14	15	1	1	1	1	1	1	1	1	1	1	1	1	1	1	1	1	1	1	1	
	9	4	2	6	8	4	4	4	5	18	1	9	1	1	1	1	1	1	1	1	1	1	1	1	1	1	1	1	1	1	1	1	1	
	10	2	6	4	23	1	3	27	13	0	26	5	10	14	1	2	1	1	15	1	3	5	1	1	1	8	4	5	20	15	20	1	3	
	11	3	19	1	1	1	1	3	9	3	0	10	26	1	1	6	8	12	4	2	1	1	1	1	1	1	1	1	1	1	1	1	1	1
	12	3	9	1	3	1	3	1	3	23	1	3	8	13	1	1	1	1	1	1	1	1	1	1	1	1	1	1	1	1	1	1	1	1

Table 2.2 Continued

YEAR	MON	1	2	3	4	5	6	7	8	9	10	11	12	13	14	15	16	17	18	19	20	21	22	23	24	25	26	27	28	29	30	31	
1954	1	6	1	3	9	20	3	1	10	1	1	1	5	5	21	9	11	5	24	6	6	1	1	1	1	3	3	1	3	1	1	3	
	2	24	19	28	28	1	8	1	1	1	1	1	3	21	21	3	10	3	3	19	8	13	1	3	3	13	1	1	1	1	1	3	
	3	5	1	23	2	2	2	2	2	6	2	2	1	1	1	1	1	1	1	1	14	21	5	6	1	3	4	2	6	1	6	6	
	4	1	1	1	1	1	3	5	1	3	14	1	6	12	12	4	4	4	4	5	5	5	1	6	6	1	6	6	17	1	1	1	
	5	4	11	9	0	4	17	17	23	1	1	1	6	12	17	17	10	10	10	10	0	22	9	3	16	2	20	10	6	6	6	1	
	6	1	1	1	5	3	28	16	13	16	2	5	9	16	28	27	4	1	9	3	18	11	14	28	4	7	2	14	27	0	3	4	
	7	9	23	10	10	6	1	20	18	3	3	28	12	10	10	1	1	3	27	9	20	3	3	0	8	26	4	7	7	4	4	4	
	8	4	17	1	1	2	2	2	2	17	1	23	2	2	2	1	1	20	10	6	1	1	1	26	4	2	10	2	10	1	3	3	9
	9	5	1	1	5	2	10	6	2	2	10	10	10	1	3	3	3	3	11	26	23	2	6	10	19	12	23	2	2	2	1	13	10
	10	2	1	1	1	8	1	14	1	1	9	3	27	12	4	7	16	11	20	3	9	1	28	27	20	1	3	3	5	20	1	1	10
	11	9	26	16	20	1	15	15	1	1	8	20	1	1	1	1	1	1	3	3	1	8	10	2	8	1	1	1	19	21	1	1	1
	12	1	1	27	11	0	28	9	13	10	1	9	1	27	1	6	24	13	1	18	1	3	4	2	1	1	1	9	1	3	27	11	5
1955	1	3	12	7	24	4	17	7	7	7	1	1	0	6	6	2	2	10	3	1	1	8	8	13	2	1	8	2	1	6	6	6	
	2	6	14	3	3	15	2	1	3	19	6	10	1	2	9	1	4	16	16	13	5	9	2	9	18	14	8	2	8	2	8	6	6
	3	15	20	1	1	3	8	7	2	6	2	1	10	1	3	17	2	2	2	24	0	15	23	23	20	3	24	6	24	6	6	1	
	4	1	19	8	1	1	1	6	8	12	23	1	12	2	6	6	12	4	2	17	6	17	6	6	8	8	8	13	15	15	19	12	
	5	28	28	20	10	4	4	22	9	0	12	4	4	11	9	18	18	7	2	2	6	4	2	1	1	3	3	8	1	1	15	12	
	6	12	4	4	11	4	4	4	4	4	20	1	1	23	10	10	24	14	1	1	19	19	8	17	1	1	3	15	15	2	6	11	
	7	1	1	1	1	1	20	1	15	23	20	14	1	19	3	5	15	20	1	3	1	19	27	11	2	4	20	1	1	3	27	11	
	8	1	1	27	11	5	5	5	5	27	27	2	1	8	17	19	3	28	28	11	1	19	18	3	5	9	10	3	28	16	5	9	
	9	9	1	13	1	20	1	5	14	26	4	2	5	5	5	1	6	6	1	1	19	1	1	1	1	0	18	22	25	4	2	2	2
	10	2	5	5	1	3	28	28	0	7	2	6	12	16	16	16	9	4	10	2	1	1	3	11	22	11	7	11	16	6	23	10	
	11	4	4	11	9	0	9	20	25	2	2	6	1	6	6	6	6	1	1	1	0	10	6	1	23	6	6	1	10	1	1	1	1
	12	1	1	1	9	9	7	2	10	10	10	10	14	1	1	1	6	2	6	10	10	1	1	6	6	2	1	3	9	3	1	1	1
1956	1	1	1	1	3	23	10	1	28	16	4	7	5	9	9	3	3	3	3	3	3	28	23	20	10	19	1	1	1	1	1	3	
	2	3	9	5	1	3	3	2	11	5	3	3	4	4	4	22	10	14	19	6	2	10	10	2	2	11	2	2	1	1	1	1	
	3	1	1	1	1	10	1	1	8	1	1	21	24	8	20	1	3	14	1	8	7	2	10	1	10	6	10	1	1	1	14	8	
	4	24	24	4	7	2	14	3	12	12	4	4	17	19	19	1	1	10	17	2	10	10	2	6	26	6	23	2	2	1	1	1	
	5	1	14	21	2	23	10	1	15	20	6	1	1	16	2	2	20	21	9	5	2	2	2	10	1	3	9	27	17	23	18	1	
	6	0	5	5	1	1	12	24	8	27	27	5	10	6	23	20	1	3	3	12	17	23	1	19	10	6	23	2	2	2	2	2	
	7	6	1	1	1	3	3	28	0	24	2	20	2	2	1	25	25	10	10	3	3	3	3	27	27	4	4	4	4	4	4	4	
	8	11	26	16	16	6	1	24	8	16	11	11	7	4	11	7	4	4	2	23	10	1	3	3	28	7	7	7	7	7	7	7	
	9	4	2	1	5	5	5	10	1	9	5	4	2	2	2	20	1	2	11	2	2	17	7	10	6	3	14	26	26	15	11	5	8
	10	9	4	2	6	1	15	27	2	1	9	27	5	15	4	5	9	20	1	21	1	27	20	20	1	8	13	2	2	2	2	2	
	11	24	28	28	3	3	1	1	1	1	1	1	9	15	1	1	8	0	3	3	4	2	10	1	27	21	2	1	1	1	15	9	1
	12	15	6	11	22	14	21	14	3	21	3	1	1	1	3	8	23	1	1	3	1	3	3	3	3	21	1	8	21	1	1	2	10
1957	1	1	1	1	3	23	10	1	28	16	4	7	5	9	14	3	27	16	6	8	13	1	3	14	1	8	21	1	1	1	1	3	
	2	3	21	4	7	21	27	13	1	1	1	3	12	4	4	4	4	2	10	10	10	6	6	14	14	8	23	1	6	1	1	1	
	3	2	2	23	2	10	6	4	4	7	22	16	0	2	2	17	17	0	12	4	4	2	10	1	1	19	19	8	1	14	1	1	
	4	1	10	14	1	23	2	2	6	2	2	6	1	1	1	3	5	1	8	5	1	1	14	14	15	23	23	10	6	6	6	4	
	5	1	19	10	6	1	9	5	14	2	6	14	21	1	1	1	6	10	1	1	8	12	4	4	4	4	2	10	24	17	1	8	4
	6	2	5	9	20	20	10	24	4	4	22	0	7	2	26	12	10	3	8	7	4	4	4	4	4	7	11	16	16	12	23	2	7
	7	2	22	4	4	4	7	2	5	10	10	25	2	10	1	1	12	4	5	11	18	16	3	3	27	4	0	0	2	7	10	3	
	8	9	16	23	7	7	7	4	4	4	2	2	1	1	2	2	10	1	1	5	2	1	1	1	1	1	1	14	21	3	1	1	
	9	19	19	19	3	15	20	1	0	12	4	4	4	7	7	14	20	10	24	2	7	5	16	10	5	10	1	18	6	0	11	3	3
	10	20	18	3	1	1	15	1	3	9	14	5	1	1	8	27	20	3	5	5	1	1	1	1	1	1	1	1	1	1	1	1	1
	11	17	14	9	15	20	6	1	3	20	2	9	3	9	10	1	1	19	3	27	23	2	9	4	2	2	10	9	6	6	13	2	2
	12	2	2	2	2	2	2	1	1	1	20	10	6	10	1	3	3	1	12	4	6	7	2	2	9	4	2	3	2	15	17	2	2

Table 2.2 Continued

YEAR	MON	1	2	3	4	5	6	7	8	9	10	11	12	13	14	15	16	17	18	19	20	21	22	23	24	25	26	27	28	29	30	31				
1958	1	6	10	1	1	6	1	3	2	2	1	18	6	20	1	9	9	17	23	7	7	2	7	4	16	28	28	1	1	1	1	ND				
	2	1	25	2	2	2	10	2	2	2	1	1	1	1	1	10	6	10	6	10	1	1	1	5	22	9	16	1	3							
	3	3	8	13	2	2	10	10	2	2	2	1	1	1	1	1	1	3	1	19	6	6	23	28	1	1	1	1	1	1	8	14				
	4	15	27	5	1	1	6	6	10	6	1	1	3	16	4	2	20	3	4	4	4	2	2	1	19	10	14	13	5	16	7					
	5	11	0	16	7	2	2	2	10	25	2	10	10	8	12	4	4	4	4	4	4	2	2	2	2	11	11	7	5	22	10	5				
	6	9	0	8	11	2	2	2	2	2	6	23	4	2	23	10	10	2	6	1	4	4	4	4	12	23	3	28	4	7	7	7				
	7	2	10	10	10	19	14	3	5	5	16	11	22	22	4	11	5	18	10	2	4	4	2	2	2	2	4	4	4	4	4	4	7			
	8	4	7	7	7	12	17	23	4	2	2	6	4	2	2	2	2	6	24	4	2	2	2	2	2	6	17	2	2	2	2	2	1	1		
	9	10	24	12	4	10	6	15	25	10	1	27	13	6	1	1	3	14	8	8	26	12	4	7	2	2	6	10	1	1	1	1	1			
	10	2	5	9	23	10	6	1	1	8	1	1	1	1	1	21	16	7	6	20	6	8	3	19	3	8	14	1	1	3	15	24	1			
	11	1	23	6	12	4	2	1	3	8	27	4	6	6	6	6	10	1	14	26	2	2	1	1	1	1	1	14	21	2	1	1	10			
	12	1	9	16	6	23	2	10	5	2	10	1	1	1	1	14	13	2	6	2	2	2	2	6	6	1	1	1	1	14	21	5	1	8		
1959	1	12	4	2	2	2	10	10	10	10	10	6	6	6	6	2	2	2	7	7	4	4	4	7	2	5	5	5	1	1	1	1	1			
	2	14	21	11	2	2	1	1	1	1	1	1	1	1	9	1	3	13	2	1	3	6	1	1	1	14	3	1	1	1	1	1	1			
	3	12	12	13	2	1	1	1	1	1	1	1	1	1	15	10	3	13	10	6	1	1	1	1	10	6	1	1	1	8	1	1	3			
	4	13	6	10	6	3	6	23	10	1	1	3	26	2	17	6	2	6	6	6	6	6	6	6	6	2	5	0	2	15	9	0				
	5	2	2	6	15	13	1	1	1	1	3	16	4	17	2	10	2	2	2	2	6	1	3	1	14	6	2	10	9	1	1	14	14			
	6	21	14	0	1	1	14	12	28	28	1	15	20	10	10	12	24	24	8	4	2	2	2	2	23	20	7	2	2	4	4	11	22			
	7	4	4	4	11	1	22	16	4	4	2	11	5	5	3	21	0	13	2	2	2	2	2	2	14	5	1	1	20	10	6	14	16	4		
	8	20	0	8	4	5	13	5	3	9	28	11	22	7	4	4	7	2	2	2	2	2	2	2	6	10	14	8	4	10	2	3	1	9	12	12
	9	12	8	16	2	6	12	4	2	1	20	1	20	1	10	10	10	1	1	1	1	1	1	1	3	28	28	3	12	4	2	1	3	ND		
	10	14	26	5	5	5	5	5	1	1	1	3	23	10	1	19	19	6	4	4	2	2	2	2	2	2	2	10	1	20	10	1	3	ND		
	11	1	2	5	21	9	3	1	9	0	6	23	2	2	5	10	8	4	4	4	4	2	2	2	2	2	2	2	2	2	10	1	3	27	1	
	12	8	1	3	3	20	3	12	7	2	2	1	1	8	19	12	19	10	1	1	1	3	3	3	3	14	1	3	14	1	3	3	1	1	1	
1960	1	3	21	5	6	1	1	1	1	3	8	12	24	6	2	6	2	2	2	2	17	19	1	1	1	3	22	7	7	22	1	14	ND			
	2	3	5	1	1	1	13	2	2	7	0	0	20	2	26	2	2	2	2	4	24	2	10	17	13	7	2	2	2	2	2	2	2			
	3	10	14	14	14	21	21	21	1	1	14	3	19	28	8	8	6	21	6	10	1	1	1	1	21	8	2	1	5	1	1	3				
	4	19	19	17	17	10	6	1	1	1	1	6	1	1	1	8	15	23	10	3	25	8	12	12	17	6	6	6	2	2	2	6	4			
	5	4	4	6	8	27	20	1	19	10	1	3	12	4	4	2	6	23	23	6	12	23	23	3	15	1	15	3	13	1	1	1	17			
	6	2	4	4	23	20	1	18	3	12	2	10	1	1	15	11	20	1	1	1	1	1	1	1	2	6	24	6	2	2	2	2	2			
	7	4	23	23	20	10	24	2	2	2	24	17	20	2	2	13	23	10	10	3	18	28	0	3	3	12	4	11	4	4	4	4	7			
	8	2	7	10	2	2	7	10	2	2	2	2	2	2	2	5	26	4	4	11	5	1	1	1	24	24	21	7	4	7	6	17				
	9	10	14	22	1	1	12	23	1	3	15	1	27	4	2	1	3	9	10	8	11	0	7	5	26	12	2	2	2	2	2	7	3			
	10	26	24	6	24	7	7	10	10	10	6	1	1	6	21	15	23	2	2	5	22	6	5	16	4	22	0	9	9	3	3	3	3			
	11	0	4	2	10	1	1	1	1	1	1	1	21	21	14	21	3	15	12	7	10	12	11	2	6	4	4	2	4	2	1	1	1			
	12	10	21	1	20	1	1	10	6	6	1	1	3	26	2	1	23	2	2	5	5	13	0	6	8	21	1	26	2	2	6	20	10			
1961	1	1	3	6	8	24	6	1	1	1	8	1	3	3	3	8	5	15	1	1	1	1	5	6	1	1	1	1	1	14	6	1	1			
	2	1	1	3	3	1	9	13	5	1	1	3	14	1	1	1	21	1	1	3	21	1	1	1	1	19	19	8	8	1	2	2	2			
	3	1	1	1	1	1	8	8	1	1	3	6	1	1	8	23	10	26	1	1	3	15	1	3	1	10	6	17	23	3	2	2	2			
	4	2	24	10	10	17	2	2	14	24	6	6	3	12	12	19	8	19	24	6	12	12	4	13	10	2	2	2	6	6	19					
	5	1	1	1	1	1	1	1	15	23	2	1	1	1	1	20	21	20	1	27	16	0	0	22	2	2	10	2	20	10	5	11				
	6	2	1	1	10	1	15	1	1	1	2	7	2	6	1	1	14	3	11	7	13	20	5	15	1	1	1	12	15	20	10					
	7	0	0	10	17	10	1	3	9	27	28	9	27	19	28	28	10	3	3	1	19	3	5	2	2	6	12	15	15	20	23	10				
	8	14	21	3	5	11	5	26	20	5	9	5	5	5	4	20	0	11	5	5	9	3	5	14	8	3	3	15	26	23	24	1	1			
	9	27	4	4	5	9	3	8	2	6	6	1	1	14	13	7	1	27	13	1	27	13	1	3	16	2	1	27	26	6	8	23	24	2		
	10	4	2	5	27	16	11	0	20	1	8	21	20	1	3	16	24	2	20	1	1	1	1	14	12	1	9	9	0	17	2	24	2			
	11	2	3	12	23	1	8	21	1	1	24	8	4	5	27	0	10	19	28	14	1	13	3	12	2	2	2	2	1	3	7	7	7			
	12	24	24	28	28	4	4	23	2	6	8	6	1	2	10	1	1	1	19	6	14	1	5	10	6	6	4	2	2	17	1	1	9			

Table 2.2 Continued

YEAR	MON	1	2	3	4	5	6	7	8	9	10	11	12	13	14	15	16	17	18	19	20	21	22	23	24	25	26	27	28	29	30	31		
1962	1	1	15	1	1	1	1	8	1	1	1	1	1	1	1	21	6	10	2	1	1	3	27	4	2	6	1	19	2	1	1	3	9	
	2	1	9	9	1	1	1	1	3	3	27	13	2	6	1	9	1	1	14	21	1	1	8	3	24	6	15	23	4					
	3	7	7	6	6	24	24	4	4	24	22	6	1	6	6	6	6	6	6	6	2	2	20	0	6	6	6	17	23	20	6	10		
	4	1	3	21	5	1	1	1	3	19	17	17	17	1	1	1	8	24	1	1	1	1	27	20	1	1	1	1	1	1	3	12		
	5	12	4	5	9	2	20	5	9	24	24	1	3	16	11	3	27	7	15	1	1	1	1	1	12	6	23	7	2	2	1	1		
	6	1	1	19	19	1	3	18	2	6	1	1	15	5	1	6	2	2	10	6	6	1	1	1	1	10	10	1	28	4	22	23	13	11
	7	20	24	12	16	16	16	4	7	4	4	4	4	4	4	17	1	1	2	10	6	6	1	1	1	10	10	1	28	4	22	23	13	11
	8	11	7	2	4	11	6	1	3	3	27	9	1	3	3	3	4	23	23	2	2	1	24	3	27	12	4	4	0	0	16	11	5	
	9	0	0	22	11	9	9	16	20	18	3	12	12	4	2	2	2	6	3	20	10	1	3	3	27	1	1	1	3	5	27	15		
	10	1	27	1	1	8	26	1	8	24	ND	2	2	1	1	8	23	10	1	17	10	24	2	2	23	10	1	16	19	27	1	15		
	11	23	1	1	9	26	15	1	25	4	20	1	27	4	14	22	22	10	1	3	16	4	2	10	1	27	11	9	1	19	24			
	12	8	12	17	1	13	17	2	2	2	13	2	20	5	20	5	1	1	1	1	1	3	5	5	9	24	6	6	18	26	11	11	18	
1963	1	25	4	22	9	4	4	7	11	11	10	10	5	9	11	9	27	4	21	2	26	2	2	13	0	6	9	27	25	10	9	16		
	2	4	4	7	11	0	2	6	10	10	10	1	1	20	10	10	1	1	1	1	1	1	2	2	5	1	1	1	1	1	1	1	1	
	3	1	ND	1	1	1	0	7	5	6	19	6	21	14	3	10	6	19	24	24	6	10	1	19	1	14	21	11	6	13	20	ND		
	4	21	1	3	0	10	10	25	23	17	6	6	6	6	6	24	4	4	4	4	2	23	23	10	21	6	14	1	8	11	2	5		
	5	26	15	23	2	6	1	6	1	1	1	1	3	5	1	15	1	25	6	23	23	1	3	5	5	1	9	3	27	27	7	5		
	6	5	15	14	1	1	15	2	5	10	10	10	6	1	8	ND	23	2	20	18	14	27	4	5	1	8	25	27	6	10				
	7	6	0	7	7	10	20	9	0	16	16	2	6	23	10	26	28	16	4	4	7	7	2	2	1	1	3	3	15	18	1	5		
	8	14	28	9	22	16	11	7	23	2	2	2	10	10	10	1	3	11	11	7	2	2	1	1	3	9	15	23	2	1	1	5		
	9	7	2	5	5	14	16	10	15	20	1	1	1	3	8	11	1	3	1	3	3	1	3	3	9	15	23	2	1	1	5	7		
	10	6	15	3	27	5	5	15	18	5	1	5	26	4	6	23	1	3	5	1	1	3	27	11	1	4	2	2	1	1	23	10		
	11	2	5	15	2	4	11	16	28	28	4	17	13	22	4	2	6	6	6	0	22	1	1	13	10	1	13	1	19	19	20			
	12	2	1	9	9	6	26	15	1	1	18	15	1	10	10	2	2	10	1	1	10	1	1	1	27	11	2	6	1	1	1	1	24	
1964	1	6	1	1	1	1	21	8	3	1	20	10	10	1	19	6	1	1	3	3	12	7	5	9	10	6	6	1	21	9	3	3		
	2	3	3	4	4	2	2	1	20	10	1	1	5	5	5	21	14	6	1	1	6	6	1	1	1	1	15	5	13	2	25			
	3	3	4	6	3	11	14	9	18	3	ND	3	19	8	8	20	10	1	1	19	6	1	1	1	1	1	1	21	9	10	21	1	10	
	4	6	1	10	14	1	1	1	3	ND	2	5	9	3	8	2	1	13	7	3	27	23	4	9	12	24	17	28	12	ND	3			
	5	3	1	1	8	26	6	8	12	13	23	10	10	19	12	28	7	1	1	1	1	1	0	6	15	20	0	24	10	10	2	10	2	
	6	2	17	7	4	4	7	7	4	11	11	0	1	9	18	9	11	0	1	1	3	9	20	1	ND	1	3	28	3	27	11			
	7	20	18	18	27	27	12	28	3	15	1	18	3	9	9	9	1	1	1	1	3	19	3	27	16	23	1	1	1	1	9	18	3	
	8	3	3	16	5	3	4	6	23	2	2	2	7	4	4	4	17	6	23	10	10	18	3	3	16	7	7	2	17	17	2	2		
	9	10	10	12	4	4	4	4	20	1	0	2	2	2	2	2	2	6	24	12	22	3	3	3	20	2	6	9	9	10	1	3		
	10	12	4	2	2	1	5	20	15	1	24	6	1	3	9	12	12	17	2	2	15	9	10	26	0	24	8	1	19	2	8	24		
	11	6	24	22	0	17	24	4	17	1	1	1	1	1	1	1	1	8	4	2	2	2	2	1	1	9	5	2	10	3	20	1		
	12	9	10	10	1	1	3	3	0	12	22	22	0	20	20	1	1	3	18	1	3	3	16	7	7	26	7	15	1	3	27	4	11	
1965	1	3	19	6	6	1	1	27	11	7	5	5	0	1	3	1	3	15	0	15	1	23	1	1	1	3	15	0	4	2	2	2		
	2	5	21	0	1	16	6	9	20	3	27	7	5	18	3	20	3	9	28	6	6	10	2	2	2	22	28	16	11	9				
	3	3	17	5	28	22	2	2	1	1	1	1	1	14	6	6	14	14	6	23	2	2	2	2	6	6	1	1	1	19	19	1	1	
	4	6	1	24	22	1	8	1	19	3	3	15	1	8	5	23	17	7	2	6	1	1	1	1	3	3	15	6	8	12	7			
	5	7	0	17	12	24	12	0	4	2	22	4	11	4	4	11	22	0	12	4	11	1	1	1	20	10	14	10	6	23	2	ND	1	
	6	3	3	3	15	20	1	8	12	23	2	2	2	2	19	19	3	3	1	12	24	17	20	1	1	1	1	1	1	9	20	1	9	
	7	12	6	4	25	2	7	ND	23	23	23	2	2	8	2	23	23	20	14	3	27	4	4	2	2	2	2	2	2	10	1	3	9	0
	8	11	11	11	4	2	5	14	8	20	2	5	11	2	10	14	13	23	2	20	6	20	15	10	6	1	1	2	5	9	0	27	3	
	9	16	11	0	11	21	7	26	11	6	6	1	1	8	3	21	20	3	8	5	3	3	3	20	2	23	2	2	2	5	9	10	10	
	10	20	1	1	3	24	6	6	6	6	6	1	1	10	6	1	1	27	11	5	3	ND	1	1	1	0	1	1	1	1	3	13	20	5
	11	5	1	9	20	1	1	3	21	1	1	3	21	6	6	6	6	6	6	6	6	6	6	6	6	6	6	6	1	1	1	1	10	6
	12	1	3	21	0	7	10	1	1	1	18	3	14	8	8	8	13	6	19	28	24	24	6	1	1	1	1	1	8	13	8	17	ND	

Table 2.2 Continued

YEAR	MON	1	2	3	4	5	6	7	8	9	10	11	12	13	14	15	16	17	18	19	20	21	22	23	24	25	26	27	28	29	30	31		
1966	1	1	1	1	1	1	1	21	3	5	3	1	19	24	6	2	6	6	0	5	3	3	19	7	7	24	2	2	6	23	7			
	2	2	21	21	3	19	12	22	3	27	5	1	8	21	14	14	6	6	2	10	10	1	1	15	19	14	26	4	24					
	3	6	1	10	1	1	15	2	1	ND	19	24	8	13	6	1	15	1	1	9	6	12	2	2	5	1	10	2	4	2	2	2		
	4	4	2	2	10	2	23	1	1	6	6	6	14	8	24	21	15	12	4	11	5	18	8	15	1	1	1	1	1	1	1	1		
	5	14	14	13	4	2	2	2	10	1	9	10	1	1	3	1	19	12	8	12	7	2	6	12	4	4	2	17	23	10	10	14		
	6	9	20	1	1	1	1	19	1	1	3	4	23	1	9	5	2	1	5	4	0	24	4	17	12	4	11	11	11	11	11	11		
	7	9	20	1	18	6	6	23	23	6	6	0	10	10	1	6	1	15	20	10	3	27	4	7	4	20	10	10	10	10	10	10		
	8	17	7	4	7	25	10	10	0	28	28	25	3	19	6	3	28	16	11	23	2	10	19	3	27	13	23	7	11	11	11	11		
	9	24	24	8	15	15	22	2	1	1	1	0	4	11	1	0	2	1	9	3	28	27	9	23	2	2	2	2	2	2	2	2		
	10	20	1	1	3	24	6	6	1	6	6	1	10	ND	1	9	5	1	8	4	22	22	4	2	6	23	11	4	4	2	1	5	0	2
	11	5	9	3	23	2	9	11	5	18	27	2	1	9	5	5	1	1	9	11	1	27	11	20	9	16	4	5	9	25	17			
	12	17	20	1	3	9	1	16	2	1	1	8	6	6	1	8	17	23	2	6	1	1	3	19	1	3	3	1	3	13	2	10		
1967	1	6	5	16	16	2	6	1	28	28	6	8	2	2	23	2	2	1	1	1	1	1	1	1	1	1	14	0	1	3	10	10	1	
	2	21	1	8	9	20	3	1	9	1	9	1	10	6	1	1	1	1	1	1	1	1	1	1	1	1	6	1	1	1	1	1		
	3	3	13	5	1	21	5	1	15	14	21	21	6	1	1	1	3	3	21	3	9	3	28	12	4	11	3	7	1	3	9			
	4	0	21	2	2	5	3	5	5	9	1	14	6	1	12	13	1	1	1	3	10	1	19	1	1	1	1	15	11	7	7			
	5	2	23	7	11	11	11	4	4	22	2	2	2	2	2	10	6	2	2	21	3	3	19	24	12	28	0	16	11	5	22	5	9	
	6	5	2	6	23	20	5	5	25	15	20	14	8	14	21	20	1	1	1	1	3	16	4	2	20	5	5	11	1	15	23	2	2	
	7	17	10	1	3	28	16	16	16	16	16	16	16	16	16	16	16	16	16	16	16	16	16	16	16	16	16	16	16	16	16	16		
	8	7	24	8	7	2	6	9	9	18	14	15	3	5	5	5	5	5	5	5	5	5	5	5	5	5	5	5	5	5	5	5		
	9	9	3	27	9	20	1	12	23	1	3	15	15	15	15	15	15	15	15	15	15	15	15	15	15	15	15	15	15	15	15	15		
	10	2	15	20	1	1	1	1	1	1	3	3	3	24	28	4	4	11	5	5	3	10	1	3	12	1	23	23	2	2	12	12	4	
	11	4	2	1	1	23	10	1	27	20	1	8	13	2	2	2	2	2	2	2	1	3	10	1	3	27	16	2	6	1	23	1	15	
	12	8	12	17	2	12	24	6	5	3	3	8	4	23	2	2	2	2	2	2	2	2	2	2	2	2	2	2	2	2	2	2	2	
1968	1	2	2	6	1	1	6	6	1	1	1	1	14	1	1	14	14	21	1	1	1	1	1	1	1	1	27	26	15	1	3	7	21	
	2	5	3	12	22	3	10	1	1	3	10	2	10	10	10	6	2	2	1	10	10	10	10	10	10	10	10	10	10	10	10	10	10	
	3	1	18	6	1	1	1	3	6	1	5	5	21	0	1	0	1	1	1	1	1	1	1	1	1	1	1	1	1	1	1	1	1	
	4	7	22	10	2	7	2	6	5	2	14	13	5	18	3	16	11	9	7	26	15	1	3	4	5	6	4	2	26	0	25	4	4	
	5	2	2	2	2	2	2	1	3	15	20	2	11	16	0	12	4	0	4	23	10	1	19	3	1	3	19	8	3	1	1	1	1	
	6	15	1	15	12	3	10	10	1	1	3	21	1	24	11	11	11	16	11	16	11	22	28	12	17	23	1	1	3	27	26	15	20	
	7	10	22	11	11	1	4	4	7	2	7	11	5	0	4	11	5	3	3	0	10	6	15	7	7	24	24	23	23	20	2	13	5	
	8	20	9	5	1	3	11	2	1	0	2	6	6	6	2	4	4	7	2	2	13	23	10	19	19	3	5	28	28	9	27	5	5	
	9	1	8	8	12	4	4	16	9	3	3	12	12	12	24	24	12	4	16	9	3	15	1	8	12	17	2	10	19	12	4	4	2	
	10	4	2	2	2	0	7	24	19	19	12	12	4	12	4	5	1	8	28	28	13	2	5	23	17	17	2	2	2	2	2	2	2	
	11	4	22	22	0	1	1	1	1	1	8	3	28	3	8	6	6	6	1	1	1	2	6	1	3	21	20	10	6	1	ND	4	4	
	12	2	1	1	15	17	10	1	1	3	1	1	1	1	1	1	8	12	7	10	19	1	1	1	1	20	2	2	2	2	2	2	2	
1969	1	1	2	2	2	4	4	22	7	2	6	2	6	1	1	15	12	4	22	22	14	3	1	1	1	23	2	1	27	27	14	23		
	2	6	1	3	17	2	2	2	2	15	7	2	5	18	0	28	17	4	9	3	3	3	1	14	1	3	3	1	0	2	6	1	2	
	3	5	1	1	1	10	10	10	2	10	19	1	1	15	1	1	1	19	28	4	4	22	16	2	1	0	2	6	1	6	1	2	1	
	4	15	21	21	1	3	19	1	1	1	10	6	1	15	12	17	1	1	1	19	12	5	26	4	2	6	1	6	1	1	1	1	1	
	5	16	4	7	10	24	12	4	2	7	2	2	2	10	15	9	5	5	21	9	20	1	5	5	5	18	4	11	25	17	2	2	2	
	6	23	0	4	4	8	0	20	2	10	2	2	15	23	2	1	5	4	23	2	2	2	2	2	2	2	2	2	2	2	2	2	2	
	7	13	23	20	10	10	10	1	3	15	3	28	12	4	4	4	4	2	10	1	1	3	3	3	3	3	3	3	3	3	3	3	3	
	8	12	16	11	7	11	25	12	17	17	25	24	28	28	12	23	23	23	10	10	10	6	9	0	20	1	15	8	13	20	12	23		
	9	10	1	1	1	1	1	1	1	3	3	20	1	20	1	1	1	1	1	1	1	1	1	1	1	1	1	1	1	1	1	1	1	
	10	19	19	19	3	28	3	4	2	2	1	1	1	21	23	1	5	11	22	2	1	1	1	1	1	1	1	1	1	1	1	1	1	
	11	19	3	5	27	20	15	20	3	28	16	16	4	23	2	4	2	15	3	17	7	11	13	5	9	16	11	0	8	20	28	1	3	
	12	24	12	25	0	1	15	1	3	9	15	8	10	1	1	14	3	8	19	1	23	2	6	10	6	1	9	27	1	10	1	10	1	10

Table 2.2 Continued

YEAR	MON	1	2	3	4	5	6	7	8	9	10	11	12	13	14	15	16	17	18	19	20	21	22	23	24	25	26	27	28	29	30	31		
1970	1	10	10	2	2	6	6	10	10	10	10	6	6	6	6	6	6	6	6	1	1	1	21	0	22	21	21	8	21	5	24	2		
	2	6	13	11	22	9	9	5	1	12	23	1	2	2	2	5	5	6	21	2	2	1	1	1	1	1	1	2	5	9	5	24	2	
	3	14	21	8	12	24	6	6	2	2	2	2	6	10	1	14	3	28	1	3	5	5	3	3	23	2	6	6	2	2	22	26		
	4	0	4	2	10	6	1	1	15	0	19	6	6	6	1	3	3	15	1	27	26	15	3	12	4	4	2	6	1	6	6	6		
	5	23	6	15	21	5	14	16	20	10	2	2	2	2	14	14	1	20	1	9	14	5	1	1	1	1	1	1	1	1	3	17	19	
	6	3	3	3	3	27	11	5	5	1	1	1	3	3	3	1	1	13	20	9	3	27	17	23	2	10	1	5	23	23	1	1	1	
	7	1	1	3	9	5	26	23	2	2	1	1	14	24	4	7	7	2	20	5	26	16	4	4	4	15	17	4	4	2	2	6	12	
	8	4	2	11	2	2	5	15	15	12	12	4	4	4	2	3	3	18	12	4	11	9	25	25	17	23	6	19	26	1	1	1	17	17
	9	28	6	1	15	12	4	4	26	27	23	2	20	1	14	21	5	20	1	15	3	6	1	15	1	8	23	1	1	1	1	1	3	3
	10	27	4	4	7	11	20	12	5	3	28	4	9	9	3	1	8	4	11	2	5	15	15	8	12	28	12	8	3	3	3	3	3	
	11	1	1	1	1	1	1	2	1	20	8	13	2	15	18	21	15	6	22	16	16	17	2	2	2	2	2	9	27	4	9	9	11	
	12	1	1	1	1	1	1	1	1	1	3	21	6	6	1	1	3	3	13	1	6	6	1	1	1	14	15	16	4	10	2	11	10	0
1971	1	6	6	6	8	23	10	1	21	21	9	18	6	1	6	6	2	6	1	1	26	4	4	2	2	2	6	1	23	2	2	4	2	2
	2	1	1	15	3	1	4	4	13	4	2	5	1	3	27	2	2	6	15	1	1	21	1	1	1	12	12	6	15	13	23	17	6	6
	3	10	14	3	12	24	6	6	6	6	6	1	8	10	6	2	2	6	6	6	6	6	1	6	1	1	6	6	8	3	17	1	1	1
	4	10	1	19	2	2	1	1	24	22	5	15	23	2	2	4	12	4	4	0	7	2	2	2	2	2	2	2	1	19	1	17	1	1
	5	1	6	8	8	28	28	3	28	22	5	9	5	2	2	5	5	21	11	1	9	20	1	3	3	3	0	6	1	1	1	1	1	1
	6	8	4	23	10	2	2	11	0	12	17	24	24	6	6	6	12	7	2	7	7	2	2	2	2	2	2	2	25	12	23	10	1	1
	7	1	3	3	12	4	4	7	12	23	20	10	26	4	11	4	7	17	17	2	2	2	2	2	2	2	2	2	2	2	2	2	2	2
	8	1	3	0	28	19	1	19	9	25	23	23	2	9	18	9	1	3	12	7	2	2	2	2	2	2	2	2	2	2	2	2	2	2
	9	15	15	1	1	3	3	16	11	2	7	22	12	12	23	23	1	9	9	27	11	5	5	9	11	2	10	1	8	12	28	1	1	1
	10	3	3	3	8	17	1	6	5	24	4	7	2	10	1	17	1	3	3	12	11	9	9	1	3	4	4	5	23	1	3	3	8	8
	11	7	14	21	20	6	15	2	5	3	0	6	24	6	27	27	4	5	23	2	9	10	15	15	3	15	3	15	2	6	2	6	6	6
	12	24	6	1	8	0	5	1	1	1	12	12	17	23	10	1	1	1	1	3	6	0	22	1	1	ND	18	6	9	9	0	1	1	1
1972	1	4	2	2	1	6	1	15	3	21	3	8	6	1	20	1	3	15	3	16	14	21	1	4	5	6	15	10	1	3	21	21	6	6
	2	1	1	8	23	23	2	10	10	1	8	12	7	2	5	10	1	19	3	3	5	1	9	3	8	3	3	5	6	19	19	17	17	17
	3	1	8	1	1	3	25	1	9	1	3	27	18	8	12	4	2	20	1	1	3	1	3	1	3	8	3	3	5	6	19	19	17	17
	4	1	1	12	4	7	2	1	14	26	4	6	15	4	6	6	6	6	6	1	3	24	24	1	1	1	10	24	16	9	0	1	1	1
	5	1	6	1	1	10	1	1	1	8	8	6	6	1	0	12	11	1	3	13	1	1	1	1	1	1	6	8	21	1	1	1	3	3
	6	10	16	20	1	27	1	10	10	1	0	6	23	0	15	5	18	5	15	9	1	1	3	9	3	8	15	15	12	17	23	1	1	1
	7	23	10	1	1	1	1	5	27	0	8	27	11	7	24	4	7	12	12	4	4	2	10	6	6	1	1	9	9	16	16	4	4	4
	8	2	11	11	0	17	17	17	17	10	12	17	19	3	3	3	15	12	3	9	1	20	1	15	9	5	24	6	23	10	1	1	1	3
	9	11	11	27	4	4	4	4	5	9	3	4	2	1	26	11	2	11	14	1	15	23	2	1	1	1	1	14	3	13	7	7	7	
	10	6	9	28	11	5	9	15	11	10	1	9	3	9	11	7	2	2	20	5	27	15	20	1	27	9	20	5	3	13	3	3	28	
	11	5	1	1	3	13	1	3	3	3	12	4	17	7	7	24	10	6	6	7	5	1	14	15	3	3	9	7	1	27	13	1	1	1
	12	11	10	1	1	1	1	8	10	1	21	1	1	1	1	1	1	1	6	1	3	3	9	21	1	1	1	1	1	1	1	1	1	1
1973	1	4	2	2	1	6	1	15	3	21	3	8	6	1	ND	1	1	1	1	1	3	8	ND	ND	ND	0	1	1	1	1	1	1	1	1
	2	27	0	4	10	1	21	9	5	20	21	9	9	20	1	1	ND	ND	ND	ND	ND	ND	ND	ND	ND	6	1	1	1	1	1	1	1	1
	3	1	8	8	23	14	8	22	5	3	27	13	1	10	ND	21	23	1	6	6	19	14	25	15	1	1	1	1	1	1	1	1	1	1
	4	15	15	15	23	10	10	2	2	2	6	10	1	5	9	0	0	ND	8	15	19	17	17	2	2	2	2	2	2	2	2	2	2	2
	5	5	9	3	1	1	3	27	4	23	17	23	10	6	13	1	4	11	9	16	17	12	ND	28	5	5	2	2	2	2	2	2	2	2
	6	20	1	1	8	27	23	2	5	17	2	4	7	7	23	6	ND	15	5	5	23	1	9	27	16	6	1	1	1	1	1	1	1	1
	7	13	4	ND	4	7	2	6	1	20	3	3	12	25	10	2	2	4	11	18	3	3	3	3	3	9	1	1	5	2	2	2	2	2
	8	3	28	28	8	12	12	28	3	3	21	28	9	28	16	4	4	2	15	12	22	9	18	7	7	2	ND	1	6	19	12	4	26	1
	9	27	20	1	8	16	23	2	10	18	4	2	2	1	1	3	0	13	11	20	20	1	14	ND	8	4	1	1	1	1	1	1	1	1
	10	3	5	1	8	4	22	28	12	12	28	11	16	4	4	7	2	2	20	5	3	21	15	1	1	3	2	1	3	8	27	23	23	23
	11	23	2	2	2	2	2	2	1	1	1	1	1	1	1	1	1	1	6	14	8	12	4	2	2	2	2	2	6	6	6	6	6	6
	12	1	3	16	20	5	9	14	21	21	1	1	1	1	1	1	1	1	2	1	1	1	1	1	1	1	1	1	1	1	1	1	1	1

Table 2.2 Continued

YEAR	MON	1	2	3	4	5	6	7	8	9	10	11	12	13	14	15	16	17	18	19	20	21	22	23	24	25	26	27	28	29	30	31
1974	1	21	1	1	1	1	1	1	1	1	1	21	14	14	1	21	1	1	3	8	8	5	3	3	1	1	3	21	3	1	1	1
	2	10	10	1	1	1	1	1	0	2	2	6	2	2	10	10	1	1	15	12	13	10	1	1	1	1	1	3	5	1	1	1
	3	1	1	3	ND	2	6	6	ND	1	1	ND	1	1	1	1	3	5	2	6	1	1	21	3	3	10	1	1	5	1	3	1
	4	0	8	ND	3	0	2	2	5	1	1	3	3	3	3	5	10	1	3	8	19	19	1	1	ND	5	5	1	1	1	3	ND
	5	22	22	0	7	10	ND	6	12	28	19	17	6	23	2	23	2	10	1	1	14	19	19	19	28	16	27	28	15	15	12	4
	6	0	1	3	23	12	12	16	20	20	ND	17	23	17	23	1	19	28	4	4	2	2	10	11	0	27	11	11	5	16	4	1
	7	7	17	6	24	12	17	17	23	1	10	12	4	2	2	2	5	5	9	1	3	28	1	9	3	3	12	4	2	17	17	23
	8	2	2	10	2	2	6	1	1	3	12	4	1	20	18	3	4	22	7	7	11	7	1	3	8	12	4	2	2	1	13	2
	9	ND	20	1	8	16	23	2	10	18	4	2	2	1	1	3	0	13	11	20	20	1	1	14	ND	8	4	11	2	20	1	1
	10	3	5	1	8	4	22	28	12	12	28	11	16	4	4	7	2	2	20	5	3	21	15	1	1	3	2	1	3	8	27	23
	11	23	2	2	2	2	2	2	1	1	1	10	1	9	17	17	23	2	2	10	6	14	8	12	4	2	2	6	6	20	10	1
	12	1	3	16	20	5	9	14	21	21	1	1	1	10	1	1	9	1	19	10	2	1	1	10	10	1	3	1	1	15	2	2

TABLE 2.3

1946-74

PERCENTAGE FREQUENCY OF BAFFIN TYPES													
TYPE	1	2	3	4	5	6	7	8	9	10	11	12	YEAR
1	30.6	27.1	25.6	20.1	18.8	15.0	10.4	12.3	18.7	19.5	21.2	27.6	20.5
2	8.1	11.4	10.5	10.4	11.3	10.0	9.9	11.6	9.5	8.3	10.4	9.6	10.1
3	9.3	10.4	7.0	6.7	5.4	6.1	9.4	8.5	8.6	8.6	5.4	7.5	7.7
4	2.8	3.2	3.5	4.6	7.0	8.0	10.4	7.0	5.5	5.5	6.5	2.3	5.5
5	4.3	3.8	2.2	3.9	4.5	5.2	3.5	6.7	4.3	7.3	3.7	2.1	4.3
6	9.3	5.6	11.6	11.4	5.6	3.0	2.8	2.9	3.3	5.3	7.9	9.6	6.5
7	2.8	1.3	1.4	2.5	2.2	3.0	5.0	4.8	1.9	2.0	2.4	1.3	2.5
8	3.1	2.4	4.8	2.9	2.2	2.3	.8	1.5	2.6	3.6	3.5	4.1	2.8
9	2.2	3.8	1.5	1.7	2.8	2.5	3.2	4.5	3.8	4.4	4.6	3.1	3.2
10	4.0	6.4	5.4	4.6	6.6	6.0	6.9	5.1	5.0	3.0	3.9	5.9	5.2
11	.9	1.1	.6	1.1	2.8	3.6	4.4	4.6	3.8	3.6	2.1	1.7	2.5
12	1.2	1.0	1.5	4.0	3.3	3.7	2.2	2.2	3.9	3.0	1.0	2.2	2.4
13	1.3	1.9	1.0	.8	.9	.6	.8	.9	1.4	.6	1.4	1.4	1.1
14	2.5	2.5	3.3	1.9	2.1	1.8	1.0	1.5	1.7	1.2	1.3	2.4	1.9
15	2.1	1.4	1.8	3.7	2.3	3.9	1.5	2.0	3.6	2.6	2.7	1.5	2.4
16	.9	1.0	.2	1.0	1.8	1.8	2.2	1.6	1.5	1.6	1.9	.7	1.4
17	.3	.9	1.8	2.7	2.6	2.0	1.7	2.4	.6	1.0	1.7	1.3	1.6
18	.6	.5	.5	.5	.9	1.3	2.2	1.4	1.1	.2	.6	.9	.9
19	1.2	1.8	2.8	2.7	.8	1.1	1.3	1.6	1.1	1.5	1.3	1.3	1.5
20	.8	1.5	1.3	1.0	2.4	4.0	4.5	2.9	4.5	3.7	2.9	2.2	2.6
21	3.6	3.4	2.5	1.1	1.2	.5	.1	.8	.5	1.0	1.7	2.9	1.6
22	1.2	1.4	1.0	.4	1.3	1.0	1.3	.8	.8	.9	1.3	.8	1.0
23	1.7	1.5	2.0	2.6	4.6	5.4	3.3	2.6	3.0	2.1	2.3	2.3	2.8
24	1.0	.8	1.7	2.4	1.0	2.0	1.4	1.4	1.4	2.1	1.8	1.3	1.5
25	.3	.1	.1	.4	.3	.4	1.4	.9	.4	.1	.2	.1	.4
26	.7	.6	1.0	1.2	.5	.5	.8	1.3	2.0	1.0	.7	.8	.9
27	1.3	1.3	.8	.7	1.0	1.8	2.6	1.4	3.0	2.9	2.9	1.0	1.7
28	.9	1.0	1.3	1.0	1.0	1.4	2.1	2.6	.6	1.8	1.2	.6	1.3
29	1.0	1.0	1.2	2.1	2.6	2.4	3.0	2.1	1.9	1.6	1.7	1.6	1.9
30	100.0	100.0	100.0	100.0	100.0	100.0	100.0	100.0	100.0	100.0	100.0	100.0	100.0

TABLE 2.4 Names & Codes of Baffin Objective Types

<u>Number</u>	<u>Name</u>	<u>Circulation</u>
1	Davis St. L	NEC
2	Ungava L	E
3	Devon Is. L	W
4	Hudson Bay L	SEC
5	Central L	C ₁
6	Thule H	NE
7	Hudson St. L	SE
8	Ungawa Ridge	SEA
9	N - Central L	Wc
10	Foxe Basin Ridge	EA
11	Southampton Is. L	Sc
12	SE - NW Ridge	NWA
13	SW Low Transition	Col
14	N - S Col	Col _C
15	Baffin Bay L	N _C
16	N. Baffin L	SWc
17	Central H	NEA
18	SW - NE Col	Col _A
19	Foxe Basin H	A ₁
20	E - W Col _C	Col _C
21	Boothia L Transition	Col
22	Foxe Basin L	S
23	E - W Col _A	Col _A
24	N - S Ridge	NA
25	S. Baffin H	WA
26	S. Baffin L	Ec
27	Thule L/Hudson Bay L	NWc
28	Central H/SE ridge	A ₂

TABLE 2.5

1946-74

MEAN MONTHLY FREQUENCY OF BAFFIN TYPES

TYPE	1	2	3	4	5	6	7	8	9	10	11	12	YEAR
1	9.5	7.6	7.9	6.0	5.8	4.5	3.2	3.8	5.6	6.0	6.4	8.6	75.0
2	2.5	3.2	3.3	3.1	3.5	3.0	3.1	3.6	2.9	2.6	3.1	3.0	36.7
3	2.9	2.9	2.2	2.0	1.7	1.8	2.9	2.6	2.6	2.7	1.6	2.3	28.2
4	.9	.9	1.1	1.4	2.2	2.4	3.2	2.2	1.6	1.7	2.0	.7	20.2
5	1.3	1.1	.7	1.2	1.4	1.6	1.1	2.1	1.3	2.3	1.1	.6	15.6
6	2.9	1.6	3.6	3.4	1.8	.9	.9	.9	1.0	1.6	2.4	3.0	23.9
7	.9	.4	.4	.8	.7	.9	1.5	1.5	.6	.6	.7	.4	9.3
8	1.0	.7	1.5	.9	.7	.7	.3	.5	.8	1.1	1.0	1.3	10.3
9	.7	1.1	.5	.5	.9	.8	1.0	1.4	1.1	1.4	1.4	1.0	11.6
10	1.3	1.8	1.7	1.4	2.0	1.8	2.1	1.6	1.5	.9	1.2	1.8	19.1
11	.3	.3	.2	.3	.9	1.1	1.4	1.4	1.1	1.1	.6	.5	9.3
12	.4	.3	.5	1.2	1.0	1.1	.7	.7	1.2	.9	.3	.7	8.9
13	.4	.5	.3	.3	.3	.2	.3	.3	.4	.2	.4	.4	4.0
14	.8	.7	1.0	.6	.6	.5	.3	.5	.5	.4	.4	.8	7.1
15	.6	.4	.6	1.1	.7	1.2	.5	.6	1.1	.8	.8	.5	8.9
16	.3	.3	.1	.3	.6	.5	.7	.5	.5	.5	.6	.2	5.0
17	.1	.3	.6	.8	.8	.6	.5	.8	.2	.3	.5	.4	5.9
18	.2	.1	.1	.1	.3	.4	.7	.4	.3	.1	.2	.3	3.3
19	.4	.5	.9	.8	.3	.3	.4	.5	.3	.5	.4	.4	5.6
20	.3	.4	.4	.3	.8	.2	1.4	.9	1.4	1.1	.9	.7	9.6
21	1.1	1.0	.8	.3	.4	.1	.0	.3	.1	.3	.5	.9	5.8
22	.4	.4	.3	.1	.4	.3	.4	.3	.3	.3	.4	.3	3.7
23	.5	.4	.6	.8	1.4	1.6	1.0	.8	.9	.6	.7	.7	10.2
24	.3	.2	.5	.7	.3	.6	.4	.4	.4	.6	.5	.4	5.6
25	.1	.0	.0	.1	.1	.1	.4	.3	.1	.0	.1	.0	1.5
26	.2	.2	.3	.4	.1	.1	.3	.4	.6	.3	.2	.3	3.4
27	.4	.4	.3	.2	.3	.5	.8	.4	.9	.9	.9	.3	6.3
28	.3	.3	.4	.3	.3	.4	.6	.8	.2	.6	.4	.2	4.8
29	.3	.3	.4	.6	.8	.7	.9	.6	.6	.5	.5	.5	6.8
30	31.0	28.2	31.0	30.0	31.0	30.0	31.0	31.0	30.0	31.0	30.0	31.0	365.2

Table 2.6 Computed daily normal temperatures (°C) at Broughton Island

	1	2	3	4	5	6	7	8	9	10	11	12
1	-23	-25	-25	-21	-12	-4	3	6	1	-5	-11	-19
2	-23	-25	-25	-21	-11	-3	3	5	1	-5	-12	-19
3	-23	-25	-25	-20	-11	-3	4	5	1	-5	-12	-19
4	-23	-25	-25	-20	-11	-3	4	5	0	-5	-12	-20
5	-24	-25	-25	-20	-10	-3	4	5	0	-5	-12	-20
6	-24	-25	-25	-20	-10	-3	4	5	-0	-6	-13	-20
7	-24	-25	-24	-19	-9	-2	4	5	-0	-6	-13	-20
8	-24	-25	-24	-19	-9	-2	4	5	-0	-6	-13	-20
9	-24	-25	-24	-18	-9	-2	5	5	-1	-6	-14	-20
10	-24	-25	-24	-18	-9	-2	5	4	-1	-6	-14	-21
11	-24	-25	-24	-18	-8	-1	5	4	-1	-7	-14	-21
12	-24	-25	-24	-17	-8	-1	5	4	-1	-7	-15	-21
13	-24	-25	-24	-17	-7	-1	5	4	-2	-7	-15	-21
14	-24	-25	-24	-17	-7	-1	5	4	-2	-8	-15	-22
15	-24	-25	-24	-16	-6	-0	5	3	-2	-8	-16	-22
16	-24	-25	-23	-16	-6	-0	5	3	-2	-8	-16	-22
17	-24	-25	-23	-16	-6	0	6	3	-3	-8	-16	-22
18	-24	-25	-23	-15	-6	0	6	3	-3	-9	-16	-22
19	-25	-25	-23	-15	-6	1	6	3	-3	-9	-17	-22
20	-25	-25	-23	-15	-5	1	6	3	-3	-9	-17	-22
21	-25	-25	-23	-14	-5	1	6	2	-3	-9	-17	-22
22	-25	-25	-22	-14	-5	1	6	2	-3	-9	-17	-22
23	-25	-25	-22	-14	-5	1	6	2	-4	-9	-17	-23
24	-25	-25	-22	-13	-4	2	6	2	-4	-10	-18	-23
25	-25	-25	-22	-13	-4	2	6	2	-4	-10	-18	-23
26	-25	-25	-22	-13	-4	2	6	2	-4	-10	-18	-23
27	-25	-25	-22	-13	-4	2	6	1	-4	-11	-18	-23
28	-25	-25	-21	-12	-4	3	6	1	-4	-11	-18	-23
29	-25	-25	-21	-12	-4	3	6	1	-5	-11	-19	-23
30	-25	-25	-21	-12	-4	3	6	1	-5	-11	-19	-23
31	-25	-25	-21	-12	-4	3	6	1	-5	-11	-19	-23
AVERAGE	-24.2	-24.9	-23.5	-16.6	-7.2	-6	5.0	3.6	-1.9	-7.7	-15.2	-21.4

Table 2.7

Mean daily departures of temperature ($^{\circ}\text{C}$) by synoptic type at Broughton Island; standard deviation (SD), standard (SE), and number of cases (N). Monthly and seasonal values are given.

MEAN DEPARTURE OF BROUGHTON I. TEMPERATURE FROM NORMAL, BY SYNOPTIC TYPE																		
TYPE	MONTH	1	2	3	4	5	6	7	8	9	10	11	12	M-A-M	J-J-A	S-O-N	D-J-F	YEAR
1	DEP	-6	-1.1	-3.7	-3.0	-2.1	-1.4	-2.4	-2.3	-1.4	-1.2	-7	-3	-3.1	-1.8	-1.1	-7	-1.6
	SD	5.2	5.5	4.7	3.7	3.0	2.9	3.7	2.4	2.1	2.8	4.0	5.2	4.1	3.1	3.1	5.3	4.3
	SE	.5	.6	.5	.4	.4	.3	.7	.5	.3	.3	.5	.5	.3	.3	.2	.3	.1
	N	102	100	105	69	64	77	30	20	68	70	71	95	238	127	209	298	872
2	DEP	3.8	4.2	1.1	2.0	-1.5	-8	-2.9	-1.0	-3	1.2	2.2	4.4	.1	-1.5	1.1	4.1	.9
	SD	6.1	6.4	5.8	6.1	4.0	2.4	2.9	2.9	2.0	2.5	5.1	6.5	5.4	2.9	3.7	6.3	5.2
	SE	1.0	1.0	1.1	1.1	.1	.4	.5	.4	.3	.4	.8	1.1	.5	.3	.3	.6	.2
	N	30	39	30	29	51	32	34	44	33	42	42	37	110	110	117	109	446
3	DEP	-8	.0	-1.6	.5	-1.2	.5	.2	.3	-5	.0	-1.1	1.0	-8	.3	-5	.2	-2
	SD	5.0	6.2	5.5	5.0	4.5	3.0	3.9	3.3	2.5	4.6	3.9	4.6	5.1	3.4	3.6	5.3	4.5
	SE	1.0	1.1	1.1	1.0	1.0	.6	.7	.6	.4	.9	1.0	.8	.6	.4	.4	.6	.2
	N	24	29	27	24	20	24	29	27	42	27	15	32	71	80	84	85	320
4	DEP	6.8	9.0	3.8	1.5	2.3	-1	.7	.4	1.3	.6	3.8	6.4	2.3	.4	2.0	7.4	2.1
	SD	6.2	4.1	6.0	5.5	4.7	2.5	3.5	2.6	4.4	3.0	5.0	1.8	5.3	3.0	4.5	5.0	4.7
	SE	1.7	1.5	2.0	1.4	1.0	.5	.5	.5	1.0	.6	1.0	.7	.8	.3	.6	1.0	.3
	N	13	8	9	16	22	22	41	27	18	22	24	6	47	90	64	27	228
5	DEP	6.0	2.4	.8	-2	-1.3	-1.9	-1.4	-1.4	-5	-3	1.4	.2	-4	-1.5	.2	3.4	.1
	SD	8.1	7.2	4.8	3.5	3.9	1.8	2.2	2.7	2.0	3.4	3.8	2.8	4.1	2.4	3.4	7.3	4.7
	SE	2.2	1.8	1.5	1.1	1.0	.4	.7	.5	.7	.7	1.0	1.1	.7	.3	.5	1.2	.4
	N	13	16	10	10	15	18	10	30	9	25	13	6	35	.58	47	35	175
6	DEP	1.7	-1.5	1.3	.9	-1.9	-1.3	-1.5	-1.8	-7	.2	-6	.9	.6	-1.6	-3	.7	.2
	SD	5.4	4.4	6.4	4.9	3.2	2.2	2.5	2.7	2.2	2.7	4.8	5.0	5.5	2.5	3.7	5.5	5.0
	SE	.8	1.0	.9	.7	.8	.7	.6	.7	.7	.7	1.0	1.1	.5	.4	.5	.6	.3
	N	44	20	46	49	17	9	15	14	10	16	21	30	112	38	47	94	291
7	DEP	4.0	9.9	5.9	3.3	-3	1.6	-1.7	1.5	-1.5	3.7	3.5	5.5	2.2	.3	2.1	5.6	2.2
	SD	6.0	6.5	6.4	7.2	3.8	1.2	3.5	2.9	2.3	2.3	3.6	6.9	6.3	3.3	3.7	6.8	5.4
	SE	1.7	2.9	3.2	2.6	1.3	.5	.9	.6	.9	1.0	1.2	2.8	1.4	.5	.8	1.4	.5
	N	13	5	4	8	9	6	16	21	6	6	9	6	21	43	21	24	109
8	DEP	-4.0	-3.4	-3.0	-2.0	-4	-1.0	-5.1	-8	-8	-1.0	-1.0	.2	-2.2	-1.1	-1.0	-1.8	-1.5
	SD	4.9	3.7	6.4	3.3	2.3	2.6	0.0	2.8	2.2	3.1	3.9	3.4	4.9	2.8	3.1	4.4	4.0
	SE	1.5	1.4	1.8	.9	1.0	1.0	0.0	1.0	.6	.9	1.2	.8	.9	.7	.5	.8	.4
	N	10	7	13	13	.5	7	1	8	12	12	11	17	31	16	35	34	116
9	DEP	2.8	.1	-2.8	.3	-7	-1.3	-1	.4	1.8	1.4	1.0	-4	-1.1	-2	1.4	.6	.4
	SD	5.8	8.2	4.9	5.6	3.4	2.9	3.5	3.2	3.3	3.1	4.1	5.4	4.7	3.3	3.6	7.0	4.9
	SE	2.0	2.2	2.0	2.5	1.1	1.0	1.0	.9	.8	1.0	1.0	1.7	1.0	.6	.6	1.2	.4
	N	8	14	6	5	9	8	12	12	17	9	17	10	20	32	43	32	127
10	DEP	4.0	4.4	-0	2.6	-2	-1.1	-6	-5	-2	-1.0	.5	2.3	.6	-7	-3	3.1	.9
	SD	6.3	6.1	4.6	6.8	4.0	3.1	2.9	2.8	2.8	2.4	4.0	5.5	5.3	2.9	3.2	6.0	5.0
	SE	1.4	1.3	1.0	1.7	.9	.8	.6	.6	.8	.6	1.1	1.2	.7	.4	.5	.8	.3
	N	20	21	21	16	21	15	27	22	12	15	13	23	58	64	40	64	226

Table 2.7 Continued

TYPE	MONTH	MEAN DEPARTURE OF BROUGHTON I. TEMPERATURE FROM NORMAL, BY SYNOPTIC TYPE												YEAR				
		1	2	3	4	5	6	7	8	9	10	11	12	M-A-M	J-J-A	S-O-N	D-J-F	YEAR
11	DEP	7.1	9.8	2.8	-1.4	4.1	1.4	-1.1	2.3	2.0	2.8	3.6	5.3	2.4	1.5	2.8	6.9	2.8
	SD	4.8	10.3	8.6	3.5	2.0	1.9	2.5	3.2	3.9	3.0	4.9	5.0	4.7	2.9	4.0	6.9	4.6
	SE	2.2	5.2	5.0	1.4	1.1	.5	.7	.7	1.2	.9	1.5	1.8	1.0	.4	.7	1.7	.4
	N	5	4	3	6	12	16	12	22	10	12	11	9	21	50	33	17	121
12	DEP	-1.6	-2.1	1.5	1.0	1.2	1.0	-3	-0	.4	-1	-9	3.4	1.2	.3	.1	1.1	.6
	SD	3.1	2.2	5.4	4.9	4.4	3.3	2.8	3.8	2.9	3.9	4.2	7.8	4.8	3.4	3.5	6.6	4.5
	SE	1.4	1.2	2.2	1.2	1.1	1.0	.9	1.2	.7	1.1	2.1	2.5	.8	.6	.6	1.6	.4
	N	5	3	6	16	15	11	9	10	19	13	4	10	37	30	36	18	121
13	DEP	4.7	-4.3	2.8	.0	-3.0	-4	-1.5	2.4	-1.5	3.4	-6	-1.2	-1	.4	.1	-2.2	-6
	SD	0.0	3.8	8.8	2.6	2.1	1.4	3.3	2.5	.9	2.1	6.2	4.3	5.8	3.1	5.0	4.6	4.9
	SE	0.0	1.4	4.4	1.2	1.3	.8	1.7	1.1	.6	1.5	2.8	1.5	1.6	.9	1.7	1.2	.7
	N	1	7	4	5	4	3	4	5	2	2	5	8	13	12	9	16	50
14	DEP	3.0	.2	.5	2.6	-2.3	-0	-1.0	.7	-2	-3.6	.5	5.6	-1	.1	-6	2.8	.7
	SD	3.2	4.5	5.8	4.4	4.2	3.2	1.7	2.2	2.7	2.4	2.3	5.8	5.3	2.7	2.9	5.1	4.7
	SE	1.1	1.5	1.5	1.8	1.2	1.1	.9	.8	1.2	1.7	1.3	2.1	.9	.6	.9	1.0	.5
	N	8	9	14	6	12	8	4	8	5	2	3	8	32	20	10	25	87
15	DEP	-2.8	2.1	-5.9	-2.7	-3.0	.3	-2.1	-3.4	-1.3	-8	-2.3	1.8	-3.5	-1.3	-1.4	.1	-1.7
	SD	4.7	6.5	3.4	3.8	3.5	3.2	3.7	2.2	2.6	3.1	2.8	5.6	3.8	3.4	2.9	5.9	4.1
	SE	1.8	3.3	1.3	1.0	1.1	.8	1.7	.7	.7	1.0	.9	2.1	.7	.6	.5	1.4	.4
	N	7	4	7	15	11	15	5	9	14	9	9	7	33	29	32	18	112
16	DEP	3.6	3.8	2.6	-2.1	-1.4	2.8	2.9	4.7	3.9	1.4	3.8	.1	-1.0	3.3	3.5	2.3	2.6
	SD	.9	4.0	0.0	0.0	3.1	1.0	3.5	2.7	4.4	1.7	4.2	4.4	3.1	3.2	4.1	3.8	3.9
	SE	.5	2.8	0.0	0.0	1.2	.6	.9	1.1	1.7	1.0	1.3	2.5	1.0	.6	.3	1.3	.5
	N	3	2	1	1	7	3	15	6	7	3	11	3	9	24	.1	8	62
17	DEP	15.5	8.1	3.2	-1.2	.3	.6	.4	2.2	-3.0	-6	.8	.8	-2	1.2	-3	4.2	1.0
	SD	0.0	7.0	6.6	4.2	4.4	1.4	2.6	2.6	.7	2.5	4.6	5.2	4.9	2.5	3.8	7.3	5.0
	SE	0.0	3.5	3.8	1.2	1.8	.6	1.0	.8	.5	1.1	1.7	1.8	1.0	.5	1.0	2.0	.6
	N	1	4	3	13	5	5	7	10	2	5	7	8	22	22	14	13	71
18	DEP	0.0	5.4	-3.9	2.1	1.1	-3	1.7	-5	-4	-2.0	3.0	2.3	-3	.5	1.3	3.2	1.1
	SD	0.0	7.5	2.6	1.4	4.4	1.1	2.8	1.7	0.0	0.0	2.1	5.6	4.1	2.4	2.7	6.4	4.1
	SE	0.0	5.3	1.9	1.0	3.1	.6	1.1	.8	0.0	0.0	1.2	2.5	1.7	.6	1.2	2.2	.7
	N	0	2	2	2	2	4	6	4	1	1	3	5	6	14	5	7	32
19	DEP	-1.2	-2.7	-2.5	-2	-2.3	2.4	.1	-6	-6	-4	-4.6	2.7	-1.5	.6	-1.8	.0	-8
	SD	8.8	3.5	5.9	3.8	3.0	2.5	2.9	3.2	3.8	4.3	2.7	4.0	4.8	3.1	4.3	6.5	4.9
	SE	3.6	1.8	1.8	1.1	1.2	1.1	1.1	1.4	2.7	1.4	1.2	1.5	.9	.8	1.1	1.6	.6
	N	6	4	11	11	5	5	7	5	2	9	5	7	28	17	16	17	13
20	DEP	-8.1	-8	4.1	2.0	-1.1	-5	-6	-2.1	.1	.3	-1.6	.2	.3	-9	-3	-6	-5
	SD	0.0	5.0	8.8	0.0	3.5	2.4	3.9	1.9	2.3	2.5	3.9	5.2	5.6	3.0	3.0	5.1	3.9
	SE	0.0	2.1	4.4	0.0	1.0	.5	1.0	.6	.6	.7	1.2	1.7	1.4	.4	.5	1.3	.4
	N	1	6	4	1	12	22	16	11	17	11	11	.0	17	49	39	17	122

MEAN DEPARTURE OF BROUGHTON I. TEMPERATURE FROM NORMAL, BY SYNOPTIC TYPE

TYPE	MONTH	1	2	3	4	5	6	7	8	9	10	11	12	M-A	M-J	J-A	S-O	N-D	J-F	YEAR
21	DEP	-3.2	-2.0	-2.9	.3	-3.2	.4	-2.3	4.3	.8	.6	-2.2	-3.0	-2.1	1.1	-1.8	-2.7	-1.8		
	SD	4.0	7.8	4.8	5.9	5.1	1.1	0.0	1.2	1.6	3.2	2.7	3.1	5.1	2.5	5.0	5.8	5.1		
	SE	1.1	2.2	1.2	2.2	2.8	.6	0.0	.9	.8	1.6	.9	1.6	1.0	.9	.7	1.1	.6		
22	DEP	5.2	10.4	5.7	13.9	4.0	2.0	2.1	3.8	3.4	1.6	5.7	1.7	6.4	2.3	3.9	5.5	4.6		
	SD	6.3	5.6	4.4	4.8	5.0	3.9	3.1	6.0	2.3	2.6	3.9	2.9	6.0	3.2	3.7	6.3	5.1		
	SE	2.4	2.8	2.2	3.4	2.2	1.9	1.3	0.0	1.1	1.1	1.3	1.7	1.8	.9	.8	1.7	.7		
23	DEP	-2.1	-2.2	-4.5	1.6	-2.4	-1.9	-1.2	.6	-6.1	-1.1	-5.1	2.9	-1.9	-1.5	-1.4	.0	-1.8		
	SD	5.4	3.9	5.2	5.2	4.4	2.7	3.1	3.5	3.2	3.4	5.1	3.6	5.2	3.2	3.9	5.1	4.2		
	SE	2.4	2.8	2.1	2.0	1.1	.7	.8	.9	1.1	1.0	1.9	1.6	1.0	.5	.7	1.5	.4		
24	DEP	-4.7	.5	2.4	3.4	2.9	-1.3	.5	.4	.3	-1.7	-4.0	.3	2.9	.2	-1.0	-1.2	.3		
	SD	4.8	5.0	5.2	3.2	4.5	2.9	1.6	2.5	3.7	3.4	2.1	4.3	4.3	2.4	3.6	5.2	4.3		
	SE	2.1	2.9	1.9	1.1	1.8	1.2	.6	1.1	1.4	1.0	1.0	1.5	.9	.6	.6	1.3	.5		
25	DEP	-1.4	0.0	0.0	3.9	-1.1	-1.1	.4	3.8	0.0	8.4	-3.6	6.4	2.1	1.9	2.4	1.2	1.9		
	SD	2.6	0.0	0.0	6.1	2.8	0.0	1.7	2.2	0.0	0.0	0.0	0.0	5.6	2.6	6.0	4.3	4.0		
	SE	1.9	0.0	0.0	3.5	2.0	0.0	.7	.9	0.0	0.0	0.0	0.0	2.5	.7	4.2	2.5	.8		
26	DEP	-2.3	4.8	.8	-1.3	-4.1	-1.5	-4.3	-3.0	-1.7	-1.5	.1	1.7	-1.0	-2.9	-1.1	1.8	-1.7		
	SD	2.9	4.6	3.3	2.1	.2	1.2	2.8	1.8	2.3	2.3	.6	6.1	2.9	2.6	2.3	5.7	4.0		
	SE	2.0	2.7	2.3	.9	.2	.8	1.6	1.0	1.1	1.0	.4	2.7	1.0	.9	.6	1.8	.6		
27	DEP	-1.3	-1.1	0.0	-2.3	-3.4	-1.1	2.9	1.9	-1.7	-1.7	.0	-3.3	-3.0	1.7	-1.8	-1.8	-1.6		
	SD	2.0	5.0	0.0	2.2	3.5	2.5	3.7	3.7	3.8	2.4	3.3	3.6	3.1	3.6	3.4	3.4	3.7		
	SE	.8	2.9	0.0	1.3	1.5	1.0	1.3	1.8	1.1	.9	1.0	1.8	1.1	.8	.6	.5	.4		
28	DEP	2.8	8.9	.5	7.1	-1.1	4.5	2.3	4.0	3.5	.4	2.9	4.3	2.0	3.3	2.0	5.6	3.0		
	SD	1.0	12.1	4.3	3.7	4.9	4.6	4.6	3.6	2.1	2.7	3.2	2.4	5.3	4.3	3.1	5.0	5.0		
	SE	.7	7.0	1.8	2.1	3.5	2.3	1.3	1.1	1.1	1.0	1.3	1.4	1.6	.8	.7	2.8	.0		
29	DEP	1.6	13.7	1.8	.6	2.0	-1.6	1.3	.8	.0	1.3	1.5	.5	1.5	.7	.9	4.6	1.7		
	SD	6.4	7.7	6.9	3.1	6.1	2.7	2.8	2.6	3.0	4.4	4.1	4.6	5.5	2.8	3.9	6.4	5.4		
	SE	2.4	3.4	3.5	1.2	1.9	1.0	.8	.8	1.0	1.7	1.5	1.9	1.2	.5	.8	2.0	.6		
30	DEP	1.1	1.3	-1.0	.1	-1.9	-1.4	-1.4	.1	-1.2	.0	.7	1.3	-1.6	-1.2	.2	1.2	.1		
	SD	6.2	7.1	6.1	5.2	4.3	2.9	3.6	3.4	3.0	3.4	4.7	5.6	5.3	3.3	3.6	6.3	4.9		
	SE	.3	.4	.3	.3	.2	.2	.2	.2	.2	.2	.2	.3	.2	.1	.1	.2	.1		
31	DEP	1.1	1.3	-1.0	.1	-1.9	-1.4	-1.4	.1	-1.2	.0	.7	1.3	-1.6	-1.2	.2	1.2	.1		
	SD	6.2	7.1	6.1	5.2	4.3	2.9	3.6	3.4	3.0	3.4	4.7	5.6	5.3	3.3	3.6	6.3	4.9		
	SE	.3	.4	.3	.3	.2	.2	.2	.2	.2	.2	.2	.3	.2	.1	.1	.2	.1		
32	DEP	1.1	1.3	-1.0	.1	-1.9	-1.4	-1.4	.1	-1.2	.0	.7	1.3	-1.6	-1.2	.2	1.2	.1		
	SD	6.2	7.1	6.1	5.2	4.3	2.9	3.6	3.4	3.0	3.4	4.7	5.6	5.3	3.3	3.6	6.3	4.9		
	SE	.3	.4	.3	.3	.2	.2	.2	.2	.2	.2	.2	.3	.2	.1	.1	.2	.1		
33	DEP	1.1	1.3	-1.0	.1	-1.9	-1.4	-1.4	.1	-1.2	.0	.7	1.3	-1.6	-1.2	.2	1.2	.1		
	SD	6.2	7.1	6.1	5.2	4.3	2.9	3.6	3.4	3.0	3.4	4.7	5.6	5.3	3.3	3.6	6.3	4.9		
	SE	.3	.4	.3	.3	.2	.2	.2	.2	.2	.2	.2	.3	.2	.1	.1	.2	.1		
34	DEP	1.1	1.3	-1.0	.1	-1.9	-1.4	-1.4	.1	-1.2	.0	.7	1.3	-1.6	-1.2	.2	1.2	.1		
	SD	6.2	7.1	6.1	5.2	4.3	2.9	3.6	3.4	3.0	3.4	4.7	5.6	5.3	3.3	3.6	6.3	4.9		
	SE	.3	.4	.3	.3	.2	.2	.2	.2	.2	.2	.2	.3	.2	.1	.1	.2	.1		
35	DEP	1.1	1.3	-1.0	.1	-1.9	-1.4	-1.4	.1	-1.2	.0	.7	1.3	-1.6	-1.2	.2	1.2	.1		
	SD	6.2	7.1	6.1	5.2	4.3	2.9	3.6	3.4	3.0	3.4	4.7	5.6	5.3	3.3	3.6	6.3	4.9		
	SE	.3	.4	.3	.3	.2	.2	.2	.2	.2	.2	.2	.3	.2	.1	.1	.2	.1		
36	DEP	1.1	1.3	-1.0	.1	-1.9	-1.4	-1.4	.1	-1.2	.0	.7	1.3	-1.6	-1.2	.2	1.2	.1		
	SD	6.2	7.1	6.1	5.2	4.3	2.9	3.6	3.4	3.0	3.4	4.7	5.6	5.3	3.3	3.6	6.3	4.9		
	SE	.3	.4	.3	.3	.2	.2	.2	.2	.2	.2	.2	.3	.2	.1	.1	.2	.1		
37	DEP	1.1	1.3	-1.0	.1	-1.9	-1.4	-1.4	.1	-1.2	.0	.7	1.3	-1.6	-1.2	.2	1.2	.1		
	SD	6.2	7.1	6.1	5.2	4.3	2.9	3.6	3.4	3.0	3.4	4.7	5.6	5.3	3.3	3.6	6.3	4.9		
	SE	.3	.4	.3	.3	.2	.2	.2	.2	.2	.2	.2	.3	.2	.1	.1	.2	.1		
38	DEP	1.1	1.3	-1.0	.1	-1.9	-1.4	-1.4	.1	-1.2	.0	.7	1.3	-1.6	-1.2	.2	1.2	.1		
	SD	6.2	7.1	6.1	5.2	4.3	2.9	3.6	3.4	3.0	3.4	4.7	5.6	5.3	3.3	3.6	6.3	4.9		
	SE	.3	.4	.3	.3	.2	.2	.2	.2	.2	.2	.2	.3	.2	.1	.1	.2	.1		
39	DEP	1.1	1.3	-1.0	.1	-1.9	-1.4	-1.4	.1	-1.2	.0	.7	1.3	-1.6	-1.2	.2	1.2	.1		
	SD	6.2	7.1	6.1	5.2	4.3	2.9	3.6	3.4	3.0	3.4	4.7	5.6	5.3	3.3	3.6	6.3	4.9		
	SE	.3	.4	.3	.3	.2	.2	.2	.2	.2	.2	.2	.3	.2	.1	.1	.2	.1		
40	DEP	1.1	1.3	-1.0	.1	-1.9	-1.4	-1.4	.1	-1.2	.0	.7	1.3	-1.6	-1.2	.2	1.2	.1		
	SD	6.2	7.1	6.1	5.2	4.3	2.9	3.6	3.4	3.0	3.4	4.7	5.6	5.3	3.3	3.6	6.3	4.9		
	SE	.3	.4	.3	.3	.2	.2	.2	.2	.2	.2	.2	.3	.2	.1	.1	.2	.1		
41	DEP	1.1	1.3	-1.0	.1	-1.9	-1.4	-1.4	.1	-1.2	.0	.7	1.3	-1.6	-1.2	.2	1.2	.1		
	SD	6.2	7.1	6.1	5.2	4.3	2.9	3.6	3.4	3.0	3.4	4.7	5.6	5.3	3.3	3.6	6.3	4.9		
	SE	.3	.4	.3	.3	.2	.2	.2	.2	.2	.2	.2	.3	.2	.1	.1	.2	.1		
42	DEP	1.1	1.3	-1.0	.1	-1.9	-1.4	-1.4	.1	-1.2	.0	.7	1.3	-1.6	-1.2	.2	1.2	.1		
	SD	6.2	7.1	6.1	5.2	4.3	2.9	3.6	3.4	3.0	3.4	4.7	5.6	5.3	3.3	3.6	6.3	4.9		
	SE	.3	.4	.3	.3	.2	.2	.2	.2	.2	.2	.2	.3	.2	.1	.1	.2	.1		
43	DEP	1.1	1.3	-1.0	.1	-1.9	-1.4	-1.4	.1	-1.2	.0	.7	1.3	-1.6	-1.2	.2	1.2	.1		
	SD	6.2	7.1	6.1	5.2	4.3	2.9	3.6	3.4	3.0	3.4	4.7	5.6	5.3	3.3	3.6	6.3	4.9		
	SE	.3	.4	.3	.3	.2	.2	.2	.2	.2	.2	.2	.3	.2	.1	.1	.2	.1		
44	DEP	1.1	1.3	-1.0	.1	-1.9	-1.4	-1.4	.1	-1.2	.0	.7	1.3	-1.6	-1.2	.2	1.2	.1		
	SD	6.2	7.1	6.1	5.2	4.3	2.9	3.6	3.4	3.0	3.4	4.7	5.6	5.3	3.3	3.6	6.3	4.9		
	SE	.3	.4	.3	.3	.2	.2	.2	.2	.2	.2	.2	.3	.2	.1	.1	.2	.1		
45	DEP	1.1	1.3	-1.0	.1	-1.9	-1.4	-1.4	.1	-1.2	.0	.7	1.3	-1.6	-1.2	.2	1.			

Table 2.8.

Broughton Island Precipitation: Contribution to Total from each Synoptic Type.

Type	Summer (June - August)		Winter (Dec. - Feb.)		Annual	
	Precip. mm.	Percent	Precip. mm.	Percent	Precip. mm.	Percent
1	154	20.6	61	12.6	720	20.9
2	106	14.1	145	29.9	616	17.9
3	58	7.7	10	2.1	147	4.3
4	22	2.9	3	.6	47	1.4
5	62	8.3	6	1.2	200	5.8
6	9	1.2	44	9.1	161	4.7
7	21	2.8	13	2.7	50	1.5
8	7	.9	0	0	44	1.3
9	21	2.8	5	1.0	97	2.8
10	7	.9	22	4.5	104	3.0
11	50	6.7	17	3.5	107	3.1
12	2	.3	0	0	27	.8
13	0	0	15	3.1	23	.7
14	5	.7	2	.4	12	.3
15	37	4.9	19	3.9	136	4.0
16	2	.3	2	.4	13	.4
17	3	.4	1	.2	22	.6
18	8	1.1	5	1.0	24	.7
19	0	0	0	0	6	.2
20	38	5.1	35	7.2	228	6.6
21	10	1.3	0	0	12	.3
22	1	.1	3	.6	4	.1
23	12	1.6	0	0	82	2.4
24	4	.5	6	1.2	60	.2
25	0	0	0	0	1	0
26	9	1.2	7	1.4	63	1.8
27	18	2.4	1	.2	42	1.2
28	5	.7	1	.2	10	.3
Untyped	74	9.9	61	12.6	374	10.8
Total	745	100.0	484	100.0	3442	100.0

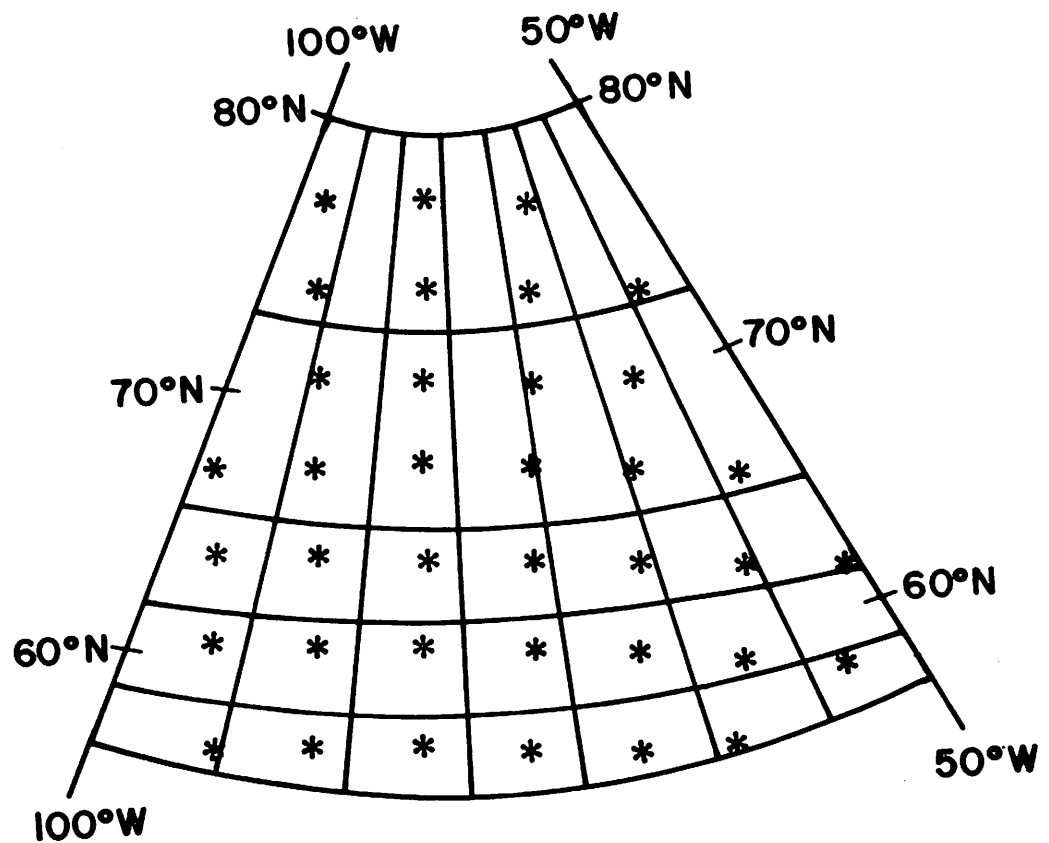


Figure 2.1. NMC 37-point grid for the sector 58°-80°N, 50°-100°W showing row and column zones.

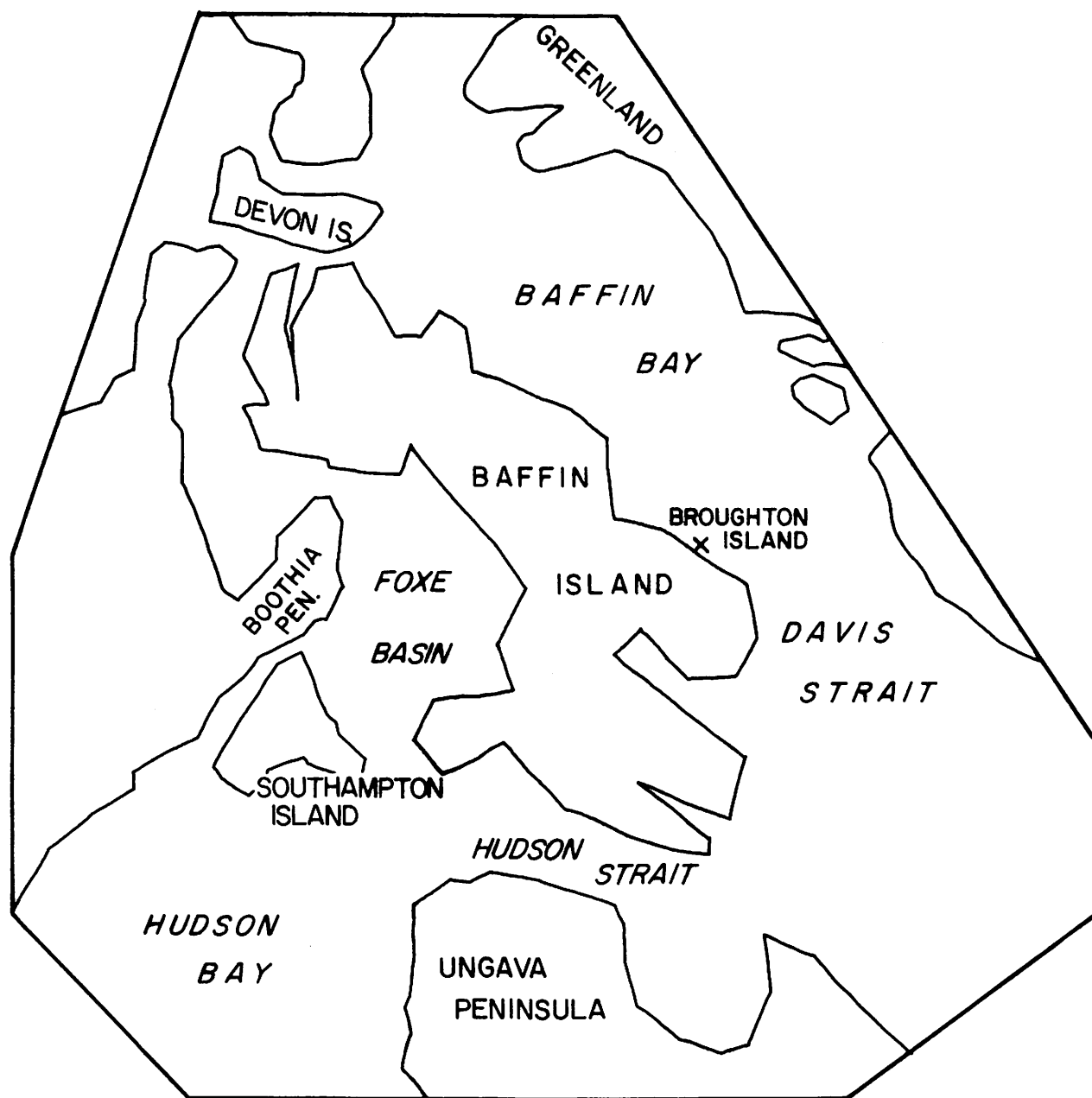
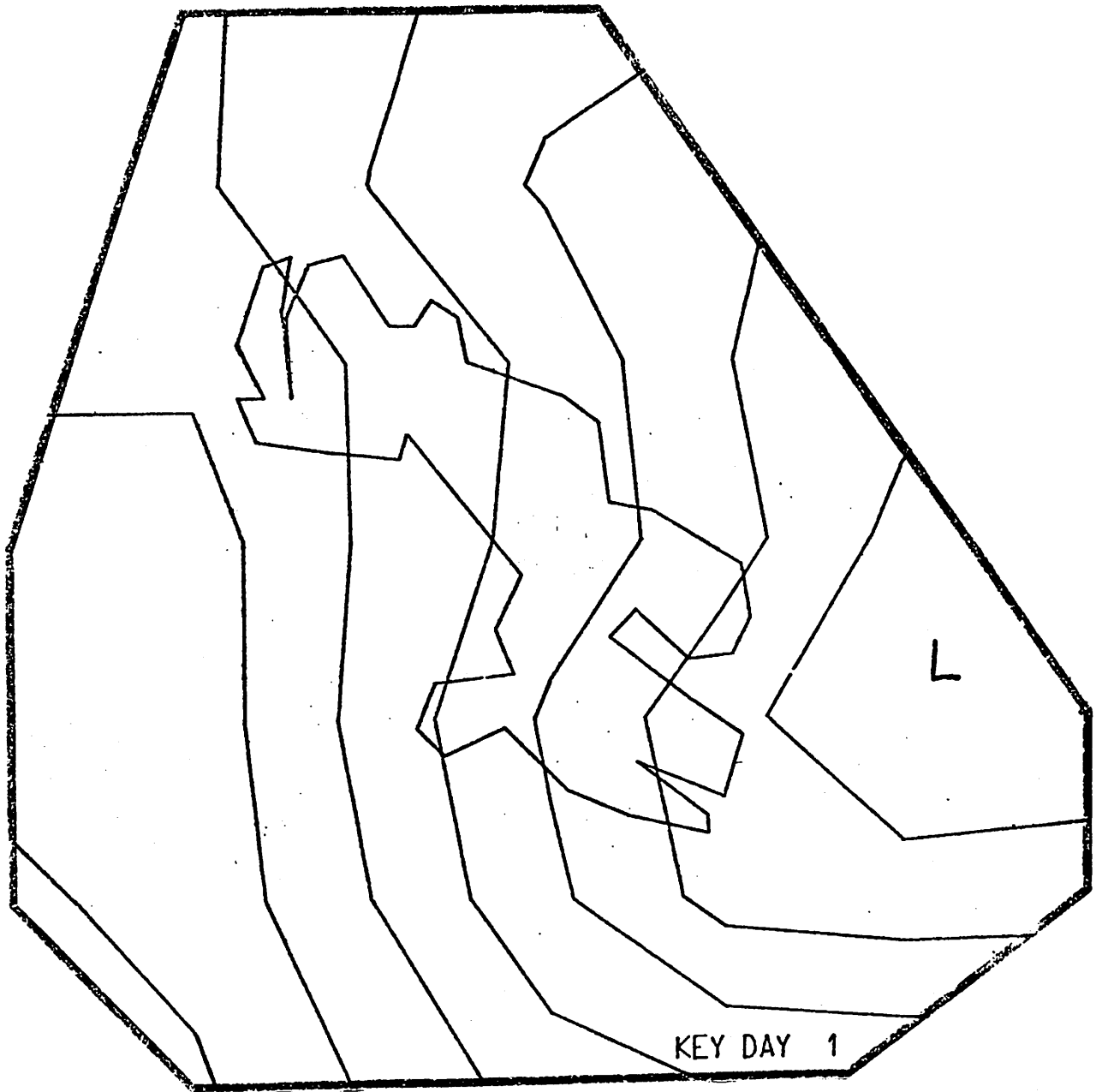
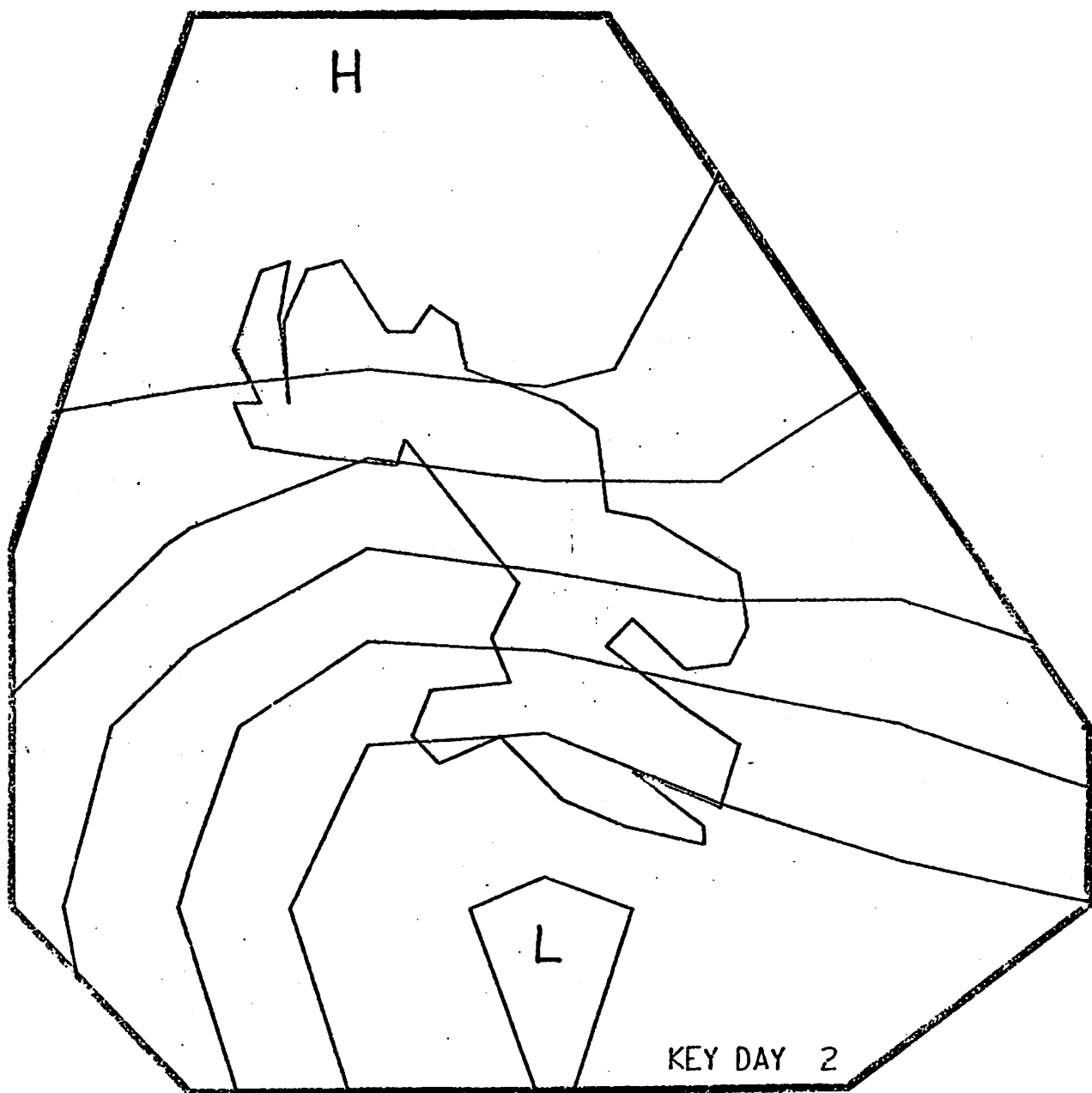
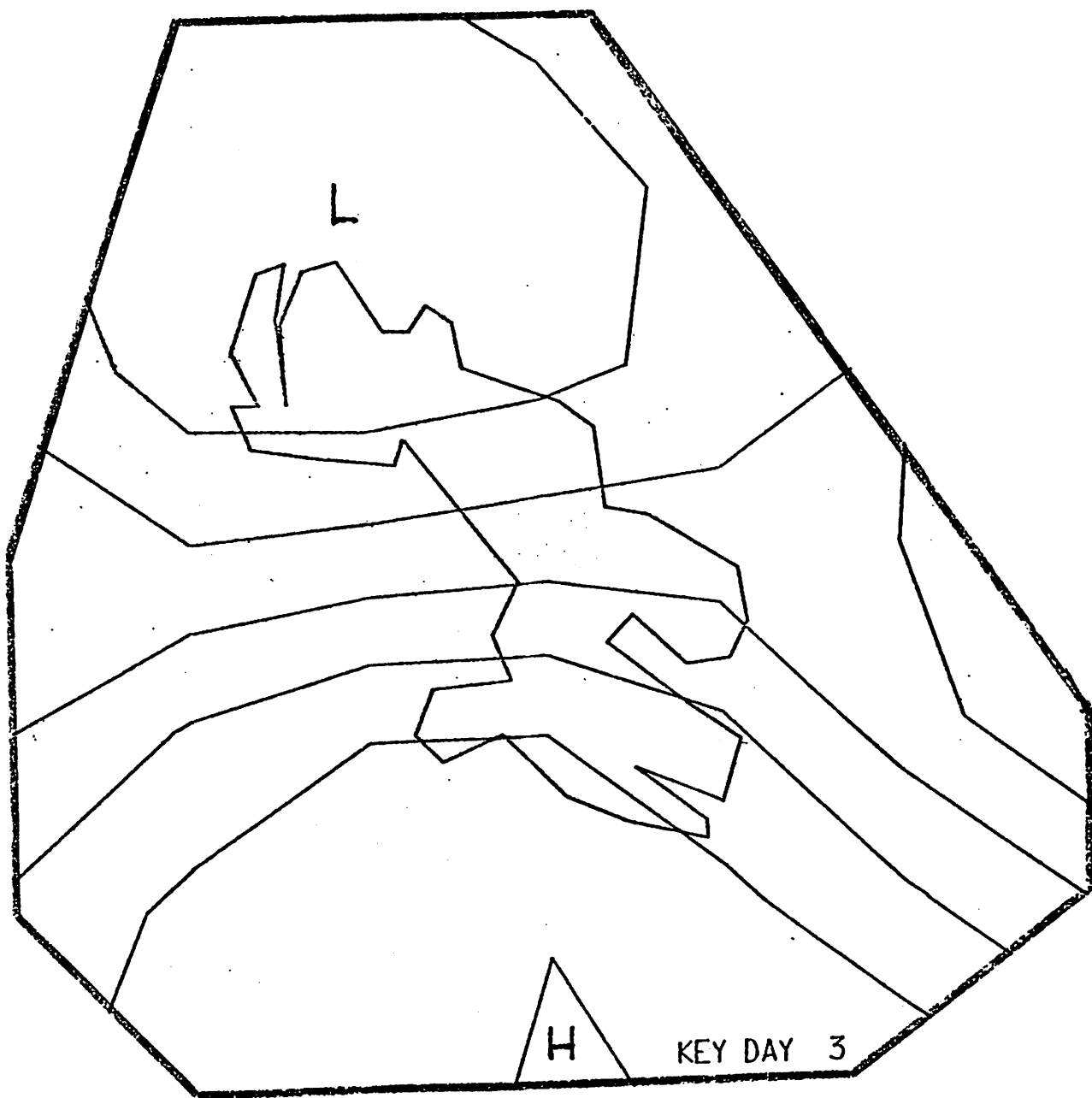
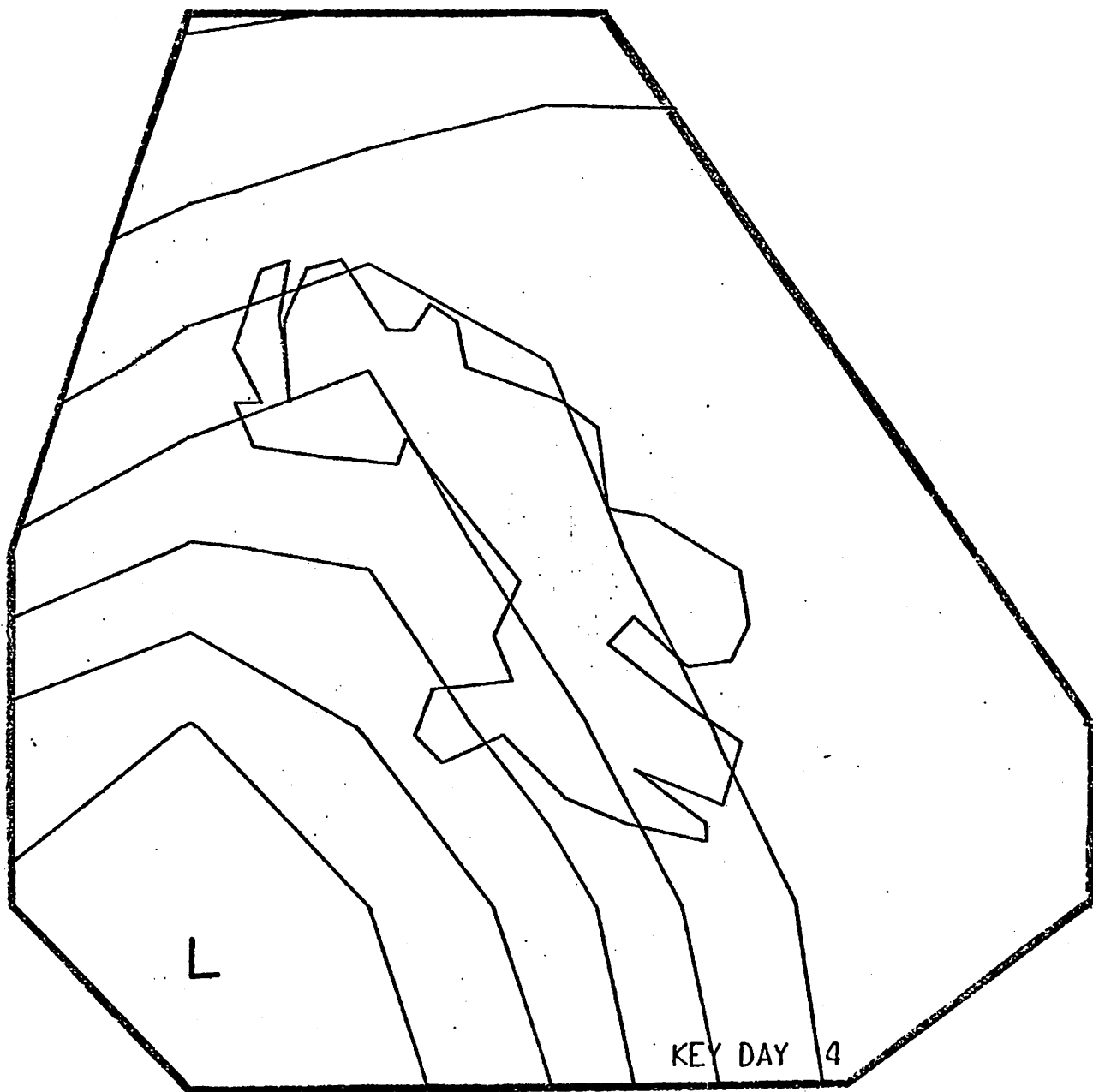


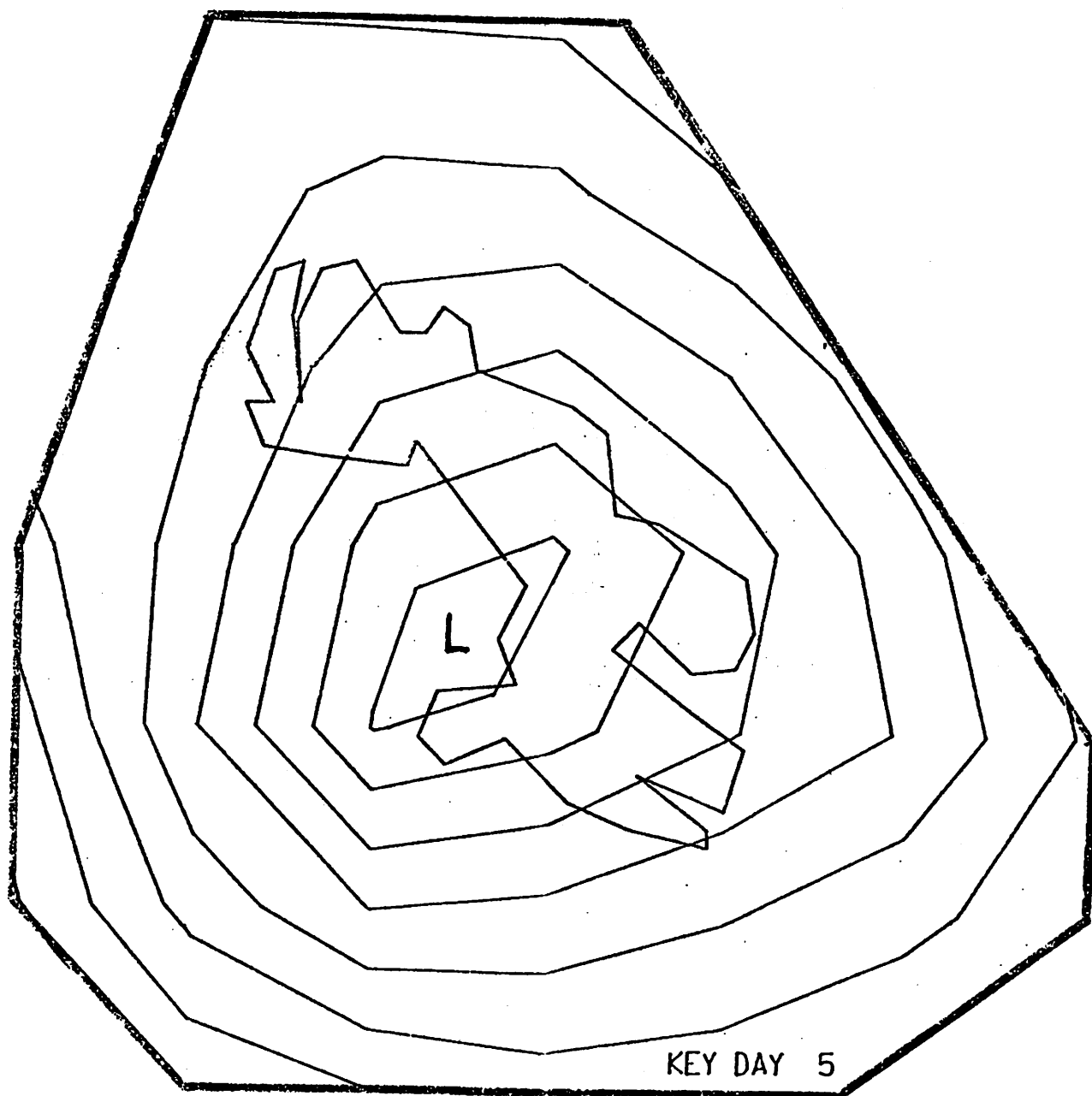
Figure 2.2. Pressure maps for the 28 key days and grid outline. Pressure units are normalized with an isopleth interval of $0.5 \times$ standard deviation.

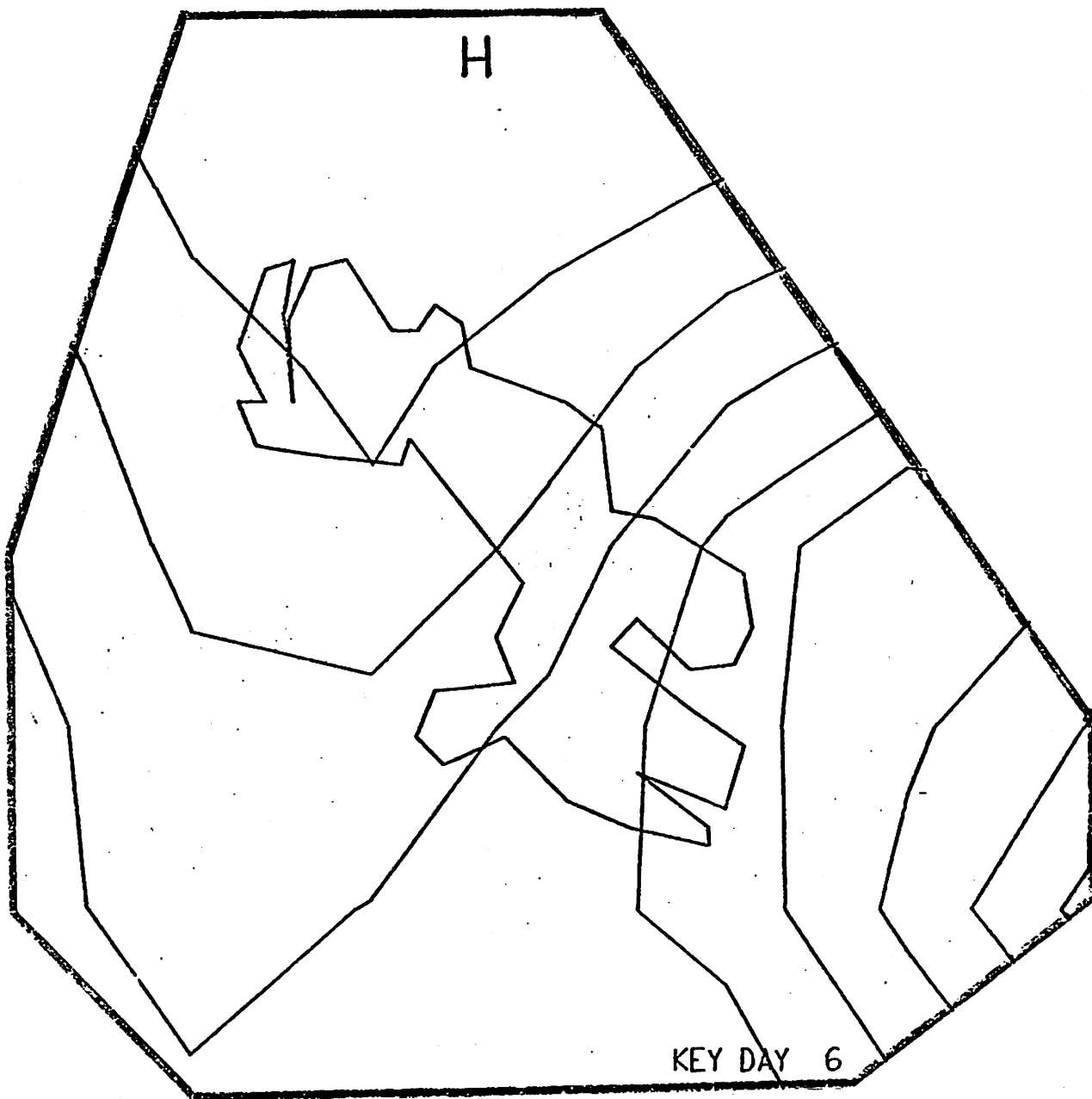


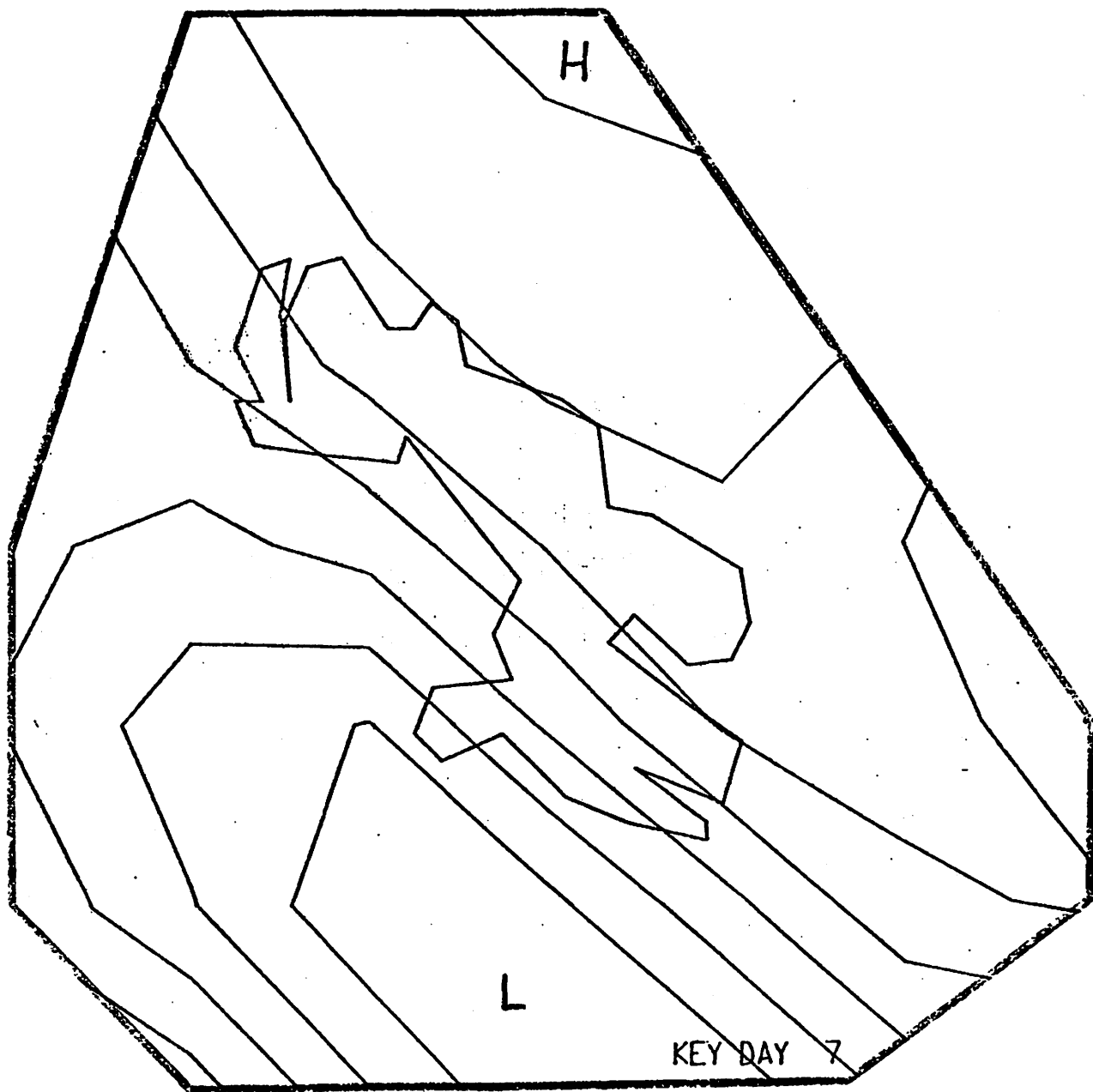


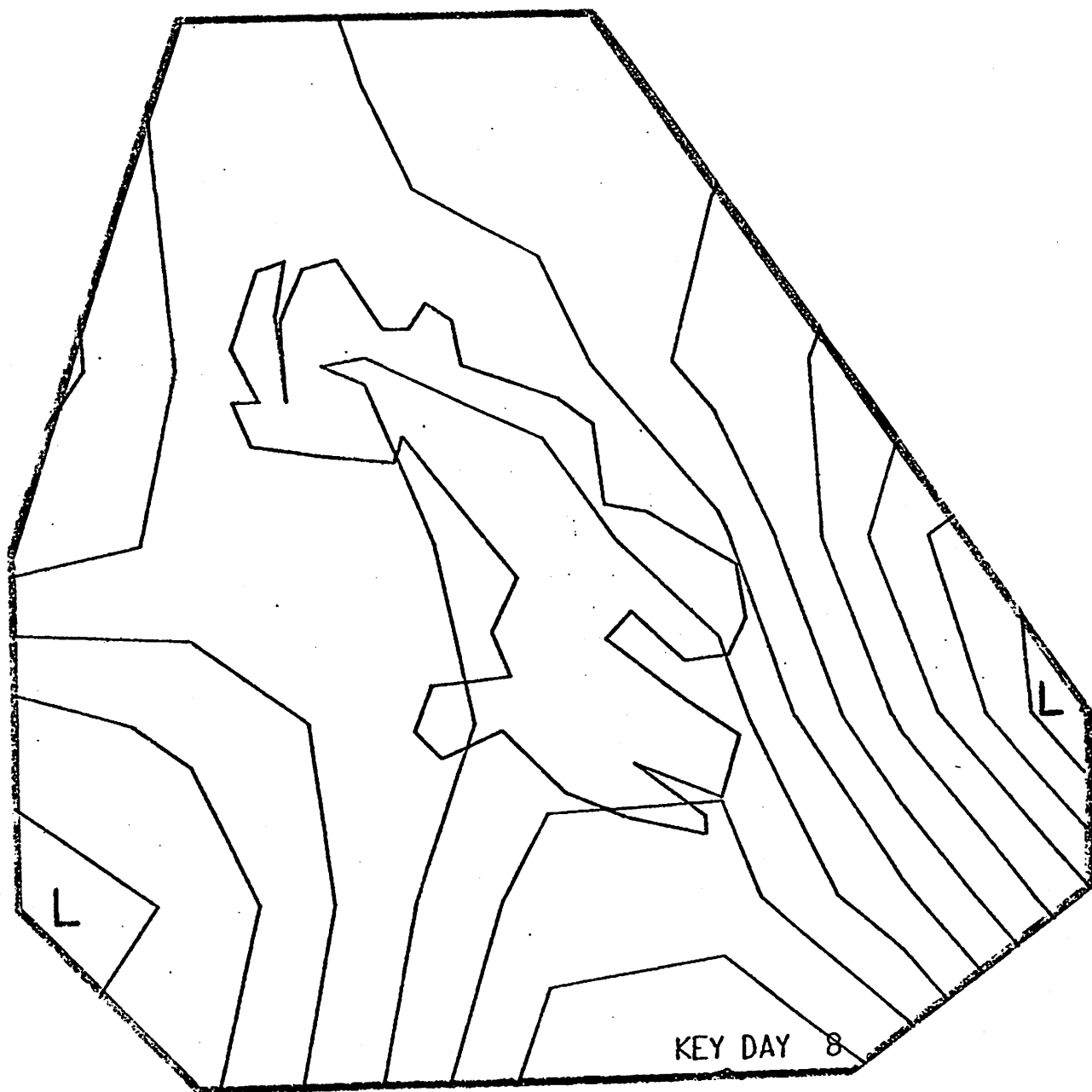


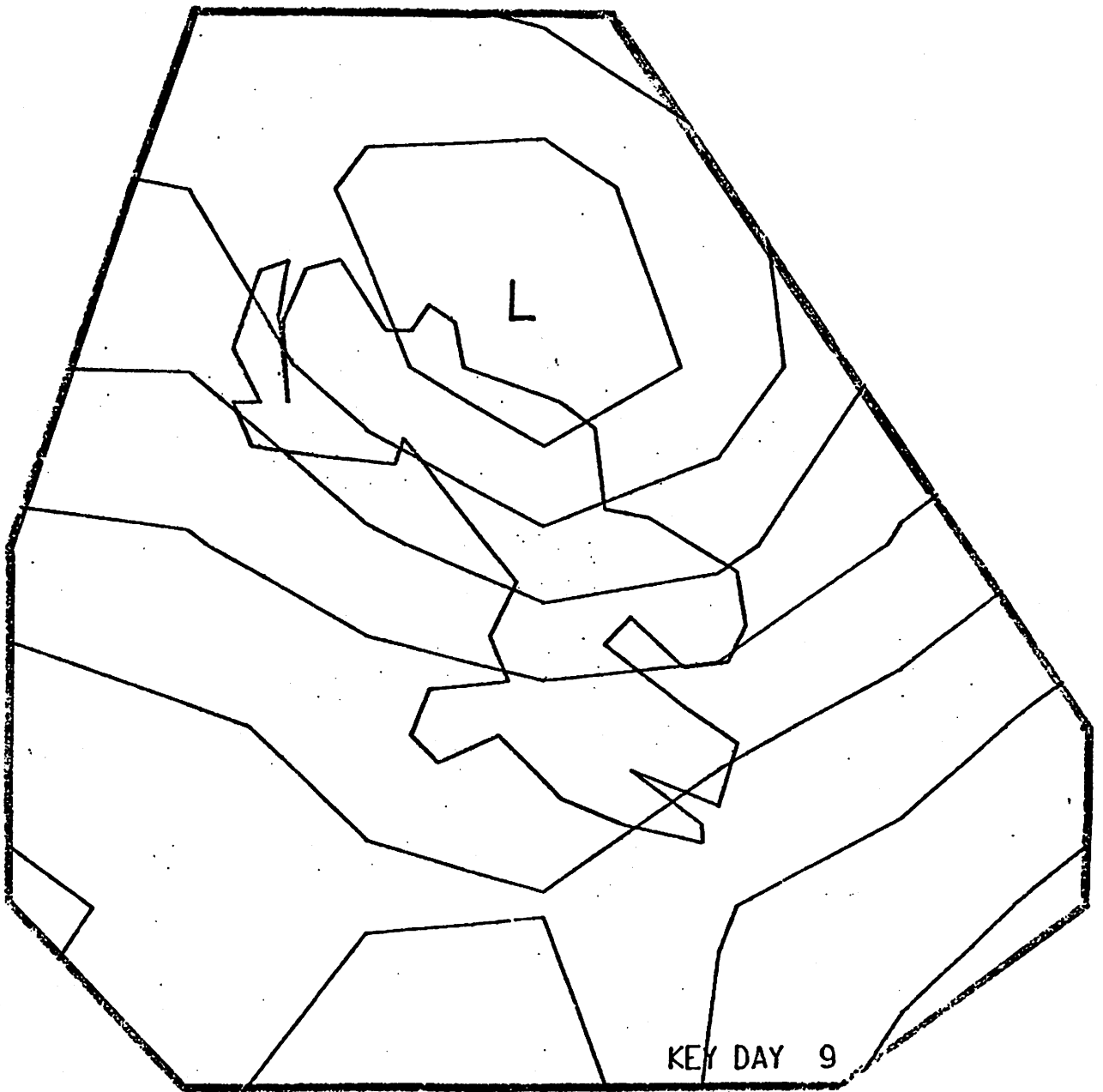


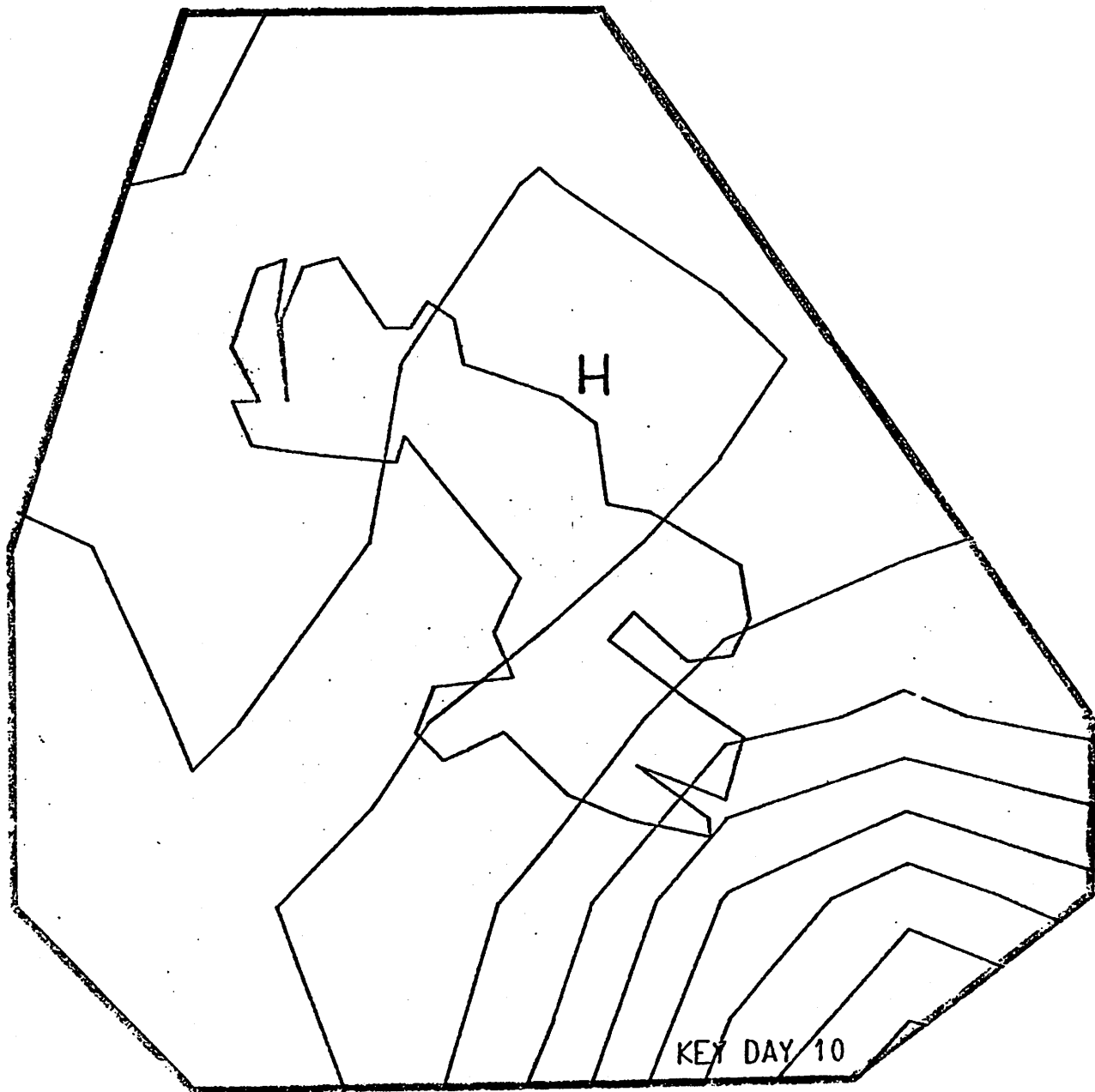


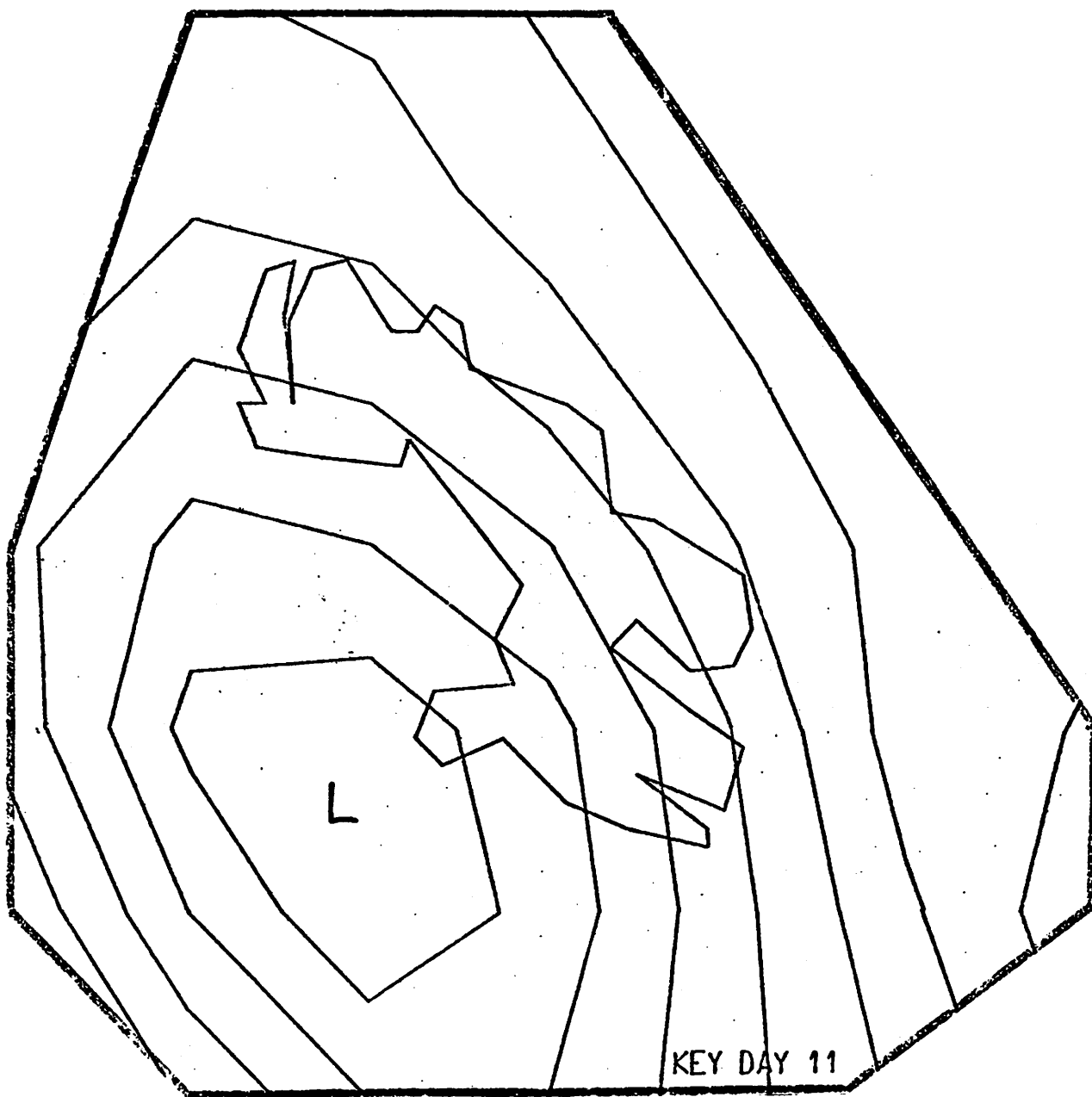


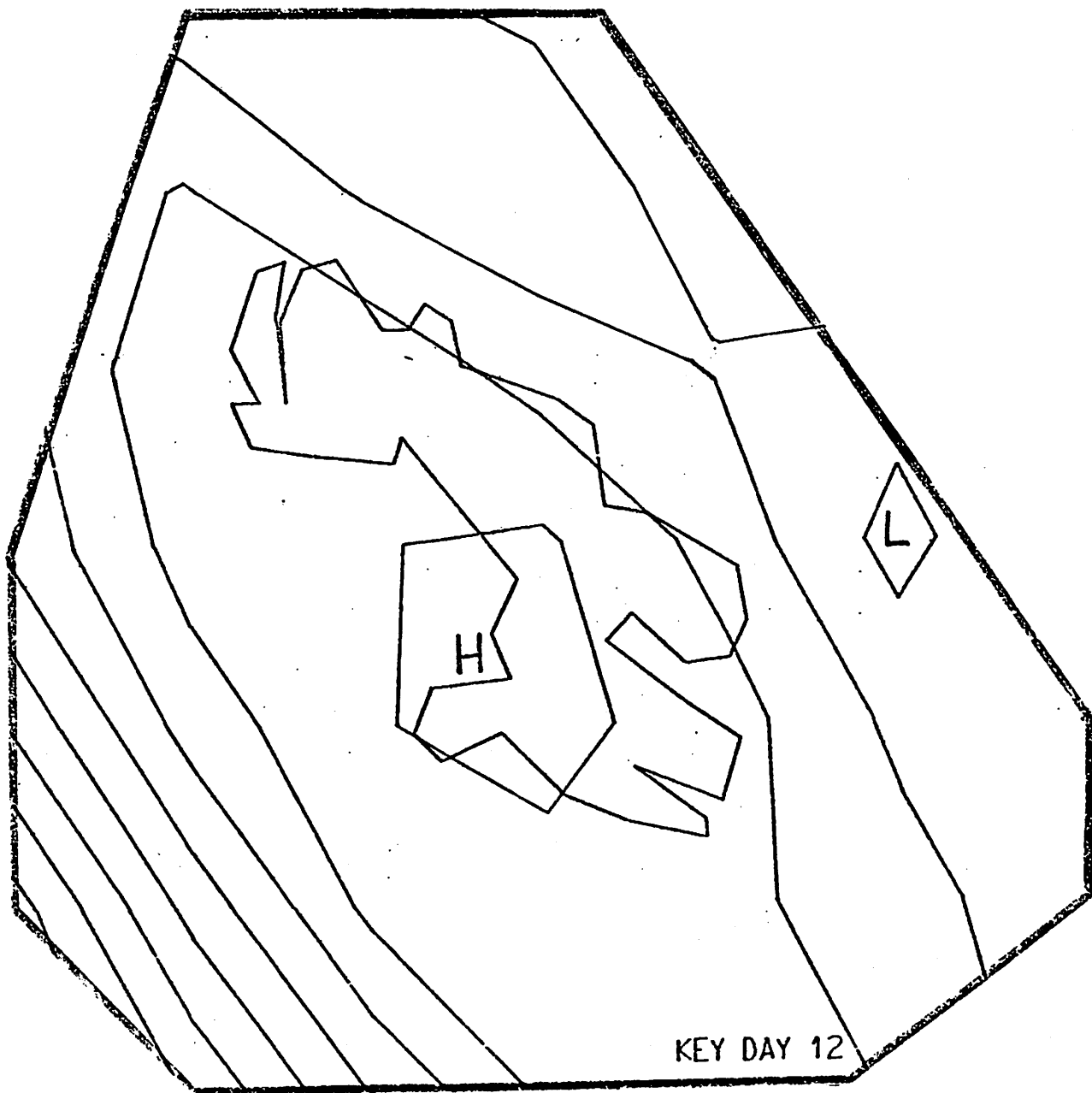


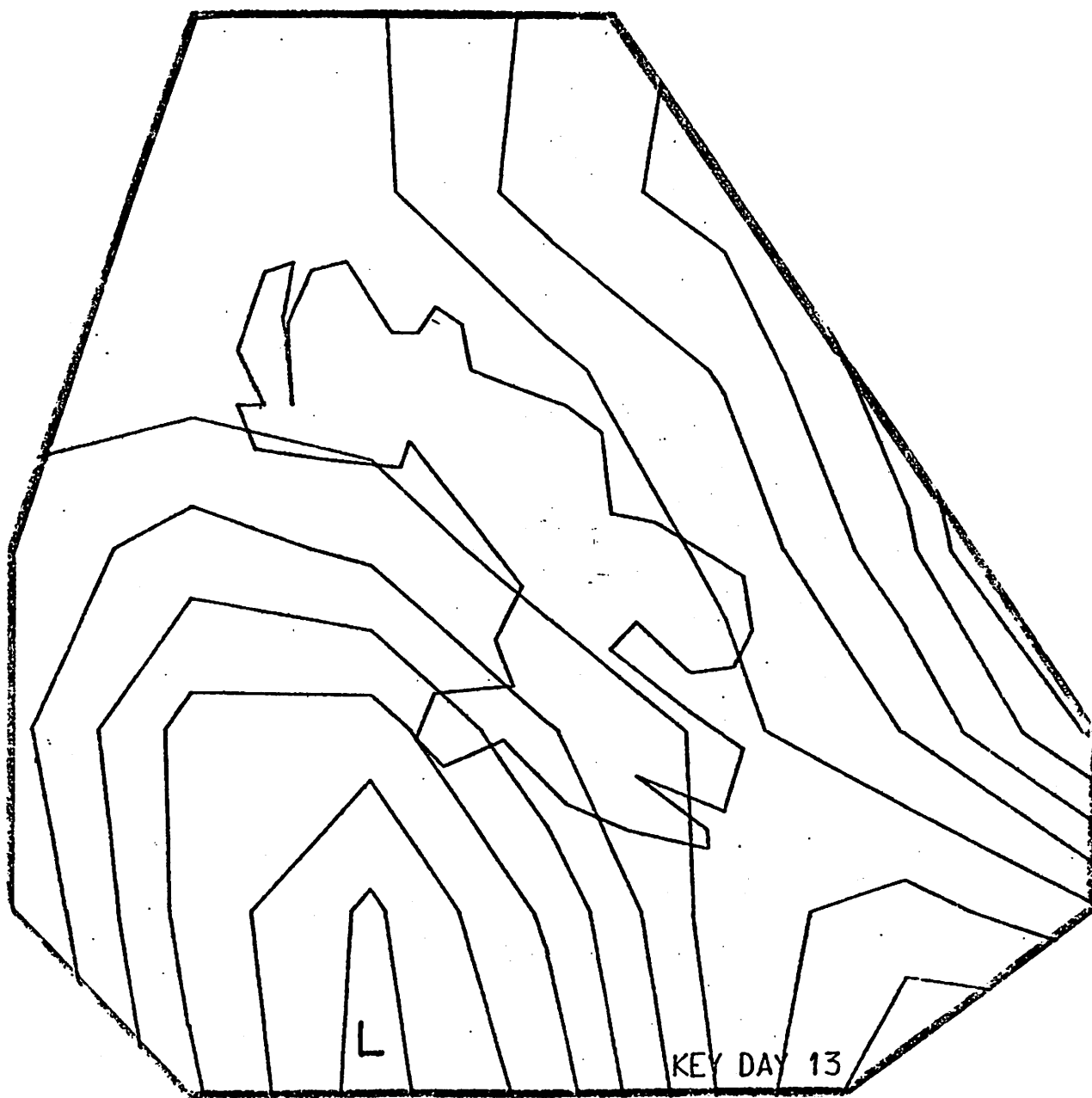




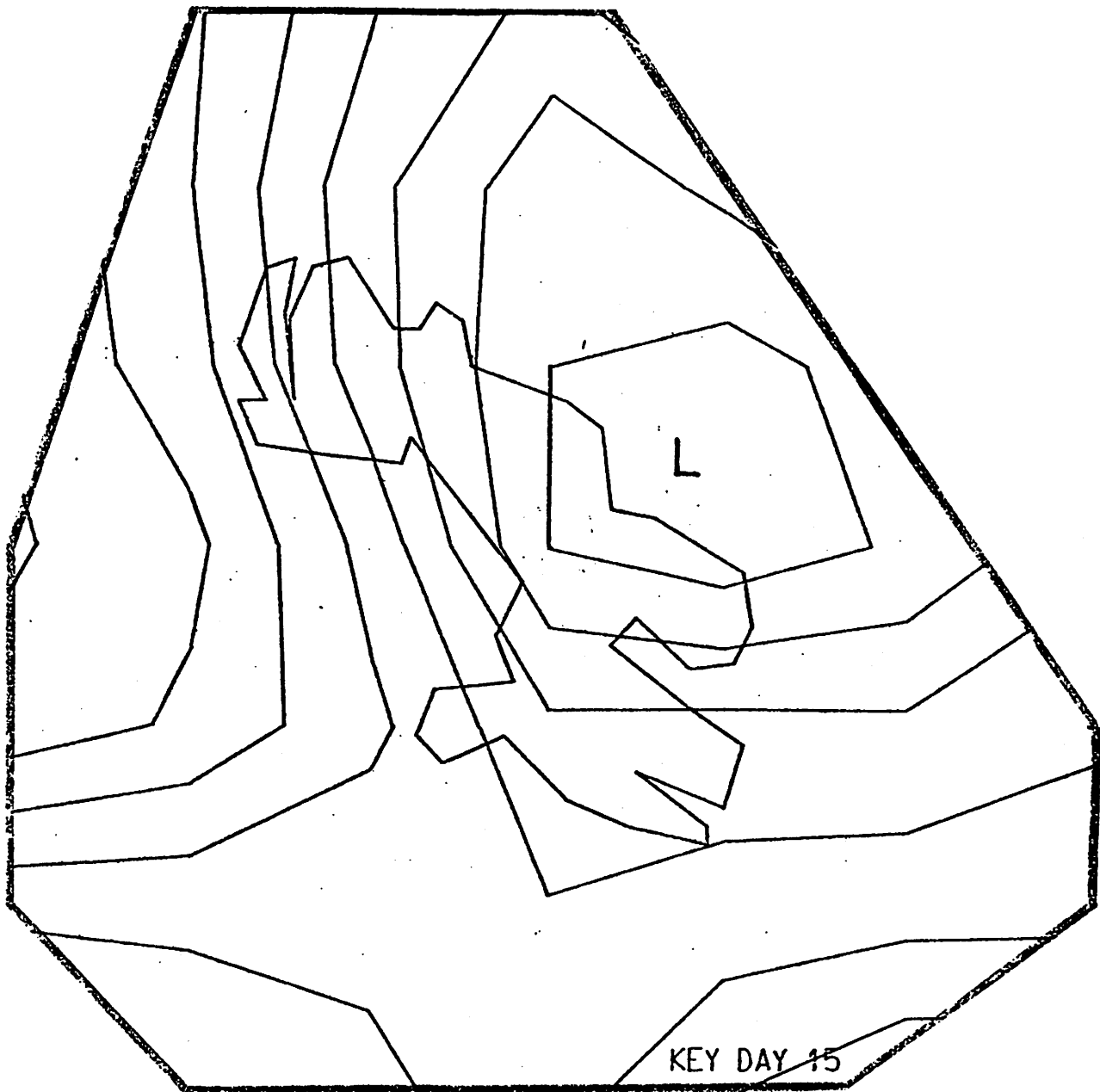


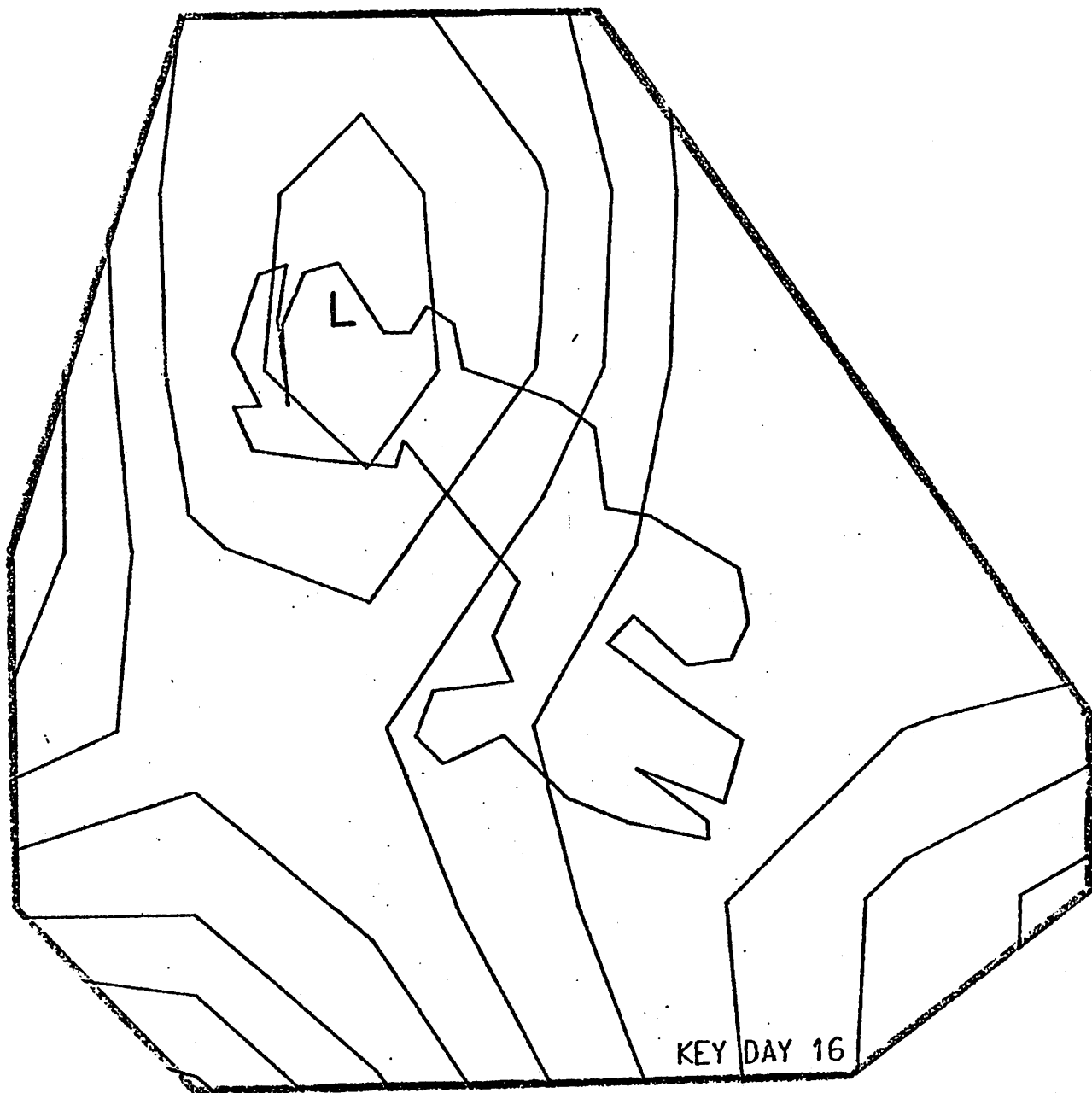


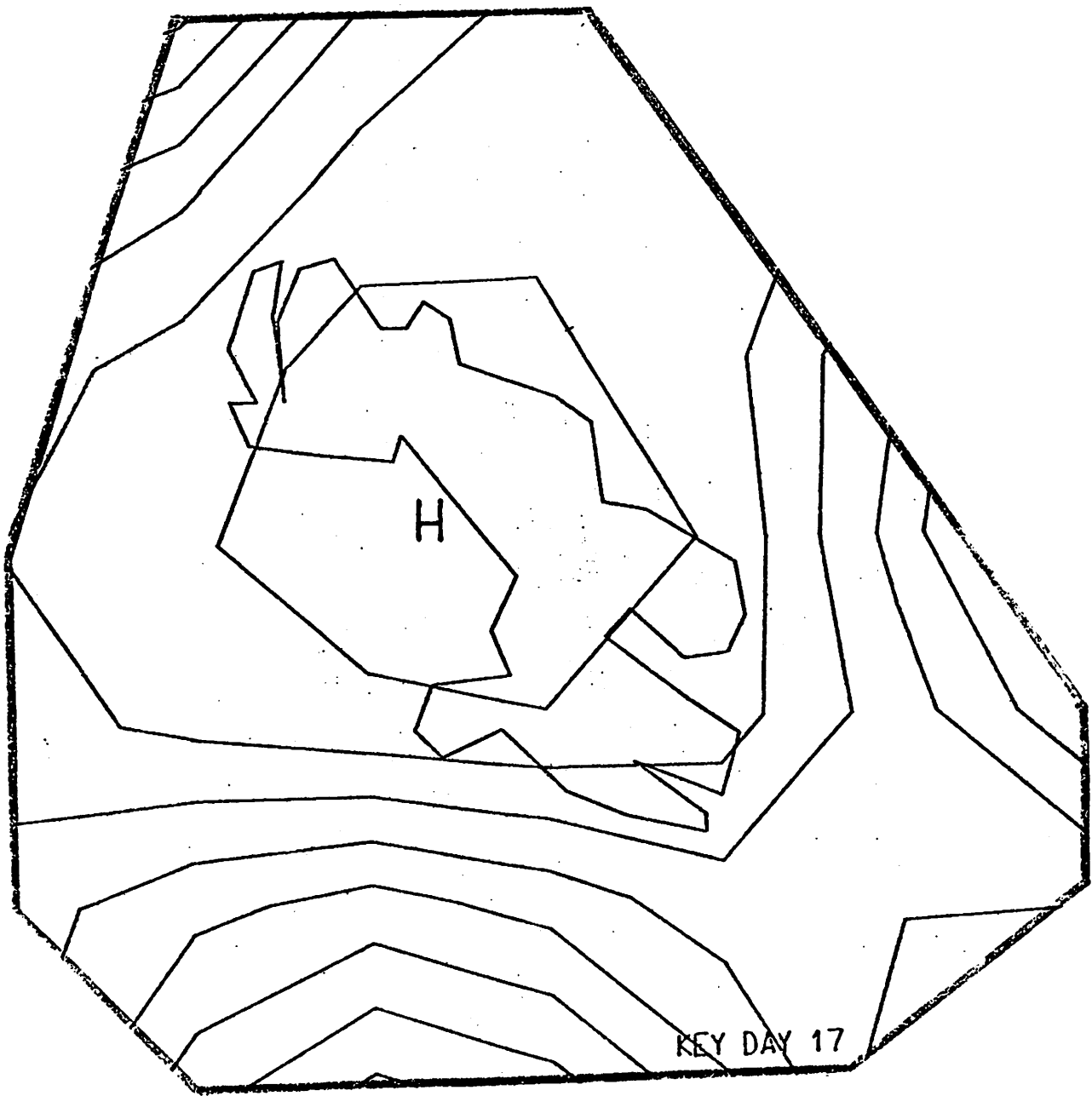


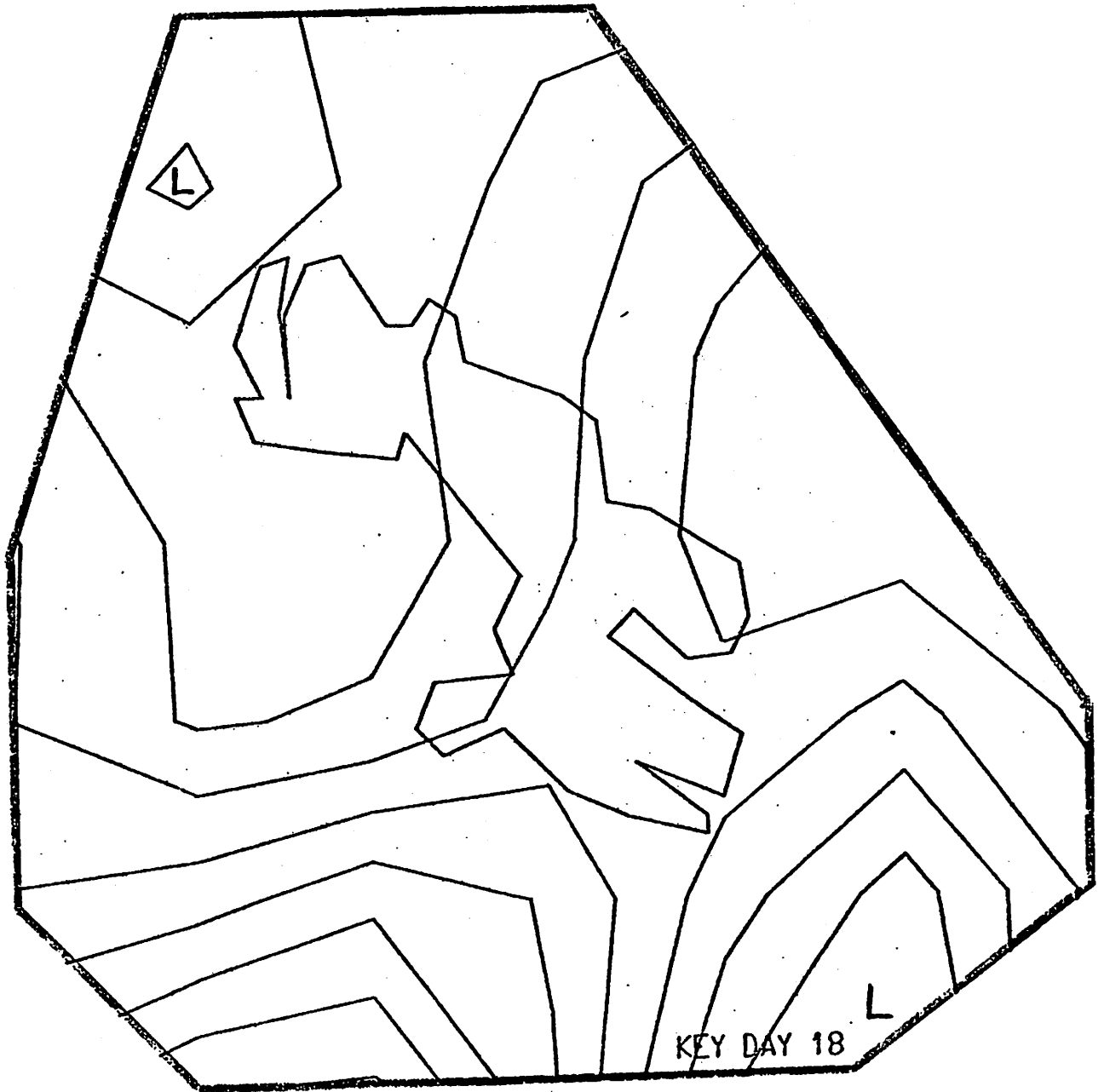


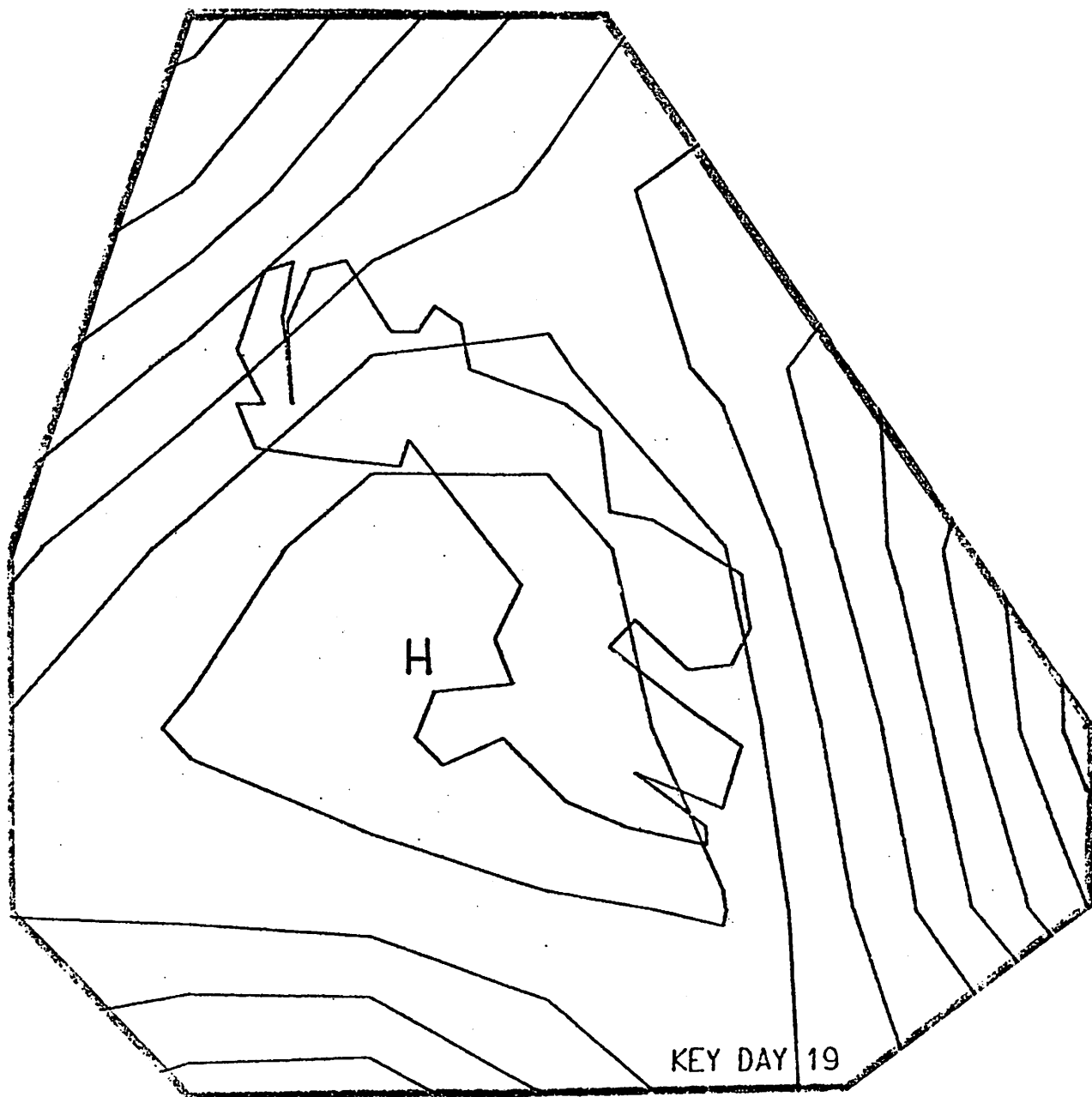


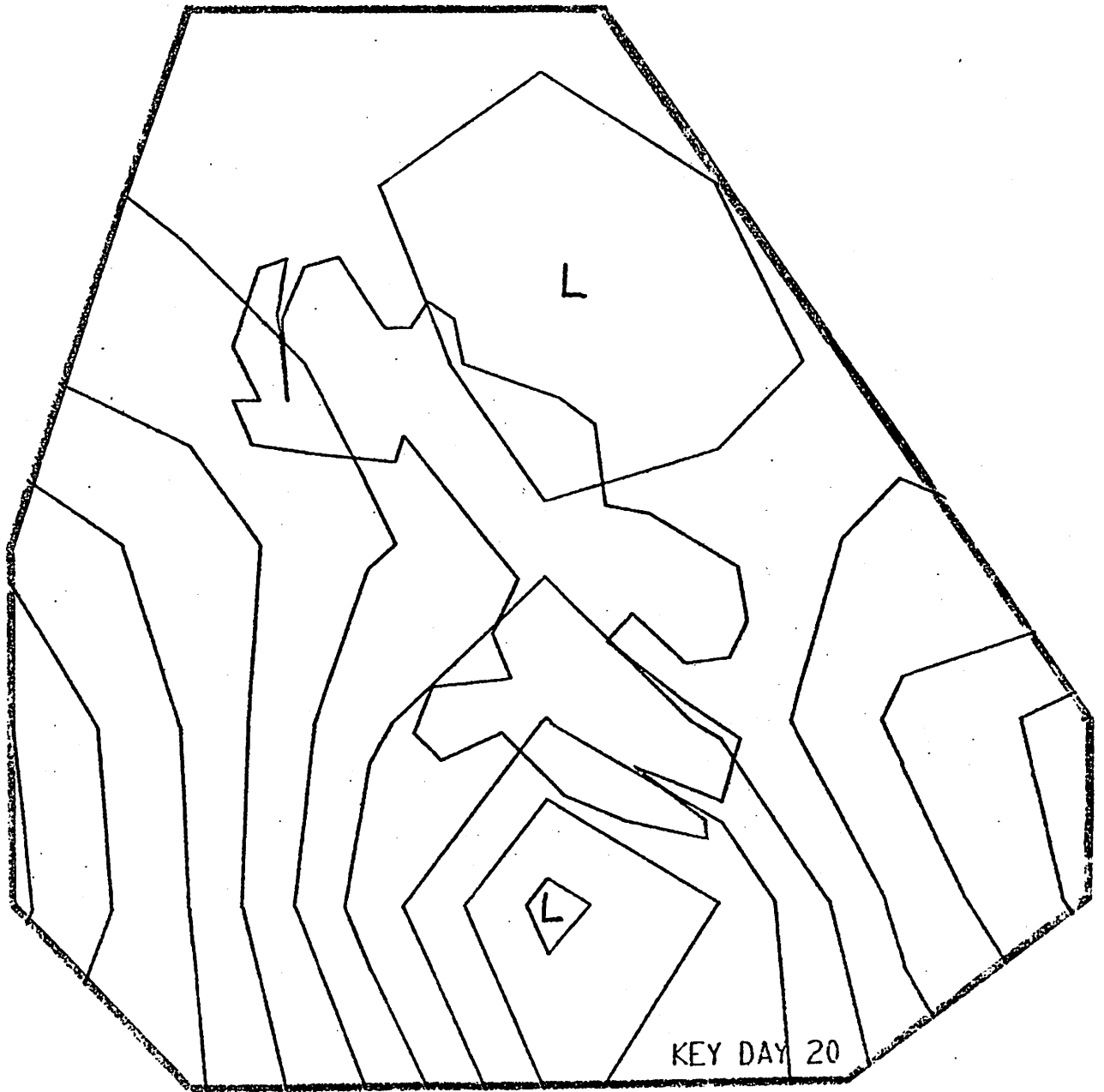


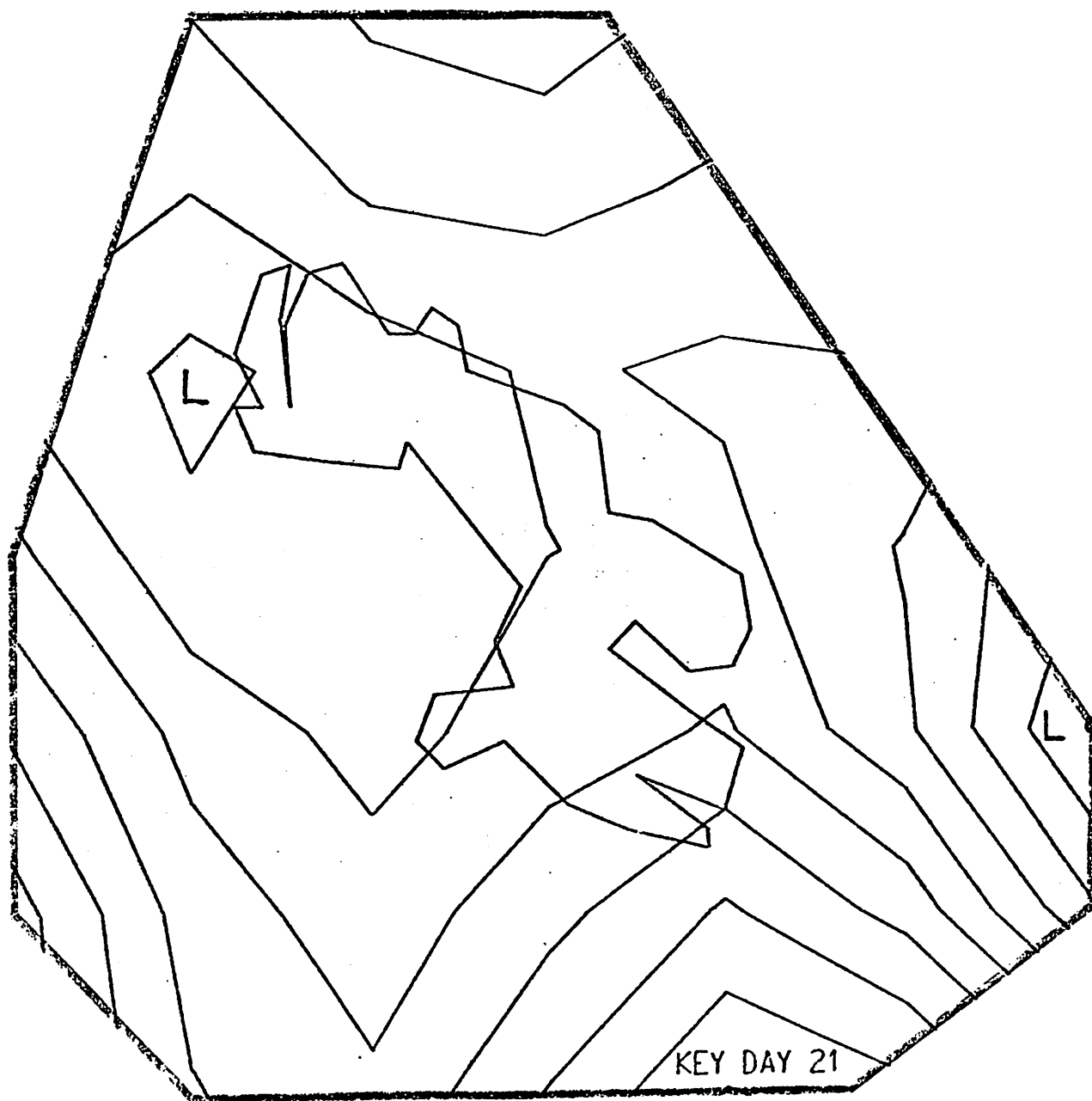


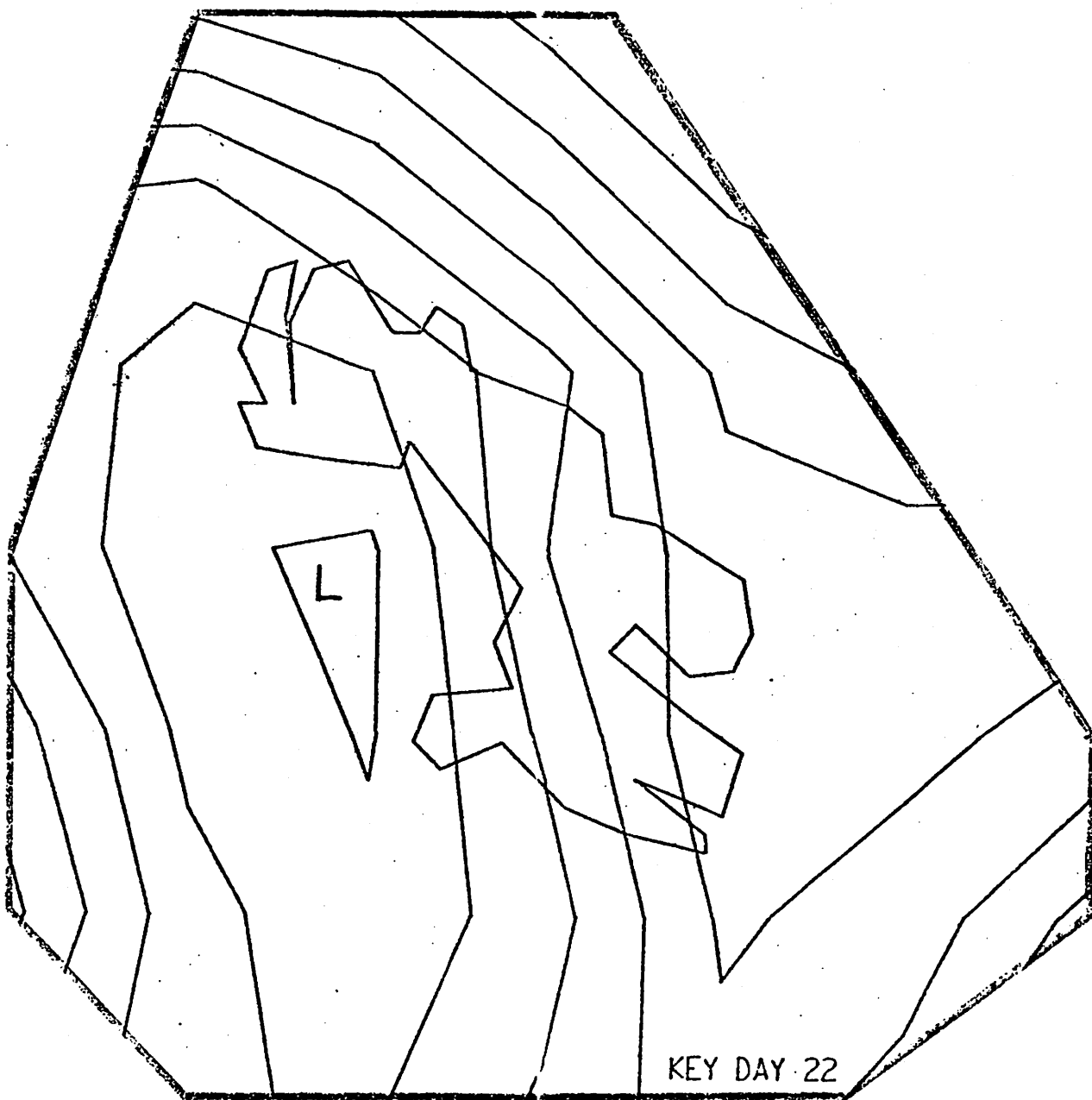


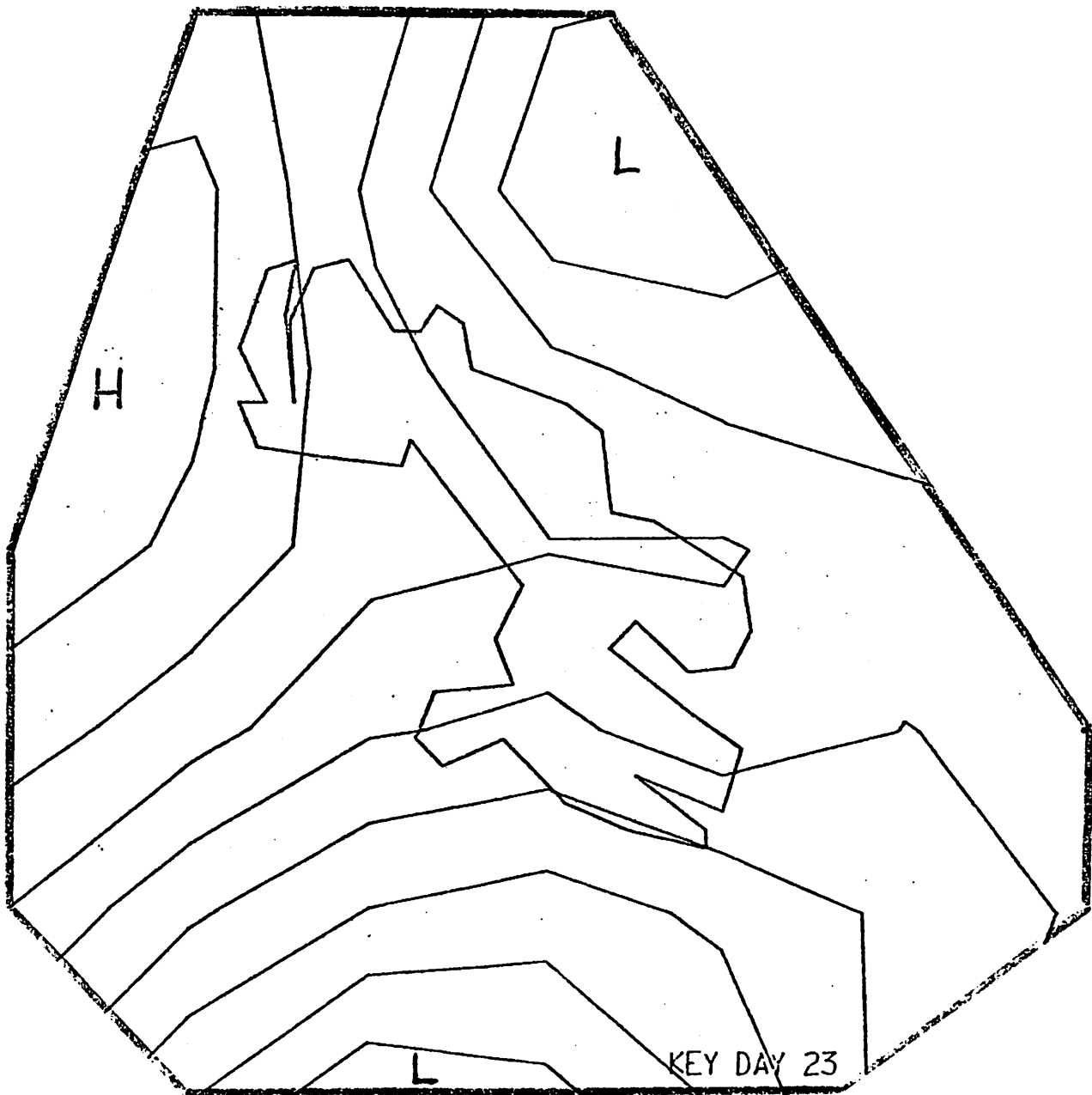


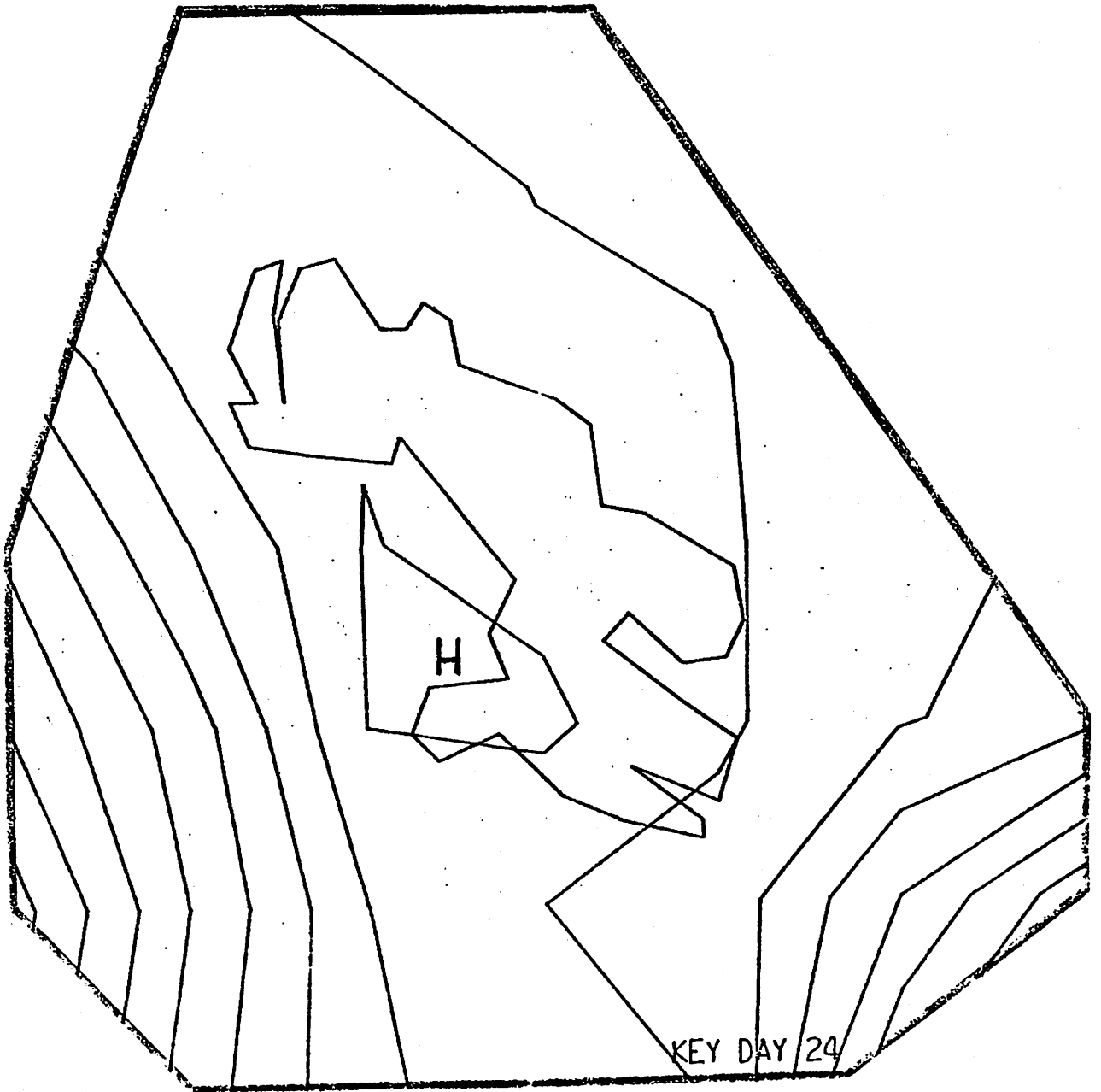


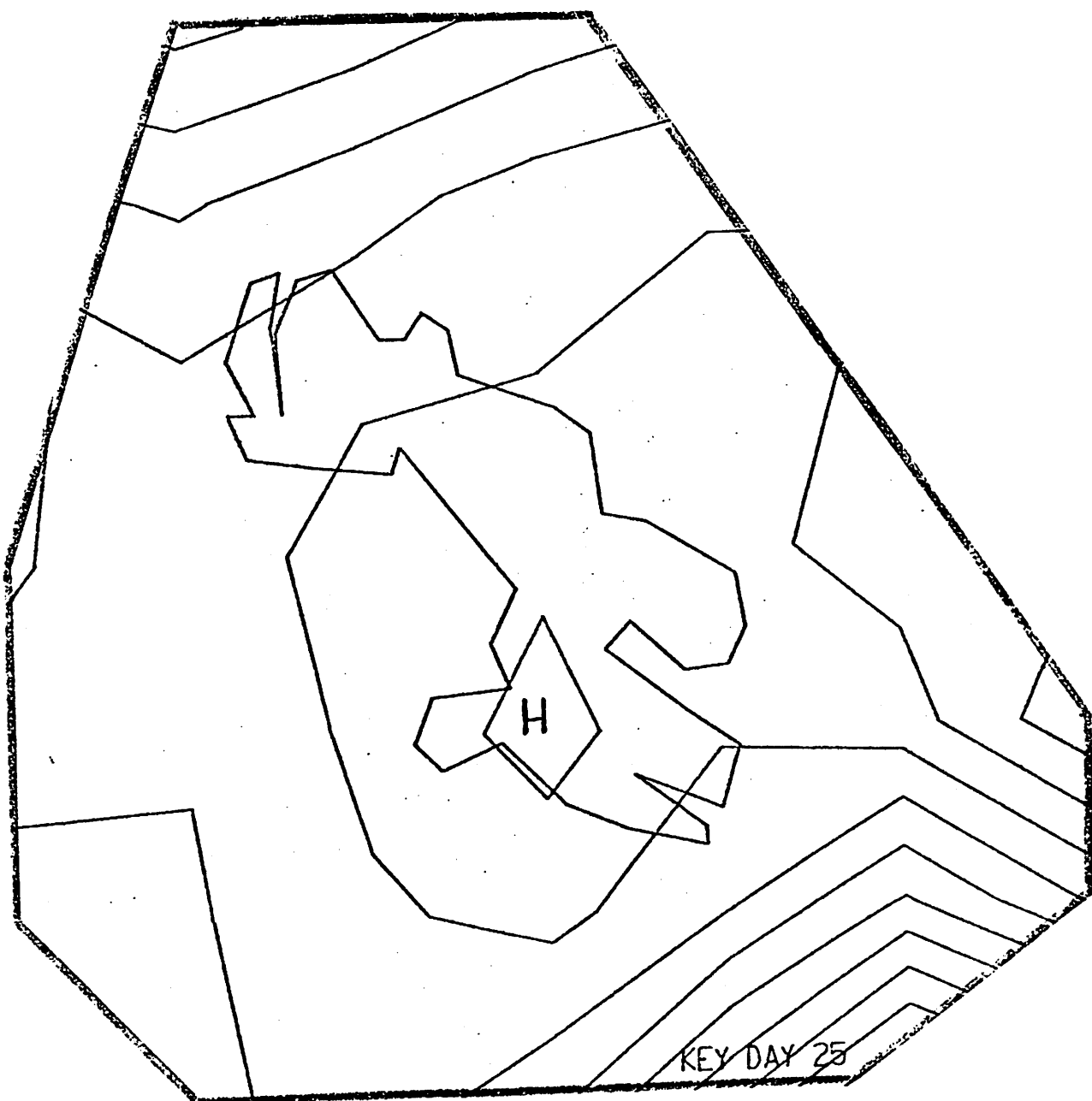


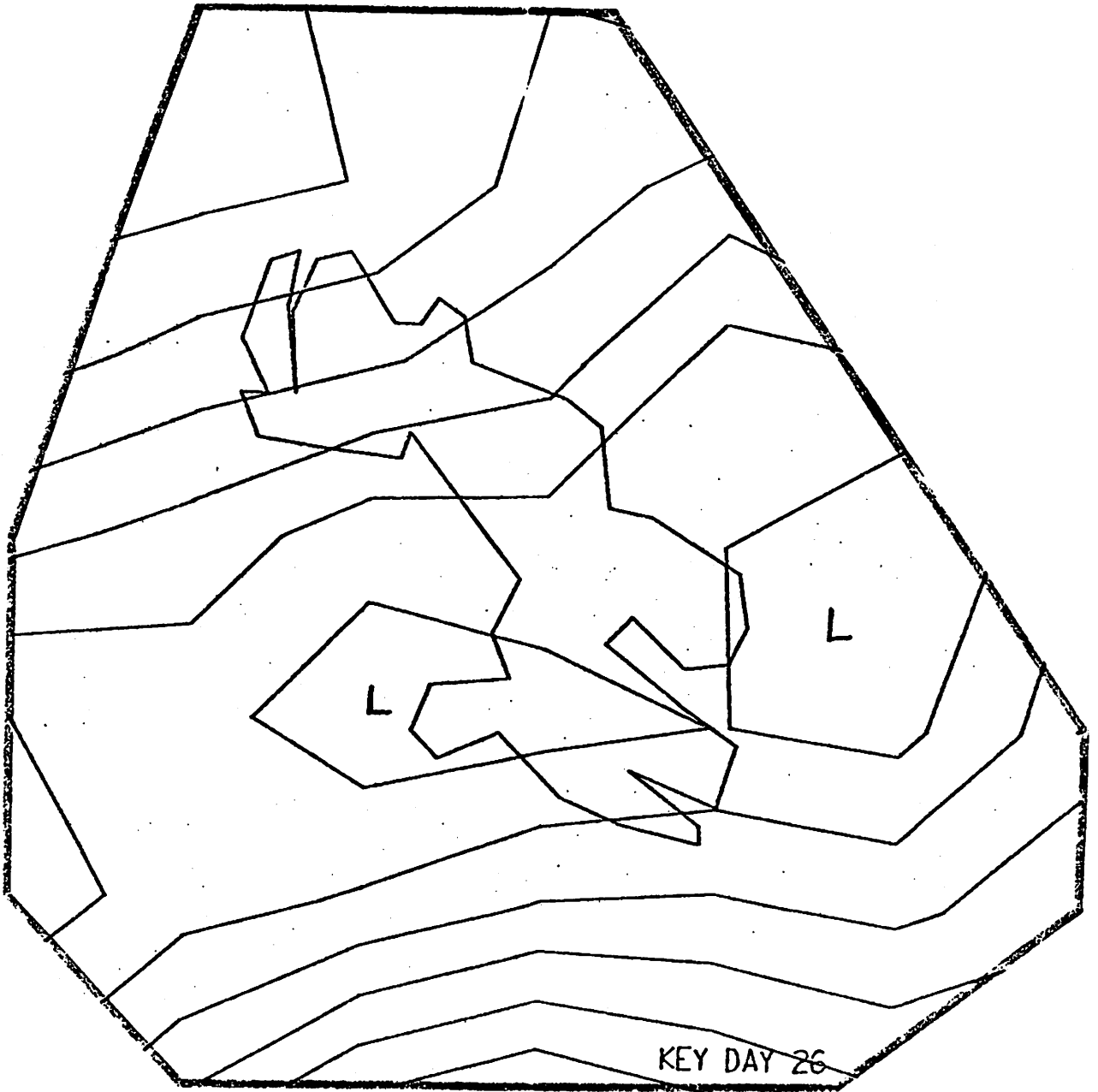


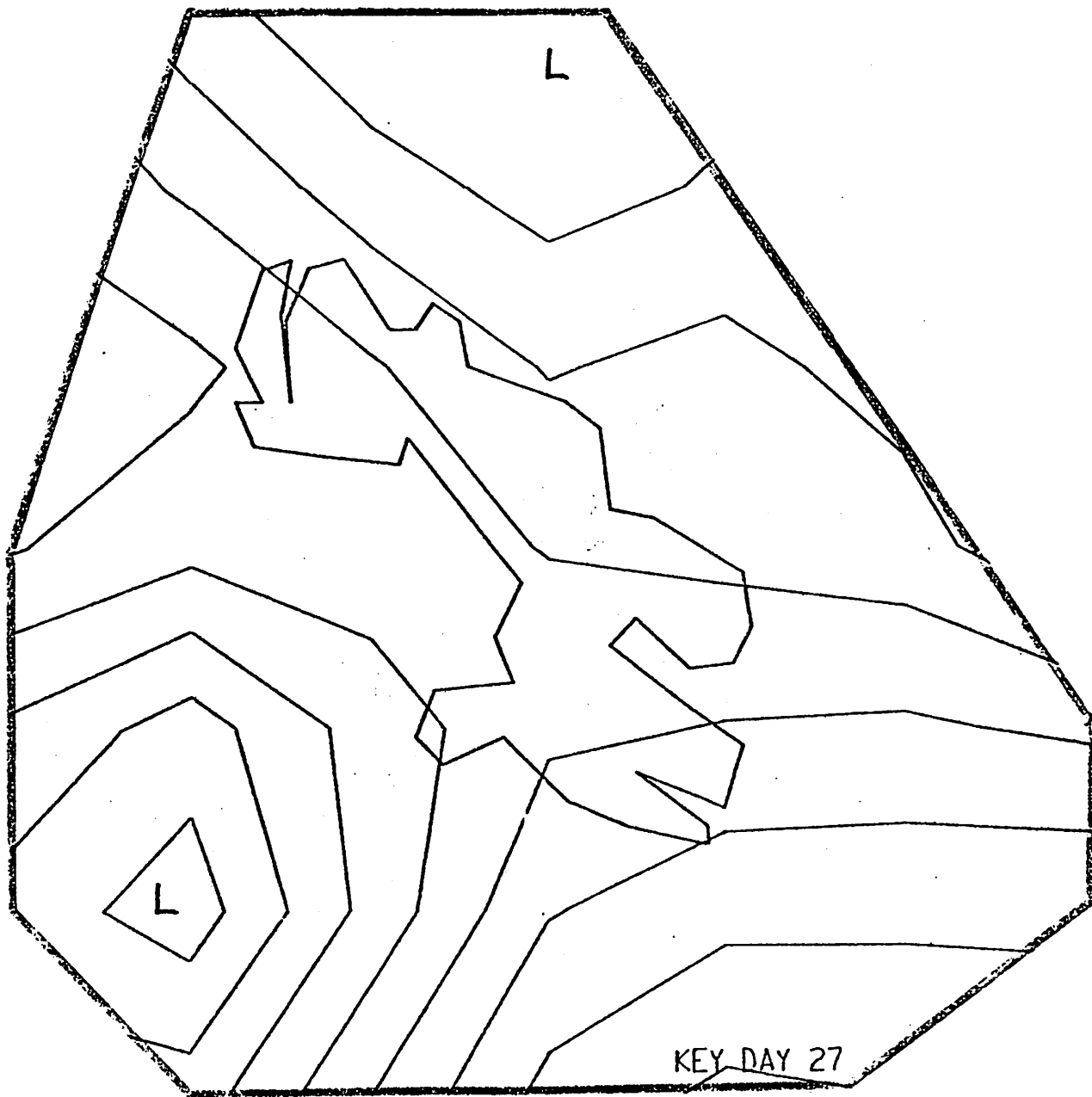


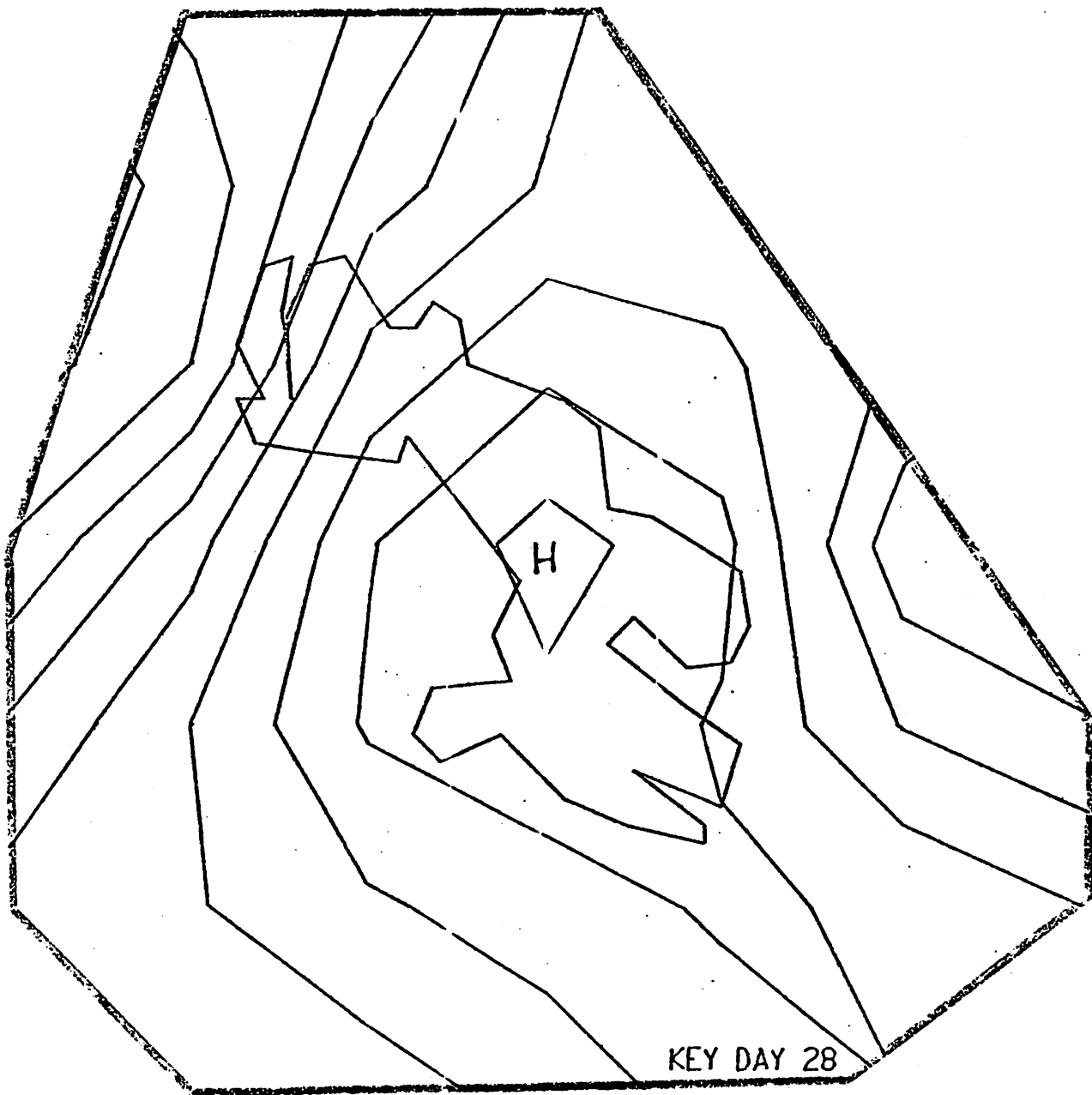


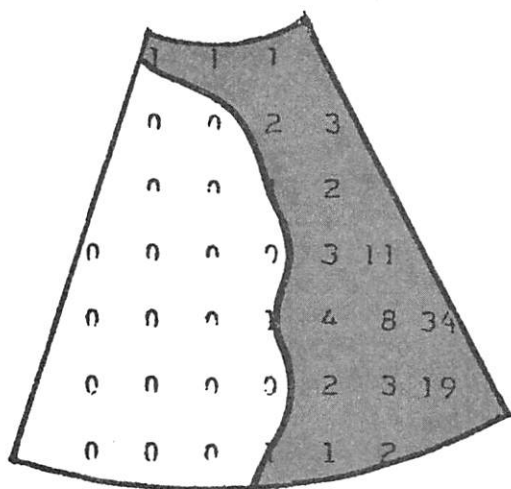




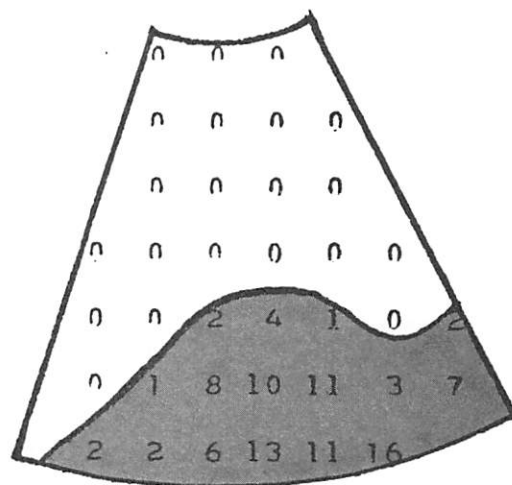




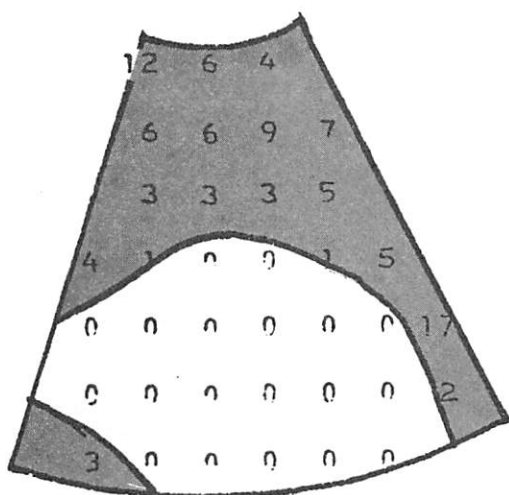




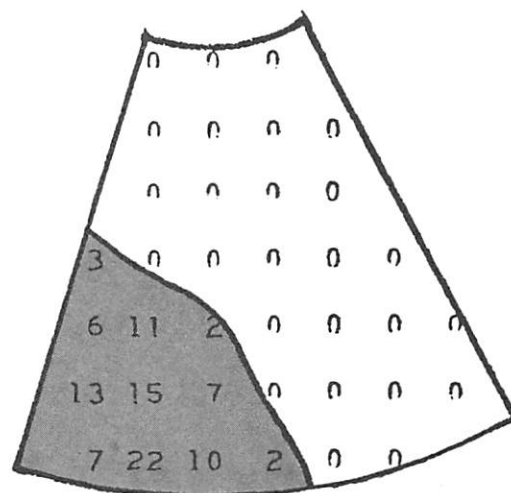
Type 1



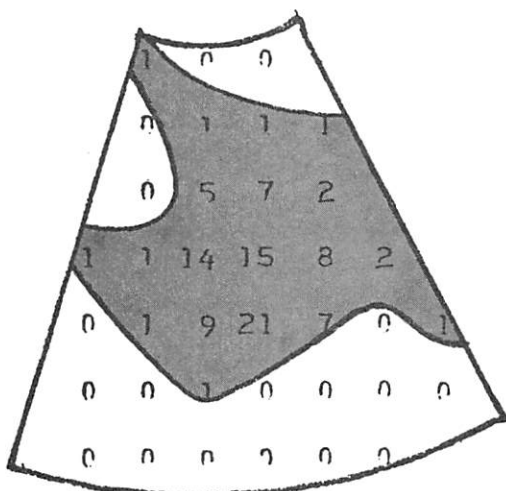
Type 2



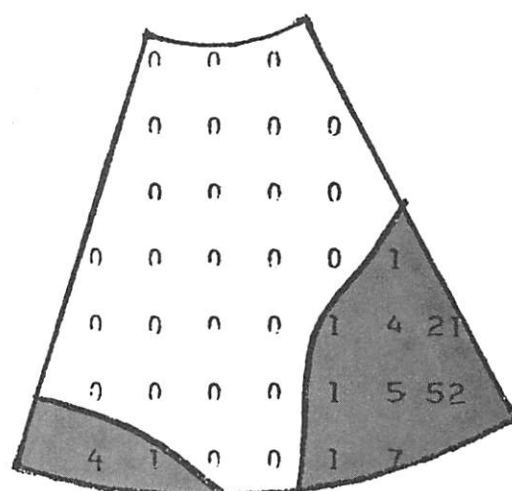
Type 3



Type 4

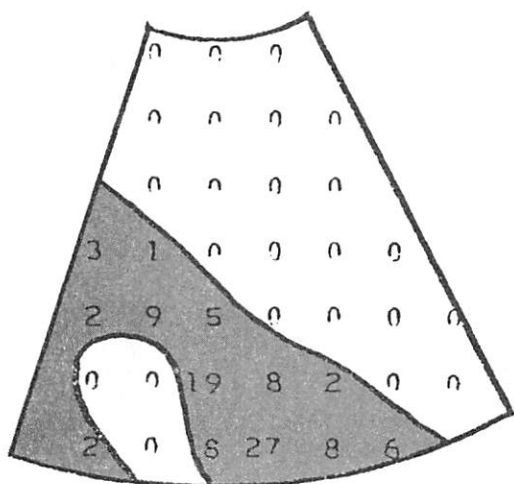


Type 5

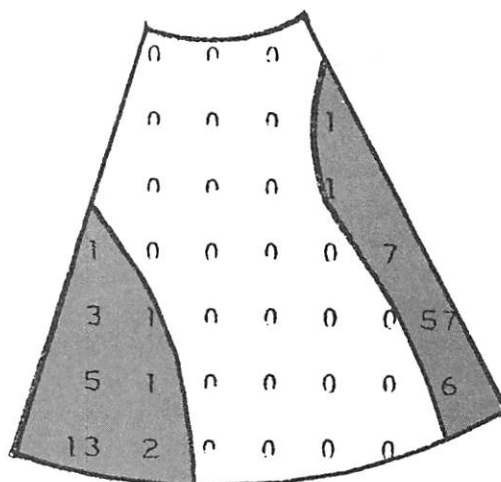


Type 6

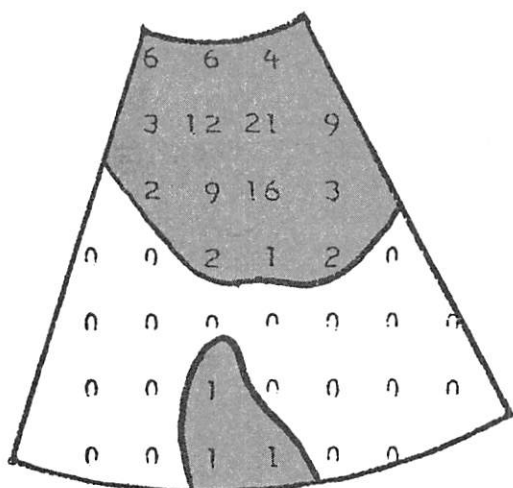
Figure 2.3 Absolute frequency of low centers (1946-74) for the first twelve symptomatic types



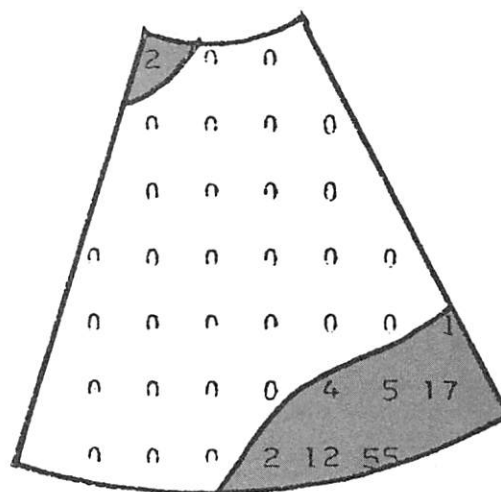
Type 7



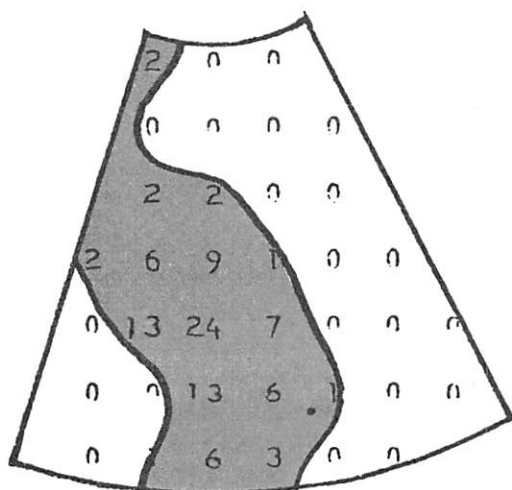
Type 8



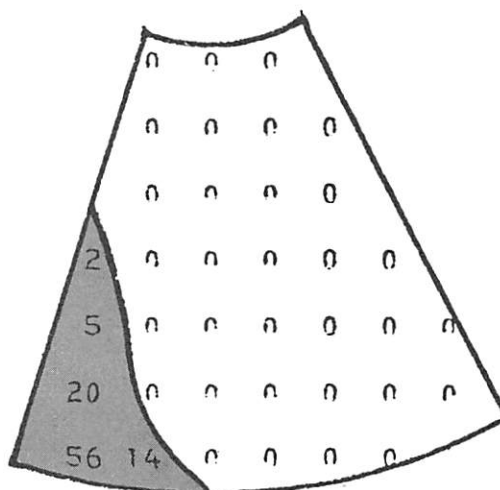
Type 9



Type 10



Type 11



Type 12

Figure 2.3 (cont.)

BAFFIN SYNOPTIC TYPES

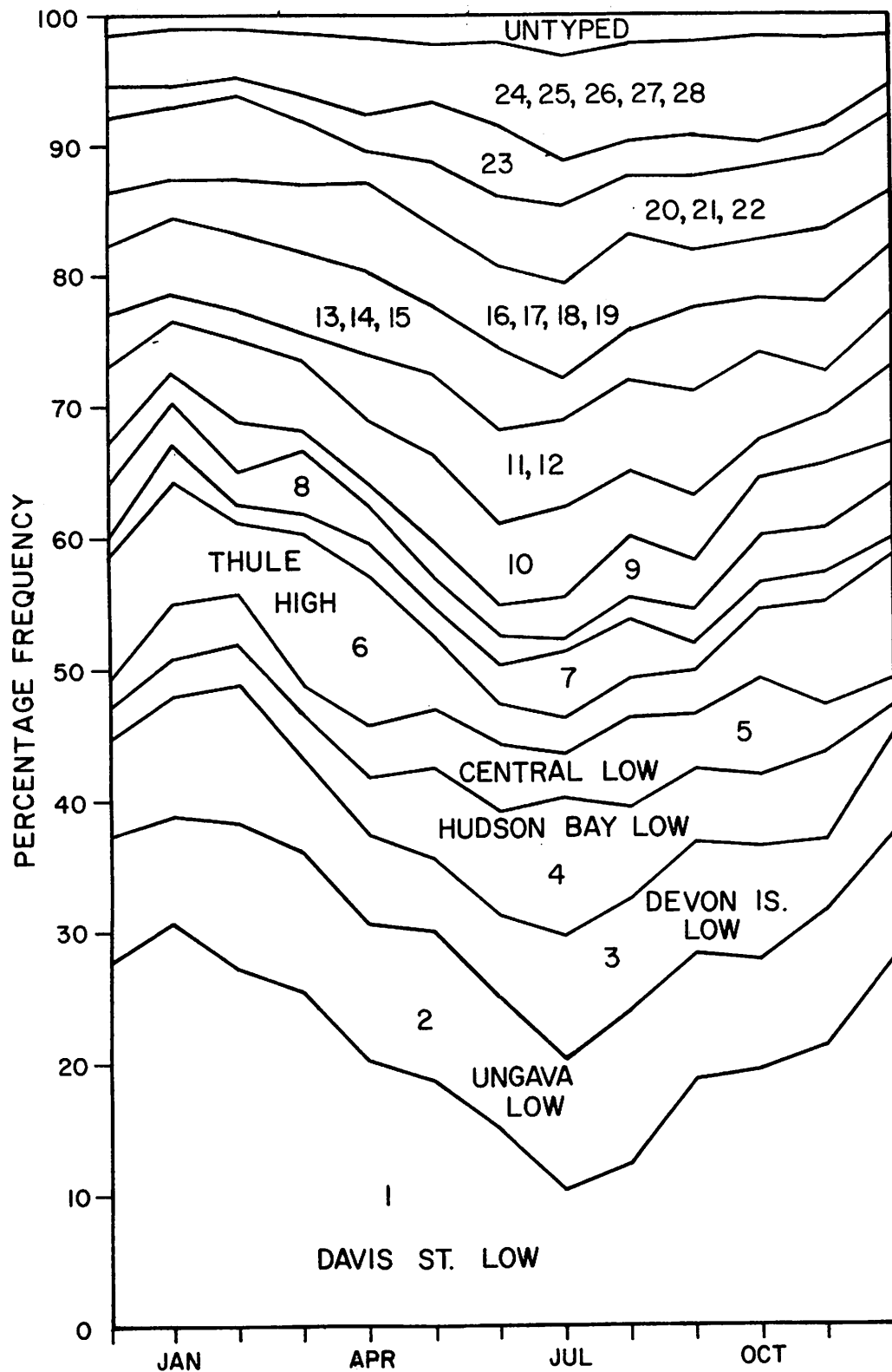


Figure 2.4. Annual frequency (percent) of the Baffin synoptic types.

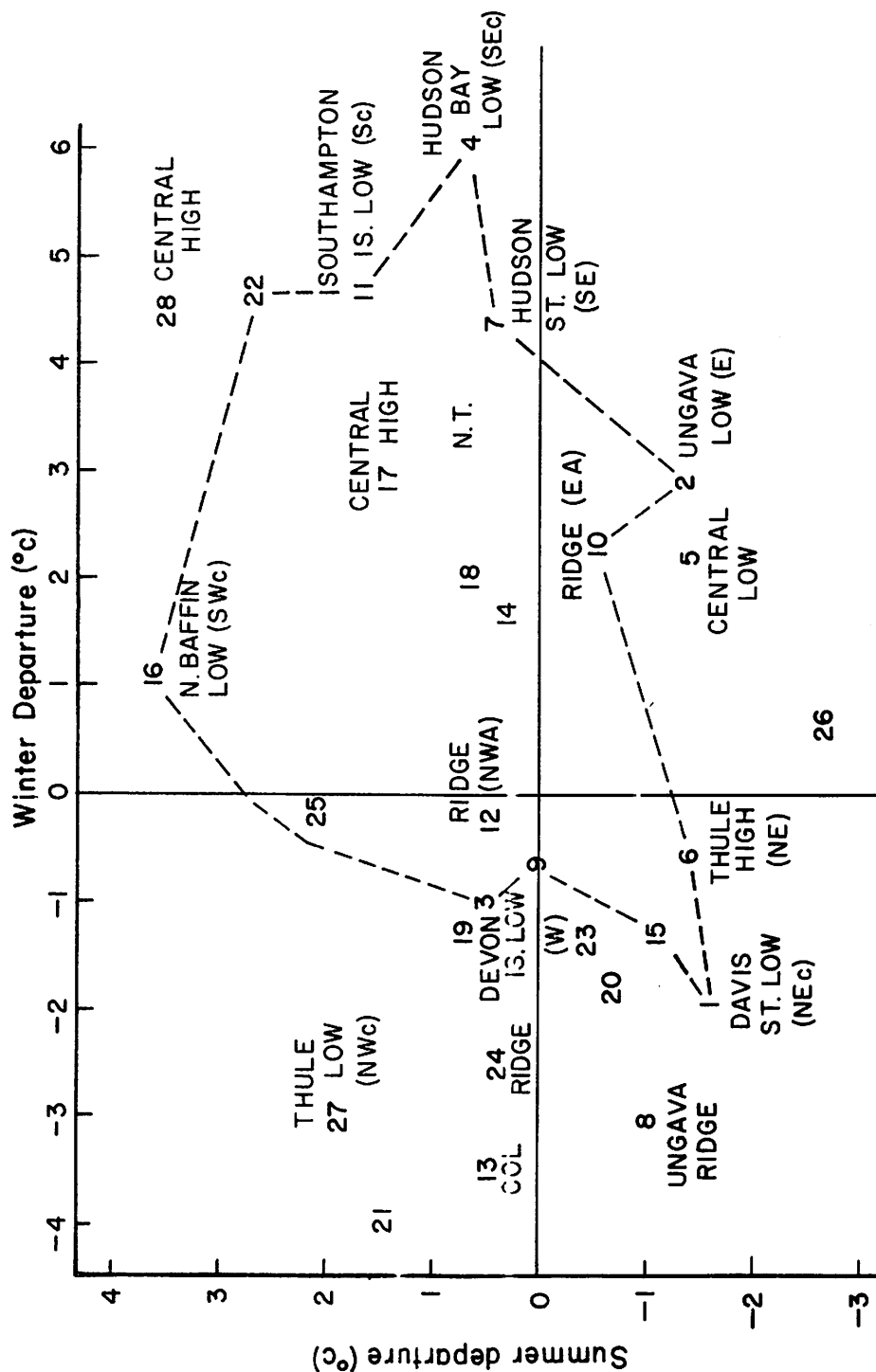


Figure 2.5 Mean summer versus winter temperature departures at Broughton Island, 1959-70, for the synoptic types.

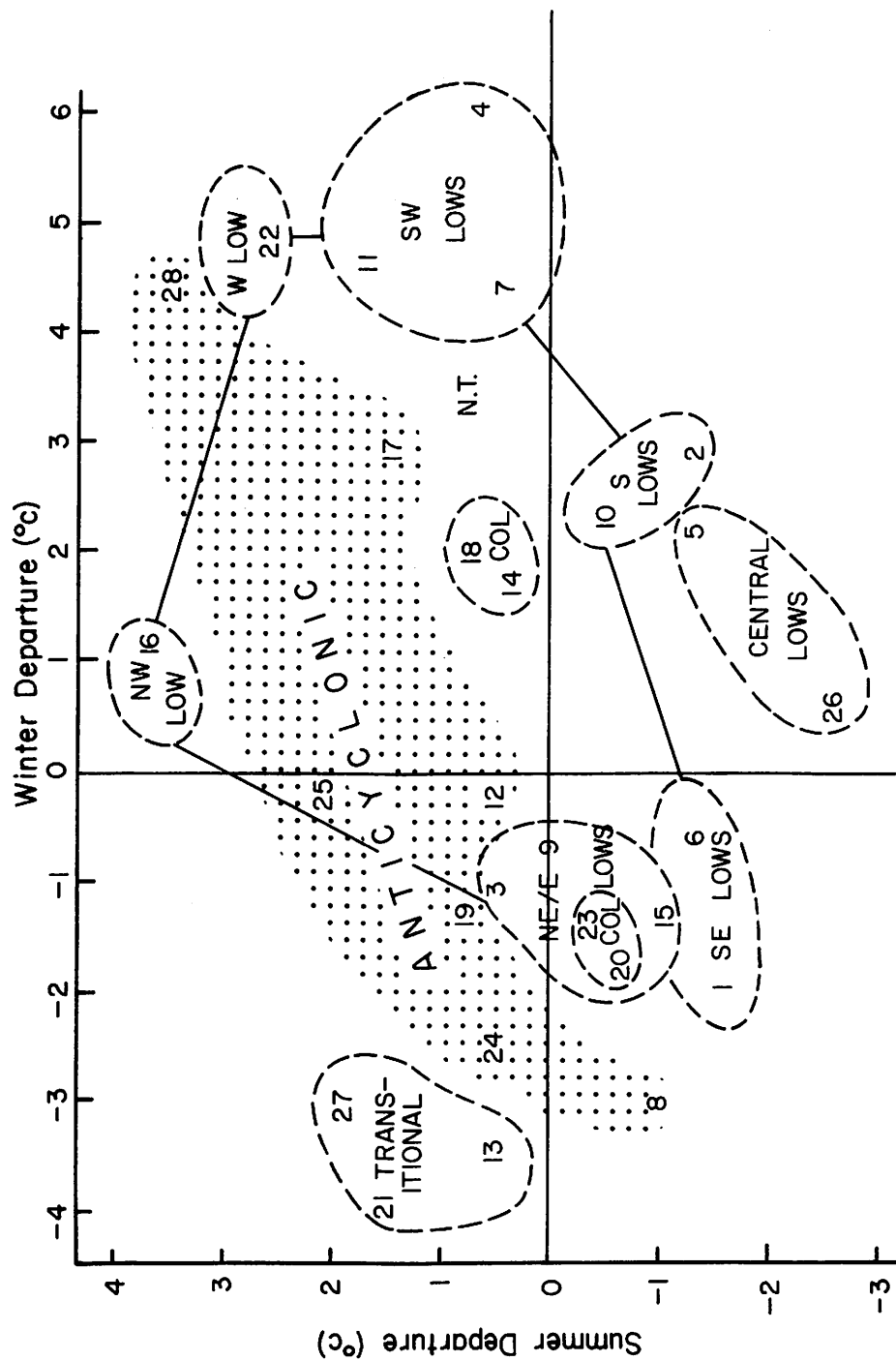


Figure 2.6. Summarization of synoptic type groups in terms of seasonal temperatures at Broughton Island, 1959-70.

REFERENCES

- Barry, R.G. 1967a. Seasonal location of the arctic front over North America, Geogr. Bull., 9, 79-95
- Barry, R.G. 1974. Further climatological studies of Baffin Island, Northwest Territories. Inland Waters Directorate, Tech. Bull. No. 65, Environment Canada, Ottawa, 54 pp.
- Barry, R.G. 1976. Study of climatic effects on fast ice extent and its seasonal decay along the Beaufort Sea coast. In: Environmental Assessment of the Alaskan Continental Shelf, Vol. 14 Ice (Alaskan OCS Principal Investigator's Annual Reports, April 1976), Environmental Research Labs., Boulder, Colo. 58-115.
- Barry, R.G., Bradley, R.S., Jacobs, J.D., Weaver, R.L. 1974. Studies of climate and ice conditions in eastern Baffin Island, 1971-73. Inst. Arct. Alp. Res., Occas. Pap. No 9, University of Colorado, Boulder, 78 pp.
- Barry, R.G., Bradley, R.S., Jacobs, J.D. 1975. Synoptic climatological studies of the Baffin Island area. In: G. Weller and S.A. Bowling (eds.), Climate of the Arctic, University of Alaska, Fairbanks: 82-90
- Barry, R.G., Bradley, R.S., Tarleton, L.F. 1977. The secular climatic history of the Rocky Mountain Area. Final Report to NSF, GA-40256, Inst. of Arctic and Alpine Research, University of Colorado, Boulder, Colo. 294 pp.
- Barry, R.G., Fogarasi, S. 1968. Climatology studies of Baffin Island, Northwest Territories; Inland Waters Branch, Tech. Bull., No. 103, Ottawa, 106 pp.
- Flohn, H. 1952. Zur Aerologie der Polargebiete, Met. Rundsch., 5, 81-87 and 121-128, (trans. the Aerology of Polar Regions, Appendix 1 to Status Report #6, Contract AF 19(604)-1141, Arctic Met. Res. Group, McGill University, Montreal, 1955).
- Fogarasi, S. 1972. Weather systems and precipitation characteristics over the Arctic Archipelago in the summer of 1968. Inland Waters Directorate, Sce. Ser. No. 16. Environment Canada, Ottawa, 116 pp.
- Kirchoffer, W. 1972. Classification of European 500 mb patterns, Swiss Meteorol. Inst., Arbeits No. 3, 16 pp.
- Müller, F., Ohmura, A., Braithwaite, R. 1976. On the climatic influence of North Water. Symposium on the geography of Polar Countries, XXII International Geogr. Congress, Extended Summaries, Hydrometeorological Publishing House, Leningrad: 55-58.
- Moritz, R.E. 1978. Synoptic climatology of the Beaufort Sea coast, Alaska, Unpub. M.A. thesis, University of Colorado, Boulder.

O'Connor, J.F. 1961. Mean circulation patterns based on 12 years of recent Northern hemispheric data. Mon. Wea. Rev., 89: 211-27.

Reed, R.J., Kunkel, B.A. 1960. The Arctic circulation in summer; J. Met., 17, 489-506.

Wilson, H.P. 1958. The West Greenland trough, Meteorol. Branch, CIR-3025, TEC-266, Dept. of Transport., Toronto, 13 pp.

3. SYNOPTIC CASE STUDIES

Ellsworth F. LeDrew
Department of Geography
University of Waterloo, Ontario

In terms of the atmospheric dynamics in the Arctic, an ice surface may be viewed as an energy sink. Energy is advected into the region with the synoptic scale air flow and transported to the surface by turbulent exchange. Here it may be utilized as melt, conducted through the ice to the ocean, or converted into radiative energy. Often the turbulent exchanges are most easily treated on a micro-scale. The energy fluxes are calculated from profiles of temperature, humidity and wind speed measured within the planetary boundary layer. On account of the precision instrumentation required, such studies usually are conducted at one location only and it is difficult to assess the spatial character of the vertical energy exchanges, or to trace the origins of the horizontal energy influx. The synoptic perspective necessary to an understanding of the linkage between surface processes and atmospheric dynamics is not available.

In this section we report on two numerical studies specifically designed to examine this synoptic scale interaction between the regional advection and surface energy exchange in the Baffin Bay-Davis Strait region. In the first study a three-dimensional limited area atmospheric model is used to analyze the energy conversion during a typical invasion of a depression system into the eastern Canadian Arctic from the Great Lakes Region. The time selected coincided with a major ice-melt event observed along the east coast of Baffin Island. The following study uses a finer resolution two dimensional model to outline the processes operating below the grid scale of the limited area model. We focus on the smaller scale advection from the warm Greenland Current to adjacent ice surfaces.

A. Diagnostic Analysis of a Synoptic Situation Causing Extreme Ice Melt

Synoptic Background for the Case Study

The synoptic record for Broughton Island during summer 1973 (Figure 3.1 partly on Jacobs, 1974) exhibits characteristic variability (Wilson, 1958). For the case study the thirteen day interval from July 13 through 25 is chosen. Records of ice thickness (R.L. Weaver) indicate a major ice melt of 25 cm within 48 hours at Broughton Island during the delayed warming interval beginning on the 19th.

Weather records from the Broughton Island station log indicate persistent low level fog with visibility restricted to less than 1 km and intermittent rain until July 22 when there was a general clearing. The ice surface quality degraded as the rain saturated the upper levels and melt holes expanded.

The period selected for detailed analysis comes immediately after an abrupt transition from weak zonal westerly flow to a convoluted meridional transport, a circulation which persisted until August 3. The trigger for this meridional flow was a low which originated over the Gulf of Alaska on July 1 and remained anchored there until July 11. It then weakened and may be traced on the maps as a small convolution in the zonal circulation which drifted eastward until it approached a major trough over Hudson Bay. On July 12 this deepened over Keewatin as a closed low, with the trough forming a closed low over the central St. Lawrence region. The large scale circulation has now developed into a deep broad trough encompassing the two systems. It is this dual depression formation which enters the Arctic along the east limb of the trough bringing the initial pressure drop to the Baffin Island area.

On July 12 the surface pressure pattern in the eastern Canadian Arctic is similar to the Thule low configuration which is a typical winter pattern (Keegan, 1958). There is an elongated trough over eastern Canada with a shallow surface low west of Thule. This is associated with a slow moving primary cyclone to the southeast of Greenland with closed isotherms in mid-troposphere. This leads a wave train over Canada with the above mentioned secondary low over the St. Lawrence region bringing southerly air into the Davis Strait sector.

The subsequent movement of the southerly depression is illustrated in Figure 3.2 for the 85 cb level (the level chosen for analysis). The low moves northward with a maximum depth on July 15. It becomes anchored over south Baffin Island until July 19 when it drifts east, with the height of the center stabilized, and leaves the grid area to the south of Greenland. During the first days of this interval the NMC charts indicate a deep depression system (120 decameters -dm- on July 12) in the central Polar Basin.

As this circulation weakens it enters the area of study from the northwest and drifts southward along the west coast of Greenland. This is a major cyclonic track during July (Namias, 1958) prompted by the thermal contrast along the margin of the Arctic Basin and resultant baroclinicity. Even though the analysis period includes the entire history of an intrusion of a southerly system through the grid area, it also includes the influence of a northern synoptic system which will be shown to have an appreciable effect of the Baffin Island thermal regime.

The Diagnostic Limited Area Model

The model used to analyze the energy exchanges throughout this synoptic episode is a form of the omega equation. A measure of development or decay is the vertical velocity (negative omega) which may be calculated from considerations of differential vorticity advection, thickness (or thermal) advection, diabatic heating, and orographic and frictional influences. The first three parameters are calculated at discrete points throughout the vertical extent of the atmosphere. In the omega equation these three terms are additive and can therefore be examined for their individual contribution to the total dynamics of the system at any model level. We can compare the contribution to the synoptic history by horizontal thermal advection and the vertical turbulence enthalpy flux from or to the surface by examination of the vertical velocity or omega value associated with each process, thereby quantifying an important linkage between the surface energy balance and the atmospheric dynamics. The surface effects of friction and orography are included as lower boundary conditions in the model.

The formulation of the equation, the numerical techniques used, and a discussion of the accuracy of the model is detailed in LeDrew (1976). The input data are from the National Meteorological centre analysis on an equidistant 350km grid network. We have selected an eight-by-eight grid sector centered on Baffin Island (Figure 3.3) for our analysis. There are six levels in the vertical (100, 85, 70, 50, 30 and 10 centibars).

Synoptic Analysis

This section is a detailed examination of the model generated data for the period July 13-25, 1973. The primary purpose of the analysis is to identify the relative importance of advected and local energy sources and sinks in the behavior of a synoptic system within the grid area.

On account of the enormous amount of data computed from the model some restrictions are necessary in the discussion. The maps presented (Figures 3.4 through 3.11) are only for the 85 cb level and therefore the interpretations are limited to lower tropospheric activity. This is a compromise so that both surface influences and features of the broad scale circulation may be included. Where appropriate, important factors from other levels are discussed verbally. To simplify the presentation further, data at 48 hr intervals only are presented in map form. For each day discussed the following data are contoured: 85 cb heights, 85 cb total vertical velocity (w_T), 85 cb vertical velocity due to vorticity advection (w_V) thickness advection (w_{TH}) and surface thermal effects (w_H), 85 cb thermal advection, total precipitation and total vapour flux divergence. The 85 cb temperature fields are in Figure 3.12.

A restriction on interpretation should be clarified. Unlike the vorticity tendency equation the omega equation is not a development model; it describes steady state fields. Explanations for development and advective processes must be conservative since they are based on a subjective examination of a sequence of maps, not on a prognosis from one map to the next. Temporal trends are not clear from one map in isolation.

On July 13 the southern depression system is in two centers, one over the Gulf of St. Lawrence (134 decameters at 85 cb) and a more vigorous vortex over southern Keewatin (131 dm). The curvature of the 50 cb flow suggests steering towards the northeast. A weak localized high over Baffin Island separates this system from a deep low (122 dm) over the Polar Basin. The steep gradient of the Polar depression extends to the northern sector of Baffin Island.

The strongest uplift (Figure 3.4) is in the southeast quadrant of the grid, in advance of the St. Lawrence low. At 50 cb the vorticity advection along the east side of the deep trough containing the two southerly depression centers is approximately $2 \times 10^{-9} \text{ s}^{-2}$ and ascent due to differential vorticity advection (w_v) is strong (1.8 cm s^{-1}). Positive thickness advection resulting from the import of relatively warm air (advective heating of $1 \times 10^{-4} \text{ kJ kg}^{-1} \text{ s}^{-1}$ in this sector) contributes additional uplift (w_{TH} approaches 1 cm s^{-1}). There is a total vapour flux convergence of $0.2 \text{ mm cm}^{-2} \text{ hr}^{-1}$ (negative divergence) and this uplift promotes intense precipitation and additional ascent of 0.2 to 0.5 cm s^{-1} due to latent heat release. These factors are augmented by strong cyclonic frictional convergence (1 cm s^{-1} at the surface) and topographic uplift from onshore flow over northern Labrador (2 cm s^{-1} at the surface). This latter factor acts to anchor the 85 cb total vertical velocity maximum (w_T is 4 cm s^{-1}) at this shore region. At this stage, the system exhibits the classical signs of a developing mid-latitude wave cyclone, as described by Krishnamurti (1968). Ahead of the vortex, in the direction of the 50 cb flow, vorticity and thickness advection as well as latent heat release act in conjunction to remove mass and promote a pressure fall with attendant development of the depression.

Over the entire grid area the surface enthalpy flux is negative. The resulting cooling is a maximum in zones of maximum warm air advection - in advance of the system - since there is a maximum air-surface temperature contrast. Since it is the spatial pattern of the surface flux that determines the vertical motion related to it (w_v) there is subsidence to the south (w_H is -0.1 cm s^{-1}) acting in mild opposition to the thickness advection, while to the north there is ascent where the cooling is a relative minimum (w_H is $+0.1 \text{ cm s}^{-1}$ over central Baffin Island).

The isotherm pattern (Figure 3.12) is of interest since, in later maps, a cold dome forms which eventually coincides with the isobaric pattern. The result is an example of the classic cold low described by Reed (1958) and Scherhag (1957). At this map time there is a decaying primary depression to the southeast of Greenland. The northwesterly flow along the east side of the St. Lawrence low sets up a strong deformation field over southern Davis Strait and the Labrador Sea. With this circulation the axis of dilation is roughly orientated northeast - southwest (cf. Palmen and Newton, 1969, pp 240) and a tongue of cold air is drawn southward over Baffin Bay. The zero degree isotherm is along the east coast of Baffin Island. The cyclonic flow from the Polar low is crossing into this tongue bringing warm air advection to the northern region ($0.5 \times 10^{-4} \text{ kJ kg}^{-1} \text{ s}^{-1}$) which acts to shift the northern sector of the tongue east. In the central Baffin Island area the circulation of the

St. Lawrence depression acts in opposition, deepening the tongue to the southwest. The interaction of these three vortices set the isotherm-isobar configuration for the development of the cold low.

By July 15 the two southern depression centers have coalesced into a deep low of 124 dm over Ungava Bay. The isobaric gradient has intensified and extends into the area of northern Baffin Island where it joins the Polar Basin low; the 147 dm isoline encircles both systems. This map (Figure 3.5, cf. also Figure 3.2) represents the maturation of the system, the center weakens noticeably in the next map. The synoptic sequence thus illustrates fully the decay of a mid-latitude system as it enters the Arctic.

The strongest ascent due to differential vorticity advection ($w_v = 0.6 \text{ cm s}^{-1}$) is weaker than on the previous map and is situated to the northeast of the vortex center over Davis Strait. The 50 cb vorticity advection is $1 \times 10^9 \text{ s}^{-2}$ here. Although the location relative to the low is similar to that of the 13th, the magnitude of the maximum vorticity advection has decreased by one-half.

The patterns of vorticity and thickness advection are no longer coincident and, within the depression, thickness advection dominates the vertical circulation. This is characteristic of the peak of development for mid-latitude systems (Krishnamurti, 1968b). Deformation of the temperature pattern has extended into Hudson Bay and the zero degree isotherm forms a closed dome immediately to the west of the depression center. The result is warm air advection (approximately $0.8 \times 10^{-4} \text{ K kg}^{-1} \text{ s}^{-1}$) to the north and west of the system with ascent of 0.6 cm s^{-1} , effectively overriding the descent due to differential vorticity advection. Where w_v is a maximum to the northeast w_{th} is zero or slightly negative.

As the patterns of w_v and w_{th} move out of phase local effects assume dominance. The maximum total ascent (1.5 cm s^{-1}) is to the north of the low over southeast Baffin Island. Since w_v and w_{th} are both zero here, this is directly related to orographic precipitation effects and frictional and topographic uplift.

For this particular case the surface vertical velocities due to frictional and topographic factors are illustrated in Figure 3.6. The onshore southeasterly flow results in an orographic uplift of 1 cm s^{-1} over southern Baffin Island. Over Foxe Basin, the lee side, descent is of the order of -0.8 cm s^{-1} and uplift is 0.1 cm s^{-1} over Keewatin. Note the marked influence of the Greenland ice cap (-1.8 cm s^{-1}) even though flow is more alongshore than offshore. Offshore descents may reach -4 cm s^{-1} on other dates. Frictional cross-isobaric convergence within the low vortex approaches 1.5 cm s^{-1} . A slight curvature of the isoline over southern Baffin Island due to onshore convergence and

differential drag is noticable. Elsewhere there is moderate descent of the order of -0.3 cm s^{-1} due to frictional divergence.

Precipitation and latent heat release in the surface (100 to 85 cb) layer is significant in response to the orographic and frictional ascent. Heat release of $3 \times 10^{-5} \text{ kJ kg}^{-1} \text{ s}^{-1}$ is calculated over southern Baffin Island which results in additional ascent of 1 cm s^{-1} at 85 cb. As before, the net vapour flux divergence is negative in this northeast sector of the depression ($-1.5 \text{ mm cm}^{-2} \text{ hr}^{-1}$).

The surface enthalpy flux results in a cooling except over Baffin Island where the warm surface coupled with negative temperature advection promotes a heating of $4 \times 10^{-5} \text{ kJ kg}^{-1} \text{ s}^{-1}$ at 85 cb with a strong local ascent approaching 0.7 cm s^{-1} over the east coast. Note that this augments local topographic, frictional and latent heat effects in this sector. Elsewhere the advective pattern is the predominant control on w_H . Generally w_H and w_{TH} are in opposition. The two are nearly equal in magnitude over Davis Strait and the Labrador Sea while over Foxe Basin and Hudson Bay, in the region of the cold dome, thickness advection has a much greater effect.

Part of the cold dome is off the grid and a complete examination of the internal energy exchanges is not possible until the next example.

This map illustrates the maturation of a mid-latitude low in the subarctic. Vorticity and thickness advection patterns are out of phase with the latter dominating the vertical motion field within the depression. Considering only these two parameters at 85 cb the vertical motion in the vortex center would be near zero. The surface frictional convergence and uplift of 0.5 cm s^{-1} would rapidly fill the system in the lower troposphere leading to decay. Any displacement would be a response to the steering of the large scale flow. However, there is strong ascent and concomitant pressure fall to the north related to local effects.

The importance of these local controls is apparent on July 17 (Figure 3.7) when the depression center has moved northward to southern Baffin Island. It has weakened to 130 dm and the regional scope of the cyclonic circulation is much more restricted as compared to July 15. The Polar low remains unchanged.

The decay of the system is reflected in the advective terms. The pressure pattern is almost in phase in the vertical (other pressure levels are not shown) such that there is very little differential vorticity advection over the system center. w_v is almost zero here. To the northeast of the system the 50 cb vorticity advection is still positive but has been reduced to $1 \times 10^{-10} \text{ s}^{-1}$ (this may be suspect on account of NMC analysis errors over Greenland) as the circulation weakens and vorticity generation and export of the depression falls.

The isobaric and isotherm patterns at 85 cb are almost coincident. The geostrophic thickness advection results in a vertical circulation

of less than $\pm 0.1 \text{ cm s}^{-1}$ within the low and acts to oppose the equally small vorticity effect. Only in the northeast sector does one factor, the differential vorticity advection, predominate, but this uplift is cancelled by orographic descent. The advective fields have a negligible net influence on the synoptic system.

The low is stabilized, however, by strong net ascent (0.8 cm s^{-1}) within the vortex, with the result that the system remains anchored here for three days. Again, this may be attributed entirely to local effects. Over the Hall Peninsula region surface orographic uplift is 0.3 cm s^{-1} , there is a strong onshore frictional convergence of 0.6 cm s^{-1} , the release of latent heat ($1 \times 10^{-5} \text{ kJ kg}^{-1} \text{ s}^{-1}$) contributes 0.1 cm s^{-1} .

The near coincidence of the isothermal (Figure 3.12) and isobaric patterns is a classic indicator of an occluding system (Palmén and Newton, 1969) and also defines a cold low which can be first discerned at this stage for this example. The zero line of horizontal advection runs through the closed zero degree isotherm which encompasses two computational grid points, one to the northwest and one to the southeast of the cold dome over southeast Baffin Island. With the circulation of July 17 there is warm air advection on the upstream (southeast) side of $5 \times 10^{-6} \text{ kJ kg}^{-1} \text{ s}^{-1}$ and cooling of $-4 \times 10^{-6} \text{ kJ kg}^{-1} \text{ s}^{-1}$ on the downstream (northwest) side. However, there is a reverse trend due to the surface enthalpy flux with a heating of $2 \times 10^{-5} \text{ kJ kg}^{-1} \text{ s}^{-1}$ over land to the northwest and a cooling of $-1 \times 10^{-5} \text{ kJ kg}^{-1} \text{ s}^{-1}$ over Davis Strait. Over land there is a latent heat release of $2 \times 10^{-5} \text{ kJ kg}^{-1} \text{ s}^{-1}$ and over water to the southeast it is $1 \times 10^{-5} \text{ kJ kg}^{-1} \text{ s}^{-1}$. Corresponding cooling rates by vertical advection (adiabatic expansion) are -3×10^{-5} and $-1 \times 10^{-5} \text{ kJ kg}^{-1} \text{ s}^{-1}$ - the orographic influence is evident. Noting the restrictions of the coarse grid resolution and approximate nature of the parameterizations we can estimate the total 85 cb energy exchange within the cold low to $6 \times 10^{-6} \text{ kJ kg}^{-1} \text{ s}^{-1}$ to the northwest and $-5 \times 10^{-6} \text{ kJ kg}^{-1} \text{ s}^{-1}$ to the southeast. Thus, there is a net intensification of the cold dome to the over advective heating. This dominance of vertical expansion was also noted by Reed and Tank (1956) and Scherhag (1957). The 85 cb cooling in this sector is approximately $-0.4^\circ \text{ dy}^{-1}$. However, the decay to the northwest is traced to the failure of the combined effects of adiabatic expansion and advective cooling to exceed heating by the surface enthalpy flux and precipitation. The heating is approximately $0.5^\circ \text{ dy}^{-1}$.

By July 19 (Figure 3.8) the depression center has shifted slightly toward the northeast - still influenced by the strong localized ascent over Baffin Island. It is no longer a closed low but forms part of a south-east trough extension of the Polar Basin low which is over the Queen Elizabeth Islands.

With this slight displacement, the flow over Baffin Island is from the northwest and there is orographic descent of -0.2 cm s^{-1} at the surface

over the east coast. The cold dome is displaced slightly eastwards, as anticipated from the energy exchange considerations on July 17, and as a result there is a broad region of negative thickness advection within the depression with a maximum that coincides with the orographic descent to produce a region of net subsidence at 85 cb within the low. On the west coast of Greenland, southerly air is flowing into the cold dome ($+2 \times 10^{-5} \text{ kJ kg}^{-1} \text{ s}^{-1}$) with a moderate positive w_{TH} of 0.3 cm s^{-1} . This adds to the positive vorticity advection along the east side of the trough ($1 \times 10^{-9} \text{ s}^{-2}$ at 50 cb, the increase from the previous day probably reflects the combined circulation of the Polar and Baffin Island low around the trough) which contributes an ascent of 0.5 cm s^{-1} . As a result, there is precipitation and latent heat release ($4 \times 10^{-5} \text{ kJ kg}^{-1} \text{ s}^{-1}$). The total uplift approaches 1.3 cm s^{-1} along the east side of the trough ahead of the depression promoting vortex development in this direction.

Two features are worthy of note. The influence of the Polar low is now evident in the positive thermal advection ($4 \times 10^{-5} \text{ kJ kg}^{-1} \text{ s}^{-1}$) to the northwest as cyclonic flow crosses the isotherms (Figure 3.17) of the cold tongue. This increases in magnitude and southward extent in the next map. There is also an 'anomalous' precipitation zone on the west limb of the trough where there should be net subsidence (cf. synoptic discussion in LeDrew, 1976) due to negative thickness and vorticity advection. However, there is significant onshore frictional convergence and orographic uplift along the west shore of Baffin Island with a total surface ascent of 0.3 to 0.5 cm s^{-1} . This is responsible for the net uplift and precipitation at 85 cb.

The configuration of the cold dome (Figure 3.12) with respect to the isobars is such that inflow is from the northwest across a very weak temperature gradient with a small horizontal advective heating of $4 \times 10^{-7} \text{ kJ kg}^{-1} \text{ s}^{-1}$. The advective cooling at the outflow, to the northeast (note the reversal of relative flow from July 17) is $-3 \times 10^{-5} \text{ kJ kg}^{-1} \text{ s}^{-1}$. The corresponding figures for the surface enthalpy flux effect are $1 \times 10^{-7} \text{ kJ kg}^{-1} \text{ s}^{-1}$ over land at the inflow and $-6 \times 10^{-6} \text{ kJ kg}^{-1} \text{ s}^{-1}$ over south Baffin Bay. The adiabatic effect is positive ($1 \times 10^{-5} \text{ kJ kg}^{-1} \text{ s}^{-1}$) over land due to subsidence in the lee side of Baffin Island, and negative at the outflow ($-6 \times 10^{-6} \text{ kJ kg}^{-1} \text{ s}^{-1}$). The net result at the outflow region is a strong cooling of $3.6 \text{ C}^\circ \text{ dy}^{-1}$, dominated by advective cooling in this situation. At the inflow adiabatic compression dominates a heating of $1 \text{ C}^\circ \text{ dy}^{-1}$. The conclusion of Reed (1956) and Reed (1958) that adiabatic cooling is the dominating factor in the maintenance of the cold low is obviously an oversimplification. The controlling parameter changes with shifts in the isobar-isotherm patterns and in relations between local features and the large scale flow. It is necessary to use more detailed grid resolution to make more confident conclusions.

With the eastward displacement of the cold dome w_{TH} becomes significantly positive to the east-southeast of the depression. This augments an increased w_v as the circulation intensity increases with the combination of the Polar and Baffin Island lows in a trough. There is a definite impetus for development towards the south of

Greenland resulting from advective effects. Note the increased thickness advection has its roots in local intensification of the cold dome on the previous map.

On July 21 (Figure 3.9) the vortex has indeed moved southeast and the height of the 85 cb surface is stabilized. It remains at 136 dm from July 19 through 21 (Figure 3.2). The Polar low has deepened to 120 dm and the increased influence is evident in the cyclonic curvature over the northern half of the grid. Over the southern section the anticyclonic curvature is part of a major high over the central Canadian plains. The net result of the two opposing systems is strong upper level diffluence over the Baffin Bay-Davis Strait region. This phase may be considered as a transition between the dominance of a southerly depression system and the Polar low, the development of the latter paradoxically initiating a period of strong positive thermal advection over the Baffin Island region.

The relative warming is a result of west - northwest flow into the cold dome (Figure 3.12), which is now stationed over Davis Strait. It is behind the southern depression and the cold low configuration no longer exists. The advective warming and adiabatic compression at the inflow of the cold dome (northwest sector) is $4 \times 10^{-6} \text{ kJ kg}^{-1} \text{ s}^{-1}$ and $1 \times 10^{-5} \text{ kJ kg}^{-1} \text{ s}^{-1}$, respectively. The corresponding figures at the outflow sector are $-6 \times 10^{-6} \text{ kJ kg}^{-1} \text{ s}^{-1}$ and $-1 \times 10^{-5} \text{ kJ kg}^{-1} \text{ s}^{-1}$. However, cooling at both locations due to downward enthalpy flux toward the water surface is strong ($-4 \times 10^{-5} \text{ kJ kg}^{-1} \text{ s}^{-1}$). The dominance of this latter factor over adiabatic and advective effects no doubt accounts for the anchoring of the cold dome over Davis Strait behind the low for the period from July 20 to 23.

The pattern of w_v opposes the ascent to the west and descent to the east due to this thickness advection. The trough containing the low along the west coast of Greenland promotes uplift due to positive differential vorticity advection and to the west the anticyclonic curvature around the mid-plains high seems to predominate. However, the combined effects of the weak opposing fields of w_v and w_{th} seems to result in a broad region of quiescent vertical circulation. With this nearly zonal flow topographic controls are again important. Over Greenland the orographic uplift (0.2 to 2.0 cm s^{-1}) and onshore frictional convergence (0.3 to 0.5 cm s^{-1}) combine to product strong ascent in this sector. This is reinforced by latent heat release with additional uplift of 0.2 cm s^{-1} at 85 cb. Over west Davis Strait-Baffin Bay there is a general subsidence due to combined topographic descent in the lee of Baffin Island (-0.4 cm s^{-1}) and frictional effects (-0.2 cm s^{-1}) as air accelerates eastward from land to sea.

The Polar low has shifted to the east and extended the cyclonic influence in the grid region by July 23 (Figure 3.10). On July 22 it had reached the maximum depth of 116 dm. The trough extension

along the west coast of Greenland on the previous map (Figure 3.9) is now almost a cutoff low between Greenland and Iceland with a relatively shallow height of 135 dm. The northwest flow along the west side of this trough has shifted the cold dome to the south near the coast of Labrador.

The contribution by differential vorticity and thickness advection is still weak. The maximum w_V of $+0.6 \text{ cm s}^{-1}$ is located over northern Baffin Island where the cyclonic circulation is analagous to a mid-latitude trough with positive vorticity advection to the east and negative advection and descent along the western limb. To the south-east the anticyclonic curvature represents an export of vorticity from the high towards the low to the east of Greenland with a corresponding descent of -0.7 cm s^{-1} .

The Baffin Bay maximum of w_V is opposed by w_{TH} (-0.7 cm s^{-1}) as cold air is transported from the temperature minimum over the Queen Elizabeth Islands. Over Davis Strait positive thickness advection and warming is associated with the same flow but which is directed into the cold tongue (Figure 3.12). It is a combination of the Polar low circulation and the position of the cold tongue (previously a part of the southerly depression system) which accounts for the marked warming interval around July 21 (Figure 3.1). The effect subsided as the cold dome shifted southward.

As on the 21st, extremes of w_V and w_{TH} are nearly self-cancelling and the major vertical motion features are related to the local effects, predominately the strong orographic ascent of 4 cm s^{-1} at the surface over western Greenland. Net subsidence over Baffin Island is clearly related topographic descent and frictional divergence of the anticyclonic curvature.

The map of July 25 (Figure 3.11) illustrates the decay of the Polar low to 133 dm as it drifts southward along the west coast of Greenland, undoubtedly prompted by strong surface orographic ascent and latent heat release in this area on the previous map (Figure 3.10).

With the southward intrusion of the low, coupled with the almost complete disappearance of the cold tongue, there is a general negative thermal advection approaching $-2 \times 10^{-5} \text{ kJ kg}^{-1} \text{ s}^{-1}$ at Baffin Island. The cold advection accentuates the effects of land-sea temperature contrast on the surface enthalpy flux. Over Baffin Island the positive heating approaches $8 \times 10^{-5} \text{ kJ kg}^{-1} \text{ s}^{-1}$ in the north and $2.5 \times 10^{-5} \text{ kJ kg}^{-1} \text{ s}^{-1}$ in the south as compared with a cooling of $-4 \times 10^{-5} \text{ kJ kg}^{-1} \text{ s}^{-1}$ over central Davis Strait. The abruptness of the change gives rise to intense gradients of $w_H \approx 1.0 \text{ cm s}^{-1}$ over Baffin Island and -0.5 cm s^{-1} over Foxe Basin and Davis Strait. Under conditions of warm air advection the fluxes over land are reduced and horizontal gradients are subdued with the result that the resultant vertical motion field of w_H does not have the intense gradients and extremes of this case.

As expected from the classical model of trough circulation there is strong ascent due to positive vorticity advection at the base of the wave (1.3 cm s^{-1}) and descent to the west (-0.7 cm s^{-1}). Both extremes are much stronger than on the previous example. However, they are opposed by the thickness advection to produce a quiescent vertical motion field, the noticeable exceptions may be attributed to local factors.

85 cb Thermal Regime for East Baffin Island, Davis Strait and Baffin Bay

Since the period studied in the preceding section was selected partly on the basis of the interesting temperature and ice melt episode it is useful to examine some thermal characteristics of the synoptic event at selected location. The model generated heating rates at 85 cb are presented in Table 3.1 and Figure 3.13 for east Baffin Island, Baffin Bay and Davis Strait. The data for Baffin Island most closely represents the synoptic data for Broughton Island in Figure 5. In Figure 3.14 the positions of maxima of horizontal thermal advection within the grid region are plotted. The "trajectories" of these centers are based on subjective interpretation of Figures 3.4 through 3.11. There is a boundary problem in that the absolute maximum for a given system may be off the grid. This map should not, therefore, be considered as a complete analysis but serve only to indicate sectors where advective influences are prominent and the probable time-space relationships of these centers.

The two warming periods identified in Figure 3.1 are evident at 85 cb (Figure 3.13) for eastern Baffin Island. There is a small warming of 4°C centered on July 16 and a major episode around July 22. At Broughton Island the recorded 48 hr ice melt (beginning on July 19) was 25 cm, the highest rate observed during the 1973 season. The interval between observations was too great to associate a definite melt rate with the first warming episode, but it was noticeably smaller.

The net heating attributed to horizontal advection, vertical (adiabatic) advection, surface enthalpy flux and latent heat release does not correspond very well with the temperature trend (Figure 3.13). This may be related to the accumulation of errors (most suspect is the surface enthalpy flux), the coarse grid resolution used to calculate the advective components and the fact that the data represent instantaneous rates at a point rather than accumulated energy (indicated by temperature) between observation. Despite these restrictions, there is some indication of a net heating increase on July 16 at Baffin Island and the maximum of July 22 is clear.

The development of the cold tongue in the Baffin Island region as a result of shear between the St. Lawrence low and the primary depression southeast of Greenland has been discussed in the previous section. The formation of this feature accounts for the unexpected sharp drop in temperature from the maximum on July 12 (Figure 3.1) while the regional pressure drops as the southerly depression moves north. The delayed warming episode on July 16 was initiated by strong horizontal advective heating (cf Figure 3.14) when the depression

intensified over north Quebec and the increased circulation brought southerly air into the cold dome over Baffin Island. The regional effect is more obvious in the Davis Strait illustration (Figure 3.13) where advective heating increased sharply on July 14 to $12 \times 10^{-5} \text{ kJ kg}^{-1} \text{ s}^{-1}$ (equivalent to $10^\circ \text{C dy}^{-1}$). The warmed air would subsequently be advected northwest under the cyclonic regime. This explains the relative delay of advection maximum and the lower rate over Baffin Island.

Over Baffin Island the horizontal advective heating is of the same scale as the surface heating during this early episode, but both values are opposed by adiabatic expansion resulting from orographic uplift. Over the ice (Broughton Island area) the rate of uplift would be smaller and advective heating would contribute to a net energy increase. The correspondence between net heating and observed temperature change would then be closer than indicated in Figure 16.

After the 19th the advective effects are related to the flow of the Polar low into the same Baffin Island cold center (Figure 3.14). The maximum rates ($14 \times 10^{-5} \text{ kJ kg}^{-1} \text{ s}^{-1}$) are comparable to those identified with the southerly system and are found to the northwest over Victoria Island. There is a strong eastward gradient of this heating (cf Figure 12) and values over Baffin Bay reach a maximum of only $8 \times 10^{-5} \text{ kJ kg}^{-1} \text{ s}^{-1}$; which is, however, greater than the maximum of the previous episode (July 16). This is augmented by heating due to adiabatic compression in the lee of Baffin Island (4 to $5 \times 10^{-5} \text{ kJ kg}^{-1} \text{ s}^{-1}$). Descent is related to the negative vorticity advection aloft and shift of the flow over the east coast so that topographic and frictional effects are reversed as the depression shifts eastward.

There is an abrupt change in the energy regime on July 23 over Baffin Island and Baffin Bay, and on July 24 over Davis Strait, as the decaying Polar depression enters the region bringing cold air with an advection rate of -4 to $-10 \times 10^{-5} \text{ kJ kg}^{-1} \text{ s}^{-1}$ and an end to the ice melt episode.

To summarize, we note that over Baffin Island the regime is a balance of a wide range of fluctuations in all the energy sources. At times the surface enthalpy heating may reach the same magnitude as the advective influences. Latent heat release is commonly an order of magnitude smaller. Over the water surfaces, however, the dominant control is the horizontal advection. In this example, there are no large surface to air temperature contrasts, nor the large enthalpy fluxes found over land. Adiabatic effects are controlled by the large scale flow which usually results in weak vertical velocities in the Arctic. Consequently, the rates of vertical advection are much less than over land surfaces where topographic and frictional uplift is important. One exception, which may be related to the grid point resolution and computational design, is the adiabatic cooling on July 23 over Baffin Bay which is related to strong orographic uplift over Greenland with the onshore flow.

In this discussion we have identified only the magnitudes and nature of the synoptic scale thermal interactions for a particular case. In particular we have speculated that the major coastal ice melt of

east Baffin Island was related to warm advection from the west, prompted by the circulation of the Polar depression, coupled with adiabatic compression in the lee of the island. With the present grid resolution (350 km) we cannot determine the perhaps significant effect of subgrid advection on the surface energy balance. This may be large at the land sea boundary. It would also be useful to determine the adiabatic contribution when the local, steep topographic gradients are considered. A meso-scale time dependent model (the three dimensional sea breeze model of Piele, 1974, for example) with a much finer grid mesh is required to investigate such situations in more detail.

Summary and Discussion

A detailed analysis of the components of the omega field at 85 cb in the eastern Canadian Arctic has been presented at 48 hr intervals from July 13 to 25, 1973. The purpose was to examine the changes in the imbalance of the physical processes contributing to omega at various points in the evolution of a typical summer synoptic system within the region. Of particular interest is the relative importance of the advected versus the local terms in the vertical circulation and their effect on the behavior of the system.

During this period a developing mid-latitude depression moved into the grid area from the St. Lawrence and drifted out, south of Greenland, as a decaying system. Following this a deep Polar low also passed through the region in its decaying stages, although its regional influence was evident from the beginning of the study period. This particular case was chosen because there were two marked warming episodes, one of which had a significant influence on the surface energy balance in that there was a major ice melt along the east coast of Baffin Island.

In June the hemispheric circulation was predominately zonal but there was a major transition to meridional flow which characterized most of July (Wagner, 1973). This was prompted by blocking over west Canada and north Europe, and a deepening of the Azores high. A trough over Davis Strait, which extended to Texas, is evident on the mean July map. In Davis Strait the 70 cb height was approximately 25 meters below (low pressure) the normal while over central Canada, north Europe and the central North Atlantic it was 40, 80 and 70 meters, respectively, above normal. In the grid area of this study the pressure surface dropped 70 meters from the June 1973 average.

As the southerly depression entered the region on July 13 it can be identified with the characteristics of a developing system as described by Krishnamurti (1968b). Vorticity and thickness advection patterns are in phase and the upward circulation in advance is augmented by strong diabatic effects. At the maximum depth of the vortex on July 15 these advective patterns are no longer coincident. At 85 cb there is almost no vertical motion and the depression would

quickly fill since there is still strong low level frictional convergence with the cyclonic circulation. This would be identified as the occlusion stage according to the classical model and indeed the NMC surface analysis indicates an occluding front.

This out of phase shift of the thickness advection relative to the vorticity advection is related to the development of a deep cold tongue through Hudson Bay - Davis Strait which was initiated by the sudden transfer to meridional circulation and the formation of a strong deformation of the isotherms between an Icelandic low, a Polar low and the mid-latitude system. The position of this cold tongue is important throughout the entire study period. In addition to prompting the destruction of the southerly system it leads to the development of a cold low.

As the two advective terms become self-cancelling the local effects become important and act to stabilize the vortex. Orographic as well as frictional ascent and a strong surface enthalpy flux produce a region of intense vertical motion over southern Baffin Island. There is also latent heat release and further uplift. The maximum 85 cb ascent of 1.5 cm s^{-1} on July 15 in this area is less than the previous maximum (4 cm s^{-1}) to the south when advective terms dominated but nevertheless it is sufficient to force the northward drift of the low.

The cold dome intensifies over Davis Strait with attendant thickness advection to the southeast of the system on July 19. This coincides with intensified vorticity advection in this area as the low becomes a trough extension of the Polar low as the two circulations combine. This rejuvenation of the advective terms initiate development towards the south of Greenland and the low eventually leaves the region by July 23.

Previous studies of the cold low feature have emphasized the role of adiabatic expansion due to uplift within the vortex in the formation of the mid-tropospheric cold center (Read and Tank, 1956; Scherhag, 1957). In this case study, however, the physical relationships are more complex. The initiation of the isotherm configuration can be traced, prior to the cold low formation, to the horizontal deformation over Hudson Bay - Davis Strait between three depression centers. The cold low forms over the east coast of Baffin Island as the southerly system moves northward and the isobars coincide with the closed isotherms. The movement is not a result of large scale flow but rather of local ascent over Baffin Island. Adiabatic cooling is important at the upstream sector of the cold low, but downstream the feature is degraded by strong surface heating and latent heat release over the island. The net result is a retrograde travel of the cold center with intensification against the direction of flow. 48 hours later the flow characteristics have changed such that intensification is in the directions of flow but horizontal advective cooling dominates. On the following map (48 hours later) the cold dome is stabilized over Davis Strait by strong cooling related to the downward enthalpy flux.

It is evident that local as well as advective effects are influential in the maintenance of the cold low, for this example. As the flow changes and the nature of the underlying surface varies, the mechanisms change. More detailed study is necessary using more examples with a finer mesh grid. It may be that this complex situation, involving imbalances of land-sea thermal effects, the large scale flow (horizontal advection) and orographic ascent, may be an anomaly, especially in light of the very high frequency of cold lows found spread over all sectors of the Arctic (cf. Flohn, 1952).

When choosing the period for this detailed study it was noted that the rapid cooling at Broughton Island at the onset of an interval of decreasing pressure is unexpected in that the reduced pressure is usually associated with advection of warm southerly air. This cold episode has been traced to the development of the cold tongue over Hudson Bay - Davis Strait. The expected warming is observed on July 16 over Baffin Island. The peak is 24 hr earlier over Davis Strait and is of greater magnitude. This is obviously the effect of warm air advection with the northward moving mid-latitude system. However, the more intense warming centered on July 22, which was coincident with a vigorous melt of the fast ice in the Broughton Island area, is associated with a different system and an additional physical process. The cyclonic flow around the Polar low has intensified in the central grid sector bringing relatively warm air from the west into the cold tongue. This advection is augmented by adiabatic compression as the air descends the east coast of Baffin Island. The two heating effects are of similar magnitude. The subgrid scale effect of surface heating of air over land and its subsequent advection over nearby ice cannot be evaluated with the present grid resolution.

The grid averages and standard deviations of the model generated data at 24 hr intervals are in LeDrew (1976). Since they are not restricted to the synoptic system they do not adequately represent the synoptic behavior and therefore are not discussed in the day by day analysis. However, some general features are worth of note. The vigor of the 85 cb vertical circulation is not comparable to that further south. The grid average for a polar outbreak in middle latitudes (on April 15) is 1.6 cm s^{-1} , with a large standard deviation of 3.2 cm s^{-1} (Le Drew, 1976). By contrast the comparable statistics for a mature Arctic system (July 15) are 0.02 cm s^{-1} and 0.7 cm s^{-1} . Krishnamurti (1968b) reports extremes of vertical circulation of $+11$ to -13 cm s^{-1} for a mid-latitude storm in the United States. The more quiescent Arctic circulation is, in part, related to the lower static stability with the lower temperatures and smaller specific volumes. For the United States a typical value is 3.13 at 50 cb (Stuart, 1970) while for the Arctic it is 2.58. At 30 cb the difference increases (11.08 and 3.54, respectively). In this respect a useful study would be a comparison of the magnitudes of the contribution to omega by the various processes (advected and local) for Arctic and mid-latitude systems to find additional causes for the different vertical circulations.

Also of interest is the relatively large grid average contribution by diabatic effects at 85 cb. In several cases (e.g. July 15, 18, 20, 23) the contribution to the total vertical motion is of the same scale as the

the advective terms. In one instance (July 19), the latent heat release dominates the total vertical circulation.

For the purposes of this study the grid format is not ideal. The eight by eight by six data grid was chosen to restrict computer storage to within reasonable limits for an exploratory study. At present the storage of the model has exceeded the core limit of a CDC 6400 computer. The size of the grid, however, is not sufficient to identify with confidence origins and maximum magnitudes of advective processes through the history of the disturbance. In the discussion of the daily features it has been noted that significant sectors are often at the edge or entirely off the grid. Sutcliffe and Forsdyke (1950) recommend a hemispheric scale to analyze adequately synoptic evolution. An alternate scheme would be to use a movable grid referenced with respect to the depression center, such as that employed by Petterssen et al. (1962). However, this would entail re-analysis of the input fields at each calculation to fit the data with the new grid position.

The results of this study have illustrated the suitability of the steady state omega equation for discussion of synoptic systems in the Arctic. The influences of advective and local energy sources and sinks can be clearly differentiated and studied. The observed synoptic behavior closely follows that expected from an examination of the model generated data and characteristics of the local climate can be interpreted adequately from these data. A more comprehensive examination of the energetics of the local climate would require a time dependent model of greater resolution to couple local surface effects with the large scale flow.

TABLE 3.1

85 CB THERMAL DATA FOR SELECTED LOCATIONS

Line 1: east Baffin Island

Line 2: Davis Strait

Line 3: Baffin Bay

Date	Heating Rates: $\text{kJ kg}^{-1} \text{s}^{-1}$				Temperature: $^{\circ}\text{C}$
July	Vertical Advection	Horizontal Advection	Surface Enthalpy Flux	Latent Heat Release	
13	2.1E-5	-2.3E-5	-5.4E-7	0	0.5
	4.4E-6	1.5E-5	-5.5E-6	0	2.2
	-5.5E-6	3.4E-5	-6.1E-6	0	2.5
14	-1.2E-5	-3.6E-5	8.1E-6	0	2.4
	-1.1E-5	2.8E-4	-1.9E-5	0	-0.8
	-4.0E-5	-1.7E-5	-3.6E-6	0	3.2
15	-4.0E-5	-5.8E-5	3.7E-5	0	3.0
	-2.6E-5	4.4E-5	-1.1E-5	1.1E-5	3.8
	-1.5E-5	4.1E-6	-6.5E-6	0	-4.0
16	-6.9E-5	3.6E-5	3.9E-5	0	4.2
	-2.1E-5	-4.0E-6	-8.8E-6	0	4.2
	2.9E-6	2.2E-5	-9.5E-6	0	2.7
17	-3.7E-5	-1.1E-5	3.3E-5	1.6E-5	0.2
	-1.7E-5	3.3E-5	-6.8E-6	6.3E-6	-1.4
	-2.3E-5	-7.8E-6	-1.9E-5	1.3E-5	3.1
18	-9.5E-6	3.3E-6	7.0E-6	4.3E-6	-0.3
	-1.9E-5	3.7E-5	-6.3E-6	9.3E-6	1.4
	-1.1E-5	-1.4E-5	-6.5E-6	0	2.8
19	-8.0E-6	4.0E-7	1.2E-7	4.0E-6	0.5
	-1.0E-5	-3.3E-5	-5.7E-6	5.2E-6	2.0
	7.6E-6	4.1E-6	-5.9E-6	0	0.3
20	-1.7E-7	1.0E-5	-1.8E-6	4.5E-7	0.5
	4.9E-6	-6.3E-5	-1.1E-5	0	-0.3
	-2.5E-5	-1.2E-5	-4.5E-6	1.2E-5	2.0
21	1.3E-5	4.5E-6	-4.3E-6	0	2.5
	3.1E-7	1.1E-6	-1.6E-5	5.2E-7	1.4
	-5.6E-6	6.9E-6	-4.4E-6	3.4E-6	0.7
22	3.8E-5	8.5E-5	-2.4E-5	0	7.1
	9.8E-6	2.2E-5	-8.3E-5	0	2.8
	-1.7E-5	4.2E-5	-3.5E-5	0	5.7
23	5.3E-5	-9.2E-5	-4.0E-5	0	3.6
	8.9E-6	-5.0E-7	-1.6E-5	0	7.0
	-1.3E-4	-4.2E-5	-1.6E-5	0	-2.0
24	-4.3E-5	-9.6E-5	7.7E-6	0	2.1
	-2.0E-5	6.0E-5	-1.8E-5	0	11.0
	-5.0E-5	1.1E-6	-4.5E-6	0	-7.1
25	-6.6E-5	-8.2E-5	6.9E-5	2.0E-5	-6.3
	-5.9E-5	-1.2E-4	-7.4E-6	2.5E-5	-0.8
	-1.4E-5	2.6E-5	-5.1E-6	0	-4.3

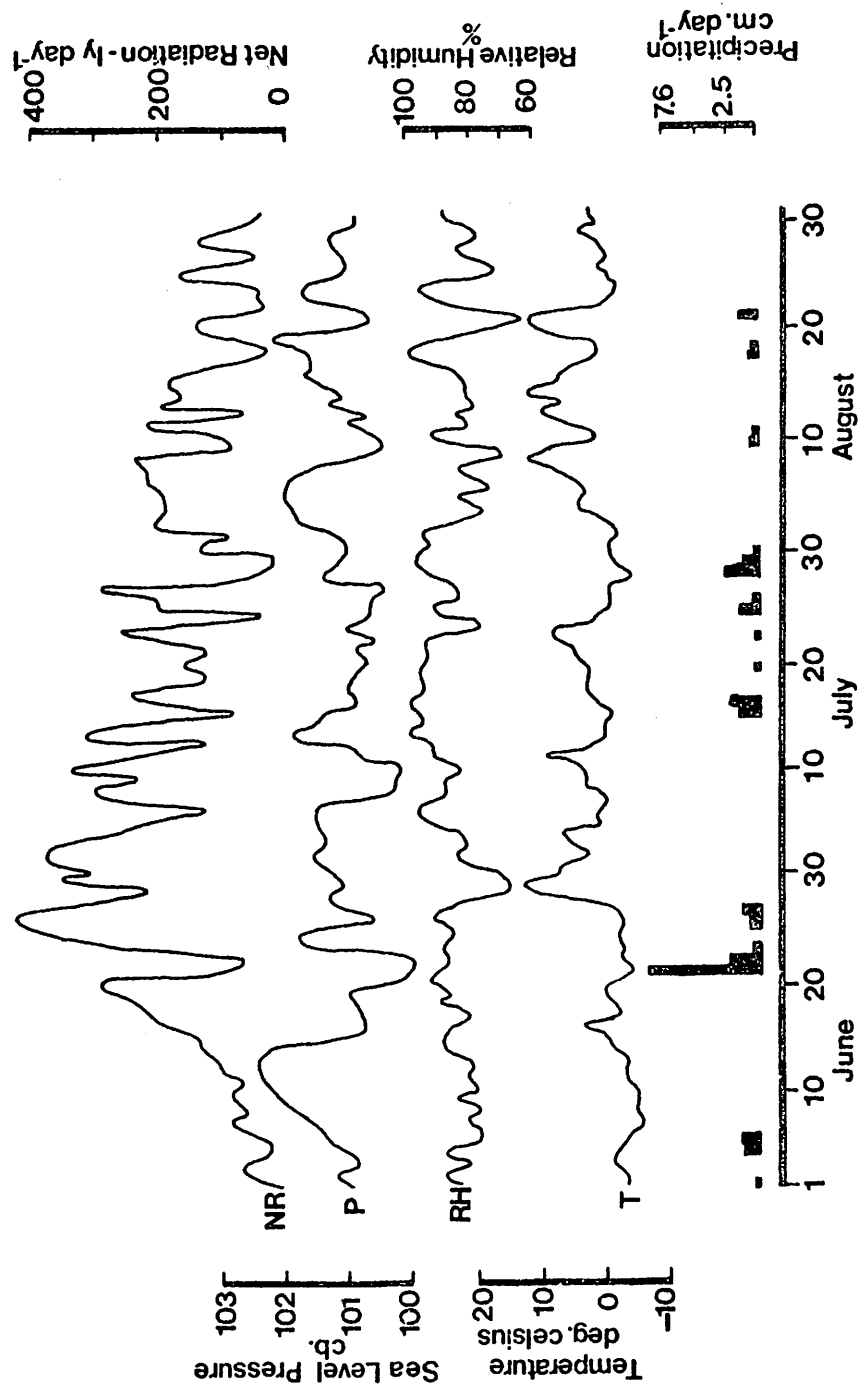


Figure 3.1. Surface synoptic data: Broughton Island, 1973.

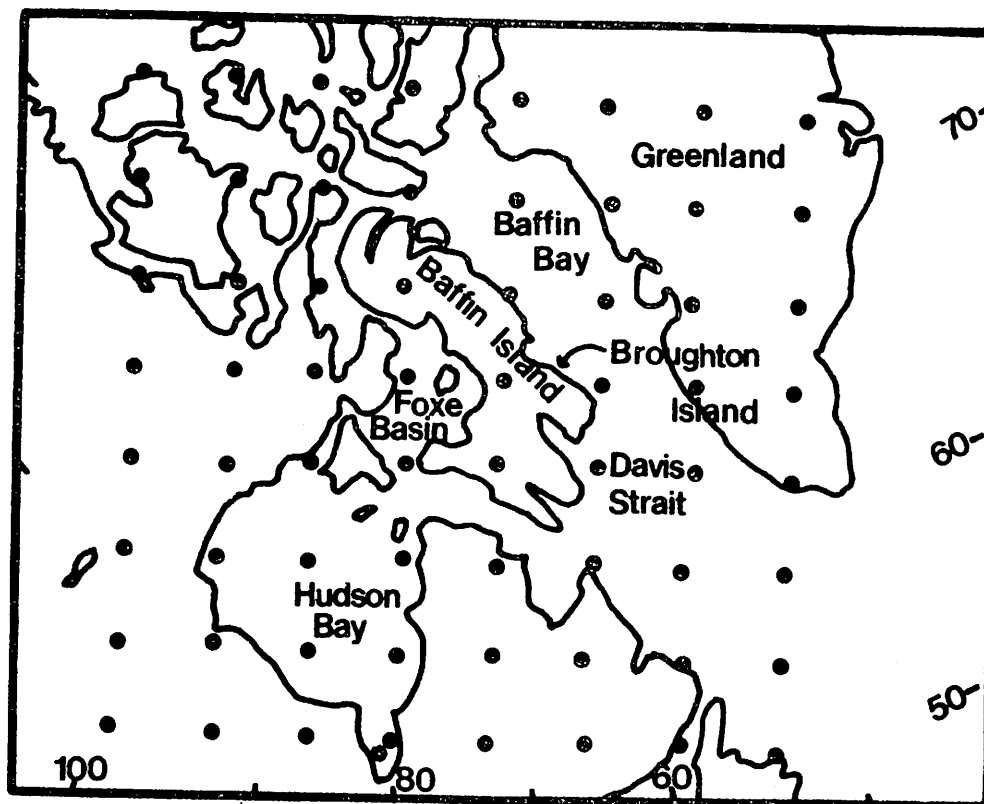
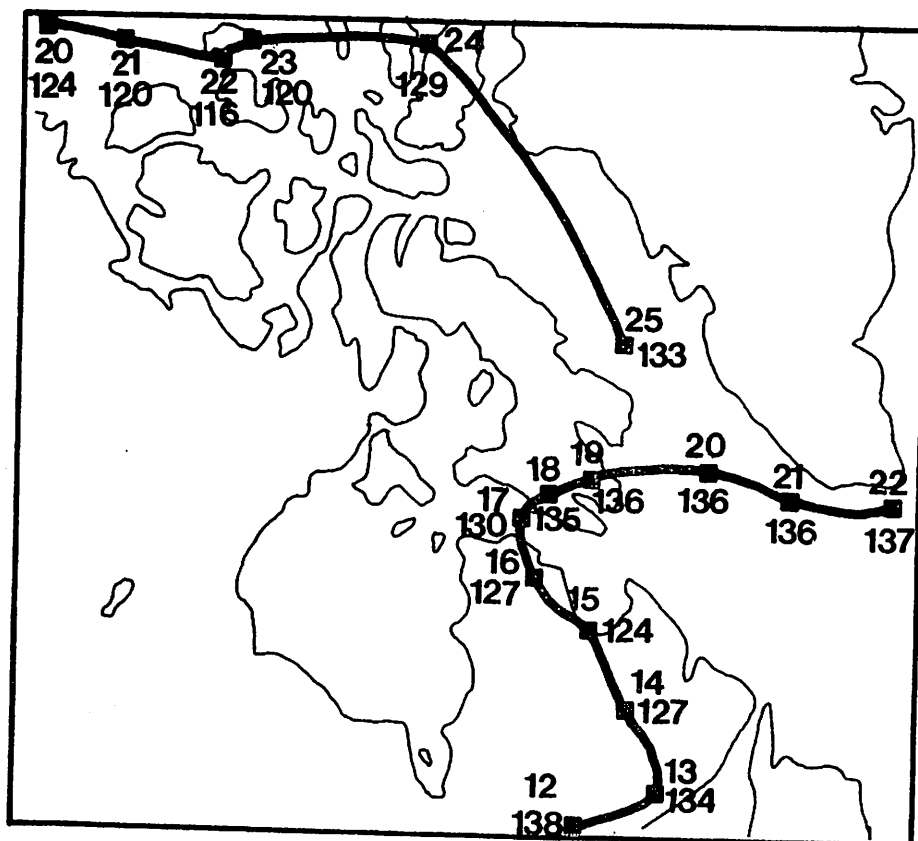


Figure 3.2. Eight x eight data grid.



22 DATE : JULY 1973
 137 HEIGHT OF CENTER - DECAMETERS

Figure 3.3. Tracks of 85 cb low centers, 12-25 July 1973.

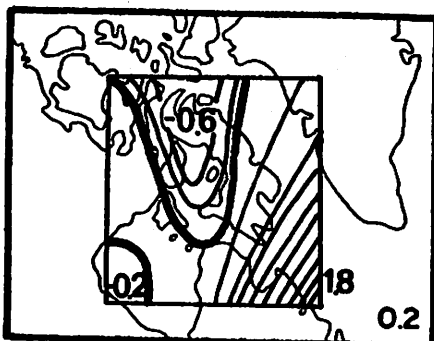
CONTOUR INTERVAL: LOWER RIGHT HAND CORNER
ZERO CONTOUR: HEAVY LINE



85 CB HEIGHT CONTOURS-DECAMETERS



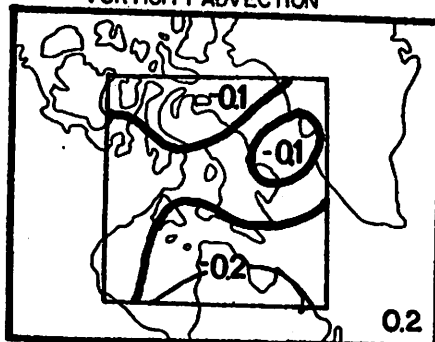
85 CB VERTICAL VELOCITY-CM.SEC.⁻¹
TOTAL



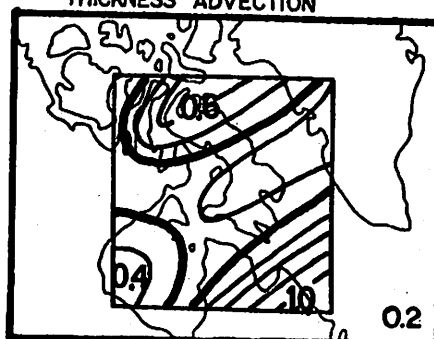
85 CB VERTICAL VELOCITY-CM.SEC.⁻¹
VORTICITY ADVECTION



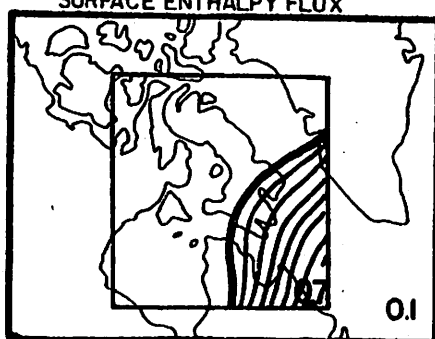
85 CB VERTICAL VELOCITY-CM.SEC.⁻¹
THICKNESS ADVECTION



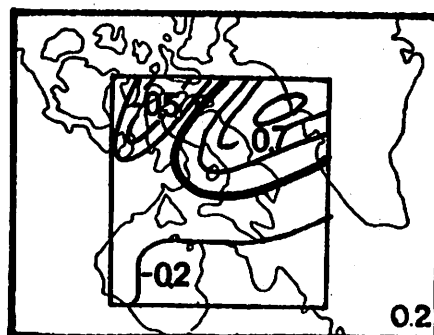
85 CB VERTICAL VELOCITY-CM.SEC.⁻¹
SURFACE ENTHALPY FLUX



THERMAL ADVECTION-KJ.KG⁻¹.SEC.⁻¹.10⁻⁴



PRECIPITATION-MM HR⁻¹



VAPOUR FLUX DIVERGENCE
MM CM⁻² HR⁻¹

Figure 3.4. **SYNOPTIC ANALYSIS**

JULY 13 1973

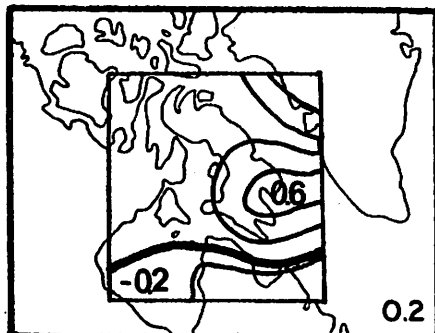
CONTOUR INTERVAL LOWER RIGHT HAND CORNER
ZERO CONTOUR: HEAVY LINE



85 CB HEIGHT CONTOURS-DECAMETERS



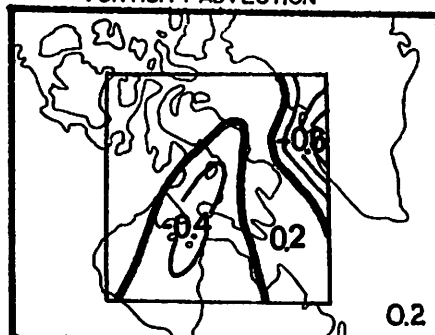
85 CB VERTICAL VELOCITY-CM.SEC.⁻¹
TOTAL



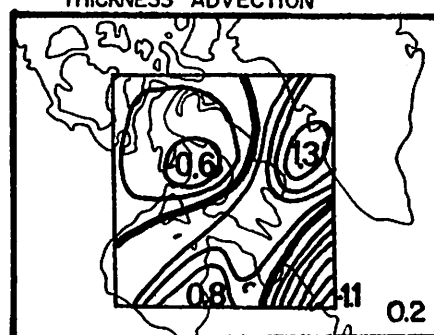
85 CB VERTICAL VELOCITY-CM.SEC.⁻¹
VORTICITY ADVECTION



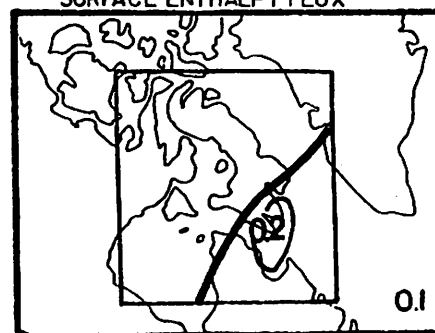
85 CB VERTICAL VELOCITY-CM.SEC.⁻¹
THICKNESS ADVECTION



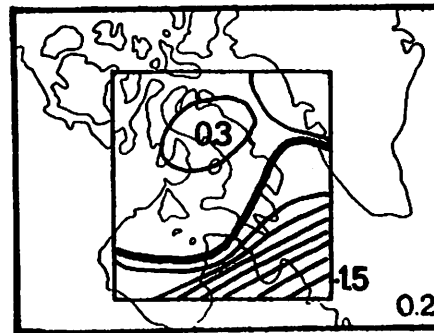
85 CB VERTICAL VELOCITY-CM.SEC.⁻¹
SURFACE ENTHALPY FLUX



THERMAL ADVECTION-KJ.KG⁻¹.SEC⁻¹.10⁻⁴

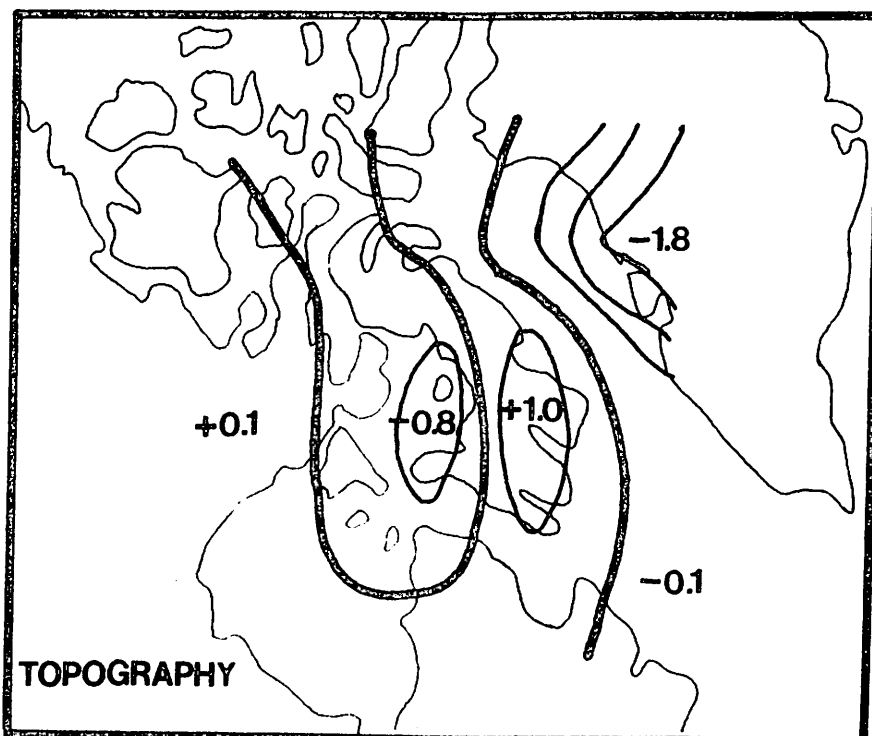
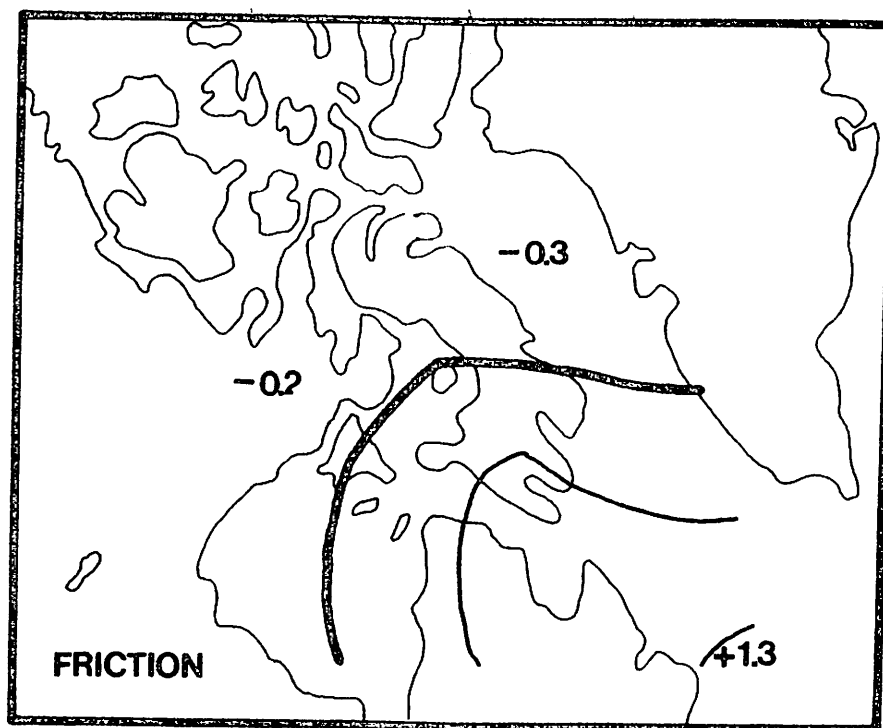


PRECIPITATION-MM HR⁻¹



VAPOUR FLUX DIVERGENCE
 $\text{MM CM}^{-2} \text{HR}^{-1}$

Figure 3.5. **SYNOPTIC ANALYSIS** **JULY 15 1973**



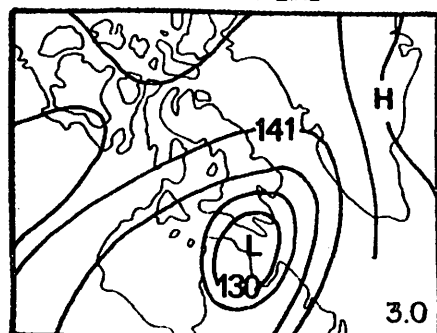
JULY 15 1973

Contour Interval -0.5

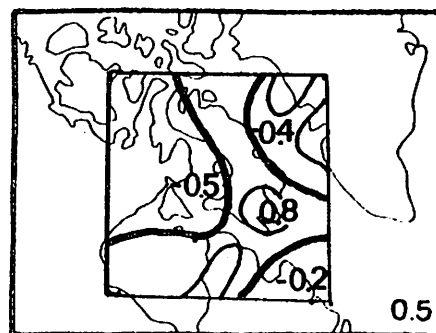
Figure 3.6. SURFACE VERTICAL VELOCITY
COMPONENTS

cm sec⁻¹

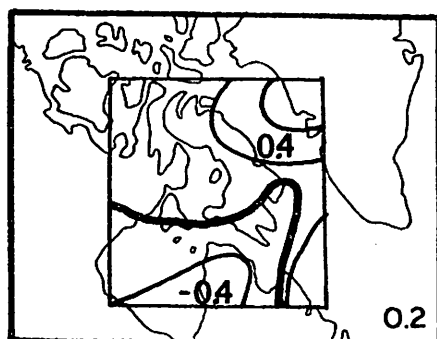
CONTOUR INTERVAL LOWER RIGHT HAND CORNER
ZERO CONTOUR: HEAVY LINE



85 CB HEIGHT CONTOURS-DECAMETERS



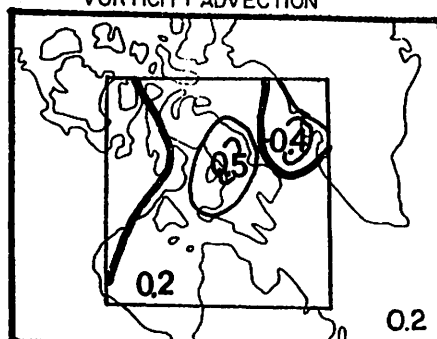
85 CB VERTICAL VELOCITY - CM.SEC.⁻¹
TOTAL



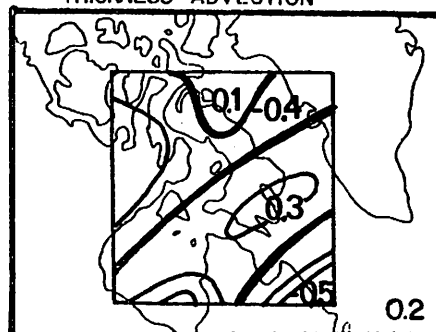
85 CB VERTICAL VELOCITY - CM.SEC.⁻¹
VORTICITY ADVECTION



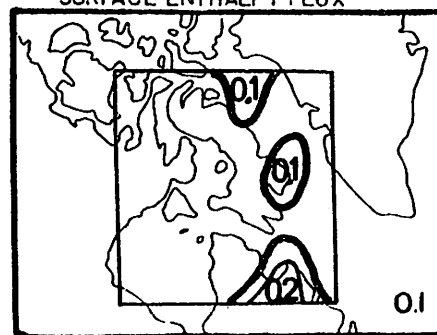
85 CB VERTICAL VELOCITY - CM.SEC.⁻¹
THICKNESS ADVECTION



85 CB VERTICAL VELOCITY - CM.SEC.⁻¹
SURFACE ENTHALPY FLUX



THERMAL ADVECTION - KJ.KG.⁻¹.SEC.⁻¹.10⁻⁴



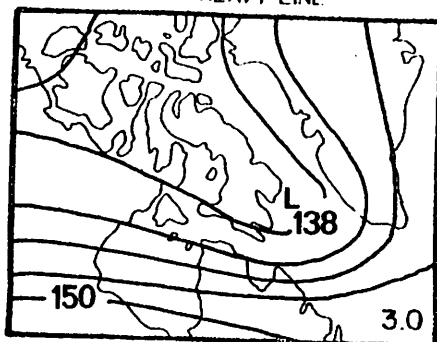
PRECIPITATION - MM HR.⁻¹



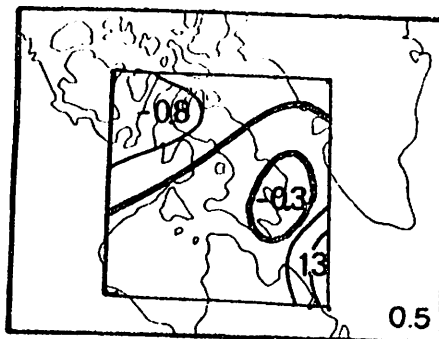
VAPOUR FLUX DIVERGENCE
MM CM.⁻² HR.⁻¹

Figure 3.7. SYNOPTIC ANALYSIS JULY 17 1973

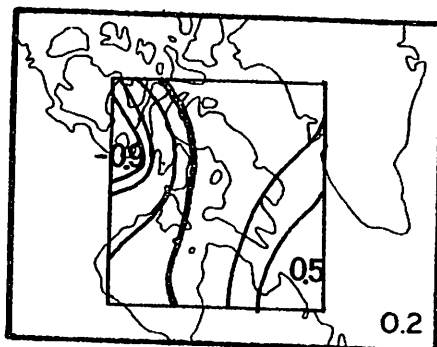
CONTOUR INTERVAL LOWER RIGHT HAND CORNER
ZERO CONTOUR: HEAVY LINE



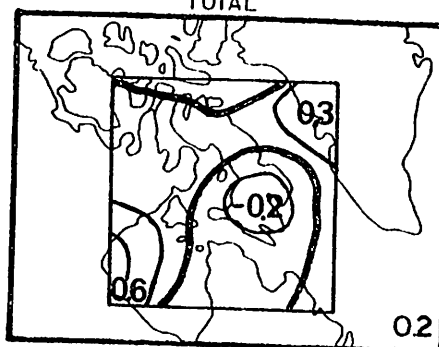
85 CB HEIGHT CONTOURS-DECAMETERS



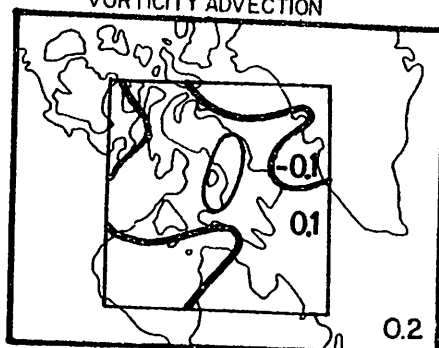
85 CB VERTICAL VELOCITY-CM.SEC.⁻¹
TOTAL



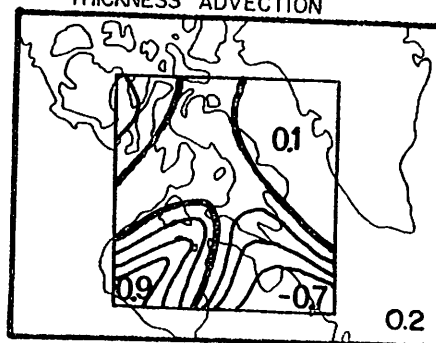
85 CB VERTICAL VELOCITY-CM.SEC.⁻¹
VORTICITY ADVECTION



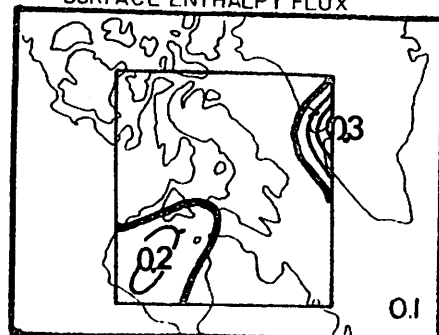
85 CB VERTICAL VELOCITY-CM.SEC.⁻¹
THICKNESS ADVECTION



85 CB VERTICAL VELOCITY-CM.SEC.⁻¹
SURFACE ENTHALPY FLUX



THERMAL ADVECTION-KJ KG⁻¹ SEC.⁻¹ $\times 10^{-4}$



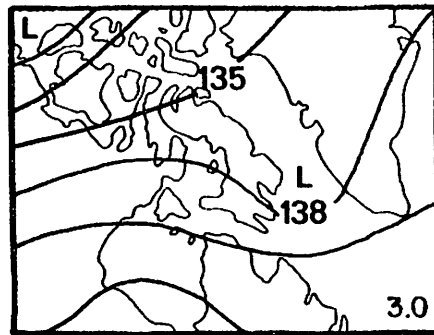
PRECIPITATION - MM HR⁻¹



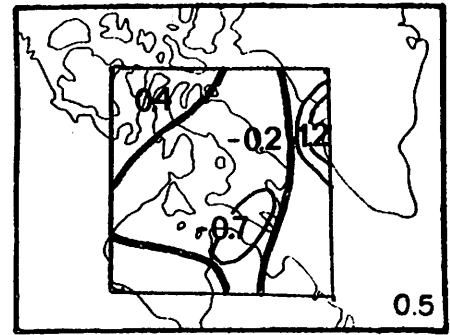
VAPOUR FLUX DIVERGENCE
MM CM² HR⁻¹

Figure 3.8. **SYNOPTIC ANALYSIS** JULY 19 1973

CONTOUR INTERVAL LOWER RIGHT HAND CORNER
ZERO CONTOUR: HEAVY LINE



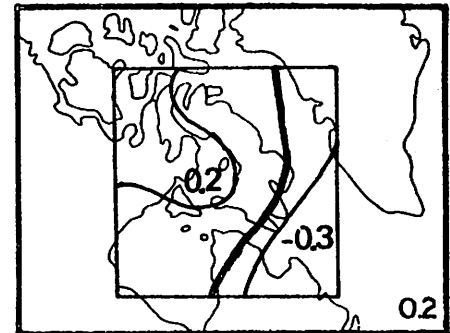
85 CB HEIGHT CONTOURS-DECAMETERS



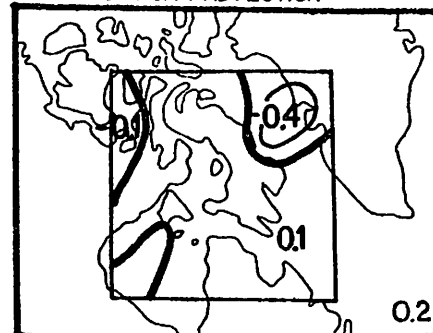
85 CB VERTICAL VELOCITY-CM.SEC.⁻¹
TOTAL



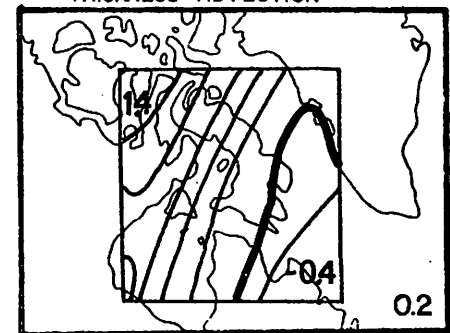
85 CB VERTICAL VELOCITY-CM.SEC.⁻¹
VORTICITY ADVECTION



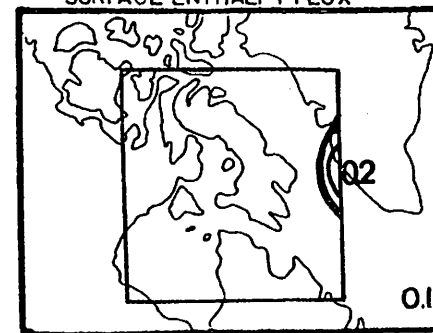
85 CB VERTICAL VELOCITY-CM.SEC.⁻¹
THICKNESS ADVECTION



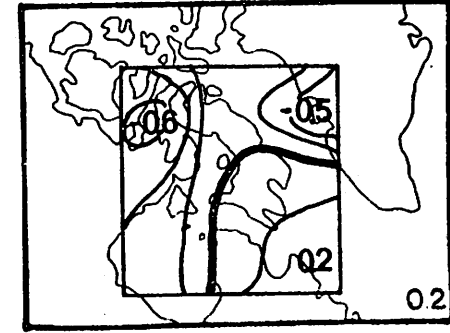
85 CB VERTICAL VELOCITY-CM.SEC.⁻¹
SURFACE ENTHALPY FLUX



THERMAL ADVECTION-KJ.KG.⁻¹.SEC.⁻¹.10⁻⁴



PRECIPITATION-MM.HR.⁻¹

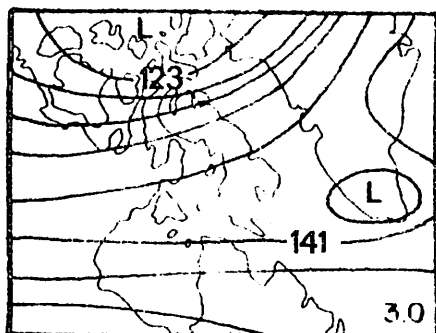


VAPOUR FLUX DIVERGENCE
MM.CM.⁻².HR.⁻¹

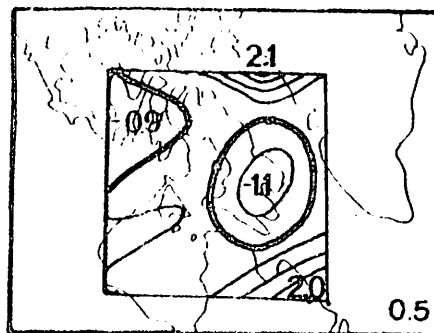
Figure 3.9. **SYNOPTIC ANALYSIS**

JULY 21 1973

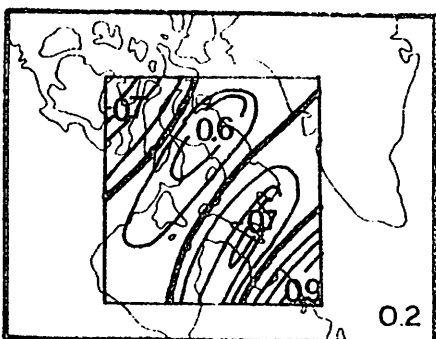
CONTOUR INTERVAL LOWER RIGHT HAND CORNER
ZERO CONTOUR HEAVY LINE



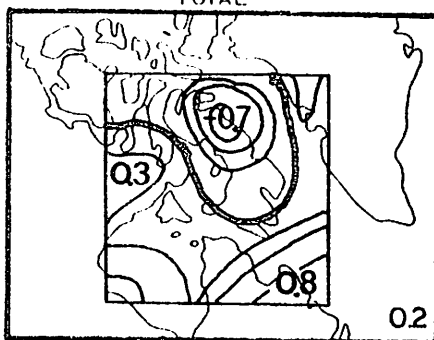
85 CB HEIGHT CONTOURS-DECAMETERS



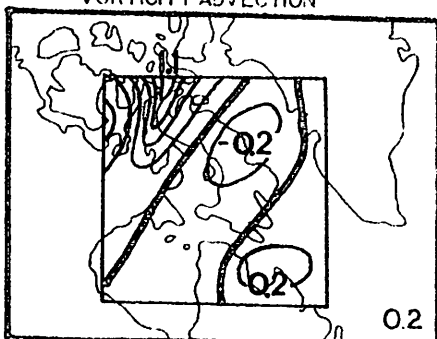
85 CB VERTICAL VELOCITY - CM. SEC.⁻¹
TOTAL



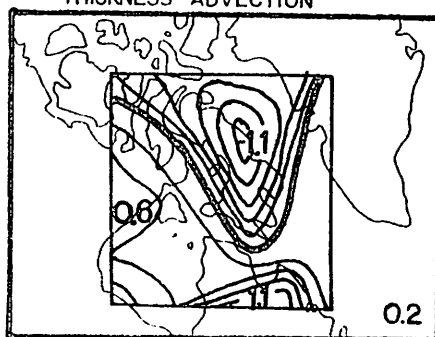
85 CB VERTICAL VELOCITY - CM. SEC.⁻¹
VORTICITY ADVECTION



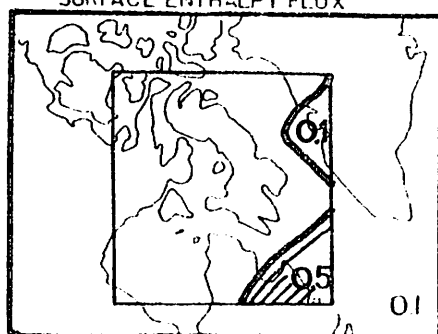
85 CB VERTICAL VELOCITY - CM. SEC.⁻¹
THICKNESS ADVECTION



85 CB VERTICAL VELOCITY - CM. SEC.⁻¹
SURFACE ENTHALPY FLUX



THERMAL ADVECTION - $\text{KJ KG}^{-1} \text{SEC}^{-1} 10^{-4}$



PRECIPITATION - MM HR^{-1}

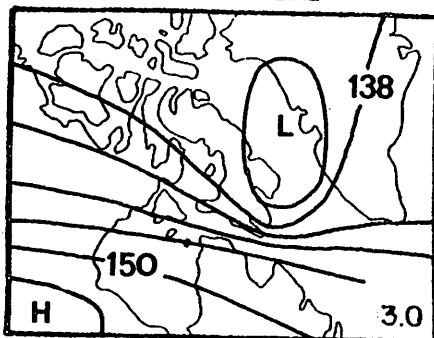


VAPOUR FLUX DIVERGENCE
 $\text{MM CM}^{-2} \text{HR}^{-1}$

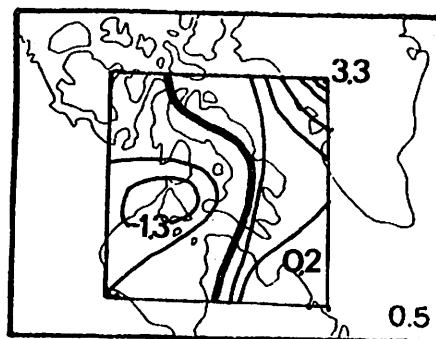
Figure 3.10. SYNOPTIC ANALYSIS

JULY 23 1973

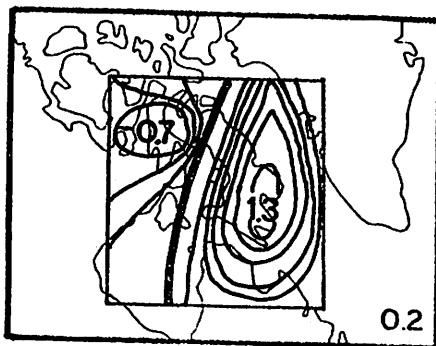
CONTOUR INTERVAL LOWER RIGHT HAND CORNER
ZERO CONTOUR: HEAVY LINE



85 CB HEIGHT CONTOURS-DECAMETERS



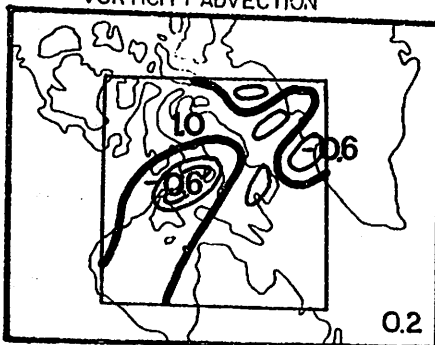
85 CB VERTICAL VELOCITY--CM. SEC.⁻¹
TOTAL



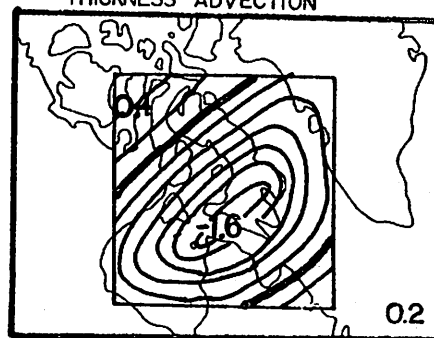
85 CB VERTICAL VELOCITY-CM. SEC.⁻¹
VORTICITY ADVECTION



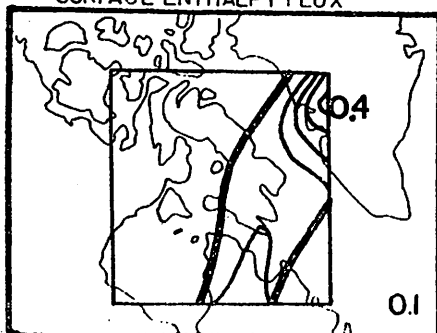
85 CB VERTICAL VELOCITY-CM. SEC.⁻¹
THICKNESS ADVECTION



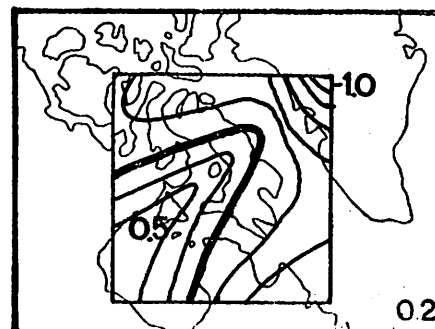
85 CB VERTICAL VELOCITY-CM. SEC.⁻¹
SURFACE ENTHALPY FLUX



THERMAL ADVECTION-KJ. KG⁻¹ SEC.⁻¹ 10⁻⁴



PRECIPITATION - MM HR⁻¹



VAPOUR FLUX DIVERGENCE
MM CM² HR⁻¹

Figure 3.11. SYNOPTIC ANALYSIS

JULY 25 1973

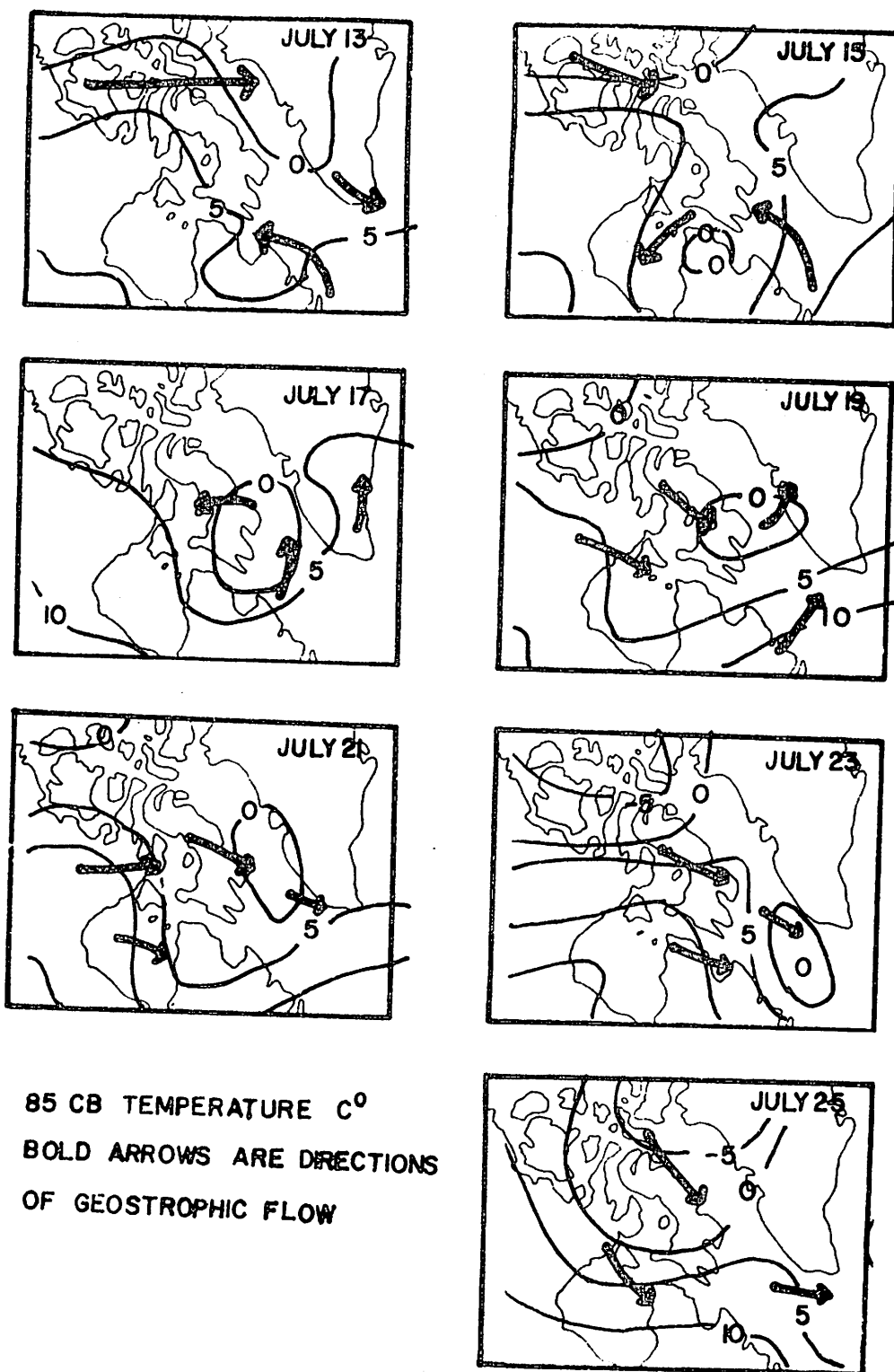


Figure 3.12. Isotherm patterns, 85 cb, 13-25 July, 1973.

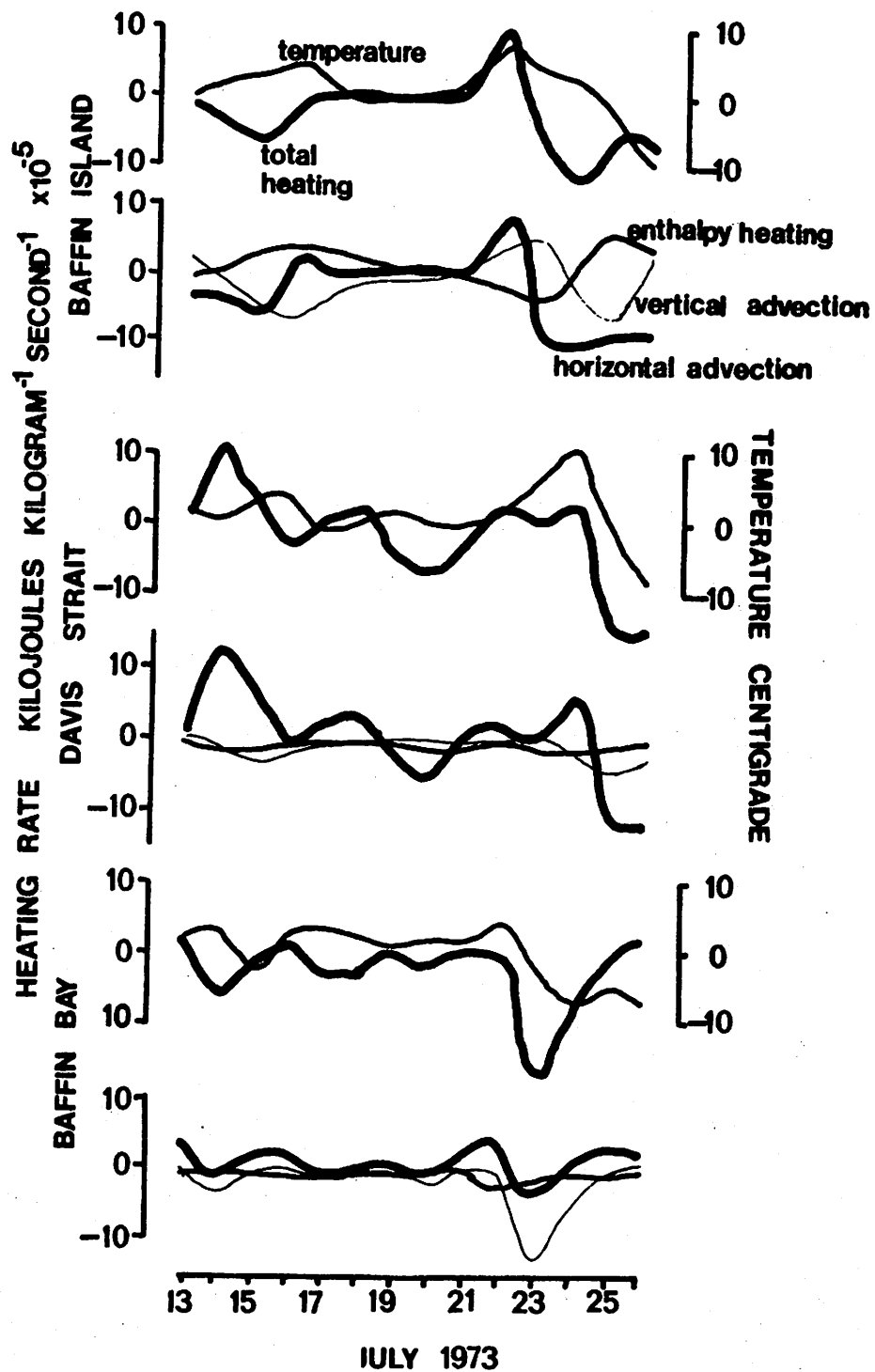
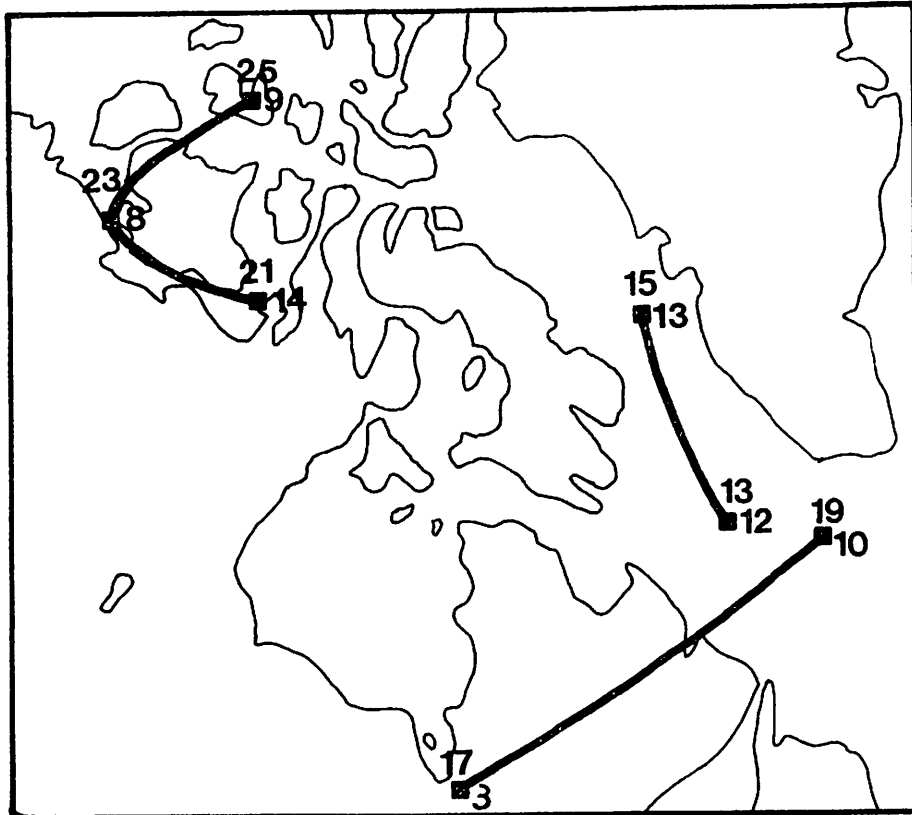


Figure 3.13. 85 CB HEATING RATES



19 DATE JULY 1973
 ■ 10 ADVECTIVE HEATING $\text{KJ KG}^{-1}\text{S}^{-1} \cdot 10^{-5}$

Figure 3.14. CENTERS OF ADVECTIVE HEATING AT 85 CB

B. Investigation of the Heat Island Effect of the West Greenland Current

As an energy source the warm West Greenland current has an influence both on the regional climate and the melt of adjacent ice surfaces. The magnitude of this "heat island" effect can be investigated by simulating the two-dimensional atmospheric circulation along a transect perpendicular to the current. The energy injected into the atmosphere through turbulent mixing over the water surface is advected downwind with the mesoscale flow and transported to the ice surface, again by turbulent mixing, where it is used for melt. We consider two experiments, each with a transect from ice to water to ice, and analyze the magnitudes and direction of the turbulent fluxes over the ice and water. In both experiments the ice surface is assumed to be in a melt stage with a temperature of 0°C . In experiment one the minimal heat island effect of the Greenland current is investigated by assigning a temperature excess of 1.3°C to the water. The maximum effect with an excess of 5.3°C is examined in experiment two.

An atmospheric stratification typical of the eastern Canadian Arctic at the beginning of summer melt (mid-June) is selected for initialization of the model (Table 3.2). The geostrophic flow is 10 m s^{-1} from the east, parallel to the transect and perpendicular to the current. The current width is specified to be 160 km (the minimum grid resolution of the model is 20 km).

Using a two-dimensional form of the sea breeze model of Pielke (1974) a meso-scale dry circulation is allowed to develop over the surfaces without a surface temperature perturbation for the first 21600 sec (6 hr). At this time the heat island is introduced by specifying a temperature excess with appropriate saturation specific humidity at the surface at all grid points over water. There is a transition from ice to warmer water to ice along the direction of flow. The circulation is allowed to respond to these revised boundary conditions up to 12 hr simulation time. With the prescribed velocity this allows time for a parcel of air to pass over the water surface to a point at least 256 km downwind over ice from the water-ice transition. At this location we have the danger of edge effects and the data are not considered for analysis. At 64000 sec (18 hr) the atmospheric structure is assumed to represent the regional climate modified by the heat island effect of the Greenland Current.

The turbulent fluxes for each grid point free from possible edge effects are presented in Table 3.3 for both experiments. These data were computed from the 18 hr profiles of wind, temperature and humidity between 25m and the surface using eddy diffusivity coefficients corrected for the atmospheric stability of this layer.

In experiment one the surface temperature excess of 1.3°C over the water is insufficient to reverse the common surface inversion and the enthalpy and latent heat fluxes are directed downwards representing an energy loss to the atmosphere at all grid points. Under inversion conditions the eddy diffusivity is very sensitive to wind shear since

mechanical turbulence dominates. The diffusivity is $2.8 \times 10^3 \text{ cm}^{-2} \text{ s}^{-1}$ over water, but increases to $3.2 \times 10^3 \text{ cm}^{-2} \text{ s}^{-1}$ over the downwind ice surface and this is reflected in the downwind increase in the fluxes. This increase is due to slight frictional convergence at the sea-ice transition. Velocity at 125m altitude over the current is 10.0 m s^{-1} compared with 9.9 m s^{-1} over the downwind ice.

⁻² Over the current the enthalpy flux varies from 0.8 to 1.2 mwatts cm^{-2} . Over the downwind ice it ranges from 3.1 to 2.8 mwatts cm^{-2} . The effect of this energy loss is a slight cooling at 25m. The change between 6 hr and 18 hr over the water averages -0.2°C over the 155 km fetch. Over the ice surface the average for 155 km downstream is -0.3°C , indicating the greater mechanical transport.

With the maximum heat island effect (experiment two) the impact upon the regional climate is more apparent (Table 3.3). As anticipated from the theory of air mass transformation, the greatest turbulent fluxes are immediately downwind of a surface transition where air - surface contrasts are great. The largest enthalpy loss is $-40.4 \text{ mwatts cm}^{-2}$, coupled with a latent heat loss of $-32.8 \text{ mwatts cm}^{-2}$ (which is equivalent to an evaporation rate of approximately 0.5 mm hr^{-1}). This is a significant source for precipitation. Although convergence zones are simulated by the model, the equations do not allow for precipitation in their present form.

The fluxes decrease in intensity with distance downstream (to the west) over the current as the air accumulates heat and water vapour and air-sea contrasts decrease. At 0 km (the downwind sea-ice interface) the maximum regional temperature modification occurs. There is a warming of 2.7°C at 25 m after an over-current trajectory of 155 km. The enthalpy flux is $-4.2 \text{ mwatts cm}^{-2}$ and the latent heat flux is similar, $-5.1 \text{ mwatts cm}^{-2}$.

This warming is advected downstream over the ice surface and transported to the surface to be used as melt. Under stable conditions, however, turbulent transfer is by mechanical mixing and is very inefficient. The heating at 25m accumulated during 155 km over water is dissipated only after a further 325 km over ice. The enthalpy flux is less than $4.0 \text{ mwatts cm}^{-2}$, approximately 1 mwatt cm^{-2} more than that calculated over the ice for a heat island of 1.3°C (experiment one). We may make the cautioned observation that the melt rate of ice surfaces is little affected by the magnitude of the regional climatic modification resulting from local advective energy import associated with oceanic advection.

Some features of this type of model are unrealistic and require further modification. Specifically, the consideration of surface temperature needs revision. Presently, one temperature is prescribed for sea and one for land. The transition is abrupt and the horizontal gradient over each surface is artificial. It would be more realistic to calculate the surface temperature for each grid point independently from energy balance considerations. The horizontal gradient over each

surface would then be a realistic response to the radiant and advective energy supply and demands.

Other points also need investigation. The land-sea friction differential apparently has an effect on mass convergence at the transition between the two surfaces which seems to affect the turbulent transfer processes downstream to a significant degree under stable conditions. The influence of various initial atmospheric stratifications on the extent of the heat island effect needs clarification, as does the influence of the moisture source on precipitation.

TABLE 3.2

ATMOSPHERE STRATIFICATION USED FOR INITIALIZATION OF TWO-DIMENSIONAL
SEA BREEZE MODEL IN THE EAST GREENLAND CURRENT
EXPERIMENT

Data are for 00 GMT, 2 July 1969, at Frobisher, N.W.T.

Geopotential Height (m)	Pressure (mb)	Potential Temperature (K)	Mixing Ratio (g kg ⁻¹)
0	1013	271.0	3.4
25	1010	273.9	4.0
125	1000	274.4	4.0
536	950	276.5	3.7
966	900	278.6	3.4
1417	850	280.5	3.0
1891	800	282.7	2.6
2392	750	286.5	2.4
2926	700	290.9	1.8
4698	600	295.9	0.9
5443	500	302.2	0.6
6500	450	305.8	0.5

TABLE 3.3
TURBULENT FLUXES OF ENTHALPY AND LATENT HEAT

Data are for grid points downstream (-distance) and upstream (+distance) from the transition from the west border of the Greenland Current to an ice surface. The upwind distance marked(*) at 184 km is an upwind transition to ice on the east border of the Greenland Current.

Fluxes were calculated from profiles of wind, temperature and humidity between the surface and 25m at 65000 seconds simulation time. The eddy-diffusivity coefficients were corrected for atmospheric stability.

Experiment One (Heat Island of 1.3° C)			Experiment Two (Heat Island of 5.3° C)	
Distance (km)	Enthalpy Flux	Latent Heat Flux	Enthalpy Flux	Latent Heat Flux
-256	2.84	1.92	3.68	2.44
-217	2.85	1.93	3.79	2.53
-184	2.86	1.94	3.88	2.60
-155	2.88	1.96	3.96	2.67
-129	2.90	1.98	4.01	2.73
-105	2.92	2.00	4.04	2.77
-82	2.95	2.03	4.01	2.77
-61	2.98	2.07	3.89	2.70
-40	3.03	2.12	3.52	2.47
-20	3.08	2.18	3.16	2.23
0	1.21	0.59	-4.20	-5.08
+20	1.19	0.57	-5.53	-5.94
+40	1.16	0.54	-7.05	-7.05
+61	1.13	0.51	-8.98	-8.53
+82	1.08	0.46	-11.6	-10.6
+105	1.03	0.40	-15.5	-13.6
+129	0.96	0.32	-22.3	-18.9
+155	0.87	0.18	-40.4	-32.8
+184	0.28	0.18	1.7	1.17
+217	0.28	0.18	1.7	1.17
+256	0.28	0.18	1.7	1.19

By convention an energy loss to the surface is negative.

REFERENCES

- Barry, R.G. 1974. Further Climatological Studies of Baffin Island
Island, Northwest Territories, Environment Canada, Inland
Waters Directorate, Tech. Bull., 65, 54 pp.
- Bradbury, D.L., Pedersen, K., Petterssen, S. 1962. The
Norwegian Cyclone Models in Relation to Heat and Cold
Sources, Geofys. Pub. 24: 243-280.
- Flohn, H. 1954. Witterung Und Klima in Mitteleuropa. Forsch.
Dt. Landeskunde 78, Stuttgart, 214 pp.
- Hare, F.K., Orvig, S. 1958. The Arctic Circulation, A
Preliminary Review, Arctic Meteorology Research Group,
Publication in Meteorology, no. 12, McGill University,
Montreal, 211 pp.
- Jacobs, J.D. 1974. Solar and Atmospheric Radiation Data For
Broughton Island, Eastern Canadian Arctic, Canada, 1971-73,
University of Colorado, Boulder, Instaar Occasional Paper
No. 11.
- Keegan, T.J. 1958. The Wintertime Circulation in the Arctic
Troposphere, in Contribution to the Study of the Arctic
Circulation, Sci. Rept. 7: 22-47, Arctic Meteorology Research
Group, McGill University.
- Krishnamurti, T.N. 1968. A Study of a Developing Wave Cyclone,
Mon. Weath. Rev., 96: 208-217.
- Namias, T.J. 1958. Synoptic and Climatological Problems
Associated With the General Circulation of the Arctic,
Trans. Amer. Geophys. Union, 39: 40-51
- Newton, C.W., Palmén, E. 1969. Atmospheric Circulation Systems,
Academic Press, New York, 603 pp.
- Pielke, R.A. 1974. A Comparison of Three-Dimensional and
Two-Dimensional Numerical Predictions of Sea Breese,
J. Atmos. Sci., 31: 1577-1585.
- Reed, R.J. 1958. Arctic Synoptic Analysis, in Contribution
to the Study of the Arctic Circulation, Arctic Meteorology
Research Group, McGill University, pp. 48-59.
- Reed, R.J., Tank, W.G. 1956. Miscellaneous Studies of Polar
Vortices, Sci. Rept. 1, Department of Meteorology and
Climatology, University of Washington, Seattle, 21 pp.

- Scherhag, R. 1957. The Role of Tropospheric Cold Air Poles and of Stratospheric High Pressure Centers in the Arctic Weather, in Polar Atmosphere Symposium, Part 1, Meteorology Section, R.C. Sutcliffe, (ed.), London, Pergamon Press.
- Stuart, D.W. 1970. Specifications of Meso-Scale Weather From Large-Scale Dynamical Calculations, Final report No. 70-5, Florida State University, pp. 1-79.
- Sutcliffe, R.C., Forsdyke, A.G. 1950. The Theory and Use of Upper Air Thickness Patterns in Forecasting, Q.J. Roy. Meteorol. Soc., 76: 194-217.
- Wagner, A.J. 1973. Weather and Circulation of July, 1973, Mon. Weath. Rev., 101: 777-782.
- Wilson, C.W. 1958. Synoptic Regimes in the Lower Arctic Troposphere During 1955, Sci. Rept. 6, Arctic Meteorol. Res. Group, McGill University, 100 pp.

4. ENERGY BUDGET STUDIES IN EASTERN BAFFIN ISLAND.

A. Radiation Climate of Broughton Island

J.D. Jacobs
(Geography Department
University of Windsor, Ontario)

Introduction

Accurate estimates of surface energy budgets in polar regions are of considerable importance both in relation to microscale and mesoscale events as well as in the more general context of surface boundary conditions in numerical modeling of macroscale and global atmospheric circulations (Committee on Polar Research, 1970; Schneider and Dickinson, 1974). Our work is concerned with surface energy budgets in eastern Baffin Island and adjacent Davis Strait, with particular attention being given the zone of shorefast ice, a feature common to many arctic regions. Measurements of radiation and of variables relating to turbulent exchange of heat and moisture were carried out on fast ice and at a shore station at Broughton Island, eastern Baffin Island, over a five year period. The general problem of energy budgets for the fast ice has been outlined elsewhere (Jacobs, Barry, and Weaver, 1975; Weaver, 1976). Emphasis here is on average characteristics of the radiation budget in summer.

Components of the Radiation Budget

The radiation budget at the surface, in its simplest form, may be expressed as

$$Q^* = K_{\downarrow} (1 - \alpha) + L_{\downarrow} - L_{\uparrow} \quad (4.1)$$

where Q^* is the net radiation, K_{\downarrow} the total incident solar flux, α is the surface albedo, L_{\downarrow} the atmospheric emittance, and L_{\uparrow} the terrestrial emittance¹. The total solar flux is the sum of the vertical component of the direct flux I and the diffuse flux D , or

$$K_{\downarrow} = I \cos \theta + D \quad (4.2)$$

where θ is the zenith angle at the sun.

Measurements of total solar radiation K_{\downarrow} and net radiation Q^* were

¹The notation used here is that recommended in the W.M.O. Guide to Meteorological Instruments and Practices (W.M.O., 1965). See also Latimer, 1972.

made at Broughton Island during the summers of 1971 through 1973, as well as in the fall and early winter of 1973. For part of the 1973 period, the atmospheric emittance L^\dagger and the direct solar flux I were also measured. Details of the measurement program and a summary of the data have been presented elsewhere (Jacobs, 1974). The present discussion is concerned with the interpretation of those results.

Solar Radiation

Clear sky conditions.

Various methods have been developed for estimating the total solar radiation at the surface. The diffuse component D is calculated as a function of the extraterrestrial flux and the amount of depletion and scattering taking place in the atmosphere. The latter may be given in the form of a single transmission coefficient (cf. List, 1968) or as a more complex function (cf. Davies, *et al.*, 1975; Hay, 1976).

In the present study direct solar radiation measured at the surface is compared with calculated values for the top of the atmosphere in order to determine the transmissivity of the atmosphere in our region. The direct flux was measured with an Eppley normal incidence pyrheliometer. Total short-wave radiation was measured continuously with an Eppley Model 2 pyranometer.

The relative transparency was first found in terms of the transmissivity q from the expression

$$I = I_0 (\bar{r}/r)^2 q^m \quad (4.3)$$

where I_0 is the solar constant, taken to be 1353 W m^{-2} (Thekaekara and Drummond, 1971), \bar{r}/r the ratio of the mean sun-earth distance to its instantaneous value, and m is the atmospheric mass which is approximated by $\sec \theta$ or, for large values of θ , by a formula given by Kondratyev (1969, p. 166).

As is generally the case in higher latitudes (Ångström, 1961), the atmosphere at Broughton Island is one of high transparency. Values of q derived from midday measurements are in the range 0.76 to 0.81 for the summer months (Fig. 4.1). On a few occasions, values less than 0.70 were measured. While some of these low values may have been due to cirrus clouds not visible from the ground, on other occasions there was obviously a reduction in visibility due to haze associated with strong advection from the south. Excluding such values (3 days out of 22), a mean value for q of 0.80 ($\sigma = 0.03$) was found for the period June through October, 1973.

The coefficient of transmissivity q is not entirely independent of the air mass m , and therefore, for large zenith angles is not a good measure of atmospheric transparency. Another parameter, the turbidity factor T of Linke (Robinson, 1966), is a more useful measure. T may be taken as equivalent to the number of atmospheres of pure air that produce the same

depletion as the actual atmosphere observed. For Broughton Island, the range of values for T was from 2.03 to 3.20 with a mean value of 2.50. There was a definite seasonal trend toward lower values in autumn and early winter. By comparison, Robinson (1966) has given values of 2.10 and 2.20 respectively, for maritime and continental arctic air.

A third measure of atmospheric transparency is Ångström's turbidity coefficient β , (Ångström, 1961; Robinson, 1966), which applies to that portion of the solar spectrum below $0.630 \mu\text{m}$ and is found by subtracting the flux measured using a Schott RG-2 filter from the total direct flux. β is a better measure of the scattering and absorbing effects of aerosols, dust, and haze than q or T because it emphasizes the longer wavelength portion of the spectrum where those effects are greatest. Values for β for the 1973 measurement period are shown in Fig. 4.1. The average June - August value for Broughton Island was 0.030, which is identical to the mean summer value for Devon Island reported by Holmgren (1971). A decrease in β and therefore in atmospheric aerosols in the autumn period is evident in the record.

Some degree of day-to-day variability was observed in atmospheric transparency, regardless of its method of calculation, with greater depletion occurring during periods of influence by southerly airflow, for example, in late June and again early in August (Fig 4.1). The Arctic Front, the mean summertime position of which is a few degrees south of this region (Barry, 1967), appears to be a boundary between air masses of quite contrasting transmissivity.

By subtracting the vertical component of the direct flux

$$S = I \cos \theta \quad (4.4)$$

from the total short-wave solar flux, measured simultaneously, the clear-sky diffuse flux D is obtained. Fig. 4.2 shows the ratio D/K_{\downarrow} as a function of the atmospheric air mass m . The general clarity of the arctic atmosphere is further indicated by the small amount of scattering of the solar beam.

Cloudy conditions.

Theoretical calculations of clear-sky flux show potentially high amounts of total radiation in summer (Fig. 4.3, solid curve). Actual measurements of K_{\downarrow} are considerably less as a consequence of frequent summer cloudiness. Table 4.1 shows the average cloud cover at Broughton Island and the average measured daily total short-wave radiation for the summer months, based on three years of observations (1971-73). During the three year period, between 50 and 70 percent of days had 8 tenths or more cloud cover. A comparison of potential clear-sky flux, estimated using the method given by List (1966), with the observed flux shows the latter to be 65 percent of the clear sky value. Using these measurements, a linear empirical relationship between total short-wave radiation and amount of cloud is obtained, or

$$K_{\downarrow} = K_{\downarrow}' (1 - k_s n) \quad (4.5)$$

Atmospheric Emissivity and Net Radiation

where K^+ is the potential clear-sky flux in the amount of cloud in tenths, and K_s a coefficient which was found to be 0.33. Average values of K^+ for various amounts of cloud in summer and winter (Nov. - Dec., 1973 only) are shown in Figure 4.4

The remaining terms of Equation 1 are the surface albedo α , and the terrestrial and atmospheric emissivities, L^+ and L^- . It is also possible to measure the net radiation Q^* directly, as was done in this study. Of these terms, α , L^+ and Q^* are unique to a particular surface, and results pertaining to the fast ice surface have been presented elsewhere (Weaver, 1976). As part of the discussion of the measurements at Broughton Island, however, both Q^* and L^+ are considered.

Net radiation Q^* was measured for three summers (1971-73) as well as in the autumn and early winter of 1973. The instrument used was a Fritschen-type net radiometer (Fritschen, 1963) mounted 4 metres above a dry tundra surface. Albedos of this surface ranged from 0.55 to about 0.90 when snowcovered and from 0.16 to 0.22 when snow-free.

The atmospheric emissivity L^+ was obtained from measurements of the total downward flux Q^+ using a pyr radiometer, where

$$L^+ = Q^+ - K^+ \quad (4.6)$$

Mean daily values of Q^* for the summer months are given in Table 4.1, and Fig. 4.4 shows average values of Q^* and L^+ as well as K^+ in relation to cloud amount. It is seen from this figure that the effect of cloud cover on the atmospheric emissivity is significant. As with solar flux in Equation 5, an empirical relationship between cloud amount and L^+ is suggested, with the effect of increasing cloud amount being positive, i.e.

$$L^+ = L^+ (1 + k_L^n) \quad (4.7)$$

The limited data suggest an average value for k_L of 0.26, with little difference between summer and winter.

Measurements of cloudbase radiant temperatures confirm the assumption often made that the atmospheric emissivity with low overcast conditions corresponds to that of a blackbody at the temperature of the cloudbase. For the PRT-5 radiometer with a 9.5 to 11.5 μ m bandpass, the contribution of water vapor to the emissivity is small. Given an instrumental error of $\pm 20^\circ K$, the blackbody emissivity calculated using Stefan's law agreed with measured values of L^+ within the limits of instrumental error.

Insofar as the total radiation balance is concerned, it is evident from Fig. 4.4 that for the tundra site where Q^* was measured, the increase in L^\downarrow with overcast conditions does not entirely offset the reduction in K^\downarrow . In other words, for this surface, as for other low albedo surfaces such as water, the absorbed solar radiation dominates the radiation budget in summer. In winter, on the other hand, when there is little or no solar radiation and the surface albedo is high, Q^* is almost entirely dependent on L^\downarrow , and the net surface cooling is substantially reduced during overcast periods.

A comparison was made between measured values of atmospheric emittance L^\uparrow and estimated based on the empirical equations of Swinbank (1961) and Idso and Jackson (1969). Both expressions appear to underestimate L^\uparrow , even when adjusted for cloud cover according to the method of Bolz (1949). The equations and results are shown in Table 4.2.

It is more likely that the measured values of L^\uparrow are excessive, particularly in the winter months. Apart from an experimental uncertainty of perhaps 15 per cent, the pyrradiometer may have been influenced by local conditions by virtue of its location on the roof of a heated building. Also, occasionally dense local concentrations of ice fog in the village in winter would have had some influence on atmospheric emittance in the vicinity. Actual values of L^\uparrow in winter would be expected to be generally less than the terrestrial emittance L^\uparrow , approximated in Table 4.2. as the blackbody flux corresponding to the mean 1.5 m screen temperature. These uncertainties point out the difficulty in trying to determine a small net longwave flux relative to the large absolute values of the terrestrial and atmospheric emittance.

As a further check on the measurements of the atmospheric emittance, the radiation budget (Equation 1) was used to find L^\uparrow as a residual, using measured values of Q^* and K^\downarrow , with estimated average albedos for the tundra site. As Table 2 indicates, the resulting values are less than those obtained from measurements but higher than the values given by either of the empirical formulas.

Discussion

The main features of the radiation climate of Broughton Island and, implicitly, of the eastern Baffin Island coastal environment may be summarized as follows. The relatively low arctic latitude (67.5 N for Broughton) means that the polar night is brief, less than a month. Even so, clear sky fluxes of total solar radiation fall below $0.20 \text{ kJ cm}^{-2} \text{ d}^{-1}$ by mid-October. Net radiation over the land becomes negative around the end of September and remains so until mid-May. While the atmospheric transmissivity is high, frequent cloudiness reduces the incoming solar flux by about one-third during the summer months. This is partly compensated by the relatively high atmospheric counter-radiation associated with overcast conditions.

It remains to compare conditions in the eastern Baffin Island region, where there is no long-term record of radiation measurements, with the data from other arctic locations. In terms of monthly averages for the 1973 measurement period, it can be seen from Table 4.3 that there are substantial differences among arctic stations, apart from latitudinal considerations. Differences in solar flux K_{\downarrow} should be explainable by differences in cloudiness, although this aspect has not been investigated. The variability in Q^* is perhaps not as large as might be expected, since this term is determined in part by surface conditions which differ among the various stations. The relative differences in Q^* during the autumn and winter months, when all surfaces are likely to be snow-covered, are large, however. Variations in cloud cover as it affects L_{\downarrow} might explain these differences in part, but measurement errors are probably more important.

The differences for individual months are smoothed out in the long-term record. Table 4.4 is a comparison of the average of three years of measurements of K and Q^* for July at Broughton Island with values interpolated for the area from presented by Hare and Hay (1974), which are based in part on data from the radiation station network of the Atmospheric Environment Service. The averages agree closely with the regional means; however, it is clear that significant year-to-year differences occur due to varying frequencies of cloud cover and, in the case of Q^* , in the amount and duration of the spring snowcover. This fact, coupled with the high degree of variability between stations as indicated in Table 4.2 suggests that climatological means of the radiation balance components should be used with caution. For many applications, it will be necessary to base estimates of radiation terms on synoptic data (clouds, temperatures) and surface conditions (c.f. Vowinckel and Orvig, 1969; Moritz, Section 4B).

TABLE 4.1

Percentage of days in each cloud cover class (tenths) and mean daily totals of total short-wave and net radiation ($\text{kJ cm}^{-2} \text{ d}^{-1}$) for Broughton Island, summers 1971-73.

	0 - 2	3 - 7	8 - 10	K↓	Q*
June	15	14	71	2.38	1.03
July	25	13	62	1.85	0.95
August	24	12	64	1.33	0.57

TABLE 4.2

Comparison of Measured Values of Atmospheric Emittance $L\downarrow$ with estimates using empirical formulas. Broughton Island, 1973.
(Flux values are monthly means of daily totals in $\text{kJ cm}^{-2} \text{d}^{-1}$.)

Month	Measured ¹	Idso & Jackson ²	Swinbank ³	Radiation Balance ⁴	Blackbody Flux ⁵
June	ND	2.29	2.18	2.28	2.84
July	ND	2.28	2.18	2.41	2.77
August	2.87	2.34	2.26	2.70	3.09
September	2.66	2.24	2.11	2.51	2.84
October	2.46	1.96	1.74	2.39	2.68
November	2.50	2.07	1.80	2.38	2.49
December	2.20	1.72	1.32	1.95	2.13

1. The difference between the total downward solar and atmospheric radiation as measured by a pyrradiometer and the total downward solar radiation measured with a pyranometer.
2. Idso and Jackson, 1969.

$$L\downarrow = \sigma T^4 (1 - 0.261 \exp(-7.77 \times 10^{-4} (273 - T)^2))$$

where T is the screen temperature in $^{\circ}\text{K}$, and σ is Stefan's constant = $5.70 \times 10^{-8} \text{ W m}^{-2} \text{ K}^{-4}$.

The resulting values for $L\downarrow$ were adjusted for cloud cover n using the equation of Bolz (1949):

$$L\downarrow_{(c)} = L\downarrow (1 + k_L n^2)$$

where n is the cloud cover in tenths and k_L a coefficient that depends on cloud type, taken here to be 0.20.

3. Swinbank, 1961.

$$L\downarrow = 5.31 \times 10^{-13} T^6 \quad (\text{W m}^{-2})$$

with the same adjustment for cloud cover.

4. $L\downarrow$ is found as the residual in the radiation balance equation

$$L\downarrow = Q^* - K\downarrow (1 - \alpha) + L\uparrow$$

where Q^* and $K\downarrow$ are measured, $L\uparrow$ estimated as the blackbody flux corresponding to the mean daily screen temperature, and the surface albedo α taken as representative for the given month based on occasional measurements.

5. The blackbody flux corresponding to the monthly mean of daily mean screen temperature.

TABLE 4.3

Mean daily flux of global ($K\downarrow$) and net (Q^*) radiation at Broughton Island compared with other Arctic stations^a, June - December, 1973. Units are $\text{kJ cm}^{-2} \text{ day}^{-1}$.

Station		K+										Q*					
Latitude	J	J	A	S	O	N	D	J	J	A	S	O	N	D			
Fort Chimo 58°06'N	2.01	1.44	1.44	0.72	0.43	0.19	0.11	←-----	Not Measured	Not Measured	Not Measured	-----	-----	-----			
Frobisher Bay 63°45'N	1.89	1.28	1.44	0.67	0.33	0.09	0.04	1.18	0.79	0.66	0.28	-0.06	-0.18	-0.25			
Broughton Island 67°34'N	2.44	1.65	1.25	0.66	0.28	0.03	0.02	0.68	0.84	0.54	0.16	-0.15	-0.09	-0.18			
Hall Beach 18°47'N	2.85	2.09	1.48	0.58	0.23	0.04	0	←-----	Not Measured	Not Measured	Not Measured	-----	-----	-----			
Resolute 74°43'N	2.23	1.63	1.04	0.49	0.10	0	0	1.14	0.87	0.48	0.01	-0.12	-0.14	-0.21			
Eureka 80°00'N	2.20	1.60	0.82	0.39	0.04	0	0	1.29	0.94	0.47	-0.09	-0.10	-0.18	-0.17			
Alert 82°30'N	2.25	1.72	0.74	0.35	0.02	0	0	0.41	1.04	0.41	-0.11	-0.12	-0.15	-0.12			

^aData for all stations except Broughton Island are from the Atmospheric Environment Service, Monthly Radiation Summary.

TABLE 4.4

Measured and Estimated July Values of Radiation Terms
for the Broughton Island Area

Measurements at Broughton	K↓	Q* (kJ cm ⁻² d ⁻¹)
1971	1.86	0.98
1972	2.03	1.03
1973	1.65	0.84
Average	1.85	0.95
Regional Means (Hare and Hay, 1974)	1.88	0.94

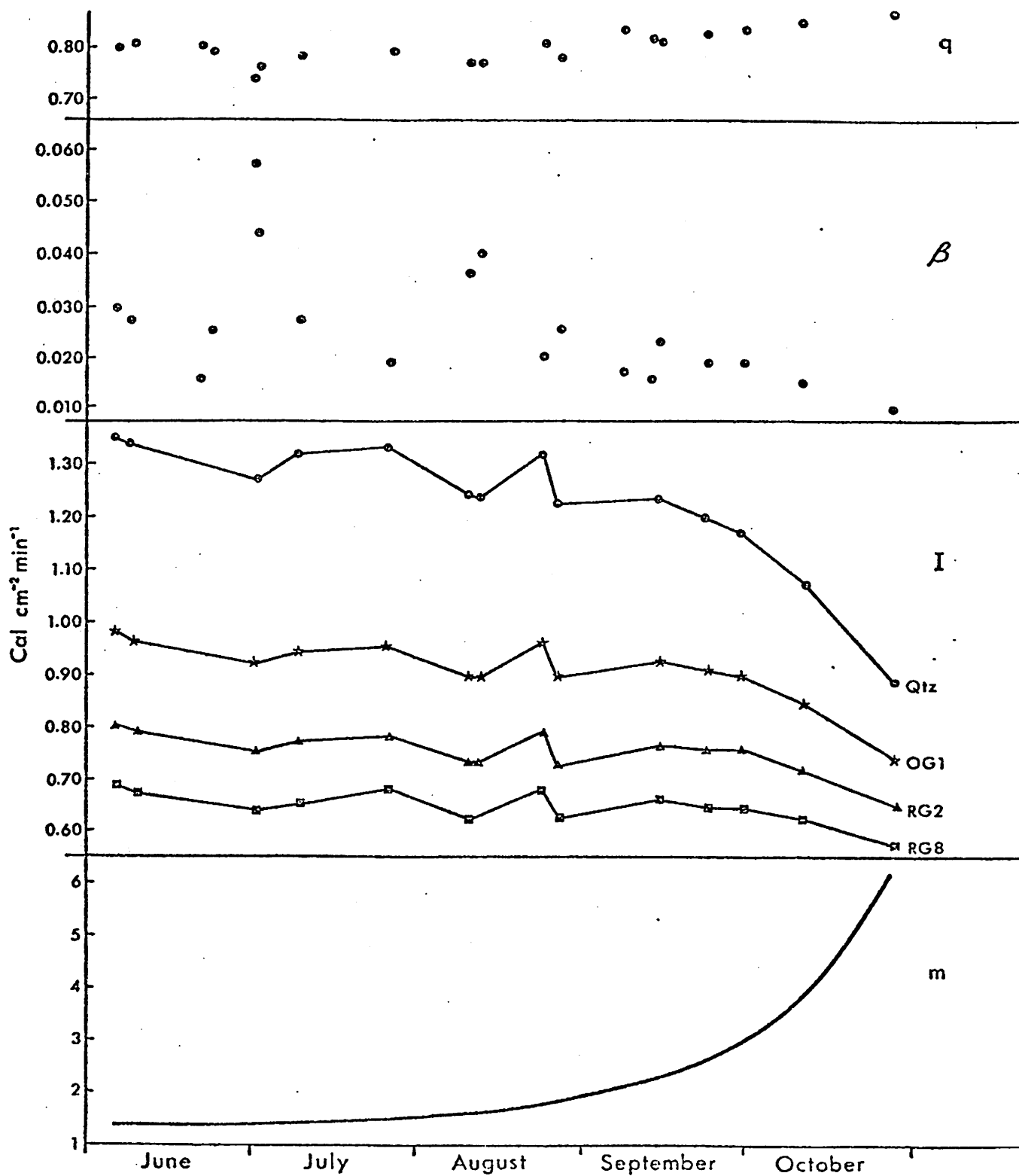


Figure 4.1 Clear day measurements of direct solar flux and derived transmission coefficients, Broughton Island, 1973. I is the measured flux using no filter (QTZ), and the Schott filter series (OG-1, RG-2, RG-8), m is the atmospheric mass ($\text{m} \cdot \text{sec}^{-1}$), q the coefficient of transmissivity, and β the Ångström turbidity coefficient.

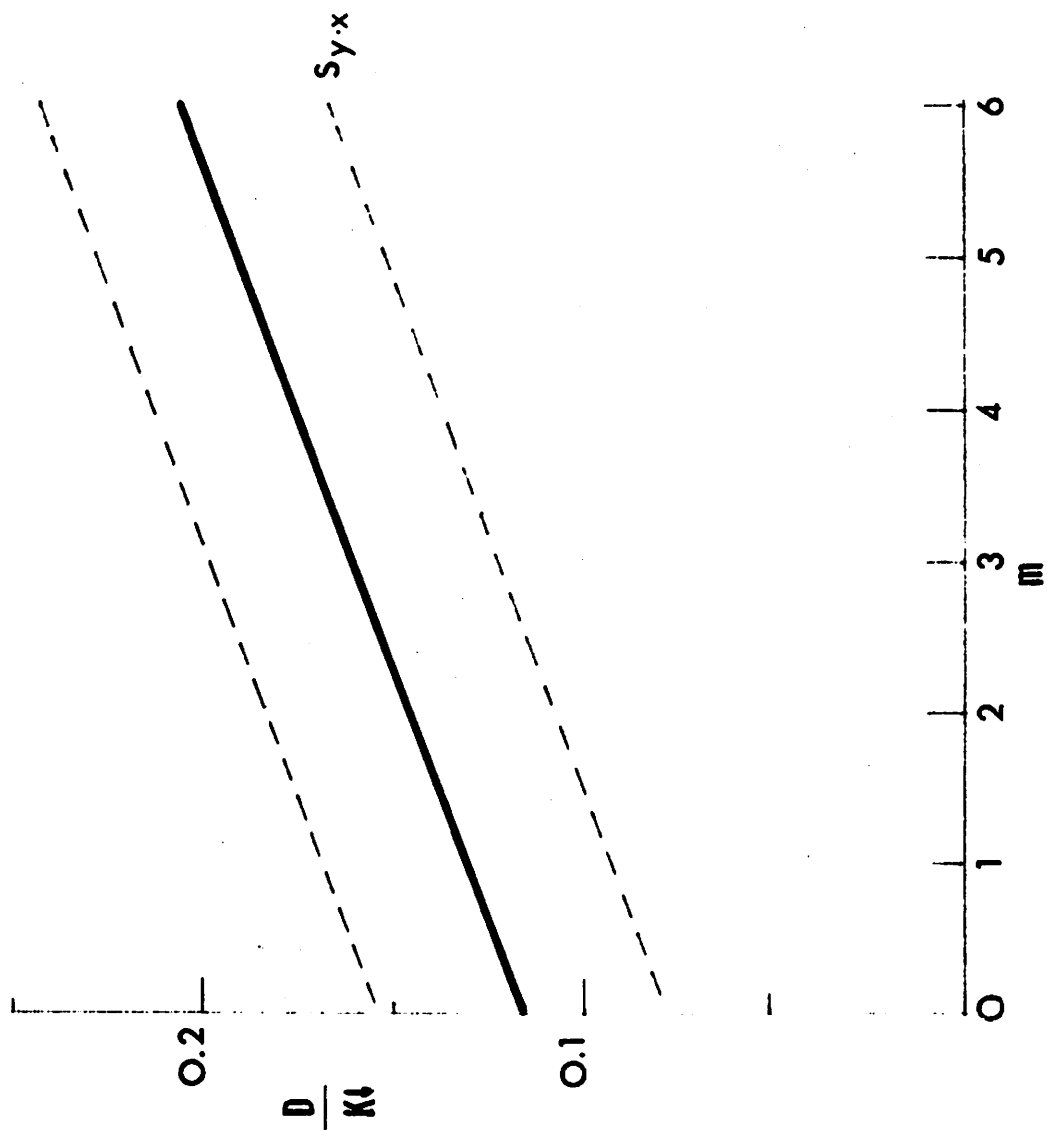


Figure 4.2

Ratio of the diffuse (D) to the total solar flux (K_t) for clear days as a function of atmospheric mass (m), Broughton Island, 1973. The solid line is the regression line and the dashed lines corresponds to the standard error.

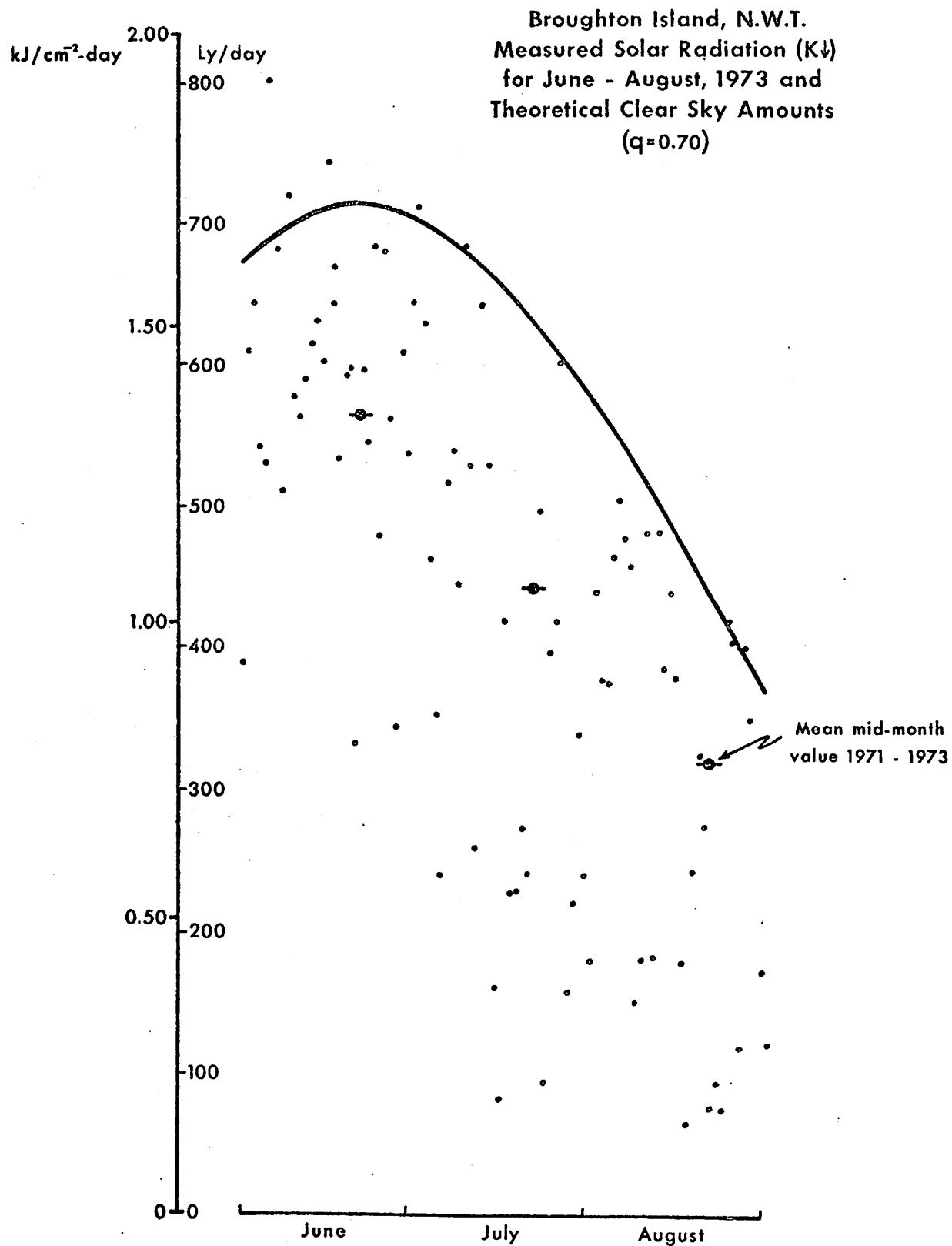
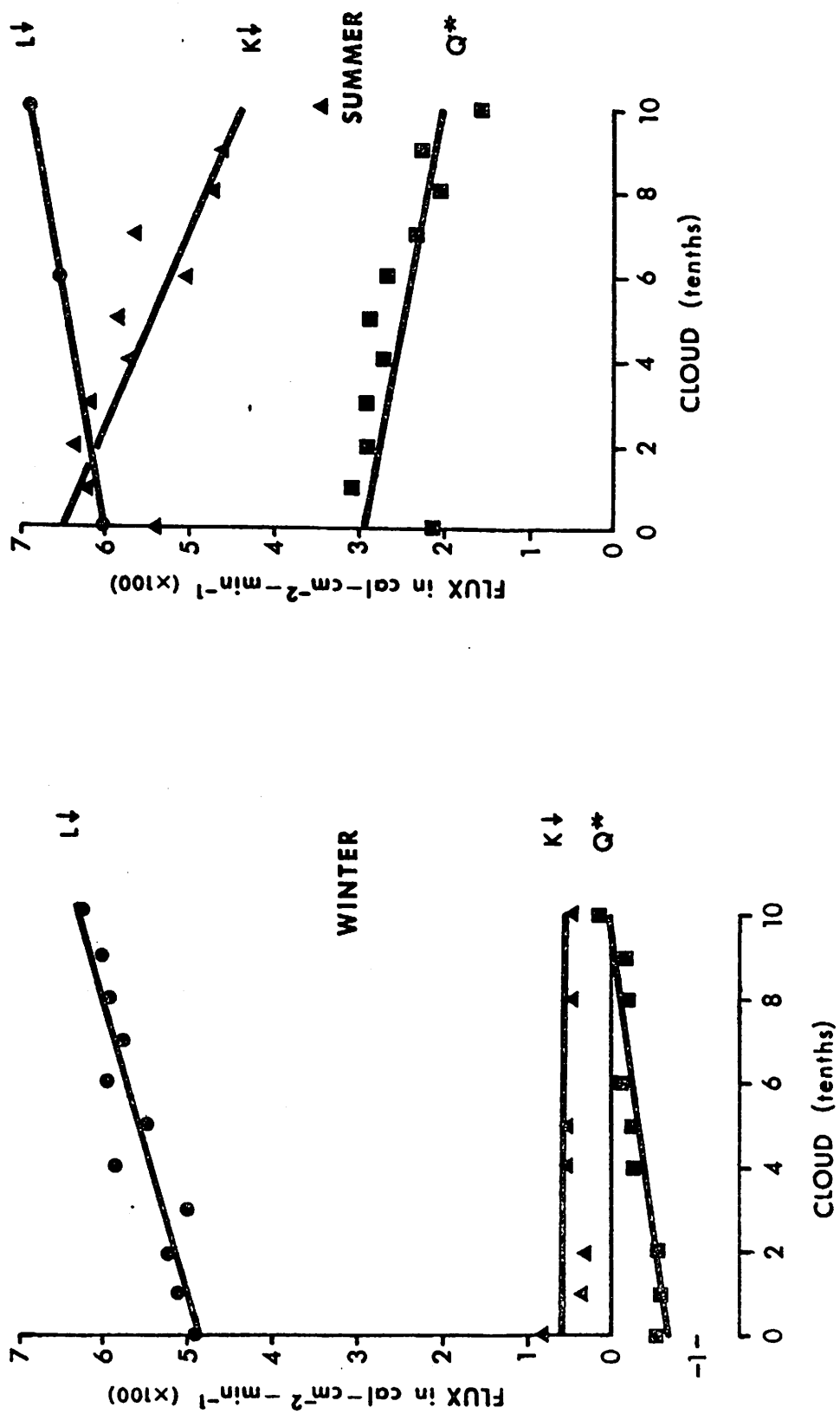


Figure 4.3



Observed effects of cloud cover on radiation budget terms at Broughton Island.

Figure 4.4

REFERENCES

- Ångström, A. 1961. Techniques of determining the turbidity of the atmosphere. Tellus, 13: 214-223.
- Barry, R.G. 1967. Seasonal location of the Arctic Front over North America. Geograph. Bull., 9: 79-95.
- Bolz, H.M. 1949. Die Abhängigkeit der infraroten Gegenstrahlung von der Bewölkung. Zeit. f. Meteor., 3: 201-203.
- Borisenkov, E.P. and Treshnikov, A.F. 1971. The Polar Experiment. Prob. Ark.i Antark., 38: 8-13.
- Committee on Polar Research, 1970. Polar Research: A Survey, National Academy of Sciences, Washington, 204 pp.
- Davies, J.A., Schertzer, W. and Nunez, M. 1975. Estimating global solar radiation. Bound Layer Meteor., 9: 33-52.
- Fritschen, L.J. 1963. Construction and evaluation of a miniature net radiometer. J. Appl. Meteor., 2: 165-172.
- Hare, F.K. and Hay, J.E. 1974. The Climate of Canada and Alaska. In: Bryson, R. and Hare, F. (eds.) World Survey of Climatology, Vol. II, Elsevier, Amsterdam, pp 49-192.
- Hay, J.E. 1976. A revised method for determining the direct and diffuse components of the total short-wave radiation. Atmosphere, 14: 278-287.
- Holmgren, B. 1971. Climate and energy exchange on a sub-polar ice-cap in summer. Arctic Inst. of North America Devon Island Expedition 1961-63. Madelanden fran Uppsala Universitets Meteorologiska Institutionen, Nos. 107-112.
- Holmgren, B., Shaw, G. and Weller, G. 1974. Turbidity in the Arctic Atmosphere. Aidjex Bull. No. 27: 135-148, Div. Marine Science, University of Washington, Seattle.
- Idso, S.B. and Jackson, R.D. 1969. Thermal radiation from the atmosphere. J. Geophys. Res., 74: 5397-5403.
- Jacobs, J.D. 1974. Solar and Atmospheric Radiation Data for Broughton Island, Eastern Baffin Island, Canada, 1971-1973. University of Colorado, Boulder, Inst. Arct. and Alp. Res., Occas. Paper No. 11, 15 pp and tables.
- Jacobs, J.D., Barry, R.G., Weaver, R.L. 1975. Fast Ice Characteristics with special reference to the eastern Canadian Arctic. Polar Record, 17, 521-536.

- Kondratyev, K. Ya. 1969. Radiation in the Atmosphere, New York, Academic Press, 912 pp.
- Latimer, J.R. 1972. Radiation Measurement: Tech. Man. No. 2, Int. Year for the Great Lakes, National Research Council of Canada, Ottawa, 54 pp.
- List, R.J. 1949. Smithsonian Meteorological Tables, 6th ed., Washington, Smithsonian Institution, 527 pp.
- Moritz, R.E. 1978. Synoptic climatology of the Beaufort Sea coast, Alaska. Unpub. M.A. thesis, University of Colorado, Boulder.
- Müller, F., Ohmura, and Braithwaite, R. 1973. The North Water Project (Canadian-Greenland Arctic). Geographica Helvetia, No. 2: 111-117. (Reprinted in Polar Geography, 1 (1977): 75-85.)
- Robinson, N. 1966. Solar Radiation, Amsterdam, Elsevier, 347 pp.
- Schneider, S.H. and Dickinson, R.E. 1974. Climate Modeling. Rev. Geophys. and Space Phys., 12: 447-493.
- Swinbank, H. 1961. Longwave radiation from clear skies. Quar. J. Roy. Meteor. Soc., 89: 339-348.
- Thekaekara, M.P. and Drummond, A.J. 1971. Standard values for the solar constant and its spectral components. Nature Phys. Sci., 229: 6-9.
- Vowinckel, E. and Orvig, S. 1966. Energy balance of the Arctic: V. The heat balance of the Arctic Ocean. Arch. Meteor. Geophys Biokl., 14: 305-325.
- Vowinckel, E. and Orvig, S. 1969. Climatic change over the Polar Ocean. II: A method for calculating synoptic energy budgets. Arch. Met., Geophys., Biokl., B, 17: 121-146.
- Weaver, R.L. 1976. Aspects of the Radiation Budget Related to Fast Ice Decay, Broughton Island, Baffin Island, N.W.T. Unpublished M.Sc. thesis, University of Colorado, Boulder, 159 pp.

B. A MODEL FOR ESTIMATING GLOBAL SOLAR RADIATION

R.E. Moritz

Department of Geology & Geophysics
Yale University, New Haven

Introduction

The direct (Q) and diffuse (q) solar radiation reaching the earth's surface at a given time and place depends on the solar constant, atmospheric path length, atmospheric 'turbidity', and cloudiness. Although most climatological formulae for calculating ($Q + q$) rely on monthly means of regional cloudiness, Lumb, (1964) shows that the net effect of all the variables may be parameterized within $\pm 10\%$ of observed values for five-day radiation totals. The formula takes the form

$$(Q + q) = Q_0 (as + bs^2) \quad (4B.1)$$

where Q_0 is the solar constant (135.3 W m^{-2}), s is the mean of the sines of the solar elevation angle at the beginning and end of the hour, and a and b are empirical constants. The constants were determined by a least-squares regression for each of nine categories of cloudiness. Although the functions were derived from data taken at $52^\circ 30'$ N lat. in the Atlantic, a comparison of predicted and observed values at stations further north showed good agreement, and no systematic variation with latitude was detected. Thus Lumb concluded that the functions were applicable between 45° and 65° in that region. These relations yielded reasonable approximations for ($Q + q$) on Baffin Island (Jacobs, *et al.*, 1972), but it is desirable to recalculate the constants a and b for our area for three reasons. First, the transmissive properties of the atmosphere may vary more with location for a given cloudiness, than between cloud-types for a given place (Vowinckel and Orvig, 1962). Second, the added complexity of multiple reflections between the surface and cloud-base is more effective in ice-infested regions such as the Baffin Island coast, causing higher values for the (q) term (Loewe, 1963; Catchpole and Moody, 1971). Third, the thickness, and, hence, the opacity of, Arctic cloud increases during the warm season, due to high moisture content when open water surfaces are available (Vowinckel and Orvig, 1962). Thus constants derived for the ablation season only should serve us better than those derived for year-round conditions.

In this study, empirical formulae for estimating Q from a knowledge of cloud characteristics are developed. It was desired to obtain equations applicable to the eastern Canadian Arctic, particularly for areas of seasonal pack ice and shorefast ice. The density of coastal

stations in the region is very low and continuous meteorological observations on the sea ice are virtually non-existent. Yet, in order to assess variations in Q associated with synoptic circulation systems, data must be available over areas the size of Baffin Bay and Davis Strait. Furthermore, the temporal frequency of observations must be at least daily, preferably higher. Only meteorological satellite data can meet these requirements. Lumb's cloud categories are dependent on observations of cloud-element morphology and the precipitation characteristics of the cloud, in addition to cloud heights and amounts. The former traits are generally not readily discerned from satellite imagery, but synoptic-scale opacity and cloud heights are identifiable (Anderson, et. al., 1974; Barrett, 1974).

Data and Methods

The cloud information was extracted from microfilm copies of the Atmospheric Environment Service's Surface Weather Record report forms for Hall Beach 'A', June, July and August, 1973. This form lists the hourly (GMT) total opacity, the opacity of each layer of cloud, and the type of cloud comprising the layer. The measured hourly (LAT) totals of global solar radiation were taken from the Monthly Radiation Summary for the corresponding months (Atmospheric Environment Service, 1973). These measurements were made with an Eppley model 2 spectral pyranometer, a temperature-compensated instrument with a nominal error of less than 3% of the measured flux (Latimer, 1972). The cosine of the sun's zenith angle was computed for each hour (GMT) according to the formula:

$$\cos \zeta = \sin \phi \sin \delta + \cos \phi \cos \delta \cos \tau \quad (4B.2)$$

where ϕ is the latitude of the site, δ is the declination of the sun, and τ is the hour angle of the sun (Sellers, 1965). The hour GMT falls within 5 minutes of the middle of the corresponding hour LAT at Hall Beach, so that $\cos \zeta$ and the cloud report can be considered as representative of mean conditions for the hour over which the radiation was measured.

The cloud reports were grouped into 12 types based on the total opacity of the sky and the height category of the layer with the highest opacity (Table 4B.1). Height categories were assigned on the basis of the observer's description. Cloud names with no prefix were classed as low (C_L), with the prefix "alto" as medium (C_M), and with the prefix "cirro" as high (C_H). When more than one level of a single height category was reported, the opacities in each category were summed. In cases where the categories with the highest opacities had equal opacities, the cloud was classed with the lower category.

The radiation incident on a unit area parallel to the earth's surface at the mean earth-sun distance (extra-terrestrial radiation) is:

$$ETR = Q_0 \cos \zeta \quad (4B.3)$$

when the relatively small variations in solar output and the eccentricity

of the earth's orbit are neglected. Of this amount, some is absorbed or scattered upward by atmospheric constituents, a part is reflected out of the atmosphere by clouds, and the remainder Q reached the earth's surface as direct and diffuse global solar radiation. The fractional transmittance of the atmosphere can then be defined as:

$$f = Q/Q_0 \cos \zeta \quad (4B.4)$$

Although scattering and absorption are not negligible processes, their space and time variations are usually much less important in determining Q than are the cloudiness and solar altitude $(\pi/2 - \zeta)$ (Kondratyev, 1969, p. 457). In the present study, f was computed for each hourly observation during the summer, 1973, and grouped with $\cos \zeta$, according to the 12 cloud categories in Table 4B.1. For each of these categories, the dependence of f on $\cos \zeta$ was evaluated by least-squares regression, such that:

$$f = \alpha + \beta \cos \zeta \quad (4B.5)$$

characterizing the fractional transmittance of each category as a linear function of $\cos \zeta$. This method was also employed by Lumb (1964). It was hoped that by allowing f to vary directly with $\cos \zeta$, the model could account for variations in transmittance due to the changing path length traversed by the direct solar beam at various zenith angles. The formulae, their standard errors of the estimate, and the number of $(f, \cos \zeta)$ pairs in each sample are set out opposite the corresponding cloud categories in Table 4B.1. Scattergrams of Q and $\cos \zeta$ are shown in Figures 4B.1-12. It will be noted that:

$$f = Q/Q_0 \cos \zeta = \alpha + \beta \cos \zeta \quad (4B.6)$$

and, multiplying the second equality by $Q_0 \cos \zeta$:

$$Q^* = Q_0 (\alpha \cos \zeta + \beta \cos^2 \zeta) \quad (4B.7)$$

where Q^* is the predicted hourly global solar radiation. Q^* is plotted as a smooth curve on Figs. 4B.1-12 according to equation 4B.7).

Model Performance and Errors

Considerable scatter is seen on the graphs for types 3 and 8. These categories represent large amounts of C_L and comprise nearly 30% of the sample analyzed. Thus they should figure prominently in any calculations of average radiation fluxes. It is believed that the scatter is due in part to the variations in cloud cover and thickness occurring in layers above the ceiling height and not observable from the surface. Also, inaccuracies will arise through the grouping of different morphological cloud types into a single category on the basis of a height classification only.

As a test on the accuracy of the model for predicting radiation fluxes at a point, based on station data, Q^* was calculated according

to the 12 equations 4B.6 for the period June 1 - July 10, 1974, again using Hall Beach data. These hourly values were then compared with observed amounts Q for the same period. The root-mean-square error ϵ , given by

$$\epsilon = \left(\frac{\sum (Q - Q^*)^2}{n - 1} \right)^{1/2} \quad (4B.8)$$

was computed for hourly, daily, two-day, three-day, and weekly average radiation totals. The results in Figure 4B.13 show that the model is accurate to $+33.9 \text{ Wm}^{-2}$ (12% of the mean daily total for this sample) when used to obtain means for 2-day or longer periods.

The effects of cloud on model performance were evaluated by computing the ratio Q^*/Q for the hourly values and finding its mean and standard deviation for cloud categories with less than 2/10 opacity, 2/10 - 5/10 opacity, and greater than 5/10 opacity. Figure 4B.14 indicates that the mean ratio exceeds unity by increasing amounts as the opacity increases. A possible explanation is that the scatter in Figs. 4B.3 and 4B.8 represent the existence of at least two families of data pairs, all recorded by a surface observer as "greater than 5/10 total opacity, mainly C_L ". Two such families might consist of cases involving thin fog or stratus of local origin on the one hand, and thick multilayered frontal or cyclonic system cloud on the other. The largest daily errors in the 1974 sample were caused by model overestimation, occurring on June 26 - 30. Ninety out of the 120 cloud observations during this period were types 3 and 8. The region was dominated at this time by an intense low pressure system and frontal cloud, with its center just west of Hall Beach on June 26. Defense Meteorological Satellite Program visible-channel satellite imagery for June 26, (Vehicle S, orbit 1446) confirms that multilayered frontal cloud was dominating the area. However, a preliminary analysis of the synoptic charts for days with mostly types 3 and 8 during 1973 showed no persistent association of either anomalously high or low values of 'f' with given circulation types. The increasingly large standard deviations associated with greater opacities in Figure 4B.14 serves to emphasize the weaknesses involved in using a surface observation to describe conditions throughout the depth of the atmosphere. Although a large error can be expected for any given hourly radiation flux for cloudy conditions, some of these errors cancel as the time-averaging interval is extended, as indicated in Figure 4B.13.

In order to apply the model on a broad spatial scale, cloud opacity and height categories must be mapped from visible and infrared satellite imagery. By assigning average opacities and heights to these maps, average radiation fluxes over areas greater than 4000 km^2 can be estimated. Some of the high frequency errors associated with point measurements might be reduced by this procedure, although the total error would likely increase. This increase would derive from high-level masking of lower clouds when viewed from space and any site peculiarities associated with the Hall Beach location. No known network of radiation stations is presently dense enough to allow the estimation of synoptic-scale average fluxes for periods of days or weeks,

hence a direct check on the accuracy of the space-extrapolation of the model is not forthcoming. In the absence of any other source of data, however, it is believed that this model can provide useful estimates of the differences in the space and time distribution of solar radiation associated with synoptic circulation systems in the Eastern Canadian Arctic.

Summary and Conclusions

Equations have been developed for estimating the global solar radiation in the eastern Canadian Arctic from cloudiness data. Despite large errors in hourly totals, 2-day means can be estimated from station data with a rms error of $\pm 33.9 \text{ Wm}^{-2}$, which is 12% of the mean daily amount for the period sampled. The cloud categories are arranged so that the model may be applied to synoptic maps of cloud opacities and height categories prepared from satellite imagery.

TABLE 4B.1

Cloud categories and statistical data for Hall Beach analysis.

<u>Category</u>	<u>Description</u>	<u>n</u>	<u>f</u>	<u>SE EST</u>
1	Total opacity less than 2/10	366	$.47 + .47\cos\zeta$.07
2	Single level C_L , Total Opac. 2-5/10	20	$.46 + .40\cos\zeta$.14
3	Single level C_L , Total Opac. 6-10/10	290	$.16 + .35\cos\zeta$.14
4	Single level C_M , Total Opac. 2-5/10	17	$.56 + .04\cos\zeta$.16
5	Single level C_M , Total Opac. 6-10/10	10	$.08 + .75\cos\zeta$.15
6	Single level C_H , Total Opac. 2-5/10	53	$.47 + .46\cos\zeta$.09
7	Multilevel, C_L , Total Opac. 2-5/10	135	$.38 + .60\cos\zeta$.12
8	Multilevel, C_L , Total Opac. 6-10/10	183	$.20 + .47\cos\zeta$.15
9	Multilevel, C_M , Total Opac. 2-5/10	93	$.43 + .48\cos\zeta$.10
10	Multilevel, C_M , Total Opac. 6-10/10	64	$.24 + .56\cos\zeta$.14
11	Multilevel, C_H , Total Opac. 2-5/10	98	$.41 + .55\cos\zeta$.10
12	Multilevel, C_H , Total Opac. 6-10/10	32	$.29 + .55\cos\zeta$.11

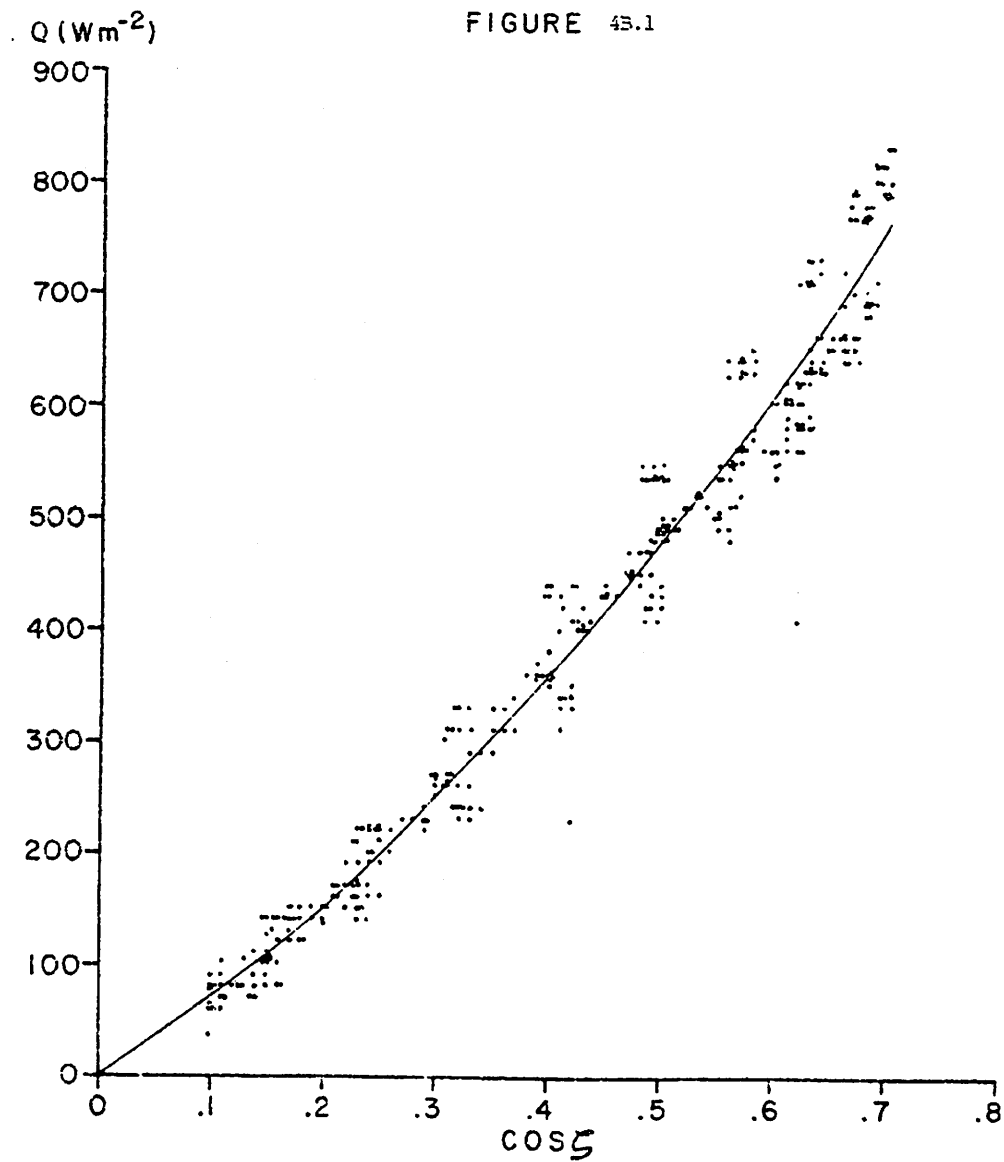


Fig. 4B. 1. Hourly global solar radiation versus $\cos \zeta$ for total opacity 2/10

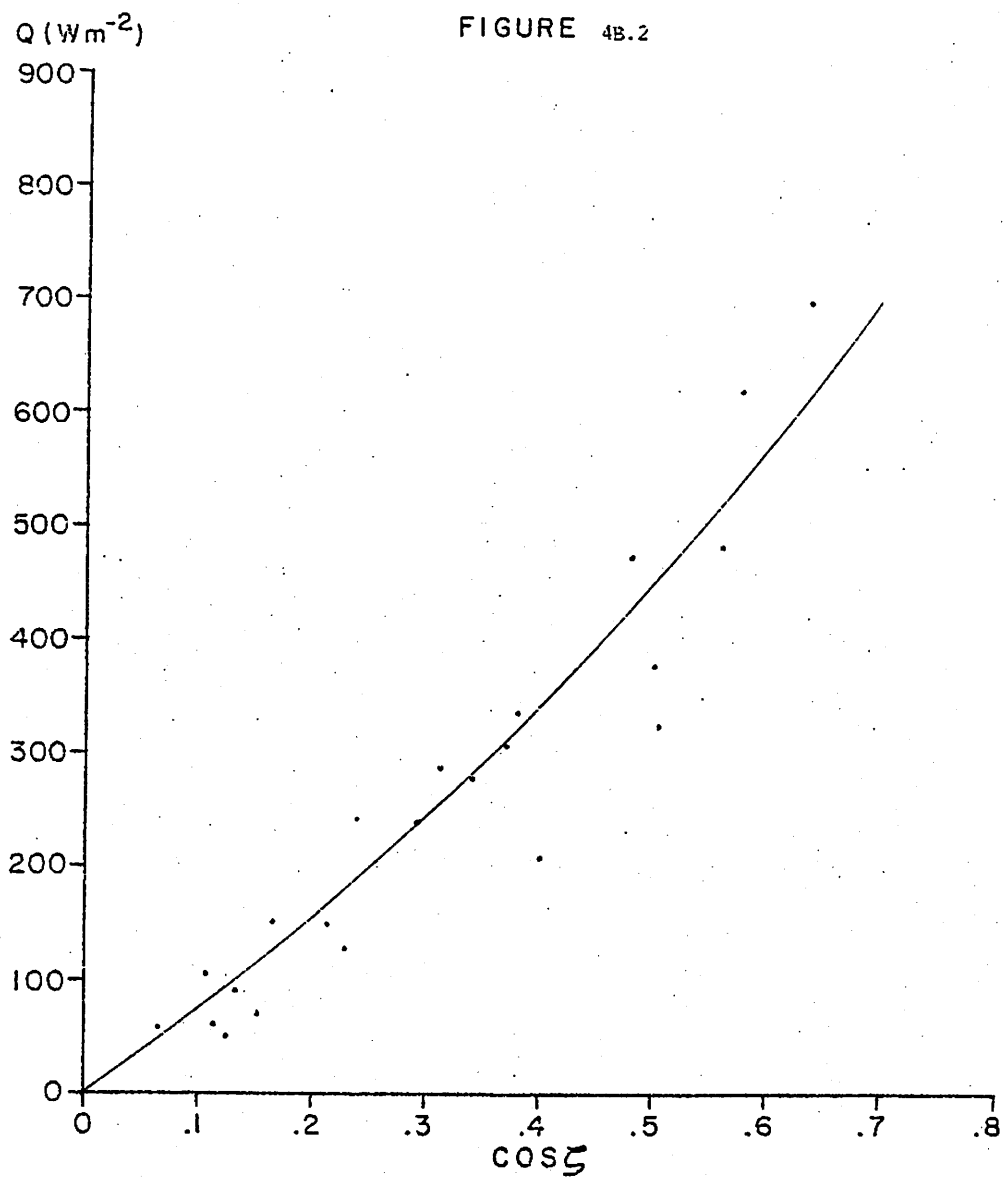


Figure 4B. 2. Hourly global solar radiation versus $\cos \zeta$, for single level C_L , total opacity 2-5/10

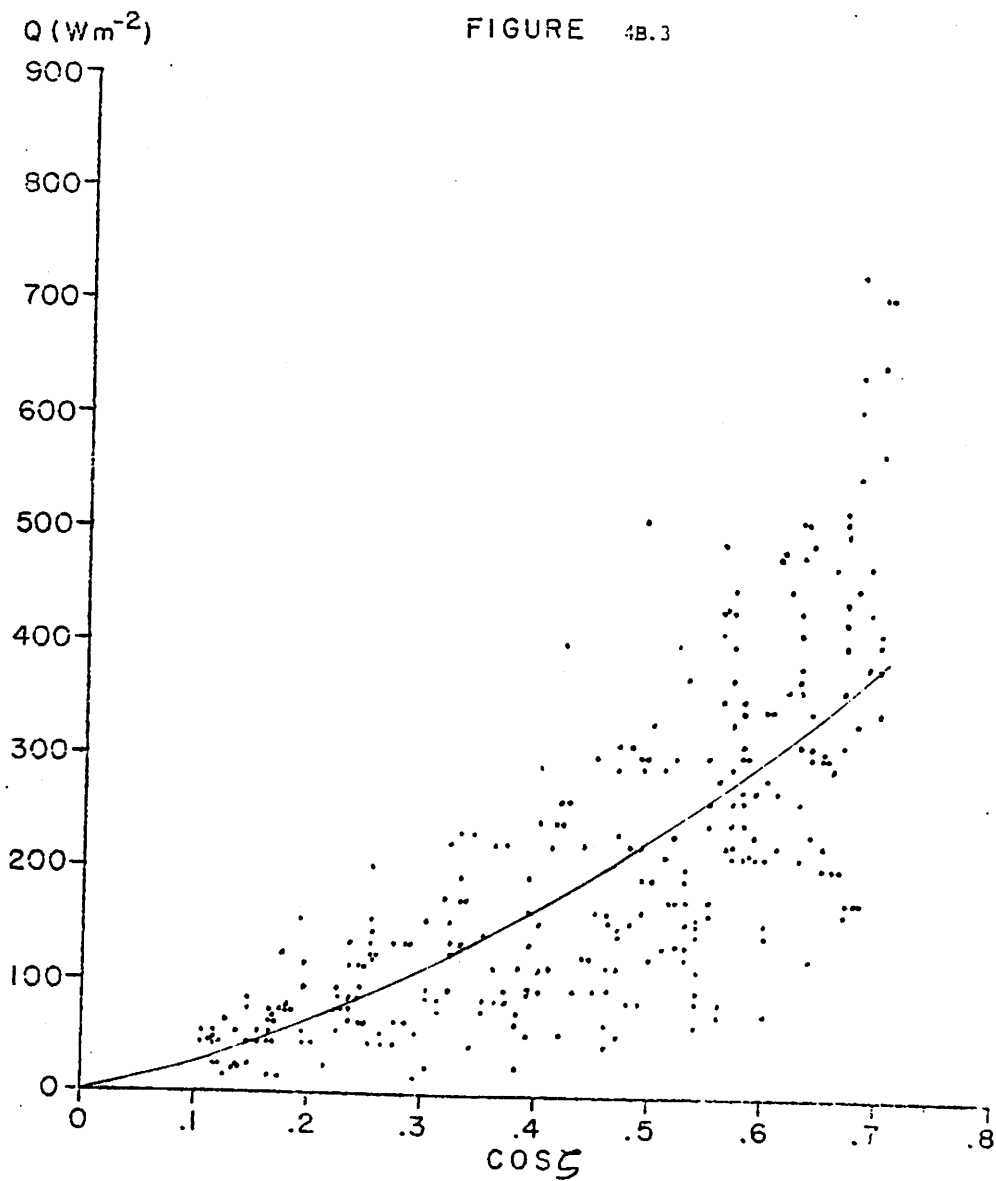


Figure 4B. 3. Hourly global solar radiation versus $\cos \zeta$,
for single level C_L , total opacity 6-10/10.

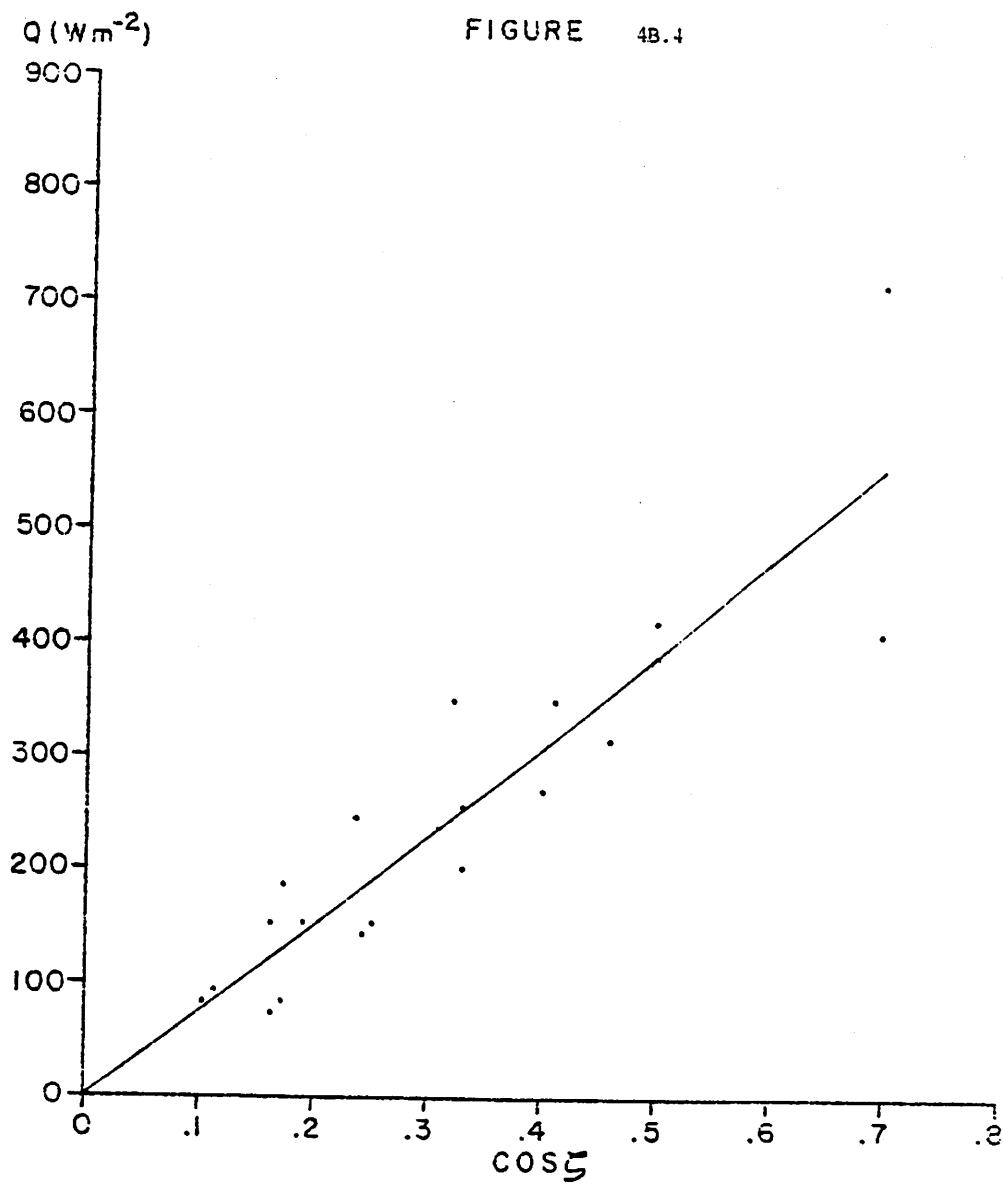


Figure 4B. 4. Hourly global solar radiation versus $\cos \zeta$, for single level C_M , total opacity 2-5/10.

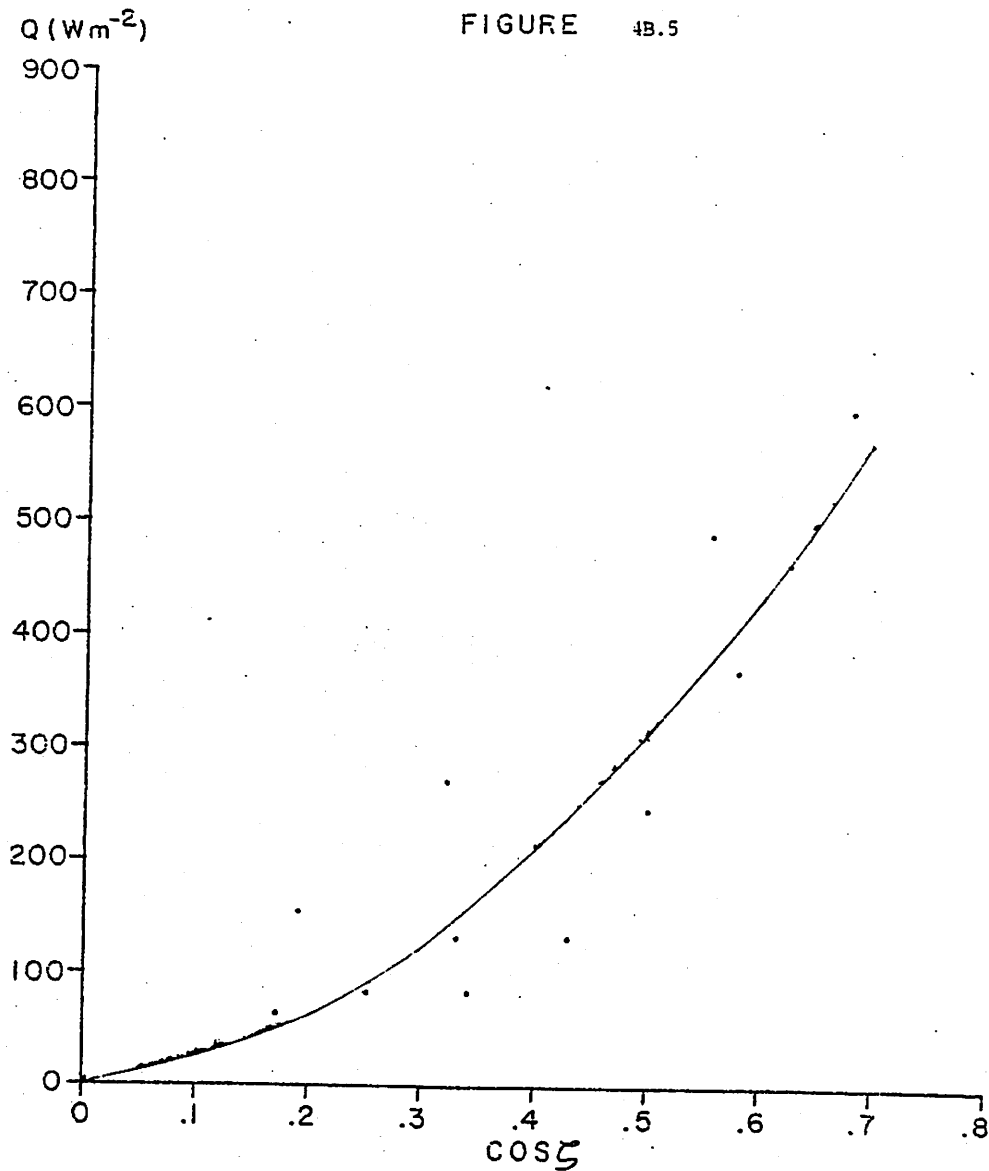


Figure 4B. 5. Hourly global solar radiation versus $\cos \zeta$, for single level C_M , total opacity 6-10/10.

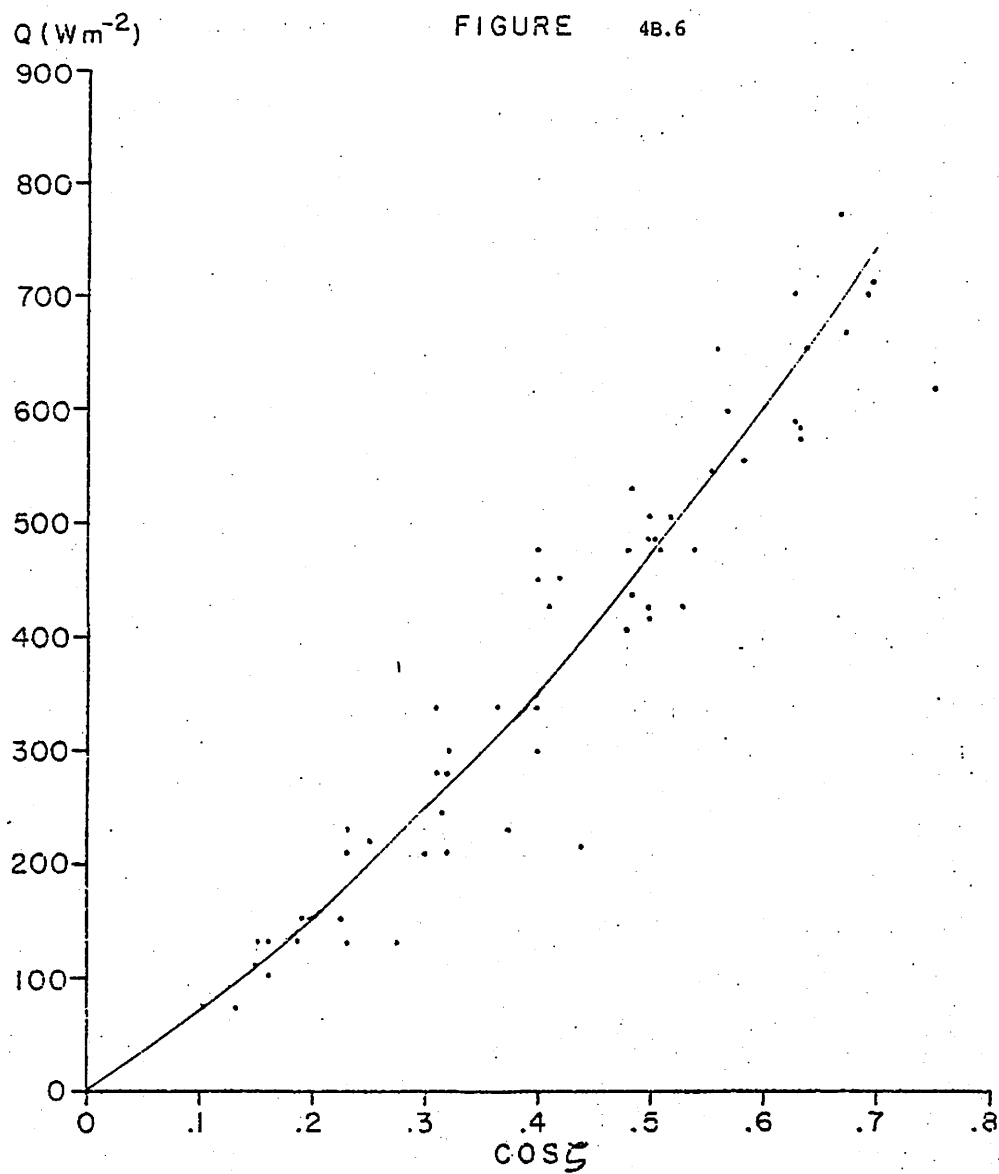


Figure 4B. 6. Hourly global solar radiation versus $\cos \zeta$,
for single level C_H , total opacity 2-5/10.

Figure 4B. 7. Hourly global solar radiation versus $\cos \zeta$,
for multilevel C_L , total opacity 2-5/10.

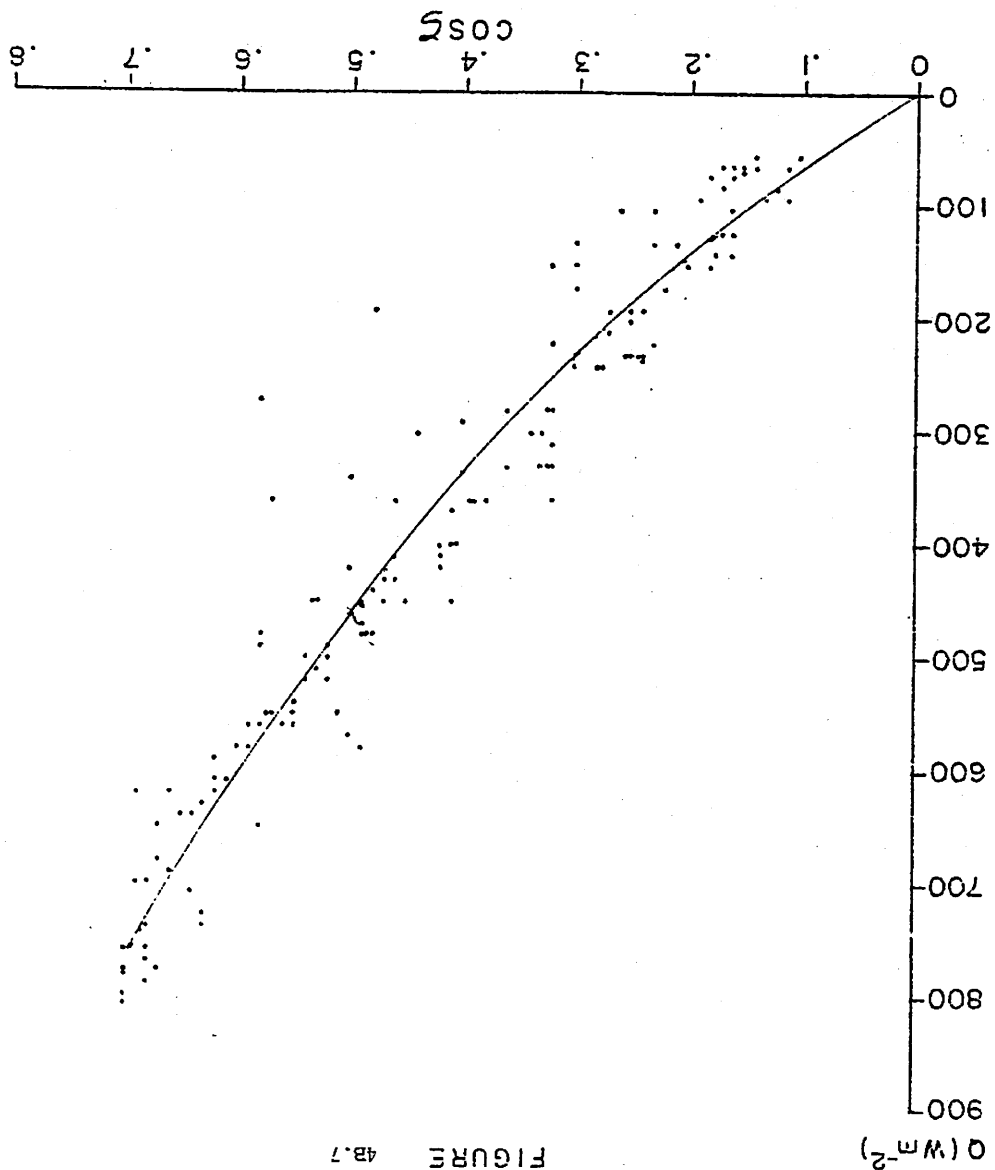


FIGURE 4B. 7

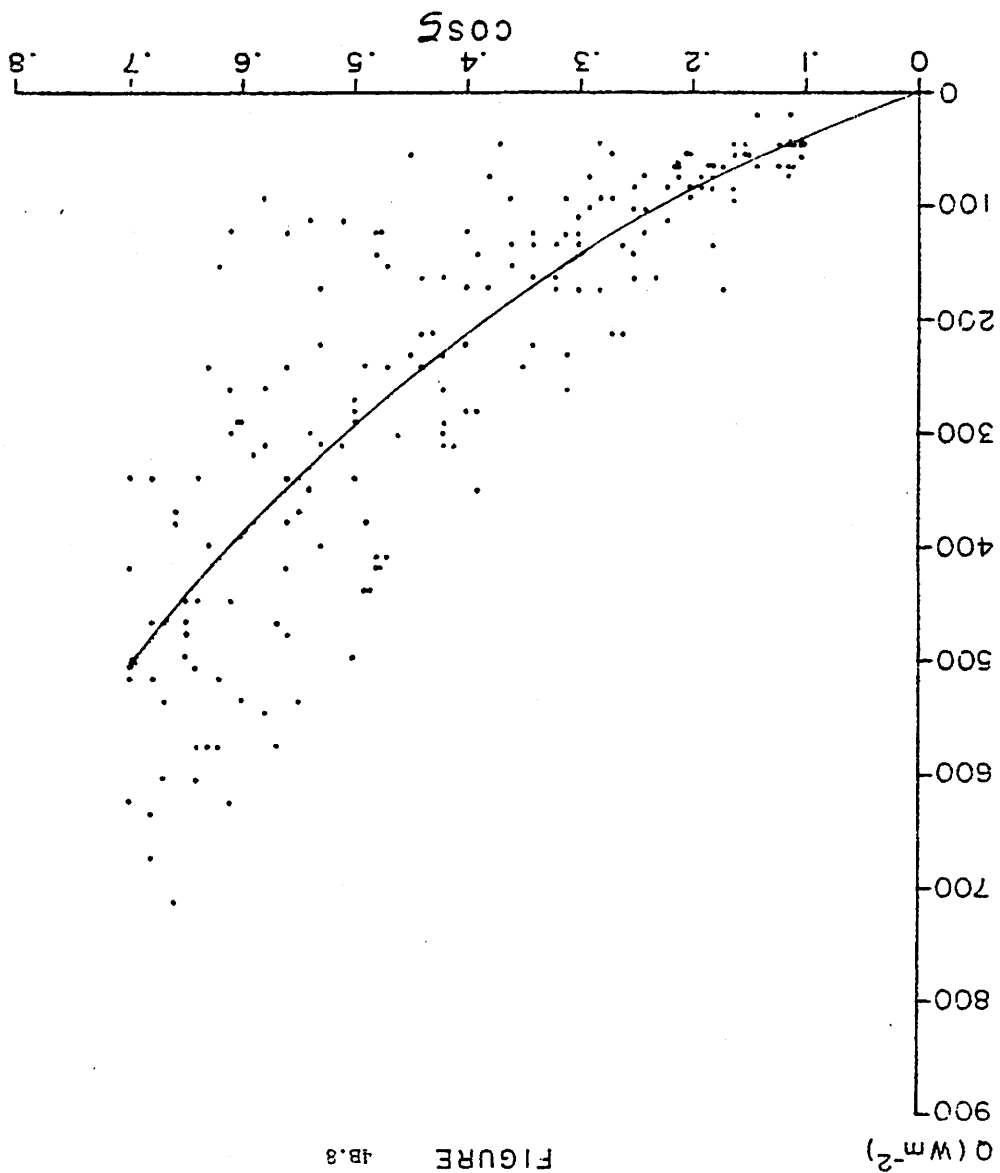


FIGURE 4B.8

Figure 4B. 8. Hourly global solar radiation versus $\cos \zeta$, for multilevel C_L , total opacity 6-10/11.

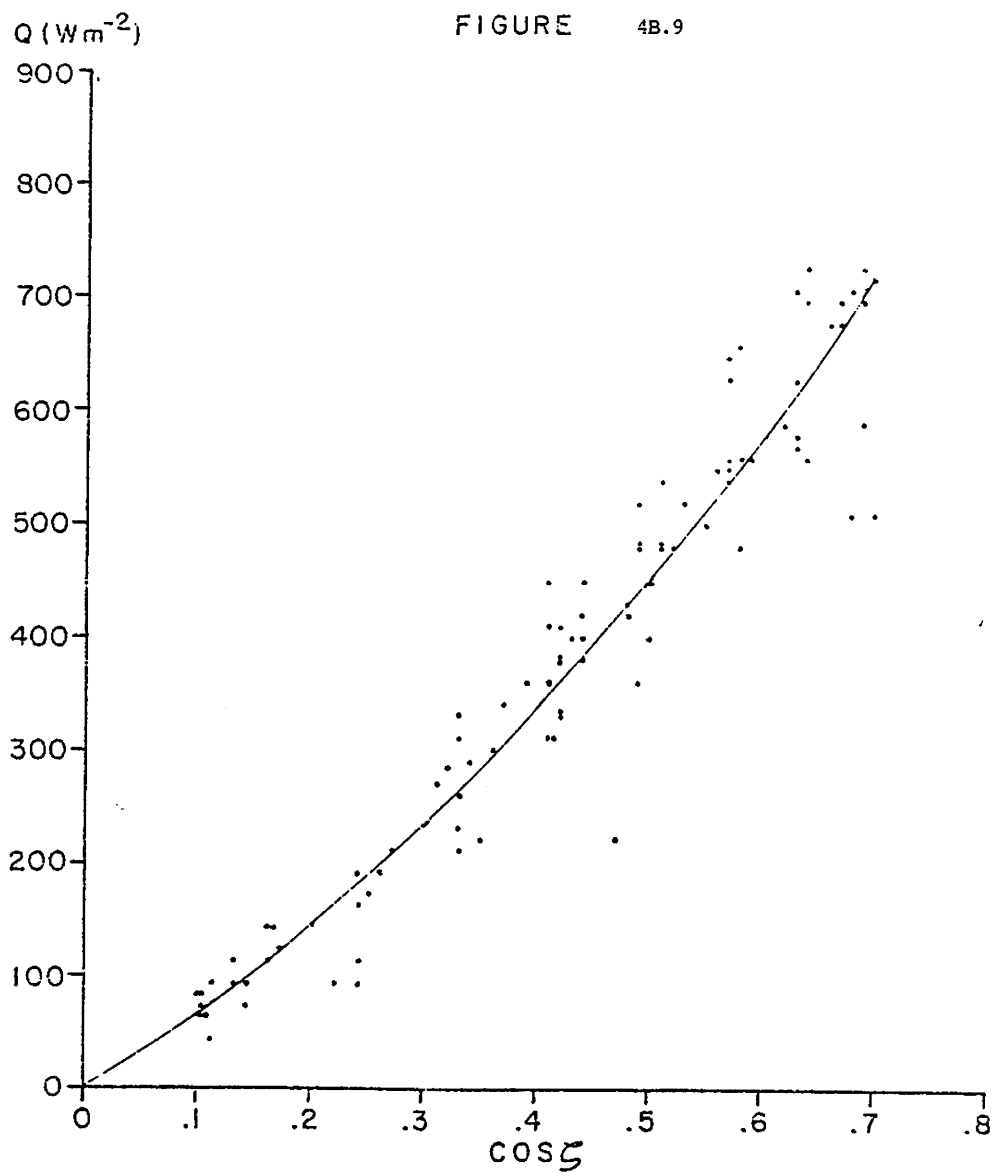


Figure 4B. 9. Hourly global solar radiation versus $\cos \zeta$,
for multilevel C_M , total opacity 2-5/10.

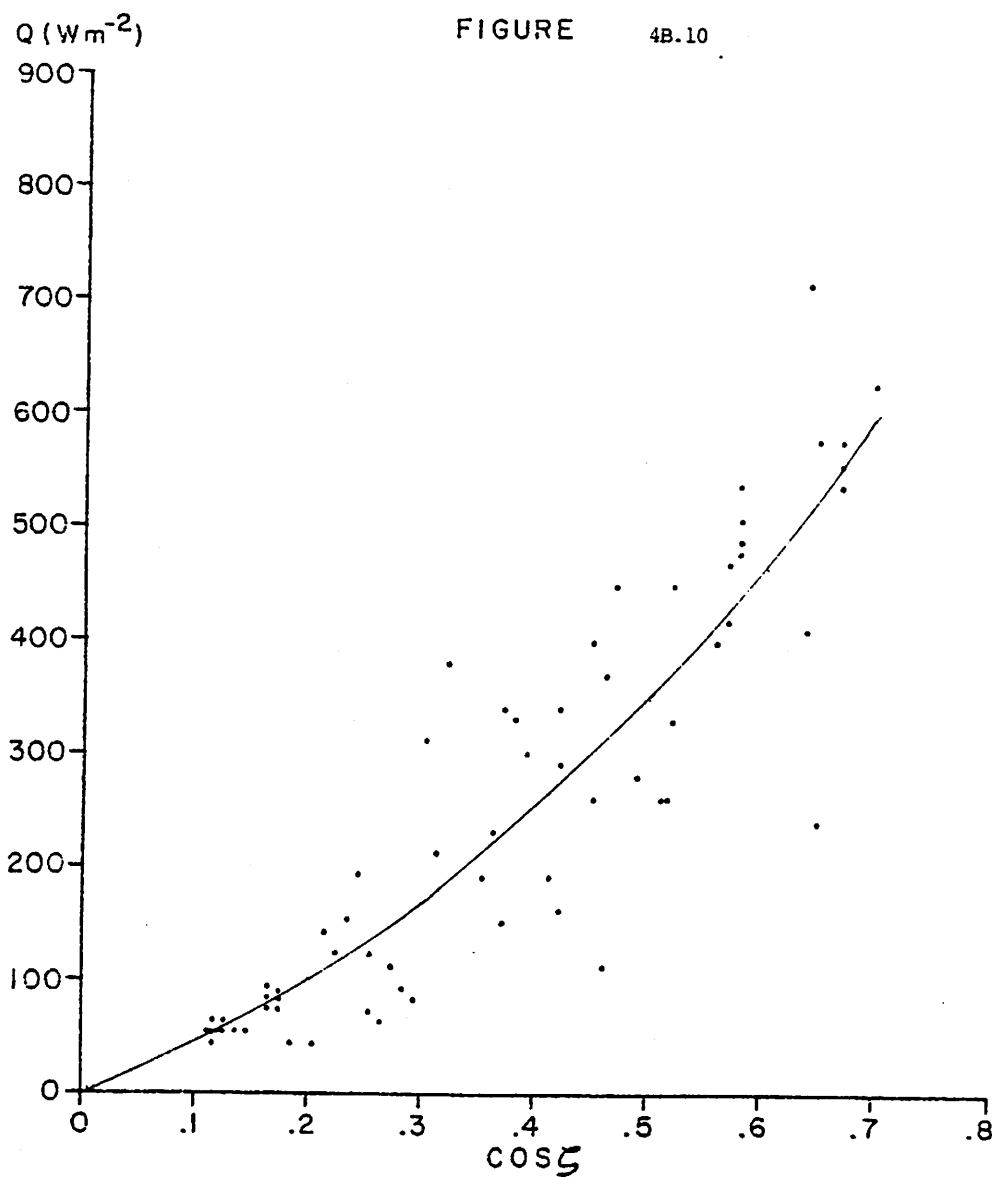


Figure 4B. 10. Hourly global solar radiation versus $\cos \zeta$,
for multilevel C_M , total opacity 6-10/10.

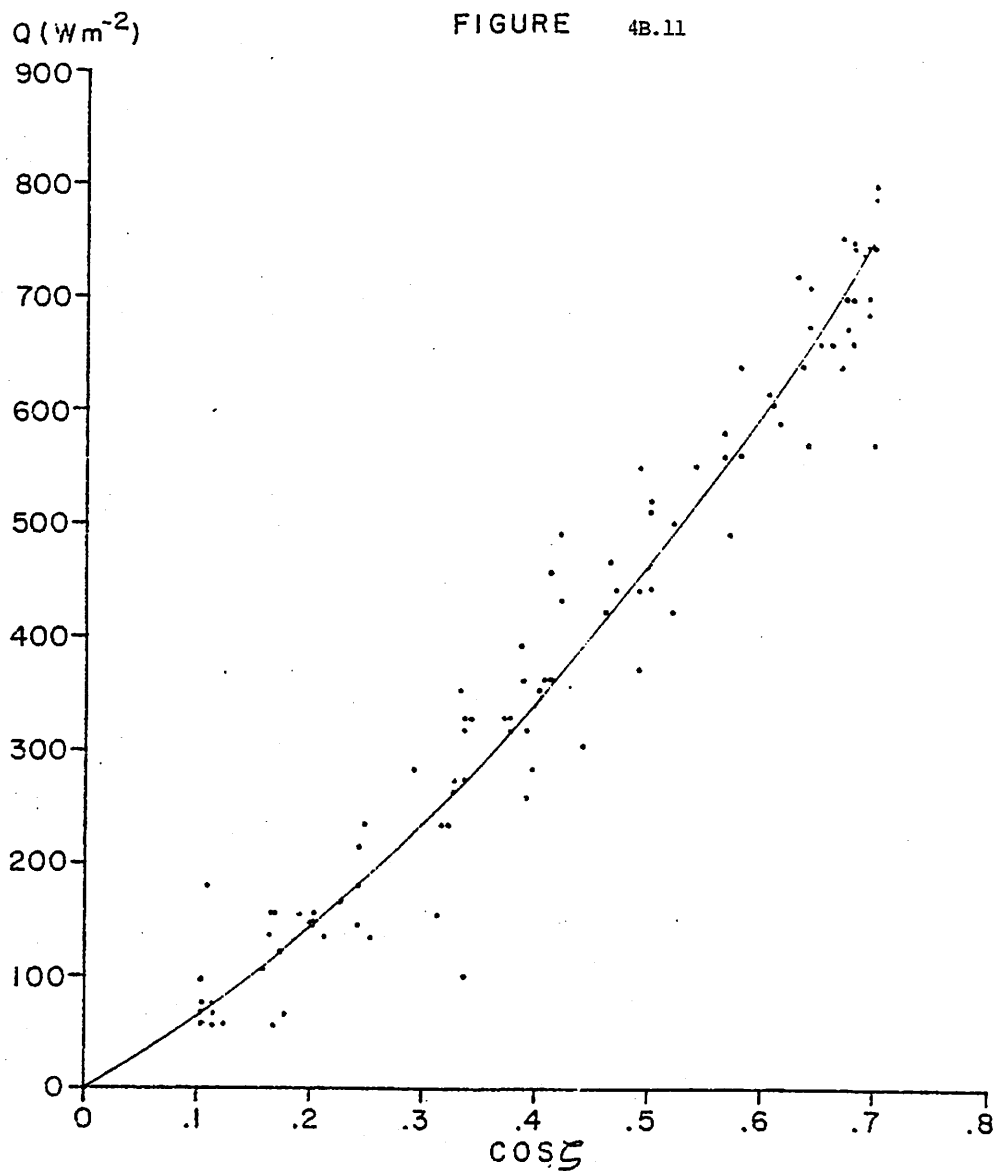


Figure 4B. 11. Hourly global solar radiation versus $\cos \zeta$,
for multilevel C_H , total opacity 2-5-10.

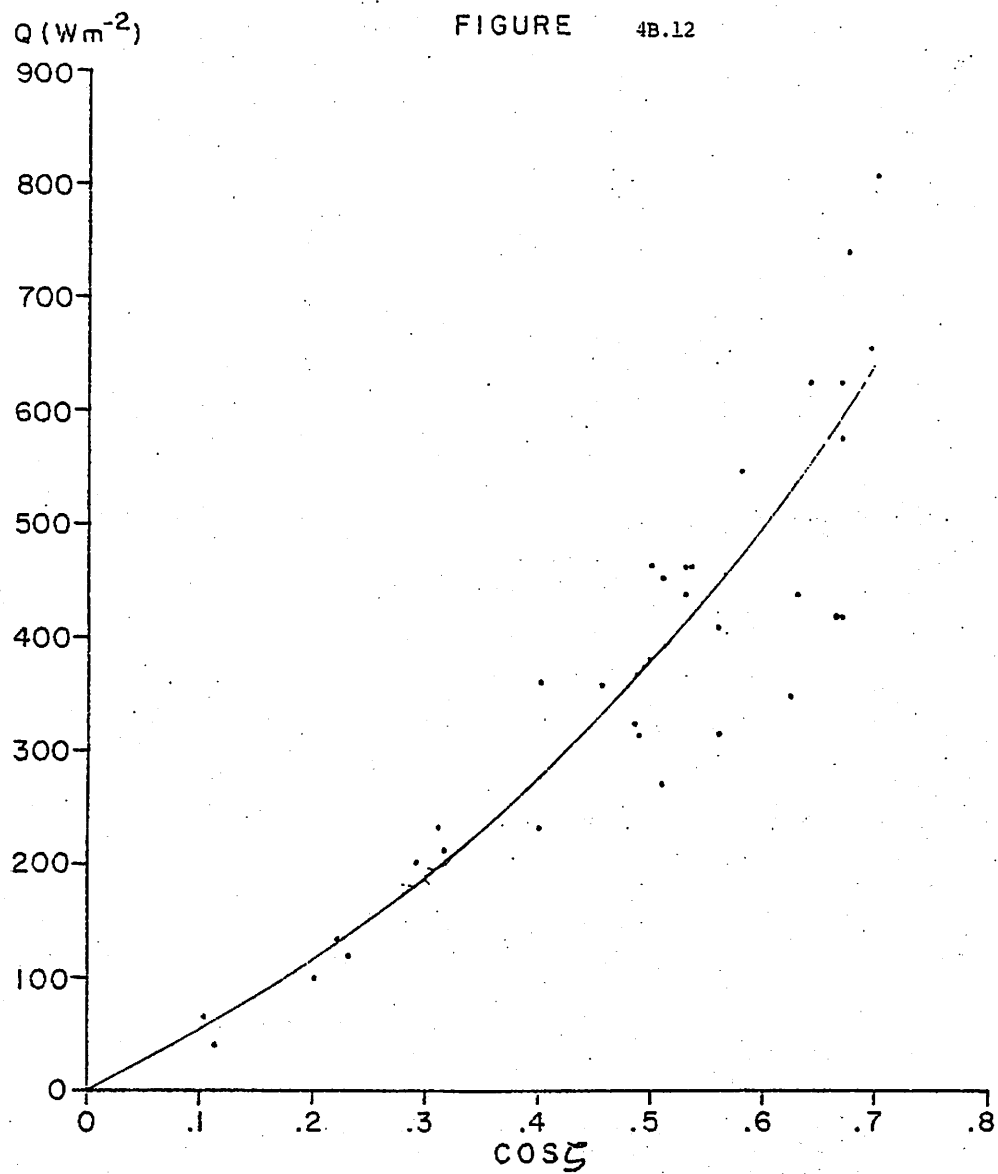


Figure 4B. 12. Hourly global solar radiation $\cos \zeta$,
for multilevel C_H , total opacity $\tau=10/10$.

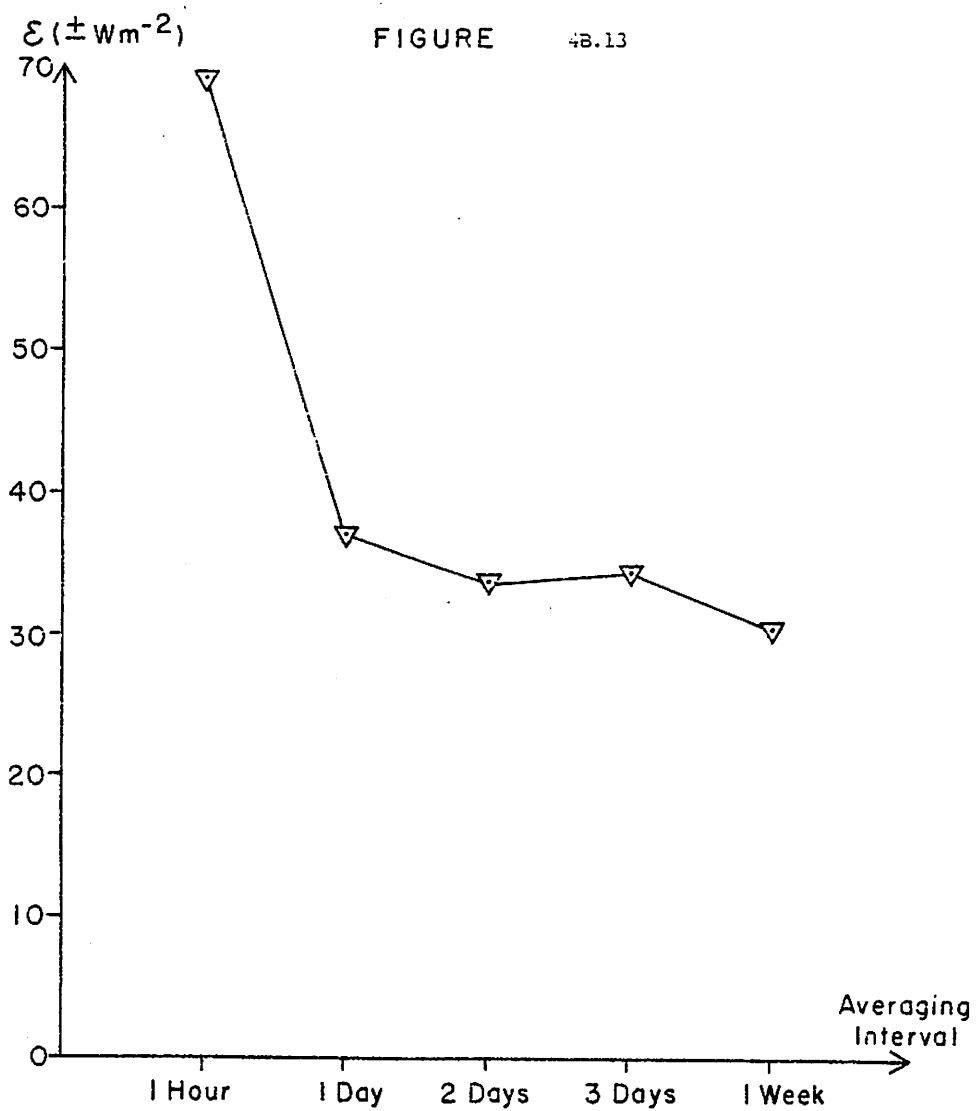


Fig. 4B. 13. Root-mean square error for estimates for different averaging intervals.

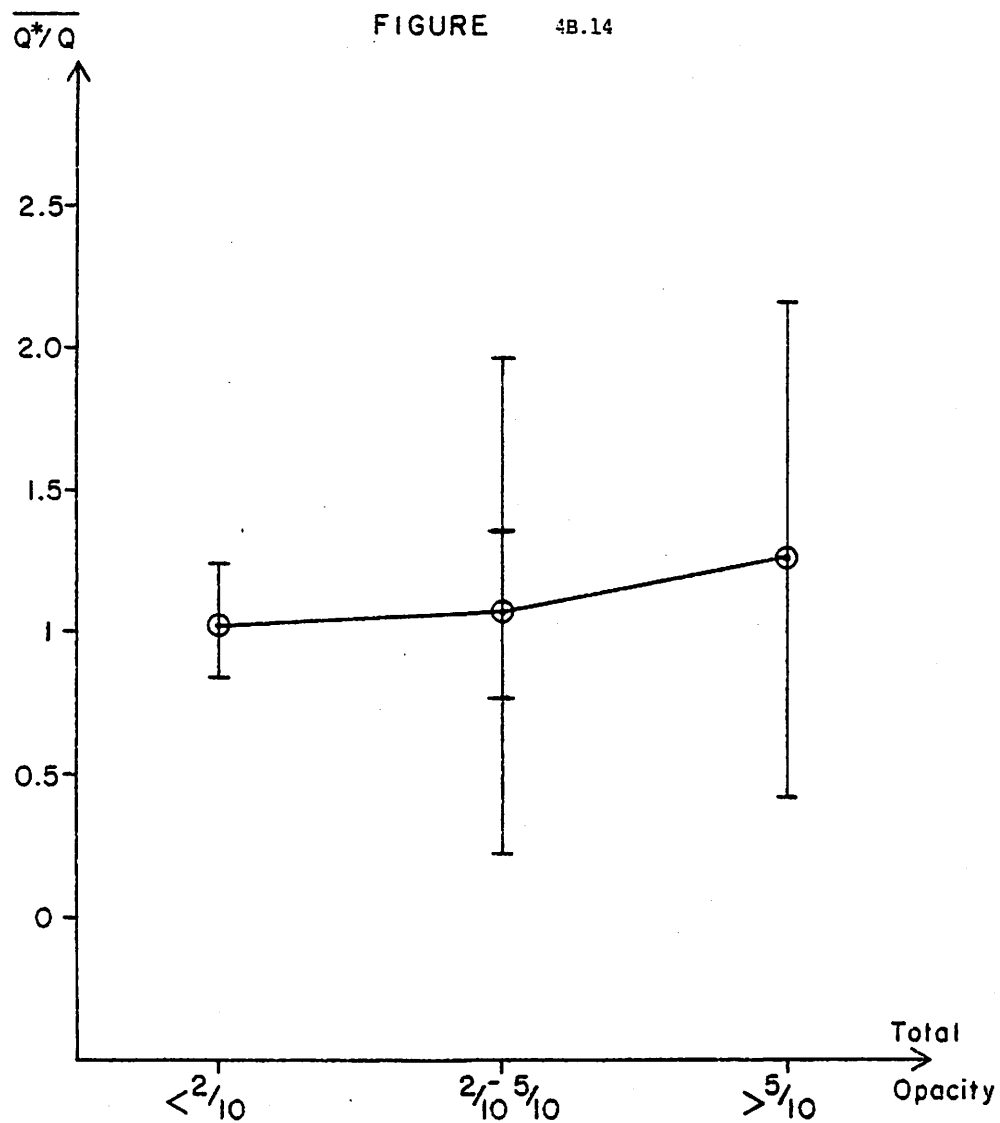


Fig. 4B. 14. Ratio of observed station data (Q^*) to estimates (Q) versus opacity.

REFERENCES

- Anderson, R.K., et. al. 1974. Application of meteorological satellite data in analysis and forecasting. ESSA TR NESC 51, sec. 2, p. 5.
- Atmospheric Environment Service. 1973. Monthly Radiation Summary. Environment Canada, Ottawa, June- August, 1973, p. 16.
- Barrett, E.C. 1974. Climatology from Satellites. Metheun, London, 350 pp.
- Barry, R.G., et. al. 1974. Synoptic climatological studies of the Baffin Island area. in: Climate of the Arctic. G. Weller & S. Bowling (eds.), University of Alaska Press, Fairbanks: 82-90.
- Jacobs, J.D., et. al. 1972. Short term air-sea interactions and surface effects in the Baffin Bay-Davis Strait region from satellite observations. Occasional Paper No. 4, Institute of Arctic and Alpine Research, University of Colorado, 80 pp.
- Jacobs, J.D. 1974. Solar and atmospheric radiation data for Broughton Island, Eastern Baffin Island, Canada, 1971-73. Occasional Paper No. 11, Institute of Arctic and Alpine Research, Univ. of Colo., Table 1.
- Jacobs, J.D., et. al. 1974. Studies of climate and ice conditions in Eastern Baffin Island, 1971-73. Occasional Paper No. 9, Institute of Arctic and Alpine Research, University of Colorado, 77 pp.
- Kondratyev, K. Ya. 1969. Radiation in the Atmosphere. Academic Press, New York, 912 pp.
- Langleben, M.P. 1966. On the factors affecting the rate of ablation of sea ice. Canadian J. of Earth Sci., 3: 431-439.
- Latimer, J.R. 1972. Radiation Measurement. IFYGL Technical Manual Series, No. 2, Ottawa, 53 pp.
- Loewe, F. 1963. On the radiation economy, particularly in ice and snow-covered regions. Beiträge für Geophysik, 72: 371-376.
- Lumb, F.E. 1964. The influence of cloud on hourly amounts of total solar radiation at the sea surface. Quart. J. of the Royal Met. Soc., 90: 43-56.
- National Academy of Sciences. 1974. U.S. Contribution to the Polar Experiment (POLEX): Part 1 POLEX-GARP (NORTH), Washington, D.C., 119 pp.
- Sellers, W.D. 1965. Physical Climatology. University of Chicago Press, Chicago, 272 pp.

- Vowinckel, E., & Orvig, S. 1962. Relation between solar radiation income and cloud-type in the arctic. J. Appl. Meteor., 1: 552-559
- Weaver, R.L., et. al., in press. Fast ice studies in Western Davis Strait. Proceedings of the 3rd International Conference on Port and Ocean Engineering under Arctic Conditions, Fairbanks, Aug., 1975.
- Weller, G. 1968. Heat energy transfer through a four-layer system: air, snow, sea ice, sea water. J. Geophys. Res., 73: 1209-1220.

5. ICE REGIME

R. L. Weaver, J. D. Jacobs and R. G. Crane

The annual regime of ice in western Davis Strait-Baffin Bay has been analyzed during the course of our program both by interpretation and mapping from satellite imagery and by field measurements in the vicinity of Broughton Island. Both aspects of this work are discussed below.

A. Regional Setting

Mapping of summer ice conditions from satellite imagery has been carried out for the pack ice and the fast ice. These analyses are discussed separately.

Areal Extent of Pack Ice

Monthly mean maps of pack ice concentration in excess of 4/10-5/10 have been prepared from the Atmospheric Environment Service (AES) ice maps, which are based mainly on aerial reconnaissance, supplemented by our own mapping from satellite information, where cloud cover permitted and imagery was available. The procedures are outlined by Weaver (1974). For 1970-73 maps were prepared for each month June through September. Based on these maps (Figure 5A.1.a-d), the following conclusions can be made:

(a) The average monthly position of the western margin appears stationary during all four years while the north and east margins fluctuate from year to year. The late season (August-September) ice tends to concentrate along the southern part of Davis Strait and the southeast coast of Baffin Island.

(b) During 1970 and 1971 the mean August pack lay offshore in the middle of Davis Strait. This contrasts with the 1972 and 1973 seasons when the mean August pack was displaced westward against the east coast of Baffin Island.

(c) The 1972 summer, characterized as a severe fast ice year, showed no major variation in pack ice distribution when compared with the other years. (Caution must be exercised here because a significant change in pack ice distribution may have occurred if areas of less than four tenths cover were considered).

(d) The general trend of pack ice concentration follows the pattern established in the severe 1960's decade (Dunbar, 1973), rather than the milder 1950's (Figures 5A.2a,b)

Separate analyses have subsequently been carried out (R.G. Crane in Barry et al., 1977) of ice growth and retreat for the area of Davis

Strait and Hudson Strait. Since these extend the spatial coverage of Figure 5A.1 southward, and span a longer record, they are included here. Figure 5A.3.a,b shows the two major types of pattern of ice growth identified for the period 1954-77, while Figure 5A.4.a,b shows analogous patterns of ice decay. These maps have been derived from the Annual Ice Summary and Analysis (1964-71) and the Southern Historical Charts (1954-63, 1972-74), of the Atmospheric Environment Service, Canada, and VHRR imagery from NOAA satellites for 1975-77. The information is not available to separate shorefast ice and pack ice.

In one pattern of ice growth, ice forms first in Frobisher Bay and on the north coast of the Cumberland Peninsula, followed by Cumberland Sound and southern Ungava Bay. Subsequently, the ice extends generally seaward from the coast. In the second pattern (Figure 5A.3.b) the ice forms first north of Cumberland Peninsula and in western Hudson Strait. It then spreads southward from Cumberland Peninsula and eastward along Hudson Strait.

Figure 5A.4.a,b shows that the Labrador Coast and Hudson Strait usually are the first areas to clear of ice. In one pattern (Fig. 5A.4.b) the ice opens up earlier in eastern Ungava Bay and the heads of Frobisher Bay and Cumberland Sound. In both cases, the last areas to clear are in central Ungava Bay, off the Hall Peninsula and off Cumberland Peninsula and northward into Home Bay.

Regional Characteristics and Extent of Fast Ice

Fast ice in the marginal arctic seas generally consists of young first-year ice, whereas it includes increasing proportions of multi-year ice northward towards the Canadian Arctic Archipelago. Along the east coast of Baffin Island fast ice grades from first-year ice in the south near Cape Dyer to a mixture of first and multi-year ice in the north.

Two areas of persistent fast ice occur in Davis Strait-Baffin Bay, the east coast of Baffin Island and Melville Bay southeast of Thule. The following case studies only concern the Baffin Coast.

The fast ice margin has been mapped for each week showing a significant change, from late May or early June until breakup for the 1970-73 seasons (Figures 5A.5.a-d). For the 1973 summer VHRR imagery was analyzed with the aid of a Zoom Transfer Scope (Bausch and Lomb) to cross-check the AES ice maps. Inaccuracies in the AES maps in the position of the fast ice edge of some 10-20 km were discovered for certain dates. The depiction in the AES maps of the north-south retreat of the fast ice and the late season margin are most probably more accurate because of the margin's close proximity to recognizable landmarks and thus greater mapping ease for an airborne observer. These reservations must be kept in mind in considering the following conclusions:

(a) The distance of the fast ice margin from the coast in late May - early June varies \pm 15-25 percent from year to year.

(b) The pattern of the breakup of the fast ice shows considerable variability from year to year. Excluding the severe 1972 season, fast ice in the Home Bay - Broughton Island area generally cleared out by about the second week of August. The region centered around Royal Society Fiord (north of Cape Adair) usually preceded the southern area by about a week. The Cape Dyer area has persistent pack ice during most of the season but little fast ice.

(c) In general, the breakup of the fast ice is associated with a decrease in pack ice concentration along the fast-pack ice boundary.

(d) A polynya occurred between the fast ice margin and the pack approximately 40 km southeast of Henry Kater Peninsula in each of the years. This feature persisted for most of June 1971 but in other years was more intermittent. Its location corresponds to the deep (circa 300 fathoms) water shoreward of the Alexander and Isabella Banks.

(e) In 1972 the fast ice persisted in the Home Bay area but broke up along the coast north of Cape Adair. General "flaw leads" and/or polynyii were noted along the fast ice margin in 1972.

In some regions of the Arctic the fast ice edge appears to conform to a particular isobath. The 18m (10 fathom) line in the Beaufort Sea (Canadian Hydrographic Service, 1970) is one example; the 10 m line in the White Sea, and the 25 m line along the Siberian Coast (Zubov, 1945) are others. For the east coast of Baffin Island, however, the fast ice edge approximates the 180 m line, which is some 70 km offshore in Home Bay and overlies even deeper waters further north along the coast. The strong southerly current off Cape Dyer is continually removing ice from the coast in other parts of western Davis Strait and obviously no general rule of depth-controlled fast ice margin can be made for the Arctic as a whole. Along most of the Baffin Island coastline, the offshore slope is steep and there is generally no bottom-fast ice or offshore zone of grounded ridges such as occurs off northern Alaska.

Fast Ice Extent and Breakup Patterns in the Vicinity of Broughton Island

LANDSAT 1 satellite Multispectral Scanner (MSS) images of the east coast of Baffin Island have been used to evaluate general changes in the fast ice surface and extent between Cape Hooper and Padloping Island since fall 1972. Preliminary case-studies and results have been reported in Jacobs et al., (1974) and Weaver et al., (1975). The regional freeze-up and decay patterns of the fast ice have been mapped, and correlations made between surface field measurements from June to July 1974 and features seen in the imagery. Images for 1973 and 1974 have been analyzed to determine (a) degree of similarity in the local

melt pattern from year to year, and (b) the feasibility of designating the relative ice melt stage from satellite imagery. (see section below on season breakup pattern.)

The LANDSAT 1 satellite repeats an identical track once in 18 days. At 65° N, however, a single point may be observed on three successive days (cloud cover permitting) because of the orbital side-lap. The MSS collects data from four wavelength bands roughly corresponding to the green, red, and photo-IR (2 channels) parts of the solar spectrum. The Instantaneous Field of View (IOV) is approximately 80m x 80m at the subpoint (ERTS-1 Users Handbook, 1972) although standard photographic products supplied by the Canada Center for Remote Sensing (CCRS) do not achieve this fine a resolution. (For analysis of sea ice characteristics visible in LANDSAT imagery, see Barnes and Bowley, 1973).

The seaward extent of the fast ice sheet in early spring 1973, as measured from Side Looking Airborne Radar (SLAR) imagery (supplied by the Canadian Defense Research Board) on March 5, 1973, roughly corresponds to the seaward margin of vast floes in the LANDSAT frame for October 14, 1973. Comparisons of young ice patches and surface ridge and/or cracks viewed in the SLAR and LANDSAT imagery suggest that movement between October and March was minimal. However, no features could be conclusively identified in both images. Better correlation exists between the March 5th SLAR and July 11th LANDSAT imagery.

Several floes imbedded in the ice sheet and two areas of first year ice were positively identified in both the March 5th and July 11th imagery. The almost coincident locations of these features strongly suggest that no deformation occurred after March 5th, but absolute proof of non-movement is not possible due to distortion inherent to the SLAR imaging system (Weaver, in Jacobs et al., 1974, p. 52).

The fast ice extent was nearly identical in 1973 and 1974 although ice composition in 1973, based on LANDSAT mapping, was generally second year in contrast to the first year ice found in 1974. The extent differed by a maximum of + 5-7 km along the margin between the two years. Although two years of data are inadequate to draw conclusions about the mean ice extent, it appears that even pronounced differences in atmospheric conditions from one year to the next have little effect on the seaward extent of the fast ice in late winter.

Regional mapping of the melt stage was attempted using the various imagery products. The coarse (1-5 km) resolution of the meteorological satellites allowed only determination of break-up; this was identifiable because of the strong reflectivity contrast between ice and water. The better resolution of the LANDSAT MSS data permitted identification of some features which might be correlated to a particular stage; however, sequential monitoring of the melt progress is not possible due to the interval between overpasses with clear frames and the rapid changes in surface characteristics.

Surface oblique photographs were taken at LANDSAT overpass times in June 1974 to provide "ground truth" for assessment of the minimum detectable size of features in the MSS imagery. The minimum detectable size varied from a lower limit of approximately 100 m to an average of 500-600 m. It depends partly on the degree of contrast between the object and its surroundings, but narrow linear patterns are more readily seen than small circular ones. The features observed, both in the imagery and on the ground, include such areas as drained puddle matrices associated with shore leads, thermal and/or tidal cracks or ice of differing age and composition. All generally relate to sub-resolution variations in puddle concentration.

The local and regional break-up process was observed quite successfully from the satellite imagery. The observations indicate that in 1972 the fast ice underwent only limited break-up in more exposed areas in the Broughton Island region (Jacobs et al., 1974). LANDSAT imagery for October 14, 1972 shows essentially 10/10 concentration of vast and giant floes out to approximately 50 km off the coast. In contrast, no ice of any type was visible on October 4, 1974 following the highest mean ablation season (June-August) temperatures on record. In the October 1972 image, some in-shore areas near Padloping Island were free of fast ice but were covered by nilas and young ice. This may be explained by tidally-induced turbulent mixing which limits ice formation. The late-freezing areas of 1972 were with some exceptions the first to clear of ice in 1973. Indeed, these late-freezing/early-melting areas apparently tend to coincide from year to year.

The local break-up proceeded along similar lines in 1973, 1974 and 1975. On this basis, the sequential progression can be outlined as shown in Figure 5A.6 for the immediate Broughton Island vicinity. In-shore areas close to Padloping and Broughton Islands are the first to clear of ice. The melt begins near the fiord heads and in a few shallow water areas further seaward, and then advances seaward toward the outer coast ice sheet, which tends to remain intact for some 10-15 days after the break-up of the in-shore and fiord ice. Generally, the retreat starts to the south of Padloping and works northward along the coast, controlled by local geographical features.

This seaward lag in break-up generally holds along the east Baffin coast. The north-south timing of break-up, on the other hand, does not appear to follow a set pattern from year to year. Instead, the break-up has been observed to begin following rapid offshore movement of the pack ice along the fast ice edge in mid- to late summer, suggesting a link to strong off-shore winds.

B. Fast-Ice Characteristics at Broughton Island

Much of our field effort has concentrated on observation of ice characteristics near Broughton Island. The following information summarizes our findings during both the season freeze-up and break-up cycles.

Ice Growth

Shore-fast ice is formed in situ from young ice during the yearly freeze-up or when drifting first or multi-year ice is frozen into a sheet which is fixed to the shore (Atmospheric Environment, Canada, 1965; WMO, 1970). Field measurements and analysis indicate that ice growth can be modelled by field measurements and analysis indicate the one-dimensional heat flow equation (Jacobs et al., 1974, p. 41):

$$\frac{\Delta H}{\Delta t} = \left[\frac{1}{L\rho} \right] \frac{T_s - T_w}{H/k_i + h/k_s} \quad (5B.1)$$

h = depth of snow	L = latent heat of fusion
H = ice thickness	ρ = density of ice
t = time	k_i = thermal conductivity of ice
T_s = temperature of snow surface	k_s = thermal conductivity of snow
T_w = temperature of water	

Theoretical curves of ice growth rate as a function of ice thickness and snow cover depth derived from this equation are shown in Figure 5B.1.

Several years of ice thickness measurements made during traverses around the island and to the north and south, and regularly in Broughton Harbor, can be used to validate the ice growth model presented above.

Mid-winter data were obtained in December 1971. For convenience of access, a restricted area in the middle of Broughton Harbor was chosen for regular ice thickness and temperature measurements. Description of field measurement procedures, weather and ice conditions are given in Jacobs et al., (1974, p. 42). Initial measurements, as well as a transect northward showed the ice thickness in mid-harbor to be less than the regional average. The "harbor" is actually a narrow strait separating Broughton Island from Baffin Island, and tidal currents of some 1-2 m/sec were observed there in summer 1971. The turbulent flux beneath the ice must therefore be large, although fairly constant. All other factors affecting ice growth rates were assumed to be the same between the mid-harbor site and the more open areas.

The 1971 freeze-up of Broughton Harbor occurred on October 31, and by November 16, the ice was sufficiently thick to support foot and snowmobile travel (J. Pearson, pers. comm.). Climatological records from the Broughton Village station show a total of 63.5 deg-days below -1.8°C through freeze-up. A week of relatively heavy snowfall occurred immediately following freeze-up, and by mid-November a 5-10 cm snowcover had accumulated.

On December 18, 45 cm of ice at the harbor site was measured using a 2 cm diameter auger. Measurements throughout the subsequent 31-day period indicated nearly linear growth at an average rate of 0.95 cm per day. The spatial variation of ice thickness in the immediate study area was tested on a single occasion by boring four holes within a 500 m radius, resulting in a range of thickness of 7 cm. Thereafter, a single hole was assumed to be representative of the area. Temperature profiles were obtained for each hole at 5 to 10 cm increments by placing a rapid-response thermistor in firm contact with the bottom of the hole. On one occasion, a larger hole was made with a chisel and ice samples taken for salinity measurements. Sample temperature profiles and a salinity profile are shown in Figure 5B.2. In addition to the salinity profile established by the "pit" method, an effort was made to recover most of the auger parings for some of the bored holes in order to determine the average salinity of the ice sheet. On one occasion this gave an average of $10.0 \text{ g/kg} \pm 2.0$ for five holes, which suggests this more rapid technique to be practicable.

The almost linear form of the measured temperature profiles (Figure 5B.2) suggested the applicability of the simple ice growth model given in Equation 5B.1. Using the reported freeze-up date and assuming an ice thickness of 25 cm when "travel" began, a regional ice growth curve was derived. Five-day intervals were considered and mean screen temperatures substituted for T_s . This latter practice seems justified by experimental comparisons of screen and ice surface temperatures reported by Doronin (1969) for winter ice.

In the initial solution, the enthalpy of ice and turbulent flux from the water to the ice were disregarded and, not suprisingly, the calculated growth rates were in excess of those measured. It was then found that the growth rate for each five-day interval could be weighted by the ratio of the measured thickness to that first calculated--a factor of 0.67--resulting in a more realistic growth curve (Figure 5B.3). These results suggest that a reasonably good growth model can be obtained from screen temperatures and snow cover alone among the meteorological variables, where ice salinity is known or assumed. Prediction of ice thickness for a specific date requires additional information: either the freeze-up date or the actual ice thickness at some subsequent date.

In June 1972, and subsequent years, more extensive ice thickness surveys were made. The sampling stations were duplicated when ice travel conditions permitted. These early June data represent the maximum ice growth for each winter season. The results are presented in Table 5B.1. Sampling station locations are mapped in Figures 5B.4-7.

Table 5B.1 shows the same pattern of variations encountered in the winter of 1971, with the greatest thickness occurring east of the island over water depths of several hundred meters: The average of all measurements east of Broughton in 1972 was 180 cm. The corresponding value in 1973 was 178 cm. The harbor area values were 148 cm (1972) and 138 cm (1973), which are some 18 to 22 percent less than the eastern coast measurements.

Stations "A" and "D" and "H" were the ones most regularly sampled during the 1972-75 period. The mean for Station A is 158 cm, Station B 186 cm and Station H 142 cm.

A form of equation 5B.1 was used to calculate fast ice thickness for the deep water area some 5 km east of Broughton Island. The predicted ice thickness by the end of May 1972 was 175 cm. Five holes drilled in the first week of June over a 20 km transect east of the island showed an average thickness of 180 cm with a range of ± 10 cm. However, model results in the 1973 and 1974 seasons were only accurate within $\pm 20\%$. In 1973, this was probably due to the presence of up to 7/10 second year ice and to abnormally heavy snow pack in the spring, which results in non-linear effects, not accounted for by equation 5B.1. In 1974, observed thicknesses were only available in the harbour area.

For 1975, the climatological data at Broughton Village were incomplete and the model could not be tested. The results suggest that a good estimate of the rate of growth of first-year ice can be made using an equation based on one-dimensional heat flow through a two-layered slab with daily mean temperatures and daily snowfall increments as independent variables. The present formulation is not applicable in shallow or constricted areas, where turbulent exchange of heat results in thinner ice. The advantage of the method presented here, over empirical expressions, lies in the fact that it can be applied widely and immediately, given the climatological data, without the need for a long series of thickness measurements.

The Break-up Pattern at Broughton Island

The ablation and break-up processes may be divided into five stages (Figure 5B.8): (1) premelt, (2) melting snow, (3) puddle formation, (4) thawhole formation and drainage, and (5) break-up (Jacobs et al., 1975). These stages generally apply to the fast ice observed during the 1971-75 summers in the vicinity of Broughton Island. Similar schemes have been reported by Zubov (1945) and WMO (1970). This sequence of events, however, probably does not occur in areas with heavily ridged or rafted fast ice.

In late May and early June, the cold, snow-covered fast-ice sheet (Figure 5B.8, stage 1) starts to warm. Lieske (1964) has reported that thermal conduction from the water beneath the ice was important during spring at Barrow, but we have no data for this early stage. Daily totals of solar radiation are large in May-June and from 10 to 30% of the incoming radiation is absorbed by the snowpack leading to melt with water percolating to the relatively impermeable ice surface (stage 2) where it coalesces to form incipient puddles. A snowcrust may persist for many days if air temperatures remain below freezing and early summer storms deposit fresh snow. Eventually, however, the snow is melted and the ice surface develops alternating hummocks and puddles (stage 3). The meltwater puddles drain through fractures, leads, and seal breathing holes to form a low density fresh water layer 0.5 to 1 m deep between the bottom of the ice and the seawater below (stage 4) in areas where the tidal or ocean

currents are insufficient to overcome the strong density inversion. A similar fresh water layer was also observed by Langleben (1966). Where runoff is restricted, extensive sheets of melt water form on the surface to depths of some tens of centimeters.

With the average albedo of the composite hummock-puddle surface now considerably reduced (from about 0.8 to 0.4), the absorption of solar radiation (with some $2.1 \text{ kJ cm}^{-2} \text{ day}^{-1}$ potentially available at mid-summer at 70°N) leads to rapid ablation. Up to 5 cm of ice melt per day was recorded during stages (3) and (4) in 1973 and since ice is a translucent material allowing solar radiation to penetrate deeply, the actual mass change was probably greater. The puddles, with an albedo of 0.25 or lower (Langleben 1969, reported values of 0.19 at Tanquary fiord), absorb ca. 15-30% more radiation than does the adjacent ice surface. The greater ice melt under the pools allows some of them finally to melt through forming thawholes (stage 4). The final break-up (Figure 5B.8, stage 5) occurs when the structurally weakened fast ice sheet is broken apart by wind and wave action. Rarely does the ice totally melt in situ. LANDSAT and NOAA-2 imagery show that at first giant and vast floes separate from the ice sheet at the edges of polynyas or along flaw leads that have persisted throughout the winter, or appeared early in the summer in regions of thin ice. Because there is little mixing of the waters between these floes, solar heating of the surface waters is intense and the final melting and break-up of the floes may occur in a matter of days.

The approximate melt stage transition dates for 1971-75 seasons are presented in Figure 5B.9. These dates are only approximate because progression from one stage to the next is a continuous gradational process. In 1974, the dates are systematically about 1 week early because the microclimatological station was located south of Broughton in an area which generally precedes break-up at the sites used in 1972 and 1973.

In the cold and stormy summer of 1972, the fast ice in the Broughton Island area did not disperse. By late August it had advanced to puddle formation, but only proceeded beyond this stage in sheltered coastal areas. By October 14, 1972 LANDSAT imagery shows that the fast ice did finally break into giant and vast floes but was already in the process of refreezing (see preceding section).

All five stages were observed in 1973. The melting snow (stage 2) to puddle formation (stage 3) transition occurred about June 26, and was associated with an atmospheric warming event when strong southwesterly airflow produced the first continuous mean daily air temperatures above 0° of the season. The transition from stage 3 to stage 4 occurred during the second week of July in the immediate area of the microclimatology station. Break-up took place during the second and third week of August.

In contrast to 1972 and 1973, the 1974 and 1975 seasons were well advanced into the melting snow and puddle formation stages (2 and 3) by the second week of June. The rapid puddle drainage observed in 1973 was not repeated in 1974, or 1975 but was replaced by continuous advancement from stage 1 to stage 4. Break-up was quite rapid and took place during mid-July in both years-- a full month ahead of 1973.

Thus, in general, 1974 and 1975 may be classed as warm summers with early break-up, 1972 and 1973 as relatively cold summers and 1971 as intermediate between the extremes. Several conclusions may be drawn from Figure 5B.10. (1) The thawhole formation and drainage stage appears about the same length in four of the five years (excluding 1972). (2) The length of the melt season between the stage two to three transition date and the four to five transition date varies + 2-3 weeks in four of the five years. (3) The initiation date of stage one to two transition is about 1 June + 10-15 days. (4) Those seasons with earlier stage one to two transition dates were also shorter melt seasons. Thus, the length of the melt season appears sensitive to the transition date from high albedo stage one to the lower albedo found in stages two and three.

In 1975, participation in the A.E.S. ice patrol flights in mid-late July provided some useful information. The fast ice around Broughton Island appears to be representative of most of the east coast and the Pond Inlet area, at least at this stage in the season. Ice in Foxe Basin appears much dirtier than in other areas (cf. Campbell and Collin, 1956) which may explain lower reflectances in NOAA imagery during the early part of the season. Relative amounts of ridging and puddling appeared similar all along the east coast of Baffin Island. However, no quantitative measure of these characteristics were possible. These observations support our conclusions based on NOAA and DMSP satellite imagery analysis.

TABLE 5B.1

Ice Thickness Measurements near Broughton Island

STATION DESIGNATION (SEE FIGURE 5B.4)

Measurements in cm

Mean all values in Traverse
A → D

	A	B	C	D	E	F	G	H	I	Harbor E → A				East of Broughton			
										\bar{x}	σ	n^*	\bar{x}	σ	n	\bar{x}	σ
June 1972	129	183	180	---	152	100	152	154	167	148	23	9	180	7	5		
3 June 1973	183(26)	188(64)	163(39)	185(47)	---	---	---	137(72)	---	138	34	4	178	17	6		
20 June 1973	---	---	---	---	---	100	130	---	---								
June 1974	137	---	---	137	133	99	148?	135	---								
7 June 1975	182	---	---	---	---	---	---	---	183								
20 June 1975	---	---	---	164	---	---	---	---	---	not possible			not possible				
Mean all years																	
σ "	158	186	172	162	143	100		142	175								
n "	29	---	---	24	---	1		10	---								

() numbers are snow depths where recorded.

* the number of measurements.

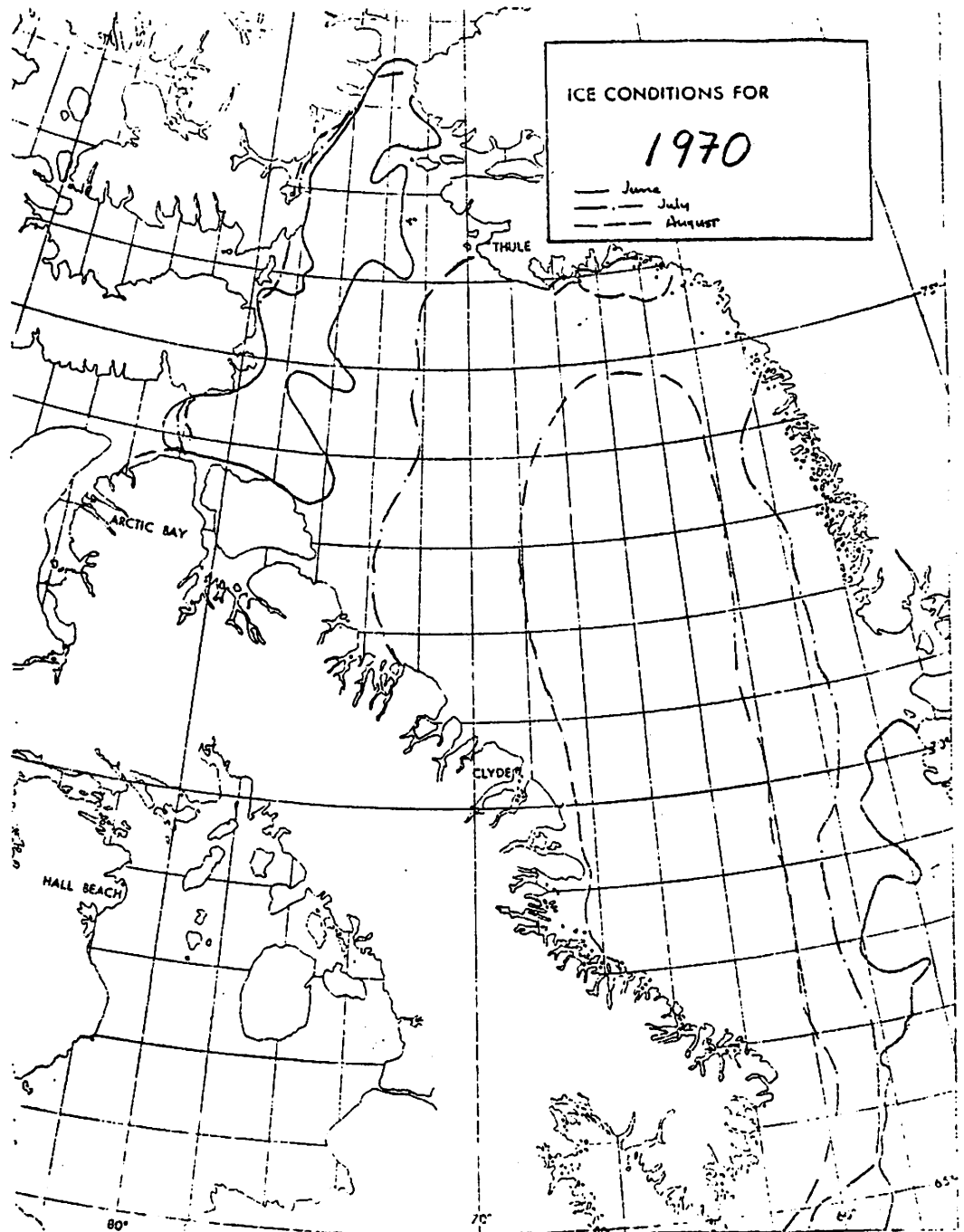


Figure 5A.1a Ice conditions in Baffin Bay, 1970

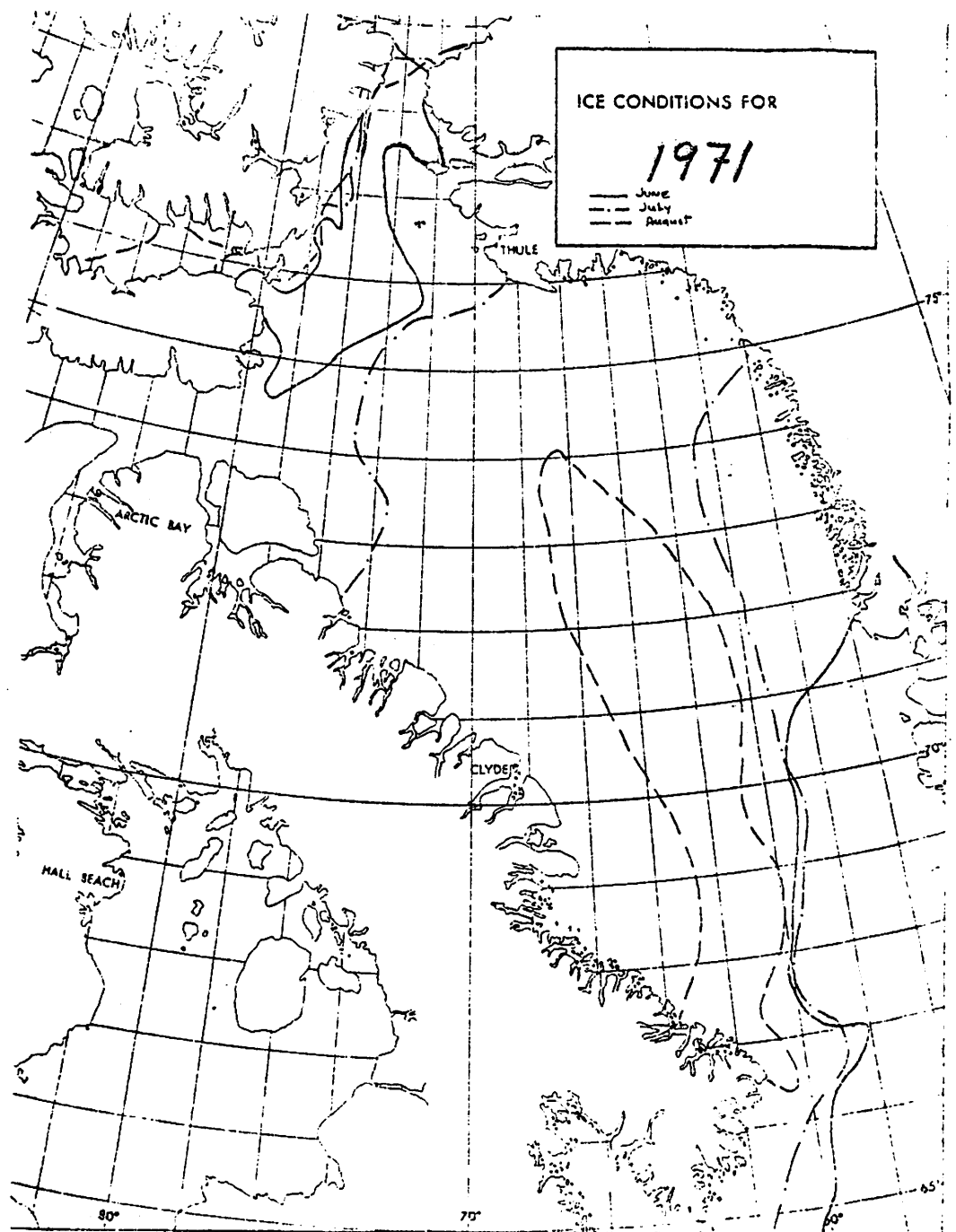


Figure 5A.1b Ice conditions in Baffin Bay, 1971

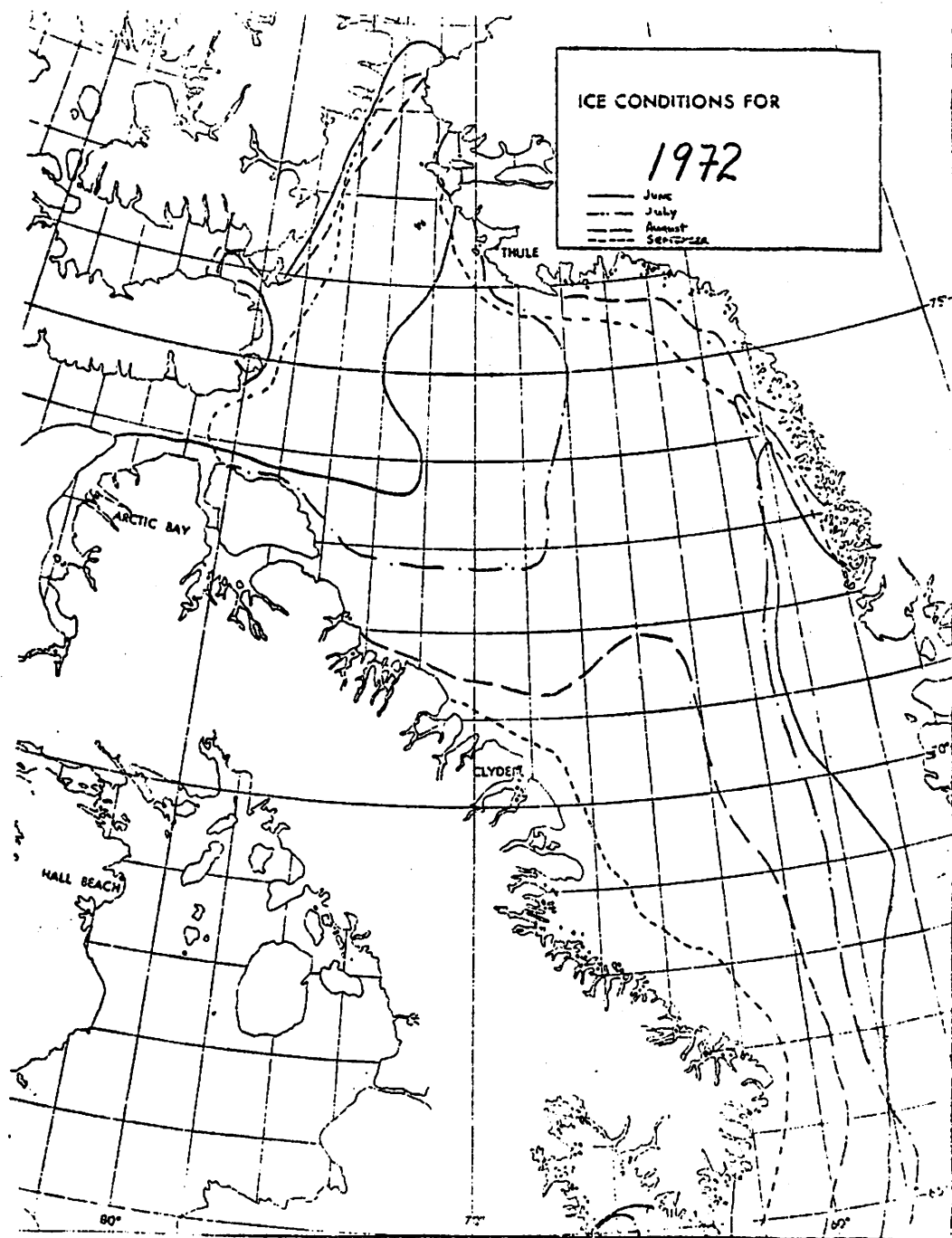


Figure 5A.1c Ice conditions in Baffin Bay, 1972

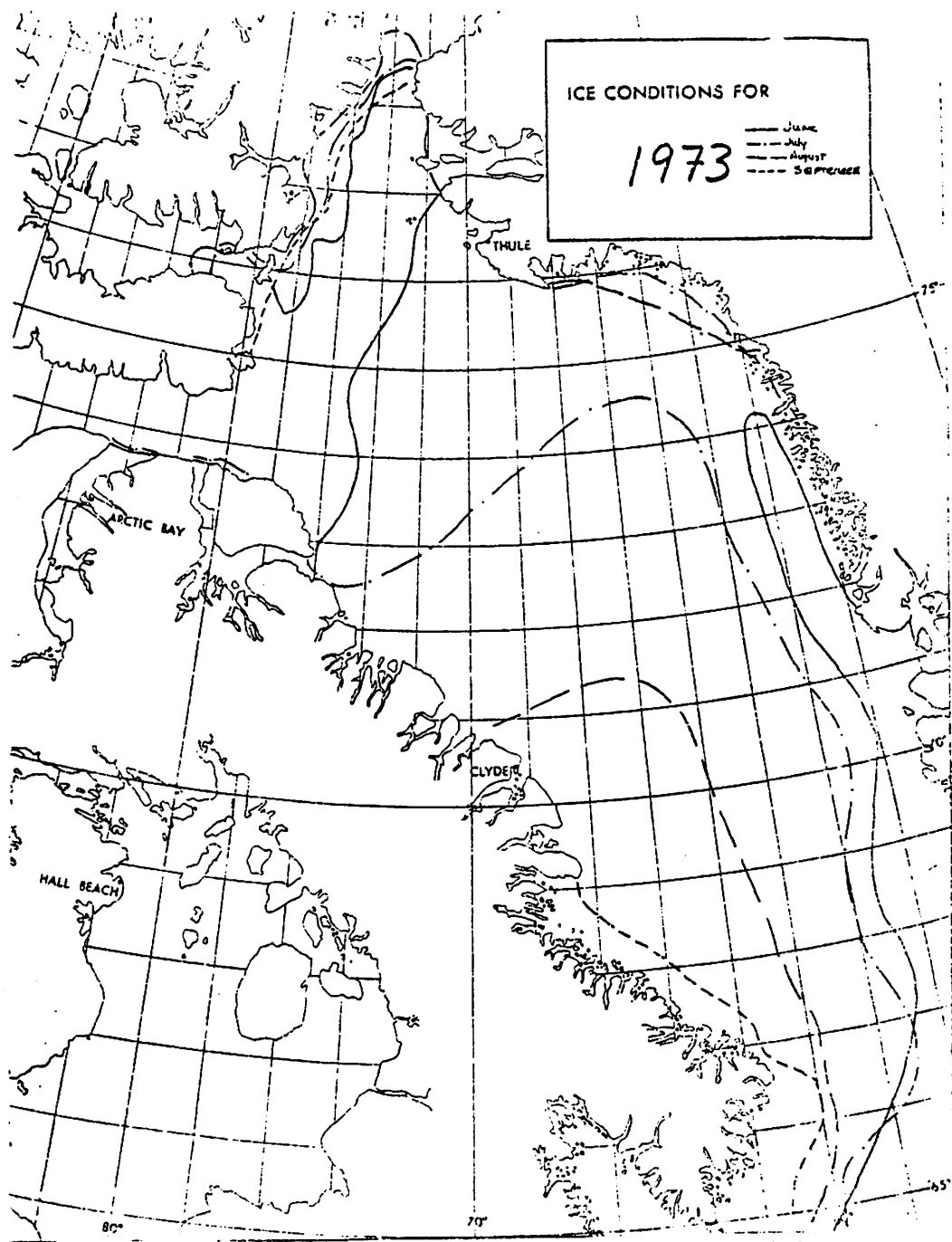


Figure 5A.1d Ice conditions in Baffin Bay, 1973

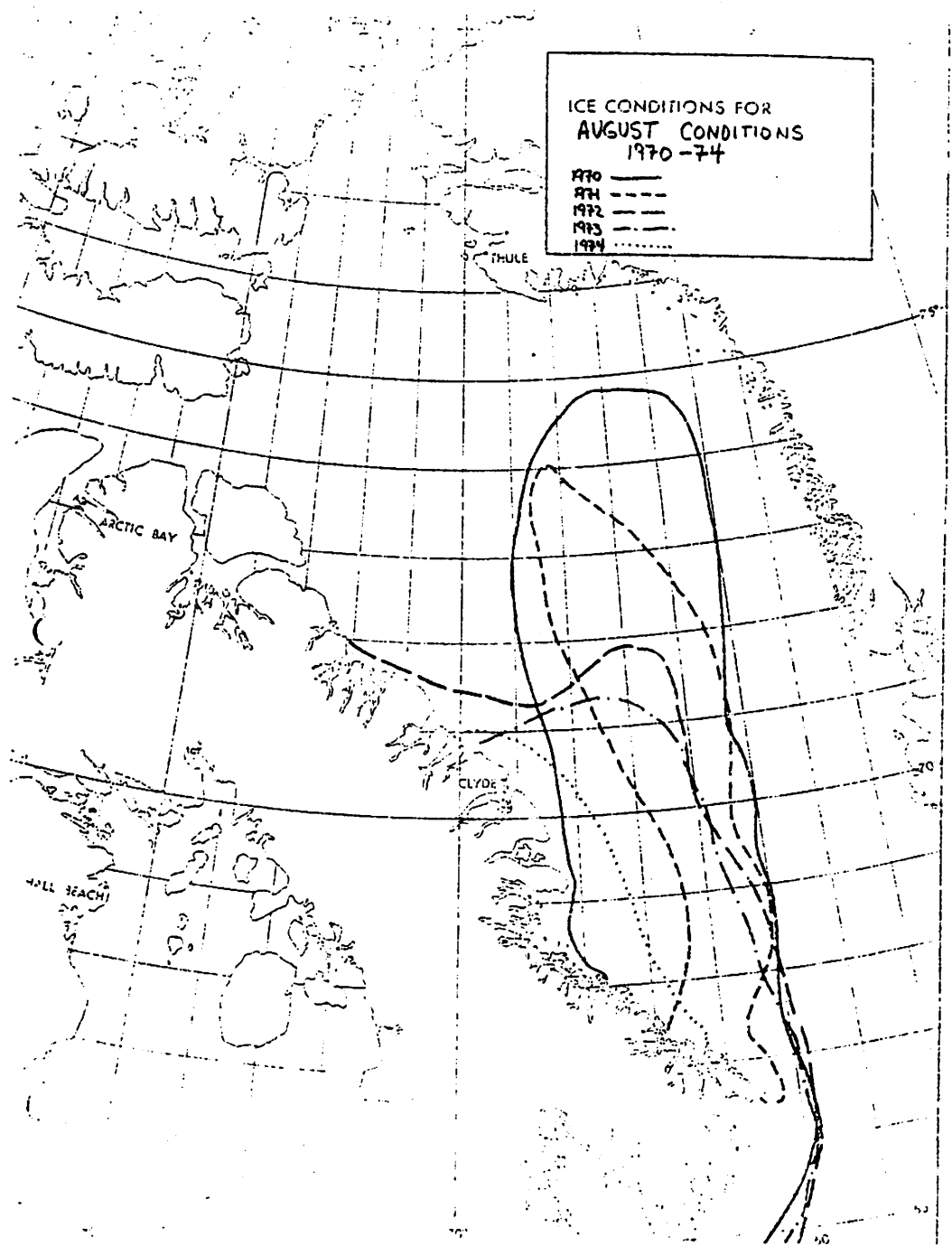


Figure 5A.1e Ice conditions in Baffin Bay, 1970-74

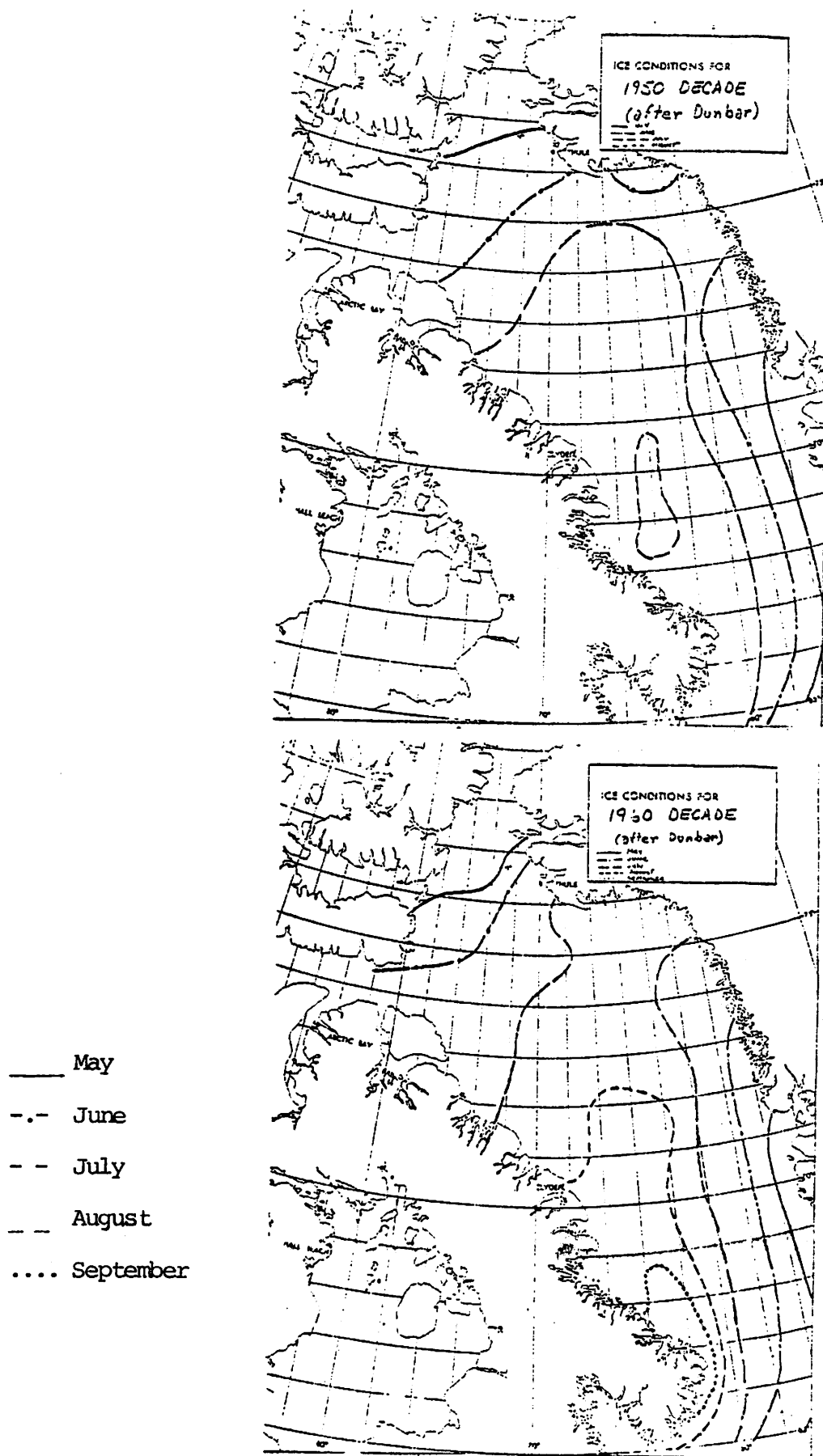


Figure 5A.2. Mean monthly pack ice extent for the 1950s and 1960s (after Dunbar 1973)

Figure 5A.3a

GENERALISED PATTERN OF ICE ACCUMULATION

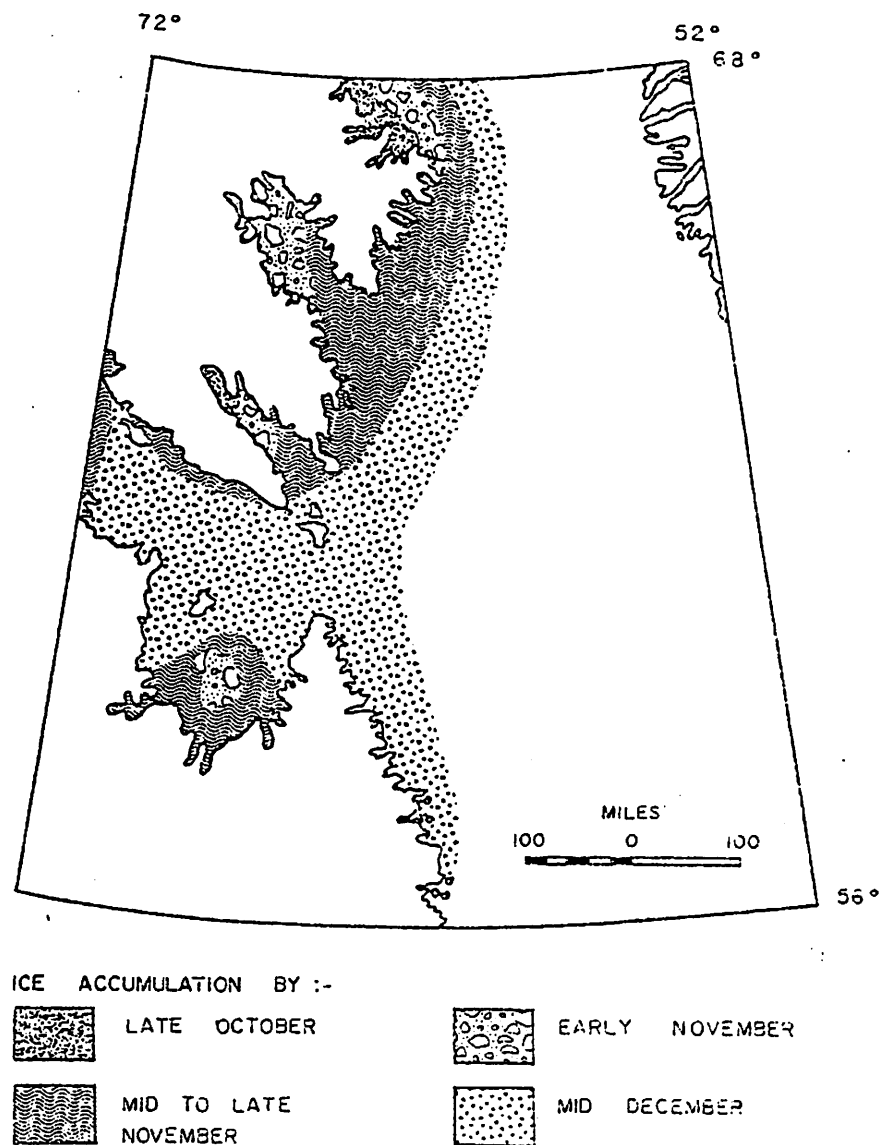
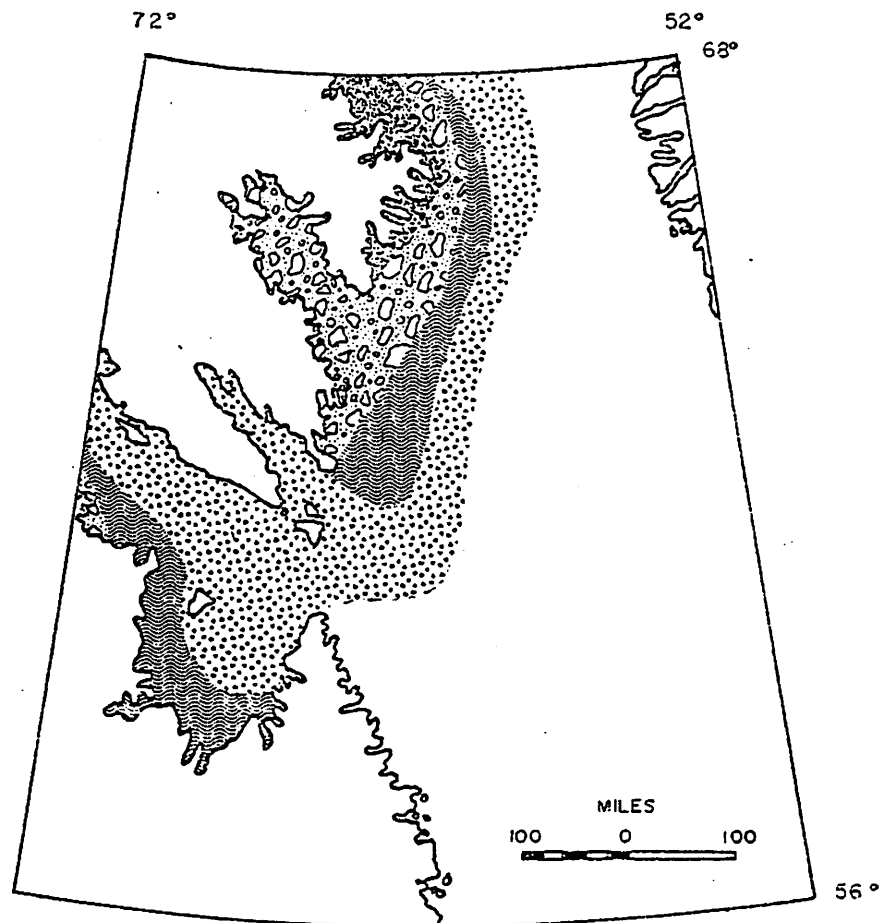


Figure 5A.3b

GENERALISED PATTERN OF ICE ACCUMULATION



ICE ACCUMULATION BY :-



EARLY OCTOBER



MID TO LATE
OCTOBER



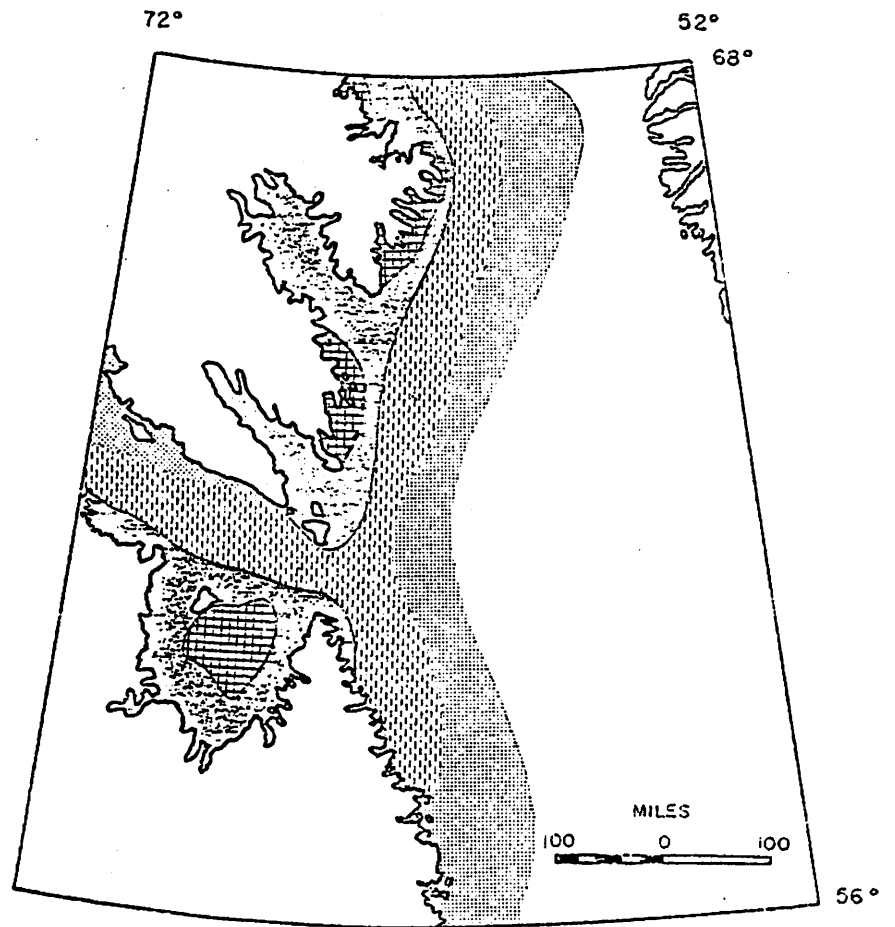
LATE OCTOBER OR
EARLY NOVEMBER



MID NOVEMBER

Figure 5A.4a

GENERALISED PATTERN OF ICE REMOVAL



SPREAD OF OPEN WATER BY :-



EARLY JUNE



MID TO LATE
JULY



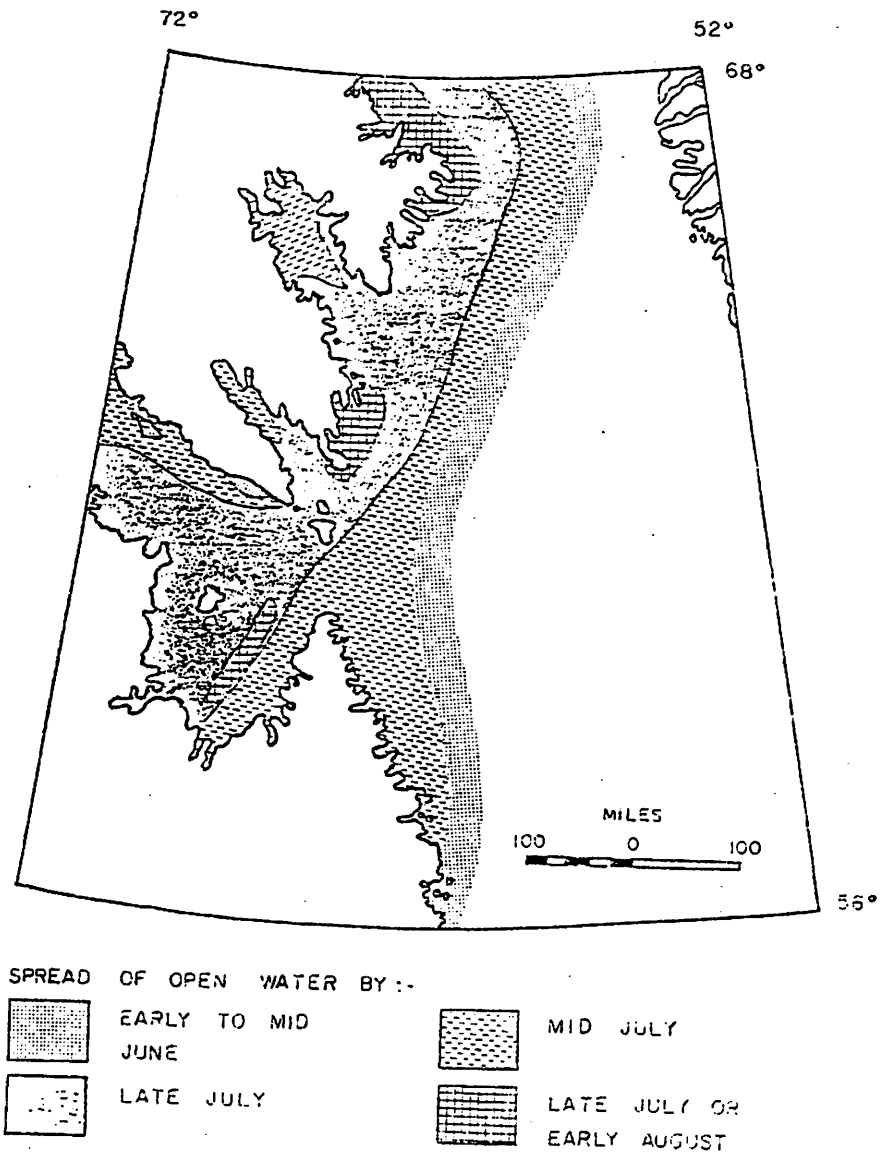
LATE JULY OR
EARLY AUGUST



EARLY AUGUST

Figure 5A.4b

GENERALISED PATTERN OF ICE REMOVAL



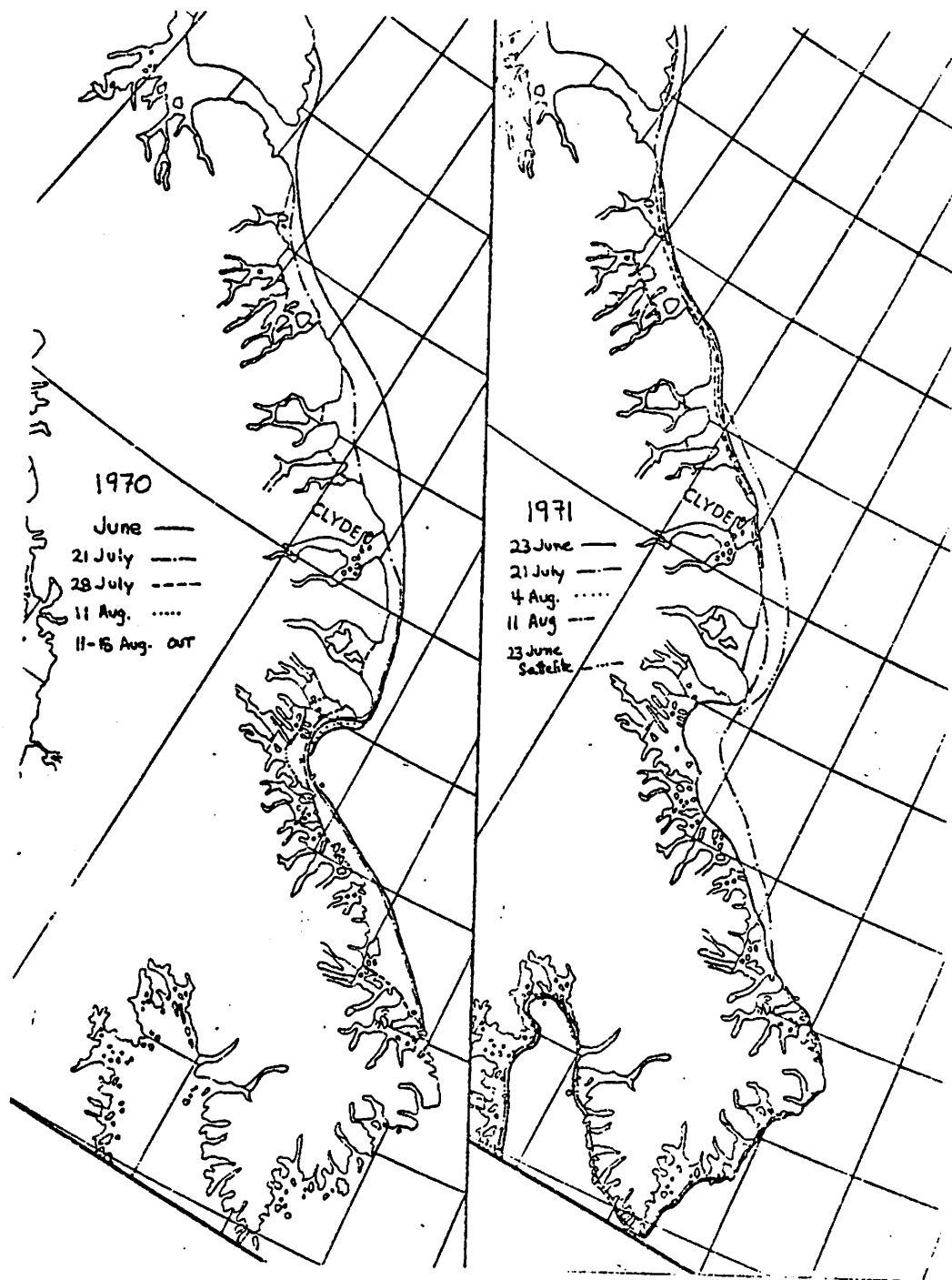


Figure 5A.5a,b Fast ice margins along the east coast of Baffin Island

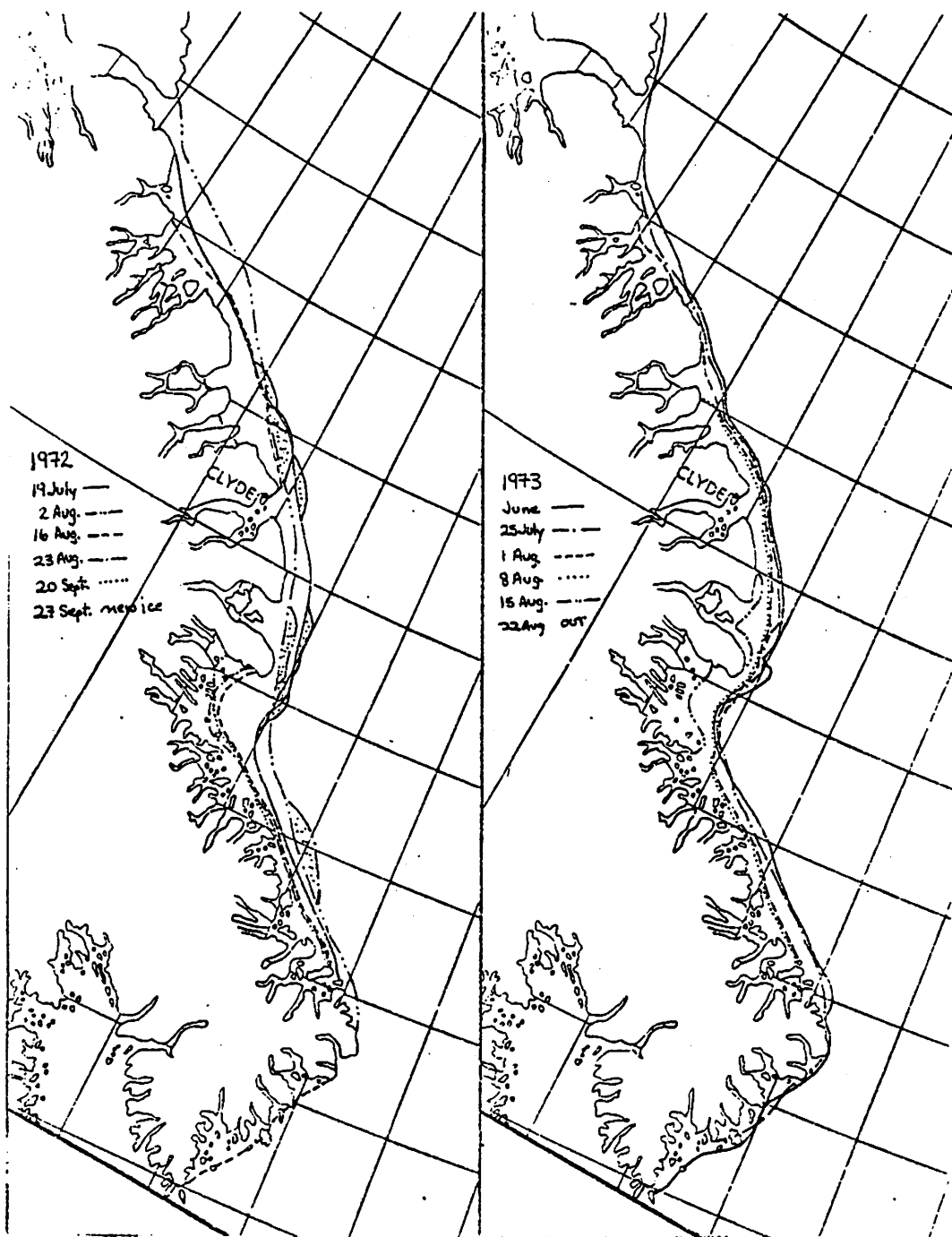


Figure 5A.5c,d Fast ice margins along the east coast of Baffin Island

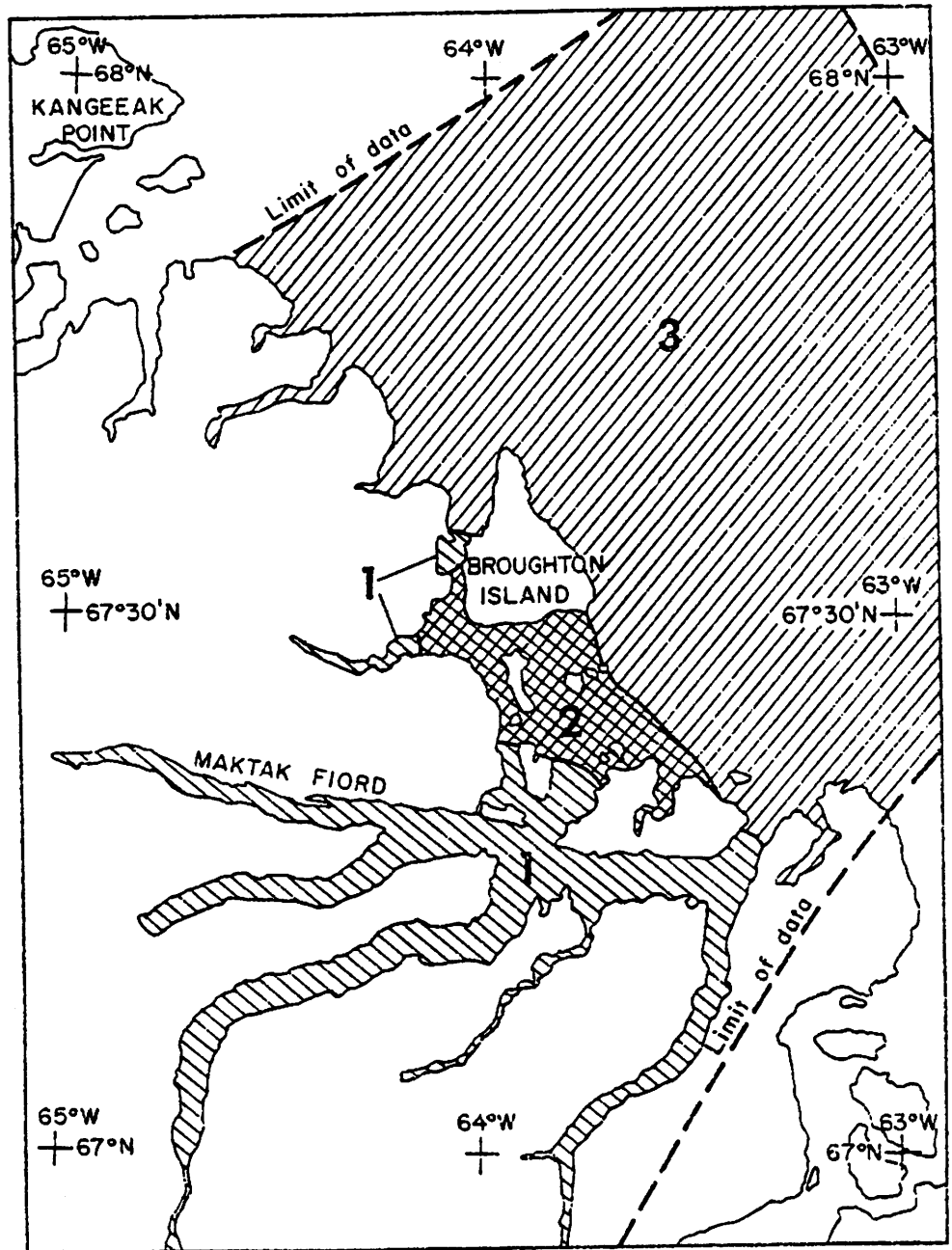


Figure 5A.6 Generalized progression of breakup in the Broughton Island area.

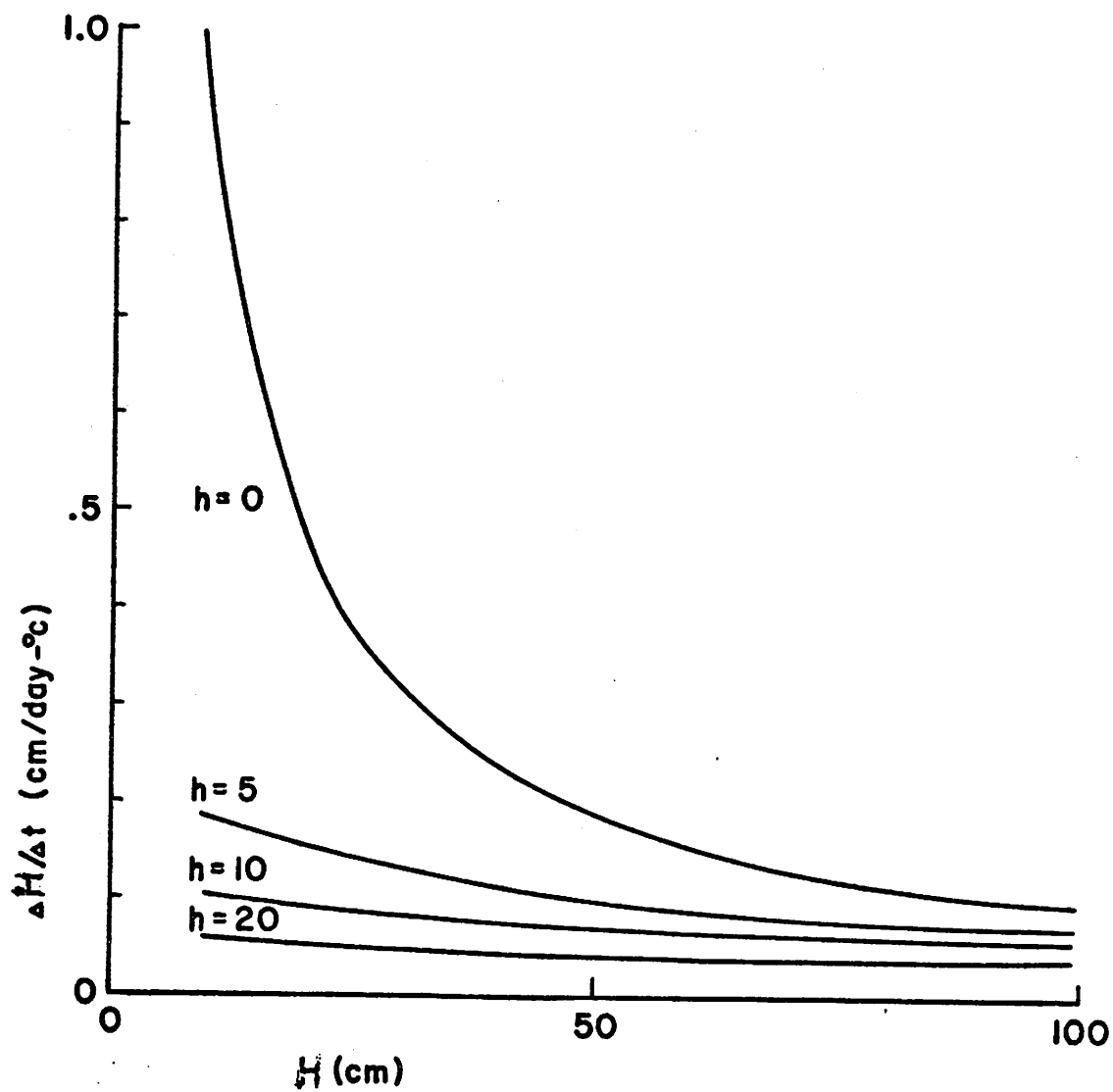


Figure 5B.1 Sea ice growth rate ($\Delta H / \Delta t$) in relation to ice thickness (H) for various depths of snow cover (h).

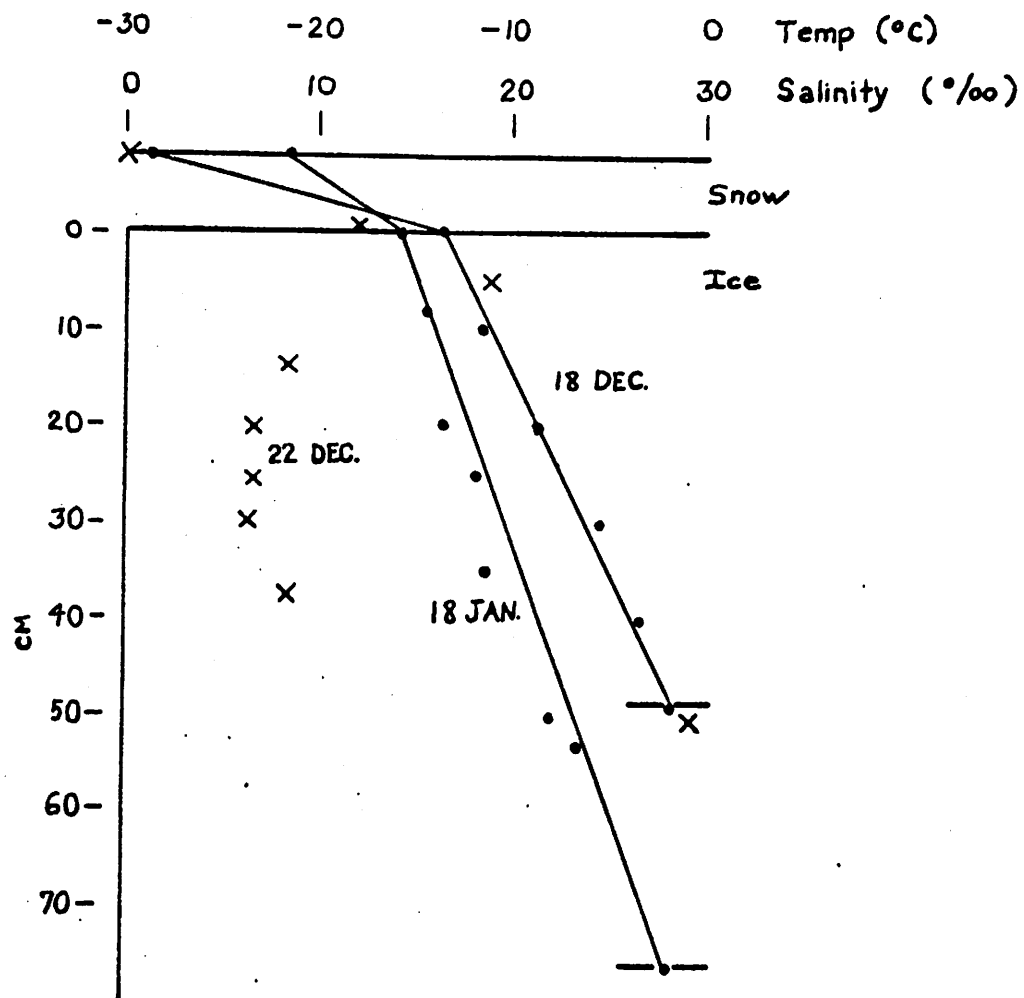


Figure 5B.2 Examples of temperature and salinity profiles in fast ice, Broughton Harbor, Winter 1971-72.

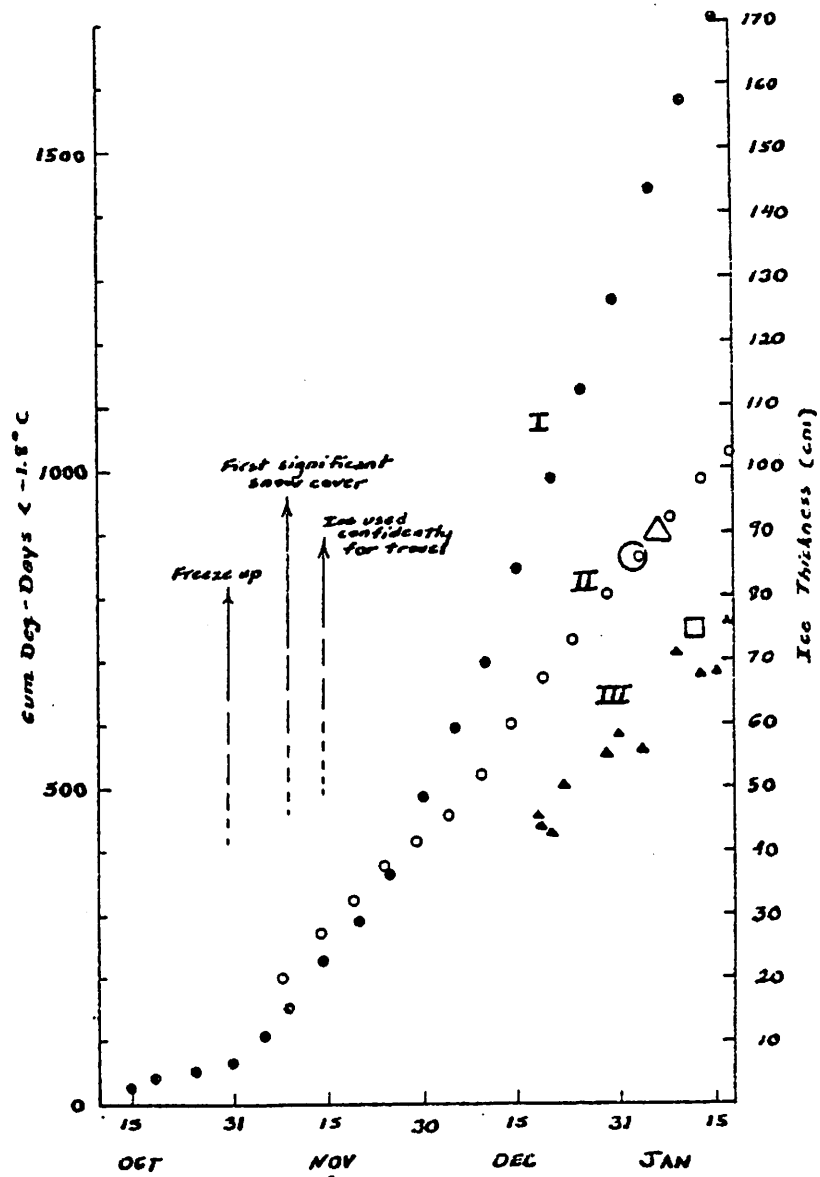


Figure 5B.3 Fast ice growth during winter 1971-72 near Broughton Island. Points I (•) show cumulative degree-days below -1.8°C , II (o) shows the calculated growth (using equation 5B.1) and III shows measured values in Broughton Harbour (▲) and Delight Harbor, Padloping Island (□).

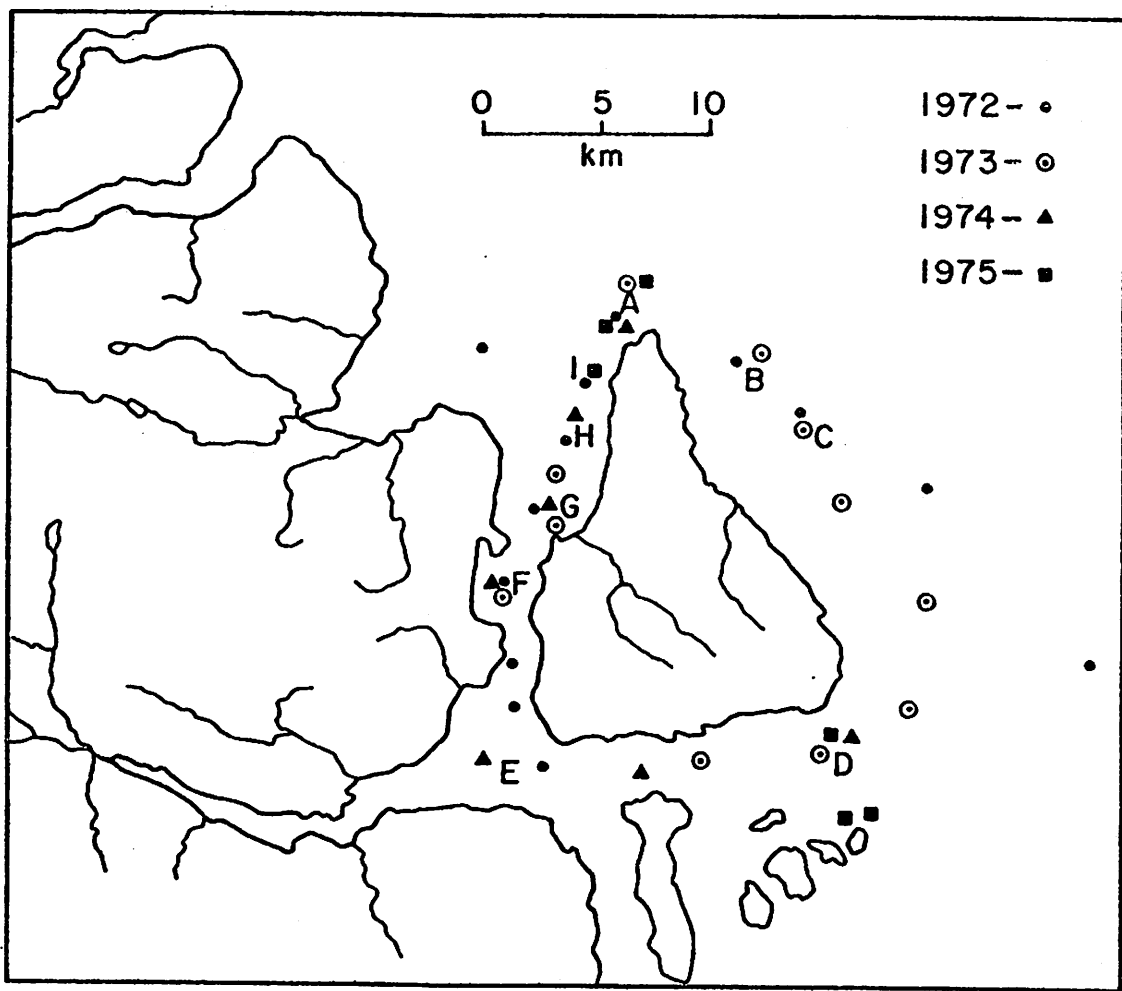


Figure 5B.4 Location of stations for ice thickness measurements around Broughton Island, 1972-75.

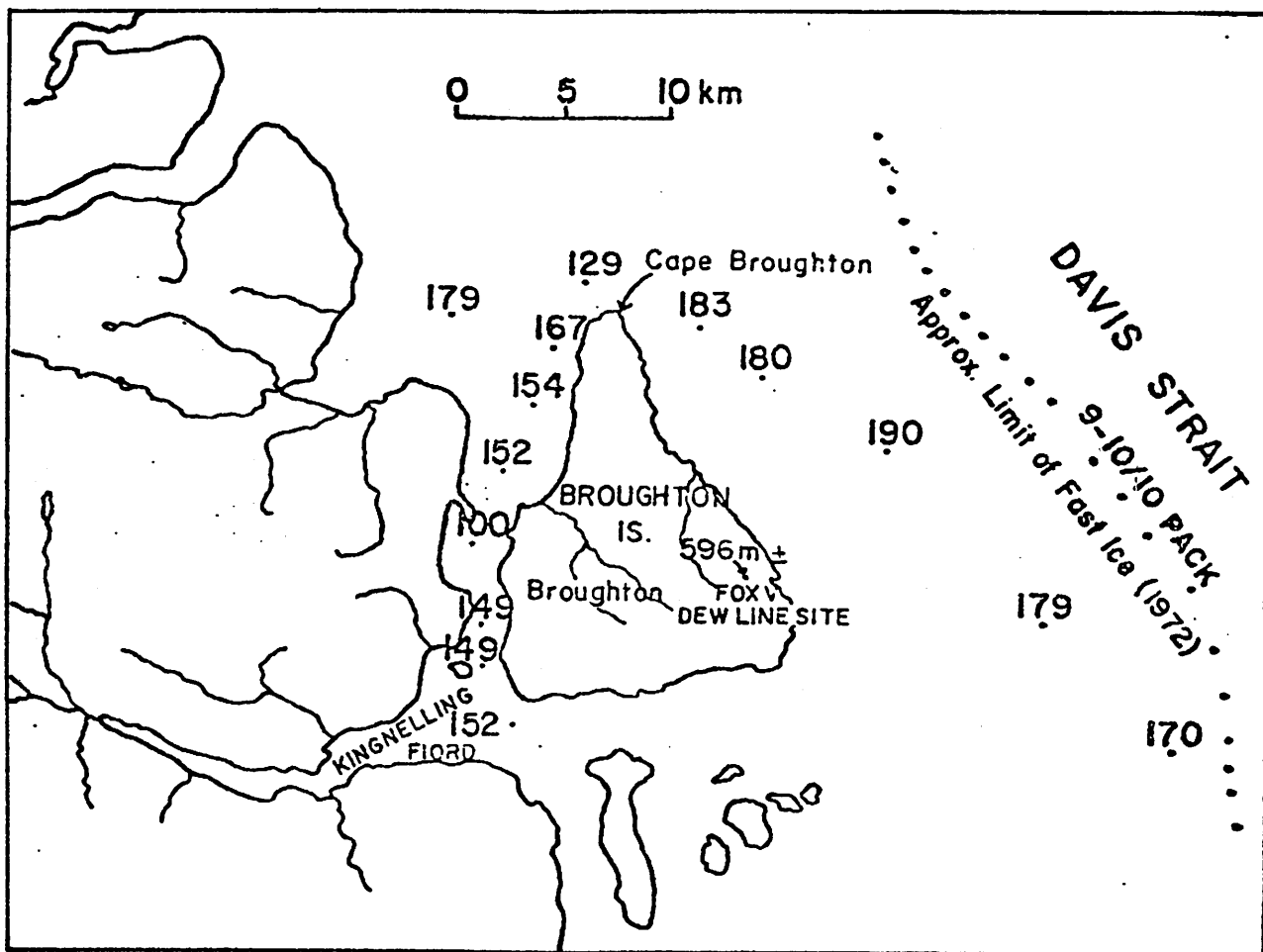


Figure 5B.5 Maximum thickness (cm) of fast ice around Broughton Island in early June, 1972.

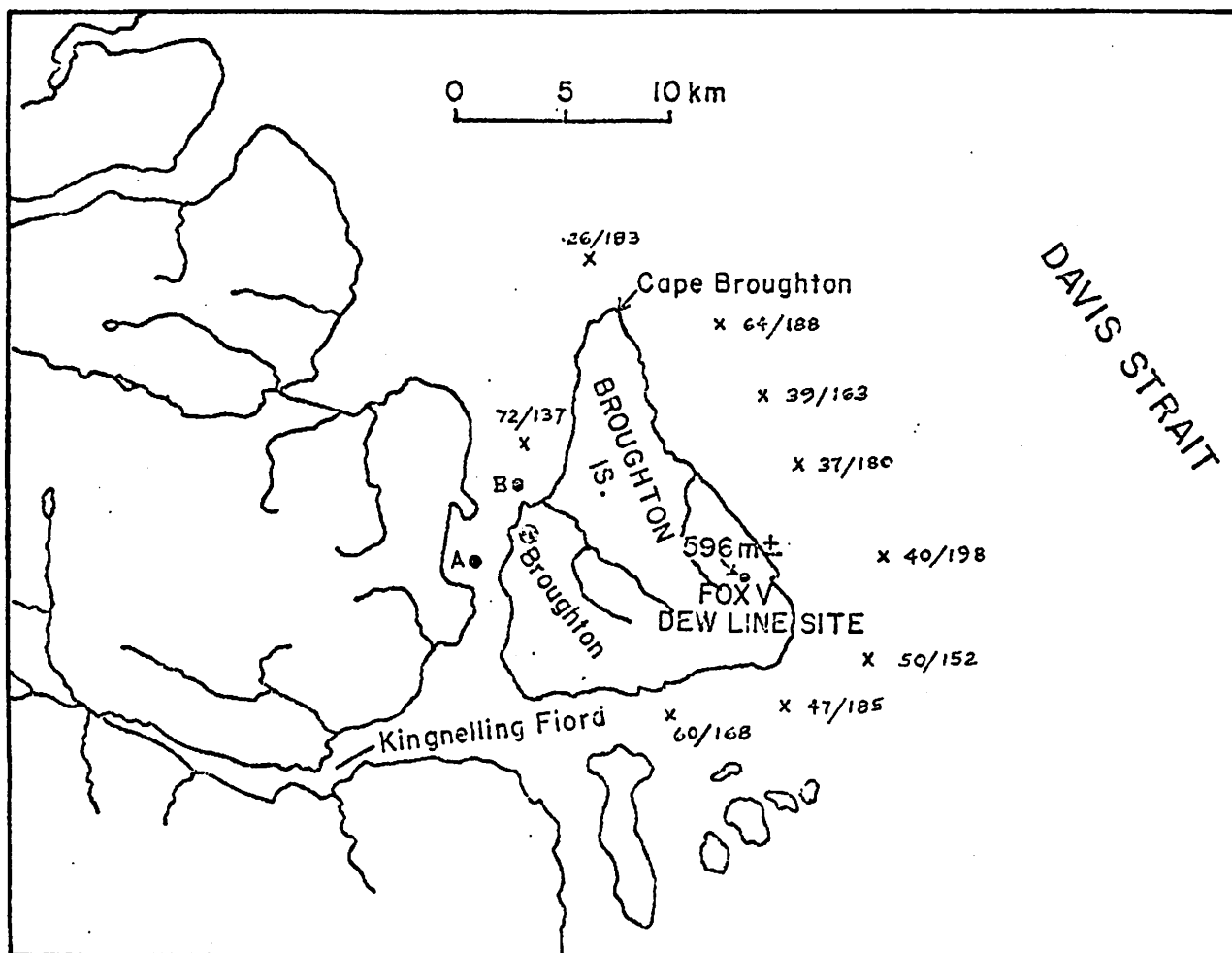


Figure 5B.6 Snow depths and ice thickness (cm) around Broughton Island in early June 1973.

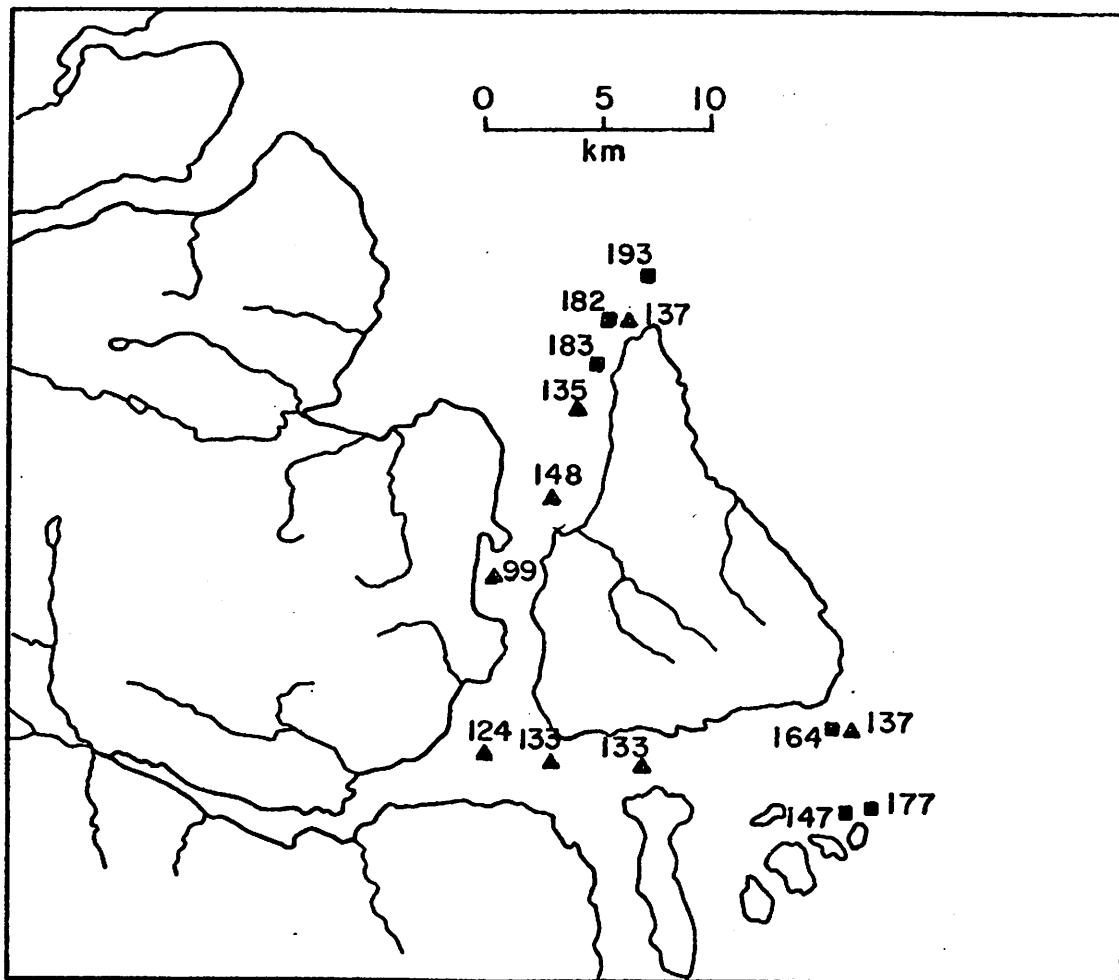


Figure 5B.7 Maximum thickness of fast ice around Broughton Island in early June 1974 (triangles) and 1975 (squares).

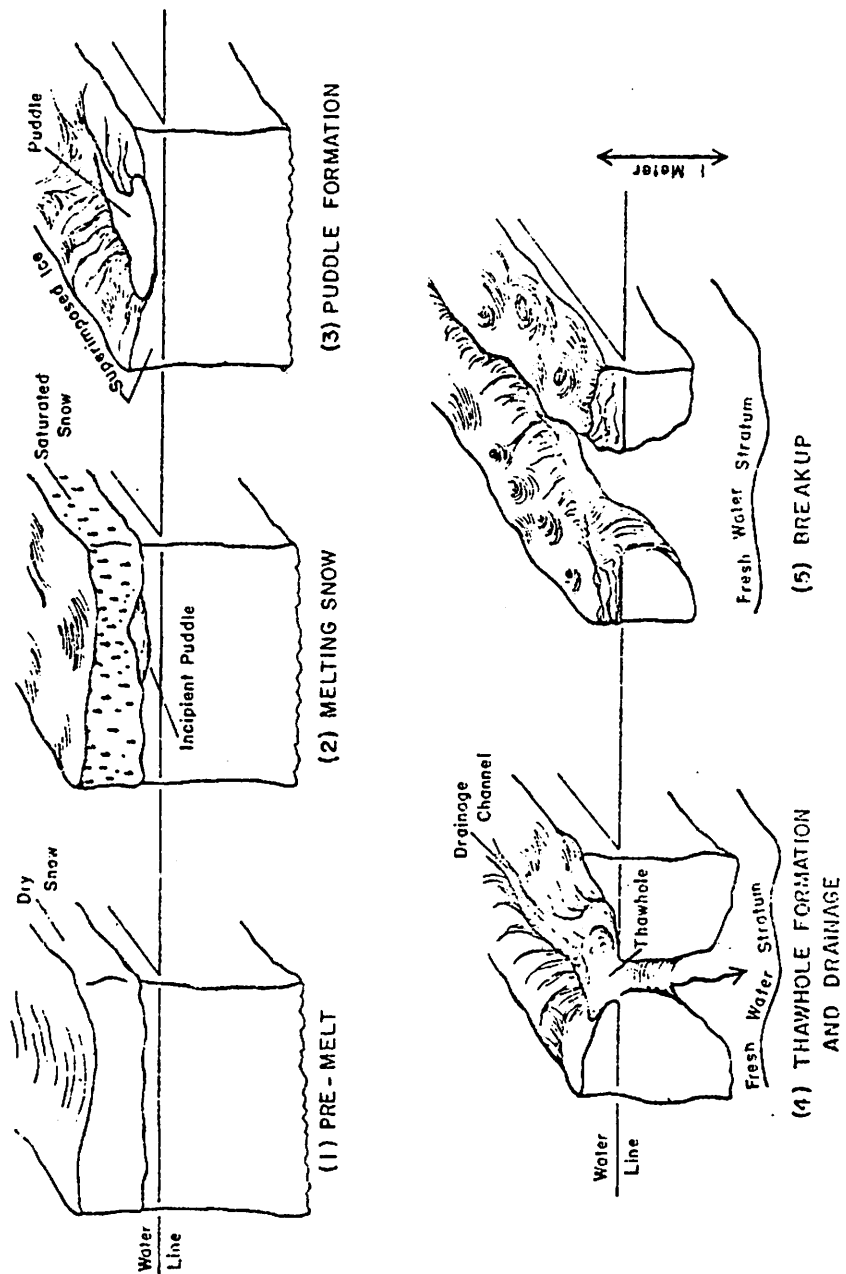


Figure 5.B.8. Five stage model of ice melt.

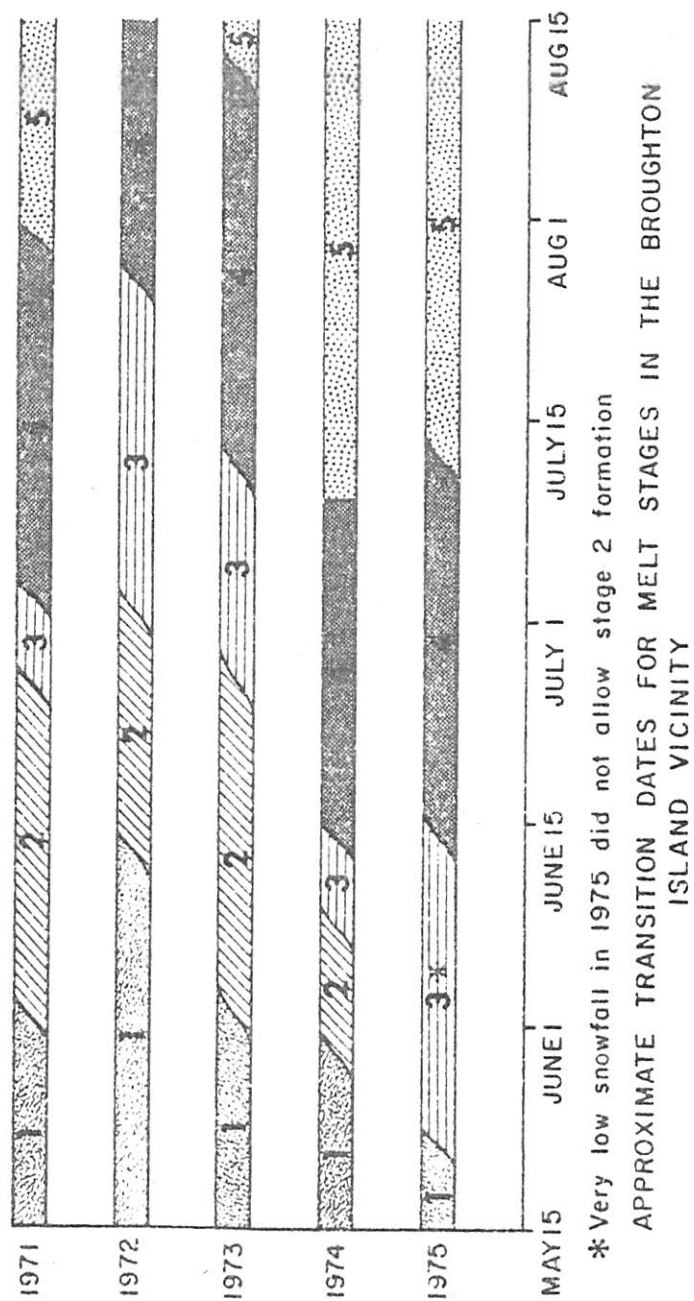


Figure 5.R. 9. The progression of the melt stages, on the fast ice at Broughton Island 1971-75.

REFERENCES

- Barnes, J.C. and Bowley, C.J. 1973. Mapping sea ice from the Earth Resources Technology Satellite. Arctic Bull. 1: 6-13.
- Barry, R.G., Crane, R.G., Locke, C.W., Locke W. W. III and Miller, G.H. 1977. The coastal environment of southern Baffin Island and northern Labrador-Ungava. Final Report, Project 138 to Imperial Oil Limited, Inst. Arct. Alp. Res., University of Colorado, Boulder, 165 pp. (Mimeo).
- Campbell, N.J. and Collin, A.E. 1956. A preliminary report on some of the oceanographic features of Foxe Basin, 1955. Atlantic Oceanographic Group, St. Andrews, N.B. Mimeo, 28 pp.
- Canadian Hydrographic Service. 1970. Pilot of Arctic Canada. Vol. 1, 2nd ed., Marine Sciences Branch, Dept. of Energy. Mines & Resources, Ottawa, 247 pp.
- Doronin, Yu. P. 1969. Thermal Interaction of the Atmosphere and Hydrosphere in the Arctic. Hydrometeorological Institute, Leningrad. (Trans. by Israel Program for Scientific Translation, Jerusalem), 244 pp.
- Dunbar, Moira. 1972. Increasing severity of ice conditions in Baffin Bay and Davis Strait. In: Karlsson, T. (ed.), Sea Ice, Nat. Res. Council, Reykjavik: 87-93.
- ERTS-1 Data users handbook. 1972. Goodard Space Flight Center document. No. 71504249.
- Jacobs, J.D., Barry, R.G., Bradley, R.S. and Weaver, R.L. 1974. Studies of climate and ice conditions in eastern Baffin Island, 1971-73. Inst. Arct. Alp. Res., Occas. Pap. No. 9. University of Colorado, Boulder, 78 pp.
- Jacobs, J.D., Barry, R.G. and Weaver, R.L. 1975. Fast ice characteristics with special reference to the eastern Canadian Arctic. Polar Record 17: 521-536.
- Langleben, M.P. 1966. On the factors affecting the rate of ablation of sea ice. Can. J. Earth Sci. 3: 431-439.
- Lieske, B.J. 1964. Net radiation over fast sea ice during spring break-up at P. Barrow, Alaska. Proc. 15th Alaskan Science Conference, 52-60.
- Weaver, R.L. 1974. Mapping seasonal changes in the fast ice and pack ice using remote sensing data. In: Jacobs, J.D. et al., pp. 47-54.
- Weaver, R.L., Jacobs, J.D., Barry, R.G. 1976. Fast ice studies in W. Davis Strait. In: Proc. Third International Conf. on Ports and Ocean Engineering under Arctic Conditions, Vol. 1, Univ. of Alaska: 455-66.
- Zubov, N.N. 1945. L'ydy Arktiki. Izdat. Glavsevmorputi, Moscow (transl. Arctic Sea Ice, U.S. Navy Oceanogr. Office, 1963, 491 pp.).

6. MICROCLIMATOLOGY OF THE FAST ICE

R. L. Weaver, R. G. Crane and J. D. Jacobs

A. Approach and Methods

The purpose of the microclimatological programs carried out on the fast ice near Broughton Island was to determine the major energy exchanges which control ice melt and to link them to synoptic-scale atmospheric systems. Energy exchanges were determined by a combination approach of energy budget analysis and aerodynamic estimates of turbulent fluxes.

The fast-ice system has interfaces with the atmosphere and with the ocean across which energy exchange can take place. The upper and lower boundary surfaces of a fast-ice sheet are considered to be planes of zero thickness through which all energy absorbed at their surfaces must pass. The instantaneous, one-dimensional energy balance equation for the ice-atmosphere boundary may be written:

$$K\downarrow(1-\alpha) + L^* + H + LE + G_a = 0 \quad (6A.1)$$

where

$K\downarrow$ = global solar radiation

α = shortwave spectral reflectance (albedo)¹

L^* = net longwave radiation

H = turbulent transfer of sensible heat

LE = turbulent transfer of latent heat

G_a = surface flux into the ice

Fluxes into the ice are positive. A similar equation may be formulated for the lower ice-ocean boundary.

$$K_w(1 - \alpha_w) + H_w + G_a = 0 \quad (6A.2)$$

K_w = shortwave flux at the lower ice surface

α = albedo of the water (i.e. water interface)

H_w = turbulent heat transfer between ice and water

K_w depends on ice composition, thickness and $K\downarrow$. The longwave radiation received at the surface does not penetrate into the ice and is therefore non-existent at the lower surface. Energy fluxes from precipitation, momentum flux and salt migration are considered

¹Some confusion exists about the exact meaning of the term albedo. Here it is specifically defined as the integrated spectral reflectance for the wavelengths between 0.3 and 2.8 μ m as a fraction of the incident flux.

negligible and are not included in the above formulae.

The net energy input to the ice sheet is derived from integration of these fluxes over time and ice depth. It is assumed that the absorbed energy is used either to warm the ice, if the ice is below salinity melting point, or to melt ice. The ice response, determined by the basic thermodynamic quantities of specific heat, thermal conductivity and heat of fusion, is complexly related to density, temperature, and most importantly salinity.

The energy balance terms may be divided into three groups: the radiative fluxes (K^+ , α , L); the turbulent fluxes (H , LE); and the surface flux (G). Estimates of the various surface energy budget fluxes by Weller (1968), Maykut and Untersteiner (1971) and Jacobs (1973) all indicate that radiative processes are more important than turbulent terms, at least for melting sea ice.

Site Location

Field microclimatological stations which provide the data base for our work were operated by the R.L. Weaver and D. Goth in 1973 and 1974, and by R.S. Bradley and R. McKnight in 1972. The station locations are shown in Figure 6A.1. The duration of station operation and frequency of observations for 1972, 1973, and 1974 are listed in Figures 6A.2-4, respectively.

In all three years attempts were made to select sites representative of the fast ice in the immediate surrounding area. All stations were between 1.6 and 2 km from shore. However, this distance is insufficient to eliminate atmospheric advection effects from the land masses. Therefore, while the results from these stations apply to the near-shore fast ice environment, they probably do not represent conditions of the outer parts of the fast-ice sheet.

In 1972 the sites were located approximately 5 km north of Broughton Village. The station was moved closer to shore in early July due to deteriorating ice conditions. The first location in 1973, the "west" site, established on 20 June, was abandoned in early July when the underlying ice became too thin for safe operation. The station was then moved to the "north" site for the remainder of the 1973 season. In 1974 the ice station was located south of Broughton Island from 6 June until 9 July when the local ice disintegrated.

The 1972 station was situated on 1.5 m first year ice after a winter of below normal temperatures. The "west" station was on 0.75 - 1.0 m first year fast ice (in early June). In contrast, the "north" site was over mixed first and second year fast ice 1.0 - 1.3 m thick. The 1974 station was situated over 1.2 - 1.4 m thick first year ice. The snow cover in 1973 was 0.4 - 0.5 m thick in early June, while snow was essentially nonexistent in 1974.

Table 6A.1. List of Microclimatological Parameters and Their Frequency of Measurement

Parameter	1972	1973	1974
Net radiation (Q*) unsaturated surface	C	C	C
Net radiation (Q*) saturated surface	P	P	C
Global solar radiation (K+)	C	C	C
Solar albedo (α)	P	PT	PT
Solar albedo under net radiation sensor (α)	Daily	Daily	Daily
Temperature @ 1.2 m (Hygrothermograph in meteorological screen)	C	C	C
Temperature @ 2 m (aspirated thermistor)	ND	ND	C
Temperature profiles @ 4 levels (Thornthwaite system)	P	ND	ND
Relative humidity (hygrothermograph in meteorological screen)	C	C	C
Relative humidity two level profiles (Assman type psychrometers)	P	P	P
Wind run at 2 m	C	C	C
Wind profiles at 4 levels	P	ND	ND
Wind run at 1 m	ND	ND	C

C = Continuous

P = Periodic

ND = No Data

PT = Periodic Transect

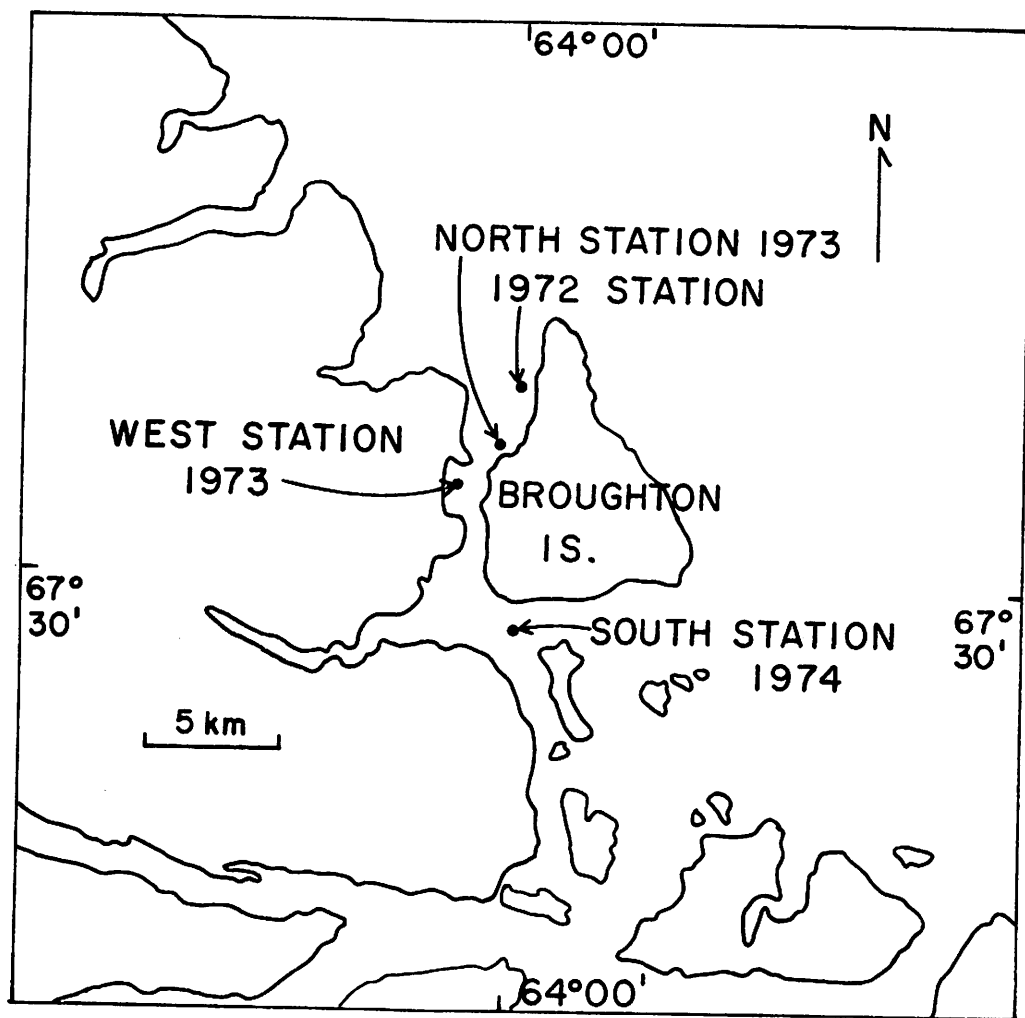


Figure 6.A.1. Location map of microclimatological stations, 1972-74.

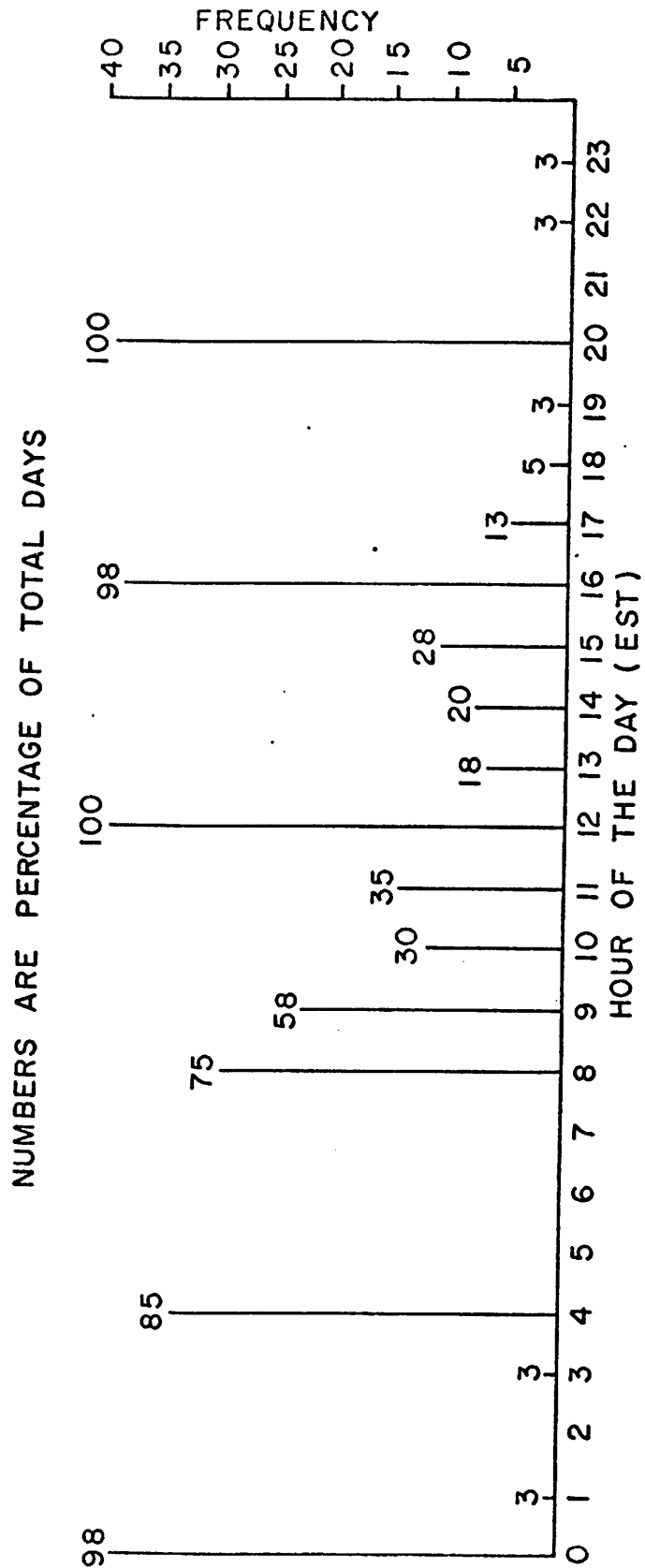


Figure 6A. 2. Summary of observation frequency, 1972.

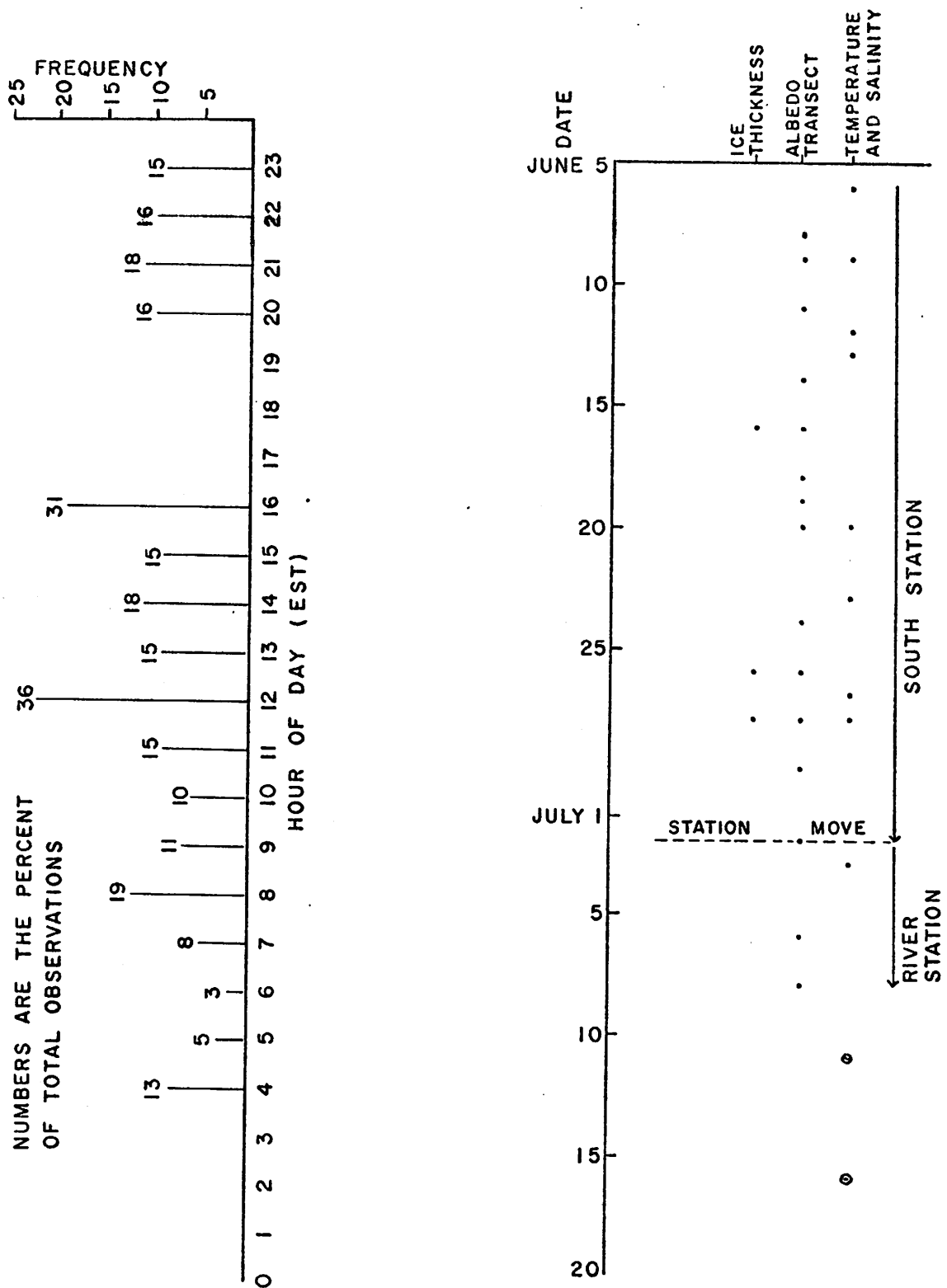


Figure 6A. 4. Summary of record duration and observation frequency, 1974.

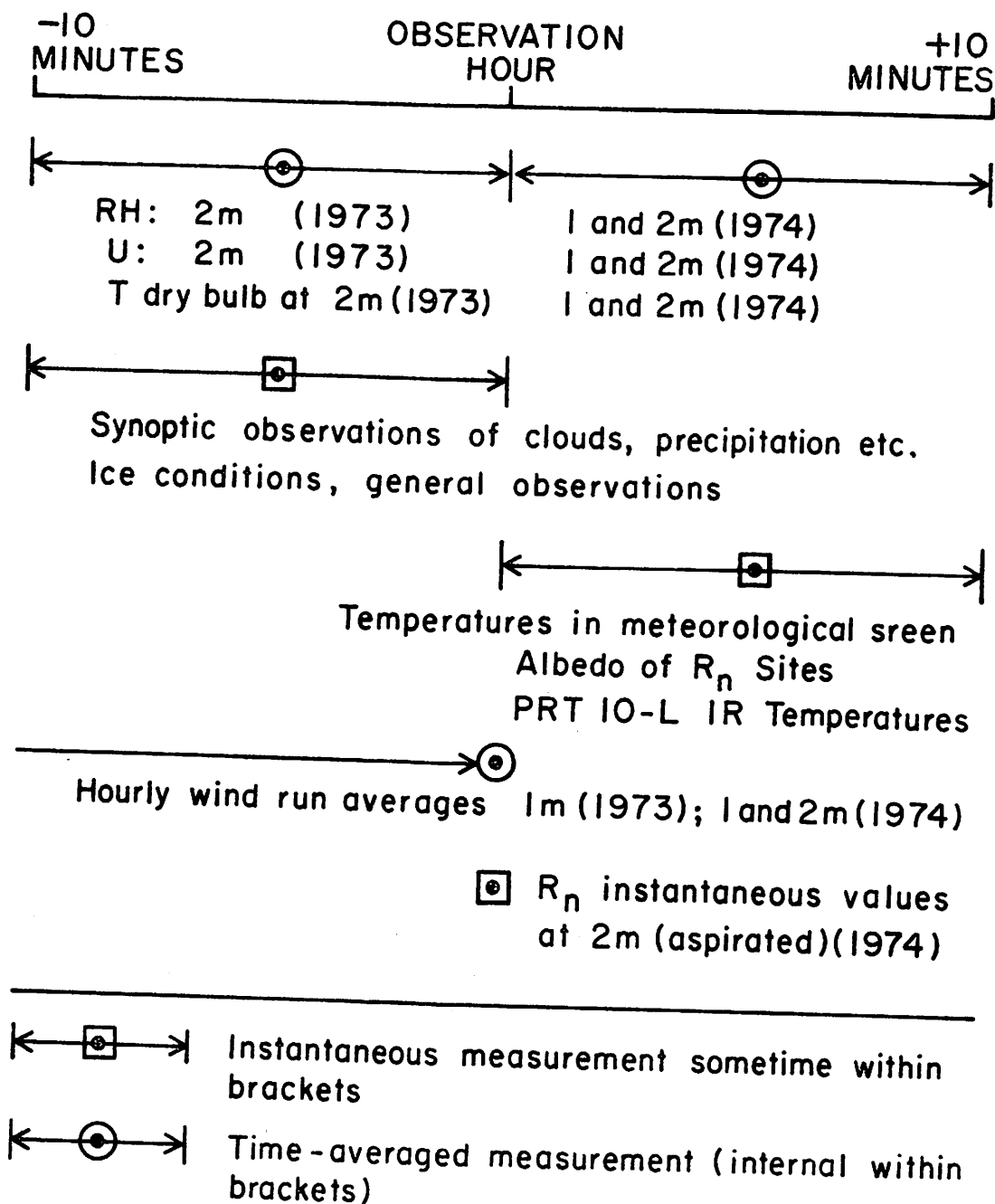


Figure 6A. 5. Hourly observation routine used at microclimatological stations, 1973 and 1974.

Tidal currents underneath each site differed, although no measurement of current velocity was made. Tidal effects were subjectively judged to be less important under the "north" stations. However, those under the "west" station certainly accelerated the ablation rate through oceanic advection affects.

Instrumentation and Measurement Procedures

The aim of the field station measurement program was to observe the dominant energy fluxes continuously and the minor contributors periodically. Based on the work of others (e.g. Weller, 1968) and our own field measurements, global solar and net radiation, and short wave albedo were judged to be the most important variables for measurement during the ablation season. The first two were recorded continuously and the third daily. Atmospheric temperature, relative humidity, wind, and surface temperatures were recorded periodically. The measured parameters and their frequency of observation are listed in Table 6A.1. The observation routine is presented in Figure 6A.5. Description of instrumentation and data collection procedures may be found in Appendix 1.

The global solar radiation sensor was located in the Broughton settlement. Since the ice station was within 5 km of the Broughton settlement measurement site in 1972 and 1973, the deviation in the integrated daily solar radiation totals should be small except on the few occasions when persistent low stratus or fog occurred over one location and not the other. No quantitative evaluation of this deviation was made. In 1974 the site displacement may have caused significant deviations since more variable cloud conditions did occur between Broughton Village and the field site some 8-10 km south. However, such cases have been excluded from the analyzed data set for 1974.

B. Radiation Results

Surface Albedo Effects

Since solar radiation is the largest energy source during the ablation season, albedo becomes the single most important controlling factor of the radiant energy absorbed by the ice. Examples of typical albedo values for various arctic surfaces are presented in Table 6B.1.

Based on work of Langleben (1969), Jacobs (1973), has suggested that the average surface albedo of sea ice may be expressed as the summation of several partial albedos weighted by the percentage of the total surface area occupied by each albedo type. This is stated mathematically as follows.

$$\alpha_t = \alpha_1 s_1 + \alpha_2 s_2 + \alpha_3 s_3 + \dots + \alpha_n s_n : s_t = \sum_{i=1}^n s_n = 1$$

(6B.1)

Thus, the albedo of fast ice may be considered as the summation of the various surface type-areas. In this study data were collected over smooth ice, surface puddles, and open water. If only smooth ice and surface puddles are considered, then equation 6B.1 may be simplified:

$$\alpha_t = (S_i S_t^{-1}) (\alpha_i - \alpha_p) + \alpha_p \quad (6B.2)$$

where $S_i S_t^{-1}$ is the fractional area covered by smooth ice.

Surface albedo data were collected in 1972-74 following techniques outlined in Appendix 1. The progression of the spatial mean albedo and albedos of unsaturated ice, and puddles are shown in Figures 6B.1-2 for 1973 and 1974, respectively. Comparison and analysis of these transect data and single point measurements under the net radiation sensors suggest the following conclusions:

(1.) A simple linear regression model can be used to represent the relationship between the "point surface estimator" (the net-radiation site value) of albedo and the spatial mean value determined by the transect data from the appropriate surface class. The regression results show a strong and significant linear relationship between the single point and transect data sets (see Figures (6B.2-3)). Single point measurements of unsaturated or puddled surface types should represent the mean albedo for the given surface type to within ± 10 percent. Therefore, given a point albedo measurement and air estimate of the fractional area for each class, the mean surface albedo may be calculated using equation 6B.2. This conclusion has not been tested for areas larger than 100-200 m², but subjective observation of smooth first-year ice indicate that it should apply to larger regions.

(2.) No overall time-dependent linear trends were evident in either the 1973 or 1974 data, (see Figures 6B.1-2). Studies of daily mean albedo variations indicate a complex interaction between surface area of the ice types, the albedo of puddles, and the albedo of unsaturated ice which can not be simplified beyond the relationship stated in equation 6B.2. It is evident from analysis of precipitation events that the large variations in mean albedo are due mainly to snowfall in the ablation season.

(3.) Results from hand-held 35mm oblique photography, used to evaluate the changes in surface puddling, indicate that 1973 and 1974 were quite different in terms of percent coverage by puddles. Coverage in 1973 was only about 10 percent throughout the ablation season, whereas in 1974 it was between 30 to 40 percent. The 1974 photographs clearly show that the puddles formed between sastrugi-type snow dunes of 10-20 cm relief on the smooth ice surface and that this early organization governed puddle shape throughout the melt season.

(4.) The relative importance of the puddles and unsaturated ice in terms of their percent contribution to absorbed solar radiation varies during the melt season. The ratio of absorbed radiation of unsaturated ice vs. puddles ice is illustrated for a hypothetical incident flux of $100 \text{ cal cm}^{-2} \text{ hr}^{-1}$ in Table 6B.2. In 1973 and 1974, unsaturated areas account for more than half of the shortwave radiative input to the ice, (i.e., ratio >1). It is not until the puddled area reached 40 percent, on June 30, 1974, when albedos dip below 0.2, that the puddled area absorbs more short-wave radiation. However, the melt puddles did account for a larger proportion of the input in 1974, than in 1973.

(5.) If the surface albedo (α_t), as represented by equation 6A.4, is considered in isolation, then it must be concluded that there are no constant relationships between the three elements. However, an overall seasonal pattern of surface albedo is apparent. There are four general albedo phases: - (a) no puddles; (b) rapid puddle formation; (c) puddle deepening, and (d) break-up. This scheme is shown schematically in Figure 6B.5. Superimposed on this general framework are meteorologically-caused variations in mean albedo; due for example, to precipitation, formation of thin nocturnal ice-layers on puddles, etc. The timing of each stage and the rate of change in mean albedo is a combination of these weather elements, oceanographic conditions, and ice history.

Net Radiation

Results of radiation measurements (global solar, net radiation and net longwave) in 1972 are shown in Figure 6B.6. During the early part of the period, there was extensive snow cover with a mean albedo of 0.82. Conditions remained, for the most part, very cloudy and net radiation varied mainly in response to albedo changes, due to snowfall, and to associated surface temperature. The higher net radiation values generally occurred on days of heavy cloud cover with lower surface albedo.

Rain and higher temperatures led to a rapid increase in melting from midnight 5 July. The surface changed from almost 100 percent snow cover, with a mean depth of 8.2 cm to over 80 percent water/slush/ice by 9 July. The albedo decreased from 0.74 to 0.53 and remained relatively low after the 9th, with a mean of 0.57. After 9 July there was a large increase in the average net radiation, with daily totals of net radiation averaging about $.65 \text{ kJ cm}^{-2} \text{ dy}^{-1}$. Fluctuations in this period appear to be due mainly to cloud cover, with net radiation increasing as the cloud cover decreased.

Net radiation measurements in 1973 have been compared to global solar radiation recorded in Broughton Village. Inspection of these data (see Figure 6B.7) that deviations in Q^* generally follow those found in K_t . However, no significant correlation was obtained

for the Q^* and K_{\downarrow} values, ($r^2 = .2$). A better correlation was found between Q^* and $K_{\downarrow} (1-\alpha)$. Additional tests using a simple linear regression model show that the covariance was not uniform throughout the melt season. Thus, even though Q^* and $K_{\downarrow} (1-\alpha)$ are shown to covary to a high degree, they do so in a manner coupled to the relative stage of the melt season.

The conclusion that Q^* is complexly related to absorbed solar radiation is further substantiated when the ratios Q^*/K_{\downarrow} and $Q^*/K_{\downarrow} (1-\alpha)$ are considered. The seasonal progression of these two ratios is presented in Figures 6B.8-9. A general increase through the melt season is noted in both data sets even though the variability is quite large. Certain segments of the Q^*/K_{\downarrow} ratio (Figure 6B.8) are suggestive of an inverse relationship with albedo although this can not be statistically substantiated from these data. Jacobs (Section 4, this report) has shown that Q^* is correlated with K_{\downarrow} over tundra during the ablation season. Results from this work confirm this relationship at least in a qualitative sense.

In 1974 two net radiation sensors were operated simultaneously; one over unsaturated "dry" and the other over "wet" fast ice. The data used were collected between 9 and 21 June 1974 at the "south" ice station. During this period the ice surface changed from unpuddled smooth fast ice to a mixture of puddles approximately 8 cm deep and unsaturated hummock areas approximately 10 cm above the general ice surface.

The hourly mean difference between these sites is presented in Figure 6B.10. Actual data values are listed in Table 6B.3. The mean difference increases in the morning hours to a maximum of $0.3 \text{ cal cm}^{-2} \text{ min}^{-1}$ at 1000 and then steadily drops off to a minimum of $0.02 \text{ cal cm}^{-2} \text{ min}^{-1}$ at 2200. The standard deviations are larger in the middle hours of the day due to variable cloud cover.

The progression of the mean hourly differences appears to follow the global solar diurnal curve. Since global solar measurements concurrent with these data are not available at this site, this conclusion could not be directly validated. However, comparisons of Q^* and K_{\downarrow} data for 1973 support this conclusion. The coefficient of determination (r^2) between Q^* and K_{\downarrow} under clear skies for 2 and 10 July 1973 is 0.91; under cloudy skies on 12 and 15 July 1973 the r^2 value is 0.75. These results agree with those found, for example, by Dunne and Price (1975), and Jacobs (Section 4, this report).

Ratio of "dry" and "wet" observations have been computed from integrated daily totals. In most instances the values used do not represent integration over a 24 hour period. However, since a ratio is a relative rather than absolute measure, it may be argued that the missing part of a day adds only a small error to the final ratio. The actual data are presented in Table 6B.4 and the chronological progression of the ratios in Figure 6B.11.

The ratios generally decrease from close to 1.0 to around .3 -.4 by the end of the period. The large decrease in the ratio about 15 June was due to snowfall which raised the "dry" site albedo while leaving the "wet" site albedo relatively unchanged. Near the end of the observations the radiative characteristics of the two surfaces are strongly divergent with the "dry" or hummocked areas receiving between 50 and 75 percent less net radiation than the "wet" or puddled areas.

Checks on linear regressions (Table 6B.5) between "wet" and "dry" site albedos and the daily ratios of net radiation show no significant results when the "wet" site albedos are compared to the "dry" site albedo and the daily ratios. The linear regression model accounts for 83 percent of the covariance. Thus, most of the variation seen in the "wet" to "dry" Q^* ratio may be attributed to fluctuations in the incoming solar absorbed radiation over unsaturated surfaces.

In summary the analysis of the net radiation data suggest the following conclusions: (1) No direct statistical link appears to exist between K^+ and Q^* . (2) A useful estimate of Q^* is possible using combined K^+ and albedo measurements. (3) The relative contribution of L^* to Q^* is small on the average. Certain synoptic situations appear to cause fluctuations in L^* up to 30-40 percent of the daily total of Q^* . (4) The mean diurnal deviation of the "wet" and "dry" sites may be attributed to the global solar diurnal cycle. The large standard deviations in the middle hours of the day are probably caused by the net longwave flux, cloud cover effects on the global solar and albedo terms, or their combined effect. (5) The daily ratios of the "dry" to "wet" net radiation values indicate a general increased difference in the two radiation balances as the puddles deepen. About 50 - 70 percent more energy is received at the puddle surface than on hummocked areas. Most likely the ice underlying the puddles absorbs most of this energy surplus. The variations in the ratio may be statistically linked to variation in the unsaturated surface albedo although the relationship through time is not simple. This implies that the net radiation totals for unsaturated surfaces are more variable than puddled areas.

Predicting Ice Melt

A simple ice response model based on radiative energy transfer has been used to predict the seasonal differences in melt rates between 1972, a cold summer, and 1973, a more normal summer. The model's input includes; global solar and net radiation daily totals and mean daily albedo. The mean ice temperature, salinity, and thickness are specified initial conditions. The model calculates four rates of ice thickness change depending on which of several albedo values are used. See Weaver (1976) for more complete derivation of the theoretical ice response equations.

The model divides the ice response into two phases depending on the mean ice temperature. If the temperature is below the salinity melting point the radiative energy is used to warm the ice, if the

temperature is at the salinity melting point then the energy is used to melt the ice. Between -2°C and the salinity melting point an alternate method to evaluate the ice warming is used due to a singularity in the equation for the specific heat of sea ice. The essential equations for the model are as follows: The energy balance equation is

$$Q = K(1-\alpha) + L^* - K_b + K_b \alpha_w \quad (6B.3)$$

where, the net longwave flux $L^* = Q^* - K(1-\alpha)$, and the shortwave flux underneath the ice $K_b = K(1-\alpha)e^{(-uZ)}$. If $T < -2$, the internal ice temperature (T) is raised to -2°C with no melt as follows:

$$\Delta T = Q C_s^{-1} Z^{-1} \rho^{-1} \quad (6B.4)$$

and $T_m = \Delta T + T_{n-1}$

In this case the specific heat of sea ice (C_s) is a function of temperature (T) and salinity (s) as follows:

$$C_s = sa^{-1} L_i T^{-2} + sa^{-1} T^{-1} (C_w + C_i) + s C_i + C_i \quad (6B.5)$$

If $-2^{\circ}\text{C} > T > s \cdot (0.018^{-1})$, the additional energy (Q_m) necessary to raise T to the salinity melting point is calculated using Q_m to remove a singularity in C_s close to the salinity melting point as follows:

$$Q_{Tm} = Q_p^{-1} Z^{-1} + Q_{Tm-1} - Q_m \quad (6B.6)$$

$$Q_m = (L_i - C_i T_o) (1 - s\beta^{-1} T_o^{-1}) + (C_w - C_i) s\beta^{-1} \ln(s\beta^{-1} T_o^{-1}). \quad (6B.7)$$

When $Q_T > Q_m$, Q is used to melt the ice and:

$$\Delta Z = Q L_i^{-1} \rho^{-1} \quad (6B.8)$$

and $Z_n = \Delta Z + Z_{n-1} \quad (6B.9)$

The individual terms in the above equations are defined as follows:

Q = amount of heat energy absorbed by the ice
 m = $.12 \text{ cm}^{-1}$, extinction coefficient for ice
 Z = ice thickness (cm)
 α_w = $.12$, albedo of water underneath ice sheet
 s = $.004$, ice salinity
 ρ = $.8 \text{ g cm}^{-3}$, ice density
 a = $0.0182^{\circ}\text{C}^{-1}$, constant of proportionality
 β = $-.018$, constant of proportionality
 L_i = $79.69 \text{ cal g}^{-1} ^{\circ}\text{C}^{-1}$, latent heat of fusion for pure ice
 C_i = $.48 \text{ cal g}^{-1} ^{\circ}\text{C}^{-1}$, specific heat pure ice
 C_w = $1.00 \text{ cal g}^{-1} ^{\circ}\text{C}^{-1}$, specific heat pure water
 T_o = -2°C , initial temperature for Q_m

Several simplifying assumptions are made in this model:

- 1) the distribution of temperature and added energy are instantaneous and uniform throughout the ice depth; 2) no energy is contributed by oceanic turbulent, H, or LE fluxes; 3) no density changes occur during the melt process; 4) the extinction coefficient (α) is constant; 5) the thermal effects of snow are ignored; and 6) energy absorbed by a melt puddle is transferred to the underlying ice.

Different measured values of the surface albedo corresponding to the various surface types and different methods of arriving at mean albedo are employed in the model. The three variations include: 1) albedo measured directly under the net radiation sensor, 2) mean puddle albedo and 3) mean unsaturated ice albedos calculated from transect data in 1973 and point measurements in 1972.

Since no continuous net radiation measurements were made over puddles in 1972 or 1973, an estimated "wet" site net radiation was used. All net radiation measurements were assumed to represent unsaturated surfaces in both years and a correction applied to the measured "dry" site net radiation to estimate "wet" site net radiation. This correction factor is based on the 1974 comparative measurements of Weaver (1976) and is as follows:

$$Q_w^* = Q_d^* (-.42 \alpha_i + .9)^{-1} \quad (6B.10)$$

where

$$\alpha_i = \text{albedo of unsaturated site}$$

The weighting factor of the combined unsaturated and puddled surface depth changes is as follows:

$$Z = Z_{ice} (S_i) + Z_{pool} (1-S_i) \quad (6B.11)$$

S_i = surface area of unsaturated ice in percent. This equation assumes that the energy absorbed underneath the puddle and "dry" areas reaches instantaneous equilibrium.

Comparison of Measured and Predicted Ice Thickness

In 1973 ice thickness was measured seven times during the operation of the ice station. The results of these measurements are given in Table 6B.6. The model was run over the same period as the field measurements. The ice thickness changes measured under the net radiation sensor and the weighted estimate of puddle-hummock ice thickness are presented in Figure 6B.12. An initial ice temperature of -5°C was used and was based on actual field measurements at the ice station. The ice salinity was estimated to be 4 o/oo and the initial thickness was 113 cm.

The model consistently over-estimates the thickness changes when compared to the actual measurements. However, the final predicted

value is within one standard deviation of the measured depth (see Figure 6B.12). Linear regression comparisons of the actual and predicted values resulted in high coefficients of determination ($r^2 = .87, .88$) for both estimates. The results of these tests are listed in Table 6B.7. These results are good considering the simple nature of this model and demonstrates the strong dependence of ice melt on the radiative sources of energy.

In 1972 the fast ice near Broughton Island did not disperse while in 1973 the ice broke up in mid-August. The abnormally cold 1972 season has been well documented at Broughton Island (Jacobs, et al, 1974). While ice conditions in 1973 were still severe, in part due to the residual ice from 1972, the fast ice did break up with heavy pack ice conditions well into the fall.

Measured values for $K+$, α , and Q^* are available for both 1972 and 1973 during the melt season. These data have been utilized in this comparative analysis of ice melt for these two seasons. No ice depth measurements are available to validate the 1972 predicted ice thickness change. The proportion of surface area covered by unsaturated ice was estimated at 70 percent from the time of first puddling in 1972.

The results of the model using the same initial conditions, ($T = -5^{\circ} \text{C}$, $s = 4 \text{ o/oo}$, $z = 113 \text{ cm}$), and the 1972 and 1973 data sets clearly show less ice melt in 1972 (see Figures 6B.12-13). The predicted ice depth in 1972 on 6 August was 76.4 cm while in 1973, it was 37.5 cm based on the albedo estimate for the net radiation site.

TABLE 6B.1

Albedo Measurements for Various Surface Types

Category	(1)	(2)	(3)		(4)
			mean	σ	
I Ice, unsaturated smooth melting ice	.52	36 - .70	-	-	.51
II Melt puddles					
undifferentiated	.23	--	-	-	-
first period 0-30 cm	--	.24 - .36	-	-	.29
second period 30-100 cm	--	.13 - .28	-	-	.19
covered with new ice	--	.18 - .37	-	-	.26
III Snow cover					
freshly fallen, dry snow	--	.72 - .98	-	-	.90
freshly fallen, wet snow	--	.80 - .85	-	-	--
fresh dry drifted snow	--	.70 - .96	-	-	.82
snow with ice showing	--	.58 - .70	-	-	.54
IV Pack ice with snow cover					
greater than .9 concentration	--	--	.91	.06	--
.9 to .71	--	--	.76	.18	--
.7 to .51	--	--	.42	.13	--
.5 to .31	--	--	.50	.21	--
.3 to .11	--	--	.32	.20	--
less than .1	--	--	.09	.09	--

data sources:

- (1) Author's data, Broughton Island, Summers 1973, 1974
- (2) Soviet drifting station data (Briazgin 1959, in Jacobs 1973)
- (3) Airborne Measurements, May 1971, (after Jacobs, 1973)
- (4) Measurements, Broughton Island, Summers 1971, 1972
(after Jacobs, 1973)

TABLE 6B.2

Relative Distribution of Potential Solar Radiation
by Surface Type

Year	Date	Radiation absorbed assuming incoming of 100 cal cm ⁻² hr ⁻¹		Ratio of Ice/Pools
		By Pools	By Ice	
<u>1973</u>	7 July	0.6	39.6	61.8
	13 July	5.8	48.8	8.5
	20 July	14.0	49.6	3.5
	23 July	19.5	42.8	2.2
	26 July	13.7	40.3	3.0
	30 July	9.4	28.2	3.0
<u>1974</u>	16 June	22.3	26.2	1.2
	18 June	21.3	28.5	1.3
	20 June	19.8	32.6	1.6
	24 June	30.2	32.6	1.1
	30 June	35.7	26.7	0.7
	2 July	41.9	24.3	0.6

Absorbed Radiation = Solar Radiation x (1 - α) x Surface Area

TABLE 6B.3

Hourly Mean Deviations Between the Q* "wet" and
Q* "dry" sites ($\text{cal cm}^{-2} \text{ min}^{-1}$)

Hour (LST)	Mean Difference	Standard Deviation (σ)	N
1	.01	.04	8
2	.03	.06	8
3	.06	.09	8
4	.05	.04	8
5	.12	.19	8
6	.14	.20	9
7	.16	.25	9
8	.23	.34	9
9	.18	.11	9
10	.31	.34	11
11	.13	.15	10
12	.19	.22	11
13	.14	.13	11
14	.11	.13	11
15	.08	.12	11
16	.19	.08	10
17	.10	.06	10
18	.09	.04	10
19	.06	.03	10
20	.06	.04	9
21	.04	.03	9
22	.02	.03	8
23	.01	.03	8
24	.01	.03	7

TABLE 6B.4

Net Radiation Data Used for Ratio Calculations
and Linear Regressions

Date	Q* "dry" (cal cm ⁻²)	Q* "wet"	N	Q* _w -Q* _d	Q* _d /Q* _w	α_d	α_w
1974 June							
9	194	201	15	7	.97	.48	.33
10	280	294	24	14	.95	--	--
11	--	--	--	--	--	.42	.30
12	216	237	15	21	.91	--	.28
13 *	193	172	12	21	1.12	.46	.27
14	214	335	24	121	.64	.68	.19
15	92	530	24	438	.17	--	--
16 *	121	316	24	195	.38	.80	.28
17	214	475	21	261	.45	--	--
18 *	226	350	11	124	.65	.64	.17
19	--	--	--	--	--	.62	.23
20 *	193	371	24	178	.52	.60	.20
21	59	153	11	94	.39	--	--
22	--	--	--	--	--	.66	.20

* indicates daily ratios based on fewer than 24 hourly samples

TABLE 6B.5

Linear Regression Tests of Albedo Data

and Q* Ratios for 1974

Slope	Intercept	r	r ²	\bar{x}	\bar{y}	S_x^2	S_y^2	D.F.	F ratio	S.E. estimate
Case I: Q* ratio vs. albedo of unsaturated site										
-.42	.91	.92	.84	.71	.61	.08	.02	4	20.49	.06
Case II: Q* ratio vs. albedo of saturated site										
.10	.17	.43	.19	.71	.24	-	-	4	.922	.063

TABLE 6B.6

Ice Depth Data 1973 (in cm)

Date	Overall mean	σ	No. samples	Ice Only mean	σ	No. samples	Pools mean	σ	No. samples
July									
4	114.3 cm	6.7 cm	3	same	-	-	-	-	-
14	101.8 cm	7.1 cm	5	104.1	-	2	101.6	2.5	3
19	87.5 cm	7.5 cm	9	91.4	-	1	87.1	8.0	8
21	85.9 cm	2.1 cm	5	83.8	2.1	4	86.0	-	1
24	62.7 cm	11.5 cm	8	61.3	7.5	4	64.1	15.7	4
31	59.6 cm	10.9 cm	16	61.3	11.4	13	52.1	3.4	3
August									
4	42.3 cm	16.8 cm	10	54.4	6.0	6	24.4	7.8	4

TABLE 6B.7

Linear Regression Comparisons

Measured and Predicted Ice Depth Data 1973

Slope	Intercept	Correlation	r^2 *	Mean Values		D.F.	F
				Measured	Predicted		Ratio
Test using net radiation site albedo							
.94	- 8.7	.93	.87	79	65.9	5	34.06
Test using weighted "wet" - "dry" depth values							
1.13	-29.8	.94	.88	79	60.1	5	36.6

* r^2 is the coefficient of determination

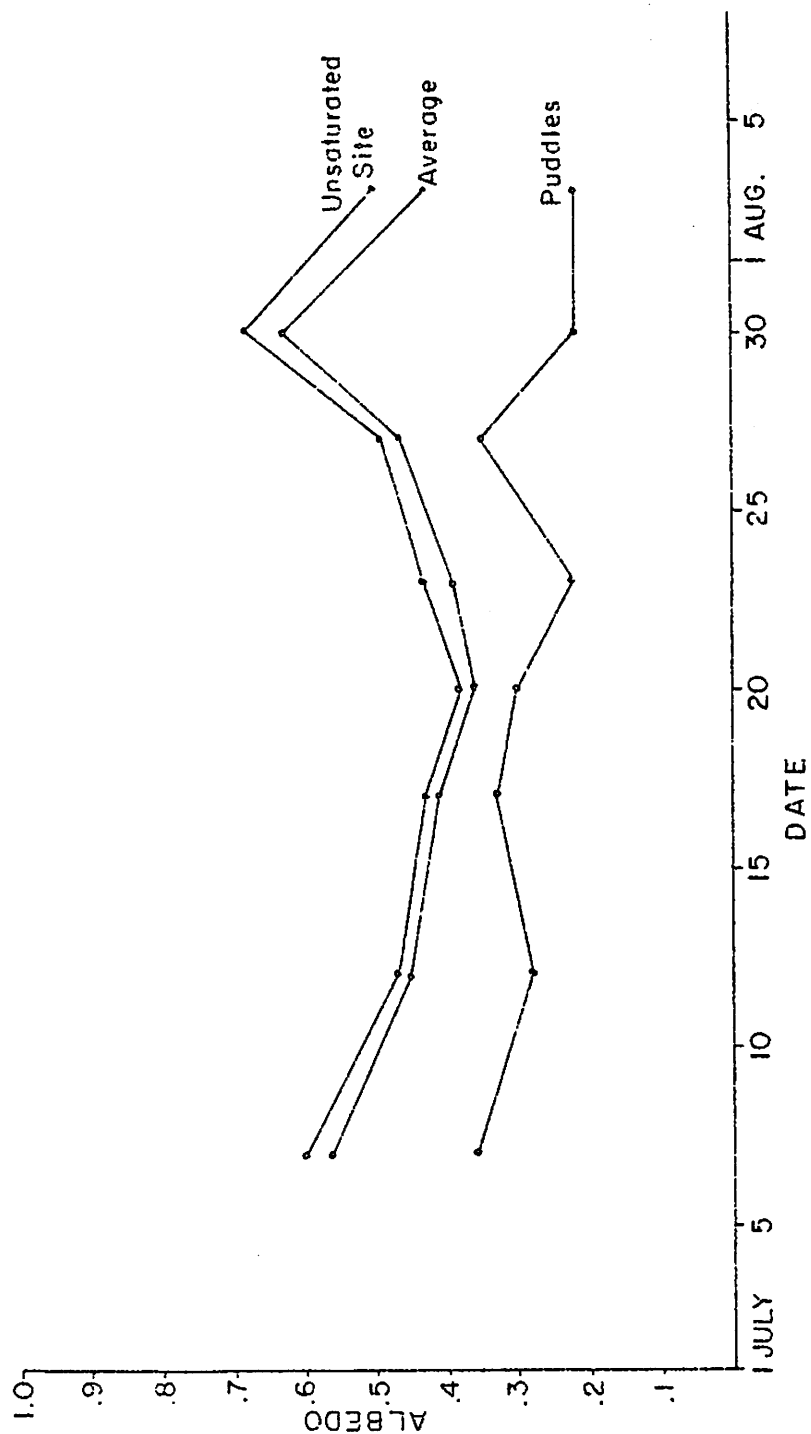


Figure 6B. 1. Mean albedos from transects during summer 1973.

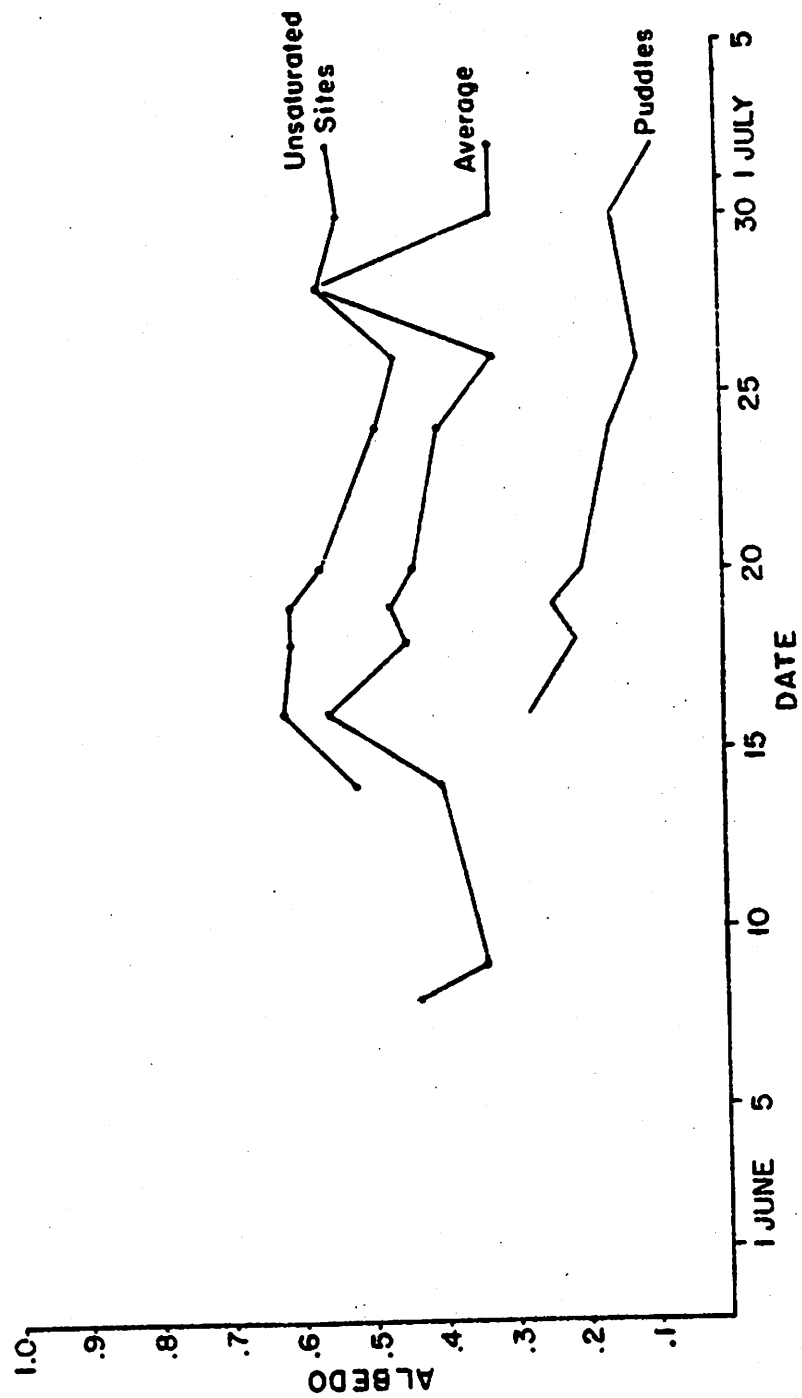


Figure 6B. 2. Mean albedos from transects during summer 1974.

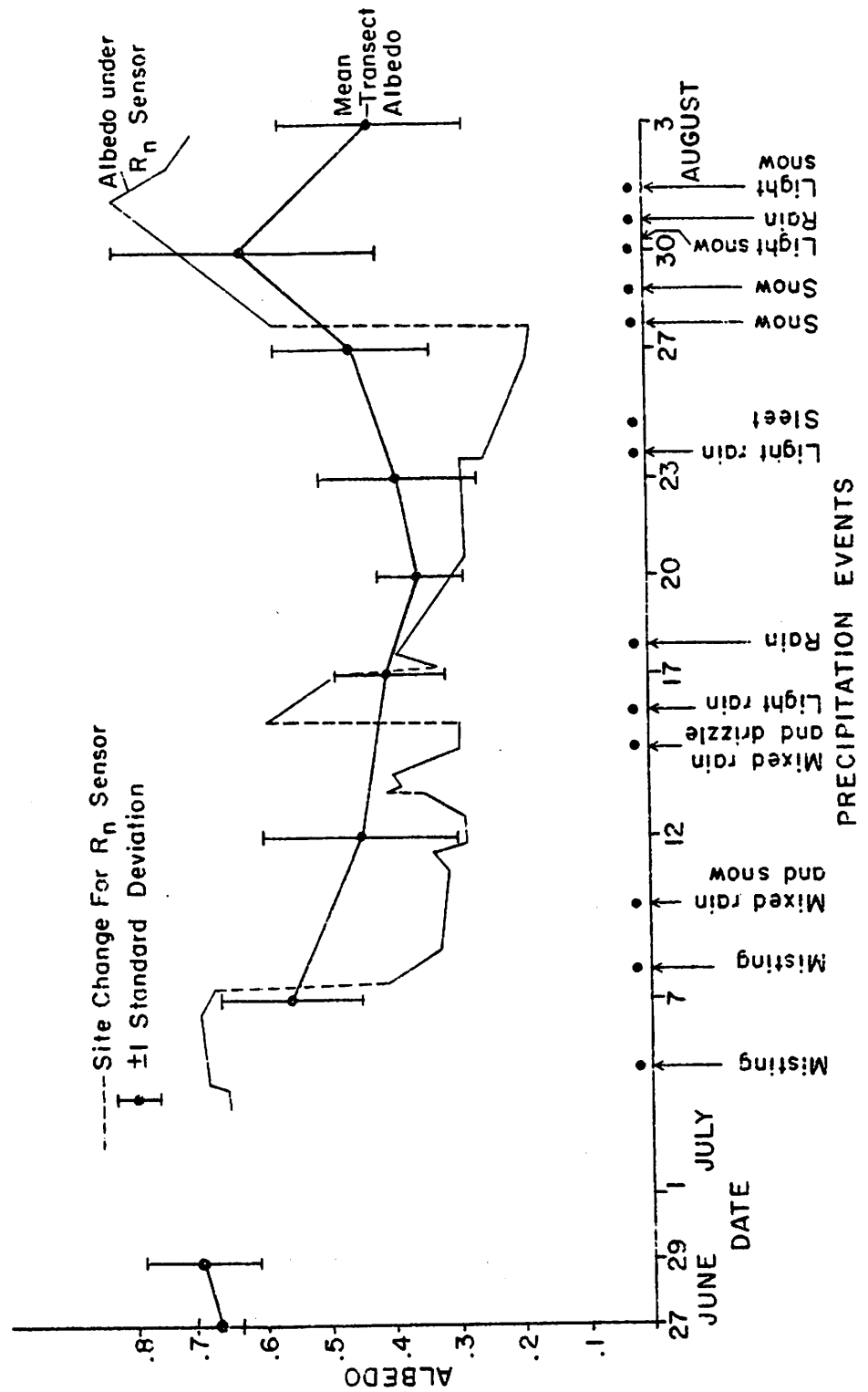


Figure 6B. 3. Point albedos under the net radiation (R_n) sensor, transect mean values, and precipitation events, 1973.

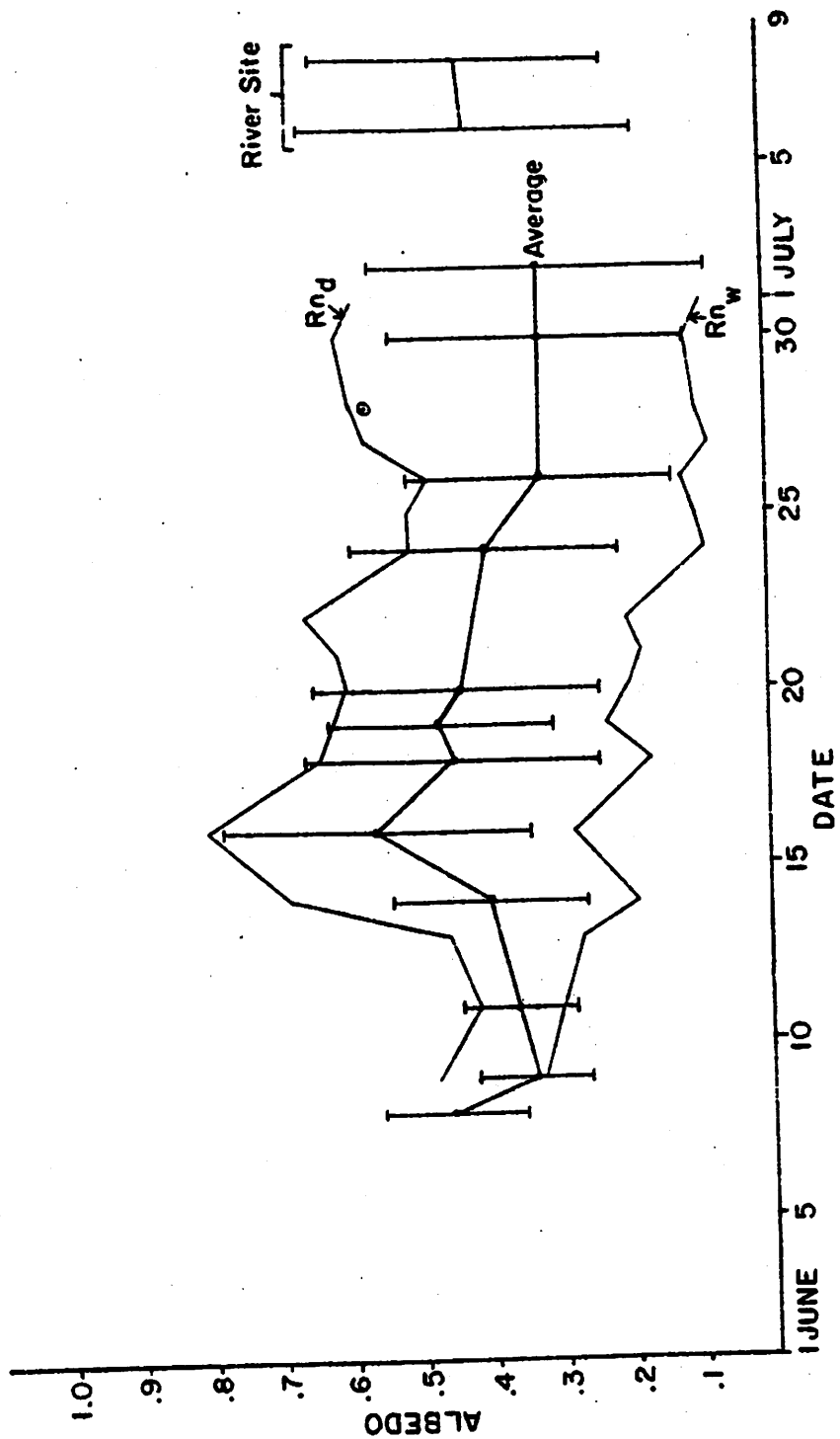


Figure 6B. 4. Point albedos at the "dry" (Rn_d) and "wet" (Rn_w) sites in relation to the mean transect values ("average") in 1974.

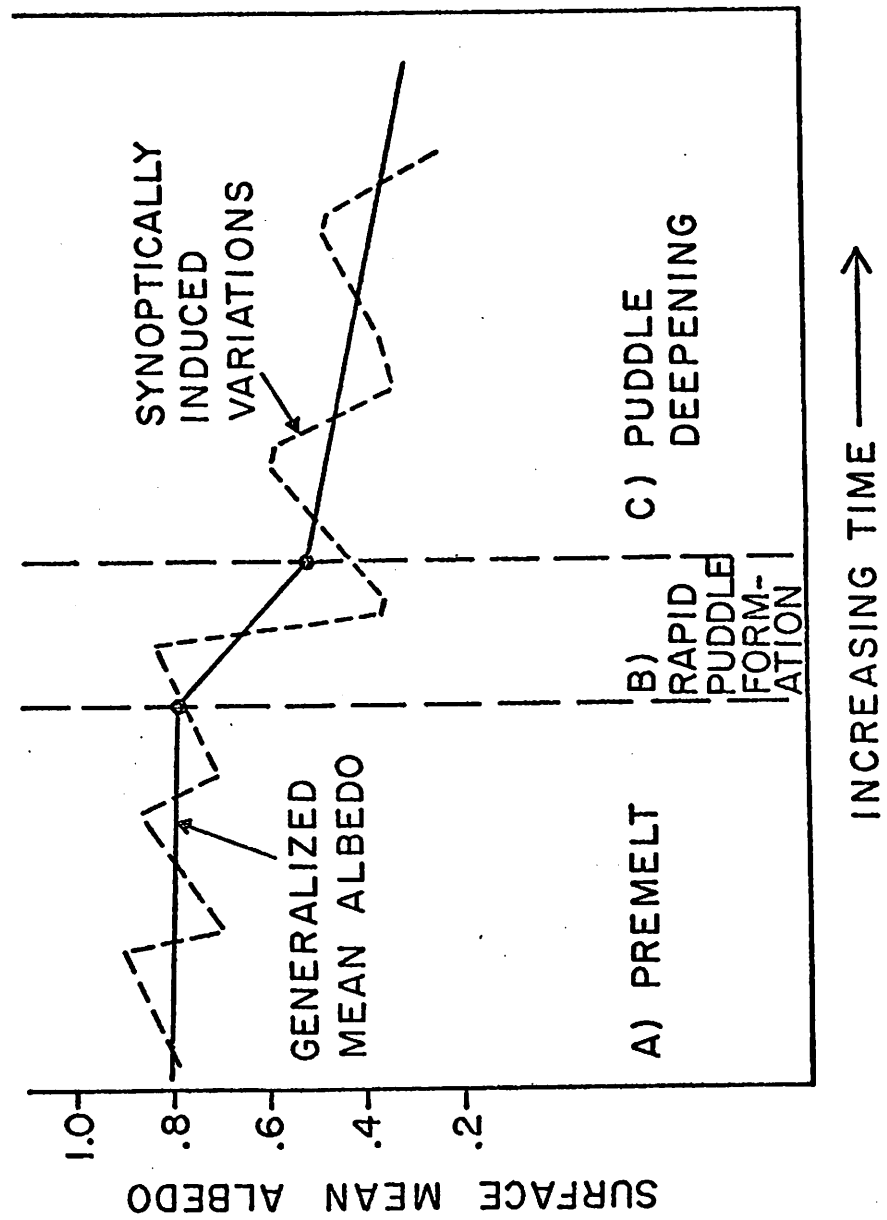


Figure 6B. 5. Schematic outline of the trend of fast ice albedo during the summer decay season.

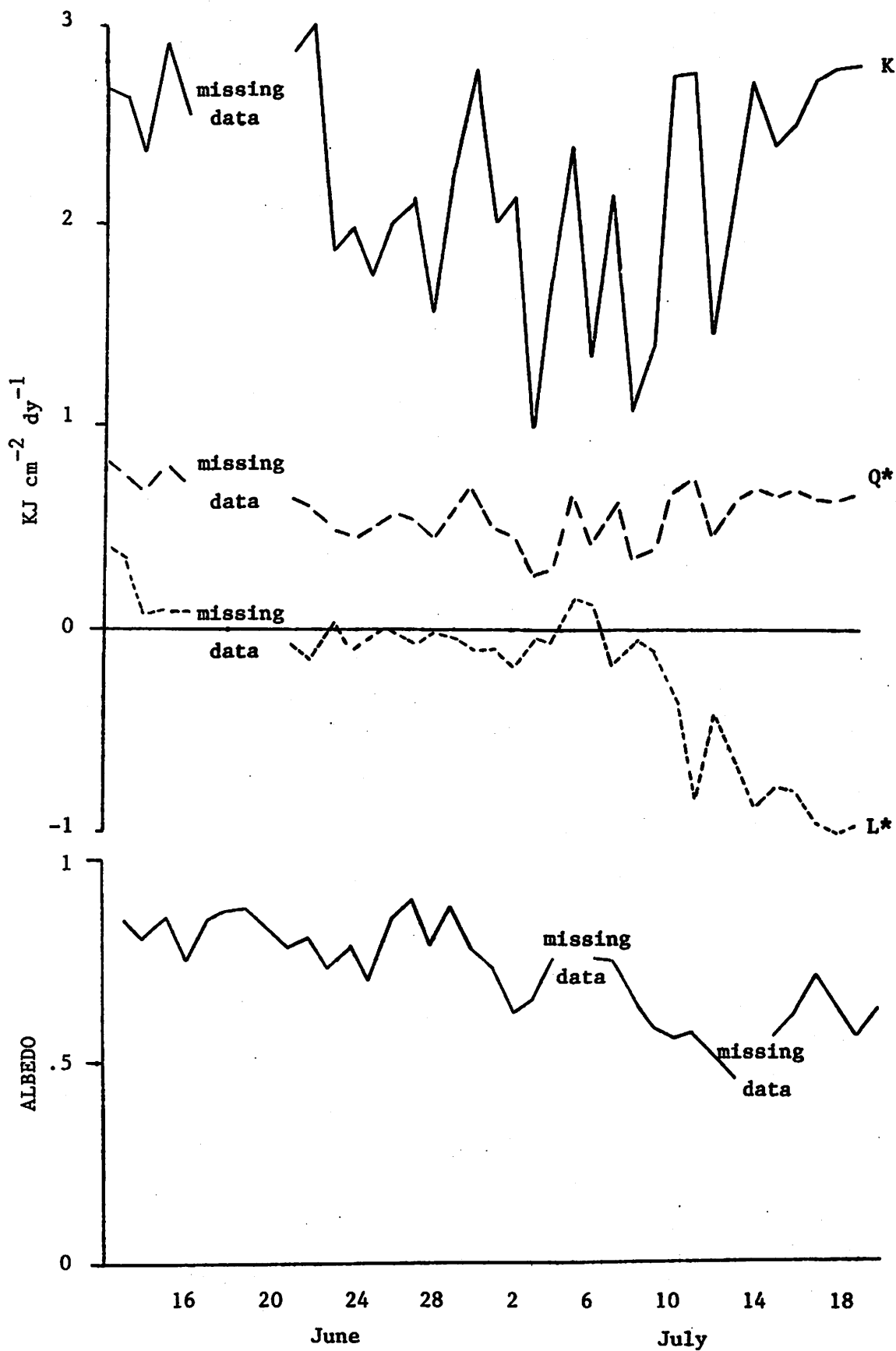


Figure 6B.6. Daily trend of (above) global radiation (K), net radiation (Q*), and net long-wave radiation (L*), and (below) albedo. Over fast ice, 1972.

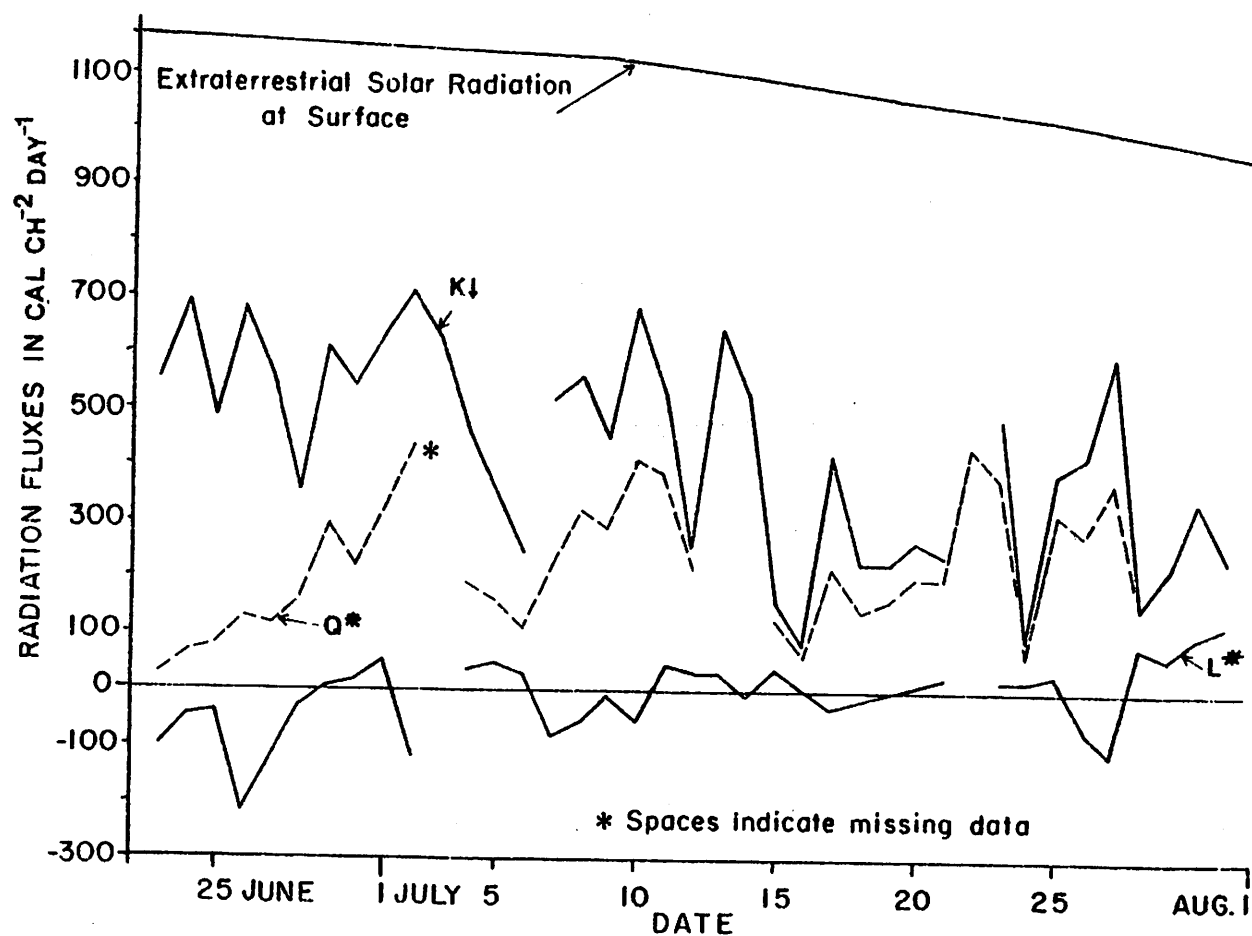


Figure 6B. 7. Net radiation (Q^*) and estimated net longwave (L^*) at the fast ice station compared with solar radiation ($K\downarrow$) at Broughton Village for 1973.

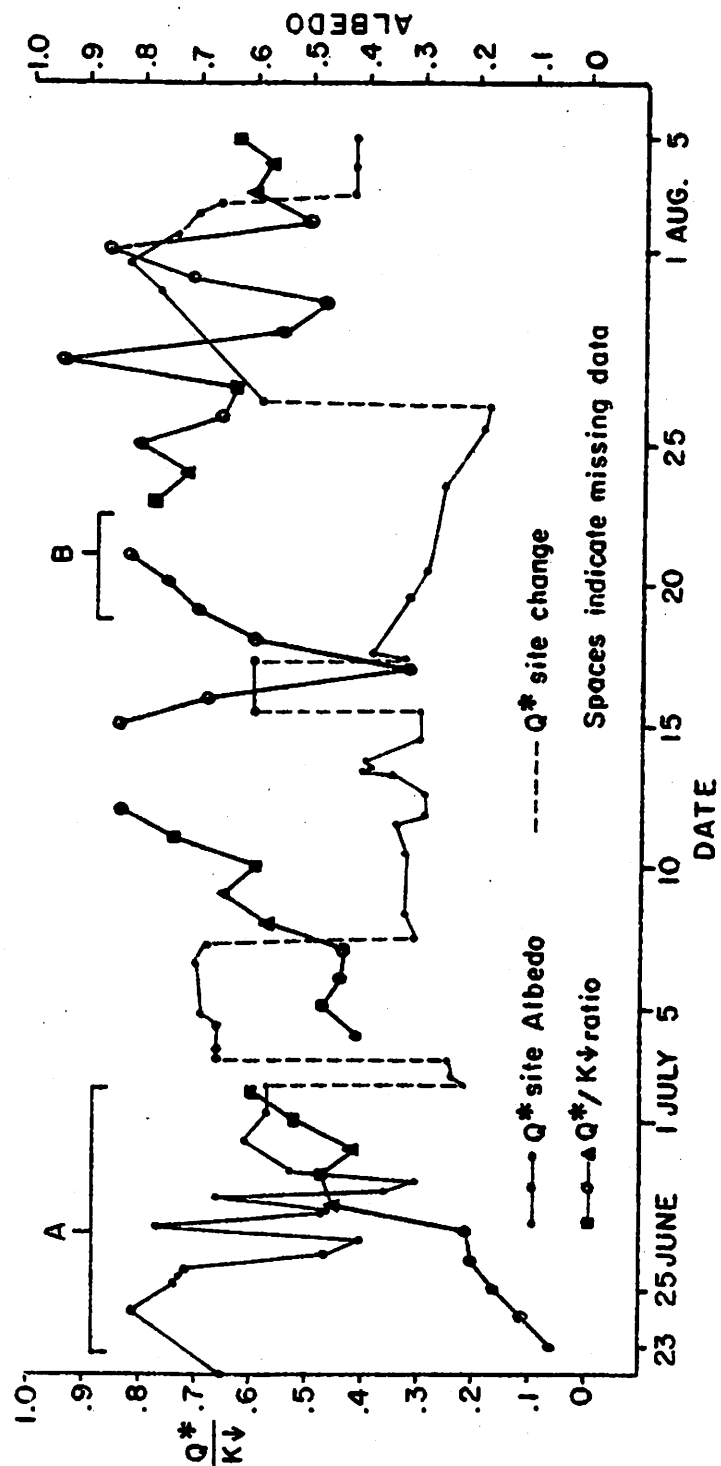


Figure 6B. 8. The ratio of daily totals net radiation (Q^*) to incoming solar radiation (K_{\downarrow}) and the mean albedo estimate for the net radiation site for 1973. Segments A and B suggest an inverse relationship with albedo. Circles denote low cloud, triangles medium cloud, and squares high cloud.

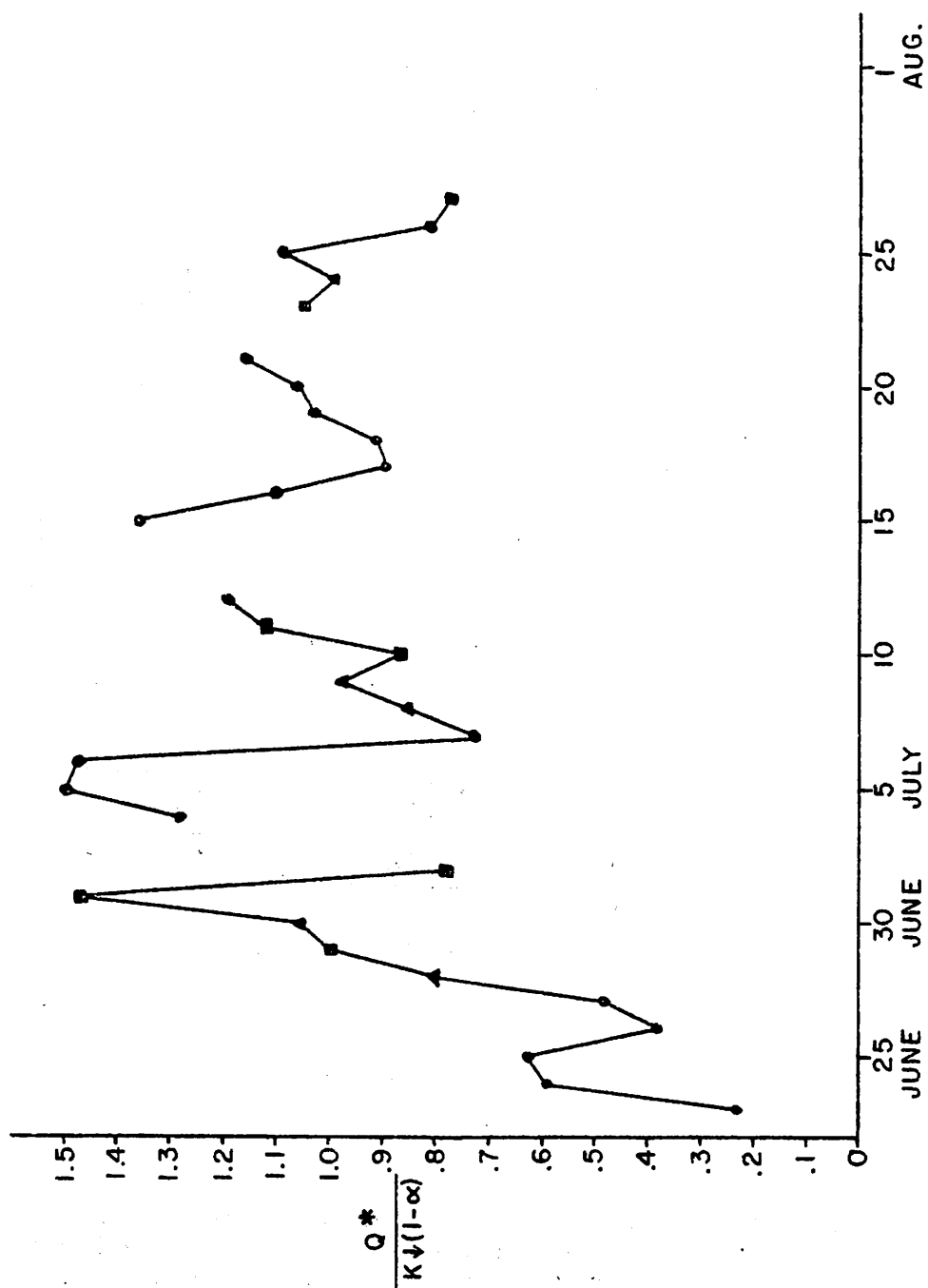


Figure 6B. 9. The ratio of daily totals of net to absorbed global solar radiation for 1973. Cloud symbols are as in Fig. 6B. 8.

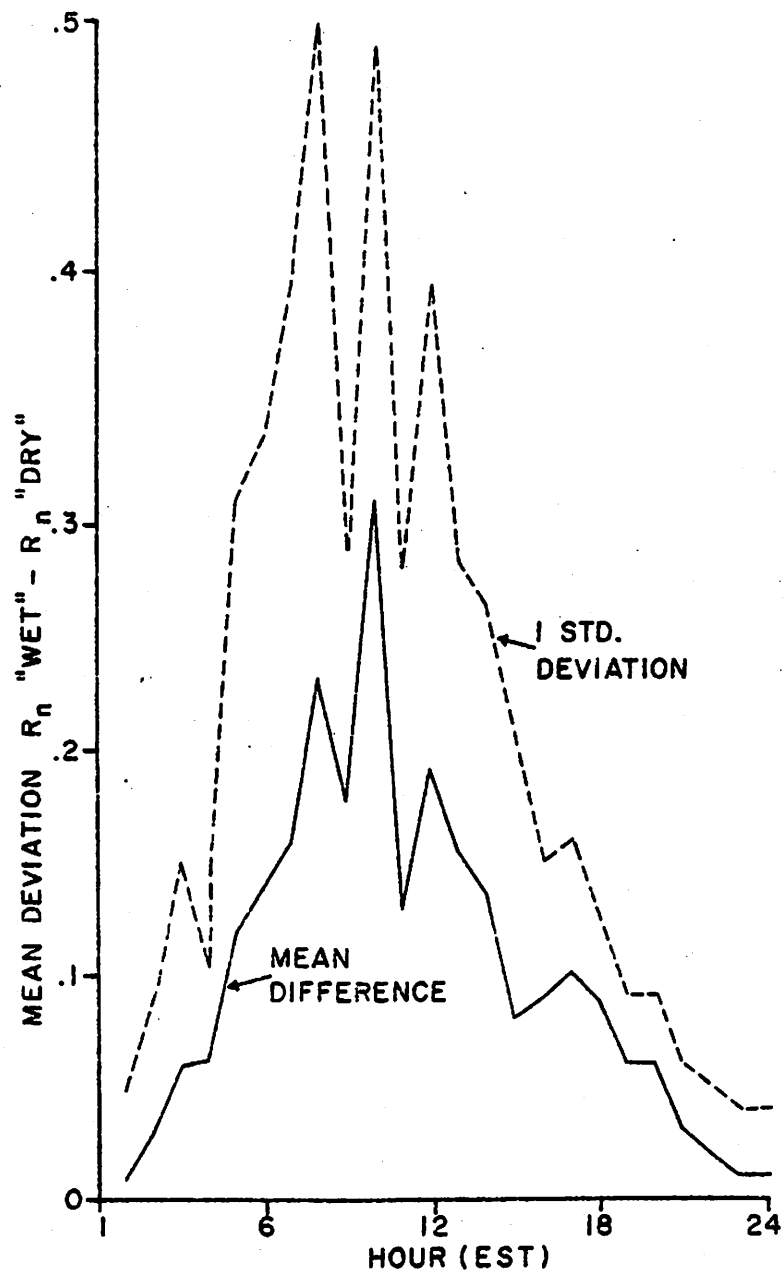


Figure 6B. 10. Mean hourly differences of the net radiation measured at "wet" and "dry" sites and the one standard deviation limit.

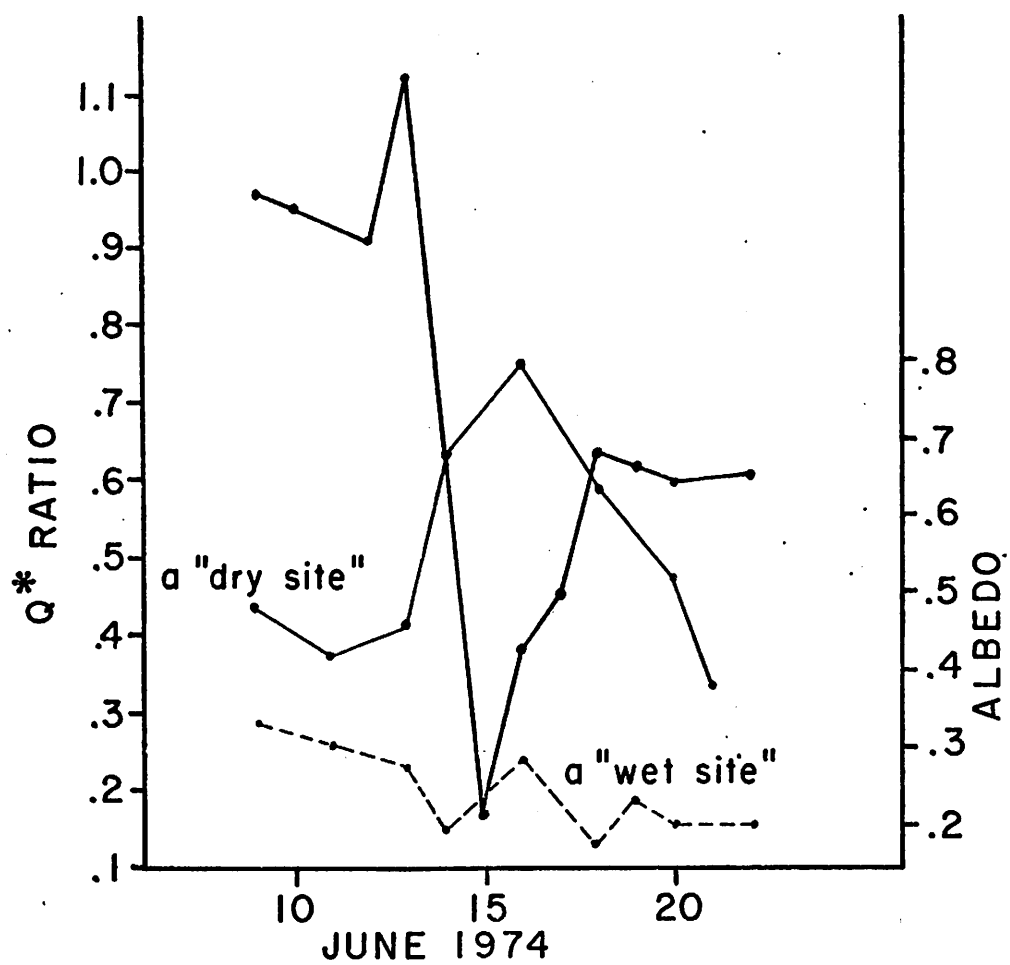


Figure 6B. 11. Ratios of "dry" to "wet" site daily totals of net radiation (heavy line) and mean daily albedos at these two sites in 1976.

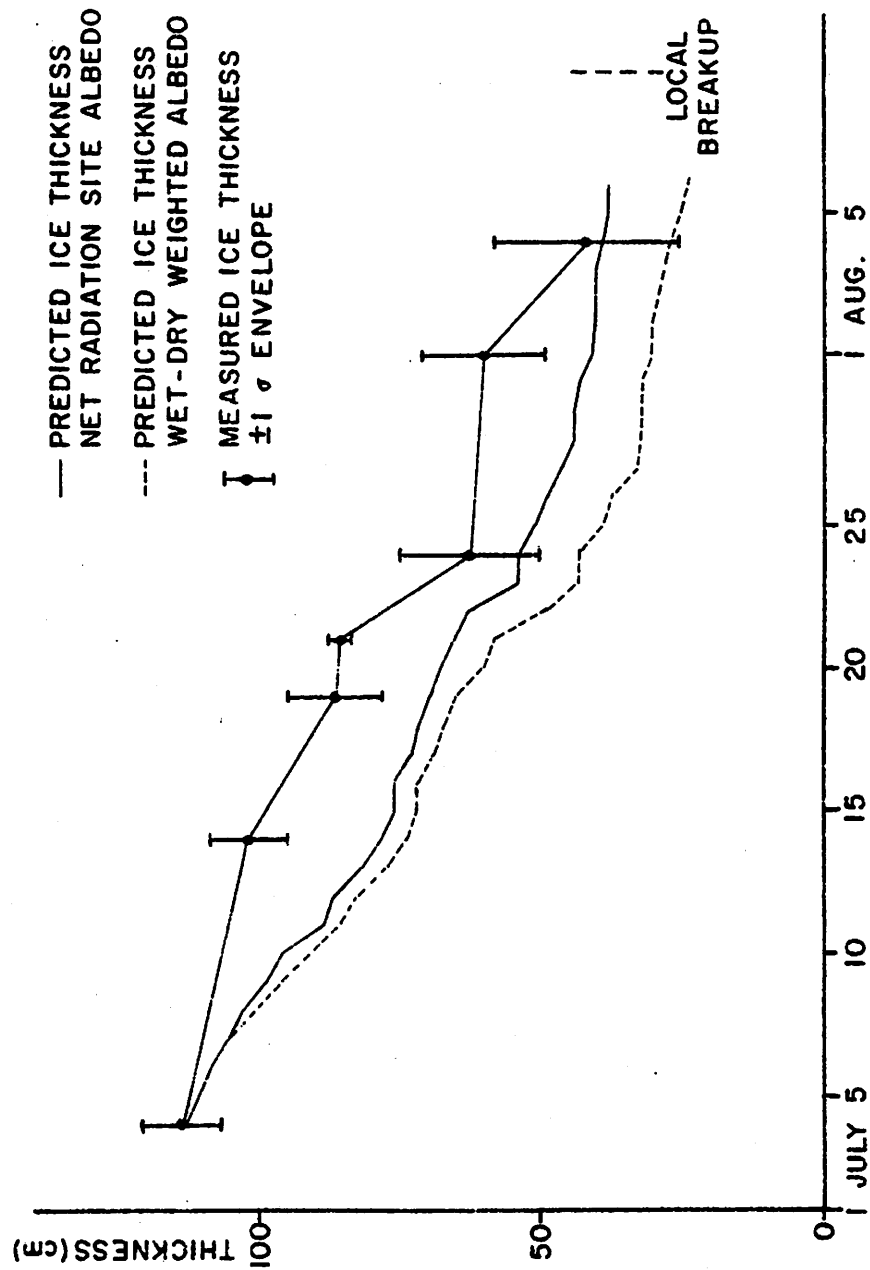


Figure 6B. 12. Predicted and measured ice melt for 1973.

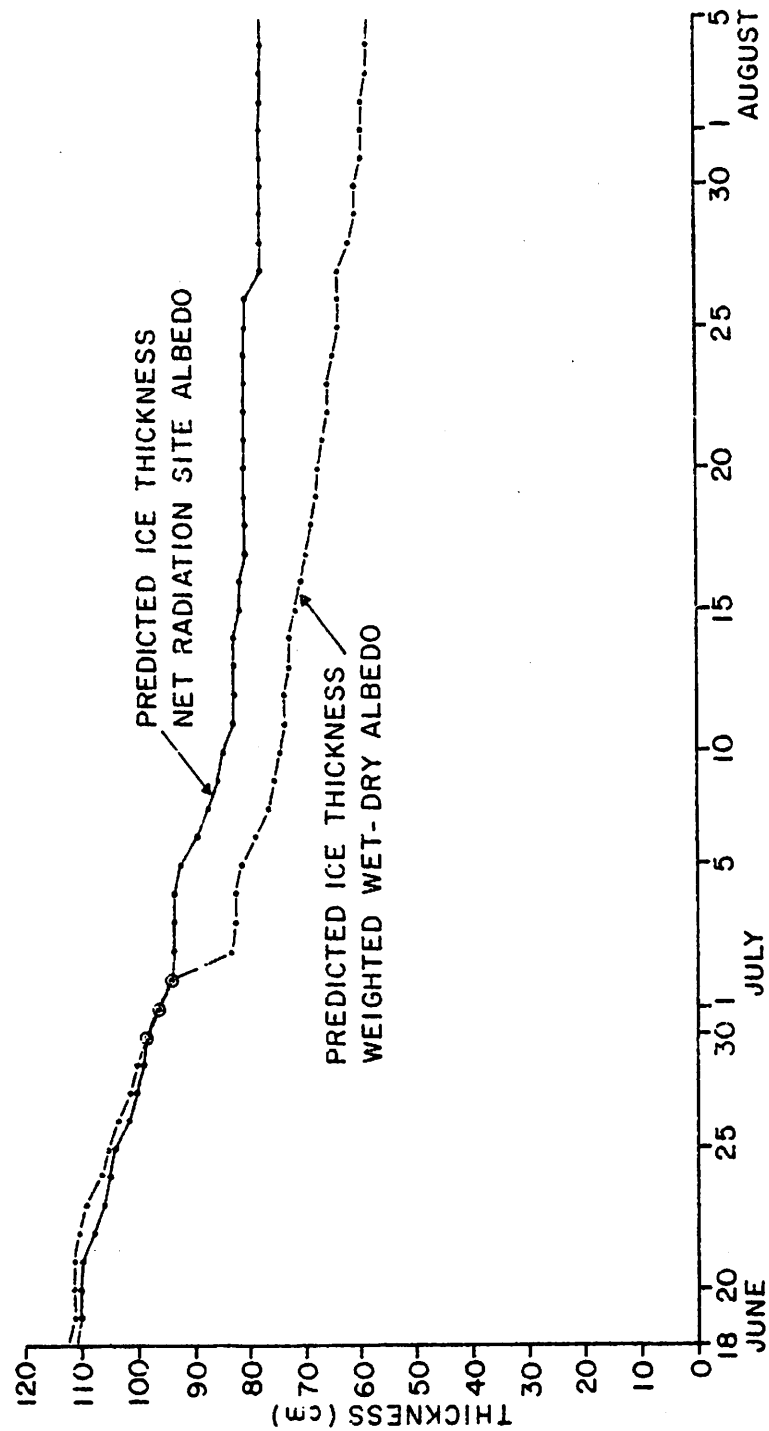


Figure 6B. 13. Predicted ice melt for 1972 based on two different albedo series.

C. Energy Budget

Basis

The energy budget for arctic surfaces can be written in the form

$$G = Q^* + H + LE \quad (6C.1)$$

where G = net flux into the surface, Q^* = net radiation, H = enthalpy flux or "sensible" heat flux, and LE = latent heat associated with the vapor flux (Jacobs, et al., 1975). All terms are considered positive downward at the surface and the net advection over the surface is assumed to be zero. For snow and ice, additional terms may be included to account for the transmission of solar radiation into or through the surface layers and for phase changes within the snow and ice (Weller, 1968).

Given accurate estimates of Q^* , calculation of the total heat flux at the surface, G , becomes a matter of determining the turbulent heat flux ($H + LE$). The general problem of turbulent transfer has been discussed by Sutton (1953) and Priestley (1959), among others. Common to these studies is an approach which treats the vertical exchanges of heat and moisture as functions of the vertical gradients of temperature and humidity, respectively, and of the vertical wind shear in the near-surface layer.

Following Priestley (1959, p. 21), the transfer of momentum between the atmosphere and surface, that is the shearing stress τ , is

$$\tau = C_D \rho u^2 \quad (6C.2)$$

where ρ = air density, u = windspeed at the reference level z , and C_D = the drag coefficient. C_D is a function of height z and the surface roughness, which may be expressed in terms of the roughness parameter z_0 .

$$u(z) = \frac{u_*}{k} \ln (z/z_0) \quad (6C.3)$$

where $u_* = (\tau/\rho)^{1/2}$ is the friction velocity, a constant throughout the layer, k = von Karman's constant, which has an experimental value of 0.41, and \ln denotes loge.

The experimental determination of C_D is accomplished indirectly by finding z_0 for a particular surface under neutral conditions from a series of simultaneous measurements of windspeed $u(z)$ at two or more levels and substituting the resulting values into Equation 6C.3 in the form:

$$\ln z_0 = \frac{(u_1 \ln z_2) - (u_2 \ln z_1)}{(u_1 - u_2)} \quad (6C.4a)$$

Alternatively, we can write (Sanders and Weber, 1970):

$$z_0 = \exp \left[\frac{u_2 \ln z_1 - u_1 \ln z_2}{u_2 - u_1} \right] \quad (6C.4b)$$

Neutrality in this case is specified by the Richardson number:

$$Ri = \frac{g (\partial \theta / \partial z)}{\bar{\theta} (\partial n / \partial z)^2} \quad (6C.5)$$

where θ = potential temperature and $\bar{\theta}$ denotes the mean value throughout the layer $z_2 - z_1$. This is closely approximated by the actual absolute temperature. For neutral conditions $Ri = 0$.

Having obtained z_0 , the drag coefficient for neutral conditions (C_{DN}) can be calculated from

$$C_{DN} = \frac{k^2}{[\ln (z/z_0)]^2} \quad (6C.6)$$

For a neutral profile the net vertical transfer of any properties of the eddying air will take place at the same rate as the movement of that air (Priestley, 1959, p. 108). This means that the turbulent fluxes H and LE can be expressed in a form analogous to Equation 6C.2:

$$H = \rho c_p C_D u (T - T_0) \quad (6C.7)$$

and

$$LE = 0.62 \frac{\rho L}{p} u (e - e_0) \quad (6C.8)$$

where C_D , u , T , and e (vapor pressure) are referenced to a particular level z , T_0 and e_0 are surface values, L is the latent heat of vaporization, and p the atmospheric pressure. The sign convention is consistent with a flux positive downward to the surface.

Although conditions over melting fast ice are generally near-neutral and we may assume that $C_D = C_{DN}$, some provision must be made for

situations in which $Ri \gg 0$, as for example in the case of advection of warm air over the ice with consequent strong stability. Conversely, over snow-free land or warm water, a superadiabatic lapse rate may sometimes be present. For arctic terrestrial surfaces, Weller and Holmgren (1974) have used a modification to the exchange coefficient, first suggested by Lettau (1949), which is a function of Ri . In our notation, this is

$$C_D = \frac{C_{DN}}{(1 + Ri)^2} \quad (6C.9)$$

where C_D reduces to the neutral value for $Ri = 0$.

Profile Data

Profiles of wind, temperature and humidity were measured on a four-hourly basis in the first 1.6m above the snow-covered fast ice north of Broughton Island during the summer of 1972. A C.W. Thornthwaite Associates wind profile system (40, 80 and 160 cm) was used in conjunction with Assmann psychrometers for air temperature and humidity (160 cm) and thermistors for surface temperature. Net radiation was also measured at 160 cm. Measurements were made between 13 June and 20 July over a surface which progressively changed from cold, dry snow to extensively puddled, melting ice.

The aerodynamic approach to estimating turbulent fluxes, outlined above, assumes near-neutral stability conditions, implying that the wind profiles are logarithmic (Grainger and Lister, 1966). The profiles in Figure 6C.1 show that this assumption is valid in all but a few cases. The stability, as indicated by the calculated Richardson numbers, also clusters around zero (Figure 6C.2) with 38 percent within the arbitrarily defined 'neutral' range of $-.0125$ to $+.0125$ (Table 6C.1). The results in this table compare favorably with those of Weller (1968) and Allison (1973). For 238 observations, the mean Ri is 0.0647 with a standard deviation of 0.264.

The distribution of average Ri values according to time of observation, for mid-June to mid-July, was as follows:

Hours (EST)	00	04	08	12	16	20
Mean Ri	.008	-.027	.004	.035	.016	.013

These data indicate a diurnal pattern that might be expected over melting snow or ice. Stability is a maximum near midday as the air warms, but the surface temperature has an upper limit of 0°C . However, this diurnal pattern was often masked by synoptic variability during the relatively stormy 1972 summer.

Roughness lengths are calculated for neutral conditions ($-.0125 < Ri < .0125$), and logarithmic wind profiles (between 40 and 160 cm),

and averaged over five or six-day periods in Table 6C.2. (Observations with very light winds or suspected errors were omitted.) Langleben (1974) cautions against assuming that a logarithmic profile is necessarily present, even under near-neutral conditions, based on his work over ice in the Beaufort Sea in April. The results in Table 6C.2 show good agreement with other studies.

The Energy Budget

Results of the turbulent flux calculations based on equations 6.c.7-9 are shown in Figure 6C.3 giving average daytime fluxes based on data for 0800, 1200 and 1600 hours. Throughout most of the period, fluxes of sensible heat are positive (i.e. downward transfer) due to the prevalence of weak inversion conditions over the ice. Latent heat flux is nearly always negative, reflecting an evaporative loss from the surface.

Table 6C.3 and Figure 6C.3 show that the pattern of average daytime sensible and latent heat fluxes changes between June and July, with the break coming at the beginning of July. The latent heat flux disposes of 53 percent of the combined net radiation and downward enthalpy flux ($0.673 \text{ Jcm}^{-2}\text{min}^{-1}$) in June compared with only 6 percent of the total ($1.663 \text{ Jcm}^{-2}\text{min}^{-1}$) in July. This division is equally apparent in the net radiation and conductive heat fluxes. (Table 6C.4 and Figure 6C.4). This large increase in net radiation and conductive heat flux coincides with the division between two classes in a simple five stage model of ice ablation and break-up. (see Figure 5B.8). The period of field measurements covers parts of stages 2 and 3, which are defined by Jacobs et al., (1975) as follows:

- Stage 2 There is a rapid increase in daily insolation values, with between 10 percent and 30 percent of the incoming radiation being absorbed by the snow and upper ice layers. Temperatures of these layers can therefore rise to near the melting point despite the fact that air temperatures are below freezing. Once melting starts, water percolates downwards through the snow cover and accumulates in hollows at the snow/ice interface.
- Stage 3 The snow cover is removed, revealing an ice surface of alternating hummocks and puddles. Surface waters drain through fractures, leads and seal breathing holes. During the early part of this period, if air temperatures remain below freezing, a snow crust may persist for some time and fresh snow may be deposited by early summer storms. Eventually however, all of the snow is removed.

The transition between stages 2 and 3 occurred at the beginning of July. During stage 2, with the ice still covered by snow, albedo averages 0.81, net radiation averages $0.47 \text{ kJ cm}^{-2}\text{dy}^{-1}$ and the conductive flux into the snow, and underlying ice, has a mean of $0.18 \text{ kJ cm}^{-2}\text{dy}^{-1}$. During stage 3, however, as the snow cover is removed and puddles form on the surface, albedo falls to 0.53, net radiation increases to an average flux of $1.66 \text{ kJ cm}^{-2}\text{dy}^{-1}$ and the conductive flux increases by 8 times to a mean of $1.55 \text{ kJ cm}^{-2}\text{dy}^{-1}$.

TABLE 6C.1

Comparison of Richardson numbers obtained over snow and ice surfaces

<u>Range</u>	<u>Percent of observations</u>	<u>Source</u>
-.01 to + .01	38.0	Weller (1968)
-.06 to + .06	84.0	
-.01 to + .01	44.4	Allison (1973)
-.07 to + .07	72.2	
-.0125 to + .0125	38.4	This study
-.0625 to + .0625	71.0	

TABLE 6C.2

Roughness Lengths for Successive 5-Day (June) or 6- Day (July) Periods,
Over Ablating Fast Ice, Broughton Island, 1972 and Comparative Values.

<u>Broughton Island, 1972.</u>			
<u>Period</u>	<u>Roughness length (cm)</u>	<u>Sample size</u>	<u>Standard error of the mean</u>
June 13-17	.070	5	.042
June 18-22	.088	17	.017
June 22-27	.144	14	.029
June 28-July 2	.114	12	.025
July 3-8	.083	10	.041
July 9-14	.071	12	.035
July 15-20	.055	6	.016
Mean	.097	76	

Fast ice, Gulf of
St. Lawrence (Seifert &
Langleben, 1972):

smooth floe	.08	74
rough floe	.34	181

Pack Ice, Beaufort Sea
(Langleben, 1972):

smooth	.05
rough	.30

TABLE 6C.3

TURBULENT FLUXES OVER FAST ICE, 1972

(Averages for 0800, 1200 and 1600 hours)

DATE	SENSIBLE HEAT ($\text{Jcm}^{-2}\text{min}^{-1}$)	LATENT HEAT ($\text{Jcm}^{-2}\text{min}^{-1}$)
June 13 to 30 (17 days)	0.152	-0.358
July 2 to 20 (16 days)	0.154	-0.096
AVERAGE MEAN	0.153	-0.227

TABLE 6C.4

NET RADIATION AND CONDUCTIVE HEAT FLUXES

OVER FAST ICE, 1972

(Averages for 0800, 1200 and 1600 hours)

DATE	NET RADIATION ($\text{Jcm}^{-2}\text{min}^{-1}$)	CONDUCTIVE HEAT ($\text{Jcm}^{-2}\text{min}^{-1}$)
June 13 to 30 (17 days)	0.521	0.336
July 2 to 20 (16 days)	1.509	1.520
AVERAGE MEAN	1.015	0.928

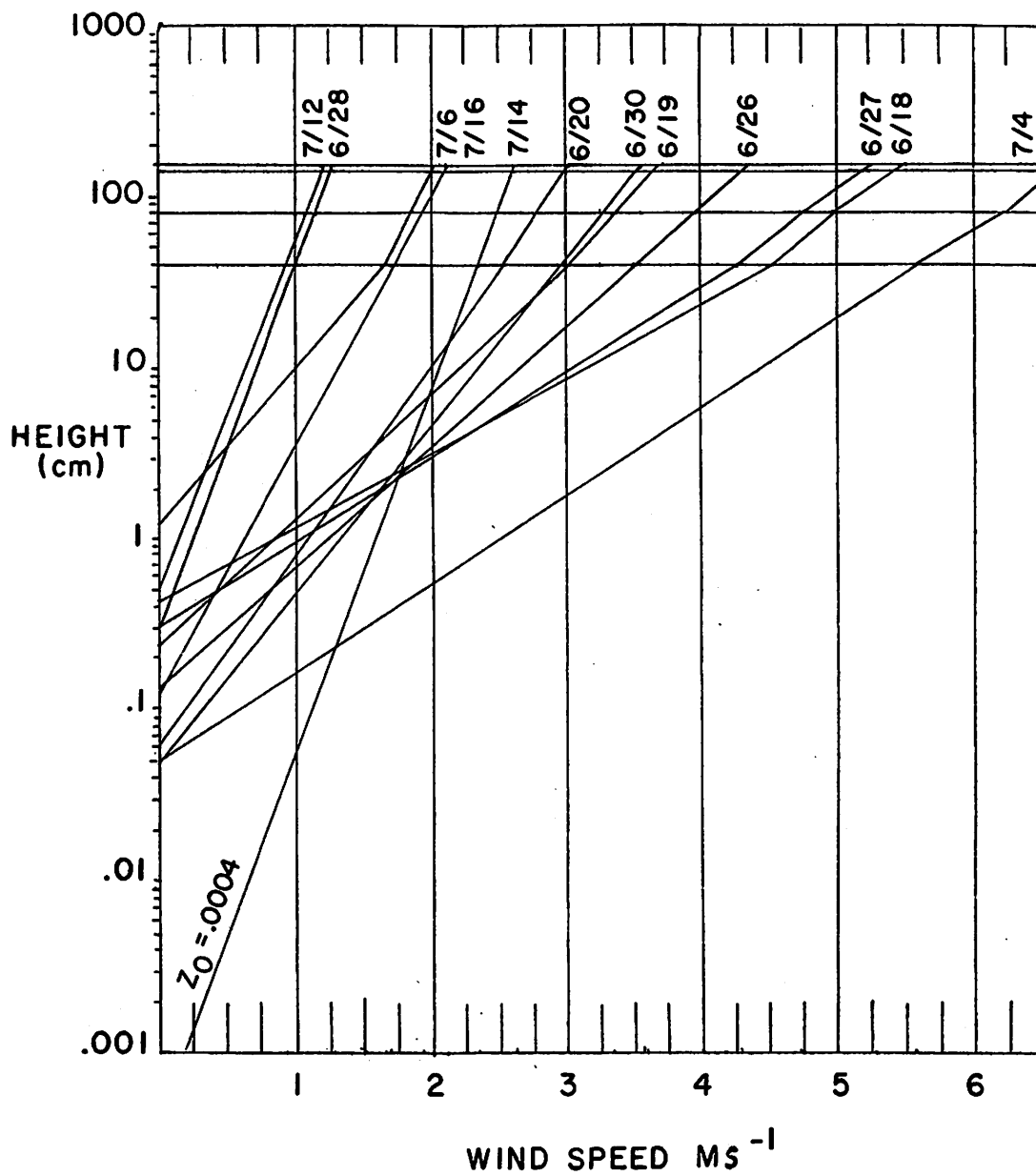


Figure 6C.1 Daily mean wind profiles over the fast ice in June-July 1972.

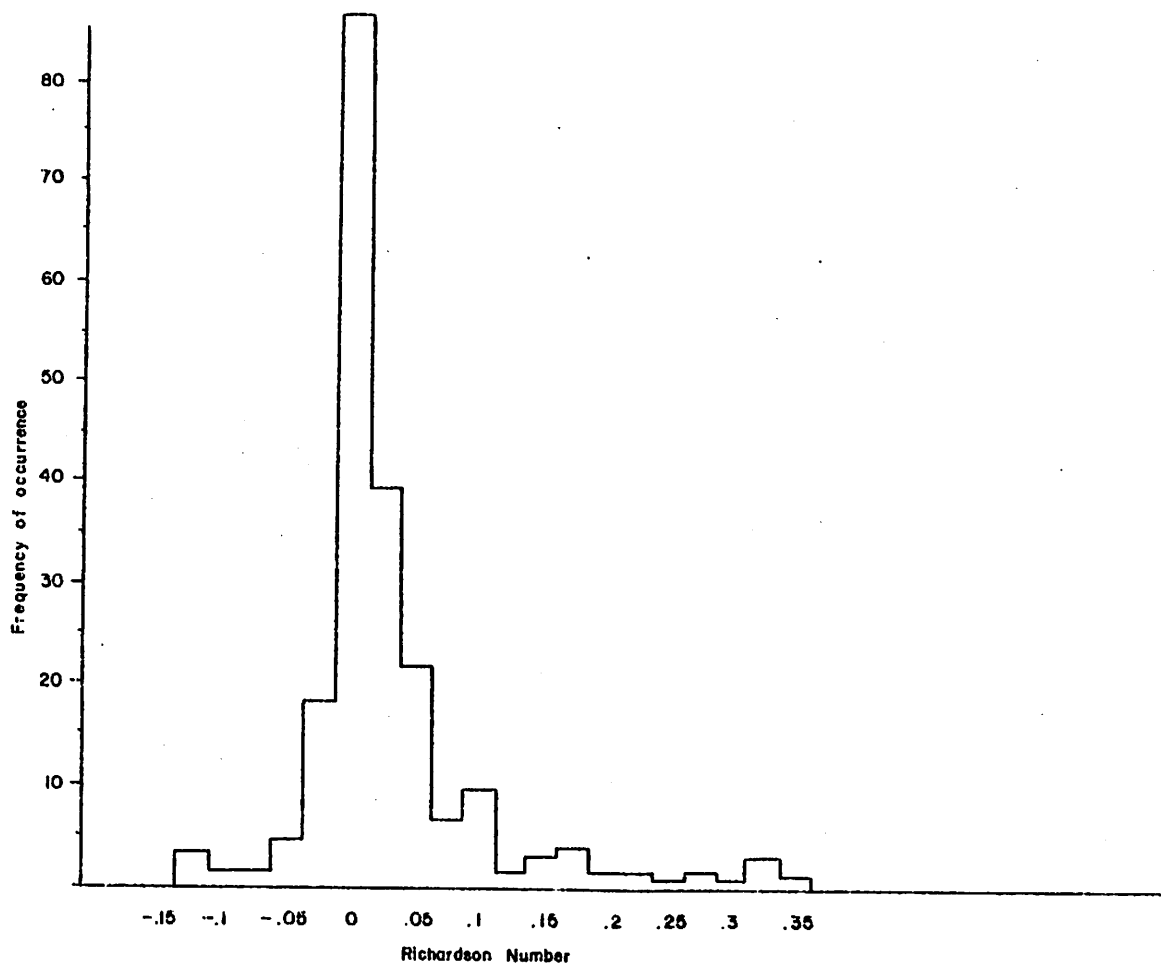


Figure 6C. 2. Frequency of Richardson numbers for June-July 1972 over the fast ice.

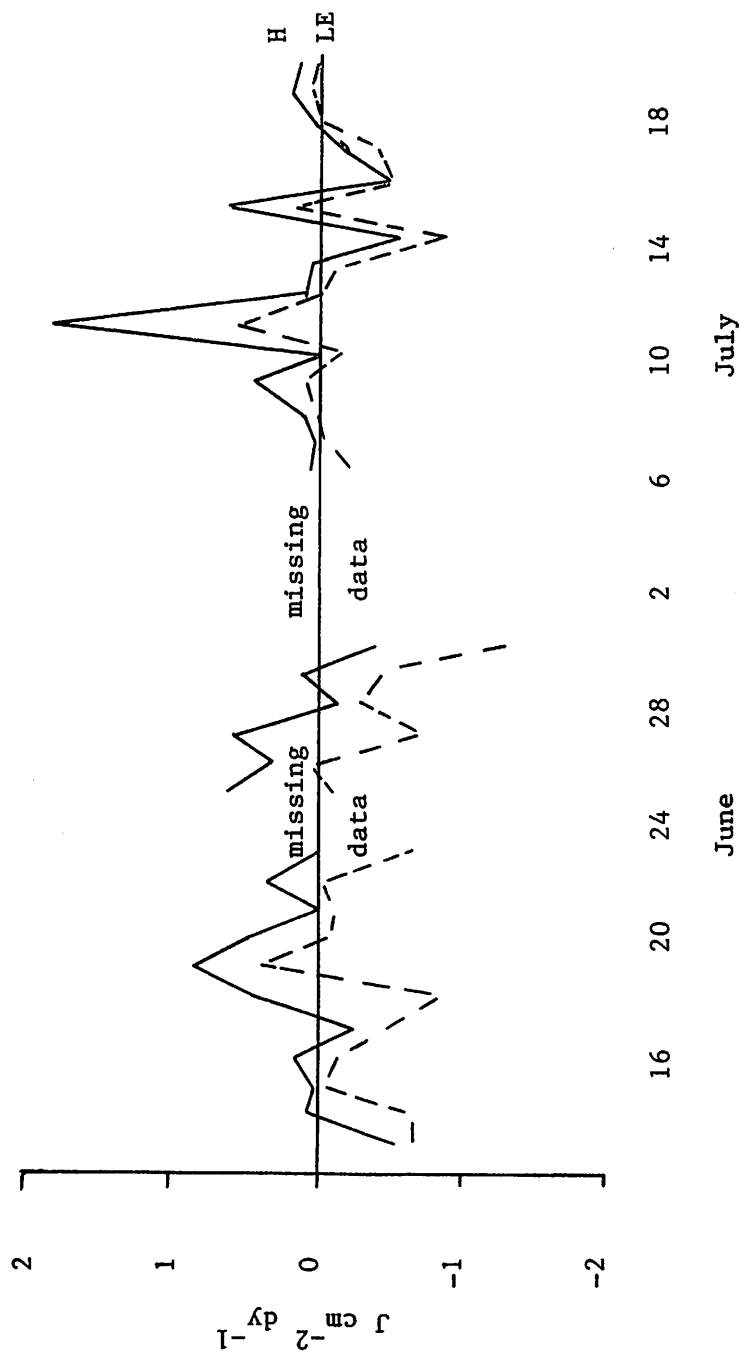


Figure 6C.3 Average daytime fluxes of sensible heat (H) and latent heat (LE), over fast ice 1972.

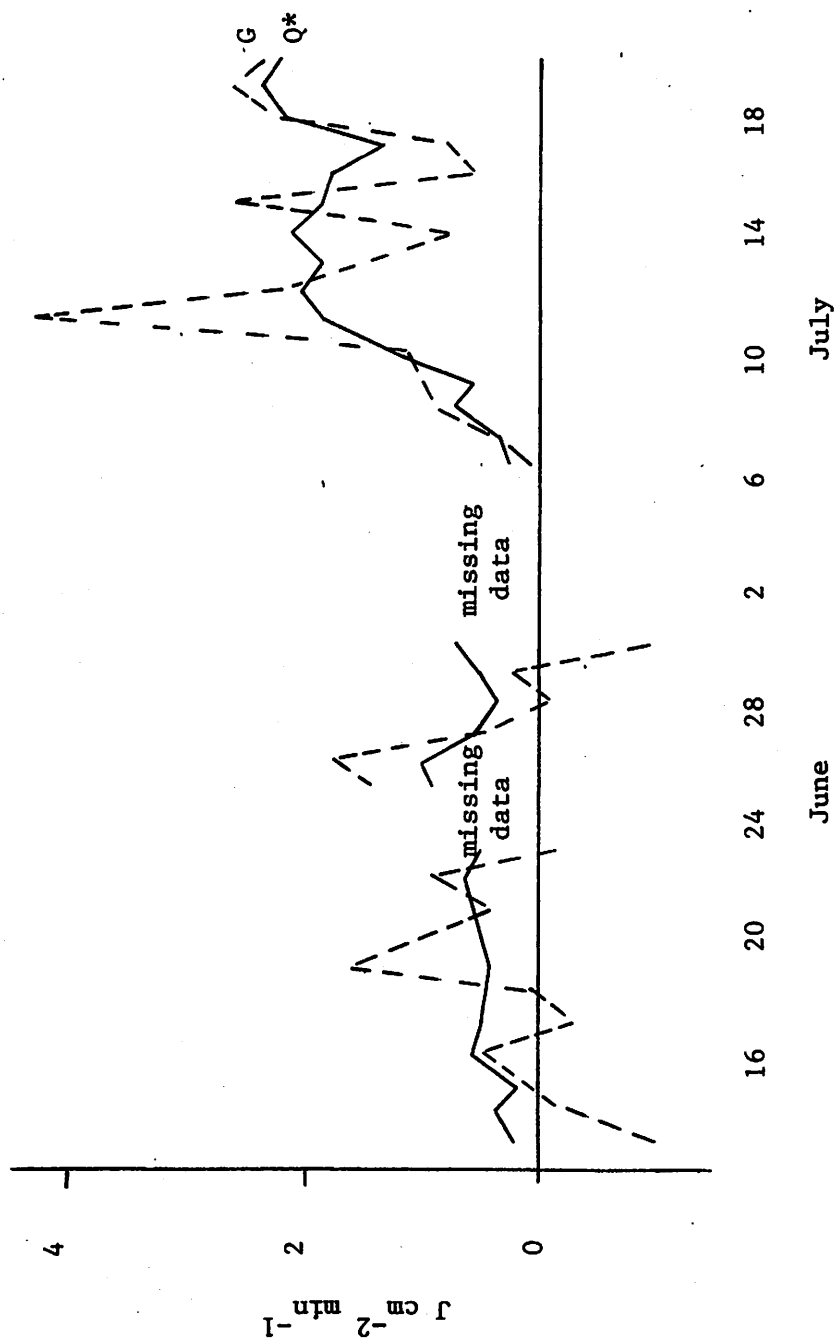


Figure 6C.4 Average daytime fluxes of net radiation (Q^*) and conductive heat (G), over fast ice 1972.

D. Synoptic Controls on the Energy Budget

Introduction

Several studies have demonstrated that periods of substantial ablation of either glacier ice or sea ice can be related to the synoptic conditions.

Jacobs (1974) illustrates how cyclonically-controlled northerly flow brought cold air over south-eastern Baffin Island, prior to the 26 June, 1973. After this date, with the development of a ridge at the 700 mb level, a cyclone moving into the area gave west to south-west flow along the northern side of the ridge. From 26 June to 1 July this caused a general warming of 10° - 16° C along the south-eastern coast of Baffin Island from Cape Dyer to Clyde. Temperatures along most of this coast rose from below freezing on 26 June to 8 - 12° C by the 29 June, by which time most of Baffin Island was in the warm sector. The progression of the system through the area caused a decrease in solar and net radiation but rapid ablation occurred due to increased advection of sensible heat. After a weakening of the ridge and a return to colder more northerly flow, temperatures fell and net radiation and solar radiation began to rise again. This sequence of events was repeated in mid-July and again in early August 1973. Both of these events were accompanied by significant periods of ice melt. The July case has been analyzed by LeDrew (section 3, this report).

Melt periods on the Devon Island ice cap are normally short and discontinuous. Appreciable summer melting can again be related to particular synoptic situations (Holmgren, 1971 and Alt, 1978). The highest melt rates are observed during cyclonic activity causing strong winds and the advection of warm and humid air over the region. Weather maps for days with the highest melt rates show the ice cap to be located beneath the warm sector of the cyclone, with a general flow from areas to the south or west. Cyclones following northeasterly tracks along western Greenland or Baffin Bay bring relatively cold weather to the area with temperatures generally below freezing.

The work of Mackay (1952) for Churchill Harbor in Hudson Bay illustrates the importance of protracted spring thaws for early ice breakup. These occur with persistent anticyclonic conditions. His results also show that the type of winter does not materially affect the breakup dates.

The four studies referred to above all indicate that there is a relationship between particular synoptic conditions and the onset of a significant ablation period.

Micro-meteorological data over fast ice near Broughton Island in 1972 allowed daily energy budgets to be calculated for the period 13 June to 20 July as described in section 6C. The sequence of synoptic events for the same period are now examined to ascertain whether synoptic changes are reflected by fluctuations in the energy budget.

Synoptic Sequence and Changes in the Energy Fluxes

The sequence of surface weather charts for 15 June - 30 June 1972 is shown in Figure 6D.1 and for 2 July - 20 July in Figure 6D.2. The charts show an occlusion entering the area in the northwest on 15 June, travelling south-eastwards across Baffin Island and leaving the area by the 19th. At the ice station mean daily temperatures rise during this period from -1.2°C to -0.5°C and winds increase by the 17th with the approach of the front, reaching a maximum on the 18th when the front is over the study site. There is also some precipitation associated with the approach of the front (Table 6D.1). Values of the latent heat flux are strongly negative, reflecting heat loss by evaporation (Table 6 D.2). Sensible heat flux is small and the conductive flux is near zero, except when net radiation values increase before the arrival of the front. Low pressure persists in the south and over Baffin Bay until the 20th causing the advection of warmer air into the region bringing above zero temperatures and this advection of sensible heat causes a large increase in the heat flux into the snow.

Colder air is brought in from the north during the building of a ridge of high pressure on the 21st. The falling temperatures lead to lower values of the Bowen ratio and generally lower values of the conductive flux. Low pressure begins to intensify again after the 24th, however, causing an increase in winds and precipitation the advection of sensible heat, and higher net radiation, resulting in a large input of heat to the surface. After the 27th, with an upper high supporting the development of a surface ridge over Baffin Island, sensible heat tends to decrease and, although net radiation remains relatively high, there is heat loss by evaporation and the conductive flux again tends to be low or negative.

Between 1-8 July the upper level high weakens and is replaced by low pressure at 500 mb and at the surface. Net radiation decreases, but temperatures increase and, although precipitation increases in the latter part of the period, (Table 6D.3) the Bowen ratio shows the dominant heat loss is by the latent heat flux; the conductive term is low as shown in Table 6D.4. High pressure forms again after the 8th, net radiation increases and temperatures increase rapidly, resulting in large increases in the conductive flux into the ice. After the 12th a well-developed, cold low forms in the west, at the 500 mb level, supporting a surface low. Temperatures decline but, as there is little frontal activity, net radiation remains high so that there is still a relatively large flux of heat to the ice.

On the 15th the development of a ridge over Baffin Island brings warm air from the south or south-west raising temperatures and giving high values of sensible heat and a large increase in the heat entering the ice. On the 16th the pattern again reverts to one of low pressure, but a weak ridge begins to form on the 17th and by the 18th the development of high pressure over the island brings in warmer air from the west.

Increased advection leads to positive values of sensible heat flux, net radiation is high due to clear conditions, and latent heat is positive. Additions of heat to the ice through the conductive flux are large, giving rise to extensive melting.

Classification of Energy Budgets

The preceding discussion shows that fluctuation in the energy budget parameters can be related, at least on a subjective level, to changing synoptic conditions over the study area. Cluster analysis has been used to try and group together days with similar turbulent flux characteristics. The increase in the energy budget terms between the melting snow stage and the puddle formation stage of fast ice ablation indicates that large variation in the turbulent energy budget can be related to the stage of decay of the fast ice. As we are here trying to demonstrate possible synoptic controls over the shorter term fluctuations in the energy budget, then the two regimes have been analyzed separately in order to remove this effect. Five variables are considered: net radiation, sensible heat, the conductive flux, Richardson number and the Bowen ratio. The daily averages of these are used as input for a principal components analysis. This analysis is used to standardize the data and to reduce the number of variables to be used in the cluster analysis. In both cases (i.e. for stage 2 and 3), the first two components explained over 75% of the total variance and clustering was based on the factor scores of these two components.

Figure 6D.3 illustrates the distribution of the factor scores for the two components from the stage 3 analysis. The similarity of the observations are measured on a linear scale, measuring the distance separating one point from another. As the space is Cartesian, then the distance is given by Pythagoras' theorem. The two closest observations are joined together to form a proto-cluster and are then represented by a single point (the centroid), or at the center of gravity where three or more points are grouped together. The next two closest points are then found and the process continued until all of the points are included within a single group.

The clustering can be illustrated using a dendrogram (Figures 6D.4 and 5). This shows cases (days) on the vertical axis versus the approximate values of $\log F$ at which each observation becomes incorporated into a particular cluster. Clusters can be picked out by eye and then tested for significance using discriminant analysis. An approximate F test shows that the groupings are significant for both regimes at <0.1 percent level.

Figures 6D.6 - 6D.8 show the results of the cluster analysis. In each regime two groups, 2a and 2b and 3a and 3b, have been recognized. The variable that contributed most to the clustering, in both periods, was the conductive flux G . Comparing the two groups for stage two (Figure 6D.6):

<u>Term</u>	<u>Group 2a:</u>	<u>Group 2b:</u>
G	low or negative	high positive
H	low or negative	high positive
LE	large negative	positive or low negative
β	-1 to +1	> +1 or < -1

There is a tendency for net radiation in 2b to be generally larger than 2a, which has some large values, but has a greater variability. Net radiation values in general, however, do not show a large difference between the groups.

Comparing the two groups for stage three (Figure 6D.8):

<u>Term</u>	<u>Group 3a:</u>	<u>Group 3b:</u>
G	relatively low	very high positive
H	low or negative	generally high positive
LE	generally high negative	positive
β	-1 to +1 generally	> +1 or < -1

Again there is a tendency for net radiation to be higher in 3b. In 3a net radiation is more variable with lower values earlier in July when snow is melting, but before the large drop in albedo caused by extensive puddle formation.

Groups 2a and 3a tend, therefore, to retard ablation, relative to 2b and 3b, for which values of G are much higher. For 2a, values of G are mainly negative, indicating a heat loss from the ice. 3a has values of G that are in fact in excess of those obtained for 2b, because of the large increase in the absolute values of the heat fluxes following the onset of puddle formation in early July. The values for 3a, however, are still low relative to those obtained for 3b.

The clustering analysis for group 2a also shows two distinct sub-groups, 2a.1 and 2a.2. The difference between these two groups, when tested using the discriminant analysis, was again significant at better than the 0.1% level. Comparing these two groups (Figure 6D.7):

<u>Term</u>	<u>Group 2a.1:</u>	<u>Group 2a.2:</u>
G	generally positive	generally negative
H	generally positive	generally negative
LE	high negative	high negative
β	-1 to 0	generally 0 to +1

Net radiation is slightly higher in group 2a.1 than in group 2a.2.

Therefore, although days in group 2a generally tend to retard ablation relative to group 2b, the group can still be divided into two groups, one of which has a negative energy budget and the other a slight positive budget, providing for some ablation. The amount of ablation however is still much less than that found in group 2b.

In both June and July the conductive flux contributes most towards the clusters, followed by the Bower ratio, Richardson number, sensible heat, and net radiation, the order of variables entered being the same in both cases. The conductive flux is therefore the most important term defining the energy budget groups. Net radiation is the last variable entered and it tends to have low correlations with other variables in the groups (except in July, where there is a relatively good within-group correlation between net radiation and sensible heat). This suggests that although net radiation supplies nearly all of the available energy to the fast ice environment, it is relatively unimportant in defining the short-term variations in the energy budget regime. It is interesting to note that variations in the conductive flux are more responsive to changes in sensible heat than to the radiation term. Assuming that, on a day-to-day basis surface conditions are little changed and that fluctuations in sensible heat are a response to advection and changing atmospheric conditions, then there is some indication that short term fluctuations in the conductive term and ice melt may also be a response to changing synoptic conditions.

Associated Synoptic Types

As a first step in determining whether or not these different energy budget regimes are synoptically controlled, the surface weather charts were compared for those days within each of the groups identified by the cluster analysis. An examination of these charts shows that the days within a particular group are characterized by similar pressure pattern or direction of flow over Broughton Island.

Although individual patterns vary in group 2a, the predominant feature in each case is a trough or a center of low pressure to the south-east, or high pressure over western Baffin Island and low pressure to the east (Fig. 6D. 9a-c) in each case, however, the flow over Broughton Island is onshore, from the north-east or south-east.

There is very little difference in the synoptic patterns between days in group 2a.1 and days in group 2a.2 (Table 6D.5b), with the exception that although the direction of flow for both groups is generally onshore, from an easterly direction, the patterns of flow in group 2a.1 tend to have more of a southerly component. This would lead to the advection of warmer air over the ice, resulting in higher values of sensible heat and thus giving rise to the positive conductive flux associated with this group.

In group 2b the dominant feature is a ridge of high pressure extending over Baffin Island from the north-west or south-west, possibly with low pressure off to the east. The main flow directions in this case are offshore from the north-west or south-west (Figure 6D.9, d-e).

Precipitation and wind speed data show little difference between the groups although, on average, windspeeds in groups 2b may be slightly higher than in 2a. Similarly high amounts of cloud cover are characteristic of the whole period, although 2a appears to have more low cloud than 2b (Table 6D.5a). However, the temperature data show a clear distinction between the groups. All of the days in 2a had below freezing temperatures and the only positive temperatures occur in 2b where the direction of flow is from a relatively warm land surface and temperatures are also increased by adiabatic warming as the air descends after crossing the mountains of Cumberland Peninsula to the west (c f. discussion in Section 3 by LeDrew). Surface wind directions for 2a tend to be north or easterly. In 2b wind directions are more variable. Some surface winds are from the north and others from the south or south-west. Local orographic factors, however, will influence these data, as the site is in a channel between Broughton Island and the main land.

For the stage 3 regime two groups were also identified and again an examination of the weather charts for these groups shows similar broad groupings of pressure pattern and direction of flow. In group 3a there is either a trough over Baffin Bay, bringing northerly flow, or low pressure centers to the south or south-east bringing easterly flow (Figure 6D. 10a-b).

In group 3b the dominant feature of the pressure patterns is a ridge over Baffin Island, bringing westerly or southwesterly flow for three out of the five days. On the 19th of July the ridge is orientated north-west to south-east, bringing south to south-east flow and on the 20th July the ridge has begun to break up, resulting in more variable flow (Figure 6D. 10c-d).

For a few of the days in group 3a pressure patterns are very weak, with small pressure gradients and little wind. These days tend to have high cloud cover, higher temperatures and some downward transfer of sensible heat. Otherwise, days in 3a have large amounts of low cloud, low or negative temperatures and some precipitation. This compares to the high temperatures, little cloud and no precipitation, associated with 3b (Table 6D.6). Wind directions also show a clear distinction between the groups with the 3a winds being mainly north or north-east and the 3b surface winds coming mainly from the south or south-west.

Relative humidity values were also compared for both 2a and 2b and 3a and 3b, but showed little variation. For the whole period, relative humidity remained high at between 85 percent and 95 percent for stage 2 and over 90 percent for stage 3.

In summary, the conditions that tend to produce the highest rates of melting, (2a and 3b), are those where a ridge forms over Baffin Island, resulting in higher net radiation values and the advection of warm southerly to westerly winds. Conditions that tend to retard ablation, (2a and 3a), are brought about by low pressure centers, particularly in the south-east, bringing in colder south-east to north-east winds. Within 2a and 3a, however, these are days when the passage of a frontal system into the area can bring higher temperatures supplying more sensible heat to the surface, relative to the other days in the group.

At this point it was hoped that the synoptic patterns for the days identified for each group could also be classified according to the subjective (Barry 1974, Barry, Bradley and Jacobs 1975) and the objective (Barry and Keen, section 2, this report) classifications that have been developed for the Baffin Island area. However, with the small number of cases in some of the groups, the variation in types within the groups was too large to make such an analysis possible.

TABLE 6D.1

Average Daytime Values of Temperature, Wind Speed, Precipitation
and Pressure for 13-30 June 1972. (Over Fast Ice)

Date	Temperature at 1.6m (° C)	Wind speed at 1.6m (m sec ⁻¹)	Snowfall (cm w.e.)	Pressure (mb)
13	-2.4	1.13	0.01	1014
14	-1.2	1.53	0	1012
15	-0.7	1.00	0	1008
16	-0.8	0.85	0	1004
17	-0.7	1.54	0.02	998
18	-0.5	5.00	0.03	995
19	0.2	3.37	0.05	1000
20	0.9	2.79	0.01	1002
21	-0.4	1.52	0	1005
22	0.6	1.11	0	1014
23	-0.8	1.65	0	1022
24	-0.1	0.87	0.02	1021
25	-0.8	1.73	0.02	1015
26	0.0	3.94	0.06	1008
27	-0.7	4.77	0.02	1009
28	-1.3	1.16	0.03	1013
29	-0.7	2.52	0.01	1016
30	-1.5	3.26	0	1016

TABLE 6D.2

Average Daytime Values of the Energy Flux Terms, over Fast ice

13-30 June 1972

Date	Net Radiation	Sensible heat	Latent heat	Conductive flux	Bowen ratio	Richardson number
	Energy units $\text{J cm}^{-2} \text{min}^{-1}$					
13	0.21	-0.57	-0.67	-1.02	0.84	-0.205
14	0.38	0.07	-0.66	-0.21	-0.11	-0.036
15	0.17	0.02	-0.06	0.10	-0.36	0.036
16	0.57	0.13	-0.16	-0.54	-0.79	0.108
17	0.49	-0.24	-0.54	-0.29	0.45	-0.005
18	0.43	0.45	-0.83	0.05	0.56	0.001
19	0.41	0.83	0.39	1.63	2.12	0.007
20	0.48	0.47	-0.07	0.88	-6.65	0.026
21	0.56	0.00	-0.12	0.44	0.12	0.003
22	0.64	0.36	-0.04	0.97	-9.97	0.099
23	0.49	-0.01	-0.63	-0.15	0.01	0.083
24	—	—	—	—	—	—
25	0.91	0.61	-0.10	1.42	-6.11	0.043
26	1.03	0.32	0.05	1.79	6.73	0.002
27	0.56	0.56	-0.68	0.44	-0.83	0.001
28	0.34	-0.13	-0.29	-0.08	0.44	-0.010
29	0.50	0.11	-0.41	0.02	-0.26	-0.001
30	0.70	-0.40	-1.28	-0.99	0.31	-0.003

TABLE 6D.3Average Daily Values of Temperature, Wind Speed,Precipitation and Pressure, 2-20 July 1972.(Over Fast Ice)

Date	Temperature at 1.6m (° C)	Windspeed at 1.6m (m sec ⁻¹)	Snowfall (cm w.e.)	Pressure (mb)
2	0.7	2.57	0	1016
4	-0.2	6.17	0.02	1009
6	0.1	1.87	0.02	1005
7	0.0	0.85	0.01	1010
8	0.9	0.92	0.03	1012
9	1.0	3.02	0.03	1013
10	0.4	0.92	0	1012
11	2.5	1.73	0	1004
12	0.3	1.07	0	1006
13	-0.2	1.10	0	1005
14	-1.1	2.48	0	1009
15	3.3	1.20	0	1016
16	-1.4	1.91	0.03	1017
17	-0.6	1.38	0	1023
18	2.0	0.72	0	1024
19	1.2	0.62	0	1020
20	0.4	0.78	0	1017

TABLE 6D.4

Average Daytime Values of the Energy Flux Terms over Fast ice

2-20 July 1972

Date	Net radiation	Sensible heat	Latent heat	Conductive flux	Bowen ratio	Richardson number
	Energy units: $\text{J cm}^{-2} \text{ min}^{-1}$					
2	0.84	0.16	-0.31	0.68	-0.50	0.042
6	0.23	0.05	-0.22	0.06	-0.24	0.044
7	0.36	0.03	-0.02	0.37	-1.48	0.085
8	0.77	0.12	0.03	0.92	4.36	0.078
9	0.56	0.41	0.11	1.07	3.84	0.115
10	1.31	-0.01	-0.14	1.17	0.07	0.015
11	1.90	1.80	0.56	4.27	3.13	0.170
12	2.08	0.08	0.00	2.16	18.75	0.020
13	1.50	0.10	-0.21	1.40	-0.48	0.069
14	2.15	-0.56	-0.88	0.71	0.63	-0.009
15	1.87	0.57	0.18	2.62	3.10	0.583
16	1.79	-0.52	-0.52	0.75	1.00	-0.019
17	1.34	-0.15	-0.34	0.85	0.44	-0.167
18	2.21	0.08	0.02	2.31	3.42	0.546
19	2.43	0.21	0.06	2.70	3.82	0.085
20	2.25	0.15	0.02	2.42	7.10	0.040

TABLE 6D.5

Comparison of Heat Flux Terms and Richardson Numbers
for Groups 2a and 2b

Term	<u>Group 2a</u>		<u>Group 2b</u>	
	Mean	Standard Deviation	Mean	Standard Deviation
Conductive Heat Flux	0.005	0.431	1.221	0.359
Bowen Ratio	-0.155	0.461	-5.152	5.142
Richardson Number	0.016	0.043	0.044	0.040
Sensible Heat	0.051	0.276	0.568	0.203
Net Radiation	0.471	0.141	0.607	0.223
Latent Heat	-0.514	0.362	0.046	0.231

TABLE 6D.6

Comparison of Heat Flux Terms and Richardson Numbers
for Groups 3a and 3b

Term	Mean	Group 3a	Standard Deviation	Group 3b	Standard Deviation
				Mean	
Conductive Heat Flux	0.784		0.406	2.747	0.774
Bowen Ratio	0.764		1.893	6.552	6.165
Richardson Number	0.025		0.080	0.241	0.256
Sensible Heat	-0.043		0.298	0.481	0.671
Net Radiation	1.120		0.670	2.121	0.215
Latent Heat	-0.239		0.295	0.144	0.221

TABLE 6D.7a

Mean Temperature, Windspeed, Precipitation
and Cloudiness for Groups 2a and 2b

VARIABLE	PERIOD	MEAN	STANDARD DEVIATION	STANDARD ERROR OF THE MEAN	SAMPLE SIZE
TEMPERATURE	2a	-0.9	0.34	0.10	11
(°C)	2b	0.2	0.74	0.37	4
WIND	2a	2.3	1.47	0.44	11
SPEED (m sec ⁻¹)	2b	2.3	1.02	0.51	4
SNOWFALL	2a	0.01	0.013	0.004	11
(cm w.e.)	2b	0.02	0.022	0.011	4
Cloud (percent)					
Low	2a	41			
Middle	2a	35			
High	2a	4			
Low	2b	54			
Middle	2b	20			
High	2b	7.5			

TABLE 6D.7b

Mean Temperature, Windspeed, Precipitation
and Cloudiness for Groups 2a.1 and 2a.2

VARIABLE	PERIOD	MEAN	STANDARD DEVIATION	STANDARD ERROR OF THE MEAN	SAMPLE SIZE
TEMPERATURE (°C)	2a.1	-1.1	0.36	0.16	5
	2a.2	-0.7	0.16	0.07	6
WINDSPEED (m sec ⁻¹)	2a.1	1.7	0.90	0.40	5
	2a.2	2.7	1.76	0.72	6
SNOWFALL (cm w.e.)	2a.1	0.01	0.01	0.006	5
	2a.2	0.01	0.01	0.005	6
CLOUD: (percent)					
Low	2a.1	36			
Middle	2a.1	44			
High	2a.1	5			
Low	2a.2	45			
Middle	2a.2	28			
High	2a.2	3			

TABLE 6D.8

Mean Temperature, Windspeed, Precipitation
and Cloudiness for Groups 3a and 3b

VARIABLE	PERIOD	MEAN	STANDARD DEVIATION	STANDARD ERROR OF THE MEAN	SAMPLE SIZE
TEMPERATURE	3a	0.0	0.78	0.22	11
(°C)	3b	1.6	1.20	0.49	6
WINDSPEED	3a	2.1	1.54	0.46	11
(m sec ⁻¹)	3b	1.0	0.41	0.17	6
PRECIPITATION	3a	0.01	0.01	.004	11
(cm w.e.)	3b	0.00	0.00	.000	6
Cloud: (percent)					
Low	3a	47			
Middle	3a	16			
High	3a	7			
Low	3b	3			
Middle	3b	3			
High	3b	11			

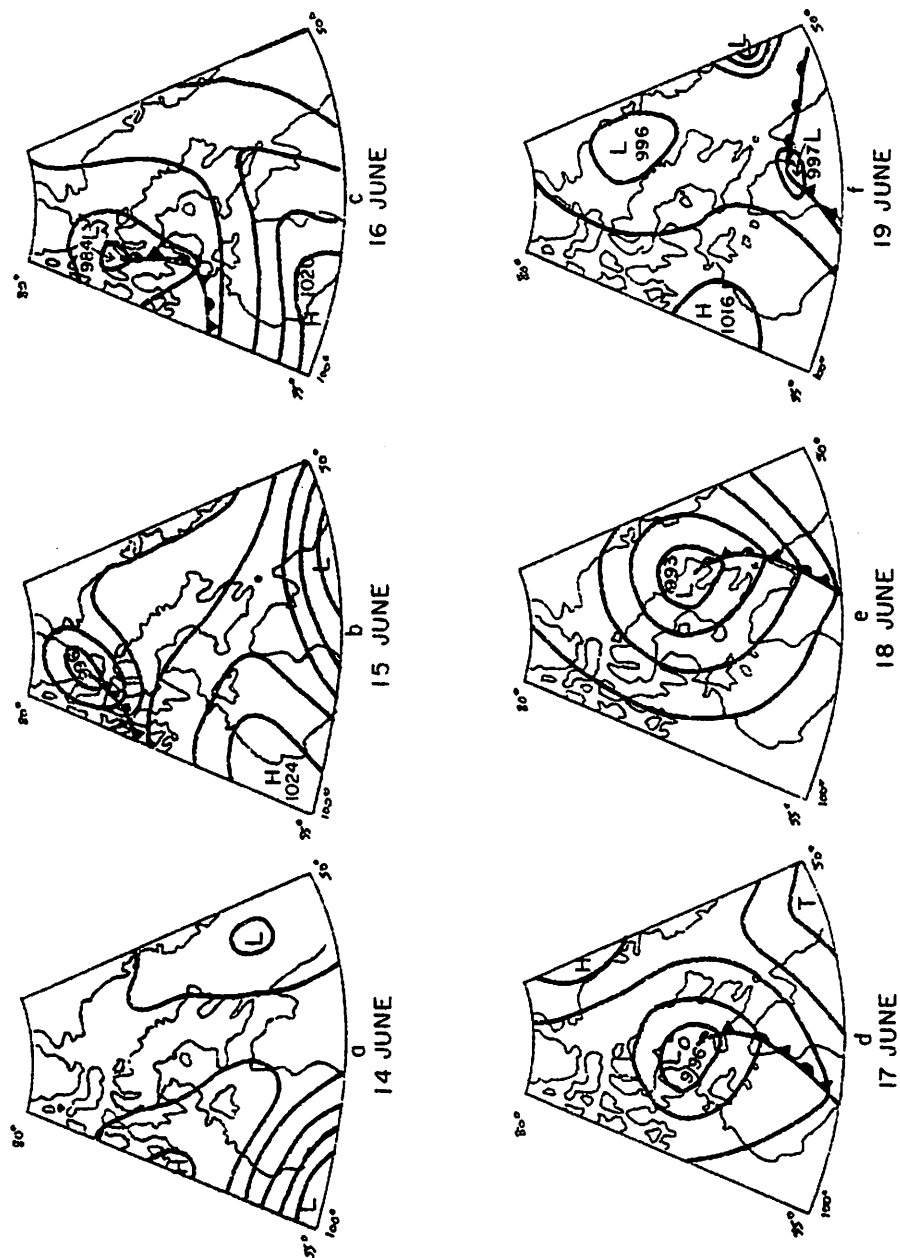


Figure 6D.1 (a-f) Synoptic charts (MSL) for 14-30 June, 1972.

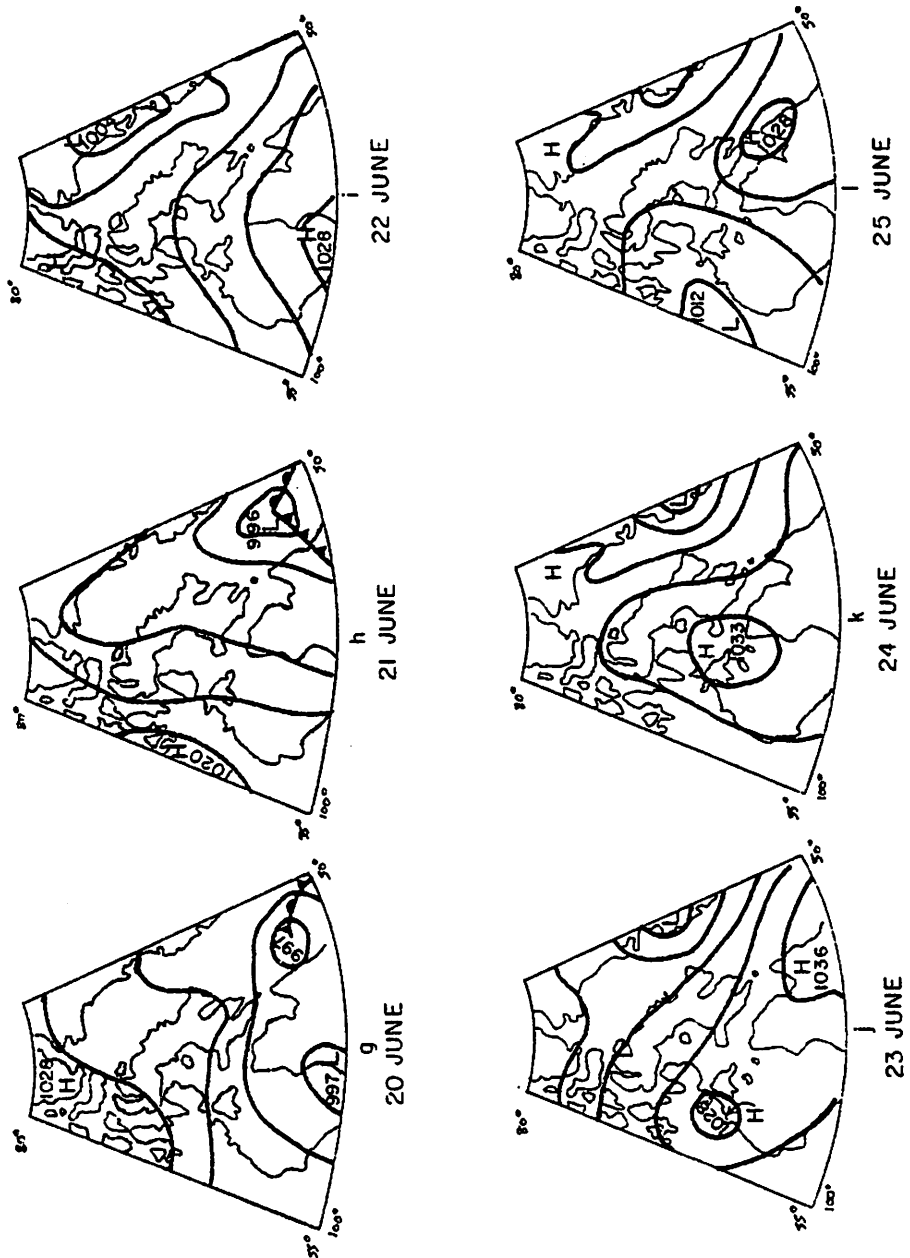


Figure 6D. 1 (g-l) Synoptic charts (MSL) for 14-30 June, 1972.

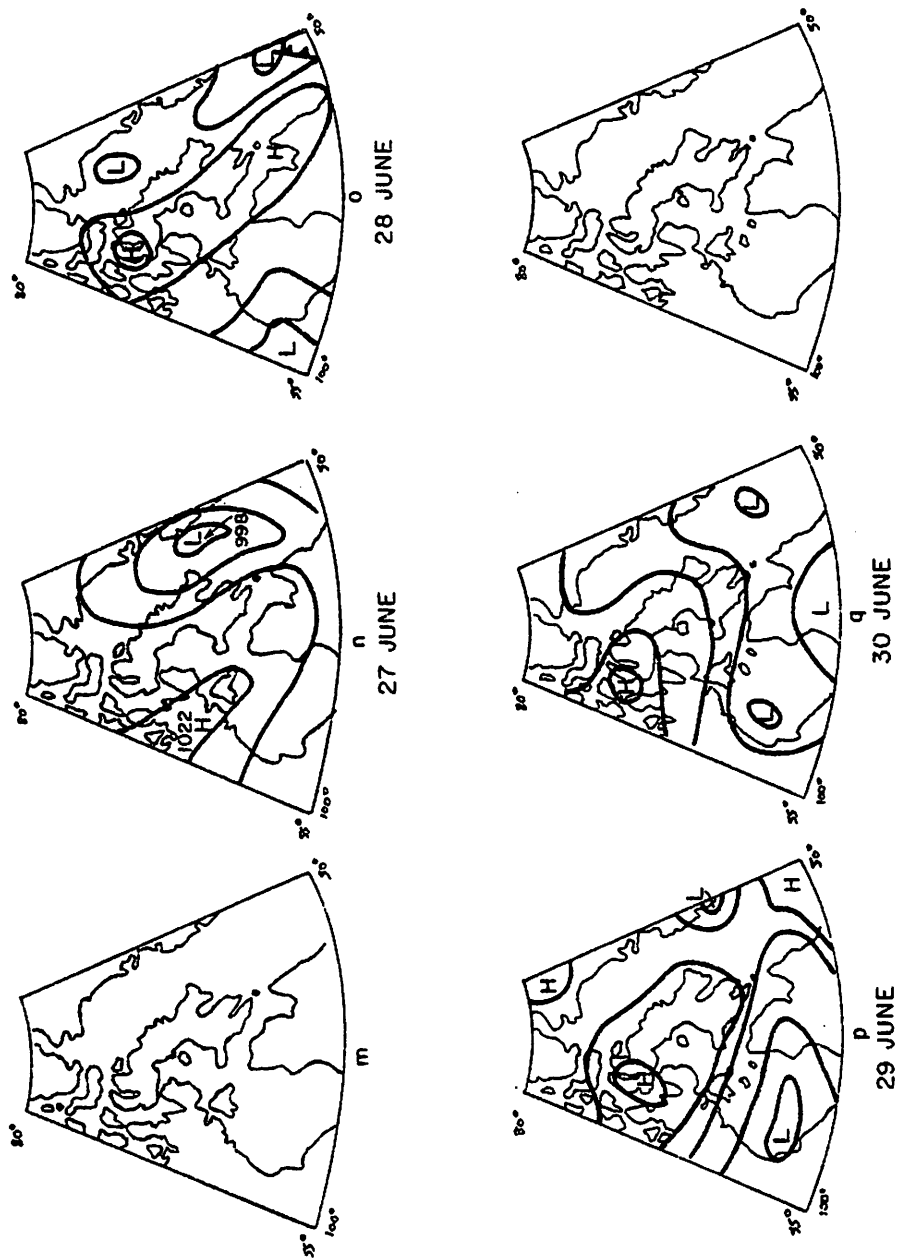


Figure 6D. 1. (m-q) Synoptic charts (MSL) for 14-30 June, 1972.

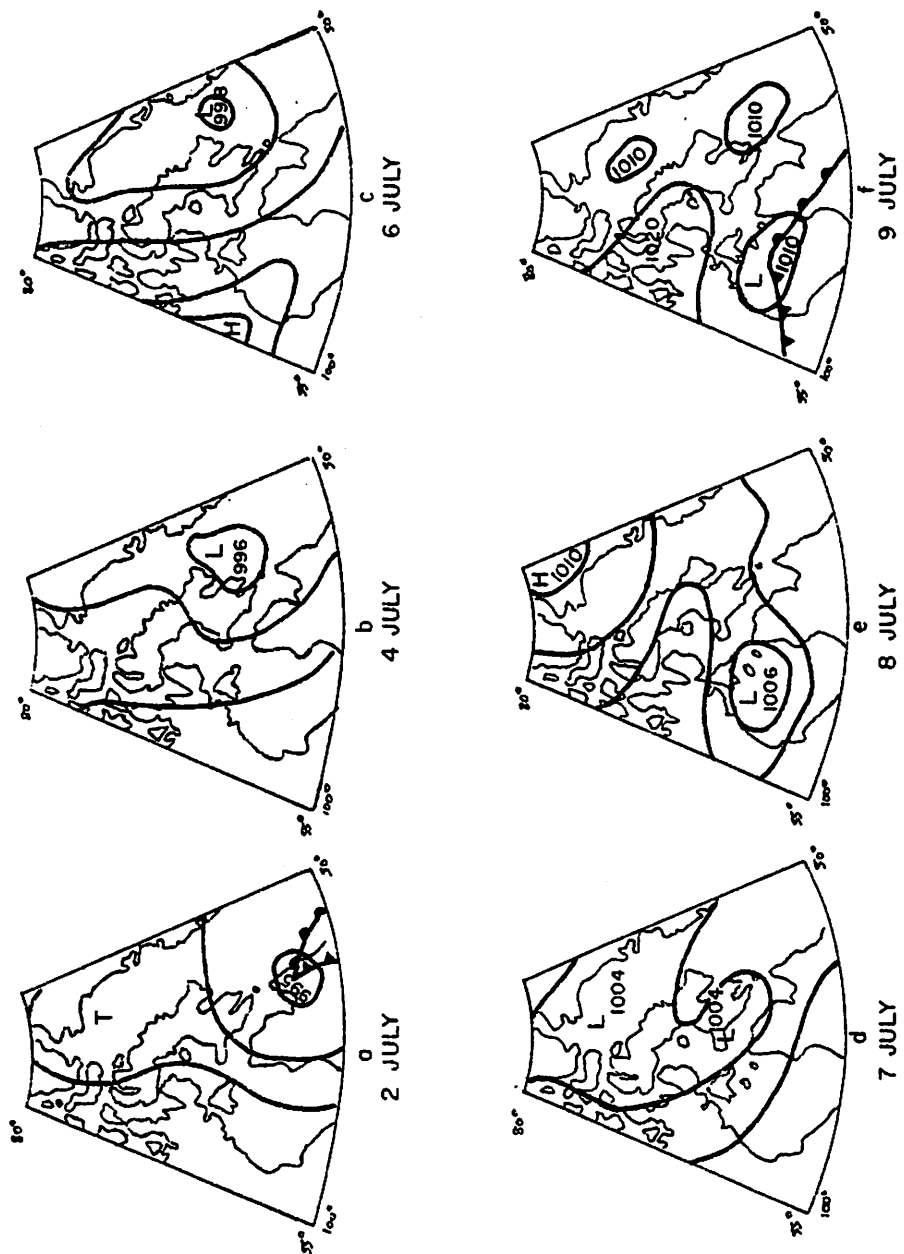


Figure 6D. 2. (a-f) Synoptic charts (MSL) for 2-20 July, 1972.

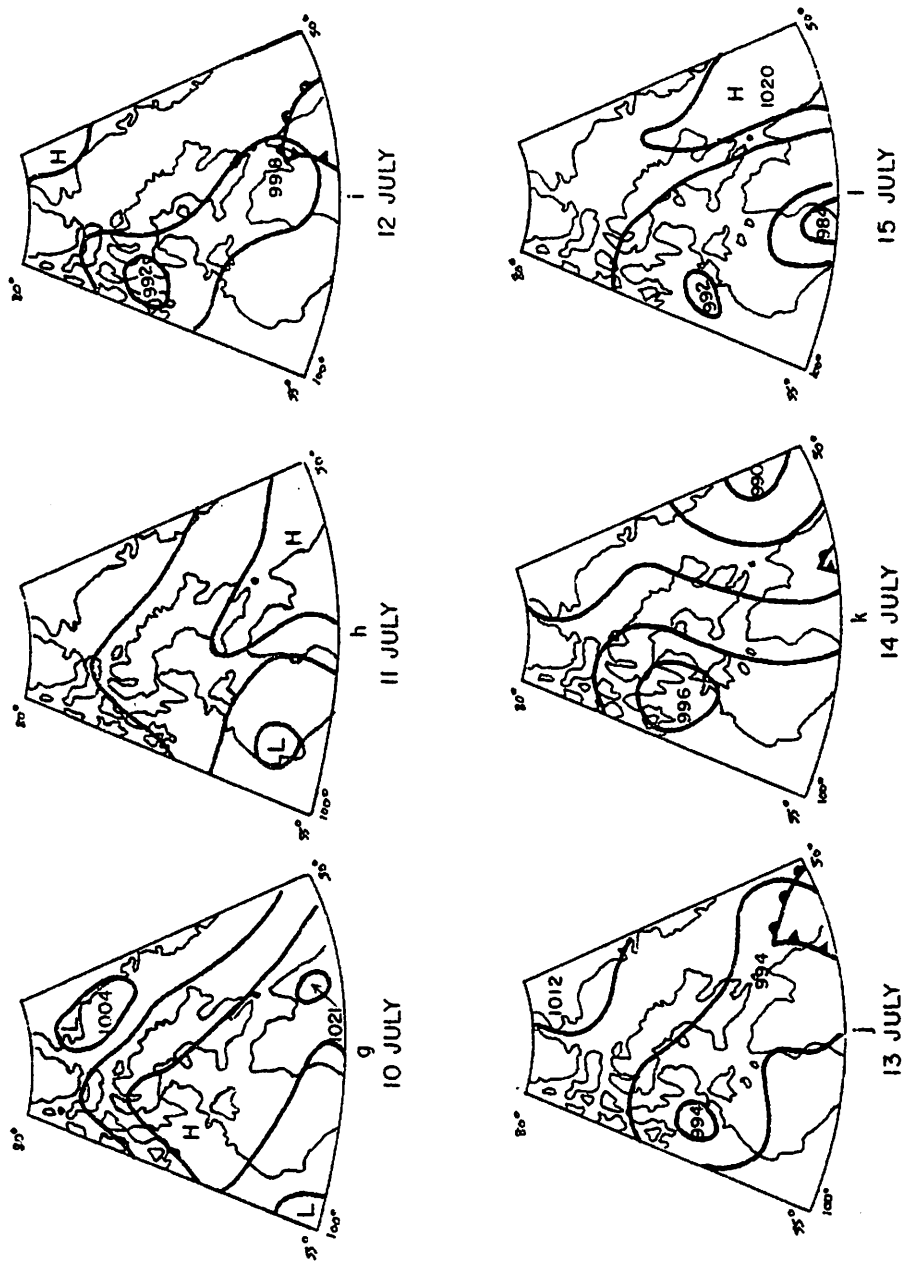


Figure 6D. 2. (g-l) Synoptic charts (MSL) for 2-20 July, 1972.

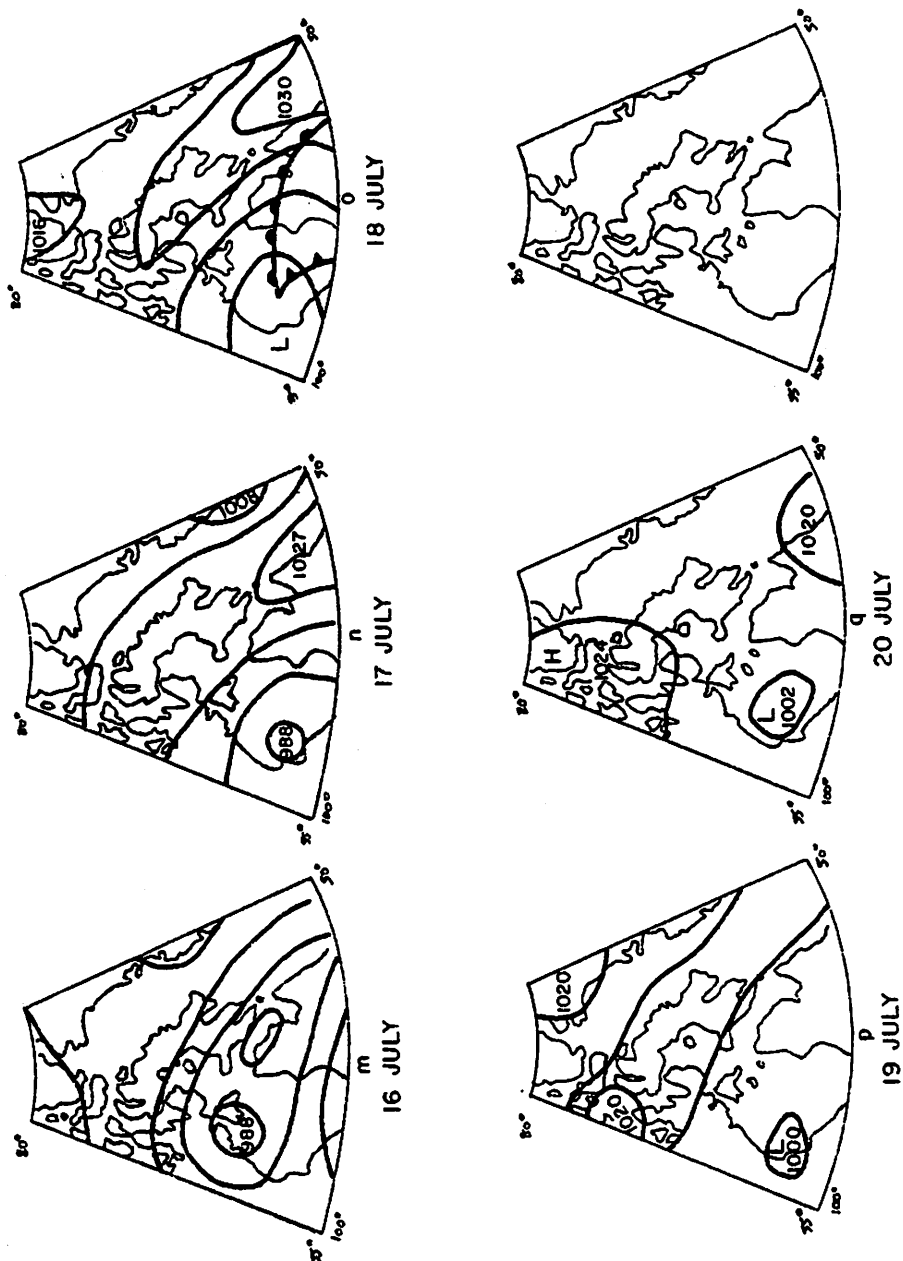
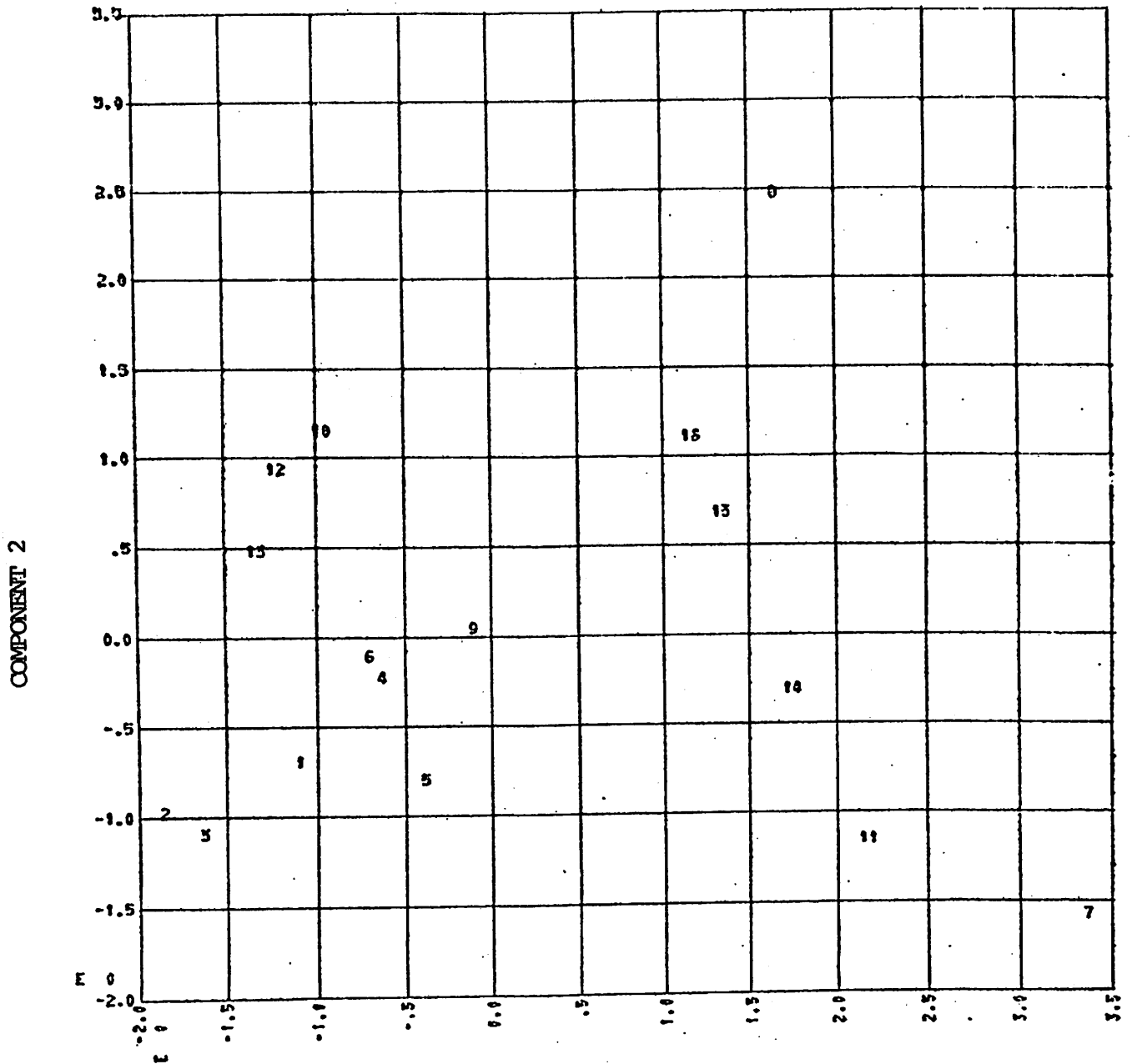


Figure 6D. 2. (m-q) Synoptic charts (MSL) for 2-20 July 1972.

RELATIVE SITE POSITIONS



COMPONENT 1

Figure 6D. 3

Distribution of factor scores for the first two principal components of stage 3 energy budget data (see text).

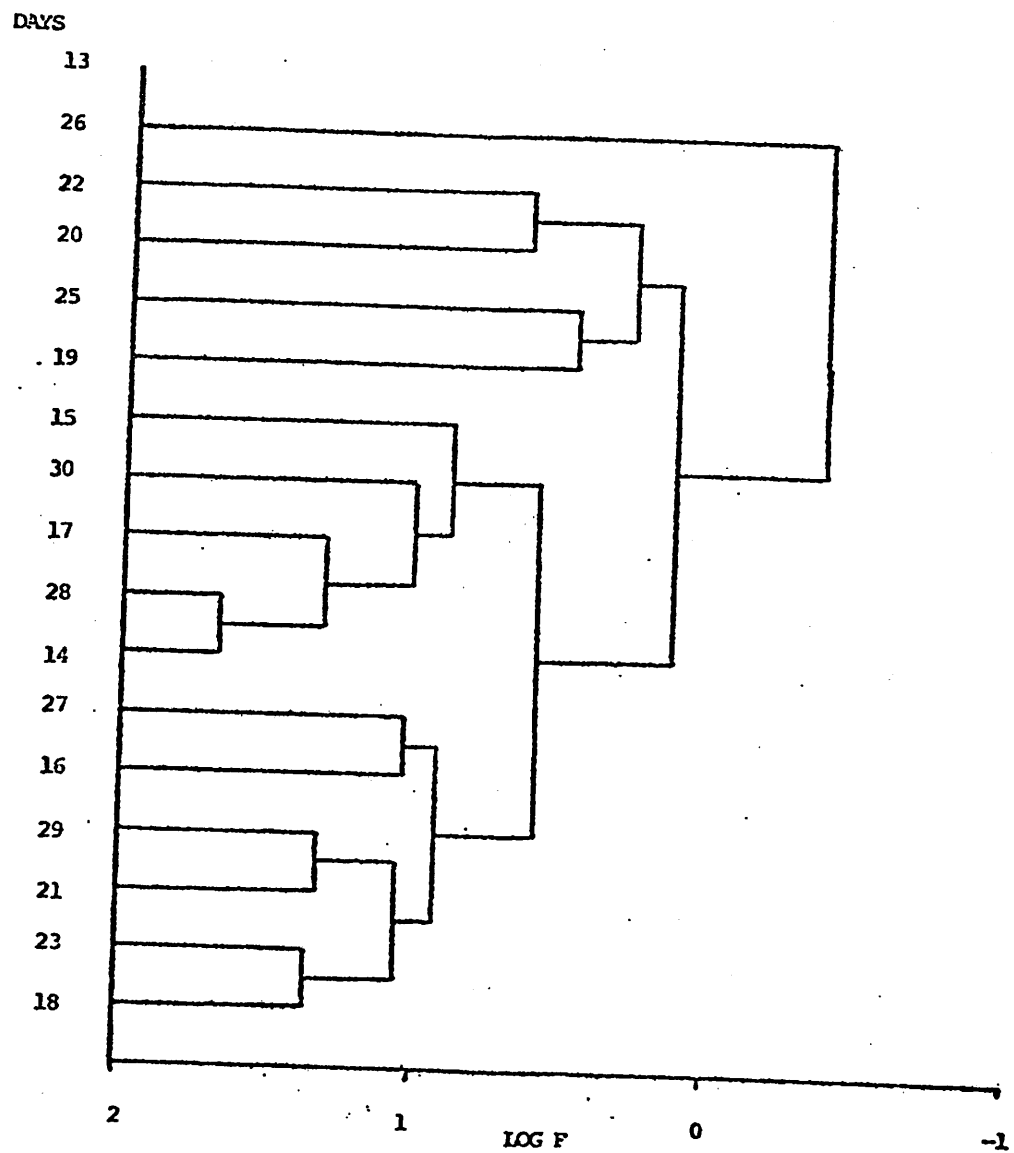


Figure 6D.4 Dendrogram of clustering analysis on June 1972 budget data.

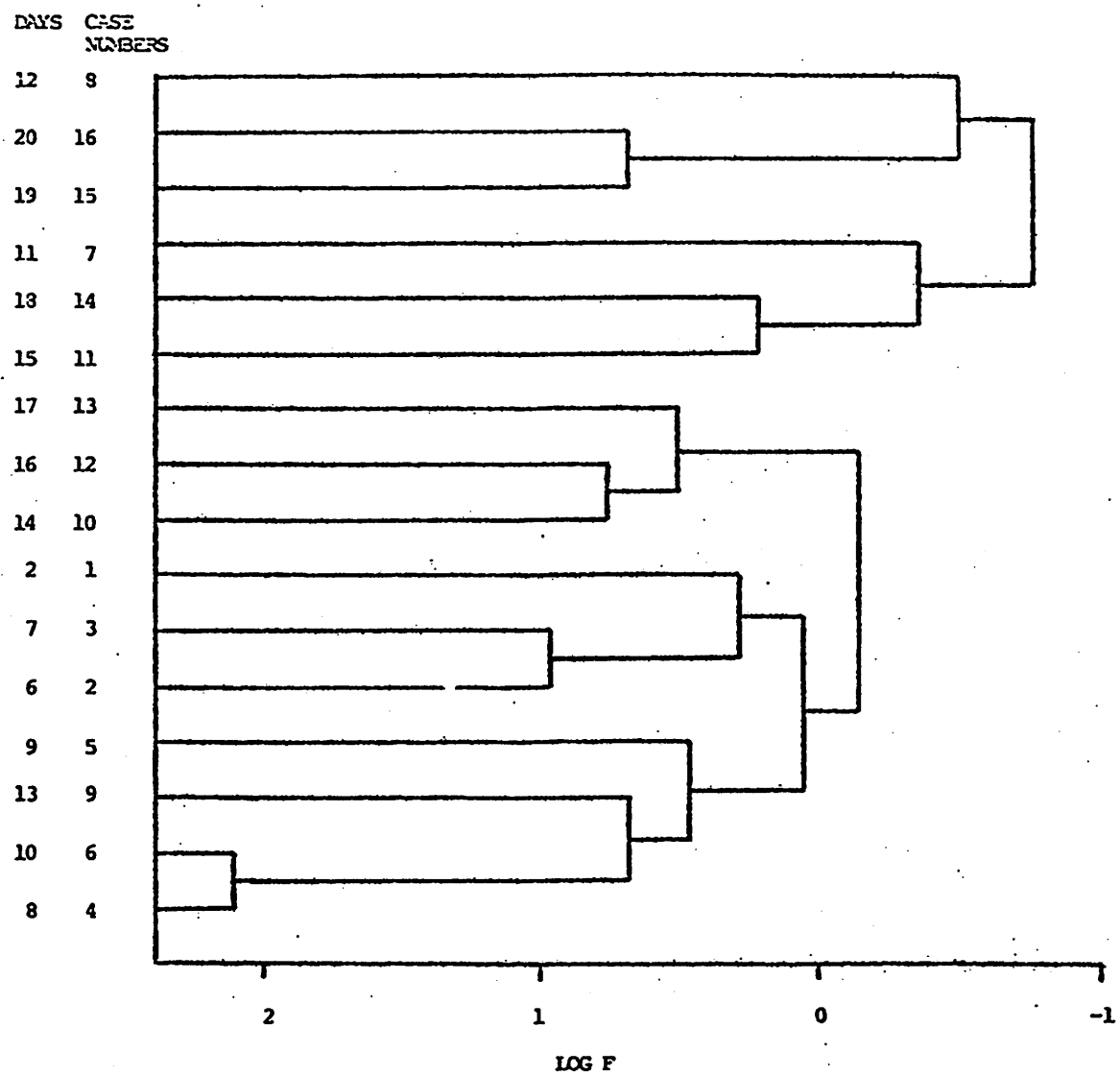


Figure 6D.5 Dendrogram of clustering analysis on July 1972 energy budget data.

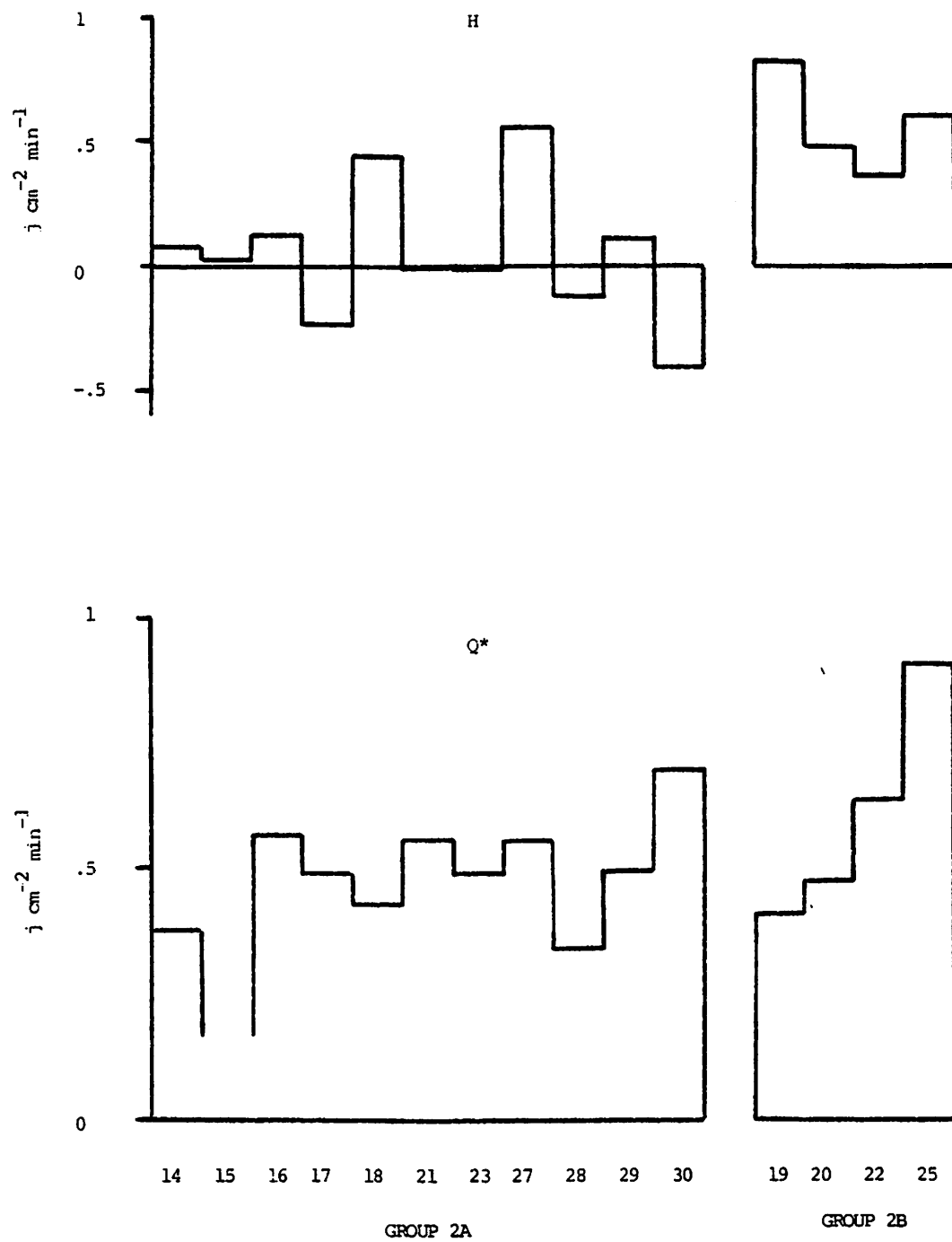


Figure 6D.6a Daytime values of H and Q*, for days in groups 2A and 2B

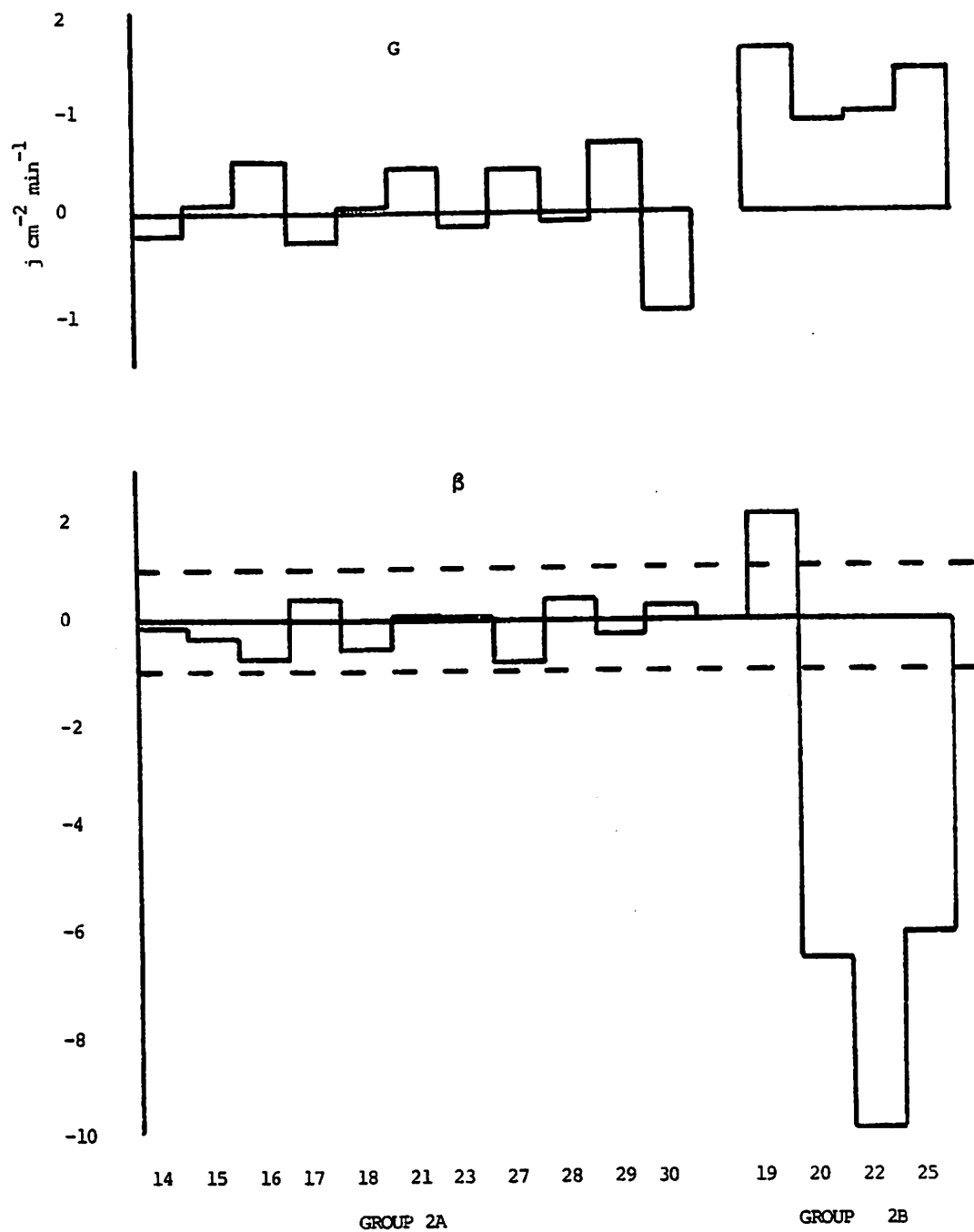


Figure 6D.6.b

Daytime values of G and β , for days in groups 2A and 2B.

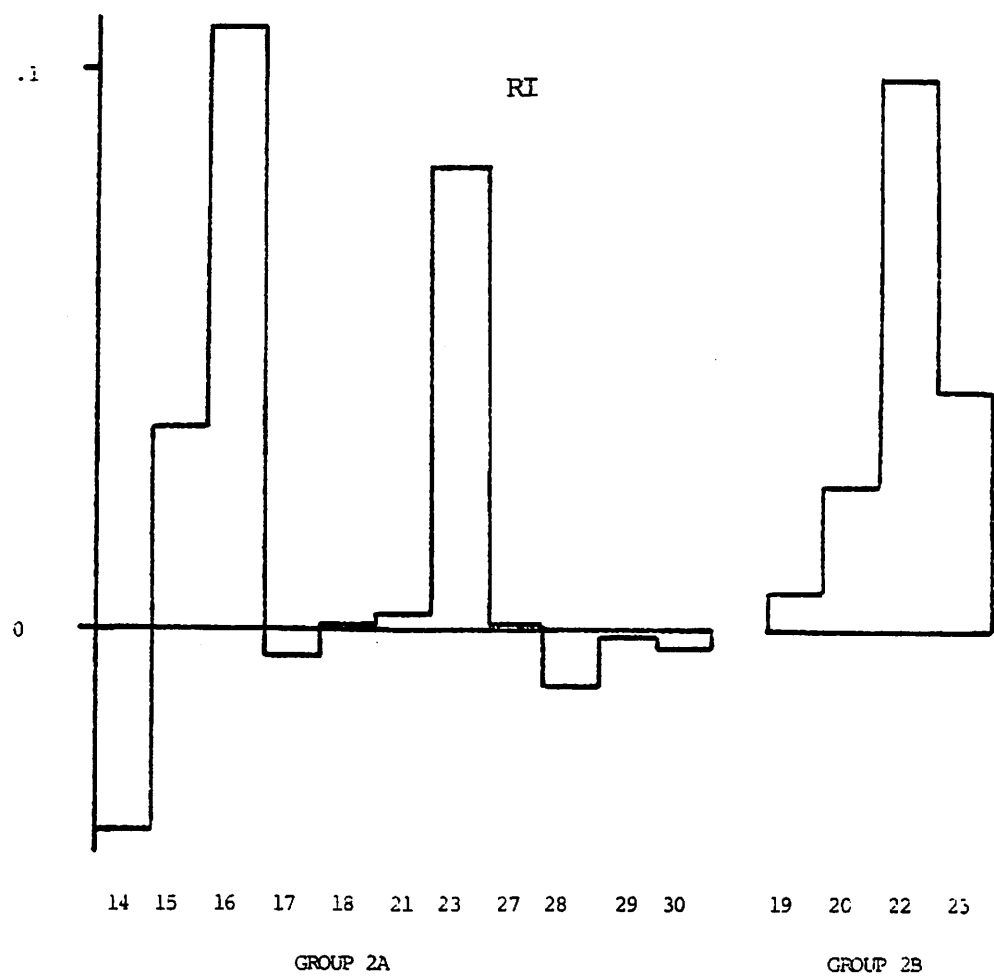


Figure 6D.6c Daytime values of R_i for days in groups 2A and 2B.

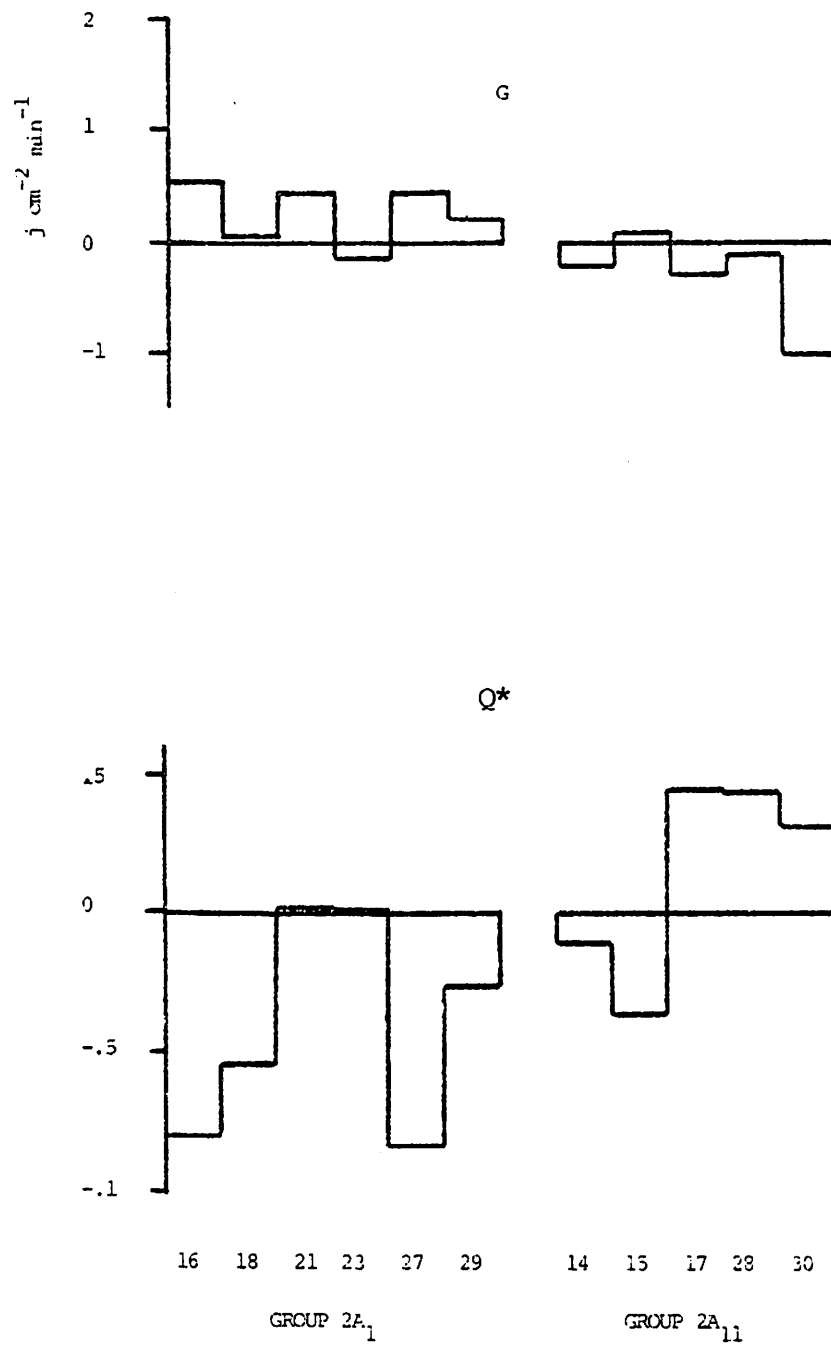


Figure 6D.7a

Daytime values of Q* and G, for days in groups 2A.1 and 2A.2

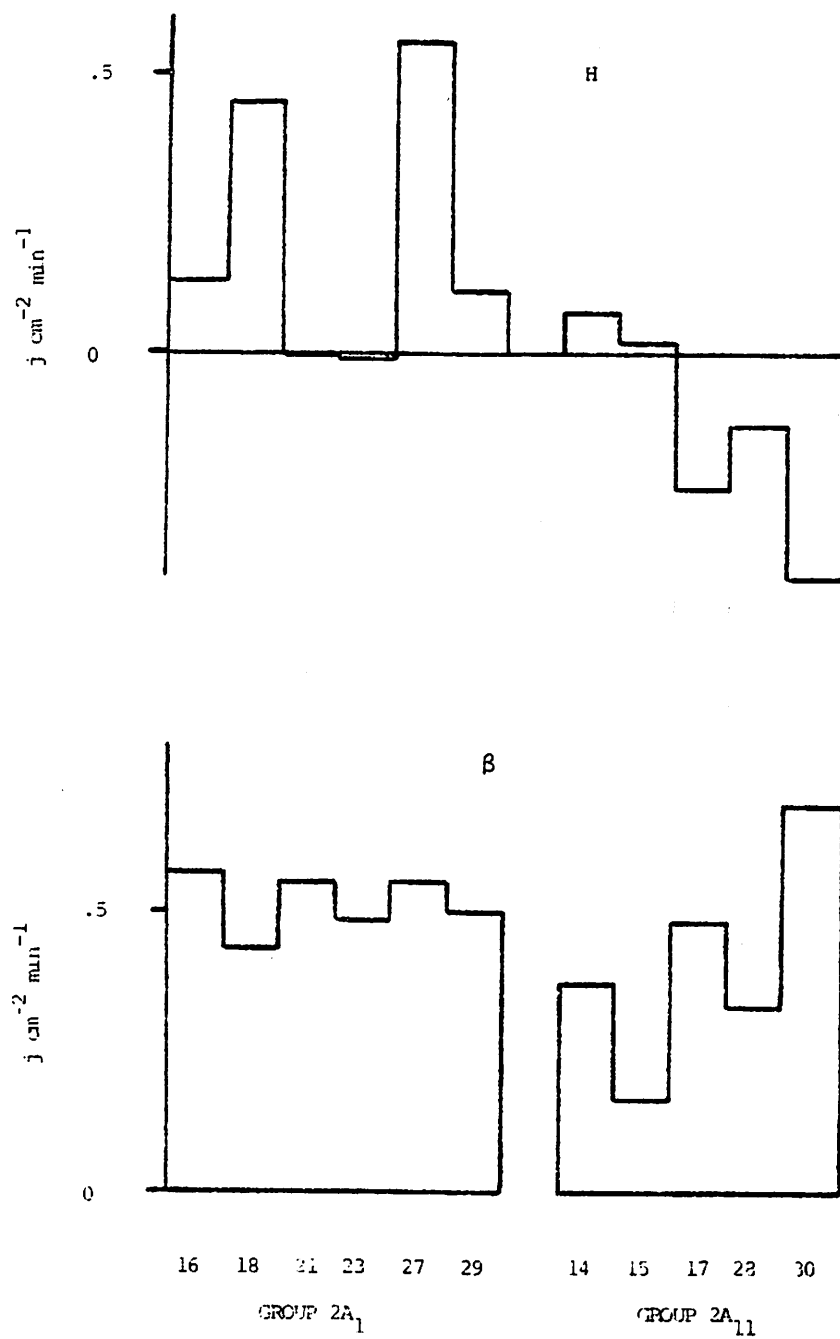


Figure 6D.7b Daytime values of H and β , for days in groups 2A.1 and 2A.2.

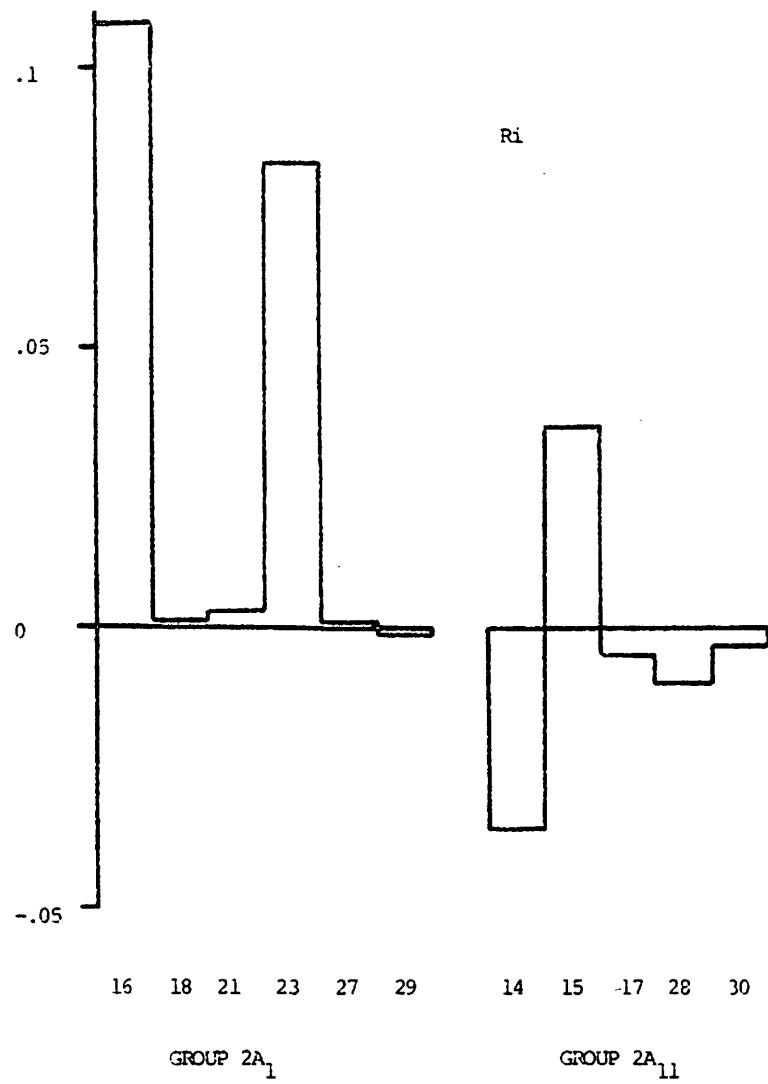


Figure 6D.7C

Daytime values of R_i for days in groups 2A.1 and 2A.2.

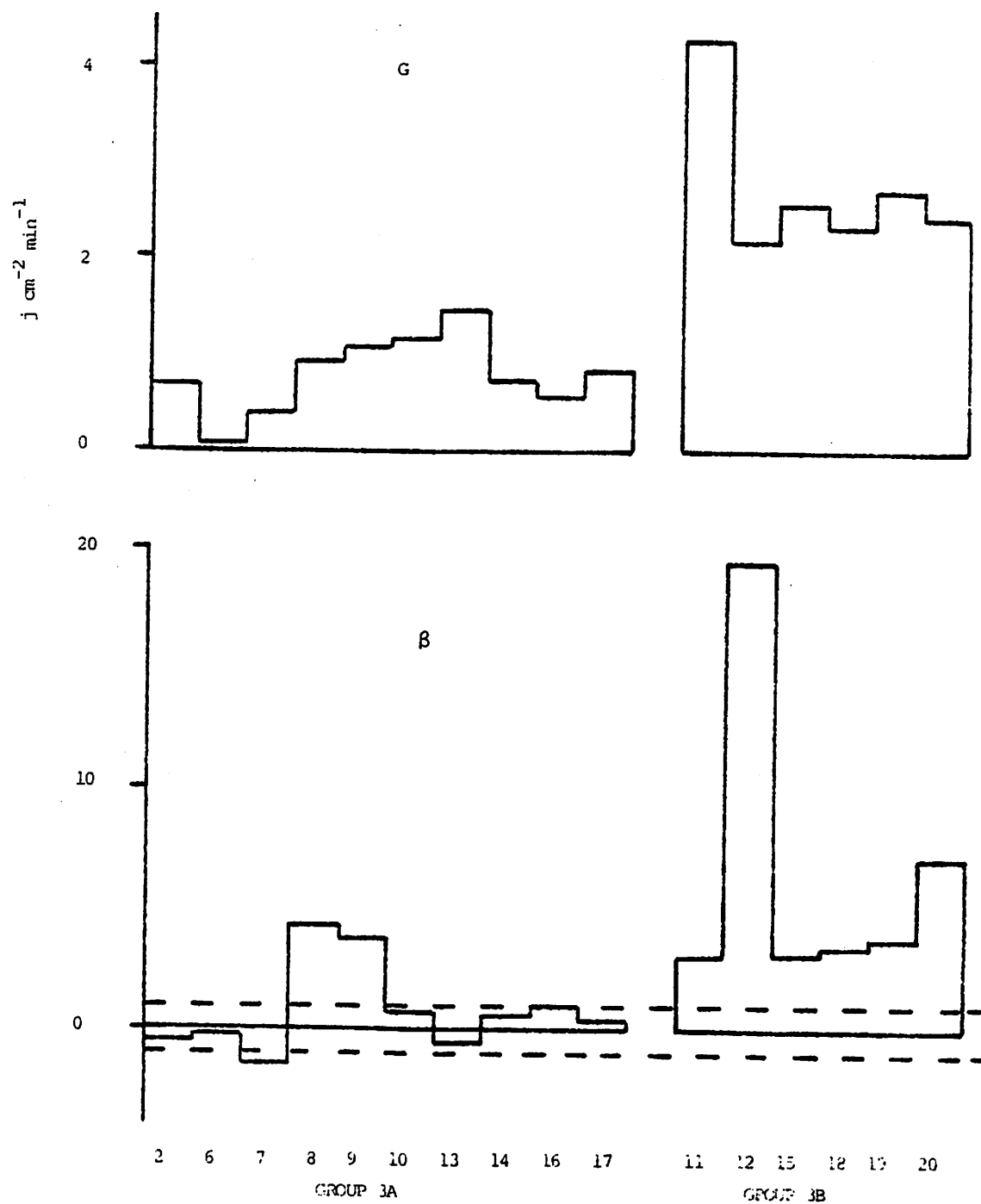


Figure 6D.8(a) Daytime values of G and β , for days in groups 3A and 3B.

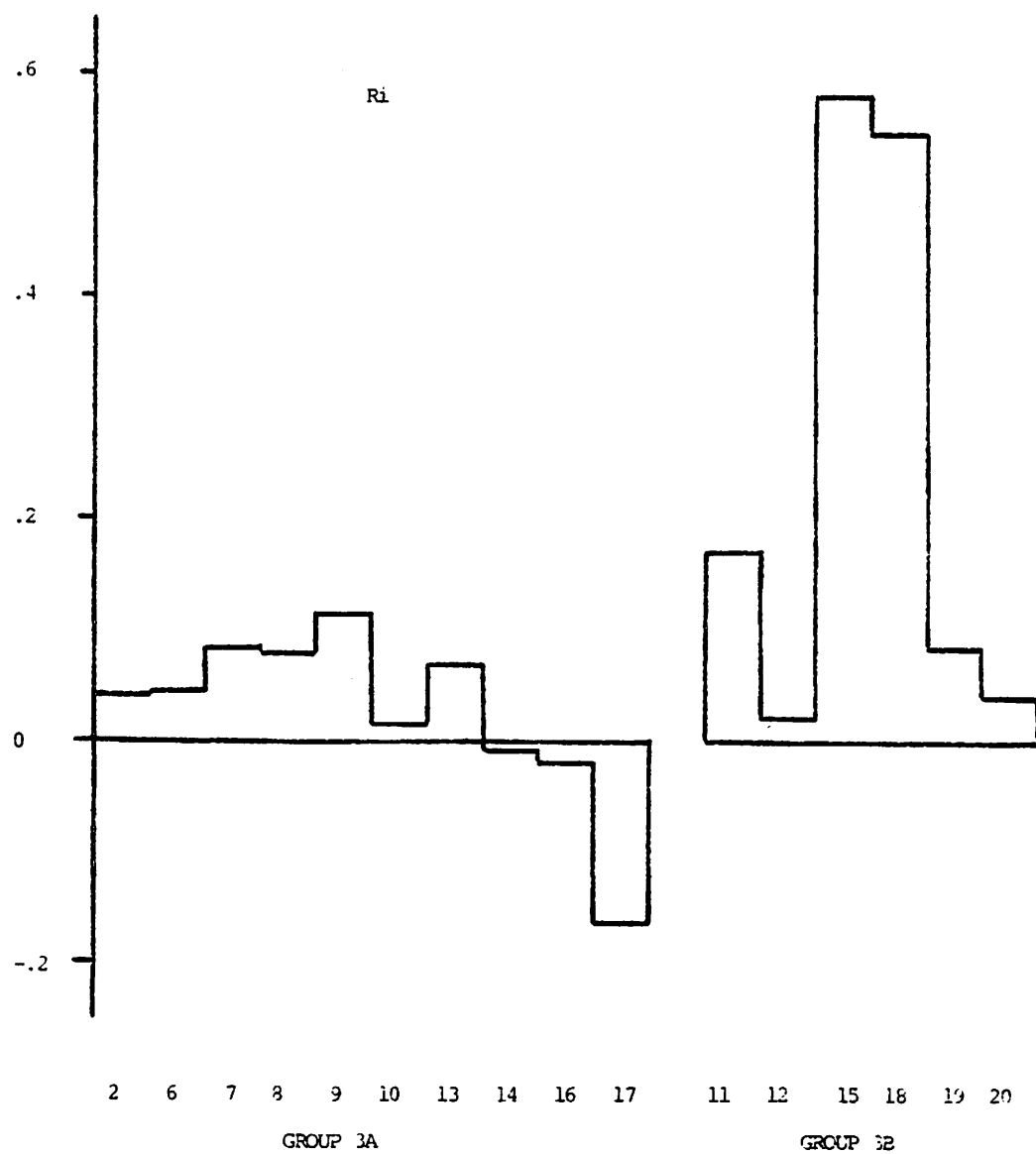


Figure 6D.8(b) Daytime values of R_i , for days in groups 3A and 3B

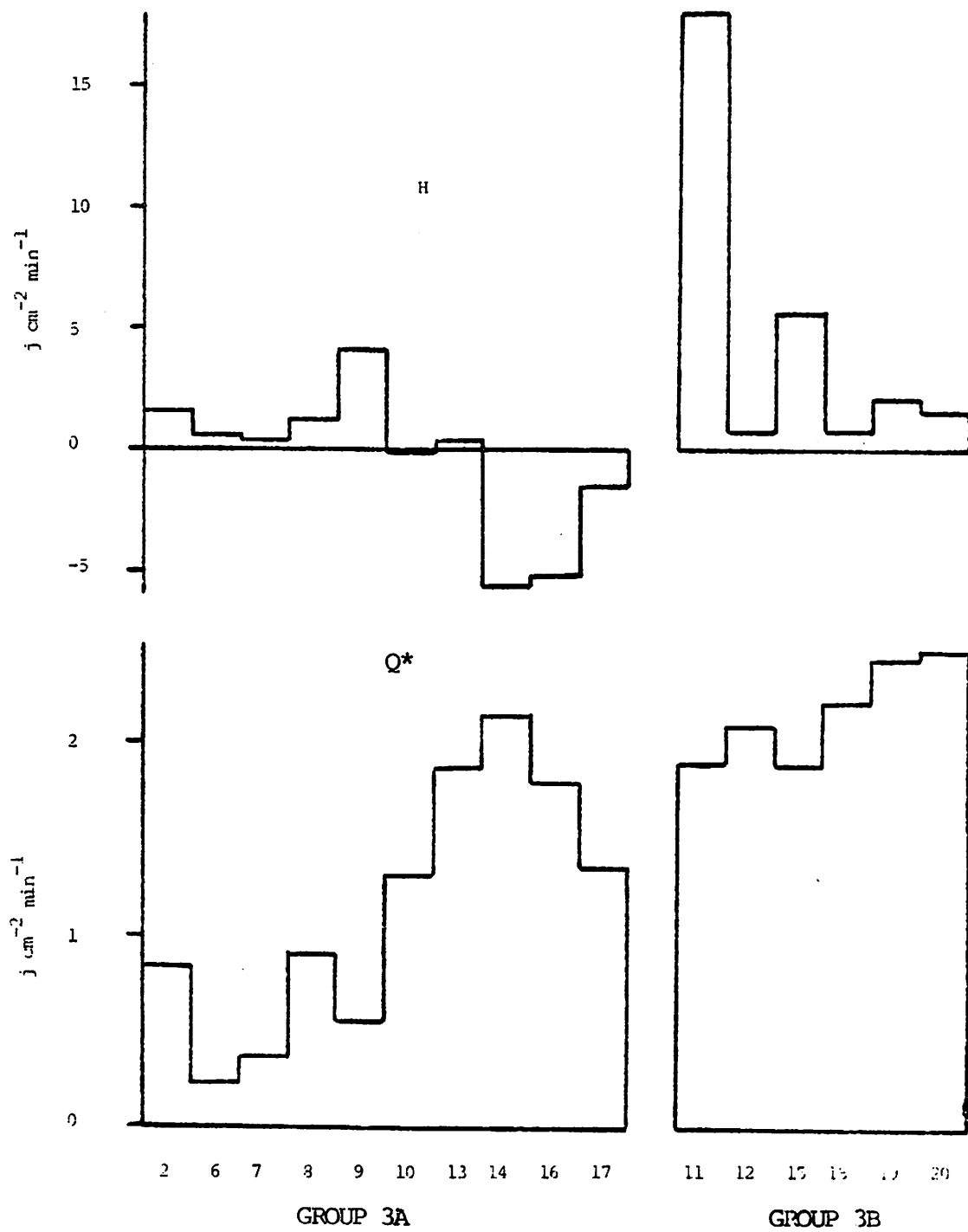


Figure 6D.8(c) Daytime values of H and Q*, for days in groups 3A and 3B.

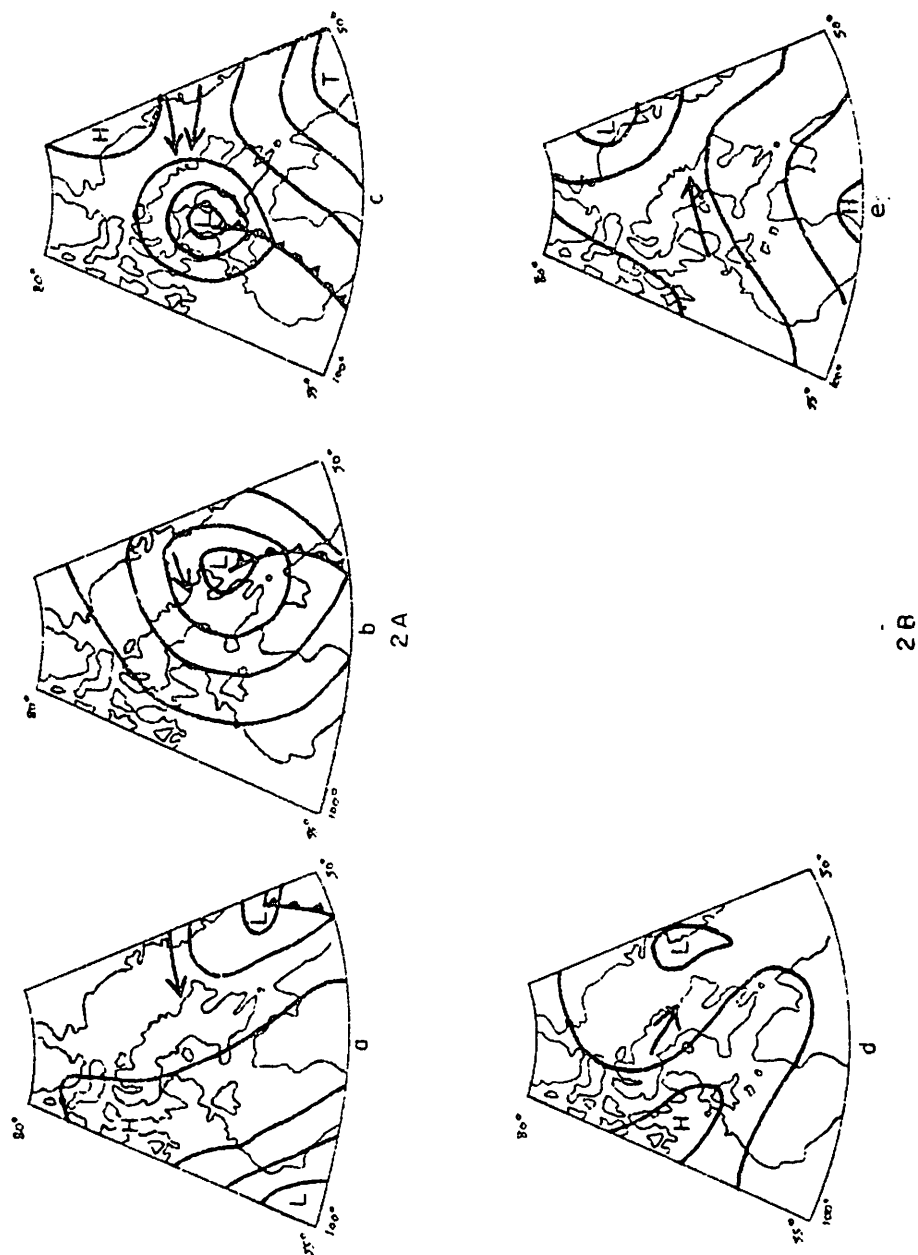


Figure 6D. 9. Characteristic synoptic patterns for days in groups 2A and 2B.

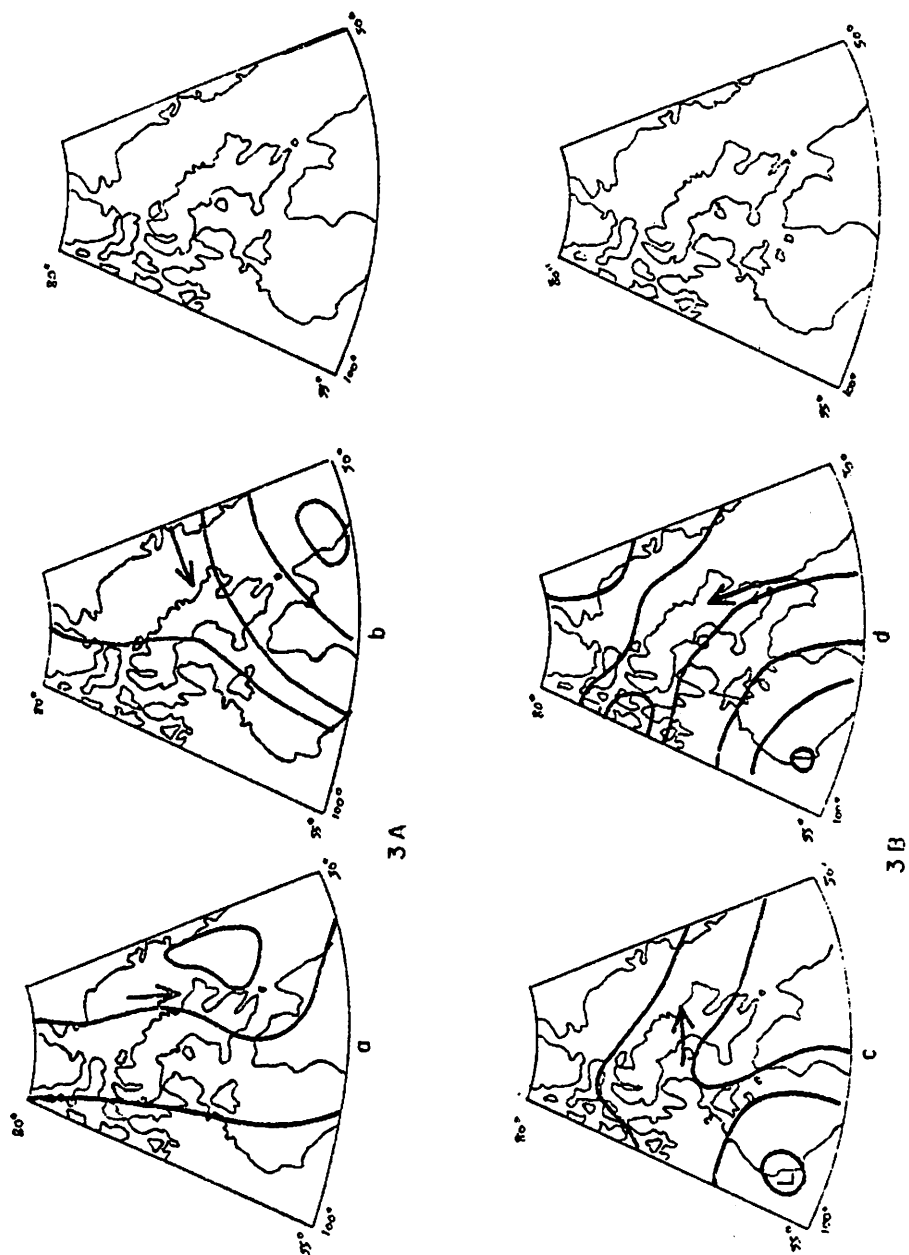


Figure 6D.10. Characteristic synoptic patterns for days in groups 3A and 3B.

References

- Allison, I.F. 1973. A sample study of the energy fluxes preceding and accompanying the formation of Antarctic sea ice. In: Energy Fluxes over Polar Surfaces, WMO Tech. Note No. 129, World Meteorol. Org., Geneva: 115-132.
- Alt, B.T. 1978. Synoptic climate controls of mass balance on Devon Island ice cap. Arct. Alp Res., 10: 61-80.
- Barry, R.G. 1974. Further climatological studies of Baffin Island, Northwest Territories. Inland Waters Directorate, Tech. Bull. No. 65, Environment Canada, Ottawa: 54 pp.
- Barry, R.G., Bradley, R.S. and Jacobs, J.D. 1975. Synoptic climatological studies of the Baffin Island area. In: Weller, G. and Bowling, S.A. (eds.), Climate of the Arctic, Univ. of Alaska, Fairbanks: 82-90.
- Deacon, E.L. 1969. Physical processes near the surface of the earth. In: Flohn, H. (ed.), World Survey of Climatology, Vol. 2, General Climatology, Elsevier, Amsterdam: 39-104.
- Grainger, M.E. and Lister, H. 1966. Wind speed, stability and eddy viscosity over melting ice surfaces. J. Glaciol., 6: 101-127.
- Holmgren, B. 1971. Climate and Energy Exchange on a Sub-Polar Ice Cap in Summer. Part F. On the energy exchange of the snow surface at ice cap station. Meteorologiska Inst., Medd. No. 112, Uppsala Univ., 53 pp.
- Jacobs, J.D. 1973. Synoptic energy budget studies in the eastern Baffin Island-Davis Strait region. Unpub. Ph.D. thesis, Univ. of Colorado, Boulder, 218 pp.
- Jacobs, J.D., Barry, R.G. and Weaver, R.L. 1975. Fast ice characteristics with special reference to the eastern Canadian Arctic. Polar Record, 17: 521-36.
- Langleben, M.P. 1972. A study of the roughness parameters of sea ice from wind profiles. J. Geophys. Res., 77: 5935-44.
- Langleben, M.P. 1974. On wind profiles over sea ice. Geophys. Res. Letters, 1: 82-85.
- LeDrew, E.F. 1976. Physical mechanisms responsible for the major synoptic systems in the eastern Canadian Arctic in the winter and summer of 1973. Univ. of Colorado, Boulder, Inst. Arct. Alp. Res., Occas. Pap. No. 22 (Cooperative thesis No. 38 National Center for Atmospheric Research) 205 pp.

- Lettau, H. 1949. Isotropic and non-isotropic turbulence in the atmospheric surface layer. AFCRL, Geophys. Res. Pap. No. 1, Cambridge, Mass, 86 pp.
- Mackay, G.A. 1952. The effect of protracted spring thaws on ice conditions in Hudson Bay. Bull. Amer. Met. Soc., 33: 101-6.
- Priestley, C.H.B. 1959. Turbulent Transfer in the Lower Atmosphere, Univ. of Chicago Press, 130 pp.
- Seifert, W.J. and Langleben, M.P. 1972. Air drag coefficients and roughness length of a cover of sea ice. J. Geophys. Res., 77: 2708-13.
- Sutton, O.G. 1953. Micrometeorology, McGraw-Hill, New York, 333 pp.
- Weller, G.E. 1968a. Heat energy transfer through four layer system: air, snow, sea ice, sea water. J. Geophys. Res., 73: 1209-20.
- Weller, G.E. 1968b. The heat budget and heat transfer processes in Antarctic plateau ice and sea ice. ANARE Sci. Repts., Ser. A(IV), Glaciology, Pub. No. 102, (Melbourne), 155 pp.
- Weller, G.E. and Holmgren, B. 1974. The microclimates of the arctic tundra. J. Appl. Met., 13: 854-62.

7. CLIMATE - ICE INTERACTION

A. Seasonal Controls of Ice Melt

R. G. Barry

The ice regime has been discussed in section 5 of the report. The purpose here is to examine the climatic controls of the normal regime and anomalies affecting its seasonal course.

While radiation input is the primary control of ice ablation (see section 6), analysis of available solar and net radiation data for 1971-73 shows no clearcut relationship with breakup. Table 7.1 summarizes radiation data for Broughton Village. It is apparent that, between 16 June and 31 July, there was a small difference in solar radiation totals favoring 1972 over 1971, whereas the ice broke up in late July 1971 but did not break up at all in 1972. However, melting-degree day totals (the positive excess of mean daily temperatures above 0°C) at Broughton Island (581 m) clearly bring out the differences between 1971-74 (Figure 7.1). This is discussed further, below. It appears that temperature conditions are particularly important in the early stages for "ripening" the snowpack on ice; the period June-July 1972 was particularly deficient in this respect. The residual effects of the cold 1971-72 winter on the sea ice temperatures, coupled with effects of the anomalous northerly wind components over Baffin Bay during the summer may have contributed to the severe ice conditions of that year (R.M.S. 1973). January-March 1972 on Broughton Island was 4°C below normal and this was not simply a local phenomenon. A colder than normal winter in Baffin Bay leads to the production of more ice to drift southward, which results in a more extensive pack. However, the effect of lower winter temperatures on the "cold content" of the ice requires only a small input of conductive heat to eliminate it. Consequently, the severity of the shorefast ice conditions, especially, is primarily determined by the summer climate.

Based on Weaver *et al.* (1976, Table 2) and the synoptic analysis in section 6D of this report, the synoptic patterns which tend to retard or advance the ablation of the ice have been tabulated in Table 7.2 in terms of the objective pressure pattern catalog (Barry and Keen, section 2, this report). Table 7.2 shows much less difference between the summer seasons of 1971-74 than might be expected in view of the contrasts in ice breakup. June 1972 is characterized by only 6 days that should favor an advancement of ablation, but this is equal to the 1946-74 mean total. The major feature seems to be the large number of days that are counted as neutral. July, 1972, however, also appears to be about average. In fact, these differences are less than those inferred previously using the subjective catalog (Barry and Jacobs, 1974; Weaver *et al.*, 1976). As noted in section 6D, there is considerable variety in the types occurring during 1972 for the period when the energy fluxes can be determined in detail. Consequently, this prevents any clear-cut relationships from being established between circulation types and energy fluxes.

Since thawing-degree days (TDDs, above 0°C) appear to be a convenient index of fast-ice breakup, their totals have been determined for the

Broughton Island (581 m a.s.l.) temperature record from 1959. Table 7.3 lists the Julian day number on which particular accumulated totals were reached and the end of September seasonal total. The results for 1971-75 (Figure 7.1) indicate that breakup around Broughton Island occurs when about 180 TDDs have accumulated at the DEW-line station (581 m).¹ Separate tabulations for the Broughton Village station suggest that the relationship between totals at the two stations is variable, but seasonal totals are generally rather higher at Broughton Village. Comparison of the years 1959-75 shows rather little year-to-year variation in the date on which 150 TDDs have accumulated. Evidently, breakup may have been later than usual (about 31 August) in 1970, which is confirmed by our general field observations, and earlier than usual (about 14 July) in 1961. The date of breakup occurs around 30 July \pm 10 days based on our observations and the TDDs in Table 7.3. Thus, breakup in 1974 and 1975 was probably about 20 days earlier than in the preceding 15 years. Table 7.3 and Figure 7.1 show also that there is considerable variation in the rapidity with which the accumulated TDDs build up. This was very rapid after early July in 1961, for example, but very slow in 1970 and 1972. An earlier examination of possible effects of onshore/offshore winds on breakup (Barry and Jacobs, 1974; Weaver et al., 1976) indicated that it may play a contributory role in some cases, but it is generally a minor factor.

Conclusions

The overall conclusion seems to be that although some substantial year-to-year contrasts in fast ice decay rates exist in this area, they are not clearly and unambiguously related to the frequency of the synoptic patterns. Certainly, northerly to easterly flow directions tend to be cool and cloudy, whereas westerly to southerly flows generally advect warm air and in association with ridge situations can give clear skies and high temperatures which can greatly accelerate melt. Once the air temperature has 'ripened' the snowpack, which may require some $8\text{--}10\text{ kJ cm}^{-2}$ of energy to melt, radiation inputs become the main control of ice ablation. Based on data in section 6, another $10\text{--}16\text{ kJ cm}^{-2}$ may be required to raise the ice temperature to 0°C and a further 50 kJ cm^{-2} to melt a 160 cm thick sheet. The 1972 data show that net radiation totalled only 10 kJ cm^{-2} in the first three weeks of July, for example. While some success in "predicting" ice thickness trends with a simple model (section 6C) has been shown, it is clear that thawing degree days still provide a simple and useful index. From the available data, about 180 TDDs ($^{\circ}\text{C}$) are required at the Broughton (DEW-line) station before breakup occurs.

¹ Wittman (1958) showed that about 500 $^{\circ}\text{F}$ TDDs (278°C) are required for the final disappearance of ice at Frobisher and Clyde, both of which stations are at sea level.

Table 7.1. Radiation Data, Broughton Village

	<u>Solar radiation</u> ($\text{kJ cm}^{-2} \text{ dy}^{-1}$)			<u>Theoretical Clear Sky</u>
	<u>1971</u>	<u>1972</u>	<u>1973</u>	
June 16-30	2.33	2.15	2.32	3.28
July 1-15	2.52	1.99	2.05	3.16
16-31	1.21	2.08	1.29	2.87
Aug. 1-15		1.64	1.56	2.46
16-31		(1.09) *	0.96	1.98

	<u>Net radiation</u> (over a tundra surface)		
June 16-30	1.29	1.15	1.04
July 1-15	1.12	1.01	1.09
16-31	0.72	1.05	0.61
Aug. 1-15		0.70	0.70
16-31		(0.28) *	0.40

* 16-26 Aug. only

Table 7.2. Objective Types in Relation to Hypothetical Ice Melt Effects

A. Categorization of Types

<u>June</u>			<u>July</u>		
<u>Retard</u>	<u>Advance</u>	<u>Neutral</u>	<u>Retard</u>	<u>Advance</u>	<u>Neutral</u>
1	3	4	1	3	7
2	7	8	2	4	10
5	11	9	5	9	
6	12	14	6	11	
10	16	15	13	12	
20	17	18	15	16	
23	19	27	20	17	
			23	18	
				19	
				27	
				28	

B. Frequency of Types (Days)

Mean	14.6	6.3	6.5	11.4	13.0	3.7
<u>1946-74</u>						
1971	15	9	2	13	12	5
1972	12	6	10	11	13	4
1973	12	10	4	10	17	2
1974	10	12	4	10	18	4

Table 7.3. Accumulated thawing-degree days (TDDs) at Broughton Island (581 m a.s.l.). (°C)

Julian day by which the following TDDs were accumulated:

<u>Year</u>	<u>50</u>	<u>100</u>	<u>150</u>	<u>Seasonal Total TDD (°C)</u> (to 30 Sept.)
1959	180	188	202	358
1960	186	195	201	382
1961	179	187	193	348
1962	187	194	202	440
1963	191	211	261	266
1964	189	204	217	281
1965	191	202	209	284
1966	192	203	213	442
1967	188	195	205	311
1968	181	198	204	293
1969	195	204	209	355
1970	202	223	245	154
1971	184	191	198	324
1972	206	219	—	141
1973	185	203	220	284
1974	175	183	189	404
1975	160	176	186	510
Mean	<u>187</u>	<u>198</u>	<u>206</u>	<u>332</u>

Note: Julian day 175 = 24 June

200 = 19 July

225 = 13 August

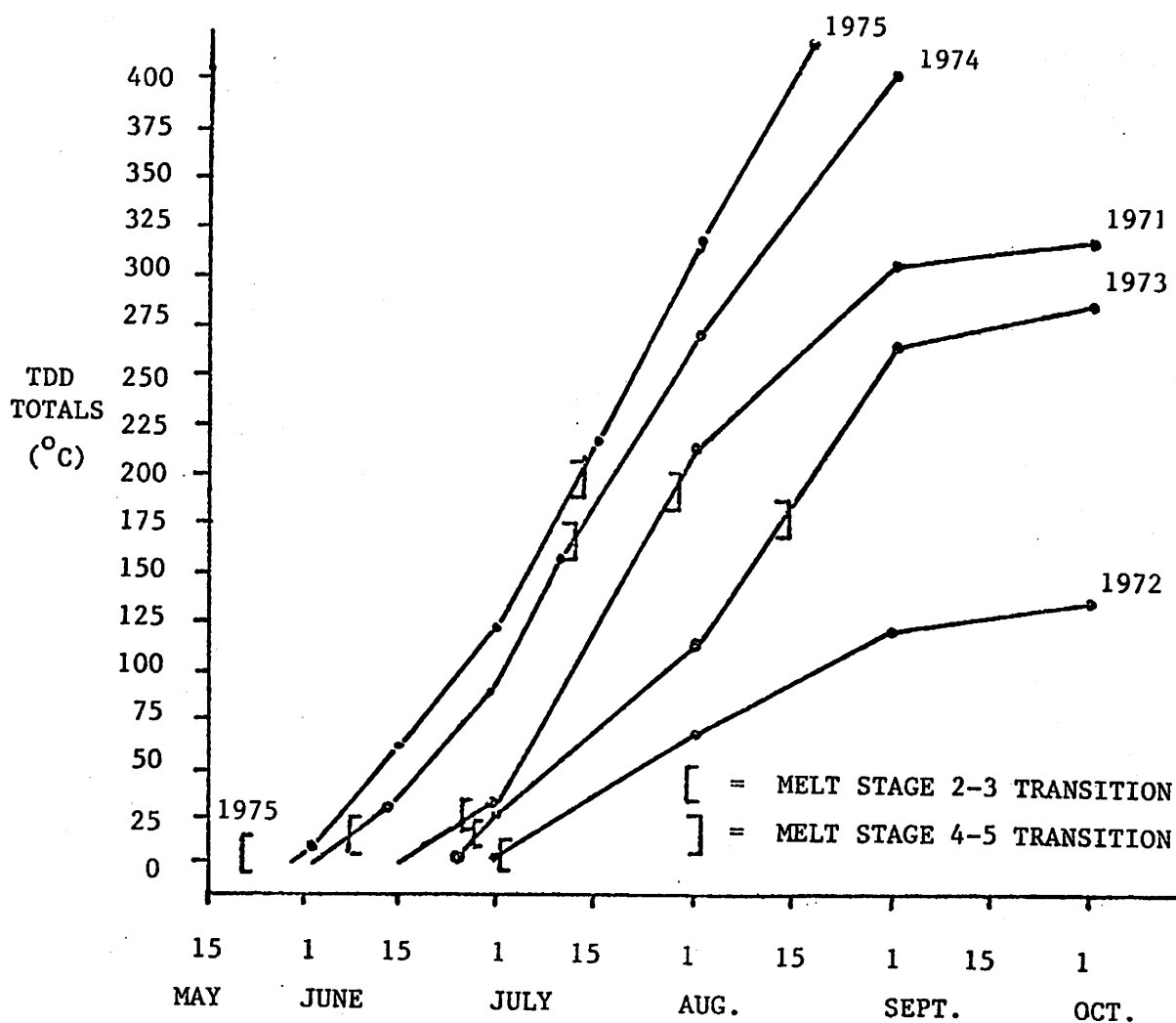


Figure 7.1

Thawing degree - day totals (°C) at Broughton Island (581 a.s.l.)
in summers 1971-75. Melt stage transitions 2-3 and 4-5 (breakup)
are also shown.

B. The Response of Baffin Bay Ice Conditions to Changes in Atmospheric Circulation Patterns
R. A. Keen

The difference in arctic ice conditions from year to year is generally largely determined by the local meteorological factors, especially summer air temperatures, which are in turn strongly controlled by the average atmospheric circulation patterns for the season. This section discusses the correlation between ice and temperature conditions for Baffin Bay and examines the associated atmospheric circulation patterns (and their variability).

The Influence of Summer Air Temperatures on Ice Conditions

The dates of the total clearing of ice from Baffin Bay for 23 seasons updated from Dunbar, 1972) are presented in Figure 7B.1. The summer (June, July, August) mean temperatures, averaged between the coastal stations of Clyde, Upernavik, and Egedesminde, are shown in Figure 7B.2. Immediately apparent in both figures is the dramatic deterioration of ice and climate conditions around 1963. During the decade preceding that year, the ice had cleared by mid-September every year but one: the decade following 1963 had seven occasions when the ice failed to clear.

When the date of ice clearing is given the numerical value of 1 for the first week in August, through 8 for the last week in September, and 9 and 10 for total clearing not occurring, its correlation with the summer temperature has a coefficient of .61. Correlating the values smoothed by a 1-2-1 running mean raises the coefficient to .79. This increase is not surprising, since the smoothing function tends to average out the component of ice breakup variability due to factors acting independently of mean summer temperature, such as sunshine, wind, storm events, and thawing during May and September. Winter temperatures, however, do not affect the correlation; their inclusion with the summer temperatures in a stepwise regression raises the correlation by less than a percent, both for the yearly and smoothed values.

The Connection between Temperature and Regional Upper Air Circulation

The variability of Baffin Bay summer temperatures may be separated into two components: the arctic mean temperature, and the local departure from the arctic mean. Summer temperatures from 44 stations were interpolated to yield values at 10° longitude intervals at 70°N latitude; these in turn were averaged to give the 70°N mean temperature, shown in Figure 7B.3. It is apparent from Figure 7B.3 that the entire arctic cooled about 0.4°C between the decades preceding and following 1963. Several authors (Dronia, 1974; Angell and Korshover, 1975; Yamamoto et al., 1975) have noted this cooling for annual average temperatures in the arctic and elsewhere, and have suggested that it may be due to volcanic dust injected into the stratosphere by the eruption of Mt. Agung in the spring of 1963 (cf. Bradley and England, 1977). This general cooling of the arctic amounts to about a third of the total cooling observed around Baffin Bay. On a yearly basis, the

variability of the arctic mean temperature is also about a third of the total variability of Baffin Bay.

The other two-thirds of the temperature variability is due mostly to changes in the regional airflow. The normal summer upper air circulation pattern in the arctic is characterized by two major troughs in the westerlies, one over extreme eastern Siberia and a somewhat stronger one over Baffin Island, and one or two lesser troughs over the North Atlantic to central Siberia sector. The longitude of the troughs is subject to changes from year to year; over Baffin Bay the prevailing upper winds can change from southerly to northerly as the trough axis shifts between west and east of its normal position over the Bay. This effect is illustrated in Figures 7B.4-7. Figures 7B.4 and 5 show the average July 700 millibar height (about 3000 meters) flow patterns for 1951-60 and 1964-73, respectively. During the first decade the trough remained, on the average, west of Baffin Bay, with resulting southerly flow. After 1963, however, the trough axis moved over the Bay, subjecting the region to more northerly flow. A map of the difference between the two decades (Figure 7B.6) shows the change to more northerly flow being strongest in a corridor from the polar ice cap over Ellsmere Island, then southeastward across Baffin Bay. This corridor coincides with the area of maximum cooling between the two decades (Figure 7B.7) as reported by Bradley (1973).

The summer mean longitude of the trough, computed as the average of the longitudes derived from the monthly mean 700 mb maps for June, July and August of each year, is given in Figure 7B.8. The major features of the year-to-year shifts in longitude compare favorably with the fluctuations in summer temperature, with the more westerly trough displacements bringing warmer air to Baffin Bay. The most notable discrepancy is that the persistent eastward shift of the trough began in 1961, two years before the start of the decade of cool summers. The correlation coefficients between trough longitude and summer temperature are .57 for the yearly values, and .75 for the smoothed values. On a local scale, the sea-level geostrophic winds over Cumberland Peninsula show a clear shift in summer wind direction about 1962-63 and a weakening compared with the 1950s (Figure 7B.9).

Changes in Cyclone Frequencies

Upper level troughs are very closely associated with cyclonic activity in the lower atmosphere; the existence of a trough on the mean upper air charts is largely due to the net effect of cyclones on the normal west to east flow. It is therefore instructive to note the changes in frequency and distribution of cyclones corresponding to the shifts in the trough. During the summer, cyclones tend to form over the central parts and off the east coast of North America, and move towards the northeast (Klein, 1957; Reitan, 1974). Some pass south of Greenland and into the North Atlantic, but many converge on the area around Baffin Island, where they weaken and dissipate. As a result, the region is under the influence of cyclones on some 85 percent of the days during the summer.

An objective scheme for classifying sea-level pressure patterns was used to tabulate the frequency and distribution of cyclones within the region

bounded by 55° and 80°N , and 50° and 100°W . The summer frequencies of cyclones over Baffin Bay, southeast of Baffin Island (over Davis Strait - Labrador Sea), and southwest of Baffin Island are compared between two decades in Table 7B.1. Also listed are the frequencies of anticyclones over the region. For comparison, the number of cyclones crossing two equal sized squares centered at 42°N , 63°W (Nova Scotia) and at 43°N , 95°W (Iowa) in July are also listed. These two areas are located in the regions of coastal and continental storm activity, and are included to illustrate the shifts in the distribution of cyclones at lower latitudes.

The cooling over Baffin Bay was accompanied by a sizeable increase in cyclonic activity over the Bay, and by a decrease in the number of cyclones to the south and southwest. The decrease in southwest cyclones is particularly significant, for these systems bring warm southerly and southeasterly winds to the region. The net effect was a shift to the north and east of cyclone activity, large enough to reverse the prevailing surface wind direction over southern Baffin Bay from easterly to westerly. The associated trough displacement increased the number of anticyclones brought into the region by the northwesterly flow on the trough's western flank. The general eastward shift was also apparent in mid-latitudes, where the cyclone activity over the central continent decreased, while coastal activity increased slightly. A similar shift in the winter storm climate has also been noted (Dickson and Namias, 1976).

The Connection between Regional and Global Circulation Patterns

The Rossby wave theory states that the length of the long waves in the atmosphere should be proportional to the square root of the speed of the westerly winds. If one of the wave features upstream (west) of the Baffin trough, such as the Alaska-Yukon ridge or the east Siberian trough, remains fixed in position, an increase in the westerly wind speed at that latitude would lengthen the wave, and push the Baffin trough eastward. The speed of the summer polar westerly winds at the 700 mb level, averaged between 55° and 70°N , and 0° to 180°W , is given in Figure 7B.10. Also shown are the mid-latitude (35° to 55°N) and subtropical (20° to 35°N) winds. The subtropical winds are actually easterly, but are presented here as negatively valued westerlies. The linear regression relations between the polar wind speed and the Baffin trough longitude is 12.1° eastward displacement for each 1 m/sec increase in wind speed, with a correlation of .74. The theoretical wave lengthens by about 15° of longitude for each 1 m/sec increase, implying that the 'fixed' feature is less than a wavelength upstream. The Alaska-Yukon ridge, whose existence is partially due to the influence of the underlying mountains, is a likely candidate, although it should be emphasized that no atmospheric circulation feature is really fixed in position.

Inspection of Figure 7B.10 reveals a general out-of-phase relationship between the fluctuations of the polar westerlies and of the subtropical easterlies, with a correlation of $-.62$, while the mid-latitude winds remain fairly constant. The average value of the wind over the whole latitude range, 20° to 70°N , is very constant, with the smoothed value always between 3.1 and 3.4 m/sec. Therefore, the variations in the polar westerlies are

due mostly to latitudinal excursions of the zone of westerlies, rather than reflecting changes in the total strength of the winds. When the westerlies shift northwards, their strength in the polar latitude belt increases.

Summary

It has been demonstrated that the severity of Baffin Bay ice conditions is largely determined by the summer air temperature. The northerly air flow prevailing during cooler summers is a result of the upper trough being east of its normal position. The trough represents part of a standing wave in the westerlies; an eastward displacement appears to be mostly a response to an increase in wavelength due to higher west wind speeds at arctic latitudes. These higher speeds are apparently due to the entire zone of westerlies being displaced northward, while the total strength of the winds remains constant. The causes of these latitudinal excursions are unclear and probably numerous. The energy balance of the tropical atmosphere is quite possibly an important factor, since a northward displacement of the zone of westerlies necessitates an expansion of the tropical circulation regime.

The essential point, however, is that the variations in ice conditions at a given arctic locality, in this case Baffin Bay, are not isolated events; rather, they are responses to changes in the largest scale atmospheric circulation patterns. This is encouraging, since it implies that any scheme capable of predicting even the simplest features of the global circulation could be applied to long-term (one to ten year) regional ice forecasting.

Table 7B.1. Average number of days in summer with cyclones and anti-cyclones around Baffin Island, and the average number of July cyclones passing through 740 km² areas near Nova Scotia and Iowa

	<u>1951-60</u>	<u>1964-73</u>	<u>Change</u>
Baffin Bay Cyclones	18	25	+7
Southwest Cyclones	35	31	-4
Southeast Cyclones	41	35	-6
Anticyclones	8	13	+5
Nova Scotia Cyclones*	3.6	4.2	+0.6
Iowa Cyclones*	3.8	2.0	-1.8

* Data provided by Dr. C. H. Reitan

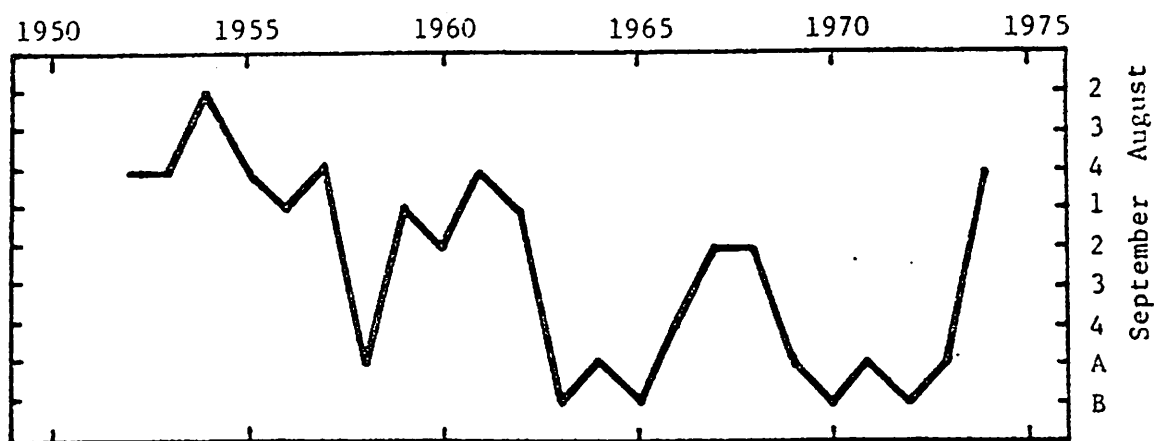


Fig. 7B. 1. Date of total clearing of ice from Baffin Bay, by week. A and B indicate ice did not clear, with, respectively, small and appreciable amounts remaining.

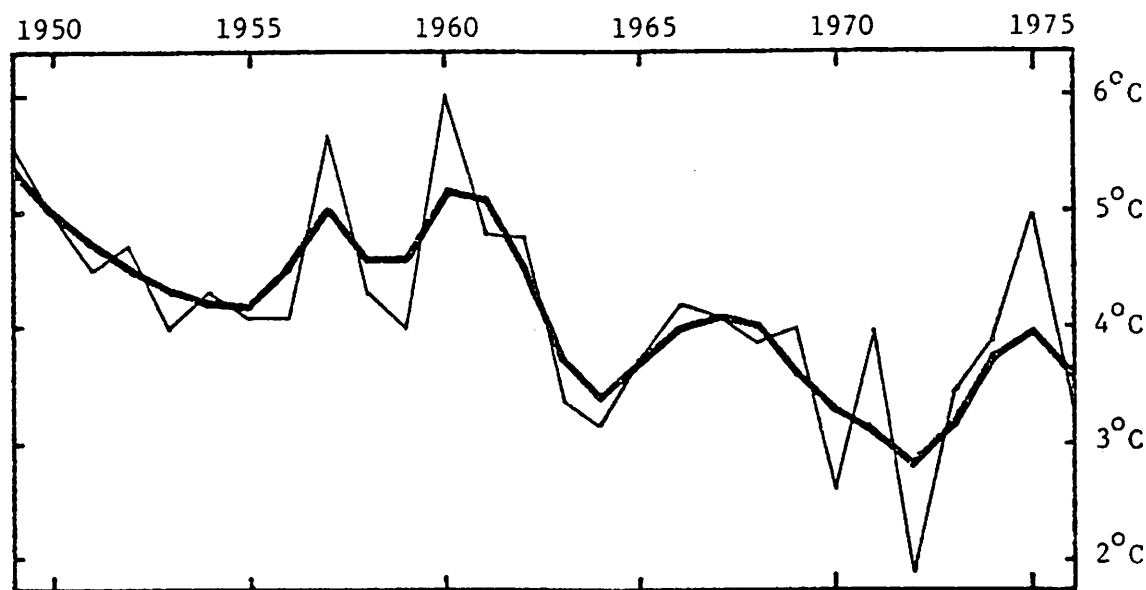


Fig. 7B. 2. Summer temperatures around Baffin Bay: yearly values (light line) and 1-2-1 smoothed values (heavy line).

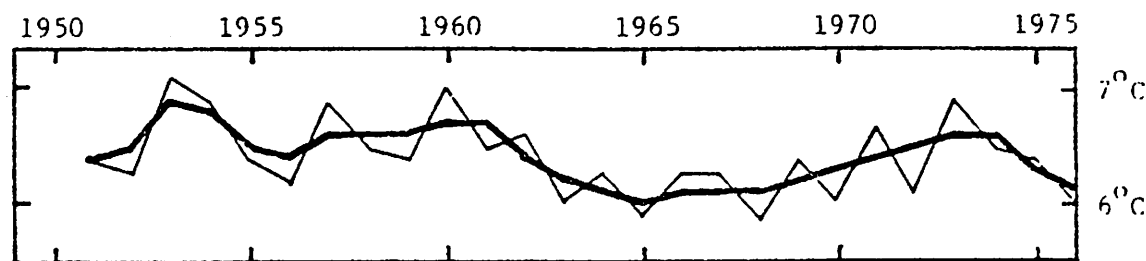


Fig. 7B. 3. Summer temperatures at 70°N, averaged around the arctic: yearly values (light line) and 1-2-1 smoothed values (heavy line).

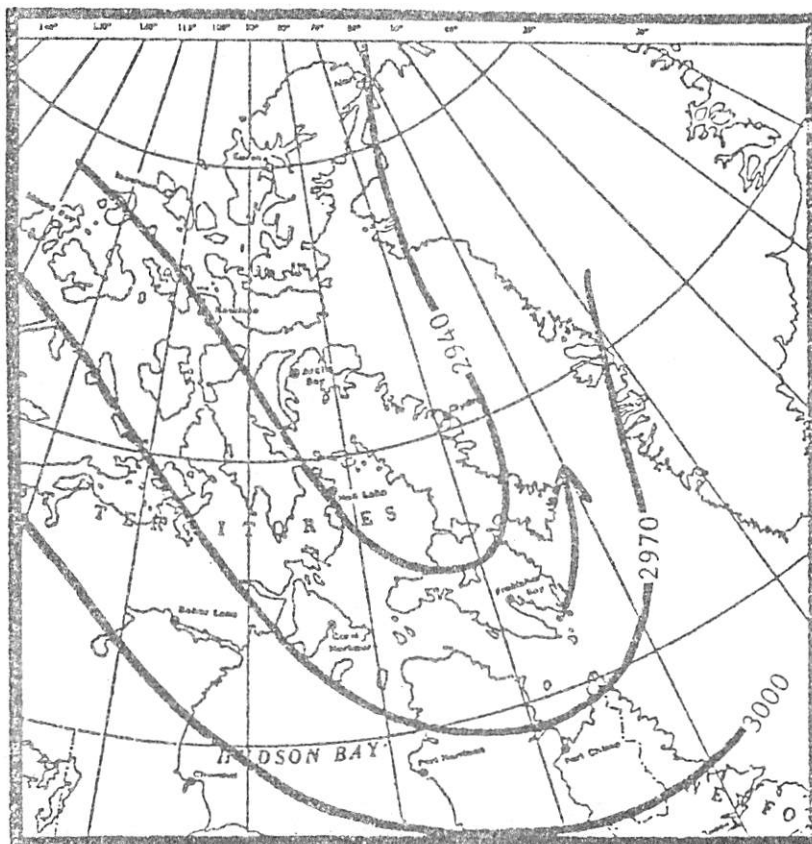


Figure 7B. 4.
Mean height of the 700
millibar level, in meters,
July 1951-60.

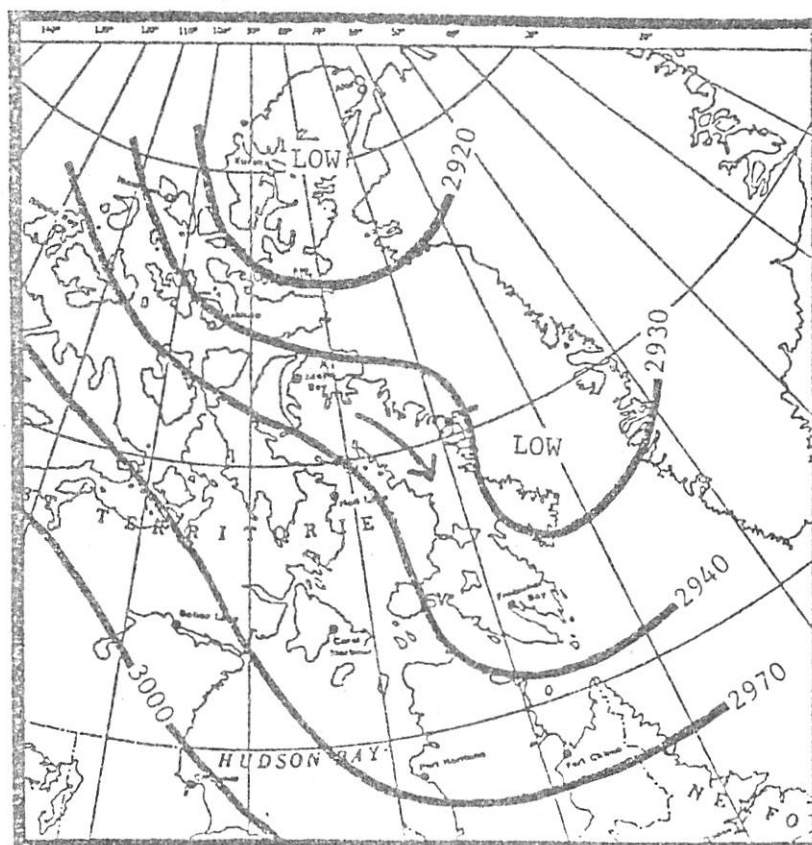


Figure 7B. 5.
Mean height of the 700
millibar level, in meters,
July 1964-73.

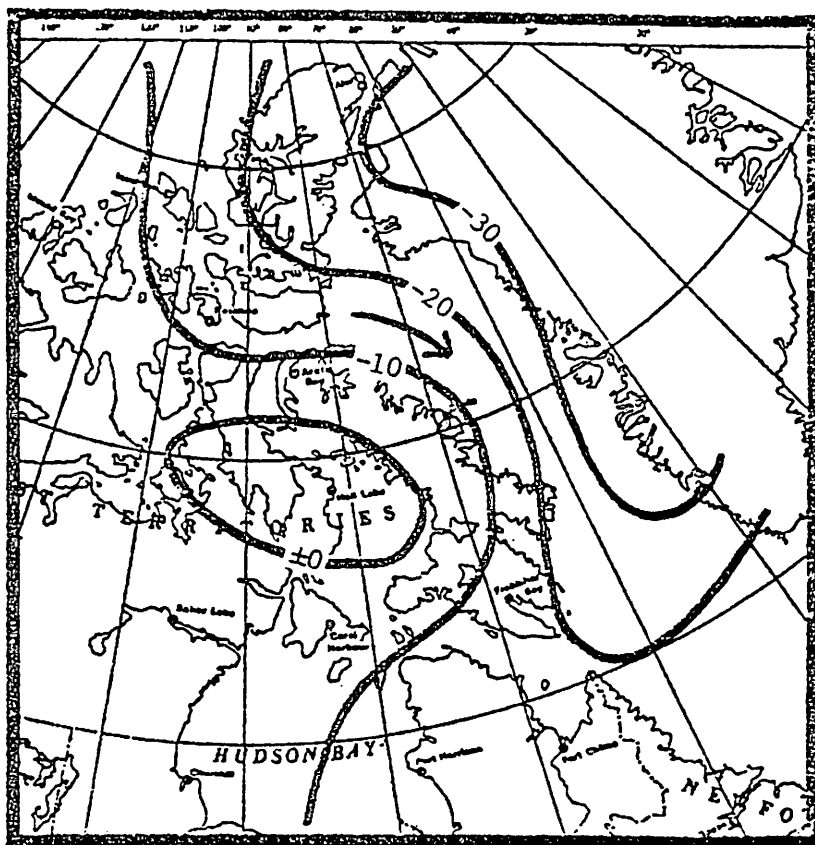


Figure 7B.. 6.

Change in July 700 millibar height, in meters, 1951-60 to 1964-73.

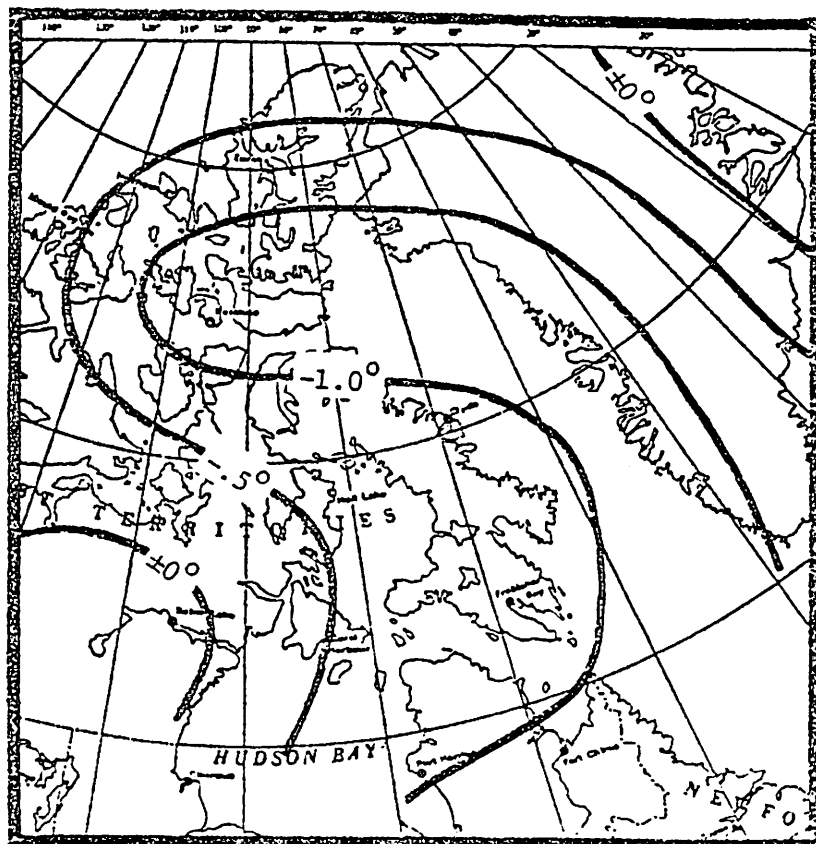


Figure 7B. 7

Change in mean summer temperatures, 1951-60 to 1964-73.

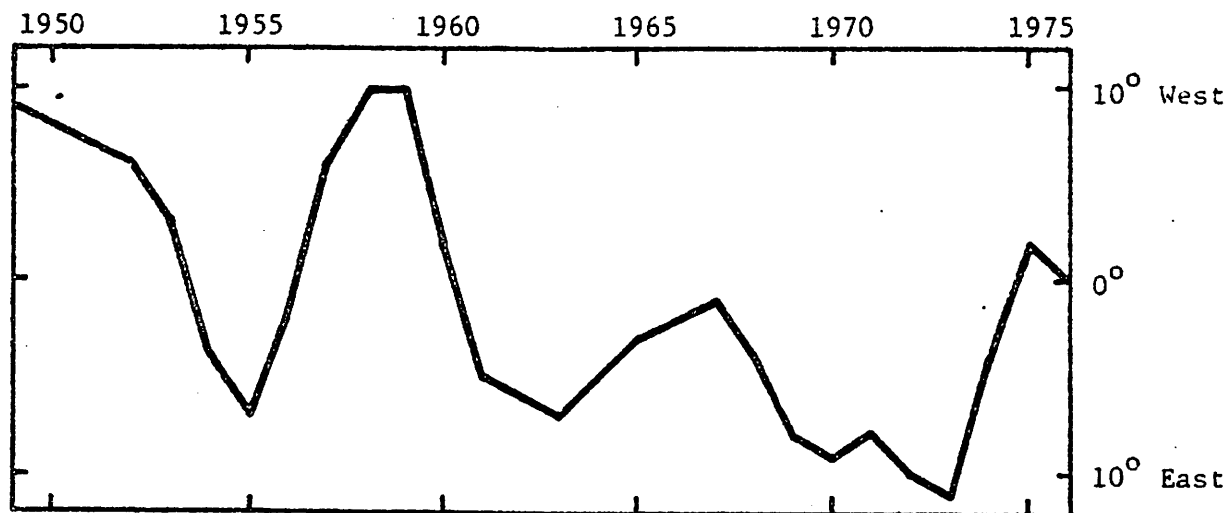


Fig. 7B.8. Displacement of the 700 millibar Baffin trough from normal position, in degrees of longitude: 1-2-1 smoothing of yearly values.

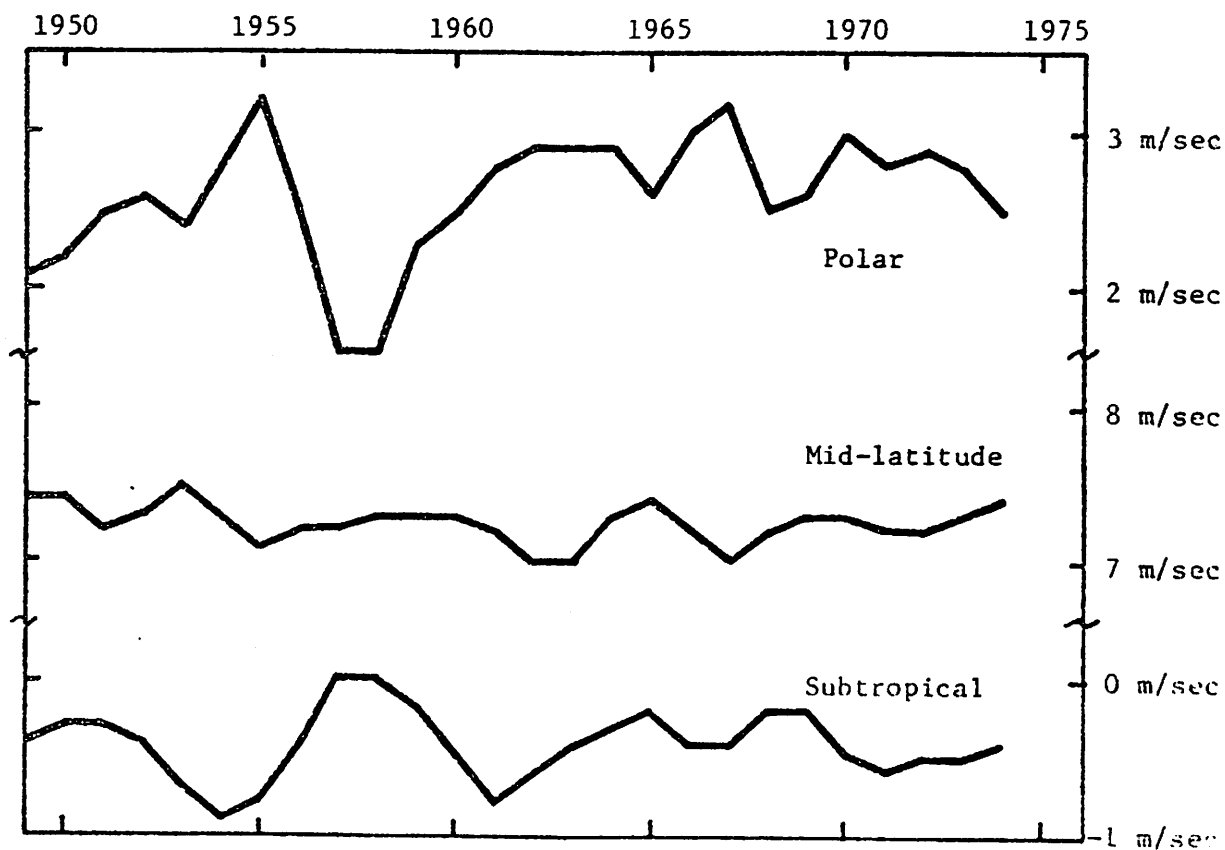


Fig. 7B. 10. Summer 700 millibar westerly wind speeds: 1-2-1 smoothing of yearly values.

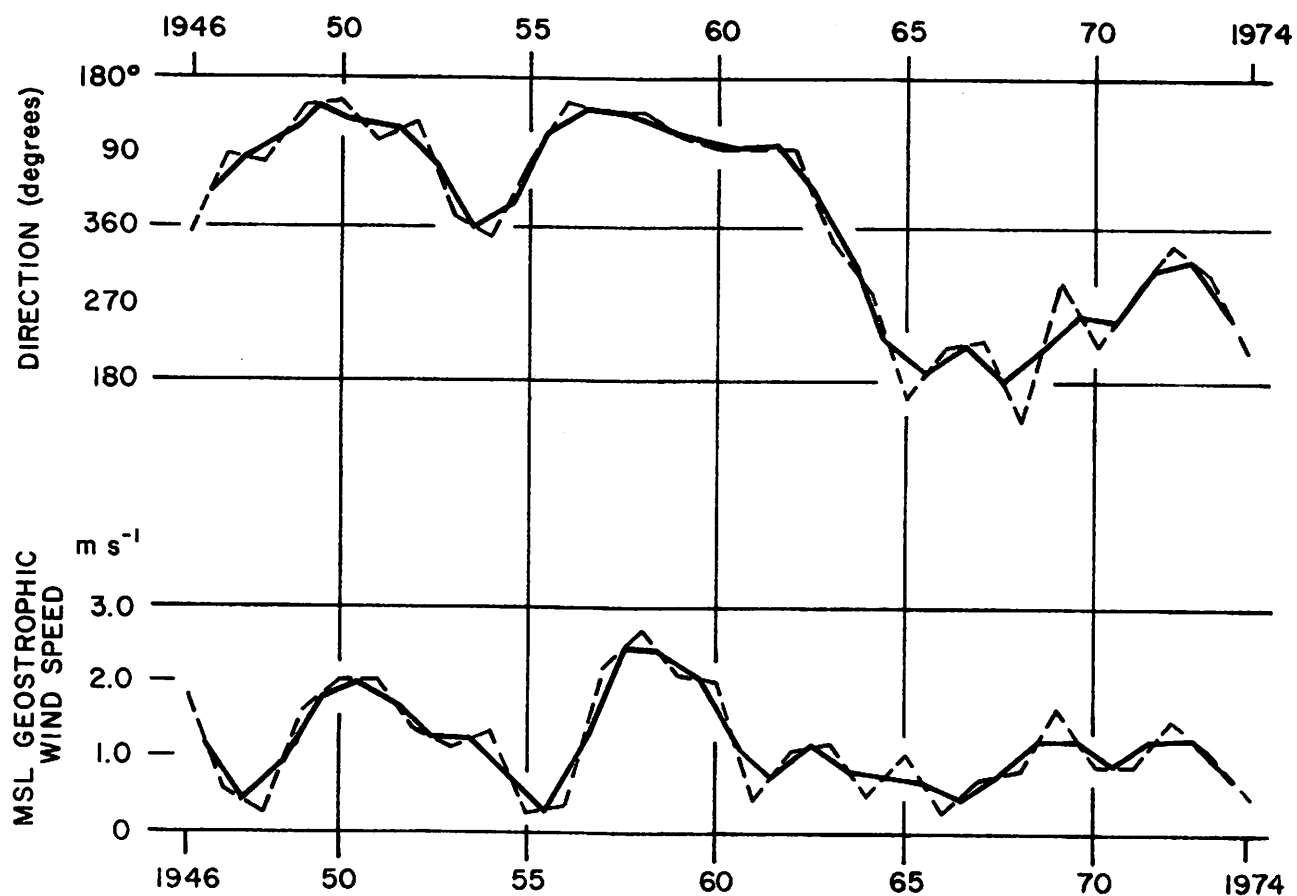


Figure 7B. 9. Geostrophic wind direction and speed for summer months over Cumberland Peninsula for 1946-74. Dashed line shows individual years, solid line 1-2-1 smoothing.

References

- Angell, J. and Korshover, J. 1975. Estimate of the Global Change in Tropospheric Temperature between 1958 and 1973. Monthly Weather Review, 103: 1007-12.
- Barry, R.G. and Jacobs, J.D. 1974. Synoptic activity, climate and ice conditions for summer 1971-1973. In: Jacobs, J.D. et al., Studies of Climate and Ice Conditions in eastern Baffin Island, 1971-73. Univ. of Colorado, Boulder, Inst. Arct. Alp. Res., Occas. Pap. No. 9, 67-75.
- Bradley, R.S. 1973. Recent freezing level changes and climatic deterioration in the Canadian Arctic Archipelago. Nature, 243: 398-400.
- Bradley, R.S. and England, J. 1977. Past glacial activity in the High Arctic. Dept. of Geol. Geogr., Univ. of Mass., Amherst, Contrib. No. 31, 184 pp.
- Dickson, R. and Namias, J. 1976. North American Influences on the Circulation and Climate of the North Atlantic Sector. Monthly Weather Review, 104: 1255-65.
- Dronia, H. 1974. Über Temperaturänderungen der freien Atmosphäre auf der Nordhalbkugel in den letzten 25 Jahren. Meteor. Rundschau, 27: 166-74.
- Dunbar, M. 1972. Increasing Severity of Ice Conditions in Baffin Bay and Davis Strait and its Effect on the Extreme Limits of Ice. In: Sea Ice, Proceedings of an International Conference, Reykjavik, pp. 87-93.
- Klein, W. 1957. Principal Tracks and Mean Frequencies of Cyclones and Anticyclones in the Northern Hemisphere, U.S. Weather Bureau Research Paper No. 40, U.S. Govt. Printing Office, Washington, D.C., 60 pp.
- Reitan, C. 1974. Frequencies of Cyclones and Cyclogenesis for North America, 1951-1970. Monthly Weather Review, 102: 861-868.
- R. M. S. 1973. Ice conditions in areas adjacent to the North Atlantic Ocean from July to September 1972. Mar. Observer 42: 187-90.
- Weaver, R. 1974. Mapping Seasonal Changes in Fast Ice and Pack using Remote Sensing Data. In: Studies of Climate and Ice Conditions in Eastern Baffin Island, 1971-73. Univ. of Colorado, Boulder, Inst. Arct. Alp. Res., Occas. Pap. No. 9, 77 pp.
- Weaver, R.L., Barry, R.G. and Jacobs, J.D. 1976. Fast ice conditions in western Davis Strait. Proc. Third Internat. Conf. on Port and Ocean Engineering under Arctic Conditions, Vol. 1, Univ. of Alaska: 455-66.
- Wittman, W.I. 1958. Continuity aids in short-range ice forecasting. In: Arctic Sea Ice, Nat. Res. Council, Publ. 598, Washington, D.C.: 244-55.
- Yamamoto, R., Iwashima, T. and Hoshiai, M. 1975. Change of the Surface Air Temperature Averaged over the Northern Hemisphere and Large Volcano Eruptions during the Year 1951-1972. J. Meteor. Soc. Japan, 53: 482-85.

APPENDIX 1

MEASUREMENTS AND INSTRUMENTATION

J.D. Jacobs and R.L. Weaver

This appendix briefly summarizes the principal instruments used in the field work supporting this study and associated instrumental and observational errors. Of primary concern are measurements made at and around Broughton Island.

1. General Climatological Observation, Broughton Village

A climatological station was established near the shore at the village, Broughton Island, in June of 1971. A program of twice-daily temperature and precipitation observations has continued regularly since that time with the assistance of cooperative observers from the village. A standard 2-meter Stevenson screen was used, with calibrated maximum and minimum thermometers supplied by the Atmospheric Environment Service of Canada mounted in the shelter. Although correction cards were supplied, the errors are less than 0.3°F in the range of normal operation and corrections have generally been neglected. The estimated error in individual temperature readings is considered to be less than 0.5°F . (0.3°C).

Precipitation measurements are difficult in Arctic regions, particularly in the colder seasons when snowfall is very light and often wind-driven. The practice at Broughton Village has been to estimate accumulation for individual storm periods by snowdepth measurements. A density of 0.2 is used in converting to a water equivalent. Summer snow and rainfall have been measured in an unshielded 10cm aperture guage with a 5:1 reduction to an interior graduated cylinder. While the catch of rainfall is reliable, that of snowfall is not. Total accumulations are therefore underestimated, a situation in common with other Arctic stations (Hare and Hay, 1971).

A recording hygrothermograph was maintained in the Stevenson screen as a backup for temperature measurements. The relative humidities measured by this instrument have been found to be within 15 per cent of psychrometric valued during the summer. For colder seasons, the hair element is an unreliable indicator of humidity. Thus, humidity measurements were not made on a regular basis as part of the climatological program.

2. Wind Measurements

Windspeed measurements at Broughton have been of two kinds, a run of wind taken at 3 m (1971) or 10 m (1972-1974), and low-level wind profiles taken periodically during intensive micrometeorological observations. Standard U.S.W.B. totalizing anemometers (Friez) with twice-daily readings were used in the former kind of measurement. In 1973 and 1974 wind measurements were recorded continuously at 10 m using a galvanometric type of sensor.

Wind profiles at the ice station in 1972 were made with a Thornthwaite four-level (20, 40, 80, and 160 cm) sensitive anemometer array for roughness parameter determinations. The factory calibration of this system was made in comparison with a National Bureau of Standards standard. Field checks showed that for air temperatures between -10° and $+10^{\circ}\text{C}$ the starting speed of the anemometers is about 0.1 m-sec^{-1} , and slight variations occur in response among the several levels. For windspeeds greater than 0.5 m-sec^{-1} , the response is uniform, and the resulting wind profiles are considered reliable.

As the basis for turbulent flux calculations using the mass transfer method, a sensitive anemometer (Casella-Sheppard, 1972, Electric Speed, 1973, 1974) and wind aspirated thermistor were installed on a 10-m tower near the shore at Broughton Island.

Wind speeds at the ice station were recorded using the Thornthwaite four level system in 1972. Four-hourly profiles were made daily throughout the summer operations. Wind run was recorded using the Cassella-Sheppard precision anemometer at 2 m in 1973. Two Bechman and Whitley light chopper anemometers at 2 m and 1 m provided continuous and short term values of wind run. The Beckman and Whitley anemometers were calibrated in the wind tunnel of the National Center for Atmospheric Research, with the assistance of Dr. Harold Baynton.

3. Temperature and Humidity Profiles

A required accuracy of 0.05°C and 0.01 mb has been given for temperature and humidity profiles used for turbulent flux calculations (W.M.O., 1966). Such accuracy is beyond the capability of conventional psychrometric methods under Arctic field conditions; however, we have been able to obtain reasonably consistent measurements having an estimated accuracy which is an order of magnitude larger than that stated above.

The technique employs one or two Assmann-type psychrometers graduated to 0.1°C . At the Ice Station in 1973 and 1974 measurements were made consecutively at two levels, e.g., 40 and 160 cm, and a gradient derived from these. An alternate method is based upon the fact that a snow, ice, or water surface is by definition saturated. Psychrometric measurements are made at a single level, 2 meters, and a surface temperature taken with a thermistor. The saturation vapor pressure corresponding to the surface temperature is then used with the value obtained from the 2 m wet and dry bulb temperatures to provide the vapor gradient.

The measurement of surface temperatures is difficult when the surface is in sunshine, since even the smallest sensor will experience some solar heating. The effect is alleviated somewhat by placing the thermistor a few cm below the surface, but even at 10 cm, an excess temperature of over 1.0°C is not uncommon under clear or partly cloudy conditions. The problem becomes somewhat less difficult once melting is underway, since a temperature of 0°C can then be assumed for the surface. However, radiative cooling occurs rapidly in the evening, even in midsummer, and surface temperatures may drop several degrees below freezing although the subsurface layers are still wet.

Neglect of such cooling means ignoring a potentially large heat influx due to condensation at the surface.

Meltwater pools provide another source of difficulty in latent heat flux estimates. A diurnal surface temperature range of as much as 10°C may occur in the upper few millimeters with solar heating during the day and cooling to form a thin skim of ice at night.

In 1973 temperature and relative humidity at the ice station were recorded continuously inside a meteorological screen and periodically on the net radiation tower. A Bendix Friez hygrothermograph was operated continuously inside the meteorological screen at a height of 1.2m. The instrument was calibrated using an Assmann Psychrometer and periodic comparisons with maximum-minimum thermometers. Screen heating of $+1-2^{\circ}\text{C}$ under calm clear sky conditions does exist within the data. Comparison of the screen and the 0.4m aspirated temperature.

Two Assmann Psychrometers were suspended on the net radiometer tower at 1.6 and 0.1m in 1973, and at 1.6 and 0.4m in 1974. Measurements were made at four-hourly intervals in 1973 and at one-hourly intervals in 1974 during station occupation. In 1974 an aspirated thermistor at 2m was employed to supplement the continuous data recorded on the Pernix hygrothermograph in the meteorological screen. The thermistor bridge output was amplified and then recorded on a Rustrack 0-1 ma recorder.

4. Radiative Temperatures

The blackbody surface temperature used in the calculation of the terrestrial flux, I_{\uparrow} , was generally obtained from measurements with thermistors, as discussed above. A commercial thermistor system (Atkins Instrument Co.) was used for this purpose and for near surface ocean temperatures and temperatures within the sea ice. The instrument was checked periodically using an ice bath, and no significant variation was found. In addition a precision resistors were substituted for the thermistors to verify meter accuracy at $\pm 25^{\circ}\text{C}$. Based upon such considerations as the firmness of thermal contact (in the case of snow) and the resolution of the meter scale, a maximum error of about 0.5°C can be given, apart from any effects of solar heating.

A Barnes PRT-5 radiometer was used on occasion in 1972 and 1973 for surface temperature measurements as well as for cloud base temperatures. The accuracy of this instrument is given by the manufacturer as 0.5°C with a sensitivity of 0.1°C . Field calibrations using a black cavity at 0°C gave an absolute error for this particular instrument of $+0.8^{\circ}\text{C}$, which corresponds to about $0.007 \text{ cal-cm}^{-2} \text{ min}^{-1}$ in the equivalent blackbody flux.

A PRT-10L Infrared Radiation Thermometer supplemented thermistor surface temperature measurements in 1974. However, little agreement was found between thermistor and IR temperatures most probably due to poor temperature calibration of the PRT-10L and unknown surface emissivity changes.

5. Solar Radiation

The principal instrument used for the measurement of global solar flux was the Kipp and Zonen pyranometer. This is a non-temperature-compensated instrument. The instrument used had been calibrated by the manufacturer at 20°C, and Robinson (1958) has shown a -0.1 to -0.2%/°C temperature was made in the field, but a post-field season (1972) mid-winter comparison with a precision Eppley pyranometer indicated that the output of the Kipp at near-freezing temperatures is 3 per cent below the rated value. This correction has been applied to the Arctic measurements. The Kipp and a Model 2 Eppley were operated side-by-side in 1973. Differences in instantaneous values for solar elevations above 20 degrees and for daily totals during the summer months were less than 3 percent. The maximum uncertainty due to temperature over a typical seasonal and diurnal range of some 25° is about 5%, Jacobs (1974).

The output of the pyranometers in 1971, 1972, and 1974 were recorded on galvanometric recorders (Esterline-Angus) with a precision d-c amplifier (Xeltex) at the interface. In 1973 a Multichannel Data logger (Esterline-Angus D2020) measured instantaneous fluxes every 10 minutes. Calibrations were made once daily. In view of the combined effects of temperature and data interpretation, an error of about 5 per cent is assumed for the solar flux data used in this study.

At the Ice Stations short-wave albedo under the net radiometer site and along transects across the fast ice surface was determined using a matched system of Monteith (Lintronic) pyranometers (Monteith, 1972). The instrument height was always one meter and therefore 90% of the radiation received by the downward viewing sensor was inside a cone approximately five meters in diameter (Latimer, 1971).

The average of three instantaneous albedo measurements comprises a single reported albedo measurement. The albedos under the net radiometers were generally measured near local noon. The linear transects consisting of between 20 and 30 individual measurements spaced 1m apart took an average of one hour to complete. the transects were most often recorded between 1000 EST and 1400 EST which reduces reflected flux errors associated with low solar angles as discussed by Langleben (1966). The predominant surface type inside a one meter radius of the instrument site was also cataloged.

Stanhill (1971) found for both Kipp and Lintronic instruments a decrease in output of about 1.5 percent when the pyranometer is inverted. In addition, when effects of spectral composition, cosine response, and solar azimuth were included, he found a range of uncertainty in reflected flux, and hence albedo, of over 20 per cent for intermediate solar elevations. Because of the large short-term variations in the albedo of snow and ice surfaces with changing conditions, it is difficult to detect any systematic error of this kind in our measurements. Nevertheless, the estimated uncertainty in albedo of 10 per cent may be too small.

6. Net Radiation

The main net radiation instrument used at the Broughton tundra site was a Fritschen-designed (Fritschen, 1963), temperature-compensated radiometer, mounted 4 meters above a representative land surface. The instrument was ventilated with dry air using a diaphragm pump with desiccant in the line. Analog records (1971, 1972, 1974) were obtained using the same recorder system described for solar flux measurements. The datalogger system recorded instantaneous fluxes at 10 minute-intervals in 1973.

A similar instrument, manufactured by C. W. Thornwaite Associates, was used for the Boas Glacier studies and on the ice at Broughton Island (1971 and 1972). Both radiometers were operated together at the same location for purposes of comparison. Using the manufacturers' calibrations, a correlation coefficient of 0.998 and an absolute difference of 11 per cent were obtained between the two. Laboratory checks over a water bath in a darkened room gave agreement within 10 per cent of the manufacturers' values. This amount of uncertainty is given as typical for this kind of instrument (W.M.O., 1965).

In 1973 and 1974 net radiation at the ice station was measured using Funk-design net pyradiometers (Solar Radiation Instruments Ltd.), and calibrated by C.S.I.R.O. The spectral response of these instruments is .2 μ m to 50 m with a linearity of $\pm 1\%$ (Latimer, 1971). These instruments are not temperature-compensated, but, the correction factor is very small ($0.05\% \text{ } ^\circ\text{C}^{-1}$). In 1973 a single net radiometer was shifted from wet to unsaturated sites to enable comparative measurements of various surfaces. In 1974 two instruments recorded continuous comparative data over wet and unsaturated surfaces. Instantaneous minute values were integrated to provide both hourly and daily net radiation totals using a Bendix datagridder at the National Center for Atmospheric Research (NCAR). The instrument height in both years was 2.0m. Ninety percent of the radiation received from the surface was inside a cone 12 m in diameter, (Latimer 1971).

7. Ice and Water Salinities and Temperatures

Ice depth and salinity-temperature profile changes were monitored throughout the melt seasons. In 1973, puddle water temperature profiles and ice salinities were recorded for only specific cases. In 1974, puddle water temperatures were included in the normal hourly observations.

A Beckman salinity-conductivity bridge model EV5 and a LaMotte water sampling bottle and chemical analysis were used to record salinity and temperature profiles in 1973 (Jacobs et. al., 1974). In 1974 a YSI Model 33 salinity-conductivity bridge was used.

Surface puddle water temperatures were measured with Atkins technical thermistor bridges in both 1973 and 1974. The bead thermistor sensor was suspended in the water and shielded from direct solar radiation. Solar heating of the thermistors imbedded in the ice was minimized by shielding the sensor burial site from direct solar radiation during the observation time.

REFERENCES

- Fritschen, L.J., 1963. Construction and evaluation of a miniature net radiometer, J. Appl. Meteor., 2: 165-172.
- Hare, F.K., and J.E. Hay, 1971. Anomalies in the large-scale annual water balance over northern North America, Canadian Geographer 15: 79-84.
- Jacobs J.D., Barry, R.G., Bradley, R.S. and Weaver, R.L. 1974. "Studies of Climate and Ice Conditions in Eastern Baffin Island 1971-73", Inst. Arctic and Alp. Res., Occasional Paper No. 9, University of Colorado, Boulder, 78 pp.
- Monteith, J.L., 1972: Principles of Environmental Physics, London Edward Arnold.
- Latimer, J.R., 1972: Radiation Measurement, Int. Field Year for the Great Lakes Tech. Manual Series No. 2 Ottawa 53 p.
- Robinson, G.D., 1958. Some observations from aircraft of surface albedo and the albedo and absorption of cloud, Archiv Meteor., Geophys., Bioklimat., B, 19: 113-117.
- Stanhill, G., 1971. Accuracy of field measurements of solar reflectivity, Archiv Meteor., Geophys., Bioklimat., B, 19: 113-117.
- World Meteorological Organization, 1965. Guide to Meteorological Instrument and Observing Practices, Suppl. No. 5, 2nd ed., Geneva, 56 pp.
- World Meteorological Organization, 1966. Measurement and Estimation of Evaporation and Evapotranspiration, Tech. Note No. 83, Geneva, 121 p.

**INSTITUTE OF ARCTIC AND ALPINE RESEARCH
OCCASIONAL PAPERS**

Numbers 1 through 5, and 11 and 12 are out of print. A second edition of Number 1 is available from the author. Numbers 2, 4, 5 and 11 are available from National Technical Information Service, U.S. Department of Commerce. For details, please write to INSTAAR.

6. *Guide to the Mosses of Colorado*. By W.A. Weber. 1973. 48 pp. Order from the author, University of Colorado Museum, Boulder, Colorado 80309. \$2.50.
7. *A Climatological Study of Strong Downslope Winds in the Boulder Area*. By W.A.R. Brinkmann. 1973. 228 pp. Order from the author, Institute for Environmental Studies, University of Wisconsin, 1225 West Dayton Street, Madison, Wisconsin 53706.
- †8. *Environmental Inventory and Land Use Recommendations for Boulder County, Colorado*. Edited by R.F. Madole. 1973. 228 pp. 7 plates. \$6.00.
- †9. *Studies of Climate and Ice Conditions in Eastern Baffin Island*. 1971-73. By J.D. Jacobs, R.G. Barry, R.S. Bradley, and R.L. Weaver. 1974. 77 pp. \$3.00.
- †10. *Simulation of the Atmospheric Circulation Using the NCAR Global Circulation Model With Present Day and Glacial Period Boundary Conditions*. By J.H. Williams. 1974. 328 pp. \$4.75.
11. *Solar and Atmospheric Radiation Data for Broughton Island, Eastern Baffin Island, Canada, 1971-73*. By J.D. Jacobs. 1974. 54 pp. (Out of print.) NTIS PB-248 955/7GA. Paper \$4.50. Microfiche \$2.55.
12. *Deglacial Chronology and Uplift History: Northeastern Sector, Laurentide Ice Sheet*. By A.S. Dyke. 1974. 113 pp. (Out of print.)
- †13. *Development of Methodology for Evaluation and Prediction of Avalanche Hazard in the San Juan Mountains of Southwestern Colorado*. By R.L. Armstrong, E.R. LaChapelle, M.J. Bovis, and J.D. Ives. 1975. 141 pp. \$4.75.
- †14. *Quality Skiing at Aspen, Colorado: A Study in Recreational Carrying Capacity*. By C. Crum London. 1975. 134 pp. 3 plates. \$5.50.
- †15. *Palynological and Paleoclimatic Study of the Late Quaternary Displacements of the Boreal Forest-Tundra Ecotone in Keewatin and Mackenzie, N.W.T., Canada*. By H. Nichols. 1975. 87 pp. \$4.00.
- †16. *Computer Techniques for the Presentation of Palynological and Paleoenvironmental Data*. By M. Nichols, M. Eccles, and H. Nichols. 1976 (in preparation).
- †17. *Avalanche Atlas: San Juan County, Colorado*. By L. Miller, B.R. Armstrong, and R.L. Armstrong. 1976. 260 pp. 60 plates. \$4.25.
- †18. *Century of Struggle Against Snow: A History of Avalanche Hazard in San Juan County, Colorado*. By B.R. Armstrong. 1976. 97 pp. 11 plates. \$4.50.
- †19. *Avalanche Release and Snow Characteristics, San Juan Mountains, Colorado*. Edited by R.L. Armstrong and J.D. Ives. 1976. 256 pp. 7 plates. \$7.50.
- †20. *Landslides Near Aspen, Colorado*. C.P. Harden. 1976. 61 pp. 5 plates. \$3.75.
- †21. *Radiocarbon Date List III. Baffin Island N.W.T., Canada*. By J.T. Andrews. 1976. 50 pp. \$2.50.
- †22. *Physical Mechanisms Responsible for the Major Synoptic Systems in the Eastern Canadian Arctic in the Winter and Summer of 1973*. By E.F. LeDrew. 1976. 205 pp. \$4.50.
- †23. *Procedures for the Study of Snow Avalanche Chronology Using Growth Layers of Woody Plants*. By C.J. Burrows and V.L. Burrows. 1976. 60 pp. \$4.00.
- †24. *Avalanche Hazard in Ouray County, Colorado, 1877-1976*. By B.R. Armstrong. 1977. 125 pp. 32 plates. \$4.50.
- †25. *Avalanche Atlas, Ouray County, Colorado*. By B.R. Armstrong and R.L. Armstrong. 1977. 132 pp. 34 plates. \$5.50.
- †26. *Energy Budget Studies in Relation to Fast-ice Breakup Processes in Davis Strait: Climatological Overview*. R.G. Barry and J.D. Jacobs with others. 1978. 284 pp. \$7.00.

†Order from INSTAAR, University of Colorado, Boulder, Colorado 80309. Orders by mail add 65 cents per title.

Occasional Papers are a miscellaneous collection of reports and papers on work performed by INSTAAR personnel and associates. Generally, these papers are too long for publication as journal articles, or they contain large amounts of supporting data that are normally difficult to publish in the standard literature.